ISCORD

12TH SYMPOSIUM ON COLD REGIONS DEVELOPMENT

17-19 JUNE 2019

PROCEEDINGS

OULU, FINLAND – ISCORD2019.COM

ISCORD 2019

12th Symposium on Cold Regions Development

June 17-19, 2019, Oulu, Finland

Symposium proceedings

Editors

Riitta Kamula and Ville Raasakka

Organizers

International Association for Cold Region Development Studies (IACORDS)
University of Oulu
Finnish Association of Civil Engineers RIL

ISCORD 2019 LOCAL ORGANIZING COMMITTEE

Ville Raasakka
Anna Järvinen
Riitta Kamula
Pekka Leviäkangas
Jarkko Okkonen
Elina Rantakallio
Pirjo Taskinen

ISCORD 2019 SCIENTIFIC COMMITTEE

Riitta Kamula, Chair
Koichi Ayuta
David M. Blake
Eun Chul Shin
Changlei Dai,
Chen Dong-feng
Pernille Erland Jensen
Ehsan Noroozinejad Farsangi
Robert E. Harris
Mitsuru Honda
Shunji Kanie
Kunihiro Kishi
Terenty A. Kornilov
Thomas G. Krzewinski
Jangguen Lee
Jong-Sub Lee
Pekka Leviäkangas
John Ma
Masaaki Minami
Zbigniew Mlynarek
Boualem Ouazia
Jarkko Okkonen
Andrzej Patalas
James Rooney
Hiroshi Saeki
Keiichi Satoh
Young Seok Kim
Anastasia N. Tseeva
David Paul Waterhouse
Wang Xinglong
Tomio Yamaguchi
Askar Zhussupbekov
Hannele K. Zubeck

ISBN 978-951-758-647-4

ISSN 0356-9403

PREFACE

International Symposium on Cold Region Development - ISCORD - is an interdisciplinary forum, organized every three years by the International Association for Cold Regions Development (IACORDS). The symposia provide cold region experts opportunities to exchange experiences and knowledge across a wide range of scientific, technological and cultural disciplines with a specific focus on the development of the cold regions. Since its establishment in 1983, ISCORD has been playing an increasingly important role in addressing challenges resulting from global warming. Cold Regions Symposium in Oulu on June 2019 is the 12th in this chain of conferences.

The ISCORD conference 2019 has brought together participants from 13 different countries around the cold and arctic areas. At the moment of the Conference, days in the Northern Hemisphere are the longest. In Oulu, the period between sunset and sunrise is less than two hours, and further North the Sun sets in July. The Nature has awakened and turning towards a summer mode.

The subjects of the conference revolve around sustainable use of resources, climate change, and traffic and infrastructure solutions in cold areas. The fundamental goal is to promote sustainable development in these delicate areas by advancing the balanced use of resources and thus minimizing the adverse effects of climate change. The presentations and discussions about the joint issues and solutions are expected to promote better future in these sensitive areas.

The contributions of all the participants are valuable for the success of the conference, especially the keynotes who have used their valuable time for the common good. The funding from all the sponsors is well acknowledged, special thanks are to our main sponsors The Federation of Finnish Learned Societies and Maa- ja vesitekniikan tuki. The organizers wish to address their compliments also to all the volunteers for their contribution.

We wish you a fruitful and enjoyable conference and hope that it will provide opportunities to foster new and intensify current cooperation in all the issues related to cold areas.

On behalf of the organizers

Dr. Riitta Kamula

IACORDS Vice President

Kvantum Institute, University of Oulu, Finland

TABLE OF CONTENTS

EDUCATION AND TRAINING

INFRASTRUCTURE

CONSTRUCTION TECHNOLOGIES

POSTER PRESENTATIONS

ENVIRONMENT AND SOCIETY

Climate Change and Assessment of Its Impact on the Engineering Design Parameters for Infrastructure in Northern Alaska

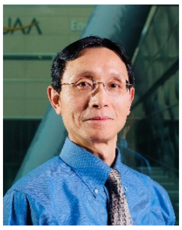

Zhaohui “Joey” Yang
Professor of Civil Engineering
University of Alaska Anchorage
U.S.A.
zyang2@alaska.edu

Mr. Kannon Lee, University of Alaska Anchorage, U.S.A., kclee3@alaska.edu
Dr. Haibo Liu, Lamont Doherty Earth Obs., Columbia University, U.S.A., haibo@ideo.columbia.edu
Dr. Caixia Wang, University of Alaska Anchorage, U.S.A., cwang12@alaska.edu
Mr. Todd Burns, University of Alaska Anchorage, U.S.A.,twburns@gmail.com

Summary

Warming climate, thawing permafrost, and subsequent ground settlement in the Arctic has become increasingly significant, posing a constant threat to the safety of underground and surface infrastructures such as energy extraction and transport assets (oil wells and pipelines), buildings, railways, highways, and bridges. Such a problem is particularly severe in Alaska where ice-rich and thaw-unstable permafrost exists extensively. This paper attempts to assess the climate change influence on the engineering parameters for the design of infrastructure in the Arctic region of Alaska. It first analyzes characteristics of the two-meter-above-ground temperature predictions from 30 models in the Coupled Model Intercomparison Project Phase 5 (CMIP5) for the next century for a study site located on the North Slope of Alaska. The air freezing and thawing indices are evaluated from the climate modeling results and compared with historical data. Then a thermal model of the top 45-m soil is presented and used to assess the ground temperature variation and degradation of permafrost table during the next century. In the end, the potential impact of the climate change and permafrost degradation on the built infrastructure including roads and buildings is discussed.

Keywords: Climate models, permafrost, thermal modelling, freezing and thawing indices, thaw penetration

1. Introduction

Alaska is at the forefront of climate change, experiencing rapid permafrost degradation on the North Slope where high quantity of oil has been produced since the late 70s. Thaw degradation is advancing with increasing air temperature resulting in subsequent ground settlement. Climate change has the effect of increasing permafrost temperature, decreasing the permafrost table, and increasing the active layer thickness [1] [2]. Anisimov et al. [3] completed a series of experiments modelling the active layer using climate models and found that climate change over the next several decades may result in 15-30% thickening over permafrost regions, but could increase to 50% over northernmost permafrost regions. In 2015, a team of United States Geological Survey (USGS) scientists completed a study on the distribution of near-surface permafrost in Alaska. Their study statistically evaluated satellite derived data and other sources to project the effects that a warming climate will have on the Arctic. Their survey found that the near-surface permafrost currently underlying 38 percent of boreal and arctic Alaska would be reduced by 16 to 24 percent by 2100. The study employed the usage of 5 IPCC climate models (i.e. cgcm31, cm2, medres, echam5, hadcm3) to account for projected climate effects [4]. Predicting the future response of northern ecosystems to climate change is dependent on understanding the distribution of near-surface permafrost and having the ability to estimate depths of thaw [4]. Thawing of permafrost and subsequent ground settlement in the Arctic has become increasingly significant, posing a constant threat to the safety of underground and surface infrastructures such as energy extraction and transport assets (oil wells and pipelines), buildings, railways, highways, and bridges. Such problem is particularly severe in Alaska where permafrost is ice-rich and thaw-unstable [5].

Increasing air temperature has direct impact on frozen soil through heat exchange at the ground surface. Decreasing depths mimic the sinusoidal variance in seasonal temperature until about 9 to 15 meters, beyond which the amplitude of ground temperature decreases with increasing depth until the temperature remains steady. From this point, the temperature increases linearly with increasing depth due to the geothermal gradient [1]. Both boundary conditions such as the surface air temperature and the geothermal gradient and Soil physical and thermal properties including ice content, unfrozen water content, and thermal properties affect the heat transfer process.

This paper attempts to assess the climate change influence on the engineering parameters for the design of infrastructures in the Arctic region of Alaska in terms of air freezing and thawing indices, and the active layer thickness (ALT). The process of prediction applies 30 models of the Coupled Model Intercomparison Project Phase 5 (CMIP5) to analyze the air temperature to the year 2100. The air freezing and thawing indices are evaluated from the climate modeling results and compared with historical data. Then a thermal model of the top 45-m soil is presented and used to assess the ground temperature variation and resulting ALT.

2. Methods

2.1 Study Area

Fig.1 Ground features at the study site including ice-wedge polygons and thermokarst lakes [8].

The study area is on the Central Beaufort Coastal Plain of the Alaska North Slope. The area extends from the Canning River west to the Colville Delta and inland to encompass the Sagavanirktok and Kuparuk river floodplains on the east and the Colville River and Itkillik River floodplains to the west. Alluvial marine deposits, floodplain deposits, and eolian sand and loess underlay the flat terrain. Features such as drained lake basins consisting of shallow wind-oriented lakes, pingos, and wet meadows comprise a significant portion of the landscape suggesting ice-wedge polygons as represented in Fig. 1 [6, 7]. Soil samples are obtained from the drill site 2M location approximately 12 air miles southwest of the Ugnu Kuparuk airport, 11.5 air miles south of the Beaufort Sea, and approximately 627 air miles north of Anchorage, Alaska. The region supports oil production activities constructed on continuous permafrost extending 100+ meter depths [7]. The Ugnu Kuparuk Airport is the nearest airport with an equipped National Oceanic and Atmospheric Administration (NOAA) [9] linked weather station.

2.2 Climate Inputs

The USGS undertook a series of borehole drillings in 1987 and collected temperature readings with advancing depth. The initial soil temperature conditions were established with WSAK-14, the nearest USGS borehole, data for modeling purposes [10]. The air temperature data set dating back to 1983 was obtained from the NOAA airport station as initial conditions. To project air temperature values, the study used a total of 30 climate models (Fig. 2) as determined by the CMIP5.

Model	Institute	Resolution (lon x lat), level
1. ACCESS1-0	Commonwealth Scientific and Industrial Research Organisation	N96 (1.25° x 1.875°), L38
2. ACCESS1-3	(CSIRO),and Bureau of Meteorology, Australia (BOM)	N96 (1.25° x 1.875°), L38
3. bcc-csm1-1	Beijing Climate Center, China	T106, L26
4. BNU-ESM	College of Global Change and Earth System Science, Beijing Normal University (BNU)	T42, L26
5. CanESM2	Canadian Centre for Climate Modeling and Analysis (CCCma)	T63 (1.875° x 1.875°), L35
6. CCSM4	National Center for Atmospheric Research (NCAR)	1.25° x 0.9°, L26
7. CESM1-BGC	Community Earth System Model	1.25° x 0.94°, L60
8. CESM1-CAM5	Contributors (NSF-DOE-NCAR)	1.25° x 0.94°, L30
9. CMCC-CESM	Centro Euro-Mediterraneo	T31, L39
10. CMCC-CM	per I Cambiamenti	T159, L31
11. CMCC-CMS	Climatici (CMCC)	T63, L95
12. CSIRO-Mk3-6-0	Commonwealth Scientific and Industrial Research Organisation in collaboration with the Queensland Climate Change Centre of Excellence (CSIRO- QCCCE)	T63(1.875° x 1.875°), L18
13. EC-EARTH	EC-Earth consortium (ICHEC)	T159(0.75° x 0.75°), L62
14. GFDL-CM3	Geophysical Fluid Dynamics	C48 (2.5° x 2.0°), L48
15. GFDL-ESM2G		2.5° x 2.0°, L24
16. GFDL-ESM2M	Laboratory (NOAA GFDL)	2.5° x 2.0°, L24
17. GISS-E2-H	NASA Goddard Institute for	2.5° x 2.0°, L40
18. GISS-E2-R	Space Studies (NASA GISS)	2.5° x 2.0°, L40
19. HadGEM2-CC	Met Office Hadley Centre	N96, L38
20. HadGEM2-ES		N96, L38
21. inmcm4	Institute for Numerical Mathematics (INM)	2.0° x 1.5°, L21
22. IPSL-CM5A-LR	Institut Pierre-Simon Laplace	3.75° x 1.875°, L39
23. IPSL-CM5A-MR		2.5° x 1.25°, L39
24. IPSL-CM5B-LR	(IPSL)	3.75° x 1.875°, L39
25. MIROC5	Atmosphere and Ocean Research Institute (The University of	T85, L40
26. MPI-ESM-LR	Max Planck Institute for	T63, L47
27. MPI-ESM-MR	Meteorology (MPI-M)	T63, L95
28. MRI-CGCM3	Meteorological Research	TL159 (1.125° x 1.125°), L48
29. MRI-ESM1	Institute (MRI)	TL159 (1.125° x 1.125°), L48
30. NorESM1-M	Norwegian Climate Centre (NCC)	2.5° x 1.875°, L26

Fig. 2 CMIP5 models used in this study [11]

The CMIP5 has produced a state-of-the-art multimodel dataset designed to advance our knowledge of climate variability and climate change. Unprecedented in scale and attracting interest from all major climate modeling groups, CMIP5 includes “long term” simulations of twentieth-century climate and projections for the twenty-first century and beyond. Conventional atmosphere–ocean global climate models and Earth system models of intermediate complexity are for the first time being joined by more recently developed Earth system models under an experimental design that allows both types of models to be compared to observations on an equal footing.

Within the core set of runs, there are two future projection simulations forced with specified concentrations (referred to as “representative concentration pathways” (RCPs)), consistent with a high emissions scenario (RCP 8.5) and a midrange mitigation emissions scenario (RCP 4.5).The radiative forcing in RCP 8.5 increases throughout the twenty-first century before reaching a level of about 8.5 W-m^2 at the end of the century. RCP 8.5 reflects current global practice, high fossil fuel use, low renewables, and fragmented cooperation. According to current consensus, the RCP 8.5 is considered as the most possible cases according to current greenhouse gas emission level. Thus, the study uses RCP 8.5 daily surface air temperature (two meters above ground) from all available models. The RCP 8.5 data is used in this study to project future air temperatures consistent with a worst case scenario [11].

The data spans 94 years from 2006 to 2100. The models output in three types of calendar formats which were normalized to a 365 day calendar ignoring leap years. Once normalized, the average daily air temperature is determined, followed by determination of the average monthly air temperature, and finally determination of the MAAT for the 30 models spanning 94 years. The air temperature data is needed to calculate the freezing and thawing indices.

2.3 Freezing and Thawing Indices

The freezing and thawing indices are important for engineering design parameters in the broad cold regions. According to Andersland et al. [1] the freezing (thawing) index is a combined measurement of the duration and magnitude of below (above) 0°C temperatures occurring during any given season. The usual design value is defined as the average air-freezing (or thawing) index of the three coldest winters (or warmest summers) during the most recent 30-year period on record. If there is not enough data to support 30 years, the index of the coldest winter (or warmest summer) during the most recent 10-year period will be sufficient. There are two types of indices for both freezing and thawing: surface index and the air index from 1.5 to 2 m above ground surface.

The air freezing and thawing indices are calculated from the air temperatures obtained from historical and CMIP5 data in this study. First the mean monthly air temperature is determined for each year. Second, within that year, a summation of all negative (positive) values provides the air freezing (thawing) index for that season. The freezing index determines the thickness of freeze-back of the active layer each year, while the thawing index determines the ALT during the summer months. There is a relation that occurs with increasing air thawing index to that of the increase of active layer thickness as presented by Nelson et al [12]. They found that a linear function exists between active layer thickness and the square root of time of cumulative thawing degree days (air thawing index).

2.4 Soil Preparation and Testing

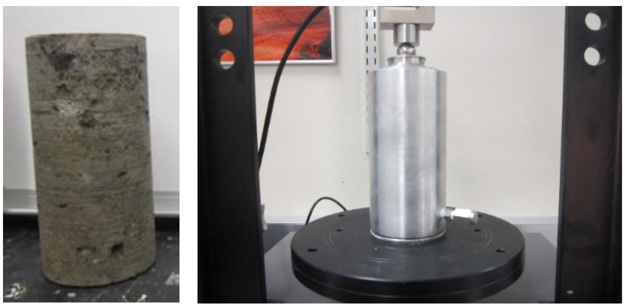

Fig. 3 An example soil specimen and the custom-designed thaw strain testing device.

This study focuses on the 2M block location where continuous frozen cores were obtained by sonic drilling. Soil testing was completed on samples from ground surface to 45 m below ground surface (bgs). Sample preparation was completed in a cold room at -10°C. Cores at chosen depths were obtained and shaped to a 63.5 mm diameter and a height that could range between 101 and 127 mm (varied due to core condition) for thaw strain testing (Fig. 3). Lab tests include index testing such as water content, bulk density, specific gravity, Atterberg limits, and grain-size analyses. An apparatus (Fig. 3) was designed to allow for one-dimensional thaw strain testing at both undrained and drained conditions with the undrained condition for thaw strain assessment and the drained condition for post-thaw strain assessment. To determine the overburden pressure in the thaw strain analysis, a linear best fit equation was obtained to evaluate the density at a certain depth based on previous testing results [13].

2.5 Unfrozen Water Content and Thermal Conductivity Modelling

Unfrozen water content (UWC) is an important property for determining frozen soil thermal properties. Li et al. [14] established a model for frozen silt, clay, and silty sands from soil samples at a near-by site (e.g. Block 2A) based on the capacitive technique. Their results were based on a temperature range of -20 to 10°C. The UWC model provides a relationship between UWC and temperature. A thermal conductivity model derived by Johansen [15] was chosen to determine values of thermal conductivity with changing temperature. The specific heat capacity was determined based on the phases in the frozen soil by the weighted average method [1].

2.6 Thermal Modelling

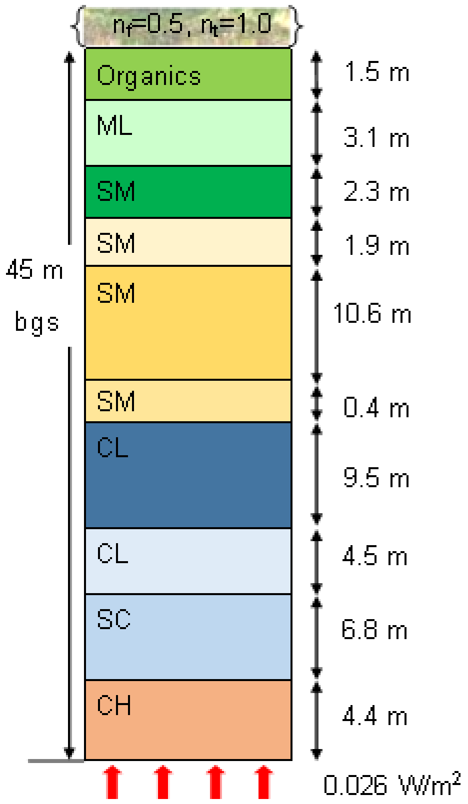

Fig. 4 Thermal model showing soil type, layer thickness, and thermal boundary conditions.

For this study, a Temp/W finite element thermal model [16] was generated to understand the impact that climatic conditions will have on ground temperature variation. Fig. 4 illustrates the soil column for this study site. The focus is placed on shallower depths to enhance the ALT modelling. For each soil layer frozen/unfrozen volumetric heat capacity is calculated and thermal conductivity and unfrozen water content vary with temperature. Average daily air temperature was used as the model input on the top boundary. The *n*-factor input defines the surface boundary condition and was calibrated for this study. Previous values were determined for Interior Alaska to account for tree and shrub ground cover [17, 18], but do not reflect the study site. A nearby active layer monitoring site that shares vegetative cover characteristics was used to determine *n*-factors for the study site [19, 20]. For this study the ground cover is represented by the thawing *n*-factor, n_t, (1.0) and the freezing *n*-factor, n_f, (0.5). The chosen ground cover reflects a ground surface with the tundra layer intact with no trees or shrubs and high wind speed. At 45 m bgs, a geothermal gradient of 2°C/100 m was applied [10]. Table 1 lists soil index properties, thermal conductivity at -10°C, and volumetric heat capacity. The model was split into two analyses: the historical analysis from 1987 to 2018 for establishing the initial temperature conditions and validation of model and the future analysis from 2019 to 2100 for prediction of climate change impact. Analysis time step was set to 1-day increment and data was stored every one step. This provides extraction of data on an annual basis spanning a 365 day standard calendar. Successful tests provide a day-by-day analysis of change in temperature with change in depth.

Table 1 Soil Properties

Soil Layer	Depth bgs m	Soil Type	Vol. Water Content %	Dry Density kg/m^3	Thermal Conductivity		Volumetric Heat Capacity	
					Frozen W/m-°C	Unfrozen W/m-°C	Frozen kJ/m^3-°C	Unfrozen kJ/m^3-°C
T	1.5	OL	60.0	531.0	1.20	0.60	1260.00	2700.00
1	4.6	ML	50.2	1511.9	2.09	1.65	3000.10	4647.10
2	6.9	SM	26.6	1621.7	2.37	1.85	2315.97	3257.79
3	8.8	SM	28.3	1420.3	2.01	1.52	2080.83	2958.42
4	19.4	SM	31.3	1330.1	1.99	1.43	2031.53	2936.68
5	19.8	SM	35.2	1394.6	2.46	1.63	2243.67	3306.87
6	29.3	CL	34.3	1487.1	1.34	1.13	2158.20	3265.67
7	33.8	CL	36.0	1546.9	1.44	1.22	2298.60	3504.47
8	40.6	SC	30.8	1466.4	2.27	1.64	2224.81	3207.73
9	45.0	CH	29.8	1527.0	1.27	1.10	2071.58	3063.52

3. Results and discussions

3.1 Mean Annual Air Temperature (MAAT)

More than 100 years of MAAT from 1983 to 2100 is displayed in Fig. 5. The average MAAT from all

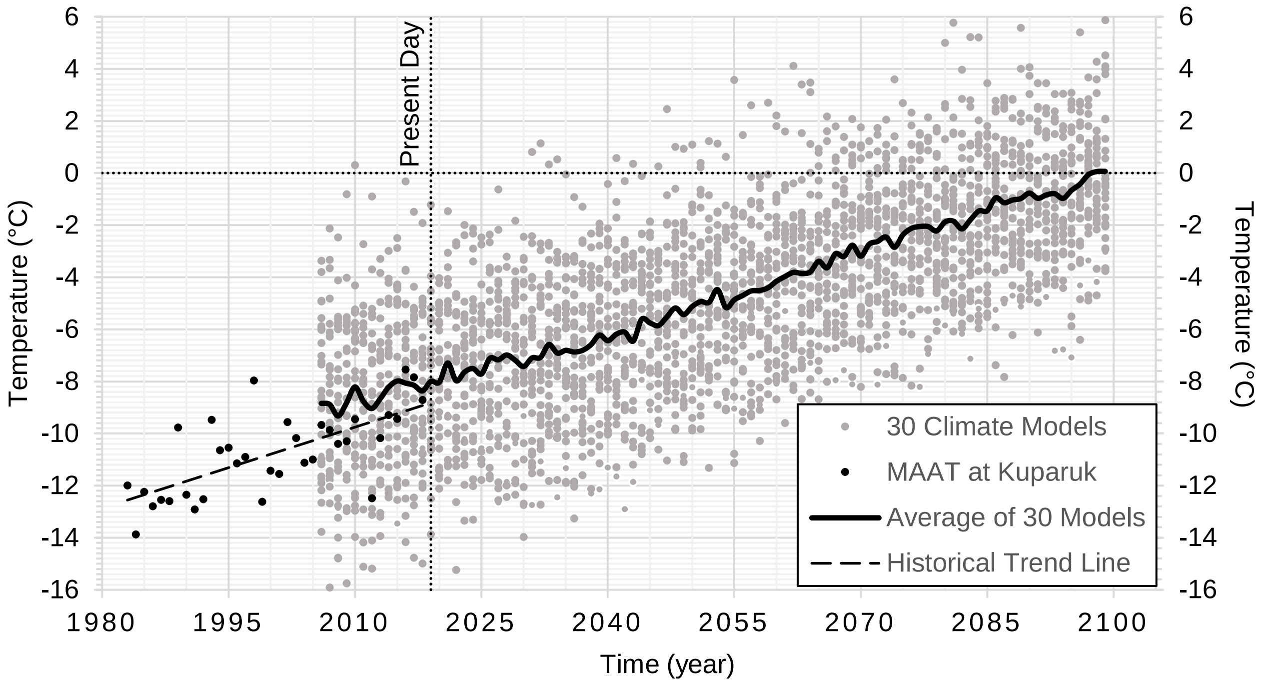

Fig. 5 CMIP5 climate model MAAT results from 1983 to 2100 at the study site.

the models was also obtained to show the trend. Each climate model is represented to show the variation in prediction for each year. The IPSL-CM5A-MR climate model is the upper bound prediction of temperatures for the study area. The CSIRO-Mk3-6-0 climate model is the lower bound representing the most conservative prediction of air temperature increase. The historical trend seen on the left portion of Fig. 5 aligns with the average MAAT of the 30 CMIP5 models, although the historical trend line does not match up with the CMIP5 average at first. The predicted MAAT result shows an eventual match if the line is extended into the future, despite that the climate models reflect the worst-case scenario for climate change. For the most part, historical air temperature data obtained from NOAA is complete. However, some years had less data than others. For example, 2011 data was removed from the analysis due to unavailable summer month temperature data. The prediction overall is that winter air temperatures are increasing resulting in longer summers.

3.2 Freezing and Thawing Indices

The thawing and freezing indices at the site are depicted in Fig. 6. An increasing thawing index, as shown, is indicative of increasing air temperature. On trend, the amount of degree-days above freezing (thawing) is increasing which correlates to a decreasing amount of degree-days below freezing [1]. The amount of days below freezing is thus decreasing leading to warmer winters. The historical trend of both the freezing and thawing indices align well with the projections. Of importance, these CMIP5 models represent the worst-case scenario of climate change.

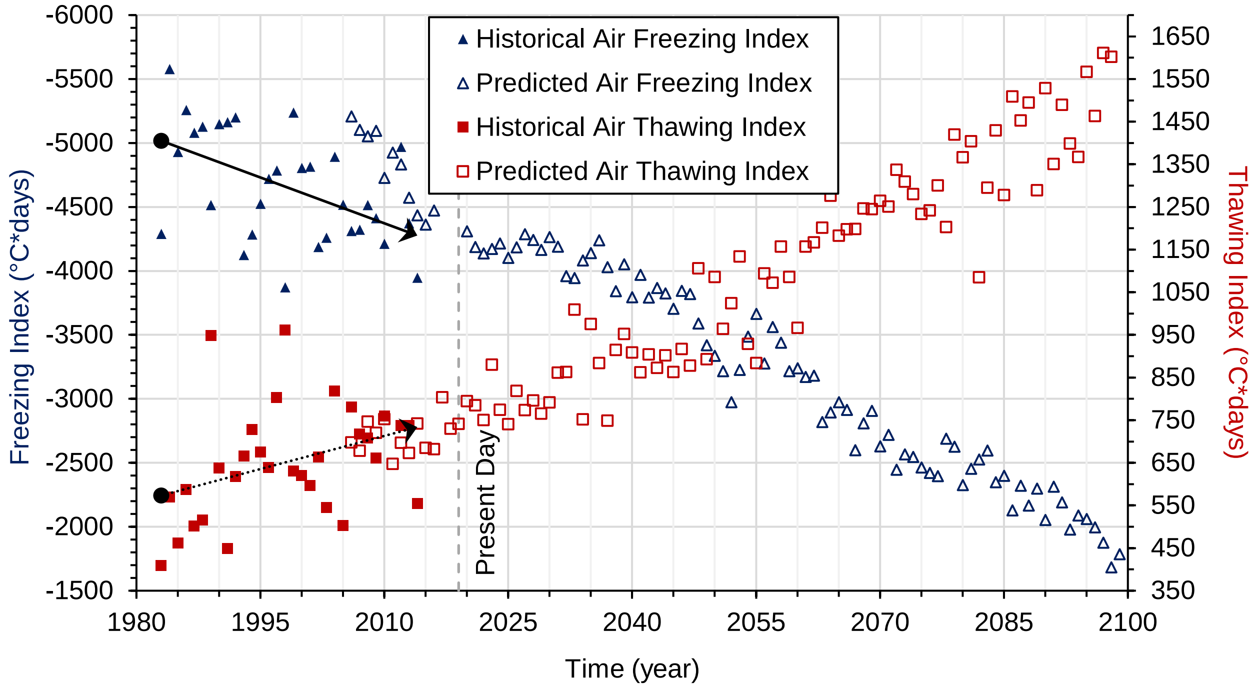

Fig. 6 Historical and Predicted Freezing and Thawing Indices.

3.3 Active Layer Thickness

The Temp/W analysis provides values for temperature with decreasing depth. However, the ALT was expected to be fairly shallow. Therefore, result processing focused on the top few meters. Temperature data was extracted from 34 data locations along a vertical line extended 4.1 m bgs at a given time step and a Matlab code was developed to process and interpolate the raw data to provide a contour map of the temperature field within each year. Fig. 7 shows the temperature fields for a few selected years with a zero-degree isotherm identified for active layer detection. It is seen from Fig. 7 that the ALT increases annually and surrounding soil becomes warmer with increasing time. One major observation is the gradual disappearance of the -10°C temperature shading at the ground surface. Despite having an insulating tundra layer, the soil is warming with increasing air temperature resulting in a degrading permafrost table. Typical winter months do not have the expectant freezing temperatures to control the reoccurring ALT. Instead, the ALT extends deeper and the soil regime remains thawed longer.

The predicted historical maximum ALT was identified from 1988 to 2018 with an increment of every 1 year and the predicted climate modelled maximum ALT was from 2006 to 2100 with an increment of every 5 years and presented in Fig. 8. Overall the ALT is expected to increase from about 1.0 m to 2.1 m, or 109% increase, in 2100. With weather systems becoming more unpredictable, more fluctuation in ALT reflected after 2040 is expected.

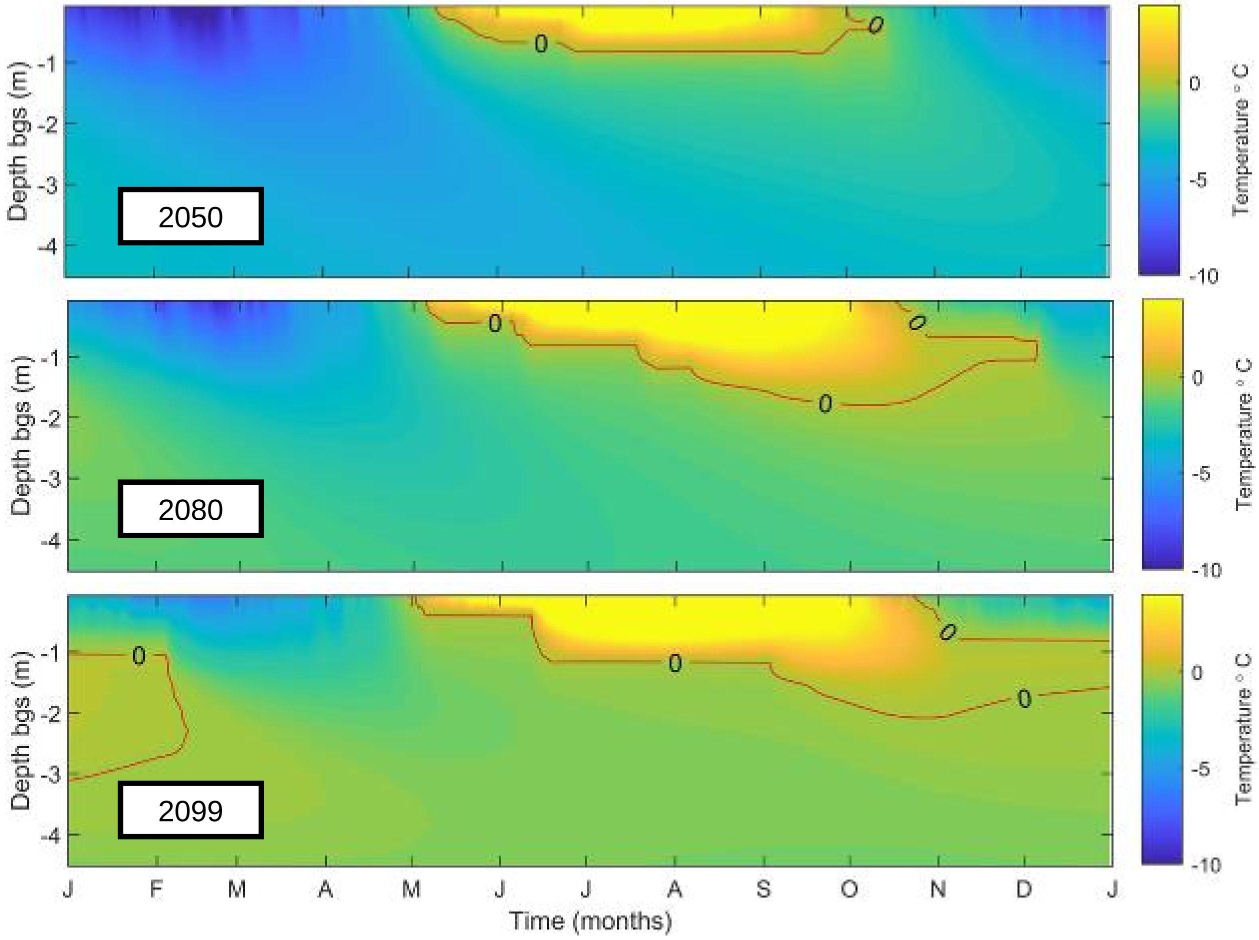

Fig. 7 Ground temperature evolution with time predicted by thermal modelling.

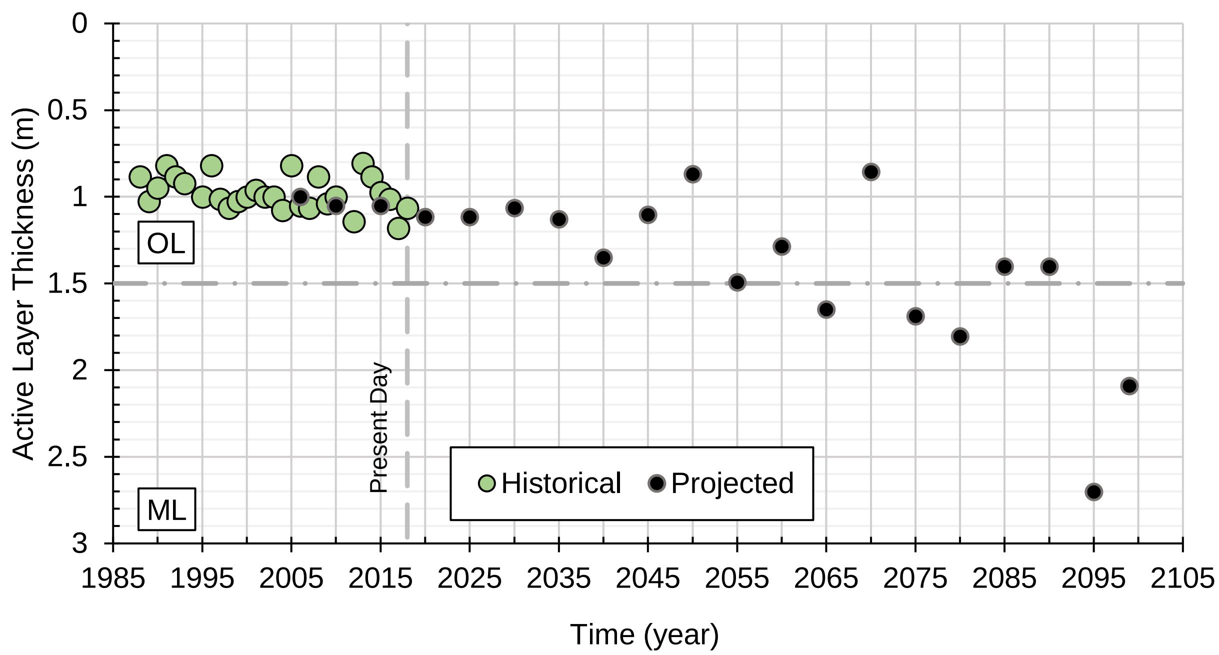

Fig. 8 Predicted active layer thickness vs. time.

3.4 Impact on Infrastructure

Increasing ALT and the associated thaw settlement on Alaska's North Slope is sure to affect oil production and negatively impact the economy. The oil industry is addressing the issue of settlement with engineering techniques such as thermosyphons to keep the ground frozen. Unfortunately, thermosyphons require cold weather to drive the process of extracting heat from frozen ground. Due to rising air temperatures, the cooling effect is steadily reduced and thermosyphons may no longer work [21]. Further engineering techniques related to foundation design will need to be developed to keep the ground frozen. In addition, this study, however, considered a ground surface that is intact. Stripping the tundra or other ground surface disturbance and placement of pavements during development only leads to further permafrost degradation and settlement. These predicted settlement values do not take into consideration the massive amounts of heat transfer into the permafrost due to oil extraction activity, which only will make the problem more severe.

4. Summary

The intent of this paper is to apply climate model air temperature data to assess the impact of climate change on the permafrost at the study site for the next century. In doing so, we predicted the effects of increasing air temperature on the MAAT, freezing and thawing indices, and the ALT. The prediction of MAAT utilized data from 30 CMIP5 climate models. In 2100, the average prediction of MAAT reached above 0°C. The freezing and thawing index predictions reflect an increase in air temperature that led to warmer winters and longer summers. The result is an increase in days above 0°C thus increasing the active layer thickness. The maximum ALT occurred in 2095 at 2.7 meters bgs. It is important to remember that this study focused on intact tundra away from oil production activity. In the most conservative of predictions, where tundra is intact and void of human activity, ALT and the associated settlement is still predicted to impact the ground surface. Suggestions for future research include analyses of disturbed tundra surfaces and ice rich soils, and the associated thaw settlement.

5. Acknowledgment

The authors appreciate the financial support by a grant from the ConocoPhillips Arctic Science and Engineering Endowment.

6. References

[1] ANDERSLAND, ORLANDO B. and LADANYI, B., “Frozen Ground Engineering,” Second Edition, ASCE Press/Wiley & Sons, 2004.
[2] KONG, YING. WANG, CHENG-HAI, “Responses and changes in the permafrost and snow water equivalent in the Northern Hemisphere under a scenario of 1.5 °C warming,” *Advances in Climate Change Research*, Volume 8, Issue 4, pp. 235-244, 2017.
[3] ANISIMOV, O.A. N.I. SHIKLOMANOV, F.E. NELSON. “Variability of seasonal thaw depth in permafrost regions: a stochastic modeling approach.” *Ecological Modelling,* Volume 153, Issue 3, 2002, Pages 217-227.
[4] OLEFELDT, D., GOSWAMI, S., GROSSE, G., HAYES, D., HUGELIUS, G., KUHRY, P., MCGUIRE, A. D., ROMANOVSKY, V. E., SANNEL, A., SCHUUR, E. AND TURETSKY, M. R., "Circumpolar distribution and carbon storage of thermokarst landscapes," *Nature Communications*, vol. 7, p. 13043, 11 10 2016.
[5] PASTICK, N.J., JORGENSON, M. TORRE, WYLIE, B.K., NIELD, S.J., JOHNSON, K.D., FINLEY, A.O., “Distribution of near-surface permafrost in Alaska: Estimates of present and future conditions. Remote Sensing of Environment, Volume 168, Pages 301-315, 2015.
[6] PULLMAN, ERIK R., JORGENSON, M. TORRE, & SHUR, Y., “Thaw Settlement in Soils of the Arctic Coastal Plain,” *Alaska, Arctic, Antarctic, and Alpine Research*, 39:3, 468-476, 2007.
[7] JORGENSON. M.T., YOSHIKAWA, K., KANVESKIY, M., SHUR, Y.L., RORNANOVSKY, V., MARCHENKO, S., GROSSE, G., BROWN, I"~ AND JONES, B., “Permafrost characteristics of Alaska.” In *Proc. of the 9th Inter. Conf. on Perm.*, 29 June - 3 July 2008, Fairbanks,

Alaska, *Edited by* D.L. Kane and K.M. Hinkel. Ins. of Northern Eng., University of Alaska Fairbanks. pp. 121-122, 2008.

[8] Study Area Map. *Google Maps*, 22 February 2019. www.google.com/maps

[9] (NOAA) National Centers for Environmental Information: National Oceanic and Atmospheric Administration, 2019. https://www.ncdc.noaa.gov/cdo-web/datasets. Retrieved 10/2018 – 2/2019.

[10] MATTHEWS, C.M., DESSEIN, T., AND YUEN, S., “Comprehensive Thaw Subsidence Assessments for Kuparuk DS-2A, Draft Final Report to ConocoPhillips Alaska Inc.,” C-FER Technologies, Edmonton, Alberta, Canada, 2015.

[11] IPCC, 2014. “Climate Change 2014: Impacts, Adaptation, and Vulnerability. Contribution to the Working Group II” to the *5th Assess. Rep. of the Intergov. Panel on Clim. Ch. (AR5)*. Cambridge University Press, Cambridge and New York. http://sedac.ipcc-data.org/ddc/ar5_scenario_process/RCPs.html

[12] NELSON, F.E., SHIKLOMANOV, N.I., MUELLER, G., HINKEL, K.M., WALKER, D.A., BOCKHEIM, J.G., “Estimating active layer thickness over a large region: Kuparuk river basin,” Alaska, USA. Arctic and Alpine Research 29 (4), 367–378, 1997.

[13] EBA (2013b). Kuparuk Core Project: Laboratory Results. EBA File: E14103016-01. EBA, A Tetra Tech Company. Technical Report to CPAI, June.

[14] LI, HAIPENG., YANG, ZHAOHUI (JOEY), WANG, JIAHUI, Unfrozen water content of permafrost during thawing by the capacitance technique, Cold Regions Science and Technology, Volume 152, Pages 15-22, 2018.

[15] JOHANSEN, O., “Thermal conductivity of soils.” Ph.D. thesis, Trondheim, Norway. (*CRREL Draft Translation* 637, 1977). ADA 044002, 1975.

[16] Geoslope, “Temp/W.” Calgary, Alberta, Canada. https://www.geoslope.com/

[17] LUNARDINI, V. J., “Theory of n-factors and correlation of data.” In *Proc. 3rd Int. Conf. on Permafrost*, Edmonton, Alberta. Ottawa: National Research Council of Canada, Vol. 1, pp.41-46, 1978.

[18] LUNARDINI, V. J., “Analytical methods for ground thermal regime calculations.” In *Thermal Design Considerations in Frozen Ground Engineering*, ed. T. G. Krzewinski and R. G. Tart, Jr. New York: ASCE, pp. 204-57, 1985.

[19] GEOPHYSICAL INSTITUTE UAF, Sites List: Deadhorse. Retrieved from Permafrost Laboratory: http://permafrost.gi.alaska.edu/sites_list, 2019.

[20] ROMANOVSKY, V. E. AND OSTERKAMP, T. E., “Thawing of the active layer on the coastal plain of the Alaska Arctic.” *Permafrost Periglacial Processes*, 8, 1-22, 1997.

[21] YARMAK, EDWARD, ZOTTOLA, JASON T., “Thermosyphon Design for a Changing Arctic.” *Con. on Tech. Adv. 2017: Cold Reg. Eng. – Proc. of the 17th Intl. Conf. on Cold Reg. Eng. at the 1st Con. on Tech. Adv.*, p 151-160, 2017.

Importance of Detailed Soil, Terrain and Geohazard Data for Cold Region Development

Dennis O'Leary, P.Ag.
Senior Terrain Scientist
Golder Associates Ltd.
Edmonton, Alberta Canada
doleary@golder.com

Thomas G Krzewinski, P.E., D.GE, F.ASCE
Golder Associates Inc.,
Anchorage, Alaska, United States of America
tkrzewinski@golder.com

Summary

Terrain conditions in polar regions are considered challenging for infrastructure development and resource exploration. These regions are perhaps most notably characterized by permafrost (soil and rock that remains frozen year-round) which varies in extent (sporadic to continuous) and thickness (meters to hundreds of meters). Where permafrost remains stable, engineering adaptations can provide reliable and secure development. Often, however, it is the dynamics of the active layer, a thin 0.5-3 m thick layer at the surface that seasonally thaws and refreezes that provides the most challenge. Understanding controls on active layer development, including parameters such as sedimentology, thickness of drift materials, slope, vegetation and snow drifting patterns are key to not only comprehending the modern environment, but predicting how it may change in the future. Widespread recent (post 1996) warming (up to 4°C / 7°F) and changes in the amount and seasonality of precipitation (increases in rain and decreases in snow), have led to a dramatic rise in permafrost terrain failures and retreat of glaciers. It appears that in some cases the environment behaves under a dynamic equilibrium, such that it can absorb a certain degree of environmental change, before it flips and attains a new equilibrium. Identifying where such changes have occurred, their impacts on the landscape and then predicting where they are likely to spread, are key components of any terrain and geohazard analysis required to inform the development process.

Too often, this kind of data is collected by costly geotechnical investigations and fly-overs of a site or proposed pipeline. Today tools such as softcopy mapping using either stereo satellite imagery or digital stereo aerial photographs allow for cost-effective desktop mapping of an environment prior to undertaking costly boreholes. Indeed, these kind of terrain assessments are best used to identify where borehole studies are most expediently applied. Softcopy allows terrain scientists to map soils, terrain and geohazard units at scales of 1:2,000 or greater (meters to 10s of meters) and provide key data that informs and instructs subsequent geotechnical investigations. This paper will present a number of examples of how softcopy mapping has been used in polar regions to identify areas of permafrost degradation and to identify critical geohazards features such as thaw slides and areas of solifluction.

Keywords: Climate Change, Groundwater Seepage, Landslides, Mapping, Permafrost Pipeline Routing, Pipeline Integrity Management, Rockfall, Rights-of-way, Terrain, Thaw Flow Slides

1. Introduction

Terrain and geohazard analyses are a critical component of all development activities that involve any disturbance of the earth's surface. A knowledge of the soil (origin, texture, drainage), depth to bedrock (overburden thickness), slope, topography and geomorphic processes is critical for the proper engineering design and construction of a project as well as on-going operations, maintenance and future reclamation activities.

In northern environments where permafrost is found it is extremely important to understand the type, depth and location of the permafrost especially in areas of discontinuous, sporadic and isolated permafrost where permafrost in not continuous across the landscape and is often associated with specific terrain conditions, including aspect, soil material, soil material texture and drainage.

Permafrost is defined as soil or rock materials that remain frozen from one year to the next. Four (4) permafrost zones have been mapped and identified in Canada [1]; each zone is defined by the percent of land area underlain by permafrost. The zones include:

- Continuous (90 – 100% of the land area underlain by permafrost)
- Extensive Discontinuous (50 – 90%)
- Sporadic Discontinuous (10 – 50%)
- Isolated Patches (< 10%)

Climate warming over past decades has caused degradation in permafrost widely and quickly. Permafrost degradation refers to a naturally or artificially caused decrease in the thickness and/or areal extent of permafrost [2]. It has the potential to significantly change soil moisture content [3] possibly resulting in (1) horizontal downslope movements due to the creep of permafrost bodies, and (2) vertical settling movements, due to the melting of ice bodies and/or interstitial ice [4]. The former tends to result in thaw flow slides (Figure 1) while the latter is more typical of thermokarst terrain (Figure 2).

Fig.1 Thaw flow slide

Fig. 2 Thermokarst terrain

A study by [5] recorded recent changes in the areal extent of permafrost at the individual peatland scale within the discontinuous permafrost zone of northern Alberta, Saskatchewan and Manitoba. This study found that at five southern sites between 30 and 65% of localized permafrost has degraded over the last 100 to 150 years and that the thaw is significantly correlated to mean annual air temperature. The same study recorded as much as 50% of peat plateau permafrost has thawed over the past 50 years in the discontinuous permafrost zone, and total thaw can be greater in the north than the south [5]. The results of the study by [5] suggest that localized permafrost at the southern limit of the discontinuous permafrost zone responds more directly to climate warming than peat plateaus in the north.

Forest cover also plays a role in the regulation of surface temperatures, and extensive logging is known to be a potential trigger of extensive permafrost melting. These effects can have a very high spatial variability due to uneven ground ice distribution (ice wedges and lenses). This effect on permafrost has been documented through numerous experiences with road construction, railways, pipelines and forest logging [4].

In the Arctic, temperature at the top of the permafrost layer has increased by up to 3ºC since the 1980s. The permafrost base has been thawing at a rate ranging up to 0.04 m yr^{-1} in Alaska since 1992 and 0.02 m yr^{-1} on the Tibetan Plateau since the 1960s. As a result, permafrost degradation is leading to changes in land surface characteristics and drainage systems [2].

The considerable impact of permafrost degradation on hydrology and water resources, ecosystems, human engineered facilities, and climate change requires us to carry out more in-depth studies and at finer spatial scales to investigate the issue [6]. It is with this challenge that this paper discusses a relatively new approach to obtaining more in-depth data at finer spatial scales. This conclusion is not only relevant to permafrost but to other terrain data, including soil materials, soil textures, depth to bedrock/overburden thickness, slope, drainage and geoprocesses including permafrost.

Simulation modelling of warm thin permafrost (mean annual ground temperature above -1ºC; 20 cm thick) has found the combined effects of Right-of-Way (ROW) disturbance and climate warming are likely to result in permafrost degradation within 20 to 40 years [7]. These ROW-disturbance effects may extend off-ROW under scenarios of climate warming. Based on the range in ground thermal conditions considered in their study, the results of the simulation indicate that the effects of ROW disturbance outweigh those associated with climate warming in the initial 10 to 15 years following disturbance, although climate warming becomes important over longer periods of time.

Permafrost degradation is projected to increase the cost of maintaining public infrastructure in Alaska by 10-20 percent (U.S. $4 billion to $6 billion) by 2030, and another 10-12 percent ($5.6 billion to $7.6 billion) by 2080 [8].

2. Areas of Study

Two areas of study are presented within this paper. The first area is in northwestern Alberta near Hay-Zama Lakes where permafrost degradation is occurring. The second area is the Healy Canyon area southwest of Fairbanks, Alaska.

Figure 3 shows the distribution and types of permafrost within northern Alberta and the southern part of the Northwest Territories. As seen in Figure 3, a narrow band of isolated permafrost approximately 50 to 100 km in width runs northwestward from the Fort McMurray area to Fort Vermilion and the High Level area immediately west of Fort Vermilion; isolated permafrost accounts for less than 10% of this land base. This band of isolated permafrost is found primarily on near level glaciolacustrine materials and is found south of two major upland areas, the Birch Mountains and Caribou Mountains [9]. Recent work by [10] have suggested that the zone of isolated permafrost extends further south than initially mapped by [1]. Indications of permafrost including thermokarst lakes are found nearly 50 to 75 km to the south along the Alberta/British Columbia border near the Chinchaga River. North of this band, the extreme northern portion of Alberta is classed as having sporadic permafrost (10 – 50% of land base). This includes area such as Bistcho Lake (‘A’ on Figure 3) and two lakes not shown on the map but south of Bistcho Lake, Hay and Zama lakes. The area of interest for this paper is shown with the letter ‘B’.

Figure 4 shows the distribution and type of permafrost in the Fairbanks – Glennallen area in east central Alaska [11]. It would appear that the permafrost distribution in this area is related to a number of factors including elevation and hydrology with continuous permafrost being found at higher elevations adjacent to glaciers and isolated permafrost being associated with river valleys.

3. WHAT TERRAIN AND GEOHAZARD DATA IS PUBLICLY AVAILABLE FOR STUDY AREAS?

Most terrain or surficial geology data is available from public websites; for example, the United States Geological Survey (www.usgs.gov/), the Canadian Geological Survey (geoscan.nrcan.gc.ca) or from state, provincial or territorial government agencies. Maps available from these sites are generally considered to be small-scale regional maps (i.e., landscape level maps) and do not provide the detailed data required for most ROW planning and engineering.

For example, mapping at 1:100,000 scale by [12] suggests the area in northwestern Alberta near the Hay-Zama Lakes complex is comprised of recent lacustrine, glaciolacustrine and fluvial materials as well as large expanses of organic accumulation. The geology mapping at 1:63,360 for the Nenana River area southwest of Fairbanks Alaska suggests that the area along the Nenana River is comprised mainly of Birch Creek schist, a quartz-sericite schist and impure marble with local disseminated pyrite with areas of landslides and outwash gravel in the valley bottom [13]. While both these data sources provide valuable data for initial high level planning, they are not detailed enough for proper ROW or corridor planning. While some ROWs such as those for transmission lines can avoid problematic terrain types through the spacing of towers, other ROWs such as roads, rail lines, pipelines and fibre optic lines cannot because the infrastructure is either on the mineral surface or buried within the soil. As a result, the location of areas exhibiting evidence of soft ground, karst topography, landslides, wetlands, areas susceptible to avulsion and channel migration, etc. is critical in the overall routing process. Many of these terrain features are too small to properly depict on small scale regional maps.

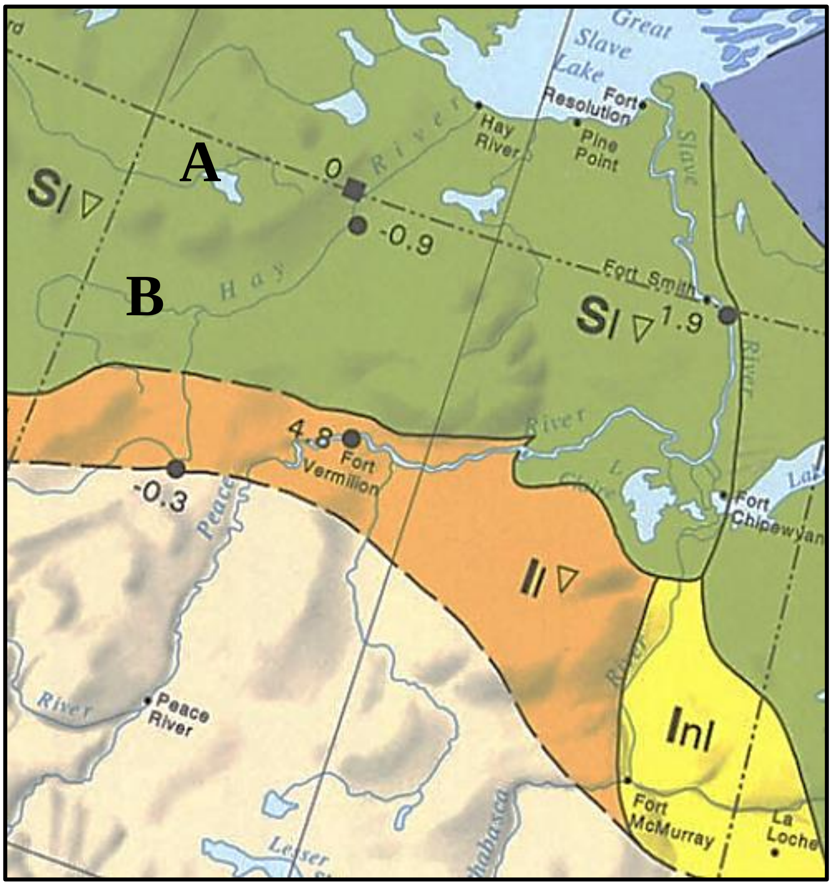

Fig. 3 Map showing distribution of permafrost zones in northern Alberta (from [1]). Areas in orange and yellow are classed as Isolated (<10% of land base has permafrost), areas in green as Sporadic (10 – 50%) and areas in blue as Extensive Discontinuous (50 – 90%) permafrost. The area of interest is shown with the letter B. The letter A represents the location of Bistcho Lake.

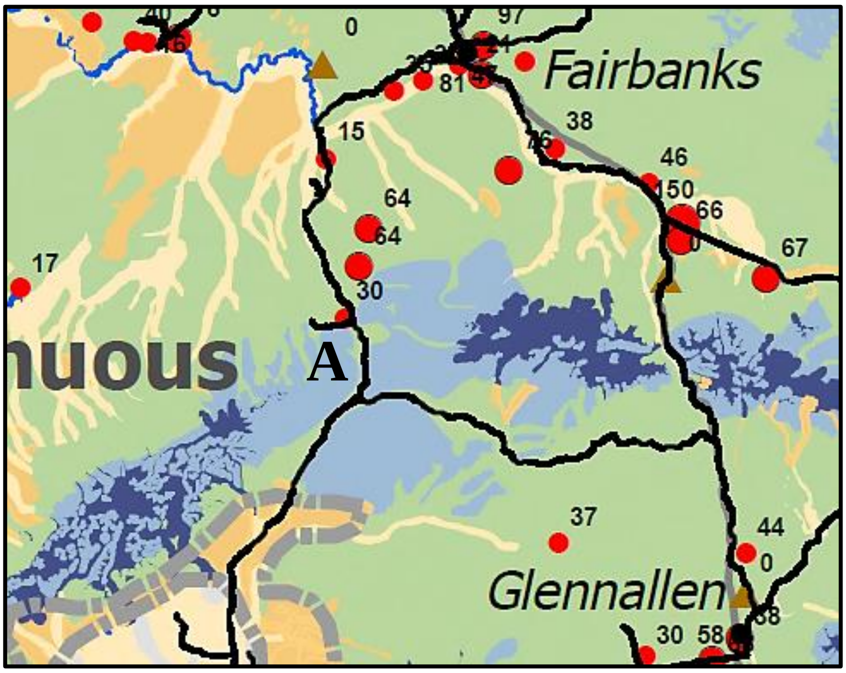

Fig. 4 Map showing distribution of permafrost in the Fairbanks – Glennallen area in east central Alaska (from [11]). Areas in beige are classed as Isolated (<10% of land base has permafrost), areas in orange as Sporadic (10 – 50%), areas in green as Discontinuous (50 – 90%) and blue areas are areas of Continuous (90 – 100%) permafrost. Dark blue areas represent glaciers. Red dots represent area of known permafrost and its depth (ft.). The area of interest is Healy Canyon and is shown with the letter A.

The level of information on permafrost varies significantly across the northern climes of northern North America and is generally presented in maps at scales of approximately 1:7,000,000 for countries such as Canada and states such as Alaska. Efforts are being made to develop better maps, but these maps that are still considered small-scale regional maps or landscape level maps. For example, the North Slope Science Initiative with the U.S. Geological Survey Alaska Climate Science Center along with the University of Alaska Fairbanks, Institute of Northern Engineering developed a new permafrost map for northern Alaska by compiling existing soil and permafrost data from available sources to create a region-wide permafrost database and landscape-level (1:1,000,000 scale) map that is suitable for regional modelling and climate impact assessments. [14] have developed a prototype map at a 1:250,000 scale to better differentiate geomorphic units because the 1:1,000,000 scale mapping typically includes complexes of geomorphic units. And similarly, in northern Alberta, work by [10] has developed a 15 m resolution raster dataset using machine learning prediction based on establishing relationships between locations where permafrost is known to be present, and a suite of predictors consisting of topographic data, satellite imagery and climatic factors to identify areas where permafrost may be located.

Other map products such as soil surveys from the Natural Resources Conservation Service (NRCS) in the United States or from Agriculture Canada or provincial soil survey agencies in Canada provide valuable starting data for initial routing purposes. However, these soil maps are generally at scales of 1:50,000 to 1:190,080 and only again provide what is referred to as small scale regional map data; the soil survey of the greater Nenana area is at a scale of 1:190,080 (1" = 3 miles). And in the case of soil surveys, small scale mapping identifies individual terrain units (polygons) with up to three soil series or components in each unit. Unfortunately, because of the small scale of mapping, the user has no idea of where the various components are to be found within the soil polygon. Is your proposed ROW going through the "*good*", the "*bad*" or the "*ugly*" components?

Besides map data, some states, provinces and territories will have public repositories of site data. The same may be true for universities and government research organizations. For example, the State of New Jersey has a database of all geotechnical boreholes and the province of Alberta has a database of all groundwater wells.

In most areas, a researcher is easily able to obtain landscape level, small-scale regional data, however the user must realize the limitations of this data and develop a plan to obtain more detailed data for their needs. [6] suggest that the considerable impact of permafrost degradation on hydrology and water resources, ecosystems, human engineered facilities, and climate change requires us to carry out more in-depth studies, at finer spatial scales to investigate the issue.

4. HOW DO WE GET DETAILED TERRAIN AND GEOHAZARDS DATA?

Today, there are a number of readily available desktop tools available coupled with field programs to help collect and produce detailed data to help in ROW planning and engineering design. These desktop tools include softcopy mapping coupled with digital stereo imagery and LiDAR data as well as Google imagery. The use of these tools allows the terrain scientist the ability to produce data at scales of 1:2,000 and larger. Data can be gathered on:

- Soil materials (e.g., till, weathered bedrock, alluvium, colluvium, etc.)
- Soil material texture (e.g., sand, silt, clay)
- Depth to bedrock / overburden thickness (e.g., bedrock at surface, within one meter of surface, between 1 – 3 below the surface or great than 3 m below the surface)
- Topography / slope (e.g., 6 – 15% slopes)
- Landform (e.g., wetlands, drumlins, eskers, outwash plain, dunes, etc.)
- Drainage (e.g., rapid, well, moderate, imperfect, poor and very poor)
- Geomorphic processes (e.g., debris flows, thaw flow slides, thermokarst, seepage, etc.)

The use of multi-year imagery allows for the examination of changes in permafrost and landslide movement over time.

The use of these tools, especially for pipeline routing and integrity management has been gaining acceptance and momentum in both the consulting world and in government agencies over the past decade. More and more scientists are using these tools to examine the ground conditions in more detail for ROW planning and site facility development [15], [16], [17] and [18].

4.1 Softcopy Mapping

Softcopy mapping is a desktop approach that allows geologists, ecologists, engineers or anyone looking at aerial photography the ability to zoom down into traditional black and white and color stereo aerial photographs on a computer monitor from their original capture scales of 1:20,000, 1:30,000, 1:40,000, etc. to scales as large as 1:1,000. Where the imagery is of good quality or has been acquired using a digital camera (e.g., 30 cm, 40 cm, 50 cm resolution), the user is able to zoom down to scales as large as 1:300 to delineate critical landscape features (e.g., permafrost, landsliding, etc.) that may affect resource development.

Softcopy incorporates 3D viewing software (e.g., PurVIEW, Summit Evolution) and ArcGIS. This combination allows the user to view the imagery in 3D and digitize linework on the fly. The mapper is able to zoom out of the imagery, for example from initial capture scale of 1:30,000 to 1:50,000, etc. to view the regional context (e.g. plains, foothills, mountains, etc.) and then zoom down to very detailed scales to examine site-specific landscape features (e.g., thermokarst features, headwall scarps of landslides, groundwater seepage zones, etc.).
The results from softcopy mapping can be used directly to refine ROW planning and assist in engineering design. Locations for borehole investigations can be properly identified and executed resulting in reduced costs for field investigations.

The following provides a number of examples of how softcopy mapping can be used to help provide not only information on soil materials, overburden thickness, slope, drainage but also geoprocesses such as thermokarst and landsliding.

Softcopy Example 1: Figure 5 shows an area in the Hay-Zama Lakes area of northwestern Alberta at a scale of 1:60,000. The area is crossed by a number of ROWs, including a major pipeline system, a road and numerous seismic lines. The soils in the area are generally a silty clay, clayey silt of lacustrine and glaciolacustrine origin. Extensive areas of shallow peat are found overlying these fine-textured materials. Fire is common within the area, thereby influencing the vegetation and the ability of an interpreter to properly interpret the landscape. At the scale of 1:60,000, an interpreter would question the area identified by the circle, wondering if the pattern is fire based, drainage based or perhaps permafrost degradation.

Zooming down to a scale of 1:2,000 (Figure 6) from the initial 1:60,000 scale image (Figure 6), the mapper is easily able to see that the area identified in the circle on Figure 6 is actually the result of permafrost degradation, thermokarst. These thermokarst lakes vary in size from less than 5 m in length to approximately 90 m in length. In addition to identifying the thermokarst lakes, the mapper is also able to delineate areas of thick peat materials around the lakes as well as upland black spruce areas. By drawing polygons around the features of concern, the individual is able to determine the area (hectares) and percent of the study area that has thermokarst lakes, thick peat deposits as well as the percent upland black spruce.

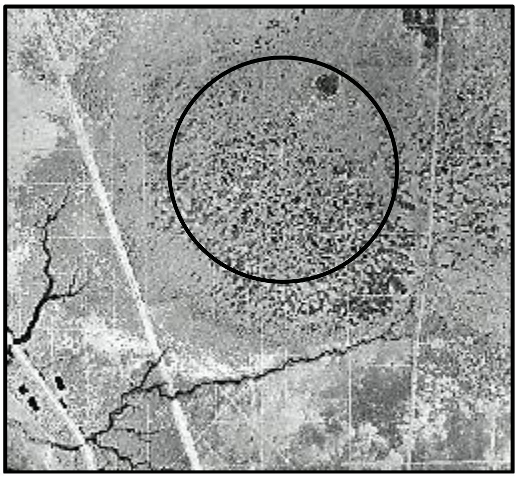

Fig. 5 1:60,000 scale black and white stereo image of area near Hay Zama Lakes, northwest Alberta. The area is in the discontinuous permafrost zone. Image is from June 18, 1994.

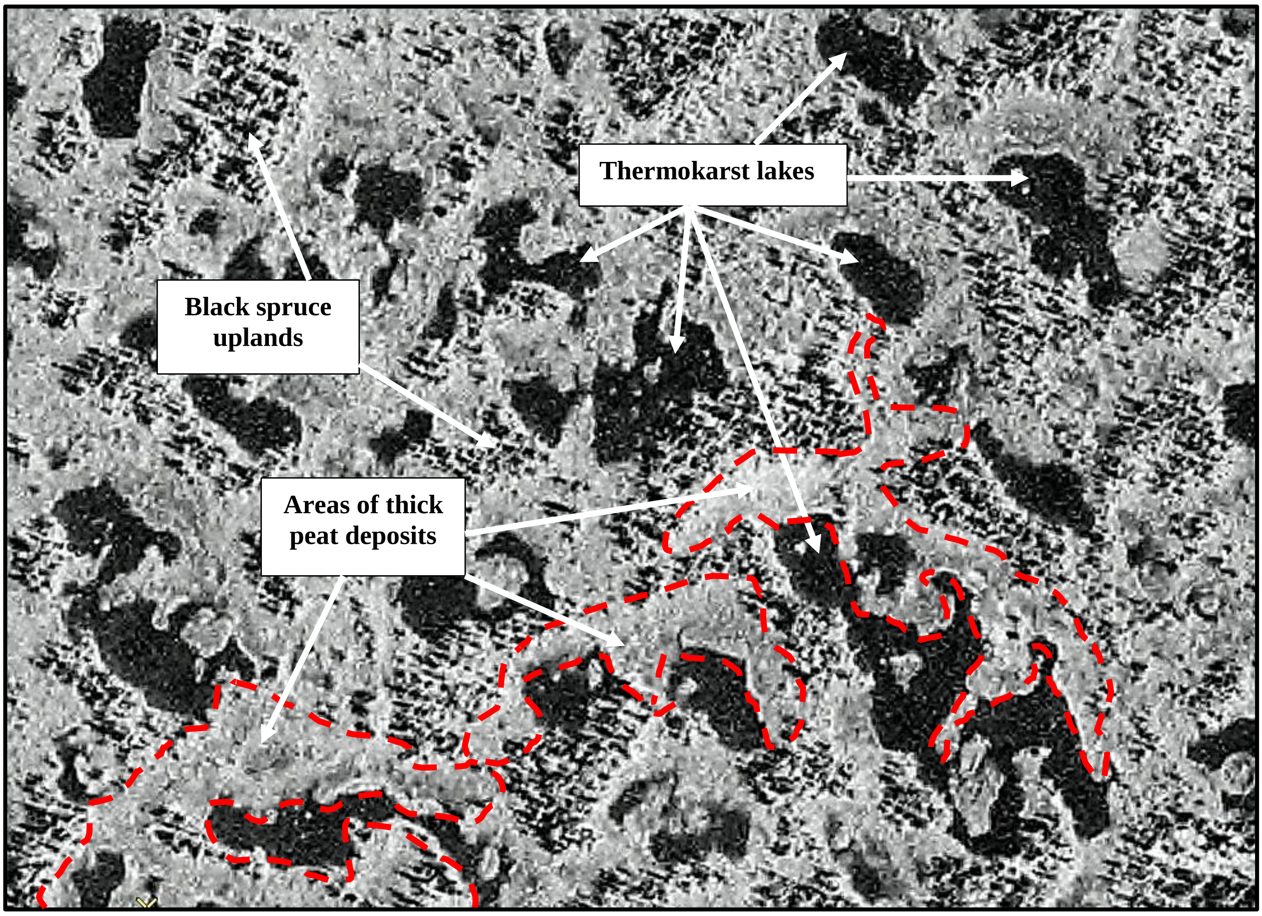

Fig. 6 The same 1:60,000 scale black and white stereo image as shown in Figure 5 zoomed into 1:2,000 using softcopy mapping tools. Thermokarst ponds vary from less than 5 m in length to nearly 100 m. Areas outlined in red indicate areas of thick peat deposits.

Softcopy Example 2: Figures 7 and 8 present similar examples of permafrost degradation in the Hay-Zama Lake area of northwestern Alberta. In Figure 7 (1:50,000) an area of bright contrast is circled adjacent to a ROW. Initially, the area within the circle would be mapped as organic terrain, however upon examination of Figure 8 (1:2,000), the mapper is able to identify a number of darker areas that are likely areas of permafrost degradation.

Fig. 7 1:50,000 scale black and white stereo image of area near Hay Zama Lakes, northwest Alberta. The area is in the discontinuous permafrost zone. Image is from June 18, 1994. Area highlighted in black circle is likely an organic fen complex with possible permafrost degradation.

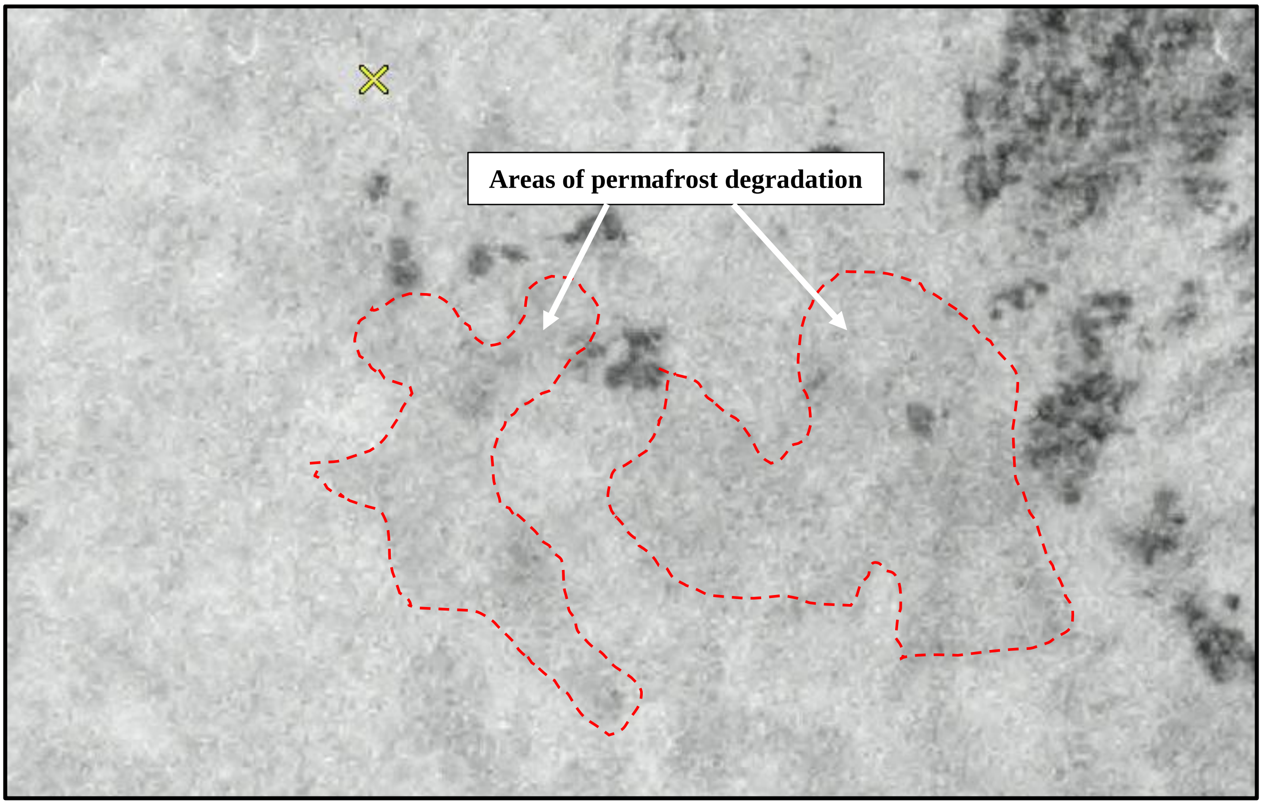

Fig. 8 The same 1:50,000 scale black and white stereo image as shown in Figure 7 zoomed into 1:2,000 using softcopy mapping tools. The darker areas delineated by the red dashed lines are the areas of permafrost degradation. The surrounding area is likely thick peat materials.

Because the imagery is rectified to either provincial DEM or LiDAR data, the user is able to quickly obtain GPS coordinates for field sampling. This then allows for a more focused and less costly field program.

Softcopy Example 3: Figures 9 and 10 are of the Healy Canyon area southwest of Fairbanks Alaska. The Healy Canyon area has a number of ROWs, including a state highway which includes a parallel pipeline and the Alaska Railway line; this latter ROW is not visible on Figure 9 but can be seen on Figure 10.

In Figure 9 (1:31,680 scale) the mapper has identified a number of features including a major deeply incised, V-shaped gully system (A), a near-vertical bedrock exposure (B) and a gently to moderately sloping upland area. While the Nenana River can be discerned at this scale it is too small to delineate as a separate unit, especially with the shadow effects from the steep north-facing slope on the south side of the river near where the gully enters the river. The mapping depicted in Figure 9 is more detailed than the landscape-level mapping of Wahrhaftig (1970) which was completed at 1:63,360 scale.

Figure 10 shows a portion of Healy Canyon at a scale of 1:2,000. At this detailed scale, the Nenana River (A) is clearly delineated and the mapper can clearly see the Alaska railway along the south slope of the Nenana River. The mapper is also able to identify the shadow of the train trestle (B) within the Nenana River. And using ArcGIS measuring tools, the mapper is able to measure the length of the train trestle (148 m). A surficial geologist trained in geohazards mapping is able to identify three types of landsliding in this image, the first being a large debris slide (C) in thick sediment adjacent to the major gully system, the second, two areas of rockfall (D) above and below the railway, and the third, a major slump (E) in the surficial materials. Being able to identify these three kinds of slides helps in establishing a proper field program and developing proper engineering practices to safeguard the railway line.

Fig. 9 1:31,680 scale color stereo image of Healy Canyon near Healy, Alaska. White lines delineate different terrain types. Terrain unit A is a deeply incised, V-shaped gully system; terrain unit B is a near-vertical bedrock exposure; and terrain unit C is a gently to moderately sloping upland area.

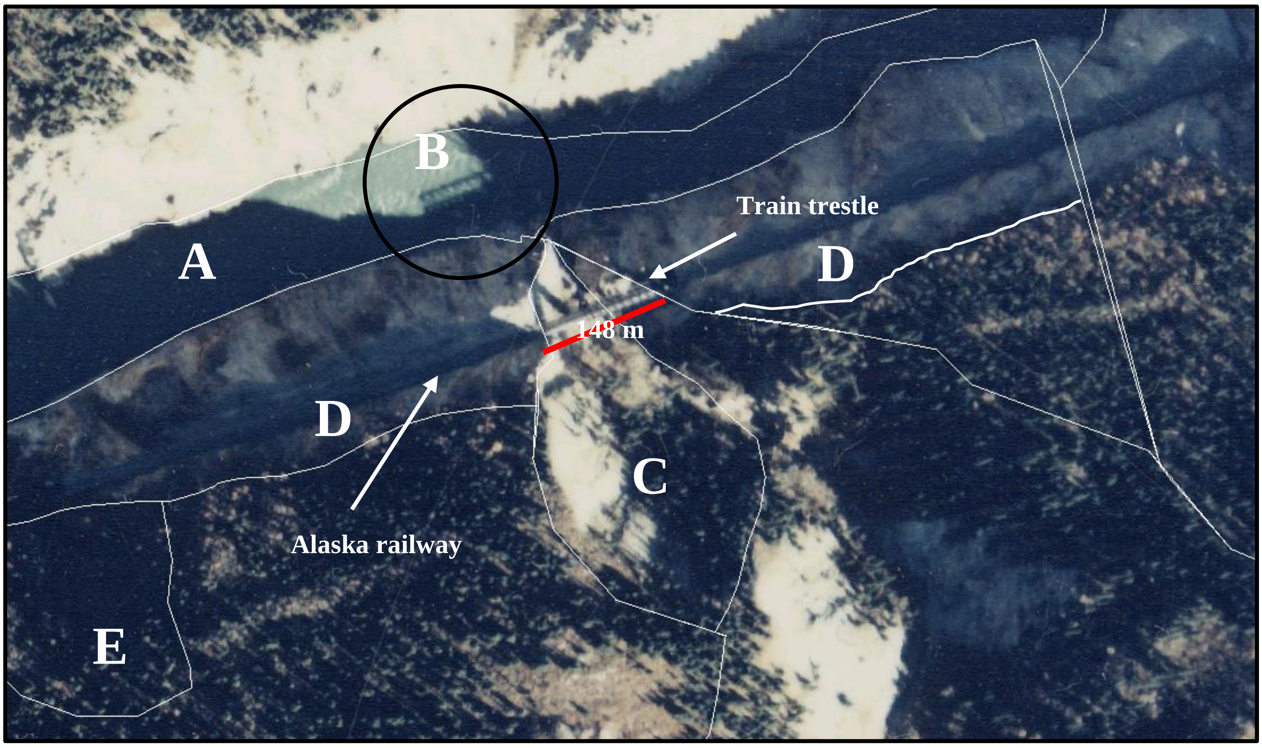

Fig. 10 The same 1:31,680 scale black and white stereo image as shown in Figure 9 zoomed into 1:2,000 using softcopy mapping tools. The Nenana River (A) is clearly seen and is approximately 32 m in width. The shadow of the train trestle is clearly seen in the river (B). Terrain unit C is a large debris slide, Area D characterized by rock fall and area E is a slump in the surficial materials.

No permafrost features are evident in the Healy Canyon imagery. This is likely due to the coarse-textured nature of the overlying materials combined with gentle to moderate and very steep slopes and bedrock being close to the surface.

5. Discussion and Conclusions

Detailed terrain data is required for proper routing along ROWs as well as for on-going maintenance of all infrastructure. Permafrost degradation represents a real challenge to ROWs in cold regions around the world. It is well documented that the climate is changing (Beilman and Robinson 2003; Dall'Amico et al., 2011; Guo and Wang 2016) and without proper knowledge of local ground conditions, the infrastructure along a ROW may be subject to failure. Pipelines buried in soils with fluctuating water tables may be more prone to stress cracking corrosion (SCC) than when buried in well drained soils. Pipelines buried in thick organic materials may be subject to floatation unless properly anchored. Roads, railways, transmission towers and pipelines built over areas of permafrost are subject to subsidence and heaving. Transmission towers built in rugged steep terrain may be subject to upslope movements including landsliding and avalanching.

A number of conclusions can be drawn from the examples provided above. These include:

1. Most publicly available data pertaining to soils, terrain, surficial geology and geohazards is of a small-scale regional landscape level basis. This kind of data is of value for initial planning purposes only and does not provide sufficient detailed information for routing, engineering design and construction purposes.

2. Data specific to ROWs or individual sites can be produced through the use of softcopy mapping tools. This is an inexpensive, desktop approach to producing detailed data that can be used for ROW planning purposes and can also be used to help identify locations of boreholes and other types of field programs.

3. Softcopy mapping can be supplemented with other data including LiDAR, data from hand augers and boreholes and other field programs including Ground Penetrating Radar (GPR).

4. The costs of knowing ground conditions upfront in a project is far less than the costs associated with failures in a system.

5. References

[1] HEGINBOTTOM J.A., DUBREUIL M.A., and HARKER P.A. 1995. *Canada - Permafrost*. In, National Atlas of Canada, 5th Edition, National Atlas Information Service, Natural Resources of Canada, MRC 4177F, 1:7,500,000 scale.

[2] LEMKE, P., REN J., ALLEY R.B., ALLISON I., CARRASCO J., FLATO G., FUJII Y., KASER G., MOTE P., THOMAS R.H. and ZHANG T. 2007: Observations: Changes in Snow, Ice and Frozen Ground. In: Climate Change 2007: The Physical Science Basis. Contribution of Working Group I to the Fourth Assessment Report of the Intergovernmental Panel on Climate Change (Solomon, S., D. Qin, M. Manning, Z. Chen, M. Marquis, K.B. Averyt, M. Tignor and H.L. Miller (eds). Cambridge University Press, Cambridge, United Kingdom and New York, NY, USA.

[3] YANG, Z., OU Y., XU X., ZHAO L., SONG M., and ZHOU C. 2010. Effects of permafrost degradation on ecosystems. Acta Ecologica Sinica, Volume 30, Issue 1, Pages 33 - 39

[4] DALL'AMICO M., CARTON A., CREMONESE E., CURTAZ M., MORRA DI CELLA U., PARO L., PHILLIPS M., POGLIOTTI P., SCHOENEICH P. SEPPI R., ZAMPEDRI G., and ZUMIANI M. 2011. Chapter 4: Local ground movements and effects on infrastructures. In Schoneich, P. et al. (eds): *Hazards related to permafrost and to permafrost degradation*. PermaNET project, state-of-the-art report 6.2. On-line publication ISBN 978-2-903095-59-8, p. 107-147.

[5] BEILMAN D.W. and ROBINSON S.D. 2003. Peatland permafrost thaw and landform type along a climatic gradient. Permafrost, Phillips, Springman & Averson (eds). 2003. Swets & Zeitlinger, Lisse, ISBN 90 5809 582 7

[6] GUO D and WANG H. 2016. CMIP5 permafrost degradation projection: A comparison among different regions. Journal of Geophysical Research Atmospheres, Volume 121, Issue 9. Pages 4499 - 4517
[7] SMITH S. and RISEBOROUGH D. 2010. Modelling the thermal response of permafrost terrain to right-of-way disturbance and climate warming. Cold Regions Science and Technology, Volume 60, Issue 1, pages 92-103.
[8] LARSEN P.H., GOLDSMITH S., SMITH O., WILSON M.L., STRZEPEK K., CHINOWSKY P., and SAYLOR B.2008. Estimating future costs for Alaska public infrastructure at risk from climate change. *Global Environmental Change*, 18: 442-457.
[9] PETTAPIECE, W.W., 1987. Physiographic Subdivisions of Alberta. Land Resources Research Centre, Research Branch, Agriculture Canada. 1:1,500,000 scale.
[10] PAWLEY S.M. and UTTING D.J. 2018. 2018. Permafrost classification model for Northern Alberta (gridded data, GeoTIFF format); Alberta Energy Regulator, AER/AGS Digital Data 2018-0008.
[11] JORGENSON T., YOSHIKAWA K., KANEVSKIY M., SHUR Y., ROMANOVSKY V., MARCHENKO S., GROSSE G., BROWN J., and JONES B. 2008. Permafrost Characteristics of Alaska. Institute of Northern Engineering, University of Alaska Fairbanks. 1:7,200,000 scale.
[12] PAULEN R.C., FENTON M.M., WEISS J.A., PAWLOWICZ J.G., PLOUFFE A. and SMITH I.R. 2005. Surficial geology of the Hay Lake area (NTS 84L/NE). Alberta Energy and Utilities Board, EUB/AGS Map 316, scale 1:100,000.
[13] WAHRHAFTIG, C. 1970. Geological map of the Healy D-4 Quadrangle, Alaska: U.S. Geological Survey Quadrangle Map 806, 1 sheet, scale 1:63,360
[14] JORGENSON M.T., KANEVSKIY M., SHUR Y., GRUMBLATT J., PING C.L. and MICHAELSON G. 2015. Permafrost database development, characterization, and mapping for northern Alaska, Final Report. Prepared for the U.S. Fish and Wildlife Service, Arctic Landscape Conservation Cooperative, Anchorage, AK.
[15] O’LEARY, D., THERIAULT B., SOMMERVILLE A. and NIXON M. 2018. The Importance of Terrain Analysis for Pipeline Planning and Pipeline Asset Management. UESI/ASCE Pipeline Conference Toronto, ON, July 15 – 18, 2018. Utility Engineering and Survey Institute/ American Society of Civil Engineers.
[16] SOMMERVILLE A., O’LEARY D., NIXON M., KUMAH A., and WILSON W. 2016. Use of softcopy technology for soil and terrain characterization. GeoVancouver 2016.
[17] O’LEARY D. and ISIDORO A. 2016. The value of using softcopy mapping tools for siting engineered tailing impoundments. Geotechnical News, December 2016.
[18] O’LEARY, D., HARRIS R., PIRAUX O., and SOMMERVILLE A. 2014. Geohazard mapping and evaluation using softcopy and LiDAR technologies. Geohazards 6, Kingston, ON. June 15 – 18, 2014.

Integrated Approach for the Regional Disaster Management Practice

Masaaki Minami
Professor
Department of Civil and Environmental Engineering, Iwate University
Japan
minamai@iwate-u.ac.jp

Summary

Since in the devastating disaster due to the Mar.11, 2011 Tohoku off-shore earthquake, Iwate University launched the Research Center for Regional Disaster Management (RCRDM) and has risen to the challenges of reconstruction and restoring these areas. The center is comprised of three divisions, which carry out research on natural disaster analysis, in community development and disaster management, and in disaster culture, respectively, to construct people centered disaster management systems and to develop infrastructures and social and educational systems to reduce the impact of disasters. The integrated approach for resilient and sustainable regional society is called the 'Iwate Model'

Keywords: Great East Japan Earthquake, Role of University, Iwate Model

1. Introduction

8 years have passed since The Great East Japan Earthquake on March 11, 2011. This article aims to describe the role of a rural university in an unprecedented disaster coping and recovery. In the case of Iwate University, it is called 'Iwate Model'. It was created and accommodated for each stage of the emergency and recovery process. Practical activities after 3.11 disaster at Iwate University, a conceptual framework for the 'Iwate Model' and a future perspective are described.

2. PRACTICAL ACTIVITIES AFTER 3.11

After the 3.11 disaster, Iwate University containing the Research Center for Regional Disaster Management took a role partially for emergency response, recovery support, and capacity building for the regional society. Figure 1 shows the outline of our activities.

Individual activity: Support activities generated spontaneously just after the 3.11 disaster. Not a few faculties and students started up support activities based on their each individual decision and specialty. The autonomous distributed activities occurred at the beginning of long term support activities. They were motivated personal relationships with the people lived in Iwate region before the 3.11 disaster.

Organized activity: Iwate University established the disaster countermeasures office just after 3.11 disaster and organized activities started up. The office examined the faculties' preferences of support activities by a questionnaire survey. According to faculties' possible commitments, the support plan of the university was built up and allocated budget for each activity. The leadership of the headquarters and the faculties' consensus building succeeded at the stage of the emergency. Rural university have an advantage to make a consensus for participation.

Collaborative activity: Long term and neighbourhood relationship between Iwate University and the region proceeded individual, organized and collaborative activities for each stage of recovery process.

And also, people at Iwate University such as faculties, officers and students had regional wide knowledge and experience about natural, physical, social, economic, and human resource. It was a reason why the regional adapted support and recovery activities proceeded.

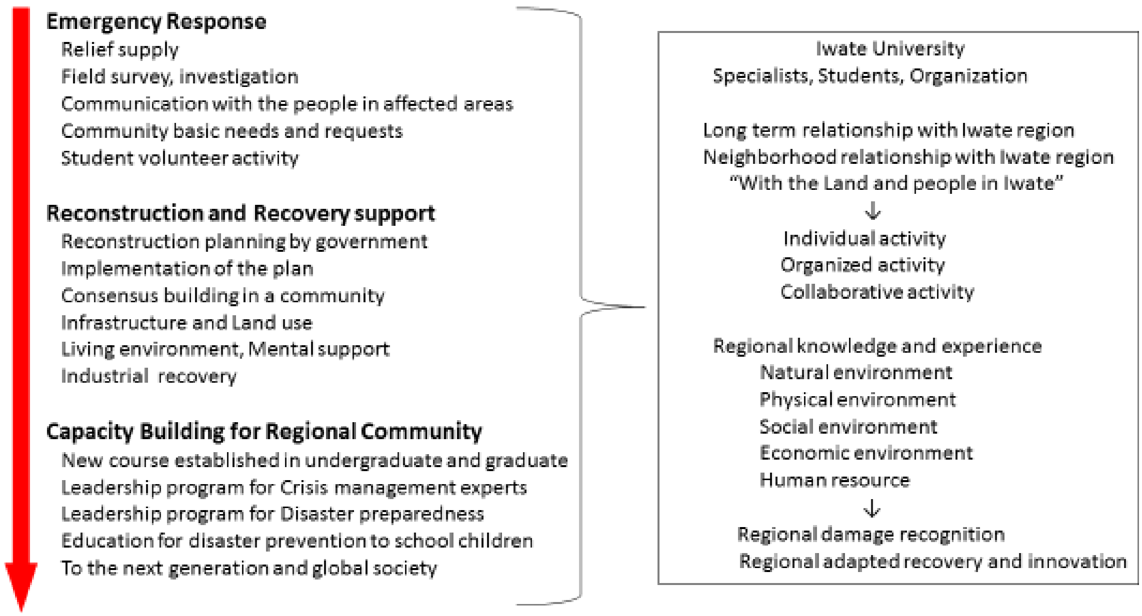

Fig. 1 Practical activities at Iwate University after 3.11 disaster

3. FRAMEWORK OF THE IWATE MODEL

Figure 2 suggests a conceptual framework of the 'Iwate Model' for recovery and social innovation which is formed by the challenges and experiences of practical activities after 3.11 disaster at Iwate University.

Regional center: The model consists of Education activity, Research activity and a Regional center which provides a platform to exchange knowledge and experience with regional and global society.

Education activity: Iwate University established a disaster management related causes in undergraduate and graduate school a few years ago. A tour of inspection is conducted for all first year students. Research center for regional disaster management at Iwate University is continuing to conduct three disaster management related education program for lifetime education, such as crisis management experts program and leadership program for disaster management for adults and children. Students and people in Iwate region can study and practice together in the education program. Faculties can learn the regional problem to be solved from the participants as well.

Research activity: Tsunami, volcanic eruption, flooding and other forms of natural disasters tend to be region specific in terms of their occurrence as well as regarding the process of recovery and reconstruction. Thus, Research center for regional disaster management at Iwate University is engaged in disaster management research and education that is built on regional characteristics specific to Iwate and the Tohoku area. Many of our faculty members value a long-term engagement with familiar fields, identifying challenges that regional problem including disaster management faces, and seeking solutions to improve the situation.

Networking: Figure 3 suggests the conceptual model of networking of rural universities coping with unprecedented disaster. It is emphasized that each rural university and region is facing severe risk for disaster. Iwate University is on a process of recovery. And also, each rural university is on a stage of preparedness, emergency response, and recovery for build back better. The experiences of 3.11 disaster at Iwate University lead to networking of rural universities to build up resilient society for future generation.

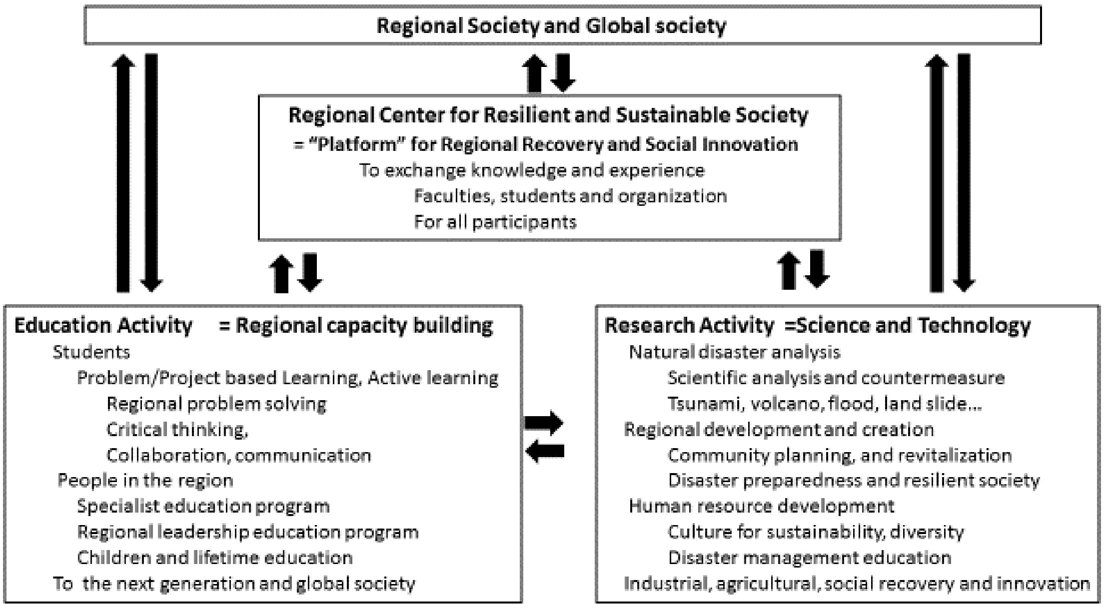

Fig. 2 Framework of the 'Iwate Model'

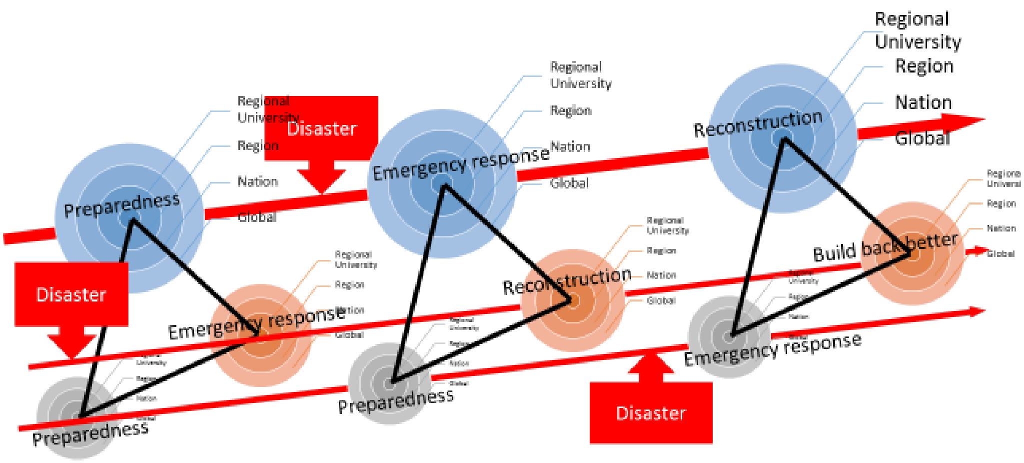

Fig. 3 Networking for each stage of rural university

4. CONCLUSIONS

Before the Sendai Framework for Disaster Risk Reduction adapted in March 2015, Support activities had been continued heuristically with courageous decisions at Iwate University. Just after the 3.11 disaster, existed personal human network and local knowledge were effective. In the organized activity, headquarters' leadership, consensus building based on participants' specialties and preferences had taken effect. Collaborative work with the region are continuing today and from now on.
We call it the 'Iwate Model' and it takes an important role for promoting regional and global resiliency.

References

[1] Masaaki MINAMI, Ayako SOETA et al.: "An Implementation Study on Community Reconstruction under Unprecedented Damage by Tsunami Disaster", J*ournal of JSCE*, F5, Vol.70, No.2, 2014, pp. 46-55. (in Japanese)

History of Cold Weather Paving in Hokkaido, Japan

-a Case of the Development of National Highway Rt.36

Masato Haraguchi, Dr. Eng.
Senior Researcher
Planning Department of Hokkaido Development Engineering Center
Japan
haraguchi@decnet.or.jp

Yasuhiro Kaneda, Hokkaido Development Engineering Center, Japan

Summary

65 years ago (1953), the construction of National Highway Rt. 36 that connects Sapporo to Chitose was completed in Hokkaido. The new technology employed for the construction work had drastically changed road construction measures in Japan's cold regions. Based on the technical accumulation before the World War II, new technologies had been produced to design roads in Hokkaido, the northern most island and the coldest region in Japan. The developed new road construction technologies were incorporated into national road construction projects. They have been handed down to today's road design standards. The purpose of this paper is introducing the technological transition of road construction in cold regions and the efforts to develop new technologies to utilized them in cold region road development toward the future.

Keywords: road, pavement, subgrade, asphalt, concrete, anti-frost-heave

1. Background of the National Highway Rt.36 development project

1.1 History

Fig. 1 National Highway Rt. 36 connecting Sapporo to Chitose

During the World War II and for some years after the war, Japan had suffered infrastructure destructions caused by the war all over the nation. Therefore road development or repair of gravel roads had not been made in northern most island Hokkaido whose population was smaller than the mainland Japan. Then, US Army of Occupation Japan that stationed in Hokkaido requested the Japanese government to improve Rt.36 (Fig. 1) that is connecting Sapporo, the capital city of Hokkaido and Chitose where the airport and one of the US Army bases then existed. The snow removal of National Highway Rt. 36 in winter was conducted by the US Army. It was the first large-scale snow removal in Hokkaido. During the Korean War, heavy vehicles ran between Sapporo and Chitose, the road surface was

Fig. 2 Opening ceremony of the improved R. 36 in November 1953

gradually deteriorated. In the spring of 1952, the US Army requested to improve Rt.36 with 34.5 km length as it could stand heavy vehicle traffics. The due of the road improvement was one year ahead. Excluding snowy winter period where the work could not greatly progress, the work had to complete for 7-8 months, actually. The Rt. 36 improvement project has successfully completed in November, 1953 as scheduled (Fig. 2). The costs for this project were budgeted based on administrative agreement between Japan and the United States; US-Japan Security Arrangements. Because different from normal road funding sources, this budget was relatively flexible to use, the large-scale project could be realized. But this was criticized domestically as Japan's cooperation for the Korean War, and every newspaper called the road as a "bullet road".

1.2 A leading engineer

Fig. 3 Toshigoro Takahashi

This project was led by an engineer, Toshigoro Takahashi (Fig.3); Manager of the Sapporo Development and Construction Department, Hokkaido Regional Development Bureau. He graduated from Department of Civil Engineering, Hokkaido Imperial University. His policy was practical enough to realize cost-efficient road engineering.
He directed the project including the planning, design, construction and supervision of the work proceedings and finally wrote a report.
His innovative research results were adopted in this road project which brought about fundamental changes in Japan's road construction. In 1958, he moved to the Nippon Highway Public Corporation and became the test director of the Meishin Expressway, the first expressway in Japan, to be responsible for setting Japan's highway design rules and standards.

2. Development of cold weather paving

2.1 Three technological points in the Rt. 36 project

First, this road project applied measures to fundamentally avoid pavement damage from frost heave which had annoyed road engineers for a long time. It was the first time that an actual road design adopted anti-frost-heave subgrade for the pavement in the Rt. 36 project. They used volcanic ash that is richly existing along the route for the subgrade construction, which significantly reduced the construction expenditures.

The second point was the adoption of asphalt pavement. Because the required period for the road development was so short, to complete the work to meet the due, asphalt pavement that needs shorter time than concrete pavement to complete was preferable. This was the époque-making event that turned the conventionally used concrete pavement to use asphalt pavement in Japan.

Thirdly, this road project established general road design standards with technical proofs. At this time when Japan was still seeking road design standards, it was vital that the road design that matched technologically modern society was shown through the Rt. 36 project to the central government.

The details of those three points follow.

2.2 Adoption of the anti-frost-heave subgrade

Fig. 4 Spring frost heaving in a national highway

Fig. 5 Ice lens taken out from the observation pit

Until when the anti-frost heave subgrade was introduced to pavement construction, frost heave which destroys road structures had been a serious problem to pavement construction as shown in Fig.4. No one understood the mechanism of frost heave generation and could find the countermeasures against this phenomenon.

Anti-frost heave measures had been researched for railway before the war. In 1939, a committee was organized in cooperation with the railway management department, the snow/ice relevant associations and Hokkaido University. The research was made from two aspects: physical soil experiments and engineering test work. The research results suggested that the replacement of pavement base, subgrade, heat insulation for the base/subgrade, drainage, drug treatment, and water barrier layer placement would be effective as the countermeasures against frost heave. However, the research results had been dissipated by war.

After the war, the frost heave problem emerged again and a committee consisting of industrial arena, academia and public sectors were organized. Some engineers including Toshigoro Takahashi attended the committee. He said that they should focus on more practical engineering methods. Led by Takahashi, observation pits for frost heave phenomenon were set up beside the all national highways around Hokkaido to find a solution to prevent frost heave (Fig. 5).

Along with those efforts, the frost heave investigation also began in the Rt. 36 project in September 1952. As a result, It was found that replacing the subgrade to the depth of 80 cm from the surface, which is equivalent to 80% of the freezing depth, about 1 m, might be effective to prevent the pavement from frost-heave damage. In other words, preventing subgrade from frost heave, aggregate replacement to this depth, is most effectively hinder the creation of ice lens. Even if frost heave occurs in the layer deeper than 80cm, it does not affect the upper layer. It also can avoid soil softening in the spring. Further, because volcanic ash was used as the aggregate for the Rt. 36 subgrade replacement, the cost came to be cheaper than a case using gravels and sand.

Cinders produced from a steam locomotive had been used for subgrade replacement in the railroad. This was led to an idea of using volcanic ash as the aggregate. It was because the physical fefatures of coarse-grained volcanic ash that is easily taken along the road are similar to those of cinder (Fig.6).

On the construction site, workers sometimes mistakenly mixed poor quality soil in the aggregate. To avoid such mistakes, simple standards to differentiate volcanic ash from soil was adopted. The features of volcanic ash follow: (A) The colour is white or almost white, (B) Particles are hard as it cannot be crushed even if it is strongly pressed with fingers, (C) When water is added and soldered or grasped, it does not become viscous.

Fig. 6 The subgrade replacement using volcanic ash

After the first winter, the subgrade replacement results identified that only 11 m of the total length of 35 km suffered frost damage. It falls on only 3% of the total road length, and the investigation of the damaged section showed that the damage cause was a construction error. It proved that there was no defect in the pavement design policy.

2.3 Adoption of asphalt pavement for the Rt.36 project

When considering what kind of pavement to use for the Rt. 36 project, the principal idea was making a thick base layer to prevent frost heave and as for the pavement, there were two options, concrete and asphalt pavement.

As you may know, the concrete pavement is rigid thereby the base/subgrade could be thin because the load on the pavement disperses over a wide area. On the other hand, since asphalt pavement is flexible pavement, the bed/subgrade needs to be thick because the pavement is flexible and the load on it yield the pavement downward. At that time, the construction cost of concrete pavement was twice as much as asphalt's (Fig.7).

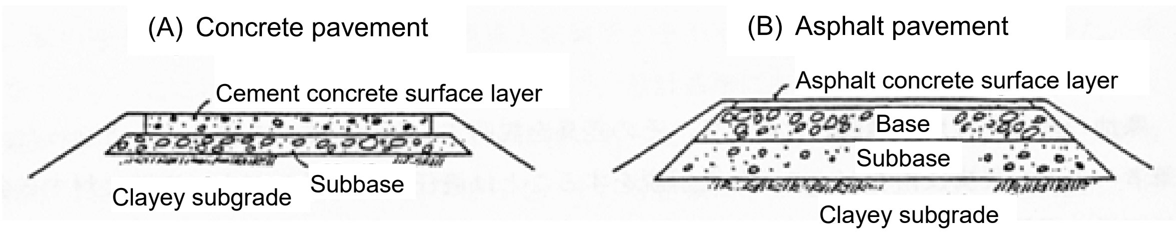

Fig. 7 Differences in subgrade structures between concrete and asphalt pavement

In Japan where curd oil is not produced, it was recommended to use concrete pavement during the war. However, because concrete pavement takes time to dry after construction, it was not suitable for this road project whose requested construction period was quite short. For time saving, flexible asphalt pavement was appropriate because while the compression of the subgrade to be replaced continued, the surface layer could be installed.

Takahashi choose asphalt pavement because it was uneconomical to install concrete pavement that took more time and cost as a road countermeasure against frost heave. Selecting asphalt pavement for the project, he showed that the road construction method in Hokkaido should be considered from the viewpoints including the design of subgrade, cost efficiency and construction period.

Fig. 8 Pavement repair using soft asphalt

This road development project over 35 km completed in 1953 as scheduled and it showed that the selection of asphalt pavement was most appropriate. The results of this project influenced all over Japan and changed the pavement from concrete to asphalt. After the first winter following the work completion, asphalt pavement's disadvantage, being subject to wear came about because vehicles' snow chains abraded the pavement surface 5-10 mm. Generally when asphalt gets worn, the oil involved in it becomes sticky and works to protect the pavement surface from physical shocks, but in cold weather because the oil becomes hard, the pavement comes to be fragile and is likely to be broken by anti-skid chains mounted on vehicle tires. However, by careful observation, some pavement parts which endured the wearing were found. They were the centre line which was painted white and the part repaired with soft asphalt. Learning from these, the pavement surface was coated with 1 mm layer of soft asphalt which was melted with oil by the next year (Fig. 8). Along with the increase in traffic volumes, the air pollution problem due to the dust created by vehicles' studded tires' pavement abrasion came about. Fortunately, studless tires solved those problems. Through such trials and errors, pavement design standards that fit a cold region were created in Hokkaido.

2.4 Road design standards adopted in the Rt.36 project

The old Rt. 36 before the development project was initially planned as a road that is mainly targeting motor vehicles while allowing the use of horse-drawn carriages that were common then even in the urban area, and there was no sidewalk. And, the Rt. 36 was designed before the war, expecting high speed traffics in populated areas and low speed traffics in rural areas. However, in the development project after the war this policy was immediately found inappropriate and changed to the opposite. It was because the objective of the Rt. 36 development project was to minimize the total travel time from Sapporo to Chitose. It is as a matter of fact now, but was not a common idea immediately after the war. To achieve this aim, the project adopted design standards that fit high speed traffics in rural sections such as those in mountainous hilly areas and in populated areas where the traffic volume is greater than in rural areas, they adopted those that fit low speed traffics.

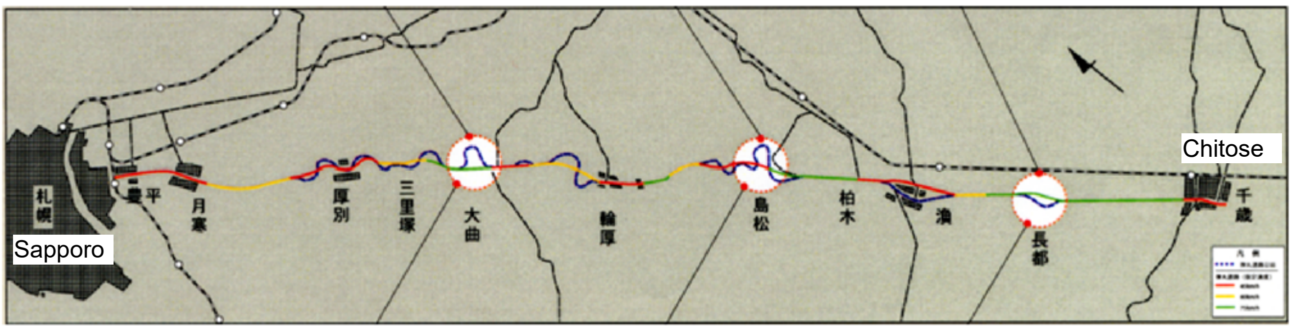

Fig. 9 Three kinds of design speed in the Rt.36 project

Therefore the road construction with a large amount of earthwork was mainly conducted in the mountainous area, and the construction work scale in the flatland was small. As a result, the cost to purchase land has been reduced so that the total construction costs were saved.

These new road design standards that were developed for the Rt. 36 project in Hokkaido had a great significance because they had influenced national road desing policies.

The colored road sections shown on Fig. 9 indicate the three kinds of design speed. The hypothetical speeds include: 45 Km / h (Red): the slow speed traffic section, 60 Km / h (Yellow): the medium speed traffic section, 75 Km / h (Green): high speed traffic section with good topography and construction environment.

In addition, as shown in Fig. 10 a, the roadway shoulder width including the curb of Rt. 36 is 1.0 m, and there is additional space 1.0 m wide outside the side groove (Fig. 10 b). This is to leave space for mounting removed snow in winter. According to the national road design standards, the road shoulder could be 0.5 m or more, however the road width wider than 0.5 m is rare.

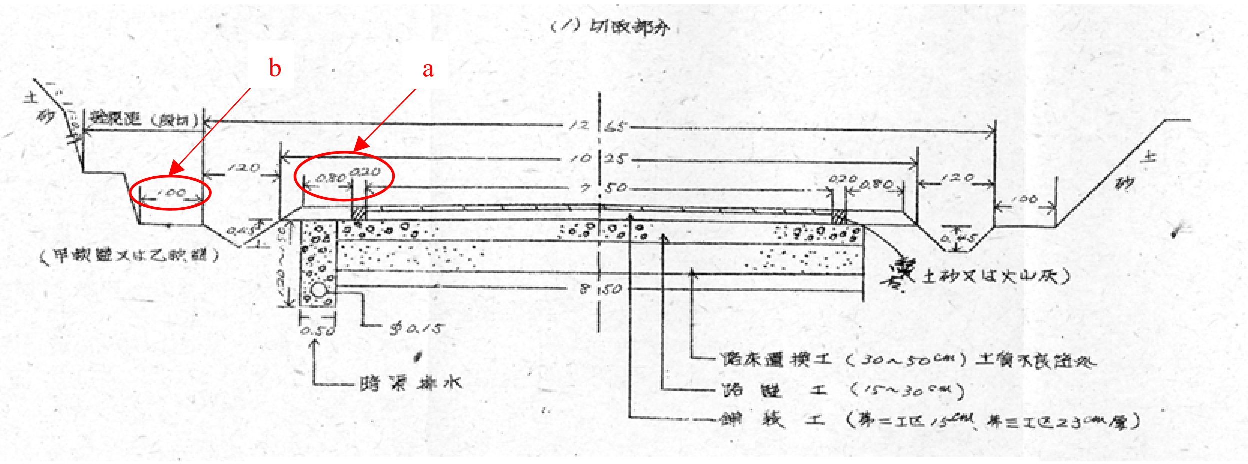

Fig. 10 Cross-sectional view of the Rt.36 roadway

3. Summary

Through the introduction of road design development in Hokkaido, a cold snowy region, taking an actual case of the Rt.36 development project, some issues have been found to be reconsidered. For example, as a time and cost saving measure, asphalt pavement was selected for the project. However, asphalt pavement's disadvantage that it is easy to wear has not yet completely solved and it needs frequent repair. The possibility of concrete pavement adoption could be re-examined, considering the recent cutting-edge technologies that may resolve the disadvantages of concrete pavement. Looking back on engineering history, there would be many things that could be used again, reviewing from the points of new technology application.

References

[1] MURAKAMI S., OBA O., SUNAMOTO F., TAMADA H., KAKU S., and OSADA J., "The aspect of dependent housing and military dispositions in the occupied japan", Japan Architect of Planning Aij. Vol.82, No.739, Sep.2017, pp.2441-2450.

[2] TAKEMOTO H., KUDOU K., MARUYAMA K., MIURA H., and KASAHARA A., "Test pit survey on national highway 36(Sapporo-Chitose): early pavement technologies in japan", J.JSCE, Ser.E, Vol.62, No.1, Mar.2006, pp.274-285.

TRAFFIC SAFETY IN COLD REGIONS

Case Studies for Traffic Safety Measures in Cold Regions

Hannele Zubeck
Professor
University of Alaska Anchorage
U.S.A
hkzubeck@alaska.edu

Dr. Vinod Vasudevan, University of Alaska Anchorage, U.S.A.

Summary

Traffic safety is one of the main considerations when designing and upgrading roads in cold regions. When compared to temperate regions, traffic safety is affected by additional issues such as incremental driving conditions and snow or ice covered road surfaces. This paper presents case studies of some recent safety measure trials around the world's cold regions. Among the case studies are Safety Corridors used in Alaska, USA, widened center line markings used in Finland, and use of rumble strips used in various cold regions. The safety measures are described, and existing before/after studies are summarized. All the aforementioned safety measures were found to reduce accidents and are feasible for use in cold regions.

Keywords: traffic safety, case studies, road markings, rumble strips, speed limits

1. Introduction

Traffic safety is one of the main considerations when designing and upgrading roads in cold regions. When compared to temperate regions, traffic safety is affected by additional issues such as incremental driving conditions and snow or ice covered road surfaces. This paper presents case studies of some recent safety measure trials around the world's cold regions. Among the case studies are Safety Corridors used in Alaska, USA, widened center line markings used in Finland, and use of rumble strips used in various cold regions.

2. Safety corridors

According to Alaska Department of Transportation and Public Facilities (AKDOT&PF), Designated Safety Corridors are segments of a state highway that has been identified as having a higher than average incidence of fatal and serious injury crashes, and the road and public safety officials have agreed to provide funding for effective education, enforcement, engineers, and support emergency response agencies for those sections of road [1]. Currently there are four designated Safety Corridors in Alaska at the various locations.

The education efforts have been conducted by providing safety messages with Alaska Statewide Highway Safety Media Campaign [2], and providing information at the Safety Corridor web page [1]. An example of the ad campaign is given in Figure 1. The enforcement efforts include citing double fines for speeds exceeding the speed limit. The speed limit traffic signs include the text "Double Fines" right under the posted speed limit (Figure 2). The emergency response agencies involved are local fire departments providing ambulance and rescue services, police and Alaska State Troopers.

The first safety corridor was imposed in May 2006 in Seward that is located in the Kenai Peninsula. The traffic volumes and traffic accidents have been monitored before and after imposing the corridors. The results show that fatal and major injury crashes are down by almost 40% overall since May 2006 [1]. The AKDOT&PF and Department of Public Safety are tasked by law with the responsibility of reducing these crashes. Long term, major road projects are needed to address traffic volume growth, but in the immediate term, cost-effective solutions such as safety corridors will be pursued to reduce severe crashes.

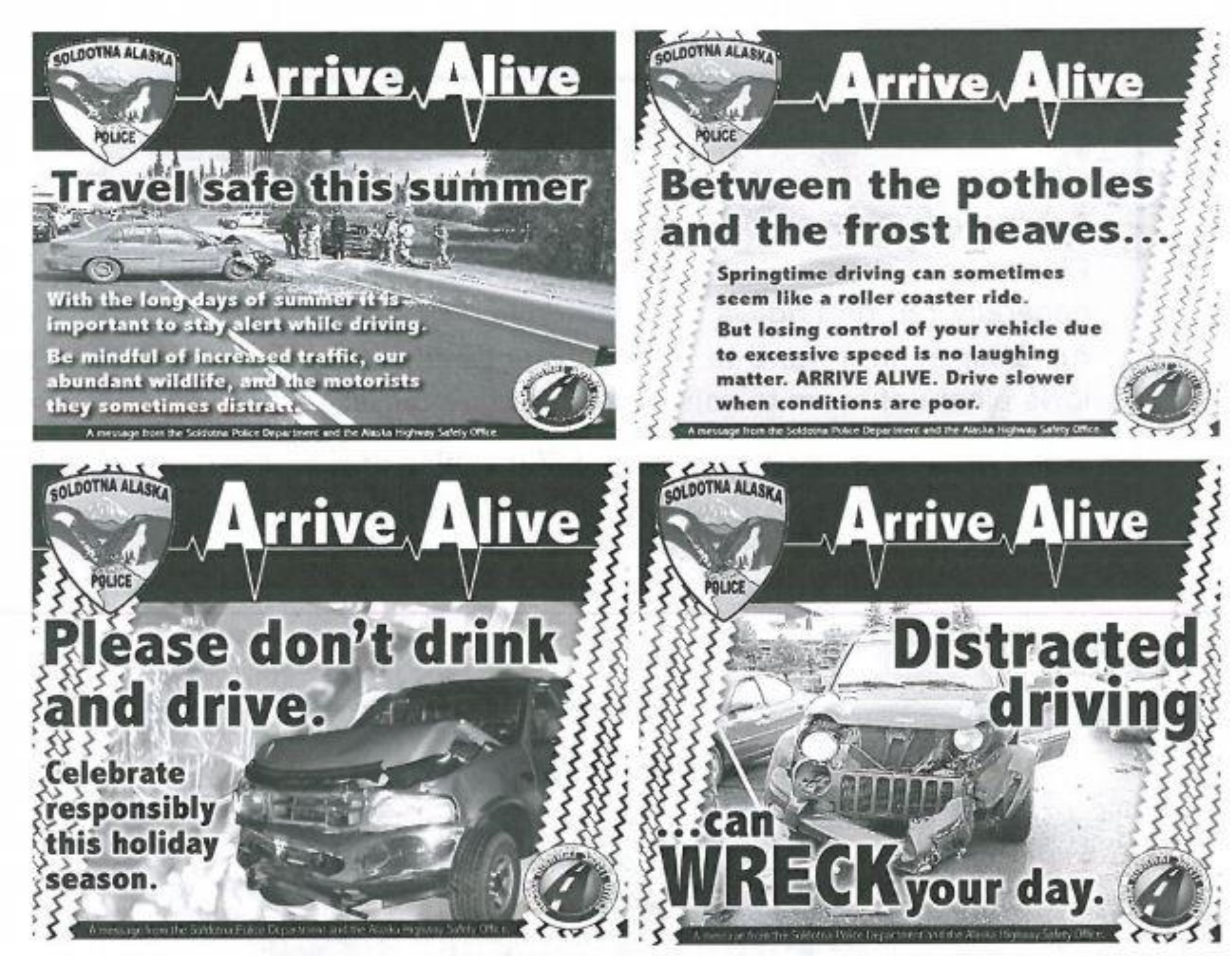

Fig.1. Example of Ad Campaign [3]

Fig. 2. Safety corridor speed limit sign with double fines warning

3. Widened center line markings

Widened center line markings have been used in Finland to improve traffic safety over a decade now [4]. An example of the widened center line markings are shown in Figure 3. Instead of a typical center line markings adjacent to each other, the lines signalling the location of the center line and possible passing restrictions are painted to the road surface with a significant cap in between. The purpose of the widened center line markings is to improve safety when passing on selected high volume road sections. The widened center increases the time to manoeuvre the vehicle after on-coming traffic is observed. According to Rasanen [4], the widened center line markings are suitable for a two lane high traffic volume road section where median guardrails are not feasible. The shoulders need to be at least 0.75 m wide for light traffic and to avoid driving off the road (right side). The total width of the paved road need to be greater or equal to 9.5 m and the speed limit of 80 or 100 km/h.

Studies summarized by Rasanen [4] indicate that oncoming traffic accidents and driving off the road at the left side have been reduced by about 10%. If median rumble strips are added, the accident reduction is about 19%. Lahtinen [5] report even larger reductions in accidents in the Southern Finland.

Fig. 3. Widened center line markings

4. Rumble strips

Rumble strips are used predominantly on rural highways where there are historically high crash rates of single crash crashes and head-on collisions on undivided highways due to lane departures. Most of these crashes result from driver errors such as inattentive driving, distracted driving, drowsy driving, and fatigued driving. Typical crashes related to drowsiness/fatigue have the following characteristics: crashes during late-night hours, crashes happen at high speed, single vehicle leaves the roadway, no attempt to avoid crashes, and driver is alone in the car [6]. These types of crashes are of significance to cold regions as most the cold regions have huge proportions of roads passing through rural areas with low traffic volume. Studies have shown that lack of other vehicles and long drives make the driving monotonous. Rumble strips have proven their effectiveness in reducing crashes and fatalities due to crashes involving roadway departures. Rumble strips induce noise and vibration to alert drivers when they leave the travelled way.

Rumble strips can be divided into four major categories: center line rumble strips, shoulder rumble strips, mid lane rumble strips, and transverse rumble strips. The purpose of center line rumble strips is to reduce head-on collisions and opposite-direction sideswipes. Shoulder rumble strips are mainly deployed to reduce run-off-the-road crashes. As the name suggests, mid lane rumble strips are deployed in the middle of lanes, but they are not popular. Transverse rumble strips are used for alerting drivers of an unexpected change in traffic condition, such as slow down or stop on a highway due to an intersection, toll plaza, horizontal curves, which may require immediate action from the driver. The dimensions and installation details are given in NCRHRP report 641 [7]. This report also shows that the reduction in head-on and opposite direction sideswipe fatal and injury crash frequency of on rural two-lane roads is 45%, whereas, on urban two-lane roads, the reduction is 64%. This report indicates that the reduction in single-vehicle run-off-the-road fatal and injury crash frequency is 36% on rural two-lane roads, whereas, on rural freeways, the proportion is 17%. The Handbook of Road Safety Measure [8] presents that the crash modification factor for transverse rumble strips was 34%. In summary, the rumble strips have significantly improved safety on highways.

Fig. 3. Rumble strips in Alaska [9]

Although the impacts of speed humps in cold regions are expected to be different due to the challenges associated with the accumulation of snow and ice on the rumble strip patterns, not much research have been conducted on cold regions to evaluate the effectiveness of rumble strips. One of the studies reported is from the state of Alaska, USA [10]. This study was conducted to review crash reduction factors (CRF) for Alaska, found that based on findings from a lower number of sites, the crashes showed significant decrease due to the implementation of rumble strips. In this study, different types of rumble strips were analysed separately. The study showed that while there were some changes in CRF values, most of these remained comparable to the values published by the NCHRP report 641 [7].

The installation of shoulder rumble strips was shown to have a crash cost reduction factor (CRF) of 50% for Alaska. On rural two-lane highways, the crash costs were reduced by 22% after the rumble strip installation. Analysis showed that the installation of rumble strips near horizontal curves yielded a CRF value of 29%, which is higher than the NCHRP reported value. For center line rumble strips, the CRF value reported in this study is 25%. As an interesting result, this study also showed that the crash risks, based on injuries and fatalities, were increased after installation of rumble strips on four-lane highways. It is important to note that the changes were noted while excluding snow and ice conditions. Most of the time the noise and vibration can still be noticed if the rumble strips are covered with snow and ice. This is a great advantage of rumble strips in warning errant drivers when the roads are covered with snow as the noise and vibration occur even though the rumble strips are not visible.

5. Conclusions

5.1 Submission

The use of traffic safety measures such as safety corridors, widened center line markings and rumble strips are feasible in cold regions. Traffic accidents including fatal accidents have been reduced using these measures.

References

[1] Alaska Department of Transportation and Public Facilities , http://www.dot.state.ak.us/highwaysafety/safety_corridors.shtml, accessed February 6, 2019.

[2] Alaska Department of Transportation and Public Facilities , http://www.dot.state.ak.us/stwdplng/hwysafety/media.shtml, accessed February 6, 2019.

[3] Alaska Department of Transportation and Public Facilities , http://www.dot.state.ak.us/stwdplng/hwysafety/assets/pdf/Soldotna_Arrive_Alive_media_2011_part_1.pdf, accessed February 19, 2019.

[4] RÄSÄNEN, M. "Leveän keskimerkinnän kokeiluista," http://pank.fi/file/511/r-s-nen_leve-n_keskimerkinn-n_kokeiluista_08_02_2012.pdf, 2012

[5] LAHTINEN, E. "Leveiden keskimerkintöjen liikenneturvalllisuusvaikutusten arviointi," "https://www.doria.fi/bitstream/handle/10024/123183/Raportteja_30_2016.pdf?sequence=2, 2016.

[6] National Highway Traffic Safety Administration (NHTSA), "Drowsy Driving and Automobile Crashes," Report HS-810 631. U.S. Department of Transportation, https://www.nhtsa.gov/staticfiles/nti/pdf/808707.pdf, 1998

[7] NCHRP, http://www.cmfclearinghouse.org/studydocs/nchrp_rpt_641-GuidanceRumbleStrips.pdf , Report 641, 2009.

[8] ELVIK, R., and VAA, T. "Handbook of Road Safety Measures," 2004

[9] Alaska Department of Transportation and Public Facilities http://www.dot.state.ak.us/stwddes/dcstraffic/rumble/index.shtml, accessed February 25, 2019.

[10] KINNEY, R. "Review of Crash Reduction Factors (CRF) for Use in the Highway Safety Improvement Program Handbook", http://dot.alaska.gov/stwddes/dcstraffic/assets/pdf/rumb-strip/crf-rpt_rum-strip_excerpts.pdf, 2009.

Study on Effects of Salt Spreading Decision and Operation Support Tools on Operator Performance

Roberto Tokunaga
Senior Researcher
Civil Engineering Research Institute for Cold Region PWRI
Japan
roberto-1097ga@ceri.go.jp

Kenji Sato, Electromechanical Chief Clerk, Hokkaido Regional Development Bureau MLIT, Japan
Akira Saida, Researcher, Civil Engineering Research Institute for Cold Region PWRI, Japan
Masaya Sato, Team Leader, Civil Engineering Research Institute for Cold Region PWRI, Japan

Summary

The efficient management of snow and ice control on winter roadways is an important task in snowy and cold regions, such as Hokkaido. For this purpose, in controlling icy roadways, the Japanese road authorities and maintenance contractors look solely to road sections where the road surface tends to be iced up and spread salt corresponding to the road surface conditions of the time. Therefore, the identification and discrimination of road surface conditions by operators who spread salt onsite is extremely important. However, as Japan has seen demographic aging in recent years, many skilled operators have been aging and retiring. It has been difficult to foster newly recruited operators.

Considering the above, technology for assisting with decision making and operating spreader machinery has been under development, while the use of ICT for salt application and its automation have been attempted in recent years. However, the technology has not achieved widespread use for reasons that include its huge cost. In addition, no research examples have been found that assessed, from the viewpoint of human factors, the effectiveness of such technology at improving the ability of operators to properly determine the road surface conditions and to properly operate a spreader machine.

The authors aim to develop technology for supporting the accurate judgment of road surface conditions and correct operation of salt spreading on the roadway. To this end, this study identifies how experienced operators differ from inexperienced operators in identifying the conditions on the road surface and/or operating a spreader when working to apply salt. Also, the effectiveness of road surface information and spreading support tools (voice command system and automated spreading system) on the spreading decision and/or operation is examined.

As a result of a series of field experiments, the following results have been obtained. The provision of information decreases the operator’s subjective mental workload regardless of skill level, and contributes to improved cognition and judgment of the condition of the road surface. However, depending on the method of information provision, the extent of observation of the road and its surroundings decreases markedly, which would affect the attention that should be given to ensure safety during the spreading task. On the other hand, by using the spreading support tool, the operator’s subjective mental workload decreased markedly, the recognition and judgment of the condition of the surface of the road became more rapid and precise, and safety during spreading task also improved.

Keywords: Winter Maintenance, Salt Spreading Operation, Support Tools, Operator

1. Introduction

Efficiency and cost cutting are issues involved in road management. Salt spreading is performed in winter "according to the surface condition of the road of the icy sections" [1] by road administrators.

Therefore, it is very important for salt spreading site operators to determine the road surface condition appropriately. However, because it has been difficult to hire and educate new operators in recent years, [2] the effect of spreading cannot help but to depend on the current skilful operators engaged in the present work. Moreover, operators are getting old, and it is assumed difficult to find suitable new operators, while cost-cuts are required from now on. We are anxious about the certainty and safety of road administration. That is, a system whereby inexperienced operators perform the road administration activities and the drivers perform spreading (one person performs driving and spreading) is inevitable. The road administrators perform the road-surface management work (spreading the salt) in winter, examining the site road surface condition and weather of the day and determining the necessary sections of salt spreading. In doing so, they refer to the following guidelines and other information: Handbook - A Practical Guide for Snow and Ice Control, [3] Minnesota Snow and Ice Control - Field Handbook for Snowplow Operators, [4] and Manual of Road-Surface Management in Winter (draft) [5] That means that, although site operators perform the spreading activities by examining the road surface condition, the validity of the determination and operation is uncertain.
On the other hand, studies of technologies that support the determination and operation, such as the use of on-board type optical road surface condition sensors and automated spreading [6] have been carried out in recent years. However, these new technologies diffusion are not progressing at sites because of the high cost at this moment.
This study has been performed, aiming at making a development proposal on supporting technologies to realize a safe-and-secure salt-spreading-work system under which one person performs both the driving and salt spreading and which is not affected by the experience or skill level of the operators. The study includes an experiment on operators' recognition and determination of the road surface condition, measurement of operating conditions of the spreading apparatus, and analysis of the psychological condition and behaviour of operators. Operators' skill levels and change in psychological condition and behaviour due to the existence and type of information, as well as the performance of the spreading operation, were investigated in 2017 and 2018.

2. Methodology

2.1 Evaluation Method

Some argue that work performed by a human being is, despite consisting of physical activities, controlled by mental load (mental workload) [hereinafter MW]. The concepts and terms in the field of MW are defined by ISO (International Organization for Standardization). [7]
Various studies of human beings' burden during operation have been performed in areas of industry, medical care, aeronautical navigation, rail, and automobiles, [8] because it is considered that issues that require an excessive load in a simple and monotonous situation for a long period lead to human error, which may result in the reduction of working efficiency and an accident. In understanding and evaluating this burden, the MW concept described above is utilized. Various studies of people's MW during car driving have already been performed overseas and in Japan, [9], [10], [11], [12] but no studies using MW to evaluate road operators' capability to resolve issues are known by the authors. This study quantifies and evaluates such capability of operators during salt spreading work using MW to construct technology to assist with on-site operation and determination on salt spreading.
A human being's MW in performing specific action can be evaluated subjectively and objectively. This study investigated operators' MW using both subjective and objective evaluation methods.
For the subjective evaluation, the NASA-Task Load Index [hereinafter NASA-TLX] developed by Hart et al. was used. [11]
For the objective evaluation, the location recognized by the operator as a section necessary to spread the agent on (recognition distance) and the locations of starting and completing the spreading were compared with the salt spreading section decided beforehand were evaluated, and the spreading conditions results corresponding to the road surface condition (hitting ratio of determination) were evaluated. Furthermore, the watching point of operators during the driving test was measured with an eye-glass type gaze tracking device.

2.2 Outline of the Experiments

The operators' testing was performed at the Tomakomai Cold Region Test Track owned by the Civil Engineering Research Institute for Cold Region at night (18:00 to 23:00) during the severe winters in 2017 and 2018. The weathers were almost fine during both the testing period. The test track consists of 2,700 m long asphalt pavement in two straight sections and two curved sections.
The testing was performed on counter clockwise driving using all sections of the test track, starting from and finishing at the KP0.3 point at a speed of approximately 40 km/h. The road surface of the test track was mostly dry, where a combination of 4 to 6 wet/icy road surface sections (100 m each one) were created artificially. The test operators performed the spreading work at these sections. It should be note that the locations of the wet road surface and the icy road surfaces were changed randomly every day.
A 2-ton truck was used as the test vehicle for the test (2017 and 2018). Moreover, to measure the test operators' behaviour, a console panel was installed between the driver's seat and the passenger seats, imitating a salt spreading control device. The console was provided with a display indicating the power button, spreading amount setup key, spreading button, and other buttons and lights so that the test operator could take actions simply by touching the screen. The actions of all buttons displayed on the spreading console panel were recorded at 10 Hz in a data recorder with GNSS (Global Navigation Satellite System). Also, during the driving on the test track, the coordinates of test operators' gaze by using a gaze tracking device.

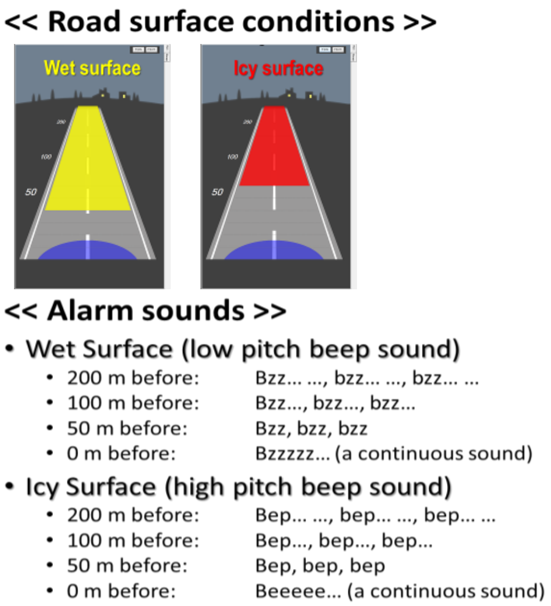

Figure-1 Example of information provided on in-vehicle information terminal

To provide the approaching road surface condition and other information to the test operators, an in-vehicle information terminal [a 7-inch tablet] was installed in front of assistant seat (2017). An application was installed to start providing the information from approximately 200 m before from the wet or icy road surface sections on the test track (Figure-1). In addition, the wet and icy sections constructed on the test track were randomly changed every day.
In 2018, an in-vehicle information terminal, which has been used since 2017, was installed as a spreading support tool between the driver's seat and assistant driver's seat. It functioned to provide the information (sound and image) and newly added voice command and automatic spreading. The test operator always observed the road surface condition while driving on the test track and set the spreading amount of the salt on the icy road surface to 30 g/m^2 and on the wet road surface to 20 g/m^2 immediately after recognizing an icy or wet road surface ahead. The determination of the road surface condition was judged to occur when the right spreading amount was set corresponding to the road surface condition. Furthermore, at the starting and finishing points of the wet and icy road surface sections, the spreading on-off operation was performed. It was permitted to use the information on the oncoming road surface and other conditions, as well as the spreading support tool, when those tools were available.
The main test procedures were as follows. Test operators were told about the important matters related to the purposes, testing items, test procedures, and ensuring of safety in the waiting room. Next, the method for wearing the eye tracking apparatus, operation procedures of the spreading apparatus, and other matters were explained to the test operators. Then, each test operator, in turn, drove the truck once from the starting point to the finishing point of the test track, performing the matters explained in the preceding paragraph. After finishing the drive, the test operator received an explanation about the subjective MW evaluation method regarding the relevant issue addressed by the test. The test operator filled in a paper questionnaire about the subjective MW perceived in the spreading operation after the explanation.

3. Experimental Results

3.1 MW as a Function of the Skill Level, Existence and Type of Information

For the 2017 experiment, four conditions were set to investigate the differences and level of MW due to the conditions. The conditions were operator skill level (not skillful or skillful) and the existence and type of information ((1) no information [hereinafter NI], (2) sound only [hereinafter SO], (3) image only [hereinafter IO], or (4) sound plus image [hereinafter S+I]). All 19 test operators were male construction workers holding a driver's license, including seven not-skillful operators [hereinafter NSOP] (43.0 years old on average with no spreading experience) and twelve skillful operators hereinafter [SOP] (57.3 years old on average with average spreading experience of 7 years). For the 2017 testing, the test operator rode in the assistant driver's seat, and the test support person performed the driving operation.

3.1.1 Operators' subjective MW

Table-1 Subjective MW as a function of skill level and information

Subjects	Conditions	Subjective MW (points)			
		Samples	Average	Median	SD
NSOP (7)	NI	7	6.3	6.7	1.7
	SO	7	4.0	4.6	1.2
	IO	7	3.2	3.2	1.2
	S+I	7	1.3	1.3	.8
SOP (12)	NI	12	5.5	6.0	1.6
	SO	12	3.5	3.7	1.1
	IO	12	1.9	1.8	1.1
	S+I	12	1.2	1.2	1.2

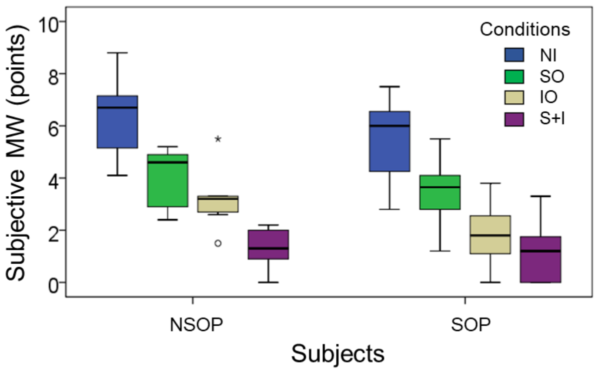

Figure-2 Subjective MW as a function of skill level and information

Table-1 shows the number of samples, mean value, median value, and standard deviation of operators' subjective MW by skill level and existence and type of information. Moreover, Figure-2 shows the results of subjective MW of the NSOP and SOP by skill level and existence and type of information with the box-and-whisker plots.
The average subjective MW with NI was 6.3 points for the NSOP and 5.5 points for the SOP, which were the highest scores for both the NOSP and SOP. In particular, the subjective MW of NOSP was the highest among the skill levels and existence and type of information. Moreover, as for the SO, average subjective MWs were 4.0 points for NSOP and 3.5 points for SOP, which means that the subjective MW of both NSOP and SOP is reduced by providing the information. Furthermore, the average subjective MW of the NSOP of the IO was 3.2 points, and that of SOP was 1.9 points, which suggested that the subjective MW in the IO case was further decreased from that of the SO case. Finally, the average subjective MW in the S+I case for the NSOP was 1.3 points, and that for the SOP was 1.2 points. The subjective MWs of both NSOP and SOP in this S+I case were the lowest among those cases of the existence and type of information. In particular, the drop of subjective MW from the case of NI of NSOP was 5.0 points, which was larger than that of 4.3 points of the SOP. Therefore, although there are some differences according to skill level, the mitigating effect of information on the subjective MW is extreme for both NSOP and SOP. The mitigating effect of S+I on the subjective MW was the largest.

3.1.2 Operators' behaviour

This testing measured the recognition distance, spreading starting and finishing distance, eye fixation point, and other behaviours of the operators during the spreading activities. Some of the results obtained by the testing are shown below.
Table-2 shows the number of samples, mean value, median value, and standard deviation of operators' recognition distance by skill level and existence and type of information. Moreover, Figure-3 shows the operators' recognition distance by skill level and existence and type of information with

Table-2 Operators' recognition distance as a function of skill level and information

Subjects	Conditions	Recognition distance (m)			
		Samples	Average	Median	SD
NSOP (7)	NI	7	-30	-32	9
	SO	7	-91	-82	46
	IO	7	-91	-90	49
	S+I	7	-140	-171	70
SOP (12)	NI	12	-44	-43	31
	SO	12	-91	-86	53
	IO	11	-87	-75	54
	S+I	12	-121	-137	60

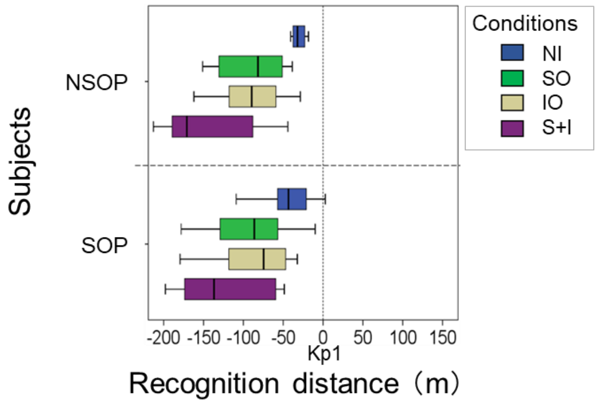

Figure-3 Operators' recognition distance as a function of skill level and information

Table-3 Eye-fixation in recognition sections as a function of skill level and information

Subjects	Conditions	Eye-fixation at recognition sections (%)					
		RB		SCD		IT	
		Average	SD	Average	SD	Average	SD
NSOP (5)	NI	89.5	2.6	7.3	2.1	3.2	1.1
	SO	76.6	22.7	16.9	17.2	6.5	6.1
	IO	59.0	24.0	12.2	7.5	28.9	18.3
	S+I	58.0	28.6	24.3	17.9	17.7	12.5
SOP (7)	NI	81.7	23.4	17.8	23.0	0.5	0.6
	SO	71.4	11.3	22.0	13.4	6.6	5.6
	IO	49.7	24.7	24.3	19.6	26.0	9.6
	S+I	52.4	24.2	31.5	23.2	16.0	2.2

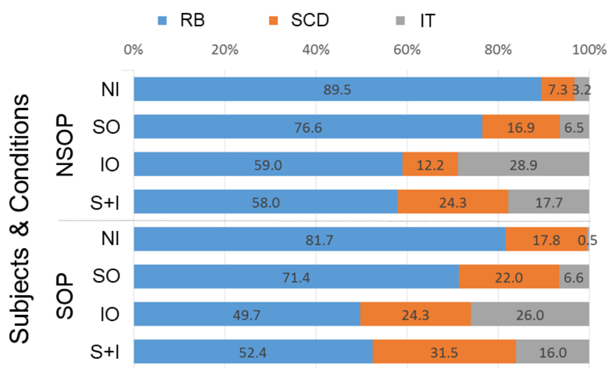

Figure-4 Eye-fixation in recognition sections as a function of skill level and information

box-and-whisker plots. For this report, the recognition distance was defined as the distance from the starting point (Kp1) of wet and/or icy road surface sections to where the test operator pushed the spreaders' power button.

The average recognition distance for in case of NI was -30 m for NSOP and -44 m for SOP. Although the average recognition distance of SOP varies a good deal, it was longer than that of NSOP. Moreover, the average recognition distance in the SO case was -91 m for NSOP and -91 m for SOP. The average recognition distance in the SO case was longer than that in the case of NI for both NSOP and SOP. Furthermore, the average recognition distance in the IO case was -91 m for NSOP and -87 m for SOP, which was almost similar to those in the SO case. Finally, the average recognition distance in the S+I case was -140 m for NSOP and -121 m for SOP. The average recognition distance in this case was the longest compared with those in other information provision cases.

The above results indicated that the information could support operators in recognizing the section that requires salt spreading earlier. The time margin to judge the spreading and take action increased. This increase was valid for both NSOP and SOP. Moreover, the method to provide the information with the sound and image was most useful for early recognition of the road surface condition, which improved the timing of starting the spreading and other actions.

Table-3 and Figure-4 show the operators' eye-fixation rates in recognition sections by skill level and existence and type of information. The recognition section means the section from the 200 m before the starting-point of wet or icy road surface section to the point at which the operator pushed the spreaders' main power button for this report.

For this testing, the areas that the operators looked at from the assistant driver's seat were divided into three eye-fixation areas; "road and background [hereinafter RB]," "spreading control device [hereinafter SCD]," and "information terminal [hereinafter IT]" areas and the rate of eye-fixation on each area was calculated. The eye-fixation-point data were obtained from a total of 12 of the 19 test operators (five NSOP and twelve SOP) who participated in this testing with naked eyes or contact lenses.

In the recognition section, the rate of eye-fixation on the RB area in the no information case was the highest for both NSOP and SOP, that is, 89.5% and 81.7% for NSOP and SOP, respectively. On the other hand, the rate of eye-fixation on the SCD was 7.3% for NSOP and 17.8% for the SOP, and that of the IT was 3.2% for the NSOP and

0.5% for SOP.
In the SO case too, the rate of eye-fixation on the RB area was the highest rate for both NSOP and SOP, that is, 76.6% and 71.4% for NSOP and SOP, respectively. The results of the SO case were similar to those of the NI case, but the rate in the SO case was less than that in the NO case. On the other hand, the rate of eye-fixation on the SCD and IT in the SO case was higher than that in the NI case for both NSOP and SOP.
That is, the rate of eye-fixation on the SCD in the SO case was 16.9% for NSOP and 22.0% for SOP, and that of the IT was 6.5% for the NSOP and 6.6% for SOP.
The results for the IO case showed a higher rate of eye-fixation on the RB area than those of other areas for both NSOP, 59.0%, and SOP, 49.7%, which were even less than those of the SO case. On the other hand, the rate of eye-fixation on the SCD was 12.2% for NSOP and 24.3% for SOP. The rate of eye-fixation on the IT was 28.9% for NSOP and 26.0% for SOP, which indicates an increase in the rate of eye-fixation on the IT for both NSOP and SOP.
The results of the S+I case showed a higher rate of eye-fixation on the RB area than those of other areas for both NSOP of 58.0% and SOP of 52.4%, which were similar eye-fixation rates to those of the SO case. On the other hand, the rate of eye-fixation on the SCD was 24.3% for NSOP and 31.5% for SOP, which were higher than those in the IO case. Moreover, the rate of eye-fixation on the IT was 17.7% for NSOP and 16.0% for SOP.
The above results show that the rate of eye-fixation on the RB area was the highest among the three areas regardless of the skill level and the existence and type of information for this section. However, the information increased the rate of eye-fixation on the SCD and IT of both NSOP and SOP. In particular, the method to provide the information with images remarkably decreased the rate of eye-fixation on the RB and significantly increased that on the IT for both NSOP and SOP. This result is considered to be caused by the increase in the frequency of eye-fixation point moving from and staying on the images that needed to be looked at. On the other hand, the information with SO increased the rate of eye-fixation on the SCD and IT of NSOP and SOP more than the NI case, but it was less than the IO case. This is because the sound information, which does not require eye fixation, suppressed the increase in the rate of eye-fixation on the SCD and the IT. Therefore, although the information, especially that including images, contributed to an earlier recognition of the road surface condition and reduction of the subjective MW, the rate of time to confirm the road surface and circumference to recognize the spreading section was less than that in the NI case, which is an issue to be consider from the perspective of safety.

3.2 MW as a Function of the Existence and Type of Spreading Support

In 2018, four testing conditions were defined for the existence and type of spreading support; (1) no support [hereinafter NS], (2) information only [hereinafter INF], (3) information plus voice control function [hereinafter INF+VC], and (4) information plus voice control plus automatic spreading function [hereinafter INF+VC+AS]. The effect of these four test conditions on the MW of operators who drive and spread the salt was investigated. The participants were eight male construction workers of 40 to 60 years old (53.0 years old on average) holding licenses for ordinary motor vehicles or larger vehicles. These test operators drove on the test track.
The voice console (VC) is a voice recognition and control apparatus that enables hands-free control of the salt spreading on the required spreading section of the test track. The test operators managed the SCD by uttering simple voice orders, such as "power on," "30 grams", "start," and "finish," while driving the truck. The automatic spreading (AS) is a device providing an automatic spreading control program that performs power supply, setting of spreading amount, and on/off of spreading the agent automatically at the wet or icy road surface sections that require the spreading of the agent according to the test track layout without operation by the driving test operators. The test operators drove the test vehicle passing through the section necessary to spread the agent, and the automatic spreading device operated automatically.

3.2.1 Operators' subjective MW

Table-4 shows the number of samples, mean value, median value, and standard deviation of operators' subjective MWs by existence and type of spreading support. Figure-5 shows operators' subjective MWs by existence and type of spreading support with box-and-whisker plots.
The average of operators' subjective MW in the NS case was 5.2 points, which was the highest

Table-4 Subjective MW as a function of the existence and type of spreading support

Conditions	Subjective MW (points)			
	Samples	Average	Median	SD
NS	8	5.2	5.3	1.6
INF	8	3.5	3.4	0.9
INF+VC	8	2.2	2.3	0.9
INF+VC+AS	8	1.2	1.0	0.8

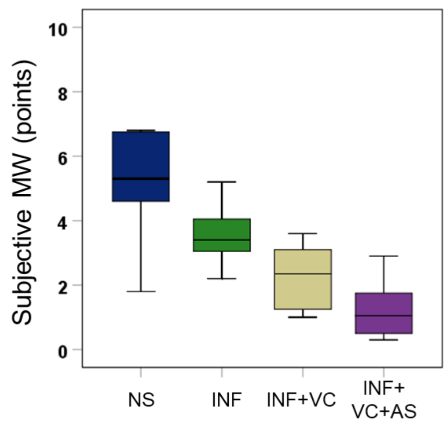

Figure-5 Subjective MW as a function of the existence and type of spreading support

Table-5 Operators' recognition distance as a function of the existence and type of spreading support

Conditions	Recognition Distance (m)			
	Samples	Average	Median	SD
NS	32	-87	-79	51
INF	32	-123	-120	46
INF+VC	32	-110	-104	35
INF+VC+AS	32	0	0	0

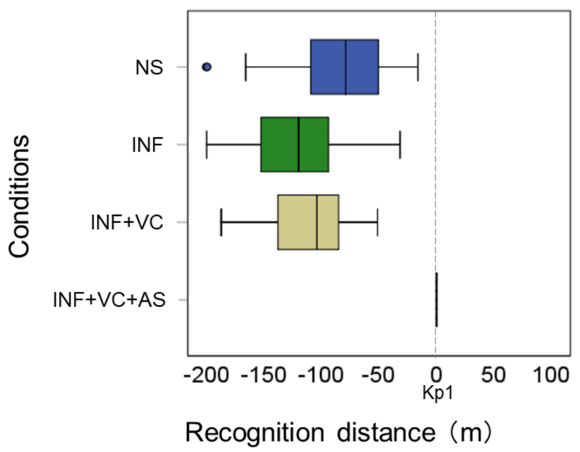

Figure-6 Operators' recognition distance as a function of the existence and type of spreading support

evaluation point among the four test conditions. Moreover, the average subjective MW in the INF case of the spreading work support was 3.5 points, which confirmed that the information reduced operators' subjective MWs, like the result of the previous year. Furthermore, when the spreading support was the INF+VC, the average operators' subjective MW was 2.2 points, which was less than the INF case. Finally, when the spreading support was INF+VC+AS, the operators' subjective MW was 1.2 points, which was the least among the cases of the existence and type of the spreading support. This is considered to be because the test operator needed to perform absolutely no spreading operation (recognition, judgment, and action) but needed to simply drive the test truck. The above results suggested that the operators' subjective MW decreases due to the spreading support, and it was found that the mitigating effect of INF+VC+AS on the subjective MW was the largest.

3.2.2 Operators' behaviour

Table-5 shows the number of samples, mean value, median value, and standard deviation of the operators' recognition distance by existence and type of spreading support. Figure-6 shows the operators' recognition distance by existence and type of spreading support with box-and-whisker plots.
The recognition distance was defined as the distance from the starting point (Kp1) of wet or icy road surface sections to the place where the spreading control device was powered on for this report.
The average operators' recognition distance in the NS case was -87 m. On the other hand, the average operators' recognition distance in the INF case was -123 m, which was longer than that of the NS case. Moreover, the average recognition distance in the INF+VC case of spreading support was -110 m. In addition, in the case of INF+VC+AS, the average recognition distance was zero because the power supply, agent amount setting and the spreading on actuated automatically and simultaneously at the Kp1 point.
From the above results, in the INF and INF+VC cases of the spreading support, operators were able to recognize sections that should be spread with the agent further from such sections compared with the case of NS. It was considered that the time margin for spreading judgment and taking action was provided like that shown by the results from the previous year.
On the other hand, when the spreading support

Table-6 Hitting ratio of judgment as a function of existence and type of spreading support

Conditions	Road Surface Judgment			
	Samples	Hit	Miss	Hitting ratio
NS	32	13	19	41%
INF	32	28	4	88%
INF+VC	32	31	1	97%
INF+VC+AS	32	32	0	100%

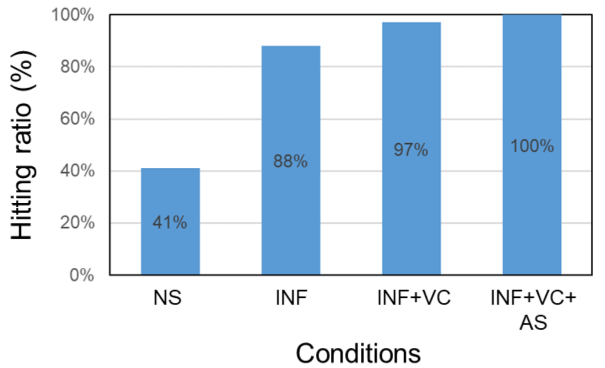

Figure-7 Hitting ratio of judgment as a function of existence and type of spreading support

Table-7 Eye-fixation in recognition sections as a function of the existence and type of spreading support

Conditions	Eye-fixation at recognition sections (%)									
	RB		SCD		IT		VI		SM	
	Average	SD	Average	SD	Average	SD	Average	SD	Average	SD
NS	83.5	5.4	7.0	3.2	0.0	0.0	0.9	1.8	8.6	3.6
INF	77.9	8.4	9.0	5.4	3.6	2.9	1.0	1.2	8.5	4.4
INF+VC	82.3	9.2	4.3	4.8	4.1	2.4	0.9	1.6	8.4	6.7
INF+VC+AS	84.9	6.2	3.1	4.6	2.8	2.7	0.8	2.2	8.3	4.1

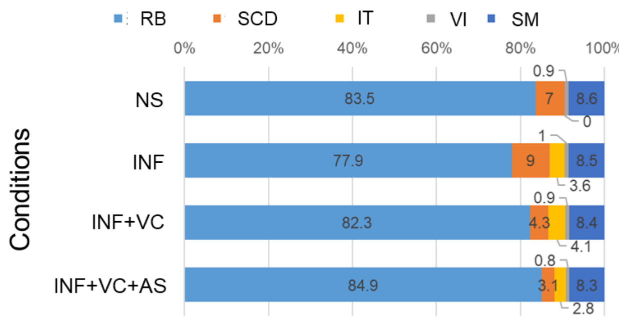

Figure-8 Eye-fixation in recognition sections as a function of the existence and type of spreading support

was INF+VC+AS, operators had not to perform the spreading, while driving the truck. In this case, the operator was able to concentrate on driving the vehicle only because it was not necessary to recognize the section, which is effective from the perspective of safety.
Table-6 and Figure-7 show the hitting ratio of judgment of the road surface condition (setting of the agent spreading amount) during the spreading. The hitting ratio of NS case was 41%, the lowest. Moreover, the hitting ratio in the INF case was 88%. Furthermore, the hitting ratio of the INF+VC was 97%. In addition, the hitting ratio of INF+VC+AS was 100%, although the operator's judgment was not performed.
The above results confirmed that the spreading support (INF and INF+VC) contributed to an improvement in the hitting ratios of the operators' judgment of the road surface condition. The spreading support of INF+VC+AS led to reliable spreading judgment. Moreover, the INF+VC+AS case enabled operators to concentrate only on driving the vehicle because operators did not need to judge the road surface condition (setting of spreading agent amount), which is effective from the perspective of safety.
Table-7 and Figure-8 show the eight operators' eye-fixation rates in the recognition section by existence and type of spreading support.
For this report, the recognition section was defined as the section from 200 m before the starting-point of the wet or icy road surface section to the point at which the operator pushed the main power button of the SCD.
For this testing, the areas that the operator looked at from the driver's seat of the test vehicle were divided into five eye-fixation areas; RB, SCD, IT, "vehicle interior [hereinafter VI]", and "speed meter [hereinafter SM]" areas, and the rate of eye-fixation on each area was calculated by existence and type of spreading support.
The rate of eye-fixation on the RB in the NS case was 83.5%, which was the highest among the five areas. On the other hand, the rates of eye-fixation on the SCD and IT in the NS case were 7.0% and 0.0%, respectively. In addition, the rates of eye-fixation on the VI and SM in the NS case were 0.9% and 8.6%, respectively, which did not differ greatly from other condition cases.
The highest eye-fixation rate among the five areas in the INF case was the same as that in the NS case, that is, the rate of eye-fixation on the RB was 77.9%, but it was less than that in the NS case and decreased most among the four conditions. On the other hand, the rates of eye-fixation on the SCD and IT were 9.0% and 3.6%, respectively, the sum of which increased from that in the no information case.

In the INF+VC case, the rate of eye-fixation on the RB was 82.3%, which was the highest among the five areas and increased from that in the INF case, approaching that of the NS case. On the other hand, the eye-fixation rates of the SCD and IT were 4.3% and 4.1%, respectively, which decreased from those in the INF case.
In the INF+VC+AS case, the rate of eye-fixation on the RB was 84.9%, which was the highest among the five areas, as with the other conditions. On the other hand, the eye-fixation rates of the SCD and IT were 3.1% and 2.8%, respectively, the sum of which was the least among the four conditions.
The above results show that the rate of eye-fixation on the RB area was the highest among the five areas, regardless of the existence and type of spreading support in the recognition sections. However, the INF increased the rate of eye-fixation on the SCD and IT from the NS case. This result is considered to be due to the fact that the information and other indications that require eye fixation increased the frequency of operators' eye-fixation point moving from the RB and staying on the IT and other areas. On the other hand, spreading support in the form of INF+VC increased the rate of eye-fixation on the SCD and IT from that in the NS case, but it was not much greater than that in the INF case. This was considered to be because the operator spread the agent without operating the spreading control device by hand, which contributed to suppress the increase of the rate of eye-fixation on the IT or SCD. Moreover, spreading support in the form of INF+VC+AS decreased the rate of eye-fixation on the SCD and IT from the INF+VC case further, and the rate of eye-fixation on the RB became the highest among the four conditions. This was considered to be because the AS function enabled the operators to concentrate on driving the spreading vehicle because the power supply on, setting of spreading agent amount, and spreading on and off functioned automatically without the operator driving the car needing to confirm the information or operate the SCD on wet and icy sections that required the spreading of the agent.

4. Conclusions and Future Issues

This study has been performed to develop technologies for salt spreading support to realize safe-and-secure agent-spreading work not influenced by the skill level of operators, even when a single operator both drives the vehicle and spreads the agent. The previous main study results and future schedule are described as follows.
In 2017, the operators' recognition and judgment of the road surface condition and the salt spreading according to the operators' skill level and the existence and type of information were analysed using the data of the testing performed by test operators on the Tomakomai Cold Region Test Track to evaluate the effect of and issues involved in the information provision method. As the results, it was confirmed that the information provision decreases the subjective MW, irrespective of the operator's skill level, to improve the capability of recognition, judgment, and other decisions regarding road surface conditions. However, it was also confirmed that the rate of eye-fixation on the road in front of the vehicle decreases remarkably depending on the information-provision method, which is an issue from the prospective of ensuring safety during the agent spreading work.
In 2018, in addition to providing the information a voice control function and automatic spreading function were designed and built. In the same manner as that of the previous year, test operators performed testing at the Tomakomai Cold Region Test Track to investigate the effect of the existence and type of spreading support methods on the operators' recognition and judgment of the road surface condition and agent spreading operation. Based on the results, it was confirmed that the spreading support technologies decreased the operators' subjective MW remarkably, that the recognition, judgment, and other decisions regarding the road surface condition became quick and exact, and the safety of spreading work improved.
Based on the results obtained so far, the following studies and works will be performed from now on: (1) design and building of a control mechanism to mount the spreading support technology to actual salt spreading apparatus, (2) testing by test operators using the above technologies on the test track and actual roads as more practical verification testing, and (3) establishment of spreading support technologies for safe-and-secure salt spreading work with due consideration of the operators' psychological condition and behaviour.

References

[1] HOKKAIDO REGIONAL DEVELOPMENT BUREAU, MLIT: “Snow-Removal Activities in FY 2016”, http://www.hkd.mlit.go.jp/zigyoka/z_doro/jyosetsu/pdf/jyosetsutaisei.pdf, November 2016

[2] MLIT: “Study Task Force Recommendation on the Way of Ensuring Road Transportation in Winter, Aiming at Ensuring Sustainable Winter Road Transportation - Cooperation and Collaboration”, http://www.mlit.go.jp/common/000997537.pdf, pp. 25-26 May 2015

[3] SALT INSTITUTE: “The Snowfighter’s Handbook - A Practical Guide for Snow and Ice Control”, http://www.saltinstitute.org/wp-content/uploads/2013/07/Snowfighters_HB_2012.pdf, 2013

[4] MINNESOTA LOCAL ROAD RESEARCH BOARD: “Minnesota Snow and Ice Control - Field Handbook for Snowplow Operators”, Second Edition, http://www.mnltap.umn.edu/publications/handbooks/documents/snowice.pdf, October 2012

[5] HOKKAIDO REGIONAL DEVELOPMENT BUREAU, MLIT: Manual of Winter Road-Surface Management (draft), September 1997

[6] THOMPSON G. et al.: “Clear Roads - Developing a Totally Automated Spreading System”, Final Report (http://clearroads.org/wp-content/uploads/dlm_uploads/11-03-Totally-automatedspreader_final_report.pdf), February 2014

[7] AOKI K. et al.: “ISO/TC159 - Concept and Definition of the Mental Workload, and Design Guideline”, Ergonomics, Vol. 29, No. 6 ('93), pp. 339-342, September 1993

[8] MIYAKE K: et al.: “Subjective Assessment of the Mental Workload”, Ergonomics, Vol. 29, No. 6, 1993

[9] DE WAARD D. et al.: “The Measurement of Driver's Mental Workload”, The Traffic Research Centre VSC, University of Groningen - The Netherlands, https://www.rug.nl/research/portal/files/13410300/09_thesis.pdf, June 1996

[10] TOKUNAGA R. et al.: “Effects of Conversation Through a Cellular Telephone while Driving on Driver’s Reaction Time and Subjective Mental Workload”; Transportation Research Record, No. 1724, Paper No. 00-1480, pp. 1-6, April 2000.

[11] HART S. et al.: “Development of NASA-TLX: Results and Theoretical Research”, Human Mental Workload, Pp. 139-183, North-Holland, 1988.

[12] HAGA S. et al.: “NASA Task Load Index - Development and Trial of Japanese Version”, Railway Technical Research Institute Report, Special Edition: Human Science, Vol. 18, No. 1, pp. 15-20, 1994

Basic Experiment Related to Technology to Detect Surroundings of a SnowPlow Using a Milliwave Radar Device under Visibility Hindrance

Takahiro Shimbo
Researcher
Civil Engineering Research Institute for Cold Region, PWRI
Japan
Shimbo-t22aa@ceri.go.jp

Summary
In order to safely perform snow removal work even in the event of visibility hindrance due to snowstorm, it is necessary to detect obstacles around the snowplow and prevent the collision accidents.
Therefore, the radar was detected during actual snowstorm by using a milliwave radar which was less affected by the weather.
As a result, it was confirmed that the detection of the vehicle 70 m ahead from the radar was possible even in the snowstorm with the visibility distance of about 50 m.

Keywords: Snow removal, Snowplow, Milliwave Radar, Visibility Hindrance, Surrounding Detection

1. Introduction

In recent years, such incidents as stuck vehicles and long-duration traffic stops are increasing due to unusual blizzards caused by climate change in the cold and snowy areas in Japan. To suppress the effect of snow and ice incidents on the socioeconomic activities of local residents, support for snowplows in performing safe snow-removal works under circumstances of visibility hindrance is greatly needed in order to facilitate road traffic. To support snowplow operation, technology to detect the surroundings, including the person, vehicle, road structure, and other physical substances around the snowplow, to prevent a collision is necessary. This paper describes the results of experiments to detect vehicles and persons under fine weather and under snowfall using milliwave radar currently used for the surroundings detection of advanced car operation support systems.

2. Surroundings Detection Experiment Using Milliwave Radar

Table 1 Specifications of the milliwave radar

Item	Performance
Minimum detection distance	< 1 m
Maximum detection distance	> 175 m (> 10 dB target) > 100 m (> 0dB target)
Direction detection distance precision	< +/- 0.5m
Distance direction separation performance in case of two targets lying at identical angles running at the same velocities	< 2.5 m
Horizontal viewing angle	> 20 deg
Horizontal angle separation performance in case of two targets lying at identical angles running at the same velocities	< 3.5 deg
Vertical viewing angle	4.2 to 4.75 deg

Because milliwave radar uses a radio wave, weather affects milliwave radar less than it affects cameras and laser not been clarified.
Therefore, an experiment was performed to verify the applicability of milliwave radar as detection technology under visibility hindrance due to a blizzard.
Available frequency bands for milli-wave radar are 24 GHz and 76 GHz at present, The 24 GHz band is often used for near and medium distances, and the 76 GHz band is often used for long distances.

For this experiment,76GHz milliwave radar, usually used for long distance,was used, assuming the distance of 70 m or more to detect obstructions in front of the snowplow.
Table 1 shows the specifications of the milliwave radar used for the experiment.

2.1 Experiment to Detect Vehicles and Persons (Fine Weather)

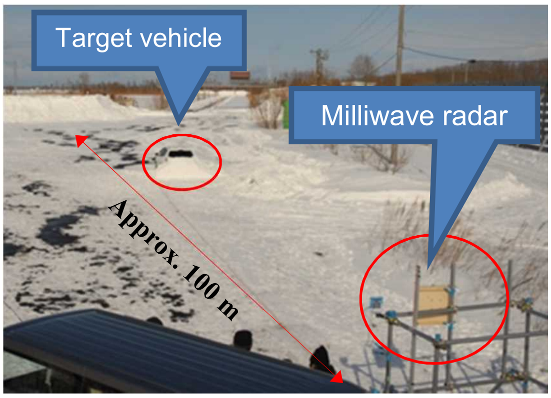

Fig. 1 Test site (Experiment (1) and (2))

The experiment was performed at the Ishikari Blowing Snow Test Field, Cold Region Public Work Research Institute.
The milliwave radar was installed in a way enabling adjustment of the height and angle. Moreover, the measuring range was set to ensure 100 m ahead of the milliwave radar (Fig 1).
The following tests were performed with basic parameters of radar installation height and angle as well as the distance to the object.

Test (1): Vehicle detectability test
Test (2): Person detectability test

2.1.1 Test (1): Vehicle detectability test

The outline of Test (1) is shown in Figure 2.

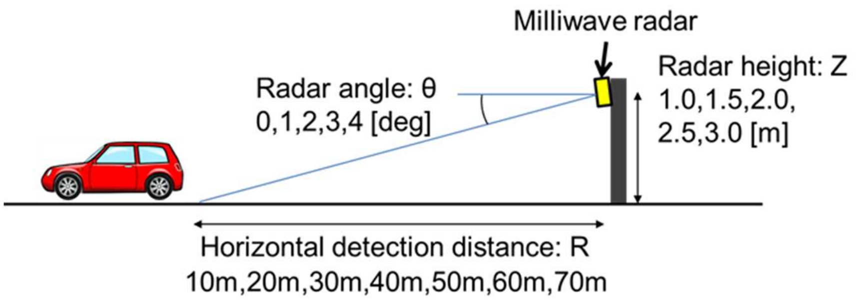

Fig. 2 Test (1) schematic view

Test (1) was performed to confirm the horizontal distance which can detect vehicles, changing the combination of installation height and angle of the radar. Based on the preliminary test results, the baseline of radar installation height and angle were decided for the following tests.
Typical examples of the vehicle detecting situation and detected results are shown in Figure 3 and Figure 4, respectively.
The test results are shown in Table 2.

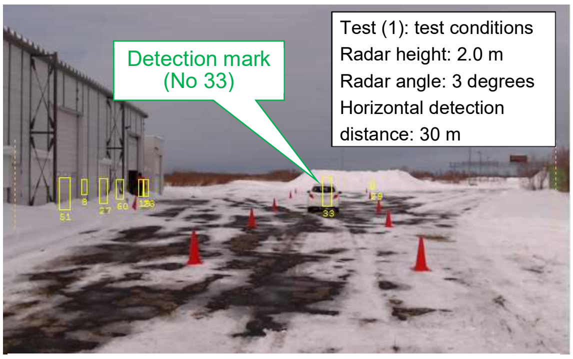

Fig.3 Test (1) Vehicle detection situation (typical)

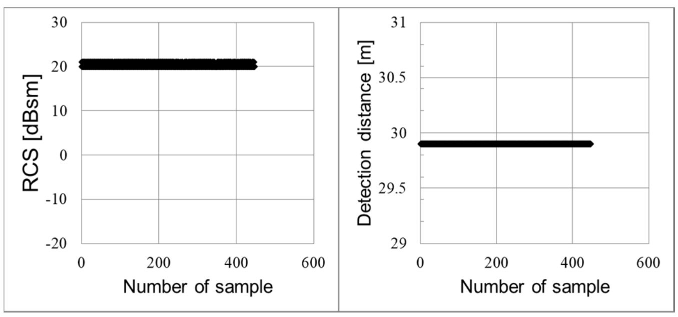

Fig.4 Test (1) Detection results (Typical)

Table 2 Test (1) Detection results

Heitht Z [m]	Angle θ [deg]	Horizontal detection distance R [m]						
		10	20	30	40	50	60	70
1.0	0	○	○	○	○	○	○	○
1.0	1	○	○	○	○	○	○	○
1.5	2	○	○	○	○	○	○	○
1.5	3	○	○	○	○	○	○	○
2.0	2	△	○	○	○	○	○	○
2.0	3	○	○	○	○	○	○	○
2.5	3	□	○	○	○	○	○	○
2.5	4	○	○	○	○	○	○	□
3.0	4	×	○	○	○	○	○	○

○: Detected
△: Partially not detected (Some data are missed)
×: Not detected
□: Detected for run 1, but not detected for run 2

Figure 4 shows the radar cross-section (RCS) and detection distance measured for 20 seconds under the conditions of 2 m radar height, 3 degree angle, and 30 m horizontal detection distance.
The RCS is the factor of the radio-wave reflectivity of the object that received the electric wave from the radar. The detectable RCS is more than approximately -10 dBsm. The average RCS was 20.4 dBsm and the variation was -0.4 to 0.6 dBsm.
Moreover, the detection distance, which is the distance from the radar to the object, measured in the test was 29.9 m on average and the variation was +/- 0 m.
As results, the vehicle was detected under all the conditions of the height, angle, and horizontal distance, except one case that was measured under the conditions of 3 m height, 4 degrees angle, and 10 m horizontal distance.
Referring to the test results, the reference test conditions were decided to be 2 m height and 3 degree angle.

2.1.2 Test (2): Person detectability test

An outline of Test (2) is shown in Figure 5.
The person detectability tests were performed to verify the detectability of persons standing, squatting down, and lying down.
Typical examples of the detection situation and results are shown in Figure 6 and Figure 7, respectively. The test results are shown in Table 3.

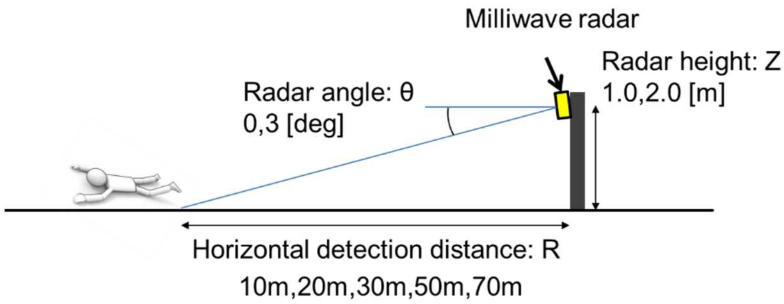

Fig. 5 Test (2) schematic view

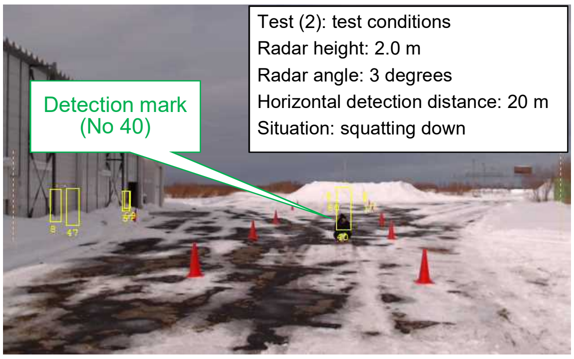

Fig. 6 Test (2) Person detection situation (Typical)

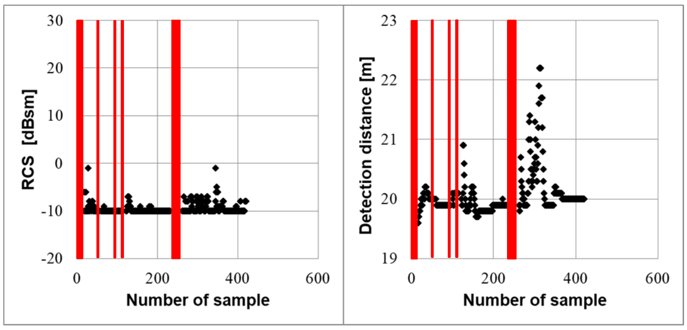

Fig. 7 Test (2) Detection results (Typical)

Table 3 Test (2) Detection results

Height Z [m]	Angle θ [deg]	Horizontal detection distance R [m]										
		10			20			30			50	70
		Standing	Squatting down	Lying	Standing	Squatting down	Lying	Standing	Squatting down	Lying	Standing	Standing
1.0	0	○	△	×	△	△	×	△	△	×	△	○
2.0	3	○	×	×	△	△	-	△	△	-	△	△

○ : Detected
△: Partially not detected (Some data are missed)
× : Not detected
- : Not tested

Figure 7 shows the RCS and detection distance measured for 20 seconds under the conditions of 2 m radar height, 3 degree angle, and 20 m horizontal detection distance for squatting persons.
The average RCS was -9.5 dBsm and the variation was -0.5 to 8.5 dBsm.
Moreover, the average of the detection distance was 20.1 m, and the variation was -0.5 to 2.1m.
As results, although the persons standing 10 m to 70 m away from the radar were detected, some standing persons engaging in slight upper body movement were undetected because of missing data.
Moreover, because the RCS of squatting persons is smaller than that of standing persons, there were many undetectable cases of the squatting persons.
The lying persons were not detected under any conditions.

2.2 Vehicle Detection Test under Conditions of Snowfall and Accumulated Snow

The following tests were performed to verify the effect of the snowfall and accumulated snow on the target vehicle on the detectability of the milliwave radar.

Test (3): Vehicle detectability test under fine weather
Test (4): Vehicle detectability test under snowfall
Test (5): Detectability test of vehicles covered with accumulated snow

The landscape of the measurement area is shown in Figure 8

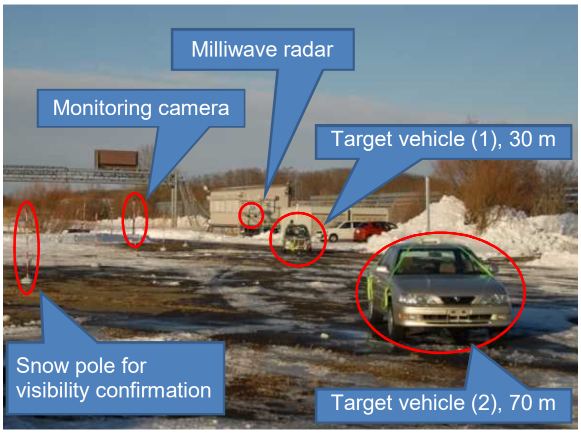

Fig. 8 Landscape of the test site (Tests (3) to (5))

To ensure an effective test under a snowstorm situation, the milliwave radar and the target vehicle were placed on the test site for 45 days, and the measurement was remotely controlled confirming the snow storm situation with the monitoring camera.
The target vehicles (1) and (2) were placed at distances of 30 m and 70 m away from the radar, respectively.
The visibility distance was measured by visual observation of the distance between the measurements of the backscattered type visibility meter placed approximately 50 m away from the milliwave radar and snow poles placed along the side of the target vehicle at intervals of 10 m.

2.2.1 Test (3): Vehicle detectability test under fine weather

Figure 9 shows the schematic view of Test (3).
The test conditions were 2 m radar height and 3 degree angle.

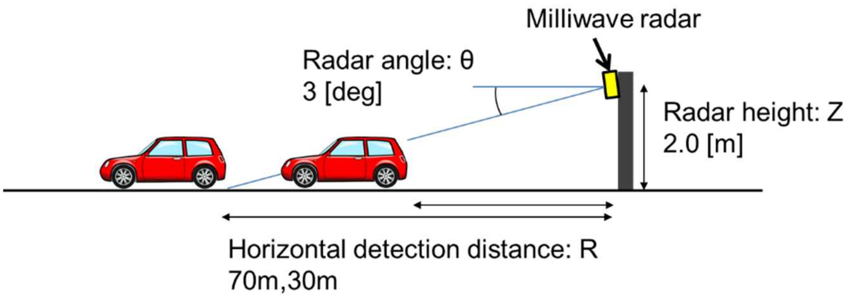

Fig. 9 Test (3) schematic view

Test (3) was performed for a 1 minute at each time of 9:30, 11:00, 13:30, 14:30, 15:30, and 16:30 on the measurement day.
Typical examples of the detection situation and results are shown in Figure 10 and Figures 11 and 12, respectively.

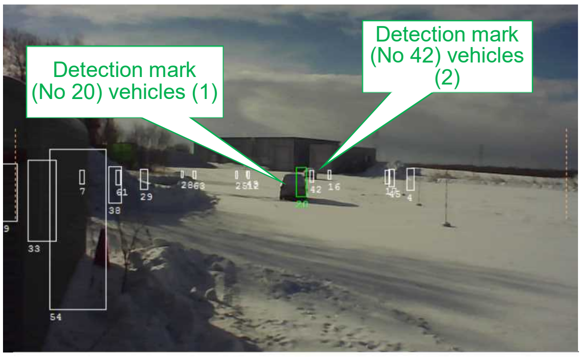

Fig. 10 Test (3) Vehicle detecting situation (Typical)

Figure 11 and 12 show the average of RCS, detection distance, detection angle, and detection rate at each measurement.
The average RCS (and the variation) of target vehicles (1) and (2) were 6.1 dBsm (-2.6 to +2.9 dBsm) and 16.3 dBsm (-0.3 to +1.7 dBsm), respectively.
The average detection distance (and the variation) of target vehicles (1) and (2) were 29.5 m (+/- 0.1 m), and 69.5 m (and +/- 0.4 m), respectively.
The detection angle of zero means a situation in which the target and the radar come face to face, the plus symbol means the target is detected on the right side, and the minus symbol means the target is detected on the left side.
The average detection angle (and the variation) of target vehicles (1) and (2) were 0.3 degrees (and -0.9 to +1.4 degrees) and 1.7 degrees (and -0.4 to +0.8 degrees), respectively.
The detection rate was 100% for both target vehicles (1) and (2) at all measurements.
The measured data under the condition of snowfall and accumulated snow on the target vehicle were compared with the reference measured under fine weather.

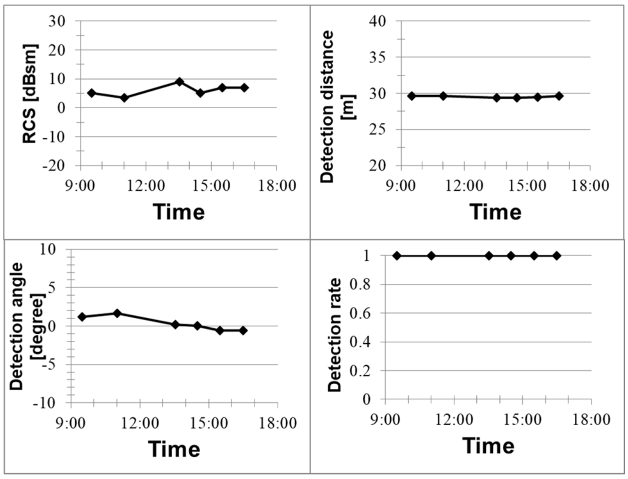

Fig. 11 Test (3) detection results (Typical) [30 m, target vehicle (1)]

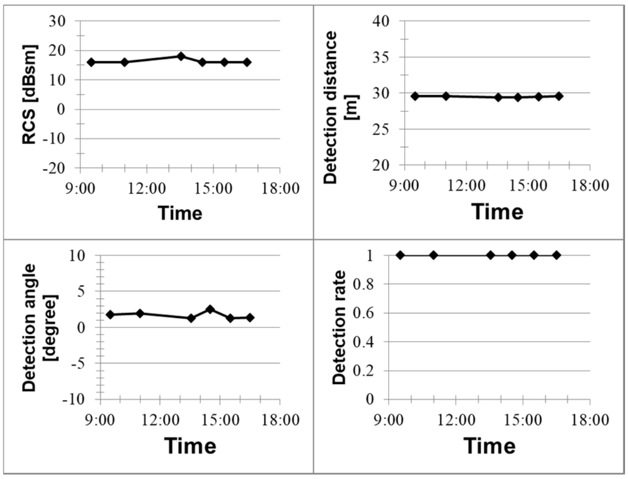

Fig. 12 Test (3) detection results (Typical) [70 m, target vehicle (2)]

2.2.2 Test (4): Vehicle detectability test under fine weather

Figure 13 shows a schematic view of Test (4).

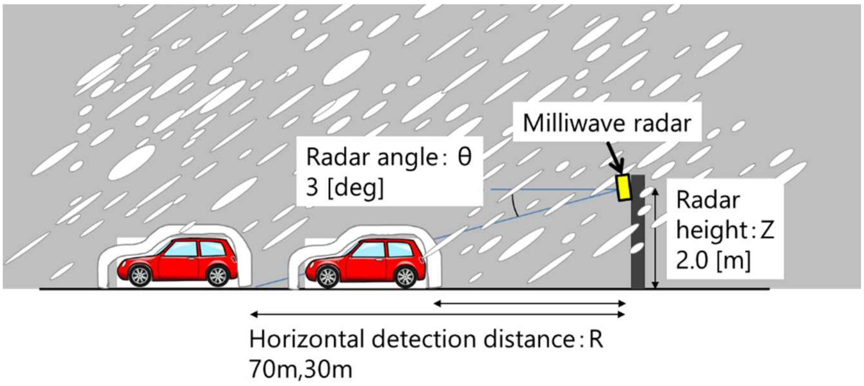

Fig. 13 Test (4) schematic view

The measurement of Test (4) was continuously performed during the snowfall to compare the variation of detectability of the difference in the visibility distance by the snowfall.
The detection situation (typical), detection result (typical), and the test results on the measurement day when the visibility distance was the worst are shown in Figures14, Figures 15 and 16, and Table 4, respectively.

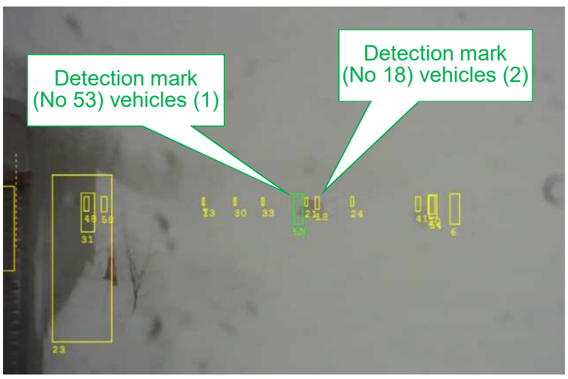

Fig. 14 Test (4) Vehicle detecting situation (Typical)

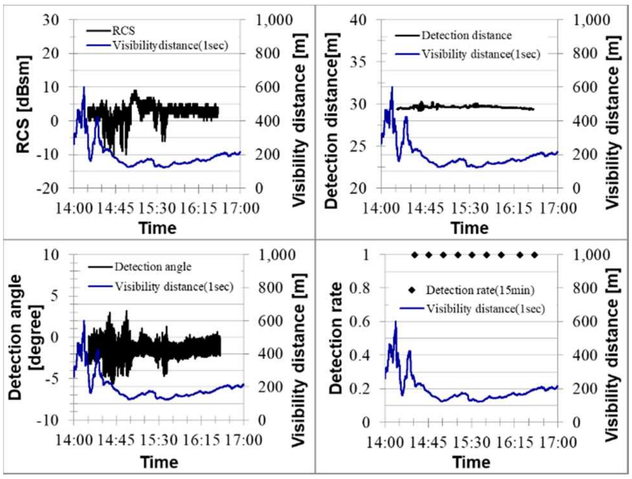

Fig. 15 Test (4) detection results (Typical) [30 m, target vehicle (1)]

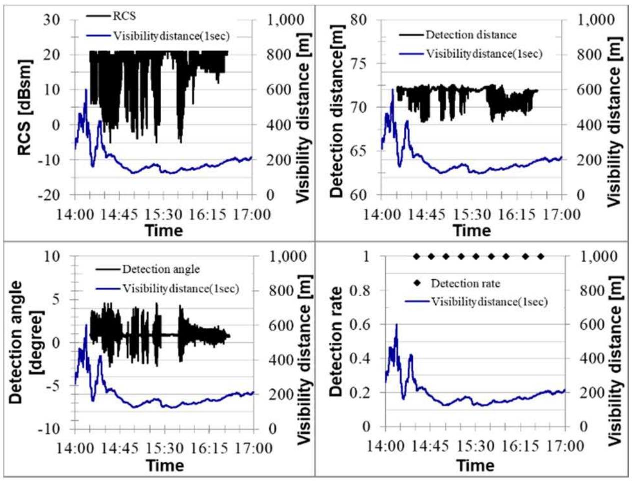

Fig. 16 Test (4) detection results (Typical) [70 m, target vehicle (2)]

The minimum visible distance of the visibility meter was 123 m at 15:36. Moreover, the visible distance of the snow pole to confirm the visibility at the same time by visual observation was approximately 50 m.

Table 4 Comparison of test results

Objects	Item	Unit	Test (3): Fine weather Average	Test (3) Min.	Test (3) Max.	Test (3) Variation	Test (4): Snow fall Average	Test (4) Min.	Test (4) Max.	Test (4) Variation
30m target vehicle (1)	RCS	dBsm	6.1	3.5	9	-2.6 to 2.9	2.7	-10	9	-12.7 to 6.3
	Detection distance	m	29.5	29.4	29.6	-0.1 to 0.1	29.6	29.2	30.3	-0.4 to 0.5
	Detection angle	Deg.	0.3	-0.6	1.7	-0.9 to 1.4	-1.5	-5.6	3.2	-4.1 to 4.7
	Detection rate	%	100	100	100	0	100	100	100	0
70m target vehicle (2)	RCS	dBsm	16.3	16	18	-0.3 to 1.7	18.1	-5	21	-23.1 to 2.9
	Detection distance	m	69.5	69.1	69.9	-0.4 to 0.4	71.6	68.3	72.6	-3.3 to 1
	Detection angle	Deg.	1.7	1.3	2.5	-0.4 to 0.8	0.9	-2.8	4.6	-3.7 to 3.7
	Detection rate	%	100	100	100	0	100	100	100	0

Comparison with the Test (3) results shows that the variation of each measurement item increases as the visible distance decreases, with the minus values especially tending to change largely. This tendency indicates that the decrease of the electric-wave reflectivity due to the snowfall causes the measurement error to increase.
However, the target detection rate exceeded -10 dBsm of the detectable threshold of the RCS for both target vehicles (1) and (2), and the detection rate was 100% for all measurements.
As results, it was confirmed that the milliwave radar of the 76-GHz band can detect the target vehicle 70 m ahead of the radar even if the visible distance of visual observation is approximately 50 m under a snowstorm.

2.2.3 Test (5): Detectability test of vehicles covered with accumulated snow

Figure 17 shows the schematic view of Test (5).

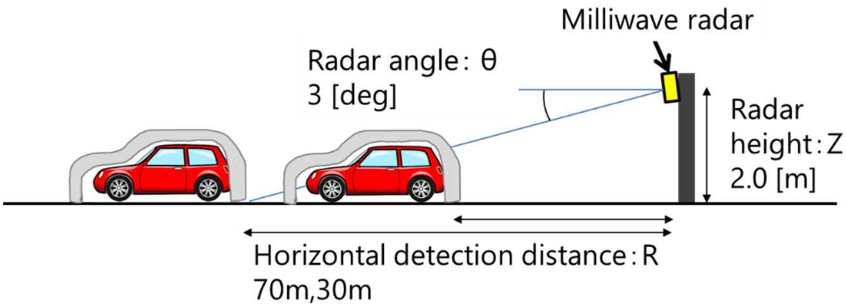

Fig. 17 Test (5) schematic view

Test (5) was performed under the conditions of the target vehicle covered with snow and fine weather six times a day (9:30, 11:00, 13:30, 14:30, 15:30, and 16:30). Measurements were taken for 1 minute in each test.
The snow accumulated on the vehicle was visually measured using the snow scale attached on the vehicle roof through the observation camera.
The detecting situation of the day when the accumulated snow on the target vehicle was the highest (typical), the situation of the snow-covered target vehicle, and test results are shown in Figure 18, Figure 19, and Table 5, respectively.
The snow coverage on the roof of target vehicles (1) and (2) was 15 cm and 20 cm, respectively, and the accumulated snow around the target vehicle was approximately 40 cm. The tail lamp on the back face of the target vehicle was uncovered.

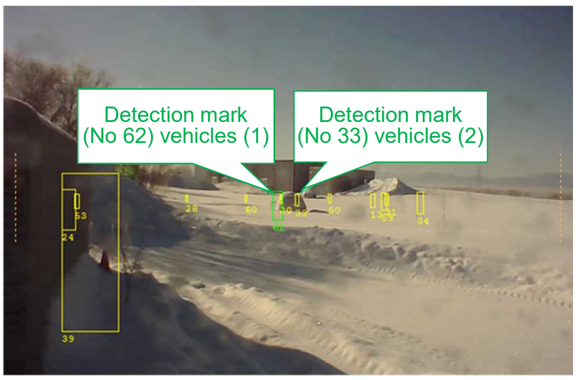

Fig. 18 Test (5) Vehicle detecting situation (Typical)

Fig. 19 Test (5) Target vehicle snow-coverage

Table 5 Comparison of test results

Object	Item	Unit	Test (3): Fine weather Average	Test (3): Fine weather Min.	Test (3): Fine weather Max.	Test (3): Fine weather Variation	Test (5): Snow coverage Average	Test (5): Snow coverage Min.	Test (5): Snow coverage Max.	Test (5): Snow coverage Variation
30m target vehicle (1)	RCS	dBsm	6.1	3.5	9	-2.6 to 2.9	2.2	-6	8.5	-8.2 to 6.4
	Detection distance	m	29.5	29.4	29.6	-0.1 to 0.1	29.7	29.3	30.1	-0.4 to 0.4
	Detection angle	Deg.	0.3	-0.6	1.7	-0.9 to 1.4	-0.5	-2.5	1.8	-2 to 2.3
	Detection rate	%	100	100	100	0	100	100	100	0
70m target vehicle (2)	RCS	dBsm	16.3	16	18	-0.3 to 1.7	15.9	8.5	21	-7.4 to 5.1
	Detection distance	m	69.5	69.1	69.9	-0.4 to 0.4	71.3	70	72.3	-1.3 to 1
	Detection angle	Deg.	1.7	1.3	2.5	-0.4 to 0.8	0.9	0.2	2	-0.7 to 1
	Detection rate	%	100	100	100	0	100	100	100	0

The RCS decreases due to the accumulated snow on the test vehicle, but exceeded 10 dBsm of the detectable threshold of the RCS, thus the detection rate was 100% for all measurements.

3. Conclusions

This paper introduces the detection test performed in cases of fine weather and snowfall utilizing 76 GHz milliwave radar, which is needed to remove the snow safely even under circumstances of visibility hindrance.
As results, it was found that some squatting down or lying persons could not be detected by the person detection experiment under fine weather.
On the other hand, it was confirmed that the detection of vehicles 70 m ahead of the radar is possible even under a snowstorm with visibility distance of approximately 50 m by visual observation.
From now on, the study of the milliwave radar loading method on a snowplow and the verification of the running detectability are planned to be implemented.

Proposal for Efficient Snow Removal System of Sapporo by Data Envelopment Analysis

Dr. Kunihiro Kishi
Associate Professor
Faculty of Engineering, Hokkaido University
Japan
kishi@eng.hokudai.ac.jp

Dr. Hiroshi Takada, Japan Urban Transportation Research Institute Co., Ltd., Japan
Dr. Yasushi Higashimoto, Nippon Data Service Co.,Ltd., Japan
Prof. Keiichi Sato, Hokkaido University, Japan

Summary

This study proposes efficient snow removal system of Sapporo. Data Envelopment Analysis (DEA) is applied for evaluation of efficiency for each district's snow removal system. This study applied DEA for Multi-zone snow removal system of Sapporo. DEA evaluates efficiency of 19 districts' snow removal system in two ways. One is that input is snow removal budget and output is numbers of operators and snow removal machines. The other is that input is numbers of operators and snow removal machines and output is road distance and total amount of snowfall. 19 districts are evaluated relatively. Carriageway snow removal, sidewalk snow removal, snow hauling and road surface leveling project are evaluated. As a result, this study clarified each district's snow removal system from the viewpoint of efficiency, that is efficient number of operators and machines, snow removal budget.

Keywords: snow removal, Data Envelopment Analysis, Sapporo

1. Introduction

It costs about 15 billion JPY (130 million USD) for snow and ice control measures in Sapporo, Japan every year. Especially it costs about 10 billion JPY for snow removal and hauling. Recently it is difficult for Sapporo to secure the budget for those projects because of decreasing of budget allocations for public works projects. Also dilapidated snow removal machines and aging of operators are serious problems.

Sapporo applies "Multi-zone snow removal system". The entire city of Sapporo is divided into districts by community associations. Several contractor groups conducting snow removal works within the cooperate with one another and combine their work, such as snow clearance from roadways and sidewalks, snow transport and other operations, into comprehensive snow removal works within the district. Numbers of snow removal machine and operators, road distances for snow removal, traffic volumes are vary among districts obviously. Snow removal machines, operators and budget should be reallocated efficiently to each district according to its situation.

The purpose of this study is to propose efficient snow removal system of Sapporo. Data Envelopment Analysis (DEA) is applied for evaluation of efficiency for each district's snow removal system. DEA analyzes efficiency from the relation between input and output, and evaluates "efficient" with small input and large output of its activity. DEA can also analyze how much should be improved for the objective that is evaluated as "inefficient".

2. Outline of snow removal of Sapporo

2.1 Summary of Sapporo

Sapporo is the northern-most city designated by government ordinance. Population is about 1.96 million, it is the 5th largest population in Japan. The first snowfall is in October and by December the city is covered in snow. There is much snowfall with the average annual snow accumulation at 600cm. However, with efficient measures for snow removal in place, there is minimum effect on daily life. It is rare by world standards that over 1.9 million people reside in an area prone to this much snowfall.

Fig.1 Location of Sapporo

2.2 Snow and ice control measures in Sapporo

In Sapporo, length of automobile expressway is 38km, that of national highway is about 152km, that of prefectural road is about 240km, and that of city road is about 5281km. Automobile expressway is managed by East Nippon Expressway Co., Ltd., national highway is managed by national government, Hokkaido Regional Development Bureau. Sapporo city manages both prefectural road and city road because City of Sapporo is designated by government ordinance.

As for snow and ice control measures in road maintenance, it costs about 20 billion JPY (179 million USD) per year recently. Especially snow removal project is about 15 billion JPY (134 million USD) per year for prefectural and city road.

Recently it is difficult for Sapporo to secure the budget for those projects because of decreasing of budget allocations for public works projects. Also dilapidated snow removal machines and aging of operators are serious problems.

Sapporo applies “Multi-zone snow removal system”. The entire city of Sapporo is divided into districts by community associations. Several contractor groups conducting snow removal works within the cooperate with one another and combine their work, such as snow clearance from roadways and sidewalks, snow transport and other operations, into comprehensive snow removal works within the district. Numbers of snow removal machine and operators, road distances for snow removal, traffic volumes are vary among districts obviously. Snow removal machines, operators and budget should be reallocated efficiently to each district according to its situation.

3. Evaluation of the efficiency of snow removal project by DEA

3.1 Application of Data Envelopment Analysis (DEA)

3.1.1 Outline of DEA

Generally, the activity of the enterprise can be regarded as the process of change that inputs resources and outputs benefits. The efficiency of the enterprise (Decision Making Unit; DMU in DEA) is compared relatively with the ratio of the output/ input. That is the basic way of thinking of DEA.

On DEA, the weight among the input or output units is allowed to be different from the weight of other DMU. The weight is determined to be convenient for DMU. Therefore, each DMU can put great weight to its good factor and put small weight to its weak factor. However, other DMU is evaluated on the same weight and the restriction is formulated, so its efficient value is not more than 1. In this way, we can say that DEA is the evaluation model that makes much of the individuality of DMU.

On the other hand, when one DMU is judged inefficiency, we can examine concretely by DEA how the DMU is inferior to other DMU and how to make DMU efficiency. DEA gives us various information in addition to Efficiency Value.

3.1.2 CCR model

The most basic model in DEA is the Charnes-Cooper-Rhodes (CCR) model (Charnes *et al.*, 1978). For DMU$_j$(j = 1,..., n), the input values are $x_{1j}, x_{2j}, \cdots, x_{mj}$ and the output values are $y_{1j}, y_{2j}, \cdots, y_{sj}$, and the efficiency of any assessment target DMU$_o$ is given by Eqs. (1) - (4).

Objective function:
$$\max\theta = \frac{u_1 y_{1o} + u_2 y_{2o} + \cdots + u_s y_{so}}{v_1 x_{1o} + v_2 x_{2o} + \cdots + v_m x_{mo}} \tag{1}$$

Constraints equation:
$$\frac{u_1 y_{1j} + \cdots + u_s y_{sj}}{v_1 x_{1j} + \cdots + v_m x_{mj}} \le 1 (j = 1, \cdots, n) \tag{2}$$

Input weight:
$$v_1, v_2, \cdots, v_m \ge 0 \tag{3}$$

Output weight:
$$u_1, u_2, \cdots, u_s \ge 0 \tag{4}$$

For the optimal solution $(\mathbf{v}^*, \mathbf{u}^*)$ and the objective value θ^* (D-efficient value), the following statements can be made.

i. If θ^* = 1, then DMU$_o$ is “Efficient”.
Ii . If θ^* < 1, then DMU$_o$ is “Inefficient”.

The value, which multiplies the optimum weight of each DMU by the data of DMU, is weighting the input and the output. We can judge by the value which factor of DMU is better or weaker.

3.2 Evaluation of the efficiency of snow removal project

3.2.1 Framework of DEA

This study analyses the efficiency of snow removal project in Sapporo. DMUs of this study are 19 groups of "Multi-zone snow removal system", City of Sapporo and 6 groups of national highway in Sapporo area of Hokkaido Regional Development Bureau, national government. That is, total is 25 groups. This study analyses not only prefectural and city road of Sapporo but also national highway at the same time, only trunk roads are focused.

Analysis objects of snow removal project are 1) snow removal of vehicle lanes and road surface levelling, 2) widening of road by snow removal, 3) snow hauling and 4) snow removal of sidewalk. And this study applied 2 types of DEA analysis as follows;

(1) Division of "system"; Input is budget, output is number of operators and snow removal machines.

(2) Division of "work"; Input is number of operators and snow removal machines, output is length of road and yearly amount of snowfall.

3.2.2 DEA analysis results

Table 1 shows data of snow removal of vehicle lanes and road surface levelling. In the same way, this study prepared data for other works, such as widening of road by snow removal, snow hauling and snow removal of sidewalk.

Table 1 Data of snow removal of vehicle lanes and road surface levelling

	DMU	Budget (million JPY)	Operator (persons)	Number of grader(vehicles)	Length of road(km)	Yearly amount of snowfall(cm)
National highway	R12, R275	41.8	28	7	21.2	615
	R36	36	36	7	19.8	615
	R230	68	18	3	44.4	770
	R5, R274	62.9	37	6	31.7	566
	R453	19	18	4	15.3	503
	R231	39.5	24	5	7	939
Multi-zone snow removal system	Chuo-1	36.2	46	18	88.3	627
	Chuo-2	26.8	32	10	62.3	627
	Chuo-3	16.3	33	10	48.9	627
	Kita-1	40	42	9	76.6	668
	Kita-2	24.5	36	11	65.4	668
	Kita-3	32.1	55	8	91.5	668
	Higashi-1	42	40	11	86.8	730
	Higashi-2	37.7	51	14	79.7	730
	Shiroishi-1	40.8	51	15	111.6	564
	Shiroishi-2	33.2	33	9	94.8	564
	Atsubetsu	21.8	51	10	73.7	700
	Toyohira	20.8	33	13	77	494
	Kiyota-1	11.5	45	10	55.1	605
	Kiyota-2	12.4	31	8	47.5	605
	Minami-1	54.6	49	11	213	626
	Minami-2	20.6	40	10	85.7	626
	Nishi-1	22	41	8	51.8	775
	Nishi-2	32.3	54	15	70.5	775
	Teine	32.1	54	7	74.5	729

These DMUs were applied for DEA analysis. However snow removal quality and service level are different between national highway and multi-zone snow removal system because national highway is more important traffic function than prefectural and city road. So national highway has disadvantage when national highway and multi-zone snow removal system were evaluated equally. This study applied CAT model in DEA, in order to consider the degree of importance for each road.

Table 2 and 3 are results of DEA analysis. Table 2 shows the analysis result of Division of "System",

Table 3 is Division of “Work”.

Table 2 DEA analysis result of Division of “System”

	DMU	Snow removal of vehicle lane, road surface levelling	Widening of road by snow removal	Snow hauling	Snow removal of sidewalk
		Score	Score	Score	Score
National highway	R12, R275	0.8616	0.3275	0.8930	0.8774
	R36	1.0000	0.6134	1.0000	1.0000
	R230	0.2647	0.3237	0.3455	0.3611
	R5, R274	0.5879	1.0000	0.8976	0.6879
	R453	0.2429		0.2368	0.4080
	R231	0.6504	0.8310		1.0000
Multi-zone snow removal system	Chuo-1	1.0000	0.6260	0.8729	1.0000
	Chuo-2	0.4299	0.3881	0.3000	0.5560
	Chuo-3	0.7092	1.0000	0.6911	0.7311
	Kita-1	0.2690	0.3159	0.1569	0.2961
	Kita-2	1.0000	0.4830	0.9538	0.4497
	Kita-3	1.0000	1.0000	0.7160	0.5554
	Higashi-1	0.3015	0.2350	0.3920	0.4612
	Higashi-2	0.4282	0.4405	0.3223	0.5127
	Shiroishi-1	0.4238	0.4645	0.4028	0.3965
	Shiroishi-2	0.3130	0.2603	0.3367	0.4177
	Atsubetsu	0.6002	1.0000	0.6843	0.6776
	Toyohira	0.7223	0.3661	0.6042	0.5720
	Kiyota-1	1.0000	0.8399	0.6285	0.8223
	Kiyota-2	0.7438	0.7625	0.4417	0.5891
	Minami-1	0.2324	0.2762	1.0000	1.0000
	Minami-2	0.5609	0.4585	0.6343	0.6286
	Nishi-1	0.4786	0.2729	0.4792	0.5651
	Nishi-2	0.5367	0.4762	0.5192	0.6271
	Teine	0.4315	0.5081	0.7417	0.7485

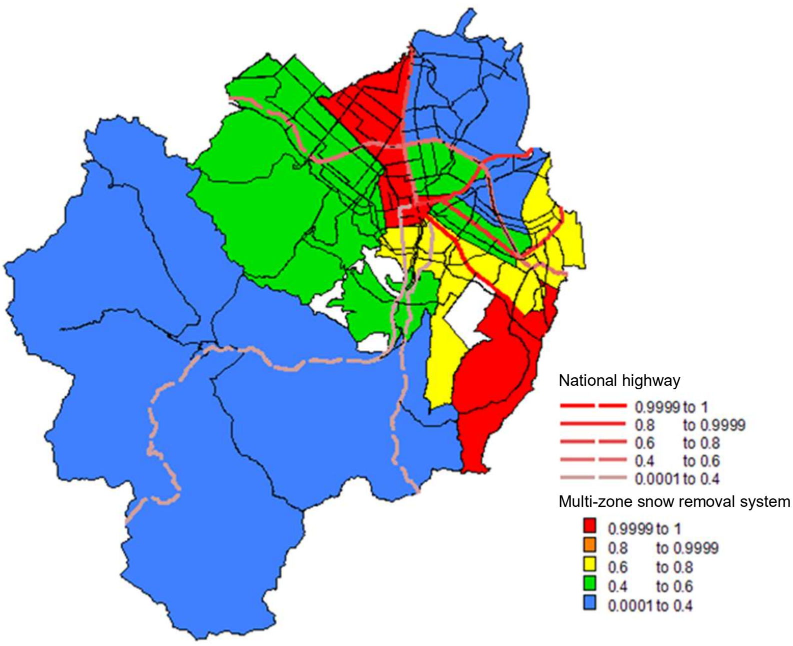

Fig.2 DEA analysis of Division of “System” for Snow removal of vehicle lane, road surface levelling

As for Division of “System”, national highway route 36 (R36) is “Efficient” for “Snow removal of vehicle lane, road surface levelling”, “Snow hauling” and “Snow removal of sidewalk”. R36 is large in traffic volume in Sapporo. In Multi-zone snow removal system, Chuo-1 is “Efficient” for “Snow removal of vehicle lane, road surface levelling” and “Snow removal of sidewalk”. Chuo-ward is the central city area and traffic volume in that area is large. Efficient of DEA means small input and large output. So small budget for large number of operator and machines in large traffic volume area can be said severe condition.

Table 3 DEA analysis result of Division of "Work"

	DMU	Snow removal of vehicle lane, road surface levelling	Widening of road by snow removal	Snow hauling	Snow removal of sidewalk
		Score	Score	Score	Score
National highway	R12, R275	0.3069	0.6916	0.6916	0.5187
	R36	0.2230	0.3938	0.3938	0.3723
	R230	1.0000	1.0000	1.0000	1.0000
	R5, R274	0.3570	0.7357	0.7357	0.8239
	R453	0.1975	no data	0.4217	0.5224
	R231	0.1182	0.1601	no data	0.2052
Multi-zone snow removal system	Chuo-1	0.7781	1.0000	1.0000	0.4868
	Chuo-2	0.4476	0.7185	1.0000	0.6974
	Chuo-3	0.3406	0.3406	1.0000	0.6478
	Kita-1	0.4396	0.8722	1.0000	1.0000
	Kita-2	0.7369	0.9471	0.8414	0.8422
	Kita-3	0.7731	0.8672	1.0000	0.5325
	Higashi-1	0.4992	0.9910	0.4669	0.8222
	Higashi-2	0.3593	0.4637	0.6872	0.7568
	Shiroishi-1	0.5034	0.6496	0.7867	0.7749
	Shiroishi-2	0.6610	0.7395	0.7274	0.7278
	Atsubetsu	0.3804	0.3322	0.4586	0.4891
	Toyohira	0.5367	0.6004	0.8955	0.7410
	Kiyota-1	0.2846	0.3221	0.4836	0.5740
	Kiyota-2	0.3527	0.3713	0.8426	0.8781
	Minami-1	1.0000	1.0000	0.3824	0.4715
	Minami-2	0.4930	0.6642	0.8074	0.7144
	Nishi-1	0.3341	0.2904	0.8801	0.7023
	Nishi-2	0.3004	0.3301	0.4988	0.6456
	Teine	0.5496	0.3174	0.5936	0.5077

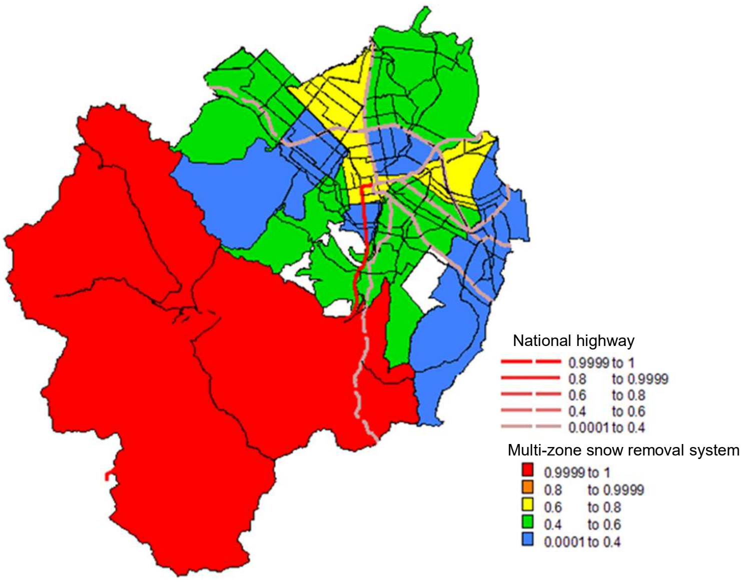

Fig.3 DEA analysis of Division of "Work" for Snow removal of vehicle lane, road surface levelling

As for Division of "Work", R230 is "Efficient" for all projects. R230 is long distance and amount of snowfall is large in that area. Small number of operators and machines for large output is efficient situation. Minami-1 has also long distance of road and snowy mountain area, so it is efficient for "Snow removal of vehicle lane, road surface levelling".

4. Rebuilding efficient snow removal system by DEA

4.1 Reallocation of the quantity of improvement by DEA to DMU

DEA can show how much inefficient DMU should improve itself in order to be "efficient". Input should be decreased and output should be increased to be “efficient”, this study focuses reducing input.

As for the quantity of improvement in “snow removal of vehicle lane and road surface levelling” in order that all DMUs become “efficient”, in Division of “Work”, 523 of 978 operators and 146 of 239 grader should be reduced. Also, in Division of “System”, 370 million of 830 million yen budget should be reduced. However, those are not realistic. This study aims at the efficiency of the snow removal system by the allocation of budget or snow removal machine among DMUs.

After distributing whole quantity of improvement into each DMU evenly, DMUs were evaluated by DEA again. In this way, DEA was applied repeatedly until the quantity of improvement was convergent.

4.2 Rebuilding snow removal system

Table 4 shows result of rebuilding snow removal system of Sapporo. Large rotary plow is used for snow hauling and widening of road, and small rotary plow is used for snow removal of sidewalk. Those were analysed by DEA for those two projects.

Table 4 Rebuilding snow removal system

	Budget (million JPY)				Number			
	Snow removal of vehicle lane, road surface levelling	Widening of road by snow removal	Snow hauling	Snow removal of sidewalk	Operator	Grader	Large rotary plow	Small rotary plow
R12, R275	45.571	27.476	138.073	13.174	23	5	3	4
R36	51.082	27.812	157.771	13.745	24	6	3	4
R230	61.582	36.620	184.036	17.744	31	7	4	5
R5, R274	67.582	32.735	169.722	20.029	35	5	3	7
R453	9.661	none	33.322	8.604	15	2	1	3
R231	15.478	9.299	none	4.605	8	1	1	1
Chuo-1	51.318	33.195	306.585	23.394	59	22	4	7
Chuo-2	31.353	25.328	128.024	18.847	45	14	4	6
Chuo-3	31.353	33.421	155.306	17.341	45	14	8	5
Kita-1	35.318	30.947	121.691	42.182	55	13	4	17
Kita-2	34.870	25.328	195.065	30.659	45	12	3	12
Kita-3	47.178	38.252	244.863	29.868	68	12	8	10
Higashi-1	25.055	21.957	86.343	27.789	39	6	3	11
Higashi-2	29.545	25.890	101.808	34.844	46	11	3	14
Shiroishi-1	33.394	29.262	115.063	35.693	52	12	4	14
Shiroishi-2	19.924	17.462	68.670	20.592	31	7	3	8
Atsubetsu	19.283	16.900	66.460	16.407	30	7	2	6
Toyohira	29.117	23.081	118.893	19.984	41	13	4	7
Kiyota-1	18.641	16.338	64.251	20.310	29	7	2	8
Kiyota-2	23.244	19.148	91.498	18.995	34	10	4	7
Minami-1	39.808	34.881	137.155	22.540	62	15	6	6
Minami-2	28.878	24.205	109.761	22.289	43	12	4	8
Nishi-1	29.545	25.890	101.808	22.713	46	10	3	8
Nishi-2	25.055	21.957	86.343	23.745	39	9	3	9
Teine	21.207	18.938	85.413	18.853	33	7	4	7

Comparison of 4 projects’ total budget between current and rebuilding snow removal system is shown in Fig. 4. Fig.5 shows comparison of number of operators.

In the city center area such as Chuo-1, traffic volume is large and importance degree of road network is also high. That is why budget and operators should be increased. On the other hand, in urban area such as Teine and Atsubetsu, budget and operators should be reduced.

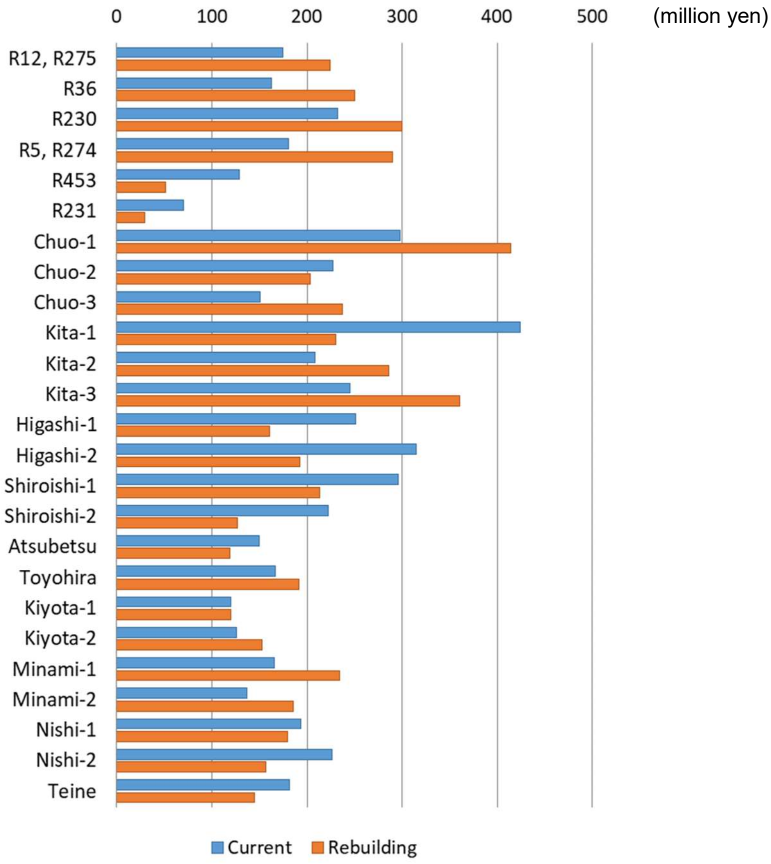

Fig. 4 Comparison of total budget

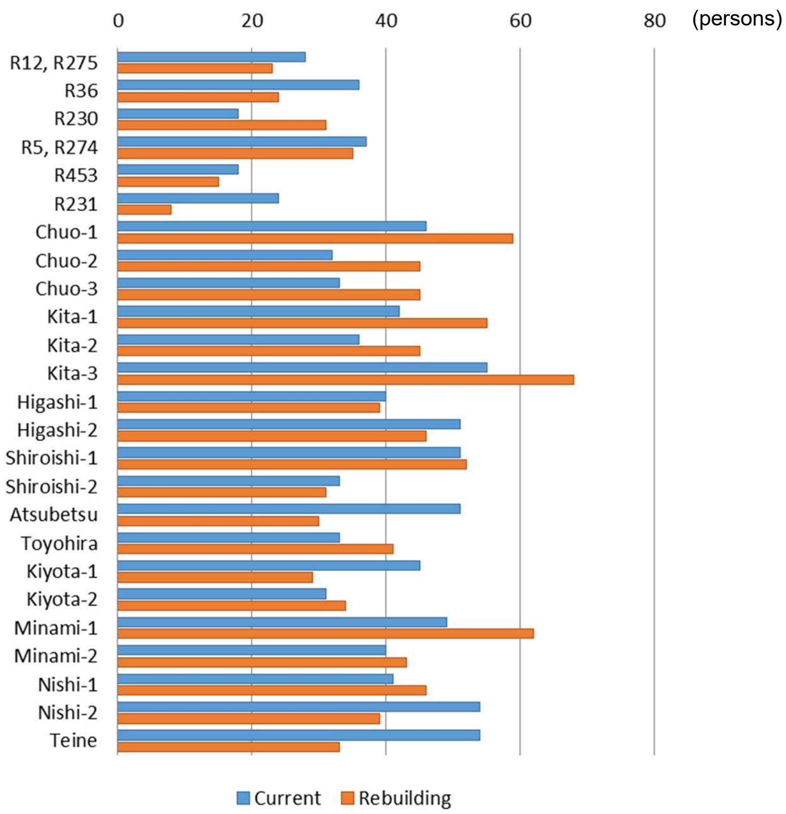

Fig.5 Comparison of number of operators

5. Conclusions

This study focused snow removal system of Sapporo. Year by year situation is becoming more severe as for securing budget and operators. In order to keep the road maintenance quality, efficient allocation of them is quite important. Currently national highways and city roads are maintained respectively. This study analysed snow removal system of both roads comprehensively by DEA. It may be necessary for national government and Sapporo City to collaborate in the future.

References

[1] Charnes, A., Cooper, W. W. and Rhodes, E. (1978) Measuring the efficiency of decision making units. *European Journal of Operational Research*, Vol. 2, 429-444.

[2] Cooper, W. W., Seiford, L. M. and Tone, K. (2007) Data Envelopment Analysis, Second Edition, Springer, New York

[3] Rukhsana K. L., Michael S. S. (1999) Resource Allocation Study for Snow Removal, *Transportation Research Record*, Vol.1672, 1, pp. 23-27.

[4] Kishi, K., Takahashi, Y., Hara, F., and Satoh, K., (2002) Level of Snow Removal Service and Residents' Willingness to Pay: Evaluation for Four Japanese Cities, *Transportation Research Record*, Vol.1794, 1, pp. 72-76.

Business Ecosystem Analysis of a Vehicular Road Weather Information System

Toni Lusikka
Research Scientist
VTT Technical Research Centre of Finland Ltd.
Finland
toni.lusikka@vtt.fi

Dr Pekka Leviäkangas, VTT Technical Research Centre of Finland Ltd., Finland
Mr Heikki Konttaniemi, Lapland University of Applied Sciences, Finland

Summary

This paper explores a concept of Industrial Internet to collect and utilise data from vehicle-installed sensors for the purpose of enhanced winter road management. Data from vehicle-installed sensors extends the coverage of road condition information from fixed Road Weather Information System (RWIS) network. Vehicle-based sensors observe similar data as fixed RWIS: road surface condition and temperature, friction values, air humidity and temperature. Some vehicles have also cameras installed to produce continuous images on the road. To utilize the vehicular data, the paper introduces an open data platform - WiRMa - that is being piloted in the Finnish Lapland. WiRMa connects the different vehicular data to be further used and processed by different maintenance management applications. The platform's data is aimed to be used for 'information service packages'. A pre-assessment on the value of data is given with some evaluation on the distributional effects of the value (i.e. benefits). Efficient utilization of sensor data, merging the data with fixed road weather station observation, and wrapping the data into usable formats and information contents requires new approaches in organizing the winter road management. The prospective value and benefits gained from the data and information are allocated to potential users or beneficiaries. These users and beneficiaries, as well as the providers of the data and information, and the suppliers of technologies and services, form a business ecosystem of winter road management. The business ecosystem is analysed through an exploratory study to evaluate the relevance and business case potential of the platform. In addition, the analysis shows what capabilities, and possible value co-creation and capturing methods should be incorporated in order to keep the ecosystem alive. The outcome of the analysis is a statement of the benefits for the ecosystem. The results can be used to justify further investments in the platform, suggesting also how the investment needs are divided between ecosystem actors. In sum, the primary condition to realize the potential benefits of the platform is the commitment of the ecosystem actors. The actors need to commit to the platform in order to realise the potential gains. Without commitments, required conditions on transactions between the parties will not take place, as do neither the co-investments in the platform. The multi-actor business case challenge is very much present. Other challenges and issues in achieving the commitments and a working ecosystem are discussed in the end of the paper.

Keywords: Internet of Things, Industrial Internet, RWIS, WiRMa, Winter Road Maintenance, Road Weather Information, Vehicular Data, Business Ecosystem, Open Data

1. Introduction

Winter road maintenance is conducted to ensure safe travelling on road network [1]. As climate changes continues, adverse winter weather and road conditions will also become more common in Finland [2]. This applies also to other countries that experience cold and snowy winters. In addition, traffic keeps increasing and thus number of accidents could rise. Increasing traffic and more adverse road conditions raise winter road maintenance costs [2]. All this makes it more and more important to have timely accurate quality assured winter road maintenance that would also be affordable.

However, currently winter road maintenance costs are rising as road users are expecting better road conditions [3], [4]. Thus, new solutions have to be researched, developed and implemented to ensure safe road network with reasonable costs.

Road weather information is one solution to improve the winter road maintenance. Road weather and condition information are estimated to reduce at least 4.6-9.2 million euros of accident costs [5]. In addition, Malin et al. [6] showed that accident risk was higher during snowfalls and rains, and highest during icy rain, slippery and very slippery road conditions. Slippery road conditions could be avoided by applying salt on the road right before ice formats on the road [7]. Hence, winter road maintenance contractors should be able to react fast and with according treatment methods, when weather changes.

Currently winter road maintenance contractors use fixed Road Weather Information Systems (RWIS) and weather service providers as information sources to help decision-making. New sensor technologies and capabilities are enabling a new way to track road weather and conditions in real time with moving vehicles. These data collection methods can have remarkable impact to decision-making and operations in winter road maintenance [8]. Vehicular road data differs from fixed RWIS information. Fixed RWIS network provides location specific, punctate, and continuous information, while vehicular system gathers information on every point of road the vehicle travels. Vehicular data collection is needed, as for example in northern Finland, network of fixed RWIS is very scattered and distances between measurement points are too long [9]. Vehicular data collection provides road condition information that is geographically superior to fixed RWIS, and thus purpose of these systems is to improve road condition information on areas, where distances between fixed RWIS stations are vast.

To implement vehicular data collection, many different business actors are needed. These actors form a business ecosystem around the vehicular data collection. Business ecosystems are complex networks that consist of multiple loosely interconnected actors, partnerships and transactions [10]. To understand business and potential ways to conduct business with vehicular data collection, business ecosystem around it has to be studied.

2. Research scope and methodology

Business ecosystem of winter road maintenance in Finland has already been studied in [11], so this paper focuses only on business ecosystem of a vehicular data collection pilot called WiRMa (Industrial Internet Applications in Winter Road Maintenance). WiRMa -project has multiple angles in developing winter road maintenance, and one of them is WiRMa platform. The WiRMa platform combines the vehicular data collection methods that are used in the project. WiRMa system setup is explained further in chapter 3. As vehicular data collection system is similar to fixed RWIS, vehicular data collection will be discussed as vehicular RWIS in the paper.

This paper presents the results of earlier research done in [12], and broadens the analysis of the ecosystem and discussion on the topic. The purpose of this paper is to study presented ecosystem and discuss feasibility and challenges of the presented business ecosystem. Outcome of the paper is network value analysis developed by [13]. Furthermore, research framework was constructed around key elements of ITS platform. Key elements of ITS platform are customers, value propositions, key partners and key resources [14]. These were used as guidelines when defining the business ecosystem of WiRMa during network value analysis as shown below in parentheses. Network value analysis consists of five steps [13]:

1. Define network (starting from customers).
2. Identify and define network entities.
3. Define the value each entity perceives from being a network member (and value proposition of each entity).
4. Identify and map network influences (who are the key partners and what are the key resources).
5. Analyse and shape.

This method is used as it shows interactions and relationships between different actors as well as provides possibility to identify problems and objectives for future development. In addition, customers, their needs and value network are identified, so it is possible to increase the created value. Network value analysis describes where value lies in the ecosystem and how it is created [13]. Hence, purpose of the method is to understand customer needs and recognize the key actors of the ecosystem [15].

3. WiRMa system setup

As discussed, WiRMa platform connects various vehicle-based sensing technologies. Thus, cloud-based IoT platform is needed to implement the system. This platform enables real time road weather data collection, analysing and visualisation. There is 19 vehicles equipped with different road condition sensing technologies to test the platform in northern Finland this year. There are five different technological solutions used: optical sensors from different hardware providers, CAN bus exploitation, telematics units, camera systems, and slipperiness detection software. Some of the vehicles are equipped with more than one technological solution to compare different techniques. With used technological solutions, all fundamental vehicle data can be observed in real time.

The necessary data to be collected with vehicles was determined by using Maintenance Decision Support System (MDSS) user requirements and quality criteria based winter road maintenance measurements. MDSS user requirements were identified in cooperation with platform test users, while the quality criteria is determined in guidelines provided by road authorities. MDSS user requirements are evolvement of road weather (situation before, now and hours ahead), dew point and dew point difference (road/air). In addition, it is required that sensor data is possible to be validated through camera images. Finnish road authorities use road friction, snowiness and evenness as the quality criteria. The data is collected with vehicles, and road weather forecasts are provided by weather service providers, who utilise vehicle data, fixed RWIS, meteorological stations, and other weather related equipment. The data list below shows the necessary data that is needed to fulfil the MDSS user requirements and quality criteria requirements [12]:

- Car data (CAN bus/mounted sensors)
    - Road surface conditions (ice, wet, snow, slush, dry)
    - Friction estimation
    - Road surface temperature
    - Water layer thickness on road
    - Air temperature
    - Relative humidity
    - Camera images from road
    - CANbus (e.g. stability control, brakes, fog lights, windshield wipers)
    - Roughness (IRI)
- Road weather forecasts
    - Road surface
    - Road friction
    - Road surface temperature
    - Water layer thickness
    - Air temperature
    - Relative humidity
    - Rain type
    - Rain intensity

Figure 1 describes simplified WiRMa platform data flows. The WiRMa platform joins vehicular and fixed RWIS data together in the cloud. Both fixed and vehicular data are also used by weather service providers to enhance the road condition forecasts. These forecasts are also delivered to the Watson IoT platform, where the data is stored, debugged, analysed and tested. So, IoT platform combines data from several sources. The analysed data is visualized in a separate web application, which can be accessed by anyone. Test users are provided with login capability, and they have more specific information available than public viewers. They can use the web application to retrieve information for maintenance operations planning, or to support their decision making, and to control road maintenance fleet according the weather. Data is also used to compare quality of different data sources.

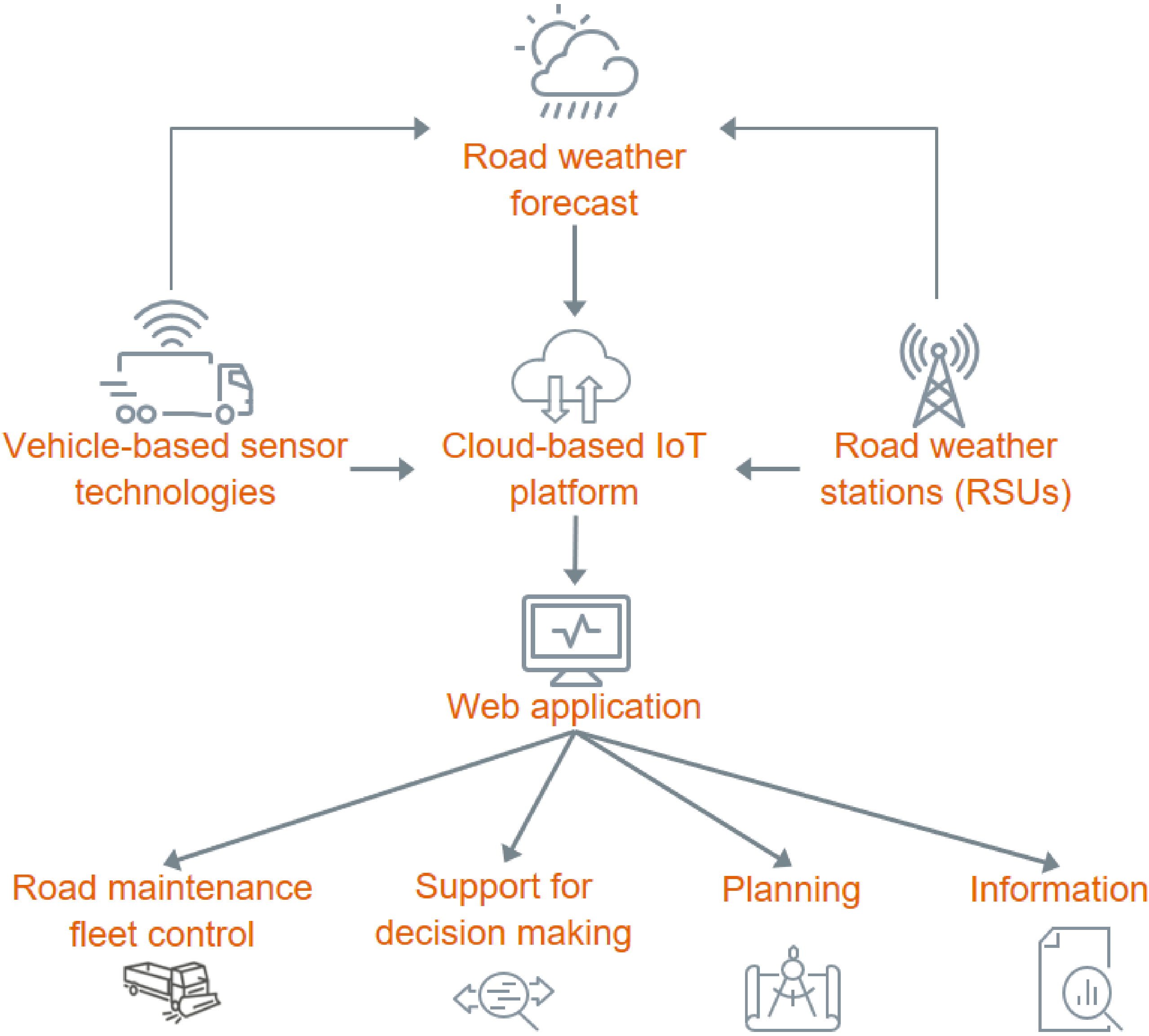

Fig. 1 Simple data flow of WiRMa system [retell 16].

Data collected to WiRMa platform is analysed and visualised to the web application. The web application is basically a map that shows fixed road weather stations and cameras, and vehicular data. The web application shows many different types of data within 24 hours of measurements. Older data is stored to IoT cloud platform. Figure 2 shows all information that can be seen from web application, and gives explanations to specific attributes of the application. Vehicular data is colour coded to present current road condition information, and it is possible to select which information is shown (road condition, friction, water on the road, road and air temperatures). In addition, when point of road is selected, it shows more specific information about road conditions in that particular point of the road. The same applies to specific road weather stations and road weather cameras that gather continuous data of the specific point on the road.

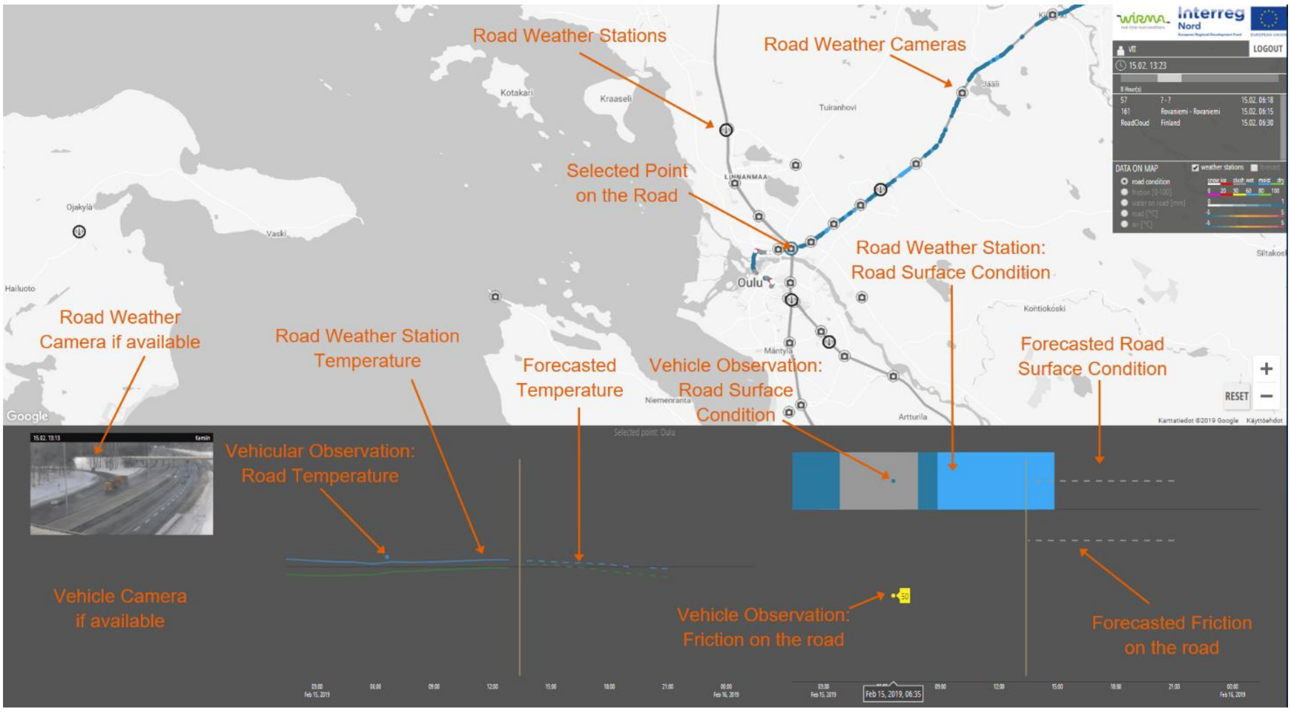

Fig. 2 WiRMa web interface with brief explanations of attributes.

Furthermore, forecasts for each type of data can be shown on the map. For example, figure 3 represents road friction forecast for Nordic countries visualised on the map. Forecasts are shown at 15-minute intervals up to three hours from current moment. Colour codes are corresponding to the

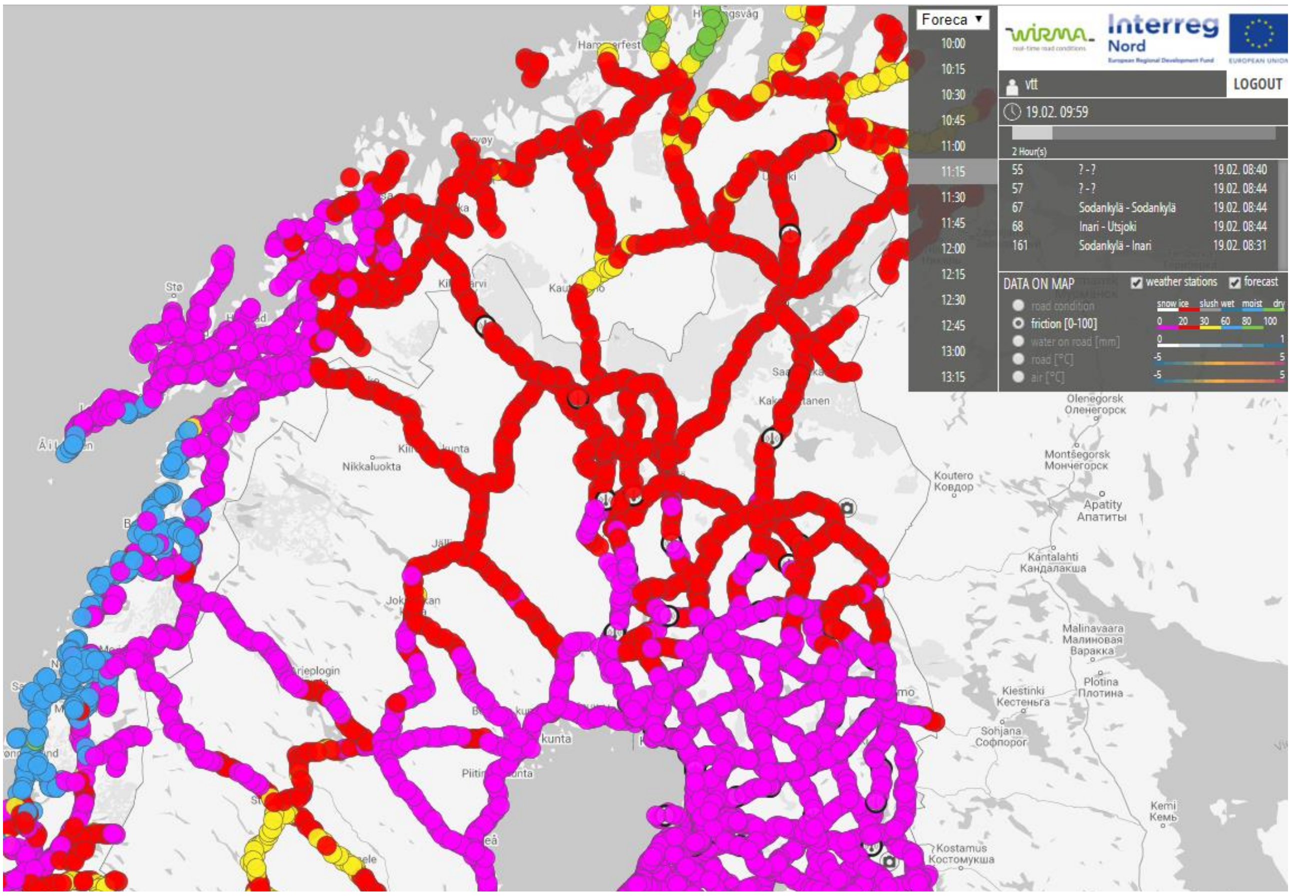

Fig. 3 Forecasted friction values on the road network of Nordic countries.

real time data representations. Two different companies provide forecasts to the platform and the desired provider can be selected to view differences in forecasts. Forecast on the road is shown with 1 to 10-kilometre spacing between specific points on the road.

4. Pilot phase ecosystem of WiRMa

Business ecosystem actors of WiRMa form a value-creating network, where value exchanges between actors consists of money, technologies and services, non-monetary benefits, and information. Value network of WiRMa pilot phase ecosystem is depicted in figure 4, in which value exchanges and offerings are also seen. Value offerings or value propositions are depicted using grey arrows, numbering and text. Monetary values are orange arrows, while dotted orange arrows are used to describe value exchanges that are possible, but might not happen in market-based ecosystem.

It is important to notice that this is only one possible way to organise business ecosystem for vehicular RWIS and it highly depends on the business model of platform owner, as they are central actors, who connect other actors and customers. In addition, as WiRMa is a research project, value exchanges do not necessarily happen in described way currently, but if the same companies would offer their services on the market in the same way, these could be the expected value exchanges between them.

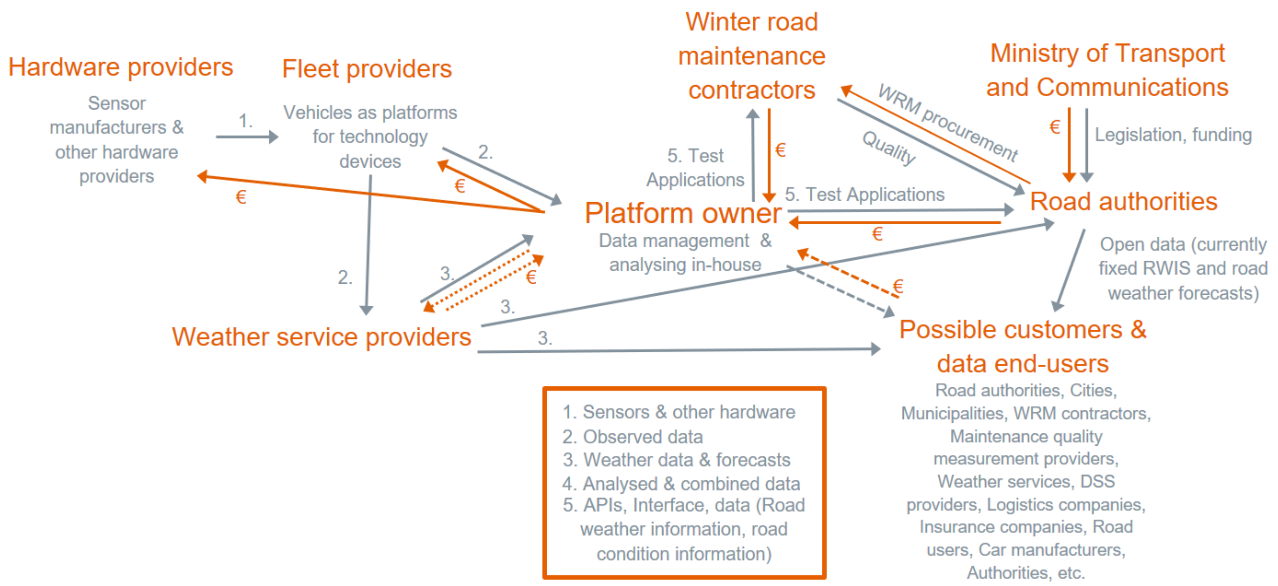

Fig. 4 Business ecosystem of WiRMa (pilot phase).

As seen in figure 4, WiRMa pilot phase ecosystem consists of eight actors: Hardware suppliers, Data collection providers, Weather service providers, Platform owners, Winter road maintenance contractors, Road authorities, Ministry of Transport and Communications, and other possible customers and/ or data end-users. Each one of them has their specific role in the ecosystem as they have different capabilities, and thus offer different value propositions. Central actor in WiRMa ecosystem is the platform owner as they are connecting other actors together, and procuring needed technologies and services as well as vending the analysed data. However, logical way to analyse the ecosystem is to start describing value creation from hardware providers, as all actors in WiRMa pilot business ecosystem are known. In market-based business ecosystem there is other actors in addition to WiRMa ecosystem actors.

Hardware providers are those actors, who provide technology solutions that are needed to provide the platform. In WiRMa ecosystem, multiple hardware providers offer their technological solutions in vehicular RWIS market, so there is plenty of options for platform owners to include in their system: Optical sensors, temperature sensors, laser scanners, breaking friction sensors, dew point sensors, cameras, and telematics units that exploit the CANbus of vehicles. Different hardware has different measuring capabilities and thus different data can be collected with them. With more high-priced sensors, more data can be collected, but with cheaper technologies good enough results for many purposes can be achieved, especially if several technologies are used simultaneously. In WiRMa ecosystem hardware providers compete with each other with sensing capabilities, for example, which technology provides the best measurement results or the best quality/price ratio. There is also competition between different technologies, such as cameras and sensors, as they provide very diverse outcomes. For other purposes, cameras are better equipped than sensors and vice versa, but winter road maintenance could benefit from both technologies.

Procured hardware is attached to the vehicles of fleet providers that platform owner should procure from various different transportation and logistics companies in order to enable geographically vast and timely accurate coverage. Fleet providers can be coach services, logistics companies, freight traffic or other professional or commercial traffic, such as taxis. On some cases, it could also be possible that private road users could offer their vehicles as platforms for technologies. Compensation for vehicles as platform is not necessarily required. Some companies or other traffic actors could provide their fleet free of charge if road conditions would be better after the data is used to enhance winter road maintenance. However, this might not be valuable enough for some fleet providers, as in their opinion, road network condition is not their but infrastructure owner's problem, so they might want monetary compensation or the rights to use the data themselves in their operative systems or they might want to retail the data further.

Observed vehicular data is transferred from On-Board Units (OBUs) to the platform owner's server, but it can be also transferred to other actors, such as weather service providers, who can utilize the data to enhance their road weather forecasts or other commercial services. This can be done in close collaboration between platform owner and weather service provider. Platform owner could exchange the rights to use the vehicular data to the rights to use the enhanced weather forecasts in platform owners application. It is also possible that vehicular data could be sold to the weather service providers, who could also sell the road condition forecasts to the platform owner as they are now selling forecasts to road authorities, winter road maintenance contractors and other customers.

Vehicular data observed by the fleet is synced in real time with platform owner's IoT cloud platform. Platform owner needs to analyse the raw data and possibly (depending on the contract with the customers) also visualize the refined data to the map or some other interface that customers can use. In WiRMa ecosystem, platform owner analyses and visualizes the data to the web interface and merges fixed RWIS data and forecasts from two different companies to the platform's interface, so that multiple essential data sources for winter road maintenance is available in one application. Basically, value proposition of platform owner is the merged and visualized data on the web interface. However, value proposition of platform owner should be thought accordingly to the customer needs to make value proposition as appealing as possible. It is important to remember that every customer have their own specific needs that they desire to be fulfilled with new vehicular data.

Value exchanges on the right side of platform owner in figure 4 are possibly the most meaningful exchanges to the platform owner. Winter road maintenance contractors, road authorities and other customers will determine the market value of vehicular RWIS as they are paying for the data in the end. However, it is not clear, who will be the customer for vehicular RWIS as many actors could use the data, but might not be willing to pay for it necessarily. These actors could anticipate that road authorities would offer vehicular data as open data. Currently road authorities procure fixed RWIS and road condition forecasts, and offer them as open data to the public and thus also to the winter road maintenance contractors. Hence, other ecosystem actors are not maybe wrong to presume that road authorities would also procure and offer vehicular data as open data in future. Currently vehicular data is not part of the open data package and it is not offered in large scale on the market though there are some platform owners already commercializing their platforms. In addition, some actors could assume that some other actor would procure and refine the data more suitable for them, and procure the data or information from that actor instead of platform owner. This is however contractual question, how platform owner allows their customers to use the procured data.

5. Discussion

Pilot phase business ecosystem of WiRMa described in chapter 4 is only one possible construction of the ecosystem. It is possible that some of the actors could have multiple different roles, which could exclude other actors from the ecosystem. For example, large logistics companies could decide to build the platform and use their own fleet as vehicle platforms for sensing technologies. Thus, there would not be need for separate platform owner, and other logistics companies might not be part of the ecosystem. However, those who are left out of the ecosystem could form ecosystem of their own or multiple ecosystems could form. Though, it is not likely that more than couple ecosystems are formed in such a small market as Finland. Furthermore, it is probable that only maximum of three ecosystems could survive on the Finnish road condition information market without strong government influence and market control. However, ecosystems should be self-sustaining without need for government intervention [17]. On the other hand, Leviäkangas et al. [11] argue that ecosystems are important in delivering societal and public services. Analysis of the WiRMa ecosystem showed that road authorities play major role in road weather information and winter road maintenance ecosystems. Hence, road authorities should choose their role and determine their position in development of vehicular RWIS.

Even though road authorities would not take other role than customer for data in the ecosystem, their commitment is still needed as winter road maintenance is the most potential use case for vehicular RWIS. If road authorities do not procure vehicular RWIS data, there might not be enough other customers so that ecosystem will survive. Or there could be enough customers, but the cost of data could be too high for separate customers to procure it. Hence, close collaboration and full commitment is needed from all participants of the ecosystem. It is also said that usually the largest and oldest business actors have important roles in sustaining and connecting relationships within the business ecosystem [18]. Thus, dynamics of the ecosystem play major role in the success of the business ecosystem.

New vehicular RWIS could have customers beyond winter road maintenance actors. Recently for example insurance companies have become interested in weather data. They could deliver notifications of poor weather conditions, such as slipperiness, to their customers, and possibly prevent accidents from happening. Thus, insurance companies would not have to pay for accident damages through insurance. This would also lower societal costs (e.g. external accident costs). Other new service businesses similar to this could emerge with new road condition data gathered with vehicles. Examples of such services include comprehensive traffic management (e.g. CAM and DENM messages) and navigation services for road users. These services would benefit society in a larger scale than just improvement of winter road maintenance. In addition, when thinking of possible future traffic solutions, such as autonomous vehicles, it is clear that more accurate weather information will be needed.

6. Conclusion

This paper viewed WiRMa platform and business ecosystem around it. Vehicular RWIS is a relatively new way to produce road condition information. Technology itself is not very new, but capabilities of sensor technologies have increased a lot in past years and cost of the technologies has also reduced. Thus, vehicular RWIS has become a viable option to gather road condition and weather data. It will not replace fixed RWIS, but the two will complement each other and provide wider angle to the road weather.

Research revealed that commitment of all actors is needed, so ecosystem will prevail. Without full commitment of the actors necessary investments might not take place. Thus, full scale vehicular RWIS could not be implemented without the full commitment. Because of this road authorities have large role in the ecosystem even though they would decide to only procure the data instead of larger influence and market control. In addition, vehicular RWIS is expected to bring new actors and produce new businesses and roles in the ecosystem as new capabilities attract other industries too.

As stated in discussion chapter, vehicular RWIS has many other possible purposes of use. Thus, for further research it is recommended that vehicular data services, such as WiRMa, would be tested in broader sense than just the winter road maintenance. Also, business actors needed to develop other services should be studied further as well as the business ecosystem that forms around the new services. When considering WiRMa, costs and benefits should be studied further and determine exact investment needed for full-scale launch. In addition, societal benefits of road weather information (especially information gathered with vehicles) need to be researched further.

7. Acknowledgements

This paper was financed through the European Union’s Interreg Nord –programme. WiRMa consortium of beneficiaries includes Lapland University of Applied Sciences (FI), The Finnish Meteorological Institute (FI), Foreca Ltd. (FI), Luleå University of Technology (SE), University of Tromsø (NO) and Casselgren Innovation AB (SE). Other partners include Destia Ltd. (FI), IMSS Ltd. (FI), Lapland Centre for Economic Development – Transport and the Environment (FI), YIT Ltd. (FI), Roadscanners Ltd. (FI), Statens vegvesen (NO) and Luleå Kommun (SE). The project is financed by the Interreg Nord Programme, Regional Council of Lapland (FI) and Region Norbotten (SE).

References

[1] PILLI-SIHVOLA E., LEVIÄKANGAS P. and HAUTALA R., “Better winter road weather information saves money, time, lives and environment”, *Proceedings of the 16th SIRWEC conference*, 2012.

[2] LIIKENNEVIRASTO, ”Talvihoidon toimintalinjat”, *Liikenneviraston toimintalinjoja 1/2018,* Liikennevirasto, Helsinki, 2018, pp. 53.

[3] TALOUSELÄMÄ, ”Teiden surkean kunnon talvihoitoon lisärahoitusta - ensi vuonna valtion väylien rahoitustaso laskee 350 miljoonaa euroa”, 2018, Available: https://www.talouselama.fi/uutiset/teiden-surkean-kunnon-talvihoitoon-lisarahoitusta-ensi-vuonna-valtion-vaylien-rahoitustaso-laskee-350-miljoonaa-euroa/70825a01-2edb-3493-a495-d2c828eaee06 [cited 21.02.2019].

[4] VALTIONEUVOSTO, ”Ministeri Berner: Teiden kunto on jo hälyttävällä tasolla”, 2018, Available: https://valtioneuvosto.fi/artikkeli/-/asset_publisher/ministeri-berner-teiden-kunto-on-jo-halyttavalla-tasolla [cited 21.02.2019].

[5] SAARINEN H., LAINE T. and METSÄRANTA H., ”Kelitiedon vaikuttavuus”, *Liikenneviraston tutkimuksia ja selvityksiä 29/2014*, Liikennevirasto, Helsinki, 2014, pp. 96.

[6] MALIN F., NORROS I. and INNAMAA, S., ”Accident risk of road and weather conditions on different road types”, *Accident Analysis and Prevention*, Vol. 122, January, 2019, pp. 181-188.

[7] BAILEY J.N.-L. and HAAVASOJA T., “Protecting groundwater: rethinking the use of road salt in modern winter maintenance”, *Geologi*, Vol. 68, 1/2016, pp. 20-25.

[8] ODELIUS J., FAMUREWA S.M., FORSLÖF L., CASSELGREN J. and KONTTANIEMI H., “Industrial internet applications for efficient road winter maintenance”, *Journal of Quality in Maintenance Engineering*, Vol. 23, No. 3, 2017, pp. 355-367.

[9] KONTTANIEMI H., ”Teollinen internet ratkaisee pitkien etäisyyksien ja hankalien sääolosuhteiden tuomia haasteita tieinfrastruktuurin talvihoidossa”, *Lumen*, Vol. 3/2016, 2016.

[10] IANSITI M. and LEVIEN R., ”Strategy as Ecology”, *Harvard Business Review*, Vol. 82, No. 3, 2004, pp. 68-78.

[11] LEVIÄKANGAS P., AAPAOJA A., KINNUNEN T., PILLI-SIHVOLA E., HAUTALA R. and ZULKARNAIN, ”The Finnish Road Weather Business Ecosystem – Turning Societal Benefits into Business and the Other Way Round”, *Engineering Management Research*, Vol. 3, No. 1, 2014, pp. 56-67.

[12] LUSIKKA T., “*Business Ecosystem Analysis of a Vehicular Road Weather Information System – case WiRMa*”, University of Oulu, 2018, pp. 81

[13] PEPPARD J. and RYLANDER A., “From Value Chain to Value Network: Insights for Mobile Operators”, *European Management Journal*, Vol. 24, No. 2-3, 2006, p. 128-141.

[14] AAPAOJA A., KOSTIAINEN J., ZULKARNAIN and LEVIÄKANGAS P., “ITS service platform: in search of working business models and ecosystem”, *Transportation Research Procedia*, Vol. 25, 2017, p. 1781-1795.

[15] HERRALA M., PAKKALA P. and HAAPASALO H., ”Value-creating networks – A conceptual model and analysis”, *Research reports in Department of Industrial Engineering and*

Management, University of Oulu, Vol. 4/2011, 2011.
[16] KONTTANIEMI H. "Wirma Project", 2019, Available: https://www.wirma-project.eu/index.php/project/ [cited 22.02.2019]
[17] PELTONIEMI, M. & VUORI, E., 2004. "Business ecosystem as the new approach to complex adaptive business environments", *In Proceedings of eBusiness research forum*, p. 267-281.
[18] LAPPI, T., LEE, T. & AALTONEN, K., "Assessing the Health of a Business Ecosystem: The Contribution of the Anchoring Actor in the Formation phase", *International Journal of Management, Knowledge and Learning*, Vol. 6, No. 1, 2017, p. 27-51.

Road Visibility Estimation Method Based on Images on the Internet

Yasuhiro Nagata, Ph.D.
Principal Researcher
Hokkaido Development Engineering Center
Japan
nagata@decne.or.jp

Toru Hagiwara, Ph.D., Hokkaido University, Japan

Yasuhiro Kaneda, Hokkaido Development Engineering Center, Japan

Masanori Mikita, Hokkaido Road Management Engineering Center, Japan

Summary

In winter, Hokkaido, the Japan's northernmost prefecture frequently experiences snowstorm-induced poor visibility that is one of the causal factors of traffic accidents. Hokkaido's national highways whose total length is approx. 6500 km are installed with about 2,000 closed-circuit television (hereinafter referred to as CCTV) cameras to monitor traffic conditions. However, obtaining area-wide visibility information that is understandable at a glance from the video images sent by many CCTV cameras is quite difficult. The Hokkaido Regional Development Bureau had sought a method to quantify the CCTV camera's video images to facilitate to speedily gain area-wide road visibility information. To meet such a demand, Hagiwara et al. studied a method for quantifying visibility state by processing CCTV digital video images. The weighted intensity of the power spectrum (hereinafter referred to as WIPS) was examined to determine its applicability as a value for identifying visibility state. Nagata et al. developed road visibility information system (RVIS) that estimates road visibility information to accumulate it, by using images transmitted by multiple CCTV cameras. In recent years, a number of still images of road conditions are provided to drivers through the Internet. In this study, the authors tried to simultaneously estimate road visibility from the CCTV camera images provided through the Internet. The assessment results have showed that the RVIS estimations enable simultaneous, timely, area-wide and accurate road visibility information. In other words, the daytime road images of CCTV cameras that can be obtained through the Internet are useful enough for RVIS to estimate road visibility ahead.

Keywords: road visibility index, CCTV camera, road still image,
weighted intensity of the power spectrum, meteorological optical range

1. Introduction

In winter, Hokkaido, the Japan's northernmost prefecture frequently experiences snowstorm-induced poor visibility that is one of the causal factors of traffic accidents [1]. There are strong calls for the provision of the information on road visibility in winter [2]. Hokkaido's national highways whose total length is approx. 6500 km are installed with about 2,000 closed-circuit television (hereinafter referred to as CCTV) cameras to monitor traffic conditions. The CCTV cameras are intensively placed at accident-prone locations such as, mountain passes. The video images recorded by the cameras are sent by means of a fiber-optic network to road maintenance offices that are responsible for monitoring road conditions including visibility. However, obtaining area-wide visibility information that is understandable at a glance from the video images sent by many CCTV cameras is quite difficult. The Hokkaido Regional Development Bureau had sought a method to quantify the CCTV camera's video images to facilitate to speedily gain area-wide road visibility information.

Several methods of assessing visibility from road images have been studied recently [3] - [6]. Hagiwara et al. proposed a method for identifying poor visibility under adverse weather conditions by processing CCTV digital images [7]. They examined the weighted intensity of power spectra (hereinafter referred to WIPS) of such images to determine its applicability as a value for identifying poor visibility from road images. WIPS reflects a band pass of spatial frequency of the image based on human eye sensitivity [8]. In this respect, WIPS differs greatly from previous image-based methods of identifying poor visibility under adverse weather conditions. Nagata et al. found that there is a high correlation between drivers' evaluations of visibility based on road images and the visibility scale assigned by WIPS and that the subjective visibility evaluation for a given road image differs little from person to person [9]. Based on these two papers, Nagata et al. developed a method for quantifying visibility state by processing CCTV digital video images. The value of WIPS was examined to determine its applicability as a value for identifying visibility state. On the basis of the results, a road visibility information system (hereinafter referred to as RVIS) was developed that estimates road visibility information to accumulate it, by using images transmitted by multiple CCTV cameras. Feasibility studies in the daytime during the winters from 2005 to 2007 were performed on national routes 230 and 231. During those two winters, the RVIS calculated visibility scale and road visibility index (hereinafter referred to as RVI) automatically, accurately, continuously, and in a timely manner from road images recorded by multiple CCTV cameras. The RVIS properly processed 90% of the images transmitted by the CCTV cameras.

Meanwhile, in the RVIS's CCTV clip image processing to obtain still images from which WIPS are gained has been a heavy work requiring time and labour. Fortunately, in recent years, a number of still images of road conditions that are produced from CCTV cameras are provided to drivers through the Internet. In this study, the authors tried to estimate road visibility from the still images provided through the Internet.
The objectives of this study follow:
1) To assess how RVIS could estimate road visibility speedily from the still images that can be obtained through the Internet.
2) To prove the accuracy of RVIS's road visibility estimations by using the still images provided through the Internet by comparing the estimations with actual road visibility identified by meteorological data.

2. Long-term investigation of the Road Visibility Information System

2.1 The Road Visibility Information System (RVIS)

Figure 1 shows the flow diagram of the Road Visibility Information System. Four sub-systems of RVIS (image collecting system, image quantification system, data accumulation system and data provision system) were originally coded in C. Each system runs automatically. The first step is to gather two-dimensional JPEG files of 720×480 pixels from website of Hokkaido Regional Development Bureau through the Internet. The two-dimensional image is stored in the database of the data accumulation system with the other data shown in Figure 1.

The second step is to crop a two-dimensional image of 256×256 pixels from the JPEG image. The grayscale intensity of each pixel is computed from the intensities of red-green-blue (RGB) components recorded in the image. The grayscale intensity ranges from 0 to 255. The image is broken down into sinusoidal gratings of different spatial frequencies using two-dimensional fast Fourier transform (FFT). The power spectrum value computed by FFT corresponds to the amplitude of spatial frequency. WIPS is calculated by summarizing the power spectrum intensity in the range of 1.5 cpd to 18 cpd [3]. Under clear conditions, the power spectra for each spatial frequency component of the road image are large and value of the WIPS is large. Under poor visibility conditions, such as those in fog or snow, the power spectra are small and value of the WIPS is small. These steps of the image quantification system are the most important in RVIS. The RVI is categorized into 5 ranks based on value of the WIPS. If the WIPS is equal to zero, the system identifies the image as an error image, and RVI are stored as non-applicable data. This problem occurs occasionally due to trouble with the fiber-optic network or the CCTV camera.

The third step is to store WIPS, RVI, and images in the database of road visibility information. The final step is to provide RVI to the public. The data provision system changes RVI into numerical ranks and symbols for provision by website of RVIS. For images defined as erroneous, the data transmission system provides the output of “N/A.” It takes approximately 1 second per image from the first step to the final step.

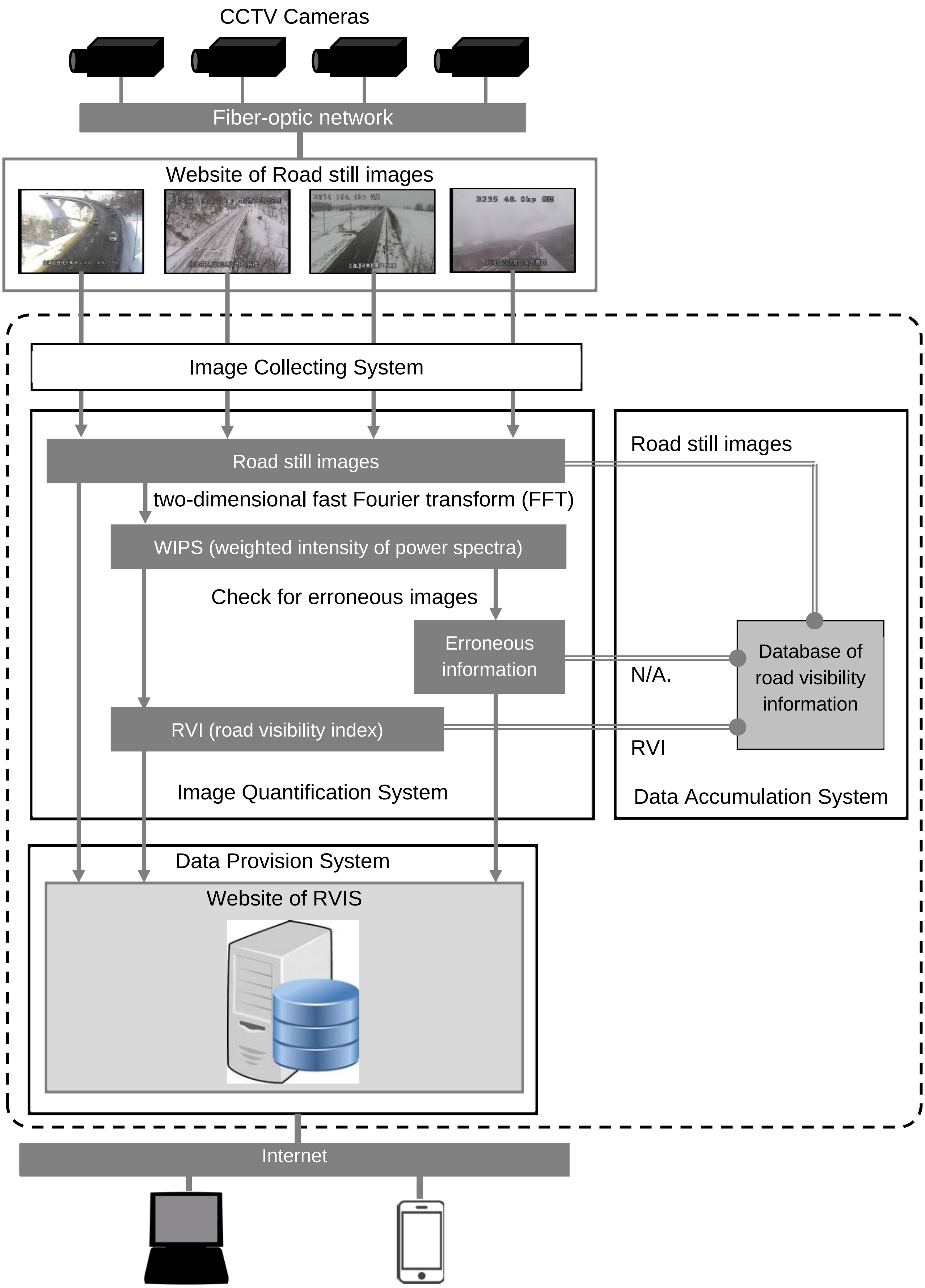

Fig. 1 Road Visibility Information System (RVIS)

2.2 Long-term investigation of RVIS

During the winter of 2018, we have conducted the feasibility study of the RVIS in Abashiri region, Hokkaido, Japan. This study chose CCTV cameras at 58 locations and RVI was calculated from the data produced from the still images recorded by CCTV cameras.

At the website operated by the Hokkaido Regional Development Bureau, CCTV cameras' still images are updated every 15 minutes. The image collecting system has automatically collected still images that are updated every 15 minutes and recorded by CCTV cameras for 90 days from January to March, 2018. As a result, the system collected still images 8640 times (4 times x 24hours x 90 days). With some errors, the system actually worked 8629 times to collect still images. If all 58 CCTV cameras worked well, the system could have collected in total 500,482 (58 x 8629) still images. However, out of 500,482; 442 images could not be collected probably because of the network's line failure. And, eight collected images appeared as those under maintenance. Further, half of the collected images after dark could not be used to calculate RVI because the images were too dark. Consequently, 322,611 still images were used to calculate RVI.

The image quantification system calculated WIPS without errors and delays from the data of 322,611 still images provided by CCTV cameras. The resulting WIPS values were categorized to five ranks of RVI for greater understandability by users. The number of still images fall on each RVI rank and their percentage to the total images follow: Level 1 (visibility range; more than 500m), 299,179, 92.7%; Level 2 (visibility range: 200 - 500 m), 21,496, 6.7%; Level 3 (visibility range: 100 - 200 m),1,268, 0.4%, Level 4 (visibility range: 50 - 100 m), 454, 0.1%; and Level 5 (visibility range; less than 50m); 214, 0.1%.

Table 1 Number of CCTV cameras' still image data

	Number of still images	Notes
Number of still images to be collected by the image collecting system	500,482	58 locations x 8629 times
Number of still images that could not be collected by the image collecting system	442	
Number of actually collected still images	499,740	
Number of still images that appeared under maintenance	8	
Number of unusable still images because of darkness	177,121	
Number of still images to be used for RVI calculation	322,611	100.0%
RVI Level 1（visibility range; more than 500m）	299,179	92.7%
RVI Level 2（visibility range; 200-500m）	21,496	6.7%
RVI Level 3（visibility range; 100-200m）	1,268	0.4%
RVI Level 4（visibility range; 50-100m）	454	0.1%
RVI Level 5（visibility range; less than 50m）	214	0.1%

3. Assessment of RVI and RVIS

3.1 Results of the comparison between values of MOR and values of RVI

In Abashiri region, two weather monitoring stations in Omu and Monbetsu of the Japan Meteorological Agency are hourly recording visibility range. Those weather stations measure visibility range by using visibility meters that measure meteorological optical range (hereinafter referred to as MOR). The values of MOR and RVI calculated from still images recorded by CCTV cameras were compared. The MOR value and RVI values for the comparison were those produced from a visibility meter and a CCTV camera whose locations are closest to the weather monitoring stations.

Figure 2 shows a time series of datasets of MOR values and RVI values. The larger a RVI value is the lower the visibility is. RVI levels follow: Level 1 (visibility range; more than 500m); Level 2 (visibility range: 200 - 500 m); Level 3 (visibility range: 100 - 200 m), Level 4 (visibility range: 50 - 100 m); and Level 5 (visibility range; less than 50m). The time series results show that the values of RVI follow the changes in the values of MOR. In the case where MOR is lower than 1000m, RVI increases to 3 or greater. RVI 3 indicates the visibility range of 100 – 200 m, where the value of RVI is significantly lower than MOR's. Such discrepancy may result from the difference in the environment where the CCTV camera and MOR are placed. The location of MOR for the feasibility test is protected by trees from strong window, which may minimize visibility deterioration due to drifting snow, while the CCTV camera's location is prone to be affected by drifting snow, which is likely to reduce visibility. The difference may also come from the features of values of MOR and RVI; the former is an average value of visibility and the latter is calculated from a momentary still image.

3.2 Assessment of RVI and RVIS by Users

The feasibility study of RVI and RVIS, RVI information was made available on a trial website for road administrators and staff working for road maintenance. Figure 3 shows the number of accesses from January to March 2018 to the website page where RVI information was available and the page where CCTV camera images are shown. The dates of the issuances of heavy snowfall warnings, heavy snowfall advisories, snow storm warnings and snow storm advisories and the dates of national highway closures in Abashiri region are also specified there. The greatest number of accesses to the website was March 1st, 2018, it was a stormy day when heavy snowfall and snow storm warnings were announced and some roads were closed. The greatest number of viewing the page where CCTV camera images are available was recorded on February 17, 2018. Heavy snowfall warnings and snow storm advisories were also issued this day and road closures were caused in Abashiri region. On other dates when heavy snowfall and snow storm warnings were issued, the number of accesses to the pages where RVI and CCTV images were provided significantly increased.

Table 2 organizes the comments given by the feasibility test attendees including road administrators and staff of road maintenance. In Abashiri region, CCTV cameras are placed at more than 200 locations. Grasping the state of visibility all over the region, viewing all CCTV cameras for a short period of time is impossible for those people. They commented because they could know comprehensive visibility state, viewing the RVI page shortly, RVI was useful. Some said that after checking the RVI page, they viewed CCTV camera images at their road stations. Those comments indicate that RVI was useful for parties concerned to know the whole visibility state momentarily. Not a few commented that they viewed RVI page by smart-phone at home or other locations that is because CCTV camera image files are rather heavy and take time to be downloaded, while RVI information is available everywhere even telecommunication environment is not good.

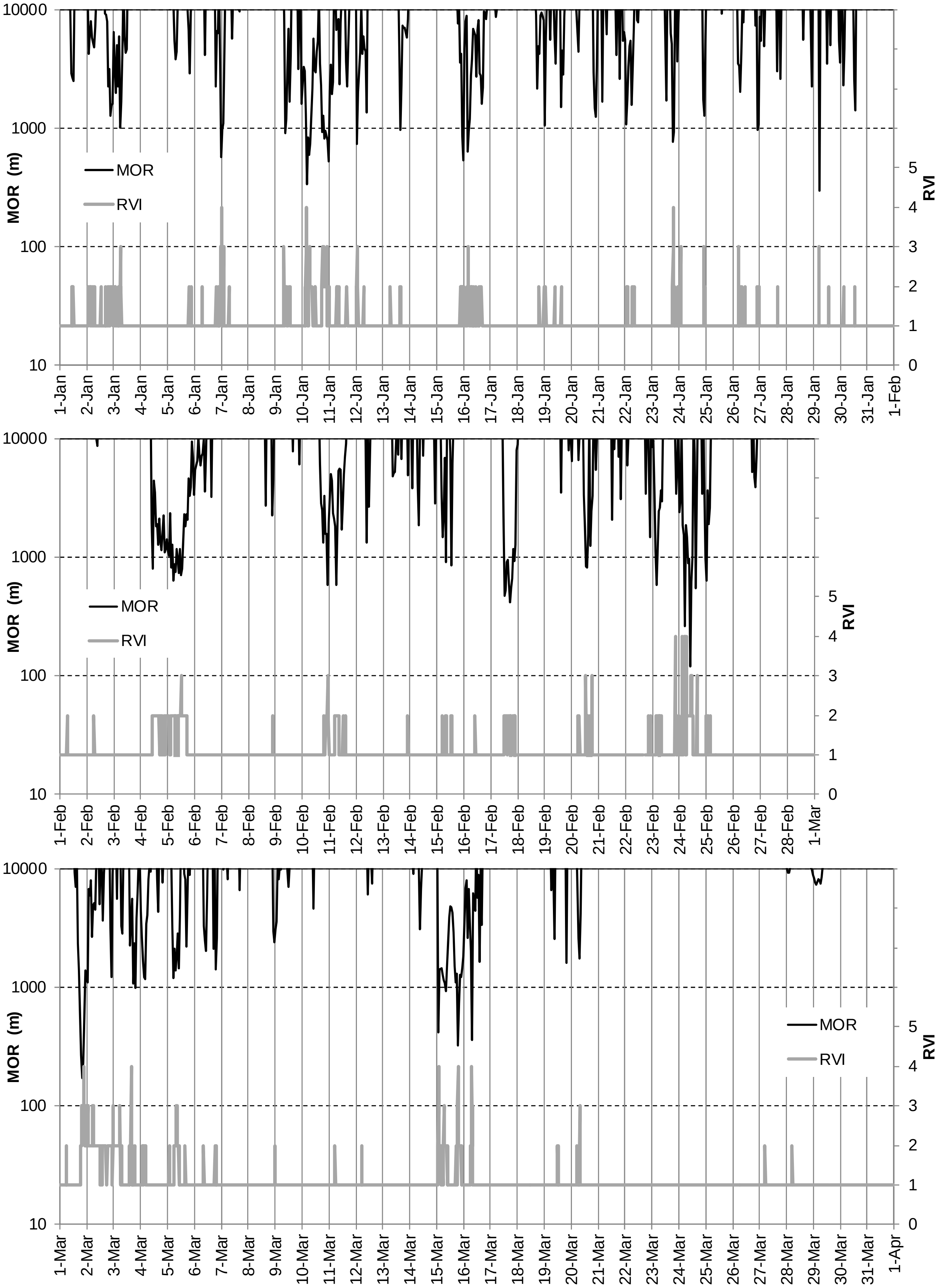

Fig. 2 Changes of value of MOR and value of the RVI.

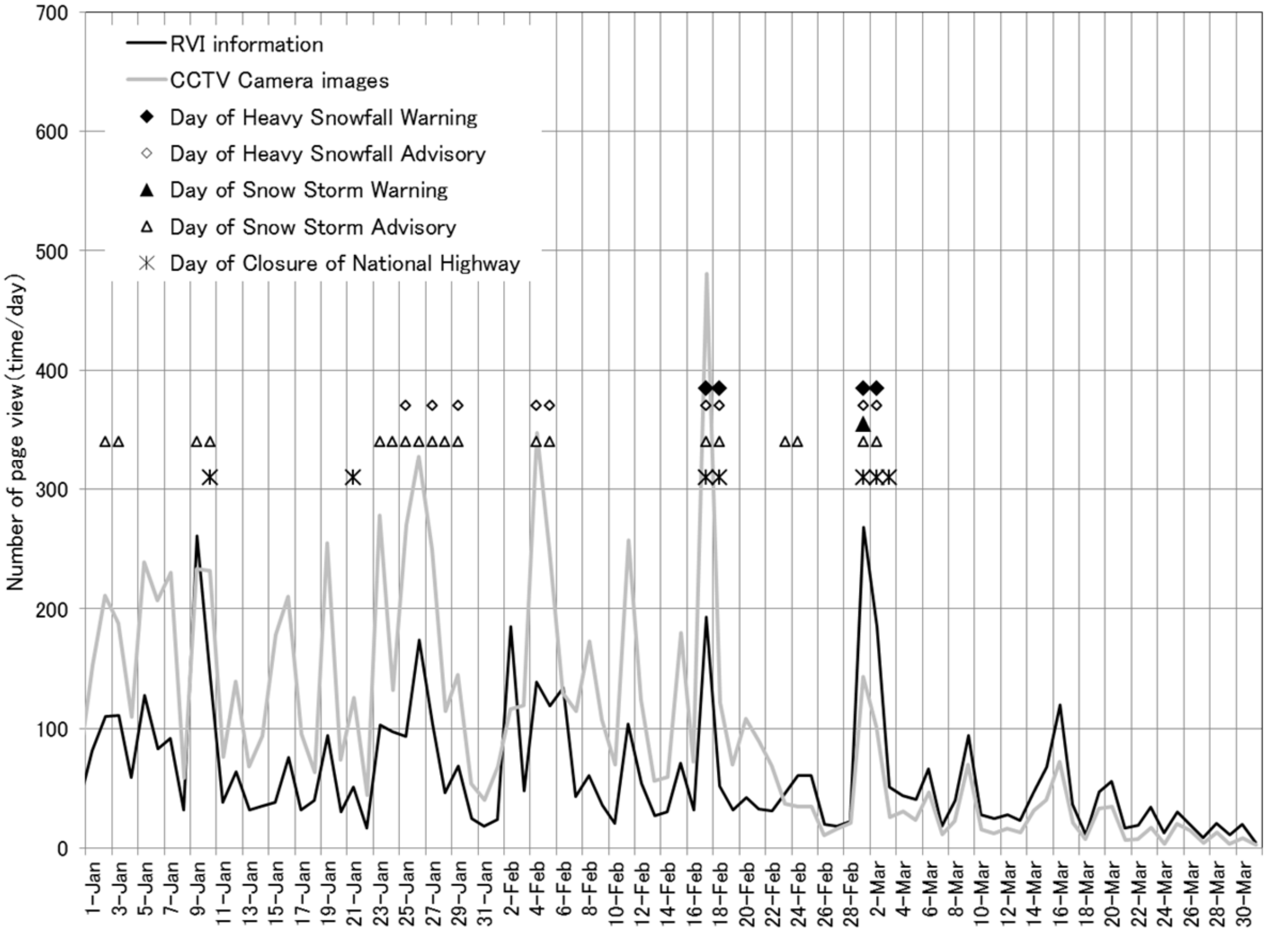

Fig. 3 Number of page view and Weather Condition

Table 2 Comments for Website

Comments	Type of staff
When no weather warning or advisory are issued, I usually viewed only RVI page.	Road administrator
I viewed RVI page first, then checked CCTV camera images at my road station.	Road administrator
Beside my office, for instance at home, I viewed RVI website. At my office, I viewed only CCTV camera videos.	Road administrator
The advantage of RVI page is that visibility information is available immediately.	Road administrator
I viewed RVI page at home or other locations beside the office.	Road maintenance staff
RVI information was useful to decide what to do first: eg. Starting patrol immediately or waiting a while.	Road maintenance staff
RVI page was useful to scan general visibility condition. I used CCTV camera images to see snow cover condition on the road surface other than visibility.	Road maintenance staff
I viewed RVI page through tablet PC at home on a stormy day.	Road maintenance staff
I used RVI page to collect visibility information on site or during the road patrol.	Road maintenance staff

4. Conclusions and Acknowledgements

Through the feasibility study of the road visibility estimation method that had been conducted from January to March, 2018, the image collection system of RVIS could collected 99.9% of still road images provided by CCTV cameras followed by the image quantification system that quantified the images and classified the resulting information to five ranks of RVI. In comparison of the RVI values with MOR value, the visibility monitoring values of weather stations were correlated: when MOR lowered, RVI values also lowered, which meant RVI was properly working.

The feasibility test participants including road administrators and road maintenance staff preferably evaluated RVI information in the points: it enabled users to scan road visibility state even if the telecommunication environment was not good. Recently, CCTV cameras and web cameras can be reasonably purchased and telecommunication technology has greatly advanced, which has enabled countries around the world to install roadside cameras. However, viewing still images provided by many cameras at a glance is quite difficult. Thus a measure to shortly obtain road visibility information is sought. RVIS introduced by this paper enables road users to shortly know general visibility state through RVI information presented on a website. The users do not need to check so many CCTV camera images. RVI which is created by quantifying CCTV cameras' still images will realize efficient road management.

One of the remained issues is the difficulty of RVI production during dark hours as shown in Table 1. Another one is that because threshold values to convert WIPS to RVI are determined on the basis of human evaluations and analyses, manual work is required for initial RVIS settings. RVIS has a potential to be utilized borderlessly around the globe if those issues could be overcome.

5. References

[1] Kajiya, Y., Kaneda, Y., and Tanji, K., “Factors Inducing Multi-vehicular Collisions During Visibility Reduced by Snowstorm”, *In Transportation Research Record: Journal of the Transportation Research Board*, No.1745, TRB, National Research Council, Washington, D.C., 2001, pp. 61-66.

[2] Uemura, T., Matsuda, Y., Kajiya, Y., and Tanji, K.,“User Needs for Road Information in Hokkaido”, *10th World Congress and Exhibition on Intelligent Transport Systems and Services*. CD-ROM. Madrid, 2003.

[3] Hagiwara, T; Kizaka, K; Fujita, S.,“Development of Visibility Assessment Methods with Digital Images under Foggy Conditions”, *In Transportation Research Record: Journal of the Transportation Research Board*, No.1862, TRB, National Research Council, Washington, D.C., 2004, pp. 95-108.

[4] Hagiwara, T; Fujita, S; Kizaka, K., “Assessment of Visibility on Roads under Snow Conditions Using Digital Images”, *In Proceeding of 11th International Road Weather Conference*, 2002.

[5] Chiba, T., Ishimoto, K and Kajiya, Y., “Spatial and Temporal Changes of Visibility in Blowing Snow and Fog”, *In 4th International Symposium on Snow Removal and Ice Control Technology*, TRB, Washington, D.C., 1993.

[6] Kwon, T. K., “Measurement of Motorist’s Relative Visibility Index (MRVI) through Video Images”, *In Transportation Research Board 80th Annual Meeting Final Program*, Washington, D.C., 2001.

[7] Hagiwara, T., Ota, Y., Kaneda, Y., Nagata, Y., Araki, K., “A Method of Processing CCTV Digital Images for Poor Visibility”, *In Transportation Research Board 85th Annual Meeting Final Program*, Washington, D.C., 2006, pp. 140.

[8] Nagata, Y., Hagiwara, T., Kaneda, Y., Araki, K., Murakami, K., “Simple Approach for Using CCTV Road Images to Provide Poor-Visibility Information”, *In Transportation Research Board 85th Annual Meeting Final Program*, Washington, D.C., 2006, pp. 71.

[9] Ginsburg, A.P., “Contrast Sensitivity, Drivers’ Visibility, and Vision Standards”, *In Transportation Research Record: Journal of the Transportation Research Board*, No.1149, TRB, Washington, D.C., 1987, pp. 32-39.

ENERGY - OIL AND GAS

Sustainable Energy for a Secure and Affordable Energy Supply:
An analysis of rural Arctic communities

Magnus de Witt
PhD Student
Reykjavik University
Iceland
magnusw@ru.is

Dr. Hlynur Stefánsson, Reykjavik University, Iceland
Dr. Ágúst Valfells, Reykjavik University, Iceland

Summary

This contribution discusses energy security for rural Arctic communities and the influence of different penetration levels of renewable energy sources. A cost benefit analysis shows how different renewable energy mixtures and penetration levels compete against diesel. Moreover, it is discussed how CO_2 pricing influences the integration of renewables.

Keywords: Energy Security, Sustainable Energy, Energy Transition, Cost Benefit Analysis

1. Introduction

Communities in the Arctic face a harsh and fragile environment (Conde Pérez and Yaneva, 2016; Skinner and Murck, 2011). In this environment human security needs a constant electricity supply (Boute, 2016). Diesel has been the main primary energy source for electricity generation and 80% of the communities exclusively depend on diesel (Bhattarai and Thompson, 2016). Besides the negative impact on the climate the use of diesel has an impact on the mid-term energy security. The short fuel transportation window can create a risk in the fuel supply chain for the next year in the communities (Bhattarai and Thompson, 2016; Canada and Natural Resources Canada, 2013). Harsh Arctic weather conditions heavily influence the transportation window – barges require open sea ways for delivery and trucks need frozen rivers, stable enough to carry them (Bhattarai and Thompson, 2016; Boute, 2016; Canada and Natural Resources Canada, 2013; Pedrasa and Spooner, 2018). The negative climate impacts of diesel arise from its burning. The emitted CO_2 is a well known greenhouse gas and particular matter leads to a special impact in the Arctic – lowering the albedo effect (EPA, 2016). The albedo effect describes the reflection of solar radiation by the white snow - a lowering in reflection increases the melting rate of snow and ice (EPA, 2016). A last point is the noise emitted by the generator, which can have an impact on life quality (McDonald and Pearce, 2013).

Energy security can be classified into short, mid and long-term energy security. Furthermore, energy security can be classified in terms of the supply chain into upstream and downstream energy security. Upstream energy security refers to the security of the supply chain before the electricity generation, such as fuel and spear parts delivery. Downstream energy security refers to the energy distribution system side. The close proximity to the end-user of renewable energy resources can increase the energy security by lowering the impact of the mid-term and upstream energy security. The introduction of local non-dispatchable sustainable resources can trigger a decrease in short-term energy security. Non-dispatchable energy sources can cause fluctuation in voltage and frequency (Hu et al., 2015). This fluctuation can result in transmission system failures (Ahmed et al., 2015). Flywheels can act as a spinning reserve and secure the very short-term energy security - seconds up to a few minutes (Bhattarai and Thompson, 2016; Muhando et al., 2010). To react on longer short-term time horizon - minutes up to hours - several storage or conversion solutions can be used such as battery storage, hydrogen production as storage or fuel for transportation / heating and converting electricity into heat for a district heating system (Murphy et al., 2009; Schaede et al., 2015). This, and a diversification of resources can increase the energy security. If one source brakes away due to a failure the others sources still can provide the basic electricity to secure the electricity supply.

This paper applies a rough cost benefit analysis to compare a set of different solutions and study how renewable energy resources can add value to the energy security. A spreadsheet based model uses cost estimations for the different technical components to calculate the approximate total cost of investment and operation. This gives an indication of a general feasibility of the different solutions to integrate renewables into an isolated grid.

2. Methodology

The methodology section is split into two parts: data gathering and modelling

2.1 Data Gathering

The data for the research was collected through a literature review. The data collection focused on mature technologies, currently available for Arctic micro-grids and the related investment, operation and maintenance cost. The already existing data (secondary data) gives a clear understanding of the costs used for the cost benefit analysis model and reflects the current status of possible solutions (Hague, 2006). Studies in Arctic areas often face a limitation of data availability. Projects in Arctic areas require higher construction costs than in lower latitudes(Baring-Gould and Corbus, 2007). This relates to the remoteness, missing infrastructure, harsh environment and in some cases permafrost. For example, the construction of a wind turbine in the Arctic is 2 – 3 times more expensive than in southern areas (Baring-Gould and Corbus, 2007). The upper end of the cost range was chosen here in absence of specific costs for Arctic areas, to take into account for the extra expenses of projects in the Arctic. An overview of the collected data is in Table 1.

Table 1: Main Data Collected for the Cost-Benefit Analysis

Name	Value	Unit	Source
Diesel price	0,85	$/Liter	(KNI, 2018)
Capacity factor Diesel generator	0,28	%	(Kasper, 2018)
Fuel Consumption	0,25	l/kWh	(Kasper, 2018)
CO_2 price	20	$/t	(Finanzen.net, 2019)
min. price ES	10	$/kWh	Selected
current time of outage	0,5	hours	(Kasper, 2018; Michael, 2018)
Installation cost Hydro	6.500	$/kW	(Tester, 2012)
Installation cost Wind	3.000	$/kW	(Baring-Gould and Corbus, 2007; Tester, 2012)
Installation cost Solar	4.000	$/kW	(Tester, 2012)
O&M Diesel	0,02	$/kWh	(HOMER, 2018)
O&M Solar	12	$/kW	(Andy Walker, 2017)
O&M Hydro	2,5	%	(IEA, 2010)
O&M Wind	3	%	(Wind Energy the Facts, n.d.)

2.2 Modelling

For the cost benefit analysis a simple spreadsheet model was set up. The simulation considers a lifetime of 20 years, which was chosen according to the shortest expected lifetime of generation technology. Solar PV cells reach a lifetime of approximately 20 years. Other technologies have a longer lifetime. The technology options must sustain the harsh Arctic environmental conditions; a detailed analysis is in section Analysis. Electricity generation with 100% diesel was used as a base case for the simulation and very often represents the current electricity mix since it is the situation in 80% of the Arctic communities. Renewables like wind and solar cells can be used in a mix together with diesel, such a system is referred to as a hybrid system (Boute, 2016; WWF, 2017). Diesel generators can handle different penetration levels of renewables with different extend of regulation equipment (Muhando et al., 2010). This ability of diesel is needed if non-dispatchable energy resources like wind, and solar cells are used. Their performance fluctuates, which leads to instability. Figure 1 shows the different penetration levels. Defined scenarios were done in accordance with the penetration levels. For all penetration levels different mixtures of energy sources have been assumed; each assumption was a scenario.

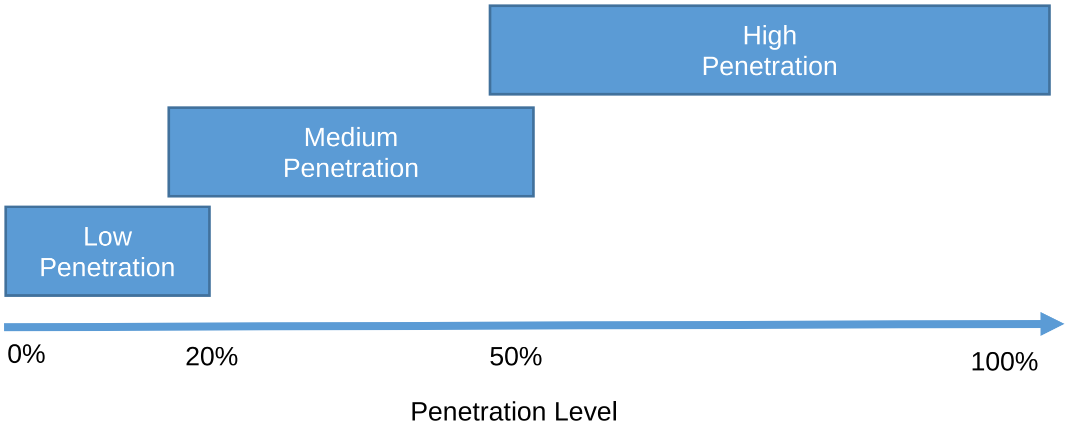

Figure 1: Penetration Levels

To encounter for the cost resulting from a lack of energy security, the value of lost load (VoLL) is calculated. The VoLL takes the economic and private loss to the society into account (Anderson et al., 2018; Schröder and Kuckshinrichs, 2015). The actual value contains a multiplication of the VoLL by the average black out duration and the changed likelihood due to technology changes. The likelihood of technology changes takes the comparison matrix as a basis, Figure 2. The total scenario cost is the sum inflation adjusted net present value over the scenario lifespan.

3. Analysis

	Hydro	Wind	PV	Tidal	Biomass	Factor
Hydro		1	1	1	1	1,00
Wind	0		1	1	1	1,25
PV	0	0		1	1	1,50
Tidal	0	0	0		1	1,75
Biomass	0	0	0	0		2,00

Figure 2: Comparison matrix of generation technologies
The matrix compares each technology with each other.
The lower the factor the securer the technology is rated

To figure out which renewable energy sources and technologies are the most feasible for arctic communities we first do an internal ranking as shown in the comparison matrix in Figure 2. The comparison matrix shows the comparison of pairs of technologies based on their security. The assumption is that the VoLL is a lower-medium value, grounds on the low value creation per kilowatt hour in the Arctic (Röpke, 2013). For longer electricity supply interruptions, the consequences can lead to severe damages on infrastructure like bursting of waterpipes and no heating (Michael, 2018). This life-threatening circumstance can add more value to VoLL. Since a long duration blackout is unlikely to happen the VoLL was slightly increased to a medium value.

3.1 Technologies

Hydropower is a mature technology with a low failure rate (Edenhofer et al., 2012; Tester, 2012). The water reservoir provides a local energy source. A dispatchable energy resource like hydropower can be a stable source of electricity to the grid. The electricity generation can be easily adjusted to the needed electricity demand (Tester, 2012).
A non-dispatchable energy resource such as wind cannot be regulated in terms of output performance (Baring-Gould and Corbus, 2007; Tester, 2012). Furthermore, wind power might require additional technology to stabilize the grid if the penetration is above 20%.
PV as a non-dispatchable energy resource is not a stable source of electricity either and similar to wind in that sense (Tester, 2012). In addition PV shows a seasonal energy distribution with high generation potential during the summer and nearly none during the winter time (Schwabe, 2016; Wu et al., 2017).
Tidal Power in the Arctic is not a mature solution yet and the risk of damages to the infrastructure by icebergs and drift ice is considerable.
Biomass technology is mature, but there is a lack of available sustainable bio resources in the Arctic. Biomass growth is barely available above the tree line in the Arctic (NSIDC, 2019), which makes a local and sustainable biomass use impossible. Imported biomass is an option to diesel but the upstream energy security issues remains.
Geothermal was not further elaborated, because of limited access among the Arctic – at the Arctic Pacific coast line and Iceland (IRENA, 2017; Sanyal, 2010). Geothermal has proven a very reliable energy source in the sub-Arctic conditions of Iceland (Georgsson and Fridleifsson, 2014).

3.2 Cost of CO_2

Two different ways can measure the CO_2 cost: the market value and the cost of harvesting CO_2 out of the air. The CO_2 market value represents the CO_2 certificates value at the stock exchanges - for the European certificate a price of approximately 20 $ per ton (Finanzen.net, 2019). In contrast to this carbon capturing creates much higher costs with approximately 1.000 $ per ton (Tester, 2012). In this case the market value was chosen for the simulation because that is the saving companies can make in hard currency. The CO_2 certificates price is expected to rise in future. Recently, several countries announced that they will not reach the targeted CO_2 reduction. For example, Germany wanted to save 40% CO_2 by 2020 but a current forecast estimates a saving of 32% by 2020 ("Deutschland versagt beim Klimaschutz," 2019). The CO_2 cost might act as a policy leverage to increase the CO_2 reduction.

4. Results and Discussion

Hydro power plays a critical role in providing sustainable electricity to Arctic communities. Especially if the community should mainly use renewables, high penetration scenarios as in Figure 3 are required. For all penetration levels hydro power breaks even with diesel at the end of the analysed time period, 20 years. In the scenarios a cost per kW installed capacity of 6.500 $ was assumed for hydro power plant below 20 MW (Tester, 2012). The upper end of the Tester estimation has proven right compared with the actual numbers from Nukissiorfiit at the Buksefjord project (Nukissiorfiit, 2018). A price below 6.000 $/kW or even 5.500 $/kW would help to make hydro power more affordable for smaller communities.

The introduction of renewables is heavily influenced by the cost of the CO_2 as shown in Figure . An increase of CO_2 prices leads to a severe reduction of the payback period. In case of a medium renewable penetration it is 6 years - calculated with an increase of 20 $/ton up to 100 $/ton for CO_2. For a high penetration it is around 5,5 years and for a low penetration case 4 years. This show that CO_2 pricing is a very useful tool for policy makers to support the energy transition. Moreover, the raised money can be used to help communities to cover the high initial upfront cost.

A low-level penetration shown in Figure of around 20% renewable shows that non-dispatchable energy sources can provide a feasible option to introduce renewables into the grid. The diesel generator can secure the grid stability (Muhando et al., 2010). Moreover, the diesel generators spare capacity can cover up for fluctuation in supply by non-dispatchable sources. Non-dispatchable energy sources need around 7 – 8 years for payback. The difference between solar and wind is very similar on the cost side. The installation of a hydro power plant requires an essential investment. Over the analysed period of 20 years the cost of hydro power is the same as diesel. The expected lifetime of 50 years or even longer can make it feasible. Renewables have a low cost during the operation time which gives them an advantage. Just operation, maintenance and electricity security cost are generated after the installation. Diesel has additional costs of fuel and emission. This analysis does not take into account replacement cost, because for the newly added renewables it is within the lifetime span. Since the diesel generators are assumed to be in place already they can create additional replacement costs in the observed timeframe.

Medium penetration shown in Figure , can be seen critically. The payback period is not significantly shorter compared to a high penetration level. On the investment side a medium penetration is not proportionally cheaper than a high penetration level. The problem of medium penetration is that the upstream energy security is not solved - fuel still has to be imported and just the amount decreases. On the downstream energy security side, the renewables have some added risks.
In case of a medium or high renewable penetration it is advisable to have a dispatchable energy source for the baseload and add to this non-dispatchable energy resources. In Figure an example for high penetration with a small diesel generator, wind turbines and a battery storage is shown. The case was created and checked with the simulation software HOMER. This case shows that it is not cost competitive (green line in Figure). To provide enough energy with wind turbines the installed capacity has to be much higher than in case of a dispatchable energy source. The installed wind capacity was 5-times higher than in the 100% diesel case.
All high and medium cases have hydropower as base load. The non-dispatchable fraction reduces the payback slightly compared to just hydro power for the renewable fraction. The orange and grey line in Figure 4 or orange compared to the grey and yellow line in Figure .

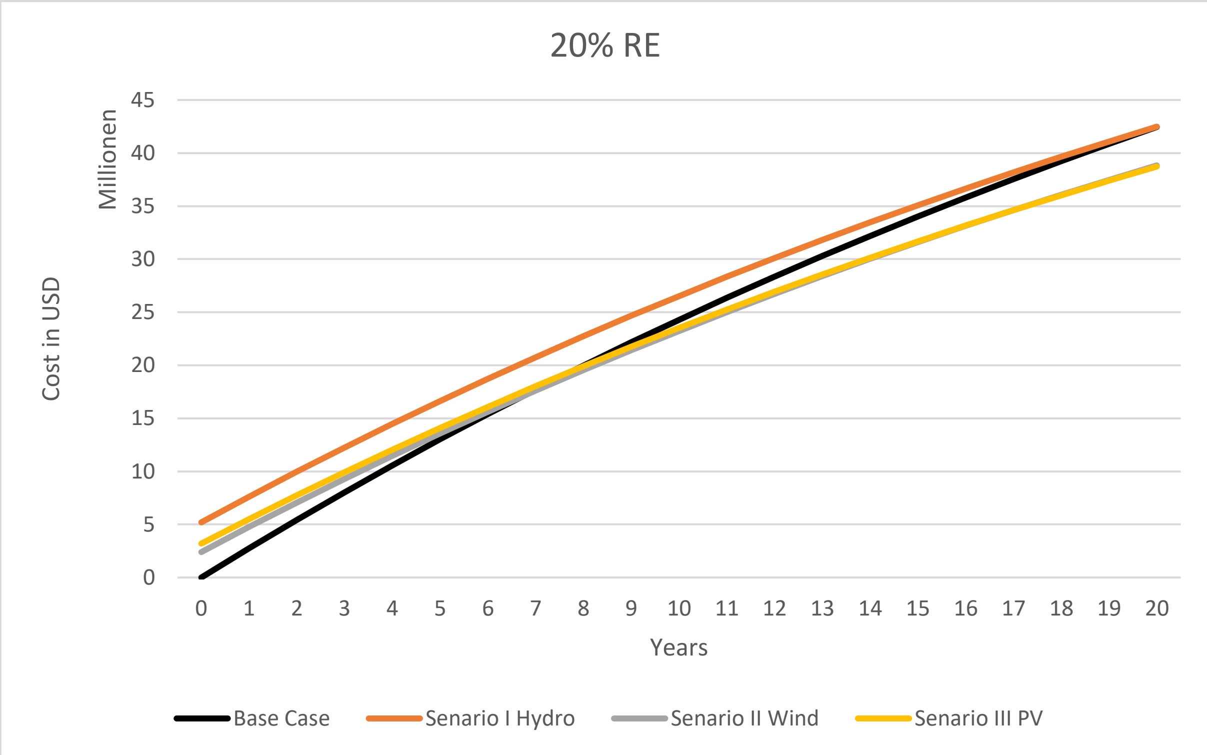

Figure 3: 20% Renewable Scenario

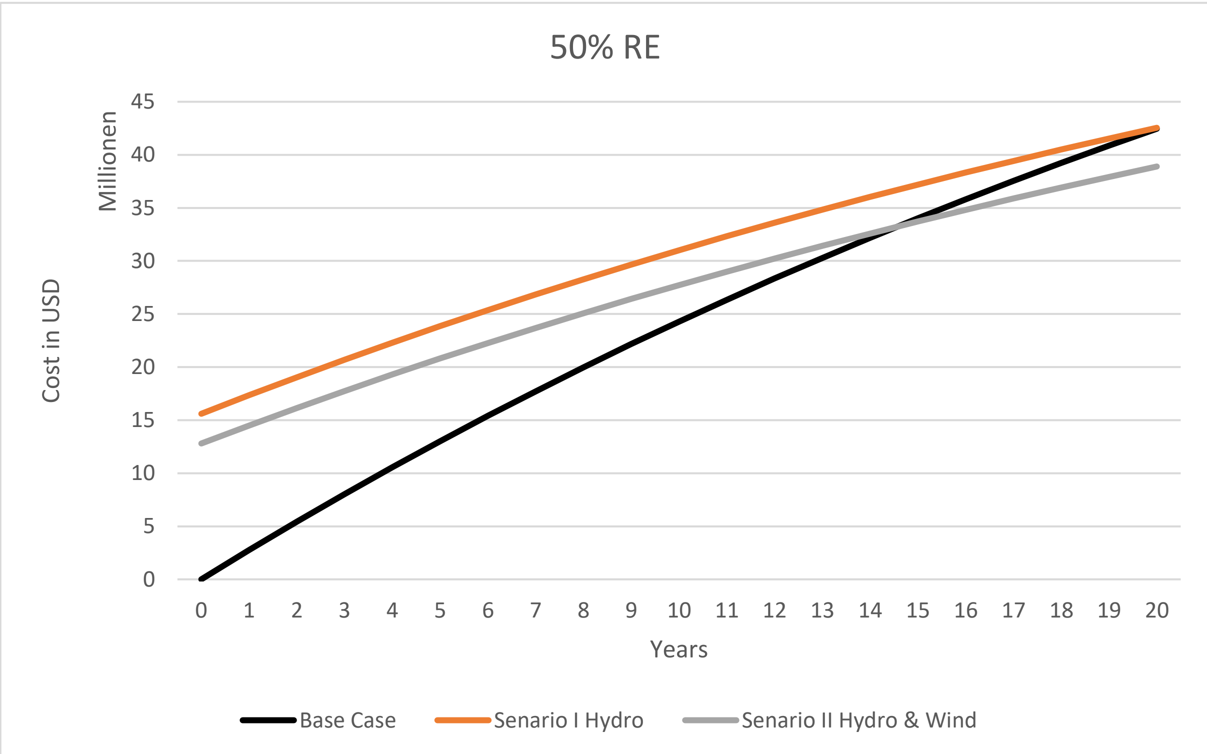

Figure 4: 50% Renewable Scenario

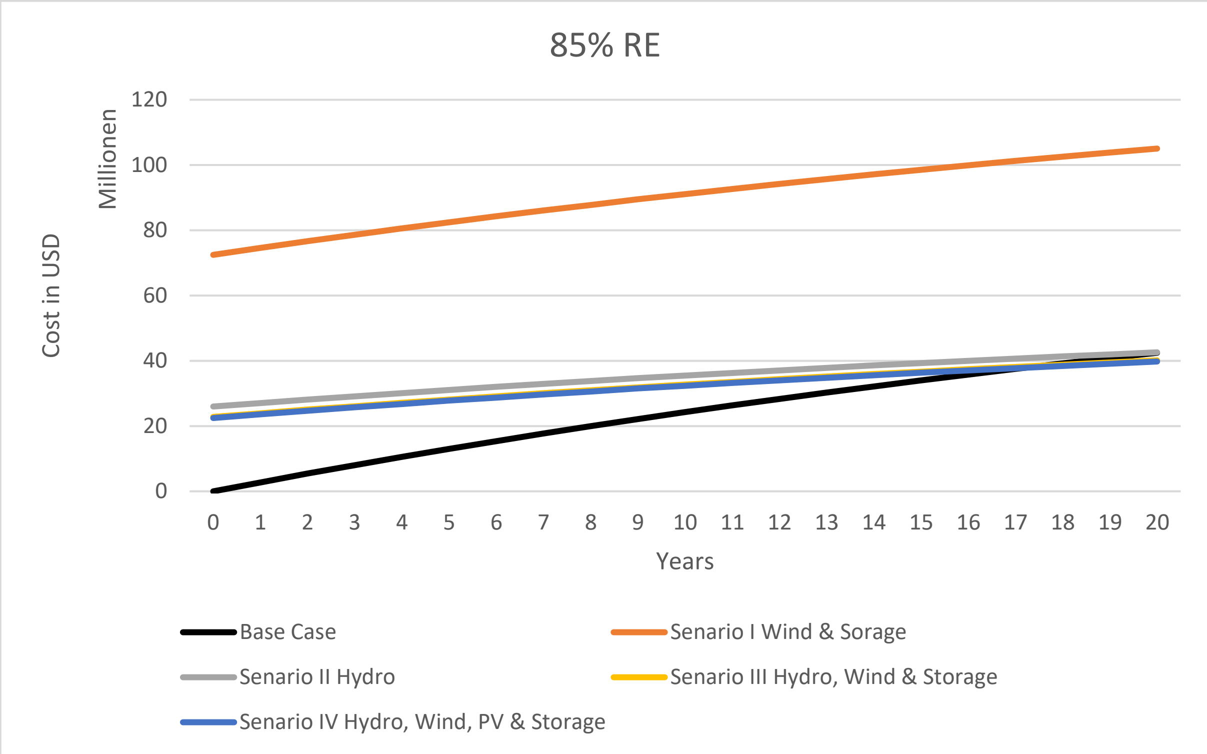

Figure 5: 85% Renewable Scenario

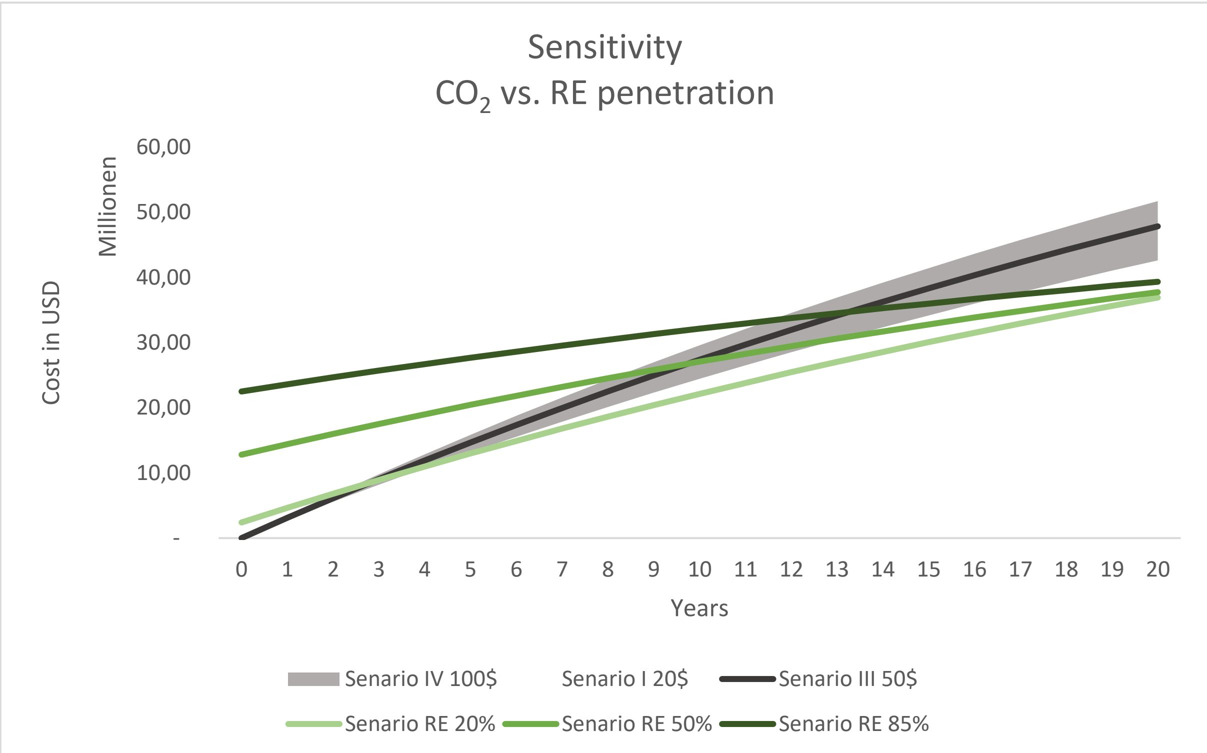

Figure 6: Sensitivity Analysis CO_2 vs. Renewable Penetration

5. Conclusion

Several technologies were examined in the study and it was shown that they have already reached a cost competitive level, but further development can improve the technologies available and lower the price. In a cost benefit analysis, scenarios with different percentages of renewables levels with several mixtures of renewables sources were analysed, as well as the influence of CO_2 pricing on the payback period of investment in renewables.

For a first integration of renewables a low-level penetration is very interesting. The electricity supply can become more secure, and the investment is relatively small and pays back in a short period. On the other hand a high penetration level with a local energy source, which gives energy independency from fossil fuels and reduces the risk of upstream energy security.

The transition process towards renewable energy can have several side effects on the environment. The reduction of fossil fuel usage can increase the local air quality around the generator side. All this leads to an increase in human wellbeing. On the other hand a few negative impacts can be associated with renewables. The technologies require more land use than diesel electricity generation. The land use can have an impact on wildlife, such as reducing grazing grounds, wind turbines can harm birds and hydro power fish migration. For further research on energy security in the Arctic it would be recommended to execute more detailed analysis on the VoLL. It can be assumed that the VoLL indicator in the Arctic differs from the VoLL in southern latitudes. The expectation is that the VoLL changes over the season and duration of the outage. The study shows that technology is available which can provide a secure and sustainable energy source
-051.

6. References

AHMED, M., AMIN, U., AFTAB, S., AHMED, Z., 2015. Integration of Renewable Energy Resources in Microgrid. Energy and Power Engineering 07, 12–29. https://doi.org/10.4236/epe.2015.71002

ANDERSON, K., LAWS, N., MARR, S., LISELL, L., JIMENEZ, T., CASE, T., LI, X., LOHMANN, D., CUTLER, D., 2018. Quantifying and Monetizing Renewable Energy Resiliency. Sustainability 10, 933. https://doi.org/10.3390/su10040933

ANDY WALKER, 2017. PV O&M Cost Model and Cost Reduction.

BARING-GOULD, I., CORBUS, D., 2007. Status of Wind-Diesel Applications in Arctic Climates. NREL, Alaska.

BHATTARAI, P.R., THOMPSON, S., 2016. Optimizing an off-grid electrical system in Brochet, Manitoba, Canada. Renewable and Sustainable Energy Reviews 53, 709–719. https://doi.org/10.1016/j.rser.2015.09.001

BOUTE, A., 2016. Off-grid renewable energy in remote Arctic areas: An analysis of the Russian Far East. Renewable and Sustainable Energy Reviews 59, 1029–1037. https://doi.org/10.1016/j.rser.2016.01.034

CANADA, NATURAL RESOURCES CANADA, 2013. Status of remote/off-grid communities in Canada.

CONDE PÉREZ, E., YANEVA, Z.V., 2016. The European Arctic policy in progress. Polar Science 10, 441–449. https://doi.org/10.1016/j.polar.2016.06.008

Deutschland versagt beim Klimaschutz, 2019. . NTV.

EDENHOFER, O., PICHS MADRUGA, R., SOKONA, Y., United Nations Environment Programme, World Meteorological Organization, Intergovernmental Panel on Climate Change, Potsdam-Institut für Klimafolgenforschung (Eds.), 2012. Renewable energy sources and climate change mitigation: special report of the Intergovernmental Panel on Climate Change. Cambridge University Press, New York.

EPA, 2016. Methane and Black Corbon Impactson the Arctic: Communicating the Science.

FINANZEN.NET, 2019. CO2 European Emission Allowances.

GEORGSSON, L.S., FRIDLEIFSSON, I.B., 2014. Geothermal Energy in the World from an Energy Perspective.

HAGUE, P., 2006. A Practical Guide to Market Research. B2B International.

HOMER, 2018. Diesel O&M costs.

HU, J., ZHANG, T., DU, S., ZHAO, Y., 2015. An Overview on Analysis and Control of Micro-grid System. International Journal of Control and Automation 8, 65–76. https://doi.org/10.14257/ijca.2015.8.6.08

IEA, 2010. Hydropower.

IRENA, 2017. Geothermal Power: Technology Brief. International Renewable Energy Agency, Abu Dhabi.
KASPER, 2018. Electricity Generation Maniitsoq.
KNI, 2018. Brændstofpriserne sænkes 10. marts 2018.
MCDONALD, N.C., PEARCE, J.M., 2013. Community Voices: Perspectives on Renewable Energy in Nunavut. ARCTIC 66. https://doi.org/10.14430/arctic4269
MICHAEL, 2018. Energy Supply in Maniitsoq.
MUHANDO, B., KEITH, K., HOLDMANN, G., 2010. Power Electronics Review - Evaluation of the ability of inverters to stabilize high-penetration wind-diesel systems in diesel-off mode using simulated components in a test bed facility. Alaska Center for Energy and Power.
MURPHY, J., HOLDMANN, G., WITMER, D., 2009. Energy Storage for Alaskan Communities Technology Summary. Fairbanks.
NSIDC, 2019. What is the Arctic?
NUKISSIORFIIT, 2018. VandKraft.
PEDRASA, M.A., SPOONER, T., 2018. A Survey of Techniques Used to Control Microgrid Generation and Storage during Island Operation.
RÖPKE, L., 2013. The development of renewable energies and supply security: A trade-off analysis. Energy Policy 61, 1011–1021. https://doi.org/10.1016/j.enpol.2013.06.015
SANYAL, S.K., 2010. Future of Geothermal Energy, in: Workshop on Geothermal Reservoir Engineering. Presented at the Stanford Geothermal Workshop, Stanford.
SCHAEDE, H., SCHNEIDER, M., VANDERMEER, J., MUELLER-STOFFELS, M., RINDERKNECHT, S., 2015. Development of kinetic Energy Storage Systems for Islanded Grids.
SCHRÖDER, T., KUCKSHINRICHS, W., 2015. Value of Lost Load: An Efficient Economic Indicator for Power Supply Security? A Literature Review. Frontiers in Energy Research 3. https://doi.org/10.3389/fenrg.2015.00055
SCHWABE, P., 2016. Solar Energy Prospecting in Remote Alaska: An Economic Analysis of Solar Photovoltaics in the Last Frontier State (No. NREL/TP--6A20-65834, DOE/IE--0040, 1239239). https://doi.org/10.2172/1239239
SKINNER, B.J., MURCK, B.W., 2011. The blue planet: an introduction to earth system science, 3rd ed. ed. Wiley, Hoboken, NJ.
TESTER, J.W. (Ed.), 2012. Sustainable energy: choosing among options, 2nd ed. ed. MIT Press, Cambridge, MA.
WIND ENERGY THE FACTS, n.d. Operation and Maintenance Costs of Wind Generated Power.
WU, Q., LARSEN, E., HEUSSEN, K., BINDER, H., DOUGLASS, P., 2017. Remote Off-Grid Solutions for Greenland and Denmark: Using smart-grid technologies to ensure secure, reliable energy for island power systems. IEEE Electrification Magazine 5, 64–73. https://doi.org/10.1109/MELE.2017.2685959
WWF, 2017. Renewable energy across the Arctic: Greenland Report. WWF.

Application of brine electrolysis process in enhanced oil recovery

Yahui Zhang
Assistant professor
Memorial University of Newfoundland
Canada
yahuiz@mun.ca

Associate Professor Lesley Anne James, Memorial University of Newfoundland, Canada
Professor Qi Liu, University of Alberta, Canada
Assistant Professor Sohrab Zendehboudi, Memorial University of Newfoundland, Canada

Summary

Usually, 60% to 80% of crude oil remains in reservoir after traditional primary and secondary recoveries. To extract the majority of original oil left, various enhanced oil recovery (EOR) technologies have been developed, which can be categorized into thermal recovery, gas injection, and chemical injection. To take advantages of the chemical properties of the oil reservoir system and combine the merits of developed EOR technologies, a novel brine electrolysis process for EOR is presented. The major products generated in brine electrolysis, i.e., alkalis, H_2 gas and Cl_2 gas, are all very effective for improving oil recovery due to their strong cleaning effects on oil reservoir. The alkalis generated can also help to mitigate the reservoir clogging of high molecular weight and viscous oil components, such as asphaltene. This brine electrolysis process combines the advantages of gas injection and alkali injection. Thermodynamically, a low applied electrical potential can realize the electrolysis process. In areas with sufficient sunshine or wind blow, a solar energy or wind energy powered electrolysis can be employed. The technological issues involved in this new process are easy to realize, which makes it economically viable and environmentally feasible. It will be an effective and promising EOR technology.

Keywords: Enhanced oil recovery (EOR), brine electrolysis, alkali injection, gas injection

1. Introduction

In oil recovery, there are usually three stages of oil extraction. In the primary recovery, oil is extracted either via the natural rise of hydrocarbons to the earth surface, or via pump jacks and other artificial lift devices. For the secondary recovery, it involves the injection of water or gas to displace the oil, force it to move from its resting place and bring it to the surface [1, 2]. Only 20% to 40% of crude oil can be extracted with the combination of primary and secondary recovery [3]. The majority of the original oil is left in reservoir, which needs to be recovered through tertiary recovery, i.e., enhanced oil recovery (EOR). There are currently three categories of primary EOR techniques: thermal recovery, gas injection, and chemical injection. By applying developed EOR technologies, production could reach about 40% to 60% of original oil in the reservoir, which is still very low [4]. Therefore, development of new highly efficient EOR processes is of great significance.

To increase crude oil recovery, decreasing oil viscosity and interfacial tension to improve its mobility is proven to be an effective approach. In thermal injection, various methods, such as cyclic steam injection, steam flooding, solar energy and combustion, are employed to heat the crude oil. As a result, the crude oil expands, its viscosity and surface tension drops, while permeability increases. Generally, these methods improve the oil sweep efficiency and displacement efficiency [5]. Thermal injection accounts for about 40% of EOR production in the United States.

Gas injection or miscible flooding, which uses gases such as natural gas, nitrogen, or carbon dioxide, accounts for nearly 60% of EOR production. It is the most commonly used approach in enhanced oil recovery. Carbon dioxide fluid is usually employed for miscible flooding due to its availability. Miscible flooding process maintains reservoir pressure and improves oil displacement. The gas molecules diffuse and penetrate into the crude oil, resulting in oil expansion, which leads to reduced oil viscosity and interfacial tension between oil and water, and allows for higher displacement efficiency [6].

In chemical injection processes, various chemicals have been used to improve oil mobility and reduce surface tension. Dilute solutions of surfactants such as petroleum sulfonates, or biosurfactants, could be injected to lower the interfacial tension or capillary pressure which impedes oil droplets from moving out of a reservoir [7]. Application of these methods is usually limited by the cost of the chemicals and their adsorption and loss onto the rock. Injection of alkalis, such as sodium hydroxide, can lower the surface tension of oil, reverse the rock wettability, improve the emulsification and mobilization of the oil, and help drawing the oil off the rock. Alkalis can also react with the organic acids naturally occurring in the oil, which will result in the production of soap that are soluble surfactants and can lower the interfacial tension to increase oil production [8]. Surfactants can also be used in conjunction with polymers [9].

Introduction of nanotechnology, i.e., injection of nanoparticle fluid into oil reservoir, is a newly proposed method of chemical enhanced oil recovery (CEOR) [10, 11]. Nano silica particles can reduce the interfacial tension between water and oil, and improve oil recovery. At present, this method is controversial and remains to be proven.

In general, the purposes of the developed EOR techniques are to improve crude oil recovery through the swelling of crude oil to reduce its viscosity and the interfacial tension between water and oil phases, and thus improve oil mobility and displacement, such as thermal injection and gas injection; or just modifying the surface property and behaviour of the oil-water-rock system, such as chemical injection.

2. Brine electrolysis process (BEP)

To extract the majority (60%-80%) of original oil in reservoir left after the primary and secondary recoveries, efforts for developing new effective EOR methods should not be given up. The best EOR process should consider and utilize the physical and chemical properties of the oil reservoir system. In an oil reservoir, the main substances are high viscosity oil, brine, and rock cores. Obviously, the developed thermal injection and gas injection processes are effective for the recovery of oil above the brine surface, while, the chemical injection processes are effective for the recovery of oil beneath the brine surface. Through analysis of the oil reservoir system and the advantages of developed EOR technologies, we present a novel process of brine electrolysis for enhanced oil recovery in this paper.

The brine in an oil reservoir is the water solution of major NaCl, and some KCl, $CaCl_2$ and $MgCl_2$ depending on the geological environment of the reservoir. During brine electrolysis process (BEP), following reaction are involved.

On the cathode, H_2 gas is generated with the reduction of hydrogen ions.

$$2H^+ + 2e = H_2\,(g) \qquad (1)$$

The standard potential of H^+/H_2 electrode E° = 0.0 v

The H+ ions are from the self-ionization of water molecules.

$$H_2O = H^+ + OH^- \qquad (2)$$

About 4% of commercial hydrogen gas is produced by electrolysis.

With the electrodeposition of H^+ ions, OH^- ions are accumulated on the cathode area, and form NaOH with Na^+, which is the industrial process for sodium hydroxide (also called caustic soda) production. Of course, KOH, $Ca(OH)_2$ and $Mg(OH)_2$ are also formed as OH^- ions combine with K^+, Ca^{2+} and Mg^{2+} ions in the brine.

$$Na^+ + OH^- = NaOH \qquad (3)$$

On the anode, the Cl^- ions are oxidized to generate chlorine gas.

$$2Cl^- - 2e = Cl_2\,(g) \qquad (4)$$

The standard potential of Cl_2/Cl^- electrode E° = 1.36 v [12]

Thermodynamically, under standard conditions, an applied potential over 1.36 v will realized the electrolysis process. It can be calculated that, for 3% NaCl solution with pH 6.5, an applied potential over 1.57 v is required for electrolysis. Therefore, the energy cost in the brine electrolysis process is reasonably low. It may even be applied to recover oil from a closed oil well.

The overall reaction of the brine electrolysis process can be summarized as:
$2NaCl + 2H_2O = 2NaOH + H_2\ (g) + Cl_2\ (g)$ (5)
Therefore, the main products obtained from the brine electrolysis are sodium hydroxide NaOH, hydrogen gas H_2 and chlorine gas Cl_2.

The sodium hydroxide NaOH, potassium hydroxide KOH, calcium hydroxide $Ca(OH)_2$ and magnesium hydroxide $Mg(OH)_2$ generated in the electrolysis of brine in oil reservoir can function as alkali injection. The NaOH solution obtained can contain over 0.5% NaOH from brine electrolysis, which is suitable for alkali flooding [8]. The alkali solution can improve the emulsification and mobilization of oil, and help in drawing the oil out of the rock due to its strong peeling off and washing ability to the oil on rock cores. It may even change the rock wettability from oil-wet to water-wet. The alkalis generated can also saponify the organic acids that naturally occur in the oil, which will result in the production of soap that consists of soluble surfactants and can lower the interfacial tension between the oil and water phases to improve oil production. Moreover, they can mitigate the reservoir oil channel clogging of high molecular weight and viscous oil components, such as asphaltene, due to pressure drop. It is known, alkali flooding is a proven high efficiency EOR technology [8]. Apparently, the brine electrolysis process is more economical than the alkali flooding process.

For conventional reservoir with a trap, the H_2 gas generated has strong diffusion ability to crude oil layer due to its smallest molecular size. This will lead to oil volume expansion, and obtain decreased viscosity and improved mobility of oil. The Cl_2 gas generated has similar effects to H_2 gas except their molecular size difference.

Cl_2 gas flowing out may also be absorbed by water on trap roof and pore wall in oil reservoir through the following reaction:
$Cl_2\ (g) + H_2O = HCl\ (aq) + HOCl\ (aq)$ (6)

If the roof rock of trap and the wall of pores contain carbonate minerals, such as calcite $CaCO_3$ and dolomite $CaMg(CO_3)_2$, the acids generated in reaction (6) will corrode the carbonates, which is beneficial to free the oil sticking on trap roof and pore walls and improve oil displacement.
$2HCl\ (aq) + CaCO_3 = CaCl_2 + CO_2\ (g) + H_2O$ (7)
$2HOCl\ (aq) + CaCO_3 = Ca(OCl)_2 + CO_2\ (g) + H_2O$ (8)
$4HCl\ (aq) + CaMg(CO_3)_2 = CaCl_2 + MgCl_2 + 2CO_2\ (g) + 2H_2O$ (9)
$4HOCl\ (aq) + CaMg(CO_3)_2 = Ca(OCl)_2 + Mg(OCl)_2 + 2CO_2\ (g) + 2H_2O$ (10)

Thus, even oil on the trap roof and pore walls may be recovered due to the corrosion of carbonate minerals. Due to the strong caustic properties of chloride-containing acids and chlorine gas, they can still weaken the oil-rock bonding even though the rock walls are not carbonate minerals.

It can be seen that the products of brine electrolysis, i.e., sodium hydroxide NaOH, hydrogen gas H_2 and chlorine gas Cl_2, are all beneficial for improving oil recovery in reservoir. Hydrogen gas H_2 and chlorine gas Cl_2 will function in the form of gas injection to improve the oil recovery on trap roof and pore walls, and sodium hydroxide NaOH will function in the form of alkali injection. They all have strong cleaning effects on oil reservoir. The brine electrolysis process integrates the effects of gas injection and alkali flooding. It is more economical and effective than the proven alkali flooding process, and will surely play a significant role in crude oil recovery.

While, the absorption of Cl_2 gas by water in the brine, is not desired. Same reaction as described in reaction (6) will occur. The generated chloric acid HCl (aq) and hypochlorous acid HOCl (aq) will react instantly with the NaOH produced in cathode through the unwanted reactions:
$HCl\ (aq) + NaOH(aq) = NaCl + H_2O$ (11)
$HOCl\ (aq) + NaOH(aq) = NaOCl + H_2O$ (12)

The overall reaction involved in reactions (6), (11) and (12) can be expressed as:

Cl_2 (g) + 2NaOH(aq) = NaCl + NaOCl + H_2O (13)

The chemical reactions involved with the generated Cl_2 gas and alkalis are all instant reactions. Therefore, the functions and reactions involved with Cl_2 gas and alkalis are mainly depend on the environmental and kinetic conditions around. Obvious, reaction (13) occurring in the reservoir brine will lower the electricity efficiency of the electrolysis process. Therefore, the efficiency of the process will be mainly affected by the flowing out rate of Cl_2 gas from the brine. To prevent the Cl_2 gas generated from the anode to react with the NaOH solution produced in cathode, i.e., to let Cl_2 gas escape from the brine with high efficiency, several factors should be considered in the design of the electrolysis system. Firstly, the working area of anode should be close to brine surface. Secondly, the anode and cathode should be separate at a suitable distance to suppress the reaction (13).

The design of brine electrolysis system can refer to the commercial production process of Cl_2 gas by electrolysis, such as diaphragm cell electrolysis process and membrane cell electrolysis process, which are mature and proven effective. In areas with sufficient sunshine or wind blow, a solar energy or wind energy powered electrolysis cell can be used [13].

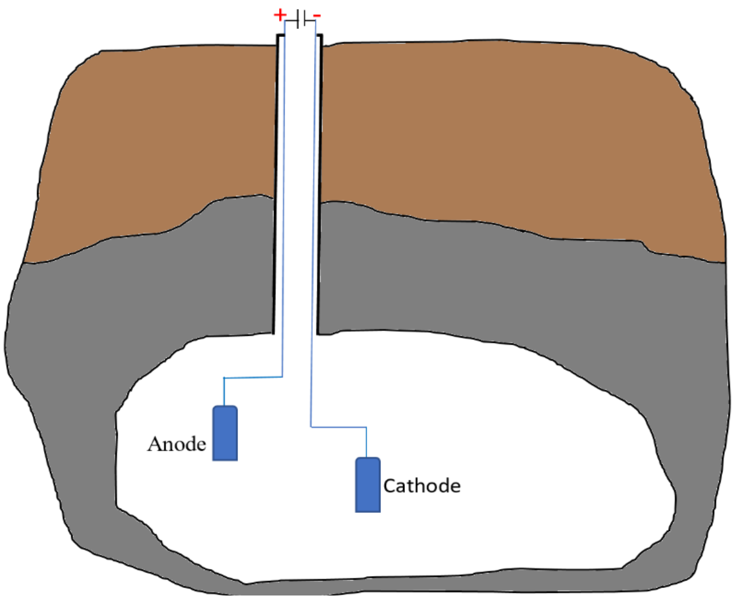

Fig. 1. Schematic diagram of brine electrolysis system for enhanced oil recovery (not to scale)

For conventional reservoirs with a trap, the brine electrolysis system can be set up as illustrated in Fig. 1. The system should be sealed to prevent the escaping of Cl_2 and H_2 gas to ground surface for operation safety and better efficiency. In practical operation, to maintain the required reservoir pressure and chloride salt supply, seawater or artificial brine can be pumped into the reservoir for enhanced oil recovery.

For an unconventional reservoir without a trap, the temperature can be above 200℃ and the pressure can be over 300 atm due to the depth of sea water and geopressure. In this case, gas injection is not feasible as the gas will be liquefied under such high pressures. Therefore, for unconventional reservoir, the brine electrolysis system can be set up outside the reservoir. Only the produced NaOH solution (containing over 0.5% NaOH from brine electrolysis) will be used for alkali flooding. The H_2 gas and Cl_2 gas produced in the BEP can be collected as by-products.

As brine (NaCl solution) electrolysis is a mature industrial process for NaOH and Chlorine Cl_2 gas production, the technological issues involved in the new process are simple, and easy to realize. The products obtained from brine electrolysis are all common chemicals, which make the process is environmentally feasible. All these advantages demonstrate that the brine electrolysis process will be a highly effective and promising EOR technology.

3. Conclusions

Only about 40% to 60% of the crude oil in a reservoir can be recovered even by applying currently developed EOR technologies. Therefore, development of new highly efficient EOR processes is imperative and of great significance for sufficient exploitation of limited oil resources. Through analysis of the oil reservoir system and the advantages of developed EOR technologies, we present a novel brine electrolysis process for enhanced oil recovery.

The main products of brine electrolysis are sodium hydroxide NaOH, hydrogen gas H_2 and chlorine gas Cl_2. They are all beneficial for improving oil recovery in reservoir, and have strong cleaning effects on oil reservoir. This brine electrolysis process combines the advantages of gas injection and chemical injection (alkali injection).

It can be calculated that an applied potential over 1.57 v will realized the electrolysis for 3% NaCl solution with pH 6.5. In areas with sufficient sunshine or wind blow, a solar energy or wind energy powered electrolysis can be employed. It is more economical and effective than the proven high efficiency alkali flooding process, and will play a significant role in crude oil recovery. Due to its low economic cost, it may even be applied to recover oil from a closed oil well.

The characteristic of the brine electrolysis process is that the chemical properties of the reservoir brine and its electrolysis products are considered and fully employed.

To obtain high efficiency of the brine electrolysis process, the design of reasonable electrolysis system is important.

References

[1] WALSH M.P., and LARRY W.L., "*A generalized approach to primary hydrocarbon recovery*", Boston, Elsevier Science, 2003.

[2] SMITH C.R., "*Mechanics of secondary oil recovery*", New York, Reinhold Publishing Corporation, 1966.

[3] Wikipedia, "*Enhanced oil recovery*", https://en.wikipedia.org/wiki/Enhanced_oil_recovery, 2019-01-16.

[4] ABUBAKER H.A., ZULKEFLI B.Y., and ABDURAHMAN H.N., "An Overview of Oil Production Stages: Enhanced Oil Recovery Techniques and Nitrogen Injection", *International Journal of Environmental Science and Development*, Vol. 6, No. 9, 2015, pp. 693-701.

[5] BYBEE K., "Forty Years of Steam Injection in California: The Evolution of Heat Management", *Journal of Petroleum Technology*, Vol. 56, No.1, 2004, pp. 47-48.

[6] MUNGAN N., "Carbon Dioxide Flooding Fundamentals", *Journal of Canadian Petroleum Technology*, No. 1, 1981, pp. 87–92.

[7] BANAT I.M., "Biosurfactants Production and Possible Uses in Microbial Enhanced Oil Recovery and Oil Pollution Remediation: A Review", *Bioresource Technology*, Vol. 51, No.1, 1995, pp. 1-12.

[8] MOHAMMAD H.S., ARASH A., MORTEZA K., and ZIBA B., "Aspects of Alkaline Flooding: Oil Recovery Improvement and Displacement Mechanisms", *Middle-East Journal of Scientific Research*, Vol. 18, No. 2, 2013, pp. 258-263.

[9] HAKIKI F., MAHARSI D.A., and MARHAENDRAJANA T., "Surfactant-Polymer Core Flood Simulation and Uncertainty Analysis Derived from Laboratory Study", *Journal of Engineering and Technological Sciences*, Vol. 47, No. 6, 2016, pp. 706-725.

[10] CHERAGHIAN G., and HENDRANINGRAT L., "A Review on Applications of Nanotechnology in the Enhanced Oil Recovery Part A: Effects of Nanoparticles on Interfacial Tension", *International Nano Letters*, Vol. 6, No.2, 2016, pp. 129–138.

[11] CHERAGHIAN G., Nezhad S.S.K., Kamari M., et al, "Adsorption Polymer on Reservoir Rock and Role of the Nanoparticles, Clay and SiO_2", *International Nano Letters*, Vol. 4, No. 3, 2014, pp. 1-8.

[12] PETER A., "*Physical chemistry*", 6th edition, New York, W.H. Freeman and Company, 1997.

[13] AHMAD W.A.O., and Abdelmaged A., "Production of Caustic Soda Using Solar Powered Diaphragm Cells", *IOSR Journal of Applied Chemistry*, Vol. 8, No. 2, 2015, pp. 9-16.

Simulating oil spill accidents with OpenDrift: cases of the Barents and Kara seas

Victor Pavlov
PhD candidate in Environmental Engineering
University of Oulu
Finland
victor.pavlov@oulu.fi

Prof. Eva Pongrácz, University of Oulu, Oulu, Finland
Assoc. Prof. Henrikki Liimatainen, University of Oulu, Oulu, Finland

Summary

The importance of the Arctic has increased because of geopolitical, economic, environmental, and transport issues, and the Arctic region has turned from the world's periphery into a centre of global attention. In perspective of risks attributed to Arctic Ocean oil spills, which are more likely to happen due to increased oil exploration activities and rise of maritime traffic, it is crucial to improve preparedness level for possible accidents.

Oil spill response (OSR) as such is not an easy process to execute, especially in the cold marine environment. It involves a great number of organizational and practical matters to deal with. From this point of view, it is also interesting to see hypothetically how oil slicks can behave in Arctic marine environments, what direction it can spread and what can be the potential damage to the local environment and the economy.

OpenDrift trajectory modelling framework makes it possible to predict oil pathways and weathering in probable spill accident scenarios, even in ice infested waters. Two Arctic seas were chosen in particular for this study: the Barents and Kara seas. Both are located along northern sea routes connecting Europe and Asia. After simulating two hypothetical scenarios of Marine Diesel Oil spills with recent conditions, May 2019, by taking account the ocean and weather conditions data, the following results were reported:

- in case of both spills, the oil drift was prevalently going towards south-west direction;
- Kara Sea weathered slick ended up stranding on the south-east coast of Novaya Zemlya as well as on floating ice blocks of high density;
- Barents Sea accident resulted in offshore marine contamination in ice free waters
- ecological damages may be possible for Beluga distribution area in the Barents Sea, Murre bird colonies in the Kara Sea, and some fish species in both seas;
- after 10-day simulations and generated oil budget graphs, domineering weathering processes of oil were mostly evaporation and dispersion.

As a recommendation, further research is still needed to test the chosen marine environments in the specified locations in different year seasons and with different types of oil. Studying other locations along the popular maritime traffic routes is also recommended. It is also recommended to develop an assessment tool for estimating potential impacts of such accidents in terms of their economic, environmental and social impacts.

Keywords: Arctic oil spill response, OpenDrift, oil drift, trajectory modelling, marine environment

1. Introduction

Accidental oil spills at sea have a long history worldwide. Since being a publicly recognized problem in the second half of the 20th century, oil and oil products, as a marine pollutant, still continue to occur in the world's oceans and seas [1]. Currently, there is a greater chance for oil spills to happen in Arctic seas. Within a recent map built by Centre for High North Logistics, the busiest marine traffic areas along the Northern Sea Route (NSR) can be noted (Fig. 1). The map shows all types of vessels at the seas.

Fig. 1 Shipping traffic of all vessels along the Northern Sea Route (NSR) in 2016

The importance of the Arctic has increased because of geopolitical, economic, environmental, and transport issues, and the Arctic region has turned from the world's periphery into a centre of global attention. In perspective of risks attributed to Arctic Ocean oil spills, which are more likely to happen due to increased oil exploration activities and rise of maritime traffic, it is crucial to improve preparedness level for possible accidents. The Barents or Kara seas are examples of maritime areas with such risks in the Arctic. [2] Growing exploration and exploitation of oil or gas resources and projected increase in Arctic shipping activities along northern sea routes explain those risks. [3-7]

Since present level of oil spill response (OSR) preparedness cannot guarantee efficient operations, bringing awareness to the problem is of adequate relevance. Two cases of hypothetical oil spill accidents at sea were considered in this study with help of OpenDrift. OpenDrift is an open access modelling tool for simulating movement of objects in ocean and atmosphere. In case of this paper, it is ocean trajectory modelling of objects. Among possible objects may be microplastics, ichthyoplankton and oil slicks suspended in the marine environment. Drifting bodies in survival suits or without it are also possible to model. However, the focus of this study was to simulate only oil spill transformation, and its slick pathway visualisation. The visualisation helps to track oil changes in time and space, and make relevant general conclusions about possible mitigation tools and clean up strategies as well as environmental or other related impacts in sea areas. The core of the tool is Lagrangian particle model module, which helps to simulate oil spills as a set of millions of particles in movement. The model works with oceanographic and atmospheric data. OpenDrift is in daily operational use for emergency response and preparedness at Norwegian authorities. [8]

The main goals of the work with application of OpenDrift were to: i) simulate two hypothetical cases of an oil spill accident in the Barents and the Kara seas, ii) describe character of oil behaviour in water as well as possible general impacts to marine ecosystems, natural protected areas as well as sea dependent industries and economic activities, and summarize the major results and provide further research recommendations.

2. Methodology

Two hypothetical oil spill accidents have the following locations. One is in the Barents Sea at 74.13º N and 46.93º E; while the other – in the Kara Sea at 71.61º N and 58.71º E as shown in Fig. 2.

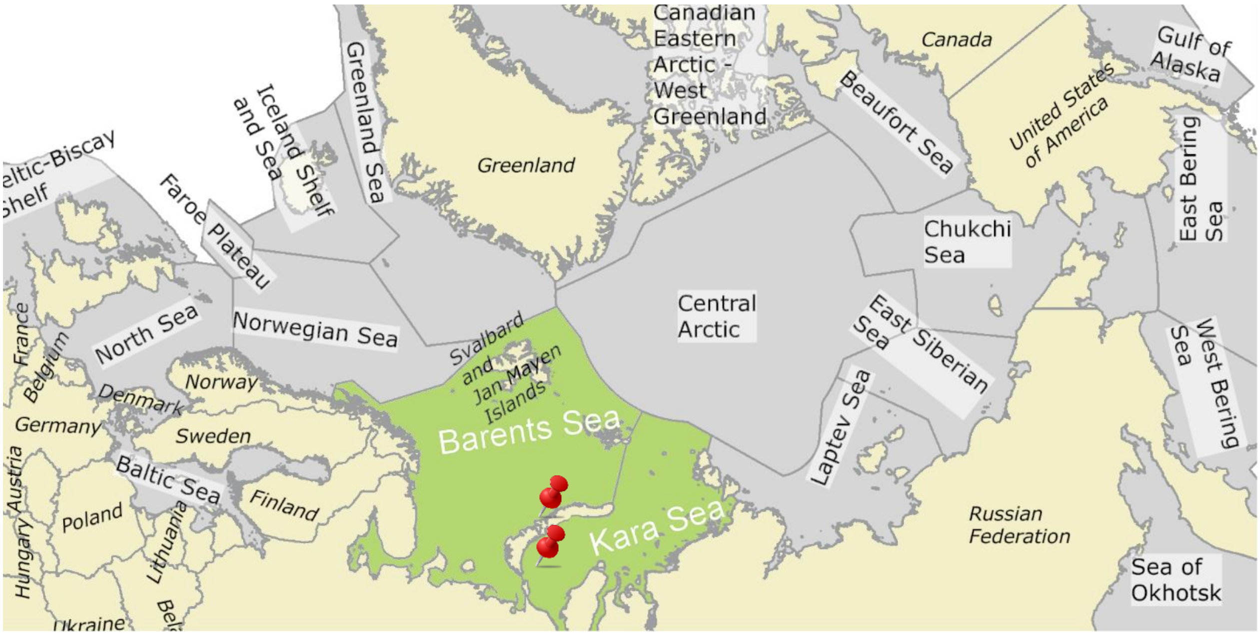

Fig. 2 Barents and Kara Sea: location of hypothetical site of accident

Both locations lie within popular maritime traffic routes, as illustrated in Fig. 1. One location is along the route, which is north round of Novaya Zemlya. The other goes along the route through the Kara Straight. Each location has an accident with one agreed oil type – marine diesel oil, Esso, with density of 851.1 kg/m^3. The amount of oil was set to be 1, 000 t. An example of ship carrying 1, 000 t of marine diesel oil may be a transit bulk carrier, similar to ice class Nordic Olympus. One consideration was to place both accident sites reasonably far from nearest OSR centers (Murmansk, Archangelsk, Naryan-Mar, Vorkuta – all located in north of Russia along the NSR to simulate challenging response operational conditions. Such distance to accident sites would mean the reaction time of marine fleet to be several days. The year season was chosen to be Spring – i.e. May, which is a transitional period with decreasing ice density after the winter season. As mentioned in EPPR report, July to October are the months of the year, when the Arctic Ocean is covered with the least amount of ice, including both the Kara Sea. The Barents Sea is usually free of ice due to influence of warm Atlantic Ocean currents – i.e. Gulf Stream. January to April, it is vice versa, the ocean is full of ice. November to December is also a transitional period with increasing ice density in the marine environment. [9] Duration of spills were set to be 10 days: May 20th-30th, 2019. Despite its recency, the oceanographic and related weather data sets were available. Time of start and end of the simulations was defined as noon – 12.00 p.m.

As a modelling tool for oil spill drifting, OpenDrift was used and in particular its sub-module OpenOil. It is linked with a library of over 1,000 oils and their properties, developed by the National Oceanic and Atmospheric Administration (NOAA), Office of Response and Restoration (ORR), Emergency Response Division. The tool is available open access and is based on knowledge of Python programming language. Once it is installed on computer, it is possible to input data with Python supporting software with direct edition of programme script, or via a simplified version of adjustable graphical user interface. The input data is provided in a summary in Table 1.

Table 1 Input data for OpenDrift simulated cases

OpenDrift input data	Values
Coordinates of the locations	Barents Sea: lat 74.13, lon 46.93 Kara Sea: lat 71.61, lon 58.71
Oil amount, t	1, 000
Oil type	marine diesel, Esso
Start release	May 20th 2019
End release	May 30th 2019
Radius, m	1

The tool is based on Lagrangian particle module, and works by simulating movement of thousands of individual particles. This can be seen in Fig. 5 and 6. The radius of 1 m means that the diameter of spill source: e.g. leaking from damaged ship hull.

3. Results and discussion

As a result of oil drift modelling, the following images were generated. Fig. 3 illustrates the scenario of oil spill accident in the Barents Sea, whereas Fig. 4 – the one in the Kara Sea.

Barents Sea. During the period of May, 20th - May, 30th, the following value ranges were reported: temperature – from -3 to +1 °C, wave height – 0.3÷1.5 m, wind speed – 2÷32 km/h, and wind direction – south-southwest. This case showed prevalent particle movement towards south-west direction. No projected contamination of the western shore of Novaya Zemlya is expected and terrestrial ecosystems are not in danger of oil pollution. According to WWF data of Beluga distribution areas as well as probability of occurrence of fish species, some damage may be expected in the area covered with the spill. [10] The generated map did not show presence of large amount of ice at sea. Minor ice presence is visible with brighter blue colour by the coast of Novaya Zemlya island. The sea is ice free for OSR operations.

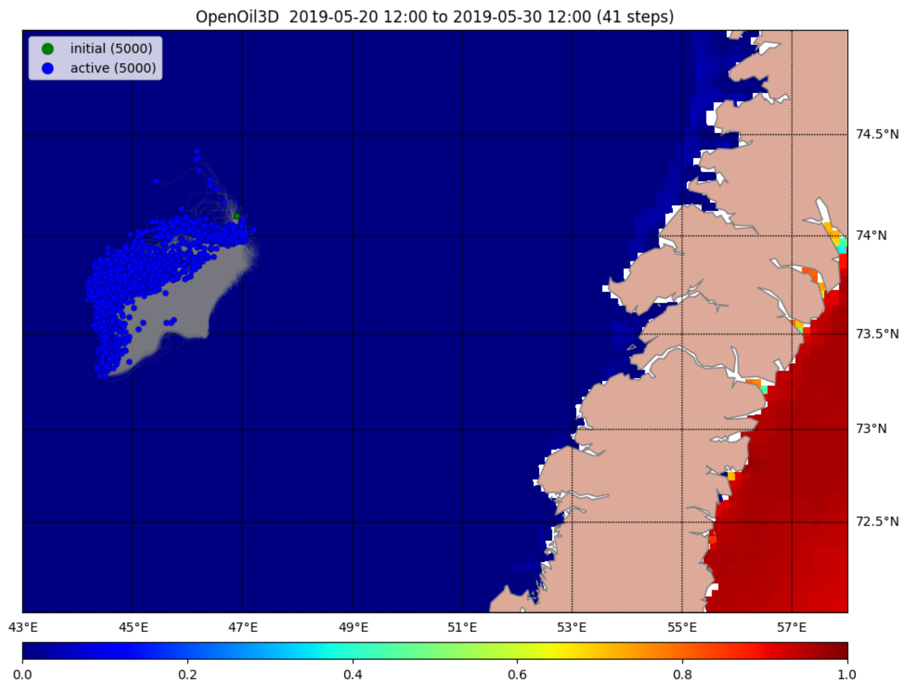

Fig. 3 Hypothetical case of oil spill accident in the Barents Sea. Map legend: green dot – initial point of oil spilling, bright blue dots – simulated movement of oil at sea, grey cloud – trajectory of oil movement, pink – land, red – ice, dark blue – sea; line below the map – ice density.

Kara Sea. During the period of May, 20th - May, 30th, the following value ranges were reported: temperature – from -4 to 0°C, wave height – 0÷1.5 m, wind speed – 6÷36 km/h, and wind direction – south-southwest. Similarly to the Barents Sea case, particles movement showed that the oil slick weathers and spreads mostly towards south-west. Interaction with ice is notable, as it is largely present at sea (see red colour in Fig. 4). Both stranding on ice and shore of the eastern coast of Novaya Zemlya are demonstrated. Damage to bird colonies or other island terrestrial ecosystems is foreseen. Examples of bird colonies in the area are thick-billed and common Murre colonies [11]. Fish species such as Arctic cisco, Arctic cod, Arctic rainbow smelt as well as marine mammals (e.g. walrus) might be also affected. [10] Hence, there may be a negative impact to local fishery.

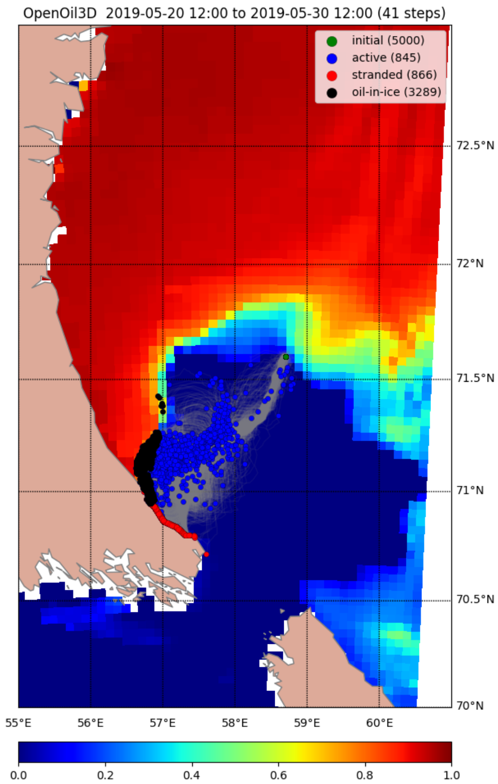

Fig. 4 Hypothetical case of oil spill accident in the Kara Sea. Map legend: green dot – initial point of oil spilling, bright blue dots – simulated movement of oil at sea, grey cloud – trajectory of oil movement, pink – land, bright red dots – stranded oil, black dots – oil in ice, red – ice, dark blue – sea; line below the map – ice density.

Oil budget for the Barents Sea case, shown in Fig. 5, is influenced by several weathering processes. The domineering effects are from evaporation, spreading and dispersion. Surface oil spreading occurs massively only in first two days. After that the effect is negligible.

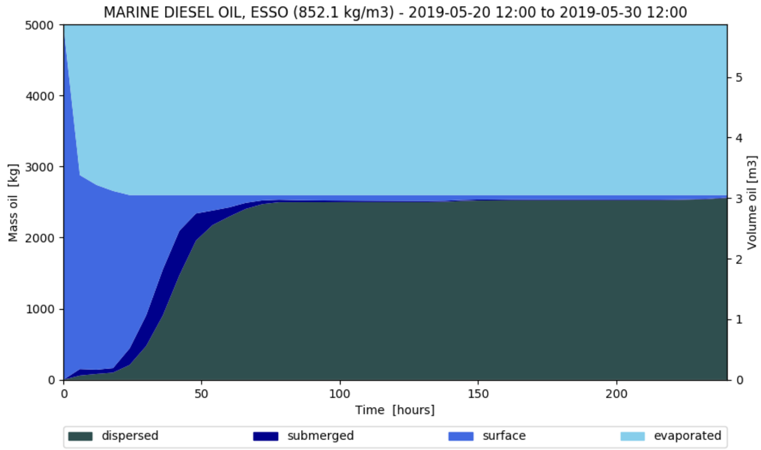

Fig. 5 Oil budget for the Barents Sea study case: 10-day simulation

Fig. 6 shows oil budget for the simulated accident in the Kara Sea. First 100 h, there is large influence of physical spreading at the sea surface. Then, on day 5 onwards, dispersion is the main weathering process. Evaporation takes place from day 1 to day 10 quite steadily.

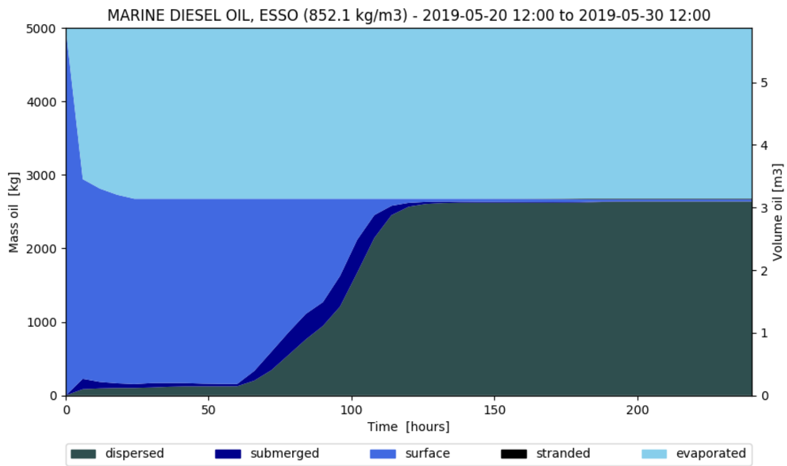

Fig. 6 Oil budget for the Kara Sea study case: 10-day simulation

In both cases, OSR techniques are applicable according to the environmental and situational conditions. On day 10, options for the Barents Sea could be natural attenuation, mechanical recovery and dispersants use. In situ burning would not be applicable due to large spreading and evaporation. The Kara Sea case would require also mechanical response, application of sorbents on shore and ice structures. In situ burning would again not be recommended due to oil state and proximity to the sensitive ecological areas.

4. Conclusions

The tool framework, in particular its sub-module - OpenOil, demonstrated what kind of oil transformations may occur within 10-day accident, as well as what direction of drifting the slick would tend to move towards, if spilled in the given conditions.

After simulating two hypothetical scenarios of Marine Diesel Oil spills with recent, May 2019, ocean and weather conditions data, the following results were reported:

- in case of both spills, the oil drift was prevalently going towards south-west direction;
- Kara Sea weathered slick ended up stranding on the south-east coast of Novaya Zemlya as

well as on floating ice blocks of high density;
- Novaya Zemlya island is rich in bird colonies, meaning a potential damage to sensitive terrestrial ecosystems;
- Barents Sea accident resulted in offshore marine contamination in ice free waters;
- damage to Arctic fish species may be expected;
- after 10-day simulations and generated oil budget graphs, domineering weathering processes of oil were mostly evaporation and dispersion.

As a recommendation, **further research** is still needed to test the chosen marine environments in the specified locations in different year seasons and with different types of oil. Studying other locations along the popular maritime traffic routes is also recommended. And last but not least recommendation is to develop an assessment tool for estimating potential impacts of such accidents in terms of their economic, environmental and social impacts

5. Acknowledgements

Special acknowledgement is due to Lars Robert Hole, Norwegian Meteorological Institute, Bergen, Norway. OpenDrift trajectory models were entirely built with his kind effort. He was the one who introduced me to the open access modelling tool and demonstrated its possibilities. My deep thanks is also to "*Arctic Preparedness Platform for Oil Spill and other Environmental Accidents*" project in particular and to Northern Periphery and Arctic Programme 2014-2020 for funding this research work.

References

[1] MCINTYRE, A.D. 1995, *Human impact on the oceans: The 1990s and beyond*.
[2] KIRBY, M.F. & LAW, R.J. 2010, Accidental spills at sea – Risk, impact, mitigation and the need for coordinated post-incident monitoring.
[3] ARNARSSON, S., DAM, K., JUSTUS, D., LATOLA, K., ŁUSZCZUK, M., SANDER, G., SCHEEPSTRA, A., STĘPIEŃ, A., STRAHLENDORFF, M. (2014). Strategic Environmental Impact Assessment of Development of the Arctic. Available: http://library.arcticportal.org/1792/1/SADA_report.pdf. Last accessed 15th Apr 2017.
[4] BAMBULYAK, A., FRANTZEN, B. and RAUTIO, R. (2015) Oil transport from the Russian part of the Barents Region. 2015 status report. The Norwegian Barents Secretariat and Akvaplan-niva, Norway. – 105 pages.
[5] OIL CHANGE INTERNATIONAL (OCI), GREENPEACE. (2015b). Frozen Future. The gaps in Shell's Arctic spill response. Available: http://priceofoil.org/content/uploads/2015/04/2015-The-gaps-in-Shells-Arctic-spill-response.pdf. Last accessed 2nd Jan 2016.
[6] VOROBIEV, U.L., AKIMOV, V.A., SOKOLOV, U.I. (2005). *Предупреждение и ликвидация аварийных разливов нефти и нефтепродуктов. (Oil and oil products spill prevention and response)*. Moscow: In-oktavo. p368.
[7] AFENYO, M., KHAN, F., VEITCH, B. and YANG, M. 2016, Modeling oil weathering and transport in sea ice.
[8] DAGESTAD, K.-F., RÖHRS, J., BREIVIK, Ø., and ÅDLANDSVIK, B.: OpenDrift v1.0: a generic framework for trajectory modelling, *Geosci. Model Dev.*, 11, 1405-1420, https://doi.org/10.5194/gmd-11-1405-2018, 2018.
[9] EMERGENCY PREVENTION, PREPAREDNESS AND RESPONSE (EPPR) WORKING GROUP OF THE ARCTIC COUNCIL. (2017). Circumpolar Oil Spill Response Viability Analysis. Available: https://oaarchive.arctic-council.org/bitstream/handle/11374/1928/2017-05-09-EPPR-COSRVA-guts-and-cover-letter-size-digital-complete.pdf?sequence=1&isAllowed=y. Last accessed 19th May 2019.
[10] WORLD WIDELIFE FUND (WWF). (2013). *Arctic Geographical Information System.* Available: http://wwfarcticmaps.org/. Last accessed 11th Jun 2019.
[11] JOHNSEN, K. I., ALFTHAN, B., HISLOP, L., SKAALVIK, J. F. (Eds). 2010. Protecting Arctic Biodiversity. United Nations Environment Programme, GRID-Arendal, www.grida.no

FROZEN GROUND AND PERMAFROST

Experimental Study of Influence factors effect on frost heave

Hyun Woo Jin
Ph.D candidate
Korea University of Science and Technology (UST)
Republic of Korea
hunu1231@kict.re.kr

Jangguen Lee, Research Fellow, KICT, Republic of Korea
Byung Hyun Ryu, Research Specialist, KICT, Republic of Korea
Yunsup Shin, Senior Engineer, NGI, Norway

Summary

Frost heave has been studied since when the mechanism of ice segregation was discovered. Laboratory frost heave test is the most direct method to investigate the influence factors effect. There are many influence factors of frost heave such as particle size, pore size, thermal conductivity, overburden pressure, etc. In this paper, laboratory frost heave tests using uniderctional freezing method were performed for studying to find out the temperature gradient, dry unit weight, and sample disturbance effect. According to the laboratory test results, it is discovered that: (1) the temperature gradient effects on silt too, specifically, the higher temperature gradient is, the more and faster frost heave amount and rate are generate; (2) the higher density is, the more dramatic frost heave behavior generates; and (3) sample disturbance has a great impact on frost heave in soils. Undisturbed soil sample does not even follow the effect of density. Additional laboratory test are required for sample disturbance.

Keywords: Frost heave, Laboratory test, Temperature gradient, Dry unit weight, Sample disturbance

1. Introduction

When soil is frost susceptible and temperature is cold enough to freeze the pore water, frost heave occurs (Zeinali et al., 2016). To investigate frost heave mechanism, unidirectional freezing method is widely used. By freezing unidirectionally, influence factors of frost heave in soils have been studied by previous researcher. Casagrande (1931) suggested that particle size determine frost heave. Jessberger (1969) presented that pore size had important role with respect to the capillarity, suction, and thermal conductivity. Penner (1972) concluded that heat extraction rate is the basic influence factor in frost heave in soils. Gorle (1980) found that the temperature gradient had a huge impact on sands, unlike silt which has no significant impact. Hill and Morgenstern (1977) suggested that there be a “shut-off pressure” at which capillary action ceases and Ueda (1977) also suggested that shut-off pressure do not exist below 465 kPa for sand, silt and clay soils, even though frost heave rate were dramatically decreased. According to the repeated freeze-thaw cycling, Konrad (1989) found that hydraulic conductivity and effective void ratio are increased after each freeze-thaw tests. There is still a lack of experimental research from the perspective of temperature gradient in clayey silt soil, density, and sample disturbance. This paper presents laboratory frost heave test results those kind of influence factor’s effect on frost heave.

2. Transparent temperature controllable cell

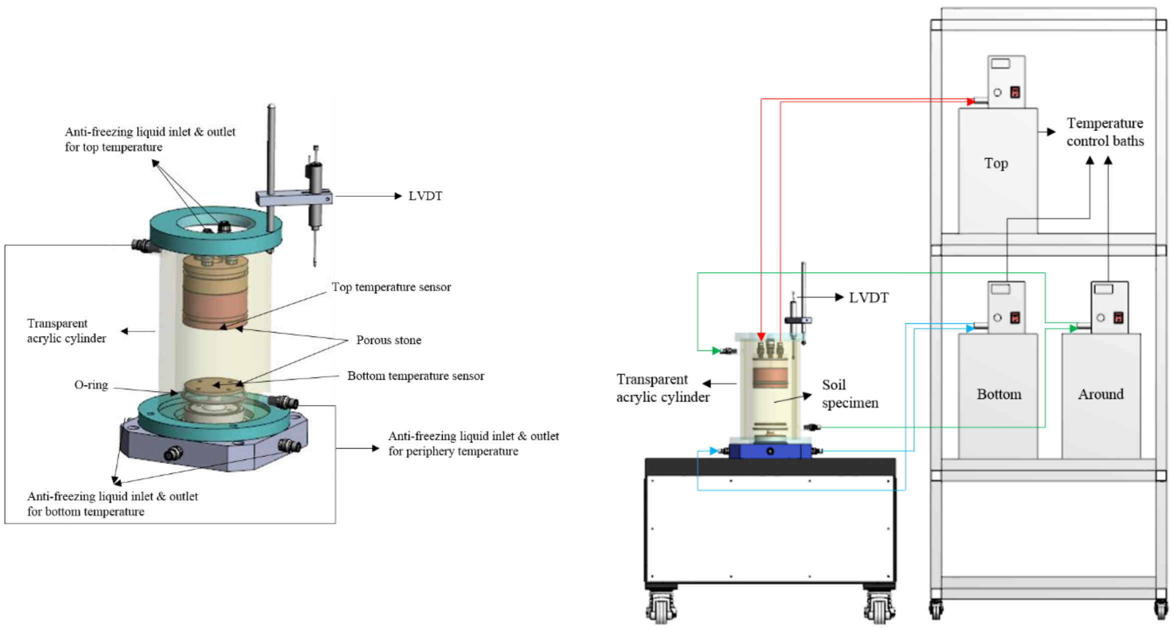

Fig. 1 Frost heave testing apparatus (Jin et al., 2019)

A simple frost heave testing method using a transparent temperature controllable cell that can control top, bottom, and periphery temperature is established by Jin et al.(2019). The temperature controllable cell consists of acrylic double rings which have different diameters, and the thicknesses of the rings are 10.00 *mm* each (Fig. 1). The spacing between the two rings is 15.00 *mm* and anti-freezing coolant is circulated inside the spacing. There are three temperature control baths. As mentioned, one of the baths connected around the cell insulates soil specimen from outside temperature and makes the soil specimen freezing unidirectionally. The other two baths are connected to top and bottom pedestals to control freezing direction. In this paper, freezing direction was set up from bottom upward to minimize side friction between soil and inner wall of the cell (Konrad & Morgenstern, 1982; Jin et al., 2019). The details of this testing apparatus including the transparent temperature controllable cell is well described in previous paper (Jin et al., 2019).

3. Soil Preparation Methods and Test Conditions

3.1 Soil properties

A frost susceptible soil is obtained from Halden in Norway, called by Halden silt. As shown in Table 1, specific gravity of a Halden silt is 2.65 and classified as SC by USCS (Unified Soil Classification System). The particle size distribution curve is shown in Fig. 2.

Table 1 Engineering properties of Halden soil

D_{10}	D_{30}	D_{30}	Uniformity coefficient, C_u	Coefficient of curvature, C_c	Specific gravity, G_s	USCS
0.002	0.01	0.032	16	1.56	2.65	SC

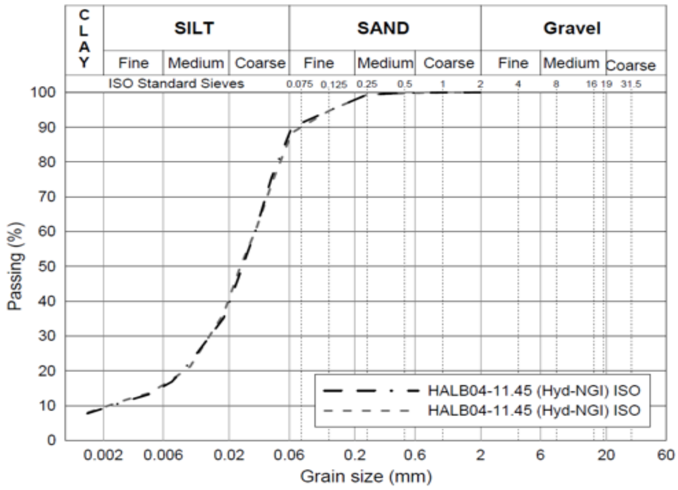

Fig. 2 Particle size distribution curve

3.2 Reconstituted soil sample preparation

In case of a reconstituted soil sample, a dry soil passing 0.50 *mm* was used to prepare soil samples. Soil samples were reconstituted to approximately 100.00 *mm* in height by dry tamping, vibration and air pluviation.

3.3 Undisturbed soil sample preparation

The process of preparing undisturbed soil sample is as follows. A wire saw and a trimming guide are used to make suitable sample hieght (100.00 *mm*) and diameter (100.00 *mm*). First, place the sample for trimming on the trimming guide and trim it with the wire saw (Fig. 3a). The diameter should be roughly 1.00 % smaller than the inner diameter of the cell. If the surface of the sample is not flat, the surface is filled with the same soil (Fig. 3b). Place the trimmed soil sample on the bottom pedestal (Fig. 3c), and then cover the cell (Fig. 3d).

a. trimming

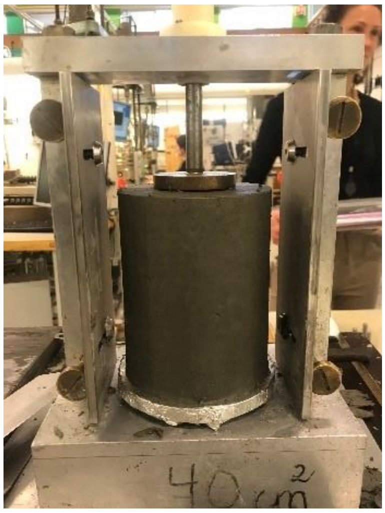

b. after trimming

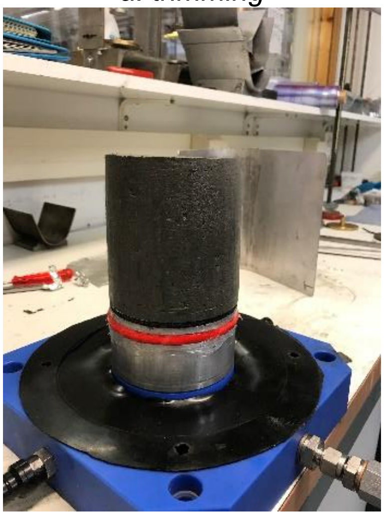

c. sample building on the bottom pedetal

d. covering the cell

Fig. 3 Undisturbed soil sample preparation

3.4 Saturation and temperature conditioning

In order to saturate the soil sample, distilled water is injected through the drainage line connected to the bottom pedestal (Fig. 4a). The overburden pressure is only 1.62 *kPa*, induced by the top pedestal filled with anti-freezing coolant. The samples are stayed for 24 *hours* in a hydrostatic condition with temperature conditioning by operating all pumps at 3.0 ℃ (Fig. 4b), and then frost heave tests are performed.

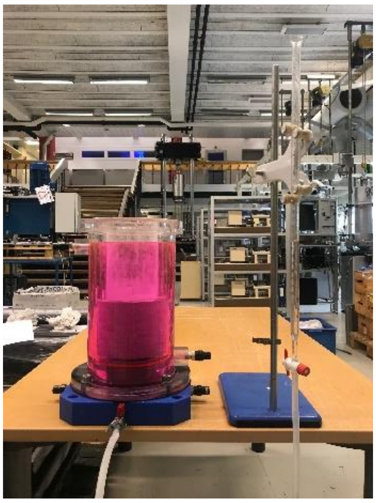

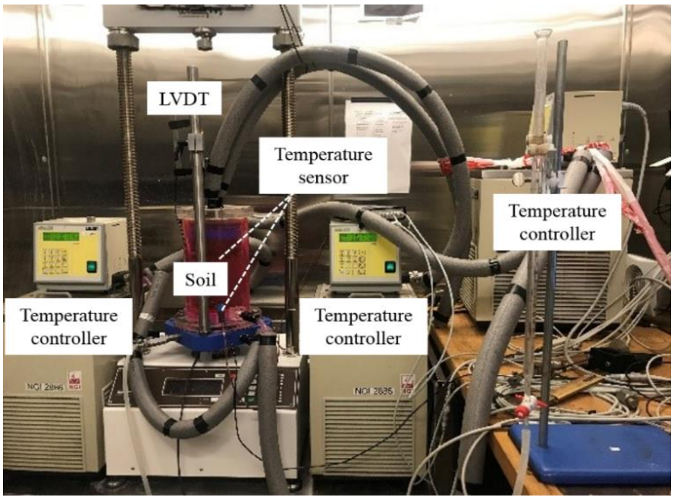

a. saturaion *b. temperature conditioning*

Fig. 4 Ready for frost heave test

3.5 Test conditions

Frost heave test conditions are shown in Table 2. This paper presents 3 influence factors effect on frost heave in soils experimentally. The 3 influence factors are consist of temperature gradient (TG in Table 2), dry unit weight (DUW in Table 2), and sample disturbance (SD in Table 2). All of the soil samples are prepared to freeze approximately 100.00 *mm* in height.

Table 2 Test conditions of Halden silt

	Soil conditions	Initial Height (mm)	Dry unit weight, γ_d (kN/m^3)	Temperature gradient (℃/mm)	Temperature (℃) Measured Top	Bottom	Setting Periphery
TG-1	Reconstituted	108.99	13.26	0.056	2.7	-3.4	1.0
TG-2		99.59	14.51	0.118	2.7	-9.1	
TG-3		97.94	14.75	0.234	2.7	-20.8	
DUW-1		105.26	13.55	0.119	3.2	-9.4	
DUW-2		99.59	14.51	0.118	2.7	-9.1	
DUW-3		107.60	13.43	0.223	3.1	-20.9	
DUW-4		97.94	14.75	0.240	2.7	-20.8	
SD-1		105.26	13.55	0.119	3.2	-9.4	
SD-2	Undisturbed	100.00	14.45	0.123	3.0	-9.3	

4. Test results

4.1 Temperature gradient effect

Frost heave test results with respect to the temperature gradient are shown in Fig. 5. The higher temperature gradient is, the more and the faster frost heave amount and rate are generated.

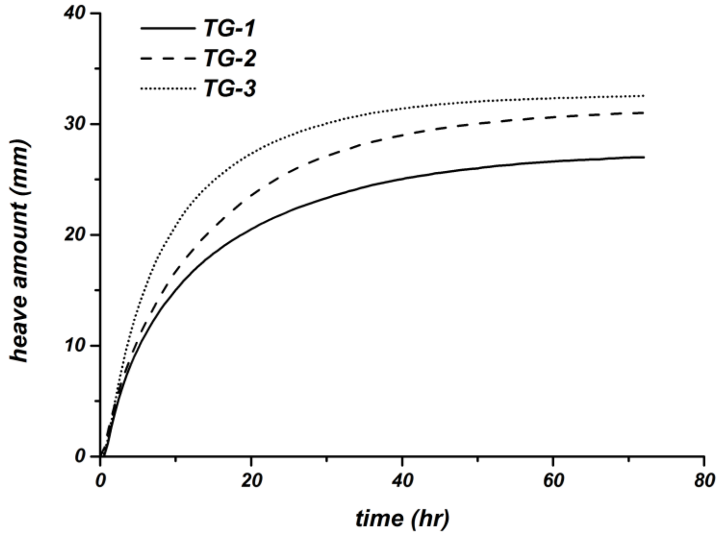

Fig. 5 Frost heave test results with respect to the temperature gradient

4.2 Dry unit weight effect

Frost heave test results with respect to the dry unit weight are shown in Fig. 6. Fig. 6 is classified into two groups with similar temperature gradients, which are Group I (Fig. 6a, DUW-1 & DUW-2 in Table 2) and Group II (Fig. 6b, DUW-3 & DUW-4 in Table 2). During the test's beginning, similar frost heave curves regardless of dry unit weights are generated. After few hours, frost heave amount and rate of high density soil samples are more and faster than those of low density soil samples. The divergence of high temperature gradient (Fig. 6b) is started faster than that of low temperature gradient (Fig. 6a).

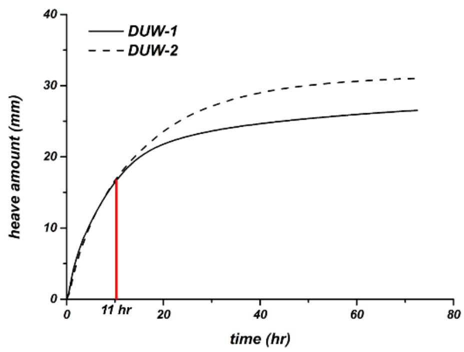

a. low temperature gradient

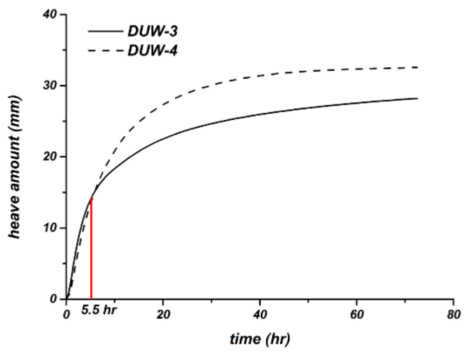

b. high temperature gradient

Fig. 6 Frost heave test results with respect to the dry unit weight

4.3 Sample disturbance effect

Frost heave test results with respect to the sample disturbance are shown in Fig. 7. During about 0-60 *hrs*, frost heave amount and rate of reconstituted soil sample are more and faster than those of undisturbed soil sample. However, two frost heave curves converged after about 60 *hrs*.

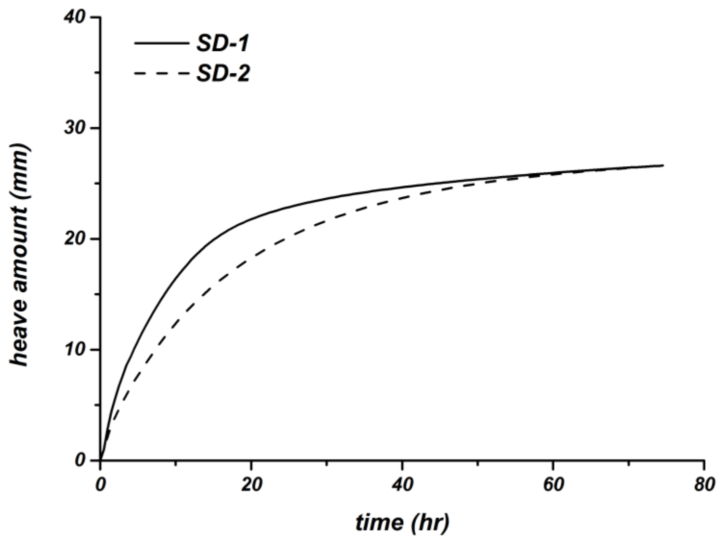

Fig. 7 Frost test results with respect to the sample disturbance

5. Discussion

In order to understand the temperature gradient effect one of the influence factors on frost heave, frost heave tests with Halden silt were performed. Fig. 8 simplifies the temperature profiles across the soil samples for different temperature gradients with the same heights. Since same overburden pressure is loaded during the tests, segregation-freezing temperature (T_s) is kept constant (Konrad & Morgenstern, 1982). According to the tests results (Fig. 5), a relatively high temperature gradient generates more and faster heave amount and rate than those of low temperature gradient's. In addition, different frozen fringe thicknesses (blue area in Fig. 8) are generated by temperature gradient. It can be concluded that temperature gradient affect the frozen fringe thickness in silt which is determines frost heave behavior. In other words, the thinner frozen fringe, the more and faster frost heave amount and rate are generated.

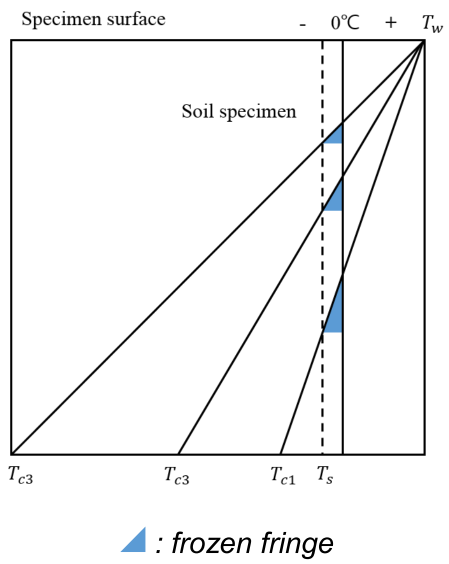

Fig. 8 Frozen fringe thickness with various temperature gradient conditions

6. Conclusion

This paper experimentally presents the effect of temperature gradient, dry unit weight, and sample disturbance on frost heave in soils. According to the frost heave tests with fully saturated frost susceptibile soil, the following conclusions were derived.

1. Temperature gradient which determines frozen fringe thickness effects on the frost heave behavior, even though the soil has approximately 80.00 % silt. Specifically, the higher temperature gradient is, the more and faster frost heave amount and rate are generated.
2. Frost heave amount and rate are dependent on the dry unit weight. After the divergence point determined by temperature gradient, frost heave amount and rate increase as dry unit weights increase.
3. Frost heave behaviours are different during about 0-60 *hrs* between undisturbed and re-constituted soil samples. After about 60 *hrs*, two frost heave curves converged. This test result does not follow the effect of dry unit weight. It is considered that sample disturbance affects the frost heave behaviour, but further research is needed.

Acknowledgment

This research was supported by the research project “Development of envirionmental simulator and advanced construction technologies over TRL6 extreme conditions” funded by the Korea Institute of Civil Engineering and Building Technology (KICT).

References

[1] CASAGRANDE A., “Discussion on ‘A new theory of frost heaving’.”, *Highway Research Board Proceedings*, Vol. 11, 1931, pp. 168-172.
[2] CWIAKALA M., GAJEWSKA B., KRASZEWSKL C., and RAFALSKI, L., “Laboratory investigations of frost susceptibility of aggregates applied to road base courses”, *Transportation Research Procedia*, Vol. 14, 2016, pp. 3479-3484.
[3] GORLE D., “Frost susceptibility of soils: Influence of the thermal variables and depth to the water table.”, *International Symposium on Ground Freezing*, Trondheim, Norway, 1980, pp. 772-783.
[4] JESSBERGER H.L., “Ground frost: A listing and evaluation of more recent literature dealing with the effect of frost on the soil.”, *Research Report V*, Vol. 44, 1969. (in German)
[5] JIN H.W., LEE J., RYU B.H., and AKAGAWA S., “Simple frost heave testing method using a temperature-controllable cell”, *Cold Regions Science and Technology*, Vol. 157, 2019, pp. 119-132.
[6] KONRAD J.M. and MORGENSTERN N.R., “Effects of applied pressure on freezing soils.”, *Canadian Geotechnical Journal*, Vol. 19, 1982, pp. 494-505.
[7] KONRAD J.M., “Physical processes during freeze-thaw cycles in clayey silts.”, *Cold Regions Science and Technology*, Vol. 16, 1989, pp. 291-303.
[8] PENNER E., “Influence of freezing rate on frost heaving.”, *Research Record*, No. 393, 1972, pp. 56-64.
[9] ZEINALI A., DAGLI D., and EDESKAR T., “Freezing-thawing laboratory testing of frost susceptible soils.”, *Proceedings from 17th Nordic Geotechnical Meeting*, Reykjavik, Iceland, 2016, pp. 267-276.

Thermal and moisture distribution of subgrade effected by the freezing

Feng Zhang
Associate professor
Harbin Institute of Technology
China
zhangf@hit.edu.cn

Ph.D. Candidate Kangwei Tang, Harbin Institute of Technology, China
Professor Decheng Feng, Harbin Institute of Technology, China

Summary

Freezing causes redistribution of moisture and temperature in subgrade, which have serious impacts on the strength and deformation behaviors of subgrade. In this research, the numerical water-heat coupling model was established based on the mass and heat conservation, and was verified by the laboratory model test of unsaturated subgrade soil moisture transfer. Then the effects of environment temperature, water supply conditions (closed system and open system), and underground water level on subgrade temperature and moisture distribution were analyzed. Numerical results show that the lower the freezing temperature, the more obvious the phenomenon is, and the deeper the water enrichment layer is. When the freezing temperature decreases from -5.6℃ to -22.5℃, the water content of water enrichment layer increases from 38.5% to 43%, and its position moves downward from 27cm to 50cm below the cold end. The freezing rate only affects the shallow subgrade (0~30cm below the cold end in this model), and its increasing can inhibit moisture migration. Adequate water supply gives rise to frost heave but has no effect on the distribution of temperature.

Keywords: Water-heat coupling model, Thermal distribution, Moisture distribution, Water enrichment layer.

1. Introduction

Freezing can cause redistribution of moisture and temperature in subgrade. A series of experiments have shown that water would migrate upward and accumulate under repeated freeze-thaw cycles, resulting in a significant increase in soil moisture content after thawing to form a water-rich layer [1-4]. In fact, the freezing-thawing process of soil is an extremely complex problem of the interaction of temperature field, water field and stress field. In addition to the experimental study, researchers began to use numerical simulation to reveal the changes of soil water and heat during freezing and thawing process.

Harlan [5] proposed a one-dimensional non-linear hydrothermal coupling equation considering water transport and ice-water phase transition based on the principles of unfrozen hydrodynamics and energy conservation, which has definite physical meaning and can be used to solve the temperature and moisture distribution. Inspired by this classical model, later researchers built a lots of more perfect and accurate models. Taylor et al. [6] improved the Harlan model on the basis of which the water and temperature fields were calculated by implicit finite difference method and compared with the experimental data. At the same time, Sheppard et al. [7] also proposed the water transfer equation in saturated or unsaturated frozen soil on the basis of Harlan model. Similarly, Celia et al. [8], Newman et al. [9], Dempsey et al. [10] also established water transfer equation of unsaturated soil during freezing. In the 1990s Guymon et al. [11] and Padilla et al. [12] found a hydrodynamic model of the interaction between heat and mass transfer and water transfer in frozen soil. But before that, O'Nell et al. [13], Gilpin et al. [14] and Konrad et al. [15] studied the formation and growth of ice lenses in frozen soil, proposed and developed a "rigid ice" model. Nixon et al. [16] proposed and developed a rigid ice model based on the hypothesis of non-deformable "rigid" ice and linear stable temperature field on the basis of sub-frost heave theory and ice segregation theory. Konard et al. [17] proposed a model describing the formation of ice crystals and water migration in frozen soils.

In recent years, great achievements have been made in the optimization of parameters in the water-thermal coupled numerical model and the analysis of water-thermal coupling factors. Kouretzis et al. [18] (2014) adopted an explicit finite element integration method for simulating seepage in sandy soils. This method can effectively use model parameters to express the compressibility of sandy soils. Zhou et al. [19] (2014) put forward the influence of temperature gradient on boundary tension and skeleton deformation in unsaturated soil-water-thermal coupled numerical model, and gave the solution of non-isothermal SFG volume change equation and non-isothermal soil-water characteristic curve. Seetharam [20] (2010) proposed a new method for the calculation of water-thermal coupled differential equations. The mass equation and energy equation of flow are expressed in general equation form, and the sequential iteration method and the non-sequential iteration method are used to solve the equations. Finally, the one-dimensional model is used to verify the method. Considering the factors of water, steam and soil skeleton, a water-thermo-mechanical coupled equation system with six main variables was proposed [21]. Masum [22] simulated the coupling problem of hydrogen migration in clay, and analysed the influence of pressure and convection on the coupling results, which is helpful to improve the disposal of waste in nuclear reactor. Gaelan [23] uses one-dimensional Hydrothermal Coupling to analyse the role of current resistance in subgrade treatment. Sanchenz [24] proposed a fully coupled formula of water and heat for unsaturated soils based on the dual porosity formula. At the same time, the paper verifies that the coupling formula has strong practicability in practical engineering. Qi [25] analysed the influence of rainfall and freeze-thaw on the stability of expansive soil slope through hydrothermal coupling, and illustrated the guiding role of the model for engineering through an example.

In this research, the numerical water-heat coupling model was established based on the mass and heat conservation, and was verified by the laboratory model test of unsaturated subgrade soil moisture transfer. Then the effects of environment temperature, water supply conditions (closed system and open system), and underground water level on subgrade temperature and moisture distribution were analyzed.

2. Theory

2.1 Hypothesis

On the basis of ensuring the accuracy of the model, in order to simplify the model, it is computability and operability. In this model, the following basic assumptions are set:
(1) In the process of water migration, water is mainly in the form of liquid, without considering the gas water migration and the latent heat of liquid water gasification;
(2) The effect of salt and other ions on water migration is not considered;
(3) Soil isotropy. It mainly includes density, diffusion coefficient, thermal conductivity and so on, which are the same in all directions;
(4) The thermal expansion and cold contraction of each phase are neglected in the freeze-thaw process, and the frost heave deformation is mainly caused by the compression of pore volume. During the freezing-thawing process, the thermal expansion and contraction of each phase and the compression deformation of soil particles during the freezing-thawing process become smaller and negligible relative to the pore volume;
(5) Water seepage in soil obeys the generalized Darcy's law;
(6) The transverse migration of vaporous water is not considered.

2.2 Water transfer equation

According to conservation of mass, the water transfer can be described by the following equation:

$$\frac{\partial \theta_l}{\partial t}+\frac{\rho_i}{\rho_l}\frac{\partial \theta_i}{\partial t}=\nabla\left[k\left(\theta_l\right)\nabla\left(\varphi_m\right)\right]+\nabla\left[k\left(\theta_l\right)\right] \tag{1}$$

Where, θ_l is liquid water content, θ_i is ice content, ρ_l is water density in kg m^{-3}, ρ_i is ice density in kg m^{-3}, $k(\theta_l)$ is the permeability coefficient of soil in m s^{-1}, φ_m is matrix potential.

2.3 Heat transfer equation

According to conservation of energy, the heat transfer can be described by the following equation:

$$C\frac{\partial T}{\partial t}-L\rho_i\frac{\partial \theta_i}{\partial t}=\nabla\left[\lambda\nabla(T)\right] \tag{2}$$

Where, C is the comprehensive volume heat capacity in J m^{-3}k^{-1}, T is temperature in °C, L is the latent heat of ice melting in J kg^{-1}, ρ_i is ice density in kg m^{-3}, λ is heat conductivity in $W\cdot\mathrm{m}^{-1}\mathrm{k}^{-1}$, θ_i is ice content, can be caculated by Eq. [3]:

$$\theta_i=\theta_0-a\left(|T|\right)^b,\left(T<T_f\right) \tag{3}$$

Where, θ_0 is initial water content of soil, a and b are regression constants, a is 17, b is -0.5,T_f is temperature of phase transition of water and ice, is -0.41 °C.

2.4 Parameter setting

2.4.1 The compressive volume heat capacity C

The compressive volume heat capacity C, reflecting the level of heat storage in the soil, is 2.785×10^6 J m^{-3}K^{-1} according to the Appendix Table K.0.1 of *the Code for Design of Building Foundation in Permafrost Region* (JGJ 118-2011).

2.4.2 The comprehensive thermal conductivity λ

The comprehensive thermal conductivity λ, indicating the heat transfer rate in soil sample under unit gradient temperature difference and the heat transfer capacity of soil sample, is related to soil composition, water content and temperature. Refer to the Appendix Table K.0.1 of the Code for Design of Building Foundation in Frozen Soil Area (JGJ 118-2011), it's 1.71 Wm^{-1}K^{-1}.

2.4.3 Matrix suction φ_m

According to VG model, matrix suction φ_m can be calculated as follows:

$$\varphi_m=\frac{1}{a_0}\left(S_r^{-1/m}-1\right)^{1/n} \tag{4}$$

Where, a_0, m, n, VG model parameter, is 0.15kPa-1, 0.697, 3.3 respectively. S_r is relative saturation which is defined in eq.[4] as:

$$S_r=\left(\theta_l\text{-}\theta_n\right)/\left(\theta_m-\theta_n\right) \tag{5}$$

Where, θ_l is liquid water content, θ_n and θ_m is residual and saturated water content respectively, which is 0.074 and 0.42 for silty clay used in this paper.

2.4.4 Permeability coefficient of soil $k(\theta_l)$

Permeability coefficient of soil $k(\theta_l)$, can be calculated in eq. [6], by :

$$k\left(\theta_l\right)=k_sS_r^{0.5}\left[1-\left(1-S_r^{1/m}\right)^m\right]^2 \tag{6}$$

Where, k_s is permeability coefficient of saturated soil, equal to $10^{-8}ms^{-1}$.

3. Numerical simulation

3.1 Geometry and Mesh

To simulate the longitudinal hydrothermal distribution of roadbed under freeze-thaw cycle, the height of the geometry model is 1 m, which is close to the real roadbed height and the width is 20cm, an extra fine mesh was applied to ensure the accuracy of simulation results.

3.2 Governing Equation in COMSOL

In this paper, the mathematical module (PDE) in COMSOL simulation software is used for it can avoid the complex process of eliminating the variables of the equations. According to the PDE module in COMSOL, the governing equation [1, 2] can be described as coefficient partial differential equation [6]:

$$\begin{pmatrix} C\text{-}L\rho_i\dfrac{\partial\theta_i}{\partial T} & 0 \\ \dfrac{\rho_i}{\rho_l}\dfrac{\partial\theta_i}{\partial T} & 1 \end{pmatrix}\begin{pmatrix} \dfrac{\partial T}{\partial t} \\ \dfrac{\partial\theta_l}{\partial t} \end{pmatrix}+\nabla\left[-\begin{pmatrix} \lambda & 0 \\ 0 & -k(\theta_l)\dfrac{\partial\varphi_m}{\partial\theta_l} \end{pmatrix}\begin{pmatrix} \nabla T \\ \nabla\theta_l \end{pmatrix}\right]+\begin{pmatrix} 0 & 0 \\ 0 & -\dfrac{\partial k(\theta_l)}{\partial\theta_l} \end{pmatrix}\begin{pmatrix} \nabla T \\ \nabla\theta_l \end{pmatrix}=0 \tag{6}$$

$$\nabla=\left[\frac{\partial}{\partial x},\frac{\partial}{\partial y}\right]$$

3.3 Boundary Conditions

Table 1 This is a Table caption

Boundary	Upper Boundary	Lower Boundary	Side Boundary
Temperature	-T(t)	1	q(T)
Moisture content		0.40	

Table 1 shows the boundary conditions of model. As the upper boundary, a Dirichlet boundary is used to determine its temperature to simulate changes in atmospheric temperature. T(t) is related to time, expressed by eq. [7]:

$$T\_t(t)=\begin{cases} -1.125t+273.15 & t\le 20h \\ 250.65 & t>20h \end{cases} \tag{7}$$

As for the lower boundary, also use Dirichlet boundary to define its temperature and moisture content to 1°C and 0.4 respectively. The heat flux of side boundary is defined by Newman boundary as q(T), which is related to Temperature of soil and can be calculated as follows:

$$q\_0(T)=2(274.15-T) \tag{8}$$

3.4 Initial Value Conditions

The initial temperature of soil is 1°C, and the initial volume water content is 0.27, which indicates that the roadbed is in the optimum humidity.

4. Results and Analysis

4.1 Thermal Distribution

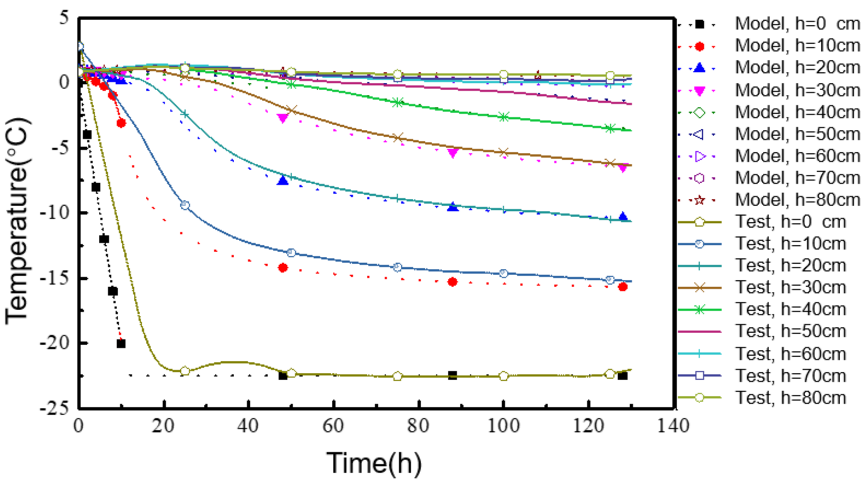

Fig. 2 Verification of thermal distribution

Figure 2 shows the comparison of temperature distributions between the model and test. It indicate that the temperature distribution of numerical simulation is in good agreement with the laboratory test results. The temperature at the top of the roadbed (h=0cm) decreases rapidly and linearly to -22.5°C in 10 hours under the freezing, then stable. Similar changes occur in other layers. The deeper the subgrade is, the higher the stable temperature is. The overall freezing depth is about 50 cm.

4.2 Moisture Distribution

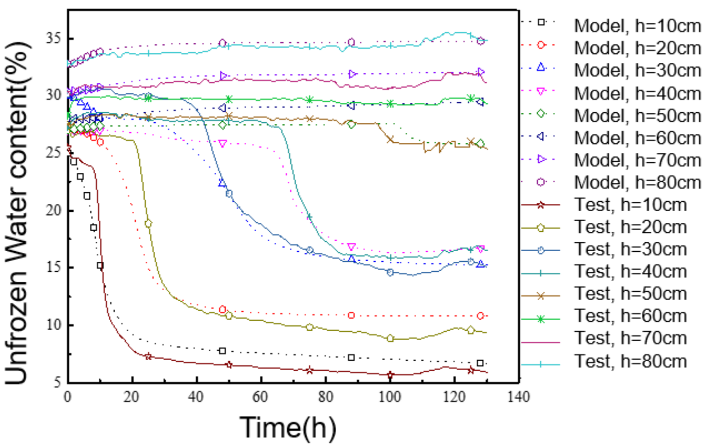

Fig. 3 Verification of Moisture distribution

Figure 3 shows the comparison of moisture distributions between the model and test. It indicateg that the moisture distribution of numerical simulation is in good agreement with the laboratory test results. The unfrozen water content at the top of the roadbed (h=0cm) decreases rapidly and linearly to -7.5% then decreases slowly. Similar changes occur in other layers. At the beginning, the other layers remain stable, then decline rapidly and finally tend to be stable. The deeper the roadbed is, the larger the stable unfrozen water content is. that of the bottom of roadbed only rises slightly, mostly stay at about 34%.

4.3 Changes of Temperature during freezing

Fig. 4 shows the curves of temperature and water with depth at four time points t = 0, 30, 70 and 100h. It can be seen from the graph that with the prolongation of freezing time, the curve gradually changes from straight line to arc curve, and then to arc curve with smaller arc. With the increase of depth, the range and rate of cooling decrease rapidly. The frozen front gradually decreases with time, and the final stable depth is 60 cm

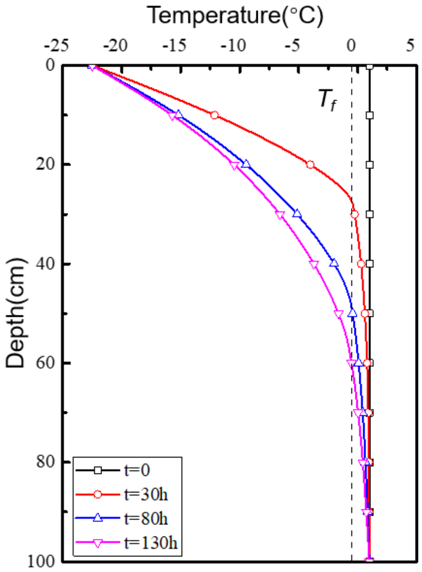

Fig. 4 Temperature versus Depth

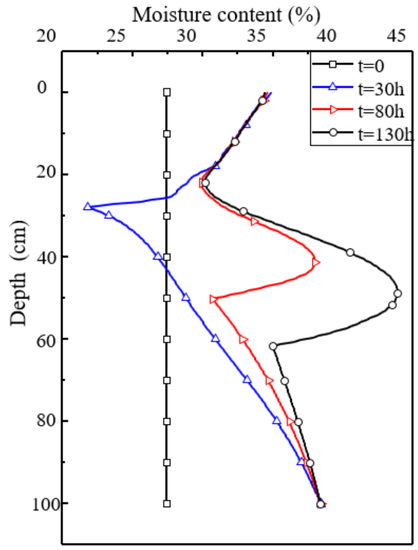

Fig. 5 Moisture versus Depth

4.4 Changes of unfrozen Water during freezing

Fig. 5 shows the variation curve of total water volume content with time and depth at four time points t=0, 30, 70 and 100h. According to the calculation results in the figure, with the prolongation of freezing time, the curve gradually changes from "<"curve to "S" curve. In the frozen area, the water-enriched layer gradually appears, and the layer develops slowly downward with time, and the water content increases slowly, and finally stabilizes. This is because under the condition of water replenishment, with the progress of water migration, when the water at the lower end migrates to the frozen front area, the phenomenon of water accumulation occurs, and then the curve begins to change from "<"type to "S" type. At the same time, the position of the enriched water layer will gradually move downward with the frozen front, and the water content will increase slowly. When the frozen front is stable, the position of the layer will tend to be stable. When the water content in this layer increases to a certain extent, the ice-bearing layer commonly seen in engineering appears. In this simulation, the position of enriched water layer is 50 cm deep, and the volume water content is 43%.

5. Effect of Boundary Conditions

5.1 Water supplement conditions

Fig. 6 and 7 show the calculation data under the condition of water supply and non-water supply, reflecting the variation of temperature and water content with time at each measuring point. The results show that the water supply condition has a great influence on the water content in the freezing process. Under the water supply condition, the overall water content of the model body increases by 9% at the time of t=130 h, and the obvious maximum aquifer appears in the maximum freezing depth. Without water replenishment, there is no obvious large aquifer in the top area of the model body, and there is no region with water content greater than 42% in the whole model body area, that is, there is no frost heave phenomenon. However, the temperature curves coincide basically under the condition of water replenishment and non-water replenishment after freezing and stabilization, which shows that the condition of water replenishment has no effect on the distribution of temperature field after freezing and stabilization

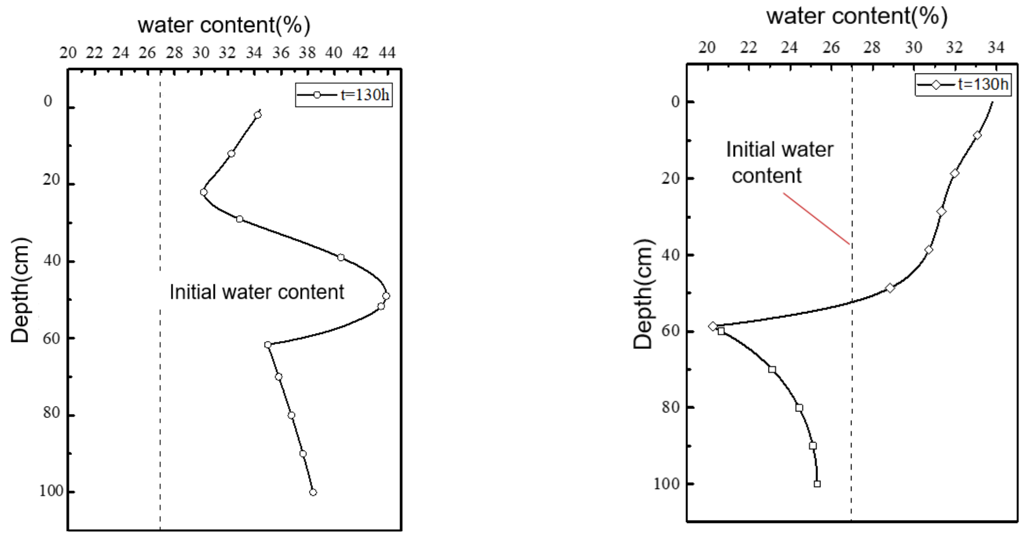

a) Water replenishment *b) No water replenishment*

Fig. 6 Water content versus Depth

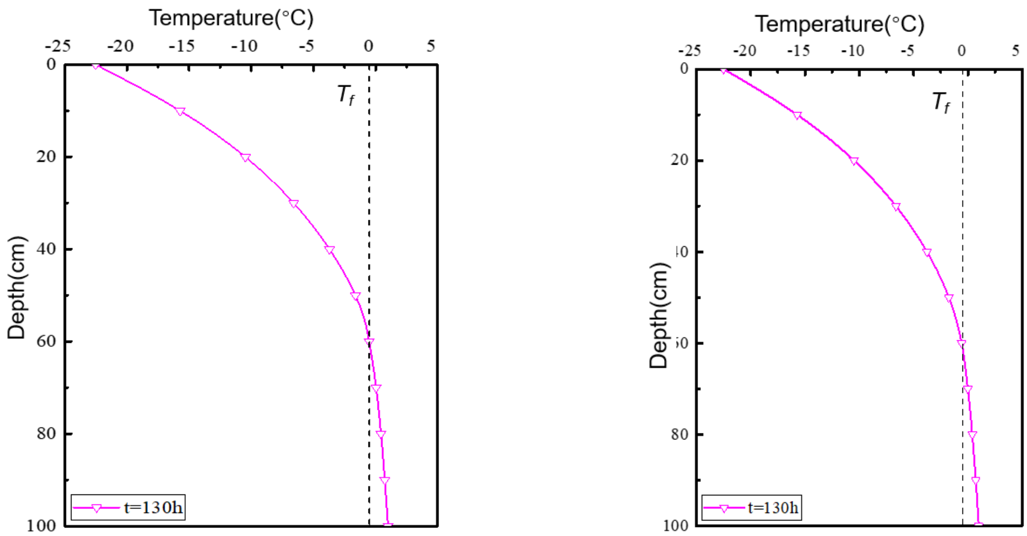

a) Water replenishment *b) No water replenishment*

Fig. 7 Temperature versus Depth

5.2 Freezing temperature

Fig. 8 shows the distribution of temperature and volumetric water content with time at the top temperature of T=-22.5 ~C, -11.25 ~C and-5.6 ~C. From the curve in the figure, it can be seen that the freezing temperature affects the whole area of freezing, but does not change the law of the curve. With the decrease of temperature, the stable temperature of enriched aquifer moves downward and the water content increases. It shows that the freezing temperature has a great influence on the water content in the freezing area. When the freezing temperature decreases from - 5.6 C to - 22.5 C, the water content increases from 38.5% to 43%, and the stable depth increases from 27 cm to 50 cm.

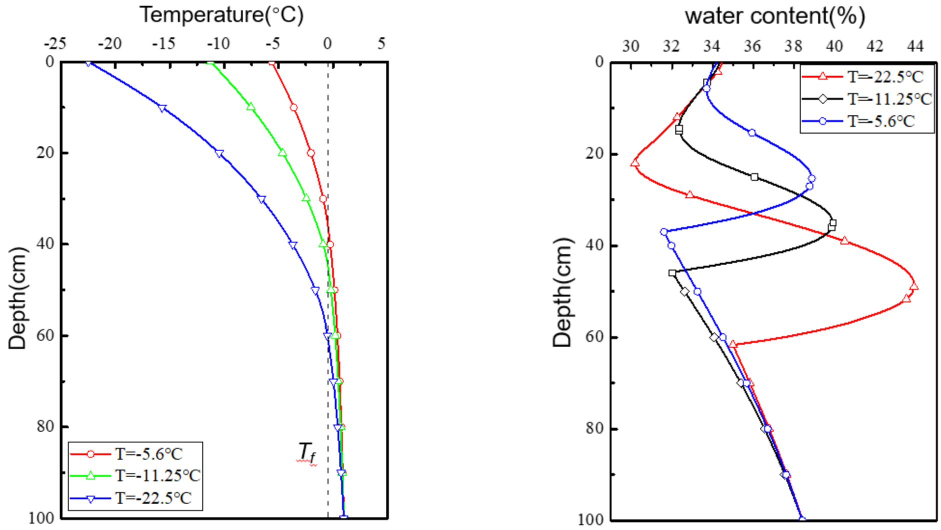

Fig.8 Temperature and water content at different freezing temperature

5.3 Cooling rate

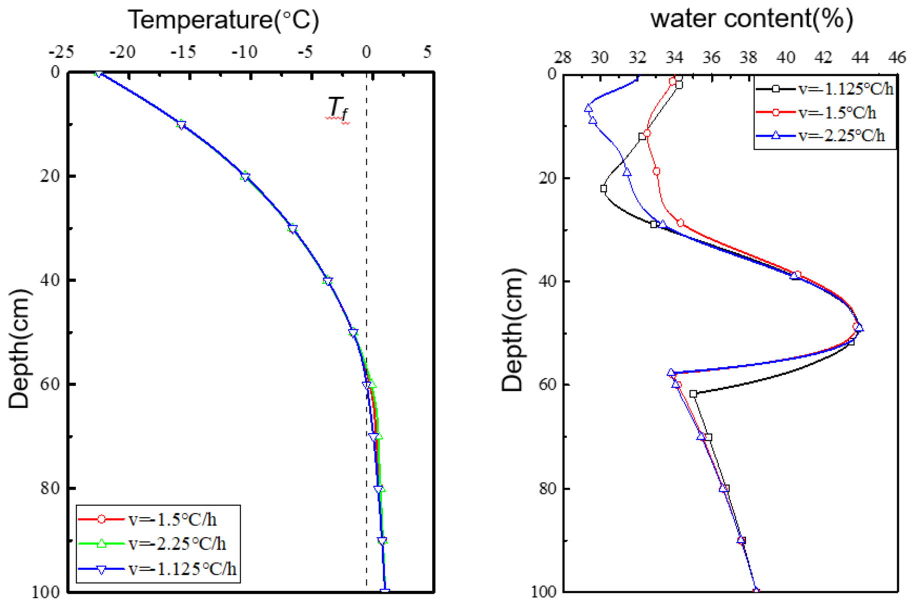

Fig.9 Temperature and water content at different cooling rate

Fig. 9 reflects the distribution of temperature and volume water content with time under the three conditions of cooling rate of -1.125 C/h, -1.5 C/h, -2.25 C/h. The final temperature of the three cases is -22.5 C. From the curve in the figure, it can be seen that the effect of freezing rate on volume water content is mainly concentrated in the shallow area, in this case, the depth is 0-30 cm. Different cooling rates have different curve forms in this area, which has no effect on the curve in deep area. In the shallow zone, with the increase of freezing rate, the distribution of water content in each layer tends to be the same, that is, the phenomenon of water migration during freezing process decreases. The cooling rate has little effect on the temperature field after freezing and stabilization.

By analyzing the influence of three factors on the total water content in the freezing process, i.e. the condition of replenishing water, freezing temperature and temperature drop rate, it is found that the condition of replenishing water affects the whole area of freezing, and there exists enriched water layer in the freezing process, with frost heave between 45 cm and 55 cm. Freezing temperature affects the distribution of water content in frozen area and the stable position of enriched water layer. The cooling rate only affects the shallow zone, and has no obvious effect on the enriched water layer. Rapid freezing can reduce the water migration during freezing process.

6. Conclusions

The differential equation of water-heat coupling and the supplementary equation of ice content are established on the basis of mass and heat conservation of differential element. Then, the coefficients partial differential equations were resolved by COMSOL, and the effects of boundary conditions on the temperature and moisture were analyzed. Some conclusions are drawn as follows,

(1) The proposed water-heat coupling model was verified based on the indoor model test. The calculated results show agree with the test results of temperature and moisture distribution.

(2)The freezing temperature and water supply conditions have great influence on the water migration of the model. Among them, the condition of water replenishment affects the whole frozen area. When there is water source replenishment, the phenomenon of enriched water layer exists in the model body.

(3) The lower the freezing temperature, the more obvious the phenomenon is, and the deeper the water enrichment layer is. When the freezing temperature decreases from -5.6℃ to -22.5℃, the water content of water enrichment layer increases from 38.5% to 43%, and its position moves downward from 27cm to 50cm below the cold end.

(4) The freezing rate only affects the shallow subgrade (0~30cm below the cold end in this model), and its increasing can inhibit moisture migration. Adequate water supply gives rise to frost heave but has no effect on the distribution of temperature.

Acknowledgments

The work is supported by the National Natural Science Foundation of China (No.51578200), the National Key Research and Development Program of China (No. 2016YFE0202400).

References

[1] Wang Yang, Liu Jingshuang, Wang Guoping, et al. The relationship between freeze-thaw and soil physical and chemical effects. Geographic and Geographic Information Science, 2007, 23(2): 91-96.
[2] Mao Yuncheng, Li Guoyu, Zhang Qinglong, et al. Study on the variation of moisture and temperature of Loess Roadbed in seasonal frozen soil region. Glacier frozen soil, 2014, 36 (4): 1011-1016.
[3] Qian Jinsong, Wang Peng, Ling Jianming, Wang Hailin. The measured characteristics of subgrade humidity in wet and rainy areas. Journal of Tongji University (Natural Science Edition), 2013, 41 (12): 1812-1817.
[4] Zongqin, Almaty, Luo Yongming, Niu Cunhuang. Experimental study on physical improvement of soil moisture in sand dunes under freeze-thaw conditions. Journal of Soil and Water Conservation, 2013, 27(01): 230-234+239.
[5] Harlan R L. Analysis of coupled heat-fluid transport in partially frozen soil. Water Resources Research, 1973, 9(5):1314-1323.
[6] Taylor G S, Luthin J N. A model for coupled heat and moisture transfer during soil freezing. Canadian Geotechnical Journal, 1978,15(4):548-555.
[7] Shepppard M T, Kaybd, Loch J P G. Development and testing of a computer model for heat and mass flow in freezing soils. National Research Council of Canada. Proceedings of the 3rd International Conference on Permafrost. Edmonton: National Research Council of Canda,1978:76-81
[8] Celia MA, Bouloutas ET, Zarba RL. A general mass-conservative numerical solution for the unsaturated flow equation. Water Resources. 1990, 26(7):1483-1496.
[9] Newman G P, Wilson G W. Heat and mass transfer in unsaturated soils during freezing. Canadian Geotechnical Journal, 1995, 34(1):63-70.

[10] Dempsey B J. A mathematical model for predicting coupled heat and water movement in unsaturated soil. International Journal for Numerical & Analytical Methods in Geomechanics, 2010, 2(1):19-34.
[11] Guymon G L, Berg R L, Hromadka T V. Mathematical model of frost heave and thaw settlement in pavements. Washington DC: Department of Transportation, 1993.
[12] Padilla F, Villeneuve J P. Modeling and experimental studies of frost heave including solute effects. Cold Regions Science & Technology, 1992, 20(2):183-194.
[13] O'Neill K, Miller R D. Exploration of a rigid ice model of frost heave. Water Resources, 1985,21(3):281-296.
[14] Gilpin R R. A model for the prediction of ice lensing and frost heave in soils. Water Resources. 1980, 16(5):918-930.
[15] Konrad J M, Morgenstern N R. A mechanistic theory of ice lens formation in fine grained soils. Canadian Geotechnical Journal, 1980, 17(4):473-486.
[16] Nixon J F. Discrete ice lens theory for frost heave in soils. Canadian Geotechnical Journal. 1991, 28:843-859.
[17] Konrad J, Duquennoi C. A Model for Water Transport and Ice Lensing in Freezing Soils. Water Resources Research, 2010, 29(9):3109-3124.
[18] Kouretzis G P, Sheng D, Wang D. Numerical simulation of cone penetration testing using a new critical state constitutive model for sand. Computers & Geotechnics. 2014, 56(3):50-60.
[19] Zhou A N, Sheng D, Li J. Modelling water retention and volume change behaviours of unsaturated soils in non-isothermal conditions. Computers & Geotechnics. 2014, 55(1): 1-13.
[20] Seetharam SC, Thomas H R, Cleall P J. Coupled thermo/hydro/chemical/mechanical model for unsaturated soils—Numerical algorithm. International Journal for Numerical Methods in Engineering. 2010, 70(12): 1480-1511.
[21] Qin B, Chen Z H, Fang Z D, et al. Analysis of coupled thermo-hydro-mechanical behavior of unsaturated soils based on theory of mixtures I. Applied Mathematics and Mechanics. 2010, 31(12): 1561-1576.
[22] Masum, Al S. Modelling of reactive gas transport in unsaturated soil:a coupled thermo-hydro-chemical-mechanical approach. Cardiff University. 2012.
[23] Van Gaelen N. Estimation of unsaturated soil hydraulic properties using a coupled hydrogeophysical inversion of inflow and electrical resistance measurements. 3rd International Cereal Cyst Nematodes Initiative Workshop. 2009.
[24] Sánchez M, Gens A, Villar M V, et al. Fully coupled thermo-hydro-mechanical double-porosity formulation for unsaturated soils. International Journal of Geomechanics. 2016, 16(6): D4016015.
[25] Qi S, Vanapalli S K. Hydro-mechanical coupling effect on surficial layer stability of unsaturated expansive soil slopes. Computers & Geotechnics. 2015, 70: 68-82.

Comparison of field data and numerical modelling of piles in seasonally freezing soils

Askar Zhussupbekov
Professor, Department of Civil Engineering
L.N. Gumilyov Eurasian National University
Kazakhstan
astana-geostroi@mail.ru

Zhanbolat Shakhmov
PhD, Department of Civil Engineering
L.N. Gumilyov Eurasian National University
Kazakhstan
zhanbolat8624@mail.ru

Gulshat Tleulenova
PhD Student, Department of Civil Engineering
L.N. Gumilyov Eurasian National University
Kazakhstan
gulshattleulenova23@mail.ru

Abstract

This paper includes short report about results of static load test, PDA and numerical modeling by driven piles of construction site “Prorva” in seasonally freezing soil ground. Cross section of piles is 40×40 cm, length 23 m. During the period from November to May, 2017 Static load tests (SLT) and PDA of pile foundations carried out in Atyrau region (Kazakhstan). Temperature was -8 ℃. Depth of freezing soil ground was 1 m. As a result of the test was obtained a graph of “load-settlement”.

Keywords: Pile foundations, static load test, load, settlement, freezing ground

1. Introduction

Issues of importance are questions about the reliability and durability of structures erected on seasonally freezing soils. In conditions of freezing and thawing of soils, pile foundations are the most appropriate. The aim of the paper is to compare the results of the SLT of pile foundations and numerical simulation of piles in seasonally freezing soils. During the period from November to May, 2017 Static load tests (SLT) and PDA of pile foundations carried out in Atyrau region (Kazakhstan). Temperature was -8 ℃. Depth of freezing soil ground was 1 m. The processes occurring in the active layer (seasonal freezing and thawing): significant temperature fluctuations; freezing and thawing of soils; frosty swelling of soils; moisture migration to the freezing front. Temperature fluctuations along the depth of the active layer are easily recorded by measuring the temperature at different depths throughout the year in the well. The greatest temperature fluctuations are experienced by the active layer. The frozen soil contains not only ice and also unfrozen water [1-3]. The purpose of this facility is to transport bulky cargo, construction materials through the Caspian Sea.

2. Geological conditions

For safety mega project deep foundations was used. Typical geotechnical conditions described by the follow soils:
Soil 1 – Silty, slightly organic, calcareous, layer thickness 0.5 m. Soil 2 – Sand, silty, calcareous, layer thickness 4.0 m. Soil 3 – Clay, silty, calcareous, layer thickness 4.0 m. Soil 4 – Sand, silty, calcareous, layer thickness 4.0 m. Soil 5 – Clay, sandy, calcareous layer thickness 5.0 m. Soil 6 – Clay, silty, calcareous, layer thickness 5.0 m. Geological conditions of construction site and details are shown in Table 1. Frost heaving swelling achieved 10 cm in Atyrau region site "Prorva".
The depth of soil freezing reaches 1 meter [1]. Table 1 presents types of soil in construction site "Prorva"

Table 1 Physical – mechanical properties of seasonally freezing soil ground

Soil	Soil name	c	φ	γ_{nat}	E_{oed}
Soil 1	Silty	0.7	29.4	19.3	2.75
Soil2	Sand	2.7	31.5	19	30
Soil3	Clay	20.8	24.5	19.1	2
Soil4	Sand	2.4	31.8	20	40
Soil5	Clay	22.7	23.8	20.6	4
Soil6	Clay	25	24.7	20.2	2

3. The methodology of pile testing

3.1 Static Compression Load Test

The Static Compression Load Test method of static loading is designed to determine the load bearing capacity of piles along the ground along the lateral surface and along the base and to establish the dependence of pile movements in the soil on the load by testing them at the construction site, carried out in a complex of design and survey works and control tests during construction. Pile testing with the SLT method is carried out with axial indentation forces applied to the pile in the form of step-increasing static loads. Tests are given without damage to the strength and carrying capacity of pile foundations. and comply with the requirements of ASTM D 1143-07.
One of the main advantages of the method is the possibility of using the tested pile in the operation of the structure. For static tests use a special stand, the load in which is created by hydraulic jacks. The stand is attached to the anchor piles. Devices are installed to record the movements of the elements of the stand and the pile. As a result of testing are obtained a graph of the "load-settlement" dependence, graphs of the resistance of the pile on the lateral surface depending on the load. Graphs of load transfer along the pile length, graphs of the specific resistance in the lateral surface along the pile length versus displacements in the soil of the test pile was obtained.
Measuring instruments used in static tests are a pressure gauge, a power measurement indicator [2-4].

3.1.1 Testing of driving piles using the SCLT method at the site "Prorva"

Static load tests conducted in accordance with the ASTM standard are cyclic. During the test using the SCLT method, the test load on the pile was 3278 kN (the first and second cycles, respectively). Vertical static pile testing with an SLT is one of the most common field tests of soils for assessing the bearing capacity of a pile. The load increment is 30%. The sequence of application of step load. In the first cycle, the test pile was loaded up to 100% of the design load, in the second cycle up to 200% (kN). The dwell time of the intermediate loading steps was 60 minutes, unloading 10 minutes. The exposure time for peak loads was 360 minutes, respectively [5-6].
The figure shows the results using the SLT method, Plaxis 2D.
The first test cycle was brought to a load of 1639 kN (curve 1, Figure 1), with a total draft of 8.64

mm. The second cycle - up to a load of 3278 kN (curve 2, Figure 1), with a total draft of 34 mm.

3.1.2 Numerical Modeling by Plaxis 2D

Numerical modelling was carried out in the “Plaxis 2D” software package. An integral part of numerical simulation is a program that allows using the numerical simulation in spatial formulation to investigate the processes of bearing capacity of pile foundations by the finite element method. Solves the problem of determining the stress-strain state of the soil and piles. Input data into the program on the geological data of the Prorva project.

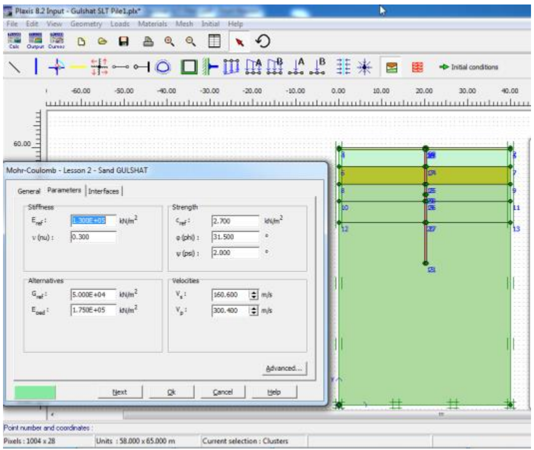

Fig. 1 Setting of program Plaxis 2D with soil types

Figure 1 shows parameters of physical-mechanical characteristics of soil types in site “Prorva” (West-Kazakhstan).

3.2 Results

Based on results of bearing capacity of pile foundation TP-02 in Plaxis 2D total displacement achieved 25 mm in seasonally freezing soil ground (Fig. 2).

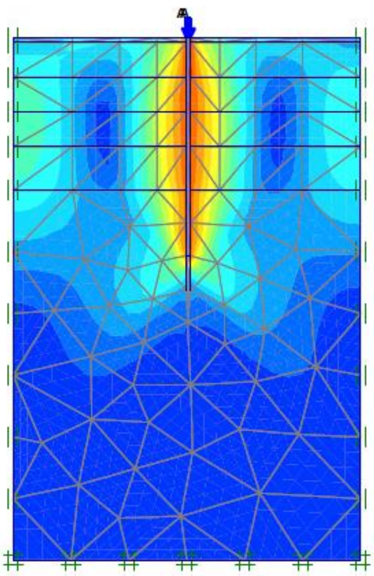

Fig.2 Graph of total displacement of pile TP-02

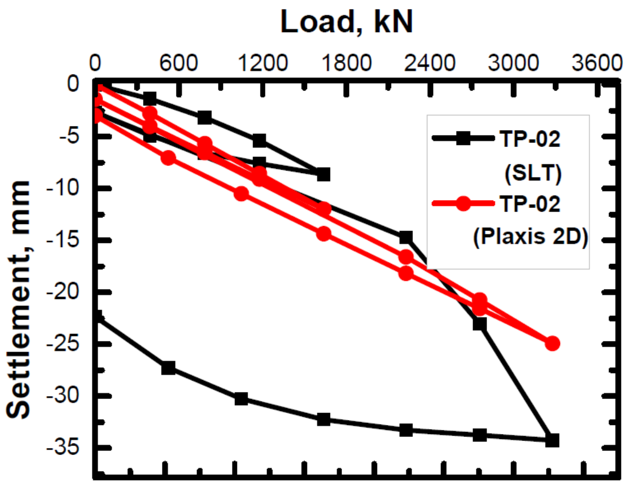

Fig.3 Graphs of SLT with numerical simulation by Plaxis 2D

Fig. 3 shows the results of the SLT of the pile TP-02 and numerical simulation Plaxis 2D pile TP-02. The curve line overlay showed that there is a change in the trajectory of the SLT curve and the numerical simulation of the SLT pile foundation TP-02. Convergence is observed when loading 2 cycles is 2650 kN, the settlement was 20 mm.

4. Conclusions

This paper presented short description of construction site “Prorva” (West Kazakhstan).
This geotechnical investigations are important for analysis bearing capacity of pile foundations by different methods. Plaxis 2D allows to analyse vertically loaded of pile in a two-dimensional space.
Test driven piles in site “Prorva” was constructed cross section 40×40 cm, length 23 m.
The vertical static loading data was maximum by using of 3278 kN, settlement was 20 mm.
These research is important for understanding of soil-structure interaction especially of behaviour driving pile in seasonally freezing soil ground in construction site “Prorva”, West-Kazakhstan.

References

[1] TELTAYEV B., SUPPES E., “Freezing characteristics of a highway subgrade”, *Proceedings of the Science in Cold and Arid regions,* Vol. 9, Iss. 3, 2017, pp. 325-330.
[2] Standard Test Methods for Deep Foundations Under Static Axial Compressive Load D1143/D1143-07’1. ASTM, 2007.
[3] SNIP RK 5.01-01-2002 “Pile foundations”, *Kazgor*, Astana, 2003.
[4] GOST 5686-1994. Soils. Field test methods piles. *Standards Publishing House.*
[5] ZHUSSUPBEKOV A., OMAROV A., MOLDAZHANOVA A., TULEBEKOVA A., BORGEKOVA K. and TLEULENOVA G., “Investigations of Interaction of Joint Piles with problematical soil ground in Kazakhstan”, *Proceedings of the 7th International* Conference on Geotechnique, *Construction Materials and Environment, Mie, Japan*, Vol. 7, No. 1, 2017, pp. 383-388.
[6] A. ZHUSSUPBEKOV , ZH. SHAKHMOV, G. TLEULENOVA , “Application of static compression load test of joint piles in seaport “Prorva” in the Caspian Sea Coastal Area (West Kazakhstan)”, *Proceedings of the First International Conference on Press-in Engineering 2018, Kochi, Japan,* 2018, pp.79-84.

Bearing Capacity of Steel Pile in Clayey Sand under Freezing Temperature

Eun Chul Shin
Professor
Department of Civil and Environmental Engr., Incheon National Univ.
Republic of Korea
ecshin@inu.ac.kr

Ju-Ho Choi, Master student, Dept. of Civil and Environmental Engineering, INU, Republic of Korea
Arum Lee, M. Eng., Dept. of Civil and Environmental Engineering, INU, Republic of Korea
Sergey Kudryavtsev, Vice Rector, Far Eastern State Transport University, Russia

Summary

The development of Sakhalin Island is necessary to cope with the demand of central government as well as local government. Currently the 6km-long bridge construction between Sakhalin Island and the mainland of Russia has been proposed by Russia central government. The preliminary test results of bearing capacity test for steel pile foundation under freezing environment have been presented in this paper. The laboratory model test conducted with the model steel pile with the diameter of 6cm and the length of 60cm in freezing ground. The temperature of frozen clayey sand was varied from –5 ℃ to –10 ℃, and –15 ℃, respectively.

Keywords: Steel pile, Bearing capacity, Freezing ground, Adfreeze bonding, Settlement

1. Introduction

As the infra-structures become bigger and higher like bridges and port facilities, there is a problem about the bearing capacity of foundation to support the load of superstructure. In general, the use of pile foundation is being increased. Therefore, it is preferable to use a steel casing pile with a large diameter which has superior horizontal stiffness and simple connection of pile head and piling, and which can secure a sufficient bearing capacity in the ground condition where the condition of soil strata changes severely. The steel casing pile has a high material strength and can penetrate into strong soil strata which having a high bearing capacity, so that a considerable load can be supported. The pile foundations in the cold region are subjected to influence of soil freezing problem around pile foundation. The moisture content of soil, types of soil, and air temperature are major sources to the freezing of soil. The adhesion strength between pile and soil under the freezing temperature is greatly influenced the bearing capacity of steel casing pile foundation for infra-structures. The bearing capacity of steel casing pile can be estimated with the summation of end bearing capacity and frictional force in unfrozen zone of soil layer, and freezing adhesion force. In this test, the freezing temperature was simulated in the freezing chamber (L=3.2 m, W=3.2m, H=2.4m) and the model test box with steel casing pile was kept inside the freezing chamber for 24 hours**.**

2. Engineering Mechanism Of Bearing Capacity

2.1 Deep foundation

The foundation is a structure that safely supports the loads acting on the upper and lower structures, and it is necessary to secure the support for the shear failure of the ground. If the foundation supporting the superstructure does not have sufficient bearing capacity, it can cause damage to the structure and destruction of the ground. The foundation can be categorized into shallow foundation ($4D_f < B$) and deep foundation ($4D_f > B$) with respect to the embedment depth of foundation (where,

D_f is embedded depth and B is width of foundation).

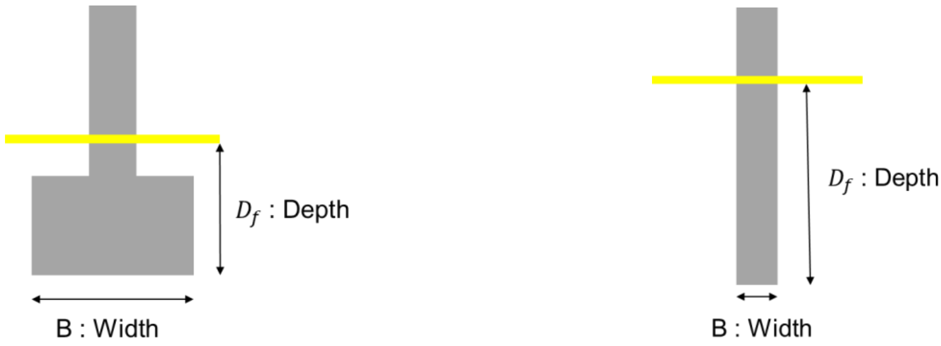

(a) Shallow foundation (b) Deep fou

Fig. 1 Classification of foundation

2.2 Bearing capacity in the frozen ground

In general, extreme bearing capacity appears as two major forces. The bearing capacity of the pile at the tip of the pile is expressed by the load acting on the pile, and the friction force of the soil due to the friction of the soil is expressed at the pile surface. But, a major force in the cold region is added with freezing adhesive force (Fig 2).

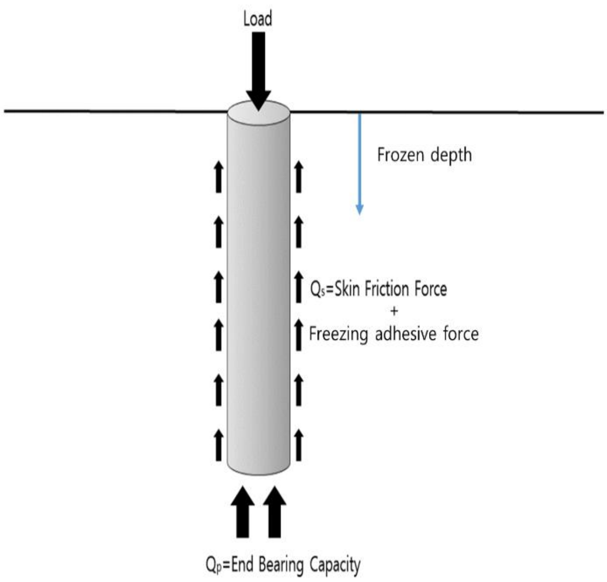

Fig. 2 Load transfer mechanism of pile foundation

The bearing capacity in the frozen ground is determined by the adhesion strength, which is the bond strength due to the interaction between the frozen soil and the pile surface.
Adfreeze bonding generally refers to a phenomenon in which moisture adheres to the surface of a heterogeneous material by freezing. Adfreeze bonding phenomenon is reported to be a typical engineering property that occurs in frozen ground with frosted soil containing pore water and volumetric expansion. Adfreeze bond strength is defined as the maximum stress at which slip failure occurs between the contact surface of the soil and the foundation in the adfreeze binding phenomenon [1]
Adfreeze bond strength is affected by various influencing factors such as freezing temperature, soil type, physical properties, and roughness constraint stress of material surface.

The main factors that have the greatest influence on the adfreeze bond strength are the freezing temperature and surface roughness. It should be taken into account when estimating adfreeze bond strength for the frozen ground foundation design [2]. Weaver and Morgensterm [2] suggested that adfreeze bond strength (τ_a) at the interface between the soil and the foundation is related to the long-term shear strength (τ_{lt}) in Eq. (1).

$$\tau_a = m\tau_{lt} \qquad (1)$$

where, m is the roughness coefficient of the surface of the pile, and τ_{lt} represents the long-term shear strength of the frozen soil.

The roughness coefficients of the pile surface are shown in Table 1.

Table 1 Coefficient for predicting adfreeze bond strength [2]

Pile material	Roughness coefficients (m)
Steel	0.6
Concrete	0.6
Uncreasoted timber	0.7
Corrugated steel	1.0

The relation between the freezing soil shear strength and the normal stress can be expressed by the Mohr-Coulomb shear strength theory of unfreezing. The relationship between the shear strength of the frozen soil and the normal stress is given by Eq. (2).

$$\tau_f = C + \sigma tan\emptyset \tag{2}$$

Where, τ_f is shear strength, c is cohesion force, σ is normal stress, and ϕ is friction angle.

3. Laboratory Experiment Work

In this paper, the bearing capacity of steel casing pile is analysis through the soil ground with the proportion of standard sand to clay of 7: 3. The pile load test was carried out on the steel casing according to the temperature change, and the bearing capacity was determined from the pile load test results using the load - settlement curve.

3.1 Soil box

The laboratory model box used in the experiment is 58 cm x 38 cm x 70 cm. It is made of iron and the insulation is attached to minimize temperature changes during the experiment. The steel pile diameter was 6 cm and the length was 60 cm. This pile is embedded in a test ground consisting of two layers, the lower layer is composed of 60 cm thick clayey soil and the upper layer is composed of 2 cm thick standard sand. Fig 3 shows the view of the model test box.

Fig. 3 View of model test box

The laboratory model test box is placed in the freezing chamber which can control the temperature down to –20 ℃. Thermocouple T type was used to check the soil temperature in model box. The soil depths are 1 cm, 2 cm, 5 cm, 10 cm, 18 cm and 19 cm respectively. LVDT was used to measure the check displacement of freezing soil. Fig 4 is shown the view of the thermocouple T type and LVDT.

(a) Thermocouple T type

(b) LVDT

Fig. 4 Thermocouple T type and LVDT

3.2 Soil condition

The soil specimen used for ground composition was consisted of standard sand (70%) and clay (30%). In order to analysis the characteristics of the soil specimen, soil laboratory tests such as particle size analysis test, specific gravity test and compaction test were conducted. Table 2 describes the soil properties of soil specimen.

Table 2 Soil properties of soil specimen

Specimen	Specific gravity, G_S	Maximum dry unit weight, $\gamma_{d.max}$ (kN/m^3)	Unified Soil Classification System, USCS
Standard sand	2.62	16.90	SP
Clay	2.66	16.25	CL

Liquid *limit and plastic limit of clays are determined as described in the Table 3.*

Table 3 Atterberg limit test result for clayey soil specimen

Liquid limit	Plastic limit
35.9 %	34.95%

For actual laboratory model tests, the soil specimen was placed in the model box and compacted with 10 cm lift thickness by using flat bottom hammer. The pile load test was conducted to determine the bearing capacity of pile under the variation of freezing temperatures (-5℃, -10℃, -15℃). The model box was placed in the freezing room for 24 hours. The temperature of the ground in the model box was checked by thermocouple. Table 4 describes the temperature variation in the ground.

Table 4 Temperature in ground by thermocouple

Temperature (℃)	
Freezing room	*Soil depth (G.L. – 10m)*
-5	*-0.4*
-10	*-0.9*
-15	*-3.3*

After freezing the soil ground, the pile load test is carried out using the test equipment shown in Fig 5. The load and the corresponding settlement were measured by a load-cell placed on the top of the testing machine and a LVDT placed along the loading shaft, respectively. The bearing capacity of soil ground was estimated from the load-settlement curve based on the experimental results. The ultimate load is selected through the load-settlement curves and the allowable load is calculated by dividing by the safety factor.

Fig. 5 View of model box set-up

4. Bearing Capacity Test Result

The allowable bearing capacity of the pile is estimated by calculating method of static bearing capacity by comprehensively examining the load condition and the settlement condition. Through the pile load test results, the allowable bearing capacity is calculated using the smallest value among the following conditions.

1. Less than 1/2 of the yielding load
2. Less than 1/3 of the ultimate load
3. Loads-settlement corresponding to allowable settlement determined by superstructure with consideration of safety factors

When determining the long-term allowable bearing capacity based on the settlement, the load bearing capacity is calculated to be 1/2 of the load corresponding to a settlement of 20 mm or 25 mm. The static bearing capacity calculation method is compared with the calculating based on the settlement, and a smaller value is selected as the allowable bearing capacity. The design load is expressed as the allowable bearing capacity. The load bearing capacity -settlement curves are shown in Fig 6.

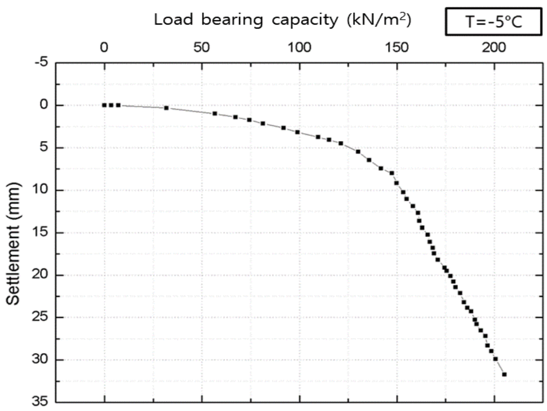

(a) P-S curve at -5 ℃

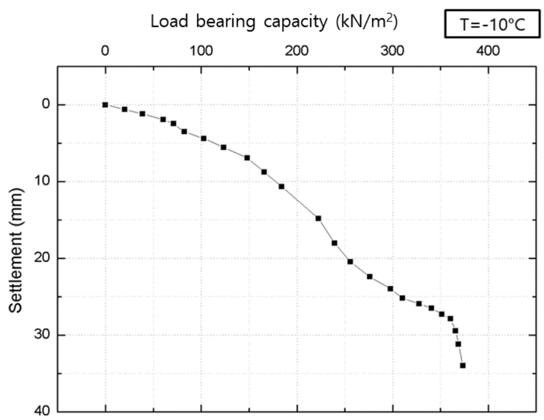

(b) P-S curve at -10 ℃

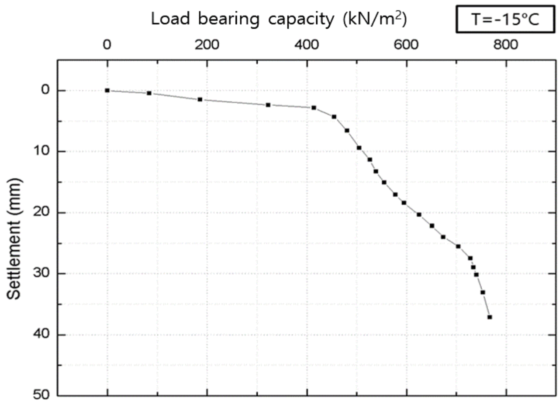

(C) P-S curve at -15 ℃

Fig*. 6 Load bearing capacity-settlement curve with temperature variation*

From the load bearing capacity-settlement curves is shown in Fig. 6. It is difficult to judge the ultimate load, and the yield bearing capacity is estimated by the static bearing capacity calculation method. Fig 7 shows the yield bearing capacity with the temperature variation *[3].*

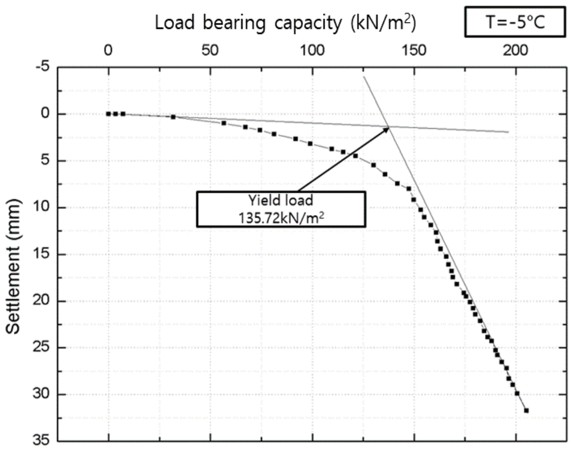

(a) Yield bearing capacity at -5℃

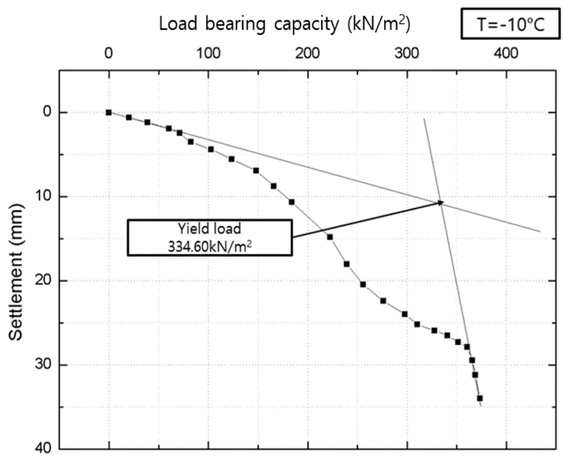

(b) Yield bearing capacity at -10℃

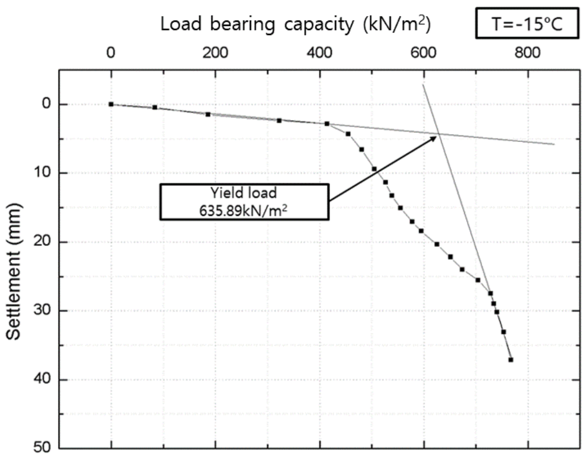

(c) Yield bearing capacity at -15℃

Fig. 7. *Yield bearing capacity from P-S curve*

The yield bearing capacity according to temperature changes are summarized in Table 5.

Table 5 Yield bearing capacity with the temperature variation

Case	Temperature (℃)	Yield bearing capacity (kN/m^2)
No. 1	-5	135.72
No. 2	-10	334.60
No. 3	-15	635.89

The allowable bearing capacity is calculated by calculating P-S curve method according to the temperature change. A value of 1/2 for each yield bearing capacity is the allowable bearing capacity. Table 6 describes the allowable bearing capacity according to the temperature change.

Table 6 Estimation of static bearing capacity

Case	Temperature (℃)	Allowable bearing capacity, q_a (kN/m^2)
No. 1	-5	67.86
No. 2	-10	167.3
No. 3	-15	317.95

It can be calculated as the ultimate bearing capacity by taking 1.5 times the yielding load. Table 7 presents the ultimate bearing capacity according to the temperature variation.

Table 7 Estimation of ultimate bearing capacity

Case	Temperature (℃)	Allowable bearing capacity, q_a (kN/m^2)
No. 1	-5	101.79
No. 2	-10	250.95
No. 3	-15	476.91

Allowable bearing capacity can be calculated from the loads-settlement curve with a settlement criterion of 25.4 mm [4]. Fig. 8 shows the of determination allowable bearing capacity.

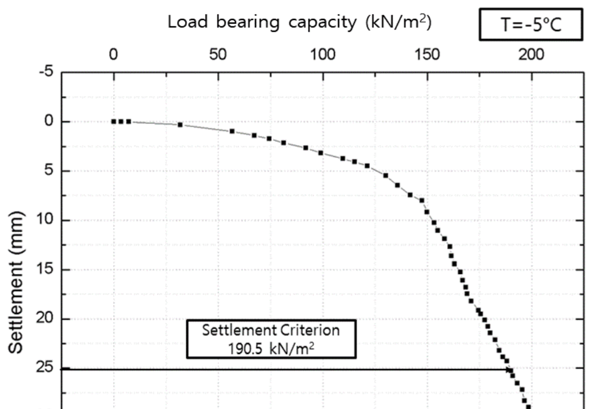

(a) Load bearing capacity at -5 ℃

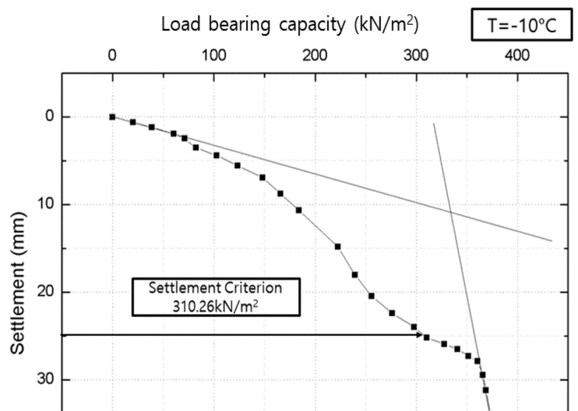

(b) Load bearing capacity at -10 ℃

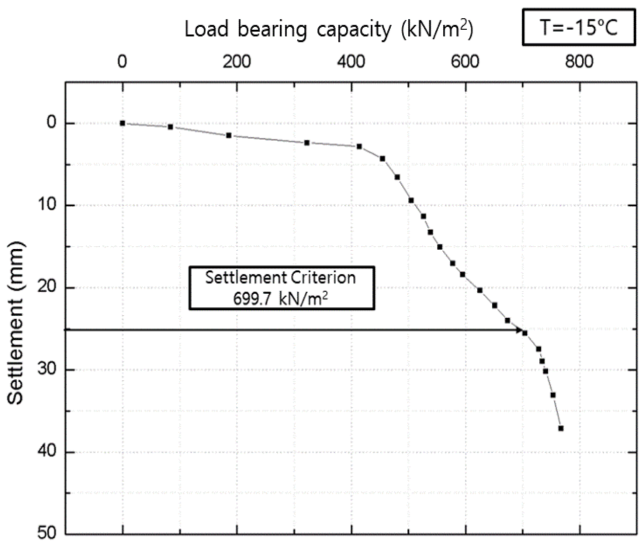

(c) Load bearing capacity at -10 ℃

Fig. 8 Load bearing capacity according to settlement criterion of 25.4mm)

The allowable bearing capacity by calculating P-S curve method and allowable bearing capacity from the settlement criterion are summarized in Table. 8.

Table 8 Estimation of settlement criterion

Case	Temperature (℃)	Allowable bearing capacity, q_a (kN/m^2)
No. 1	-5	95.25
No. 2	-10	157.45
No. 3	-15	349.85

Allowable bearing capacity from P-S curve and the allowable bearing capacity by the settlement criterion are compared in the Table 9. The allowable bearing capacity is selected by selecting smaller values from the given two results.

Table 9 Comparison of allowable bearing capacity

Temperature (℃)	Allowable bearing capacity, q_a (kN/m^2)	
	Load bearing capacity by P-S curve method	Settlement criterion
-5	67.86	95.25
-10	167.3	155.13
-15	317.95	349.85

The allowable bearing capacity calculated by the P-S curve method is lower than that of the allowable bearing capacity calculated by the settlement criterion.

5. Conclusion

In this paper, bearing capacity tests on frozen soil were conducted and analyzed the bearing capacity with temperature variation. As a result, the following conclusions were obtained.

1. The yield bearing capacity was estimated from the P-S curve based on the results of pile load test. The yield bearing capacity at -5 ℃ was 101.79kN/m^2, The yield bearing capacity at -10 ℃ was 334.60kN/m^2, The yield bearing capacity at -15 ℃ was 476.91kN/m^2.

2. As a result of estimating the ultimate bearing capacity based on the results of the pile load test, The ultimate bearing capacity at -5 ℃ is 101.79 kN/m^2, The ultimate bearing capacity at -10 ℃ is 250.95 kN/m^2, The ultimate bearing capacity at -15 ℃ is 476.91 kN/m^2.

3. When comparing the results of estimating the allowable bearing capacity by the bearing capacity estimation method, the allowable bearing capacity of the P-S curve method is lower than that of settlement criterion. Allowable bearing capacity at -5 ° C is 67.861 kN/m^2, allowable bearing capacity at -15 ° C is 317.95 kN/m^2. at –10° C, the method of estimating the allowable bearing capacity based on the settlement is 155.13kN/m^2, which is lower than P-S curve method.

4. The lower the freezing temperature, the higher bearing capacity. Also, the longer the freezing time gives the greater bearing capacity.

References

[1] CUTHBERTSON-BLACK R., *The Interaction between a Flighted Steel Pipe Pile and Frozen Sand*, Thesis for Master Degree, University of Manitoba, 2001, pp. 34-56.

[2] WEAVER, J.S., and MORGENSTERN, N.R., "Pile Design in Permafrost", *Canadian Geotechnical Journal*, 1981, pp. 357-370

[3] LEE, J.H., *Analysis of Group Behavior of Helical Piles in Sands with Inner Cone Penetration*, Thesis for Master Degree, Incheon National University, 2017, pp. 15-19.

[4] TERZAGHI, K., PECK, R.B., *Soil Mechanics in Engineering Practice*, John Wiley and Sons, INC., 2nd Ed. 1967

[5] SHIN, E.C., KIM, B.C., LEE, S.M., "The Frost Heaving Characteristics of Water-repellent Soil Using Laboratory Freezing System", *Korean Geosynthetics Society*, 2012, pp. 145-150.

[6] LEE, J.Y., KIM, Y.S., CHOI, C.H., "A Study for Adfreeze Bond Strength Developed between Weathered Granite Soils and Aluminum Plate", *Journal of the Korean Geo-Environmental Society*, 2013, pp. 23-30.

[7] KANG, S.J., JEONG, J.H., LEE, J.C., LEE, Y.D., "Bearing Capacity Analysis of Steel Pipe Pile with Loading Test Types", *Korean Society of Civil Engineers*, 2005, pp. 4328-4331.

[8] LIM, J.S., CHOI, Y. K., SIM, J.S., PARK, J.H., "A Study on the Maximum Skin Friction of Steel Piles Using the Results of Field Load Tests", *Korean Society of Civil Engineers*, 2008, pp. 1997-2000.

[9] LEE, W.J., PARK, J.H., LEE, S.W., "Bearing Capacity and Settlement of Large Scale Tubular Steel Pile with Negative Skin Friction", *Korean Society of Civil Engineers*, 2014, pp. 256-266.

[10] LEE, Y.H., KIM, M.H., "Load Transfer Characteristics and Ultimate Bearing Capacity of PHC Pile in Deep Soft Clay Layer", *Journal of the Korean Geo-Environmental Society*, 2008, pp. 41-46.

[11] LEE C.Y., KIM J.R., KANG, K.S., KANG H.B., LEE J.M., "Laboratory Comparison of Soft Ground Behaviors due to Static and Dynamic Loads", *Korean Society of Civil Engineers*, 2003, pp. 3537-3542.

[12] LEE, J.Y., CHOI, C.H., CHO, S.D., "Adfreeze Bond Strength Characteristics with Varying Normal Stress and Surface Roughness", *Korean Society of Civil Engineers*, 2013, pp. 2654-2657.

Study on the Permeability of Unfrozen Part of Soils in Artificial Ground Freezing

Go Hirose,
Section chief
Okumura Engineering Corporation
Japan
g.hirose@okumuradbk.co.jp

Yuzuru Ito, Professor, Setsunan University, Japan

Summary

Artificial Ground Freezing (AGF) is used for civil engineering works because frozen soils have many advantages such as high strength, low permeability, and excellent sealing performance and so on. For example, AGF has been used for mining sites and shield tunnel excavation for over one hounded years. Recently, AGF is also used for confining contaminated soils and shielding the destroyed nuclear reactor from groundwater inflow. In such a case, a frozen earth wall is required to be maintained for a long period.

We have been studying the mechanism of the permeability of freeze-thawed soil. The permeability of the freeze-thawed soil is significantly greater than that of the unfrozen soil but we can neither understand the mechanism nor predict them. In order to evaluate the permeability of the freeze-thawed soil, a conventional vertical freeze-thaw test (V-test) and a horizontal freeze-thaw test (H-test) have been conducted. Because in AGF, freezing pipes are installed vertically into the ground and freeze the surrounding soil horizontally. In the thawing process, the groundwater may be able to flow along the thawing frozen earth wall or into the wall inside. In the V-test, the permeability of freeze-thawed soil was influenced strongly by overburden pressure, and the relationship of the void ratio vs permeability of the freeze-thawed soil became significantly different from the unfrozen soil. The permeability of freeze-thawed soil in H-test was generally greater than that of the V-test.

So far, we understand that the permeability of a freeze-thawed soil is governed by the strength of soil structures and overburden pressure. In addition, it was revealed by the author's research [1] that increment permeability of horizontally freeze-thawed soil is caused by distribution change of the void ratio.

In this paper, we reported the recent findings on the permeability change of the unfrozen soil in front of the freezing soil. Since it is known that when a fine-grained soil is subject to freezing, shrinkage cracks (SCs) generate in front of the freezing soil by dehydration caused by ice lenses (ILs) formation. The horizontal freezing test was conducted keeping both the warmer and colder temperature sides constant and the falling head permeability test was conducted for the half-frozen specimen. In this test method, the thick last IL was generated at the ceased freezing front.

The test results were as follows. (1) Permeability of the unfrozen soil in front of the freezing soil was measured. The permeability was obtained by calibrating the volume of water intake into ILs. (2) In the case of lower test pressure, the permeability of the unfrozen soil in front of freezing soil was greater than that of unfrozen soil which was measured before the freeze-thaw test. While in the case of greater test pressure, the permeability of the unfrozen soil in front of freezing soil was decreased. (3) According to the void ratio distribution of the specimen obtained after the freeze-thaw test, a void ratio of the unfrozen soil remarkably decreased by dehydration caused by the thick ILs generation. The permeability of the unfrozen soil increased although the void ratio decreased. This result suggested that the water flowed into cracks such as SCs caused by dehydration.

Keywords: Permeability, Freeze-thawed soil, Unfrozen soil, Shrinkage crack, Ice lens, Artificial ground freezing

1. Background

In cold regions, the ice lenses (ILs) may generate when a fine-grained soil is freezing. The ILs become thicker with moisture movement from unfrozen soil. In contrast, unfrozen soil in front of the ILs is dehydrated and shrinkage cracks (SCs) may generate. It had believed that ILs and SCs caused the permeability of the freeze-thawed soil to increase [2]. Benson et al. argued that the factors affecting the increasing permeability of the freeze-thawed soil were the trace of ILs [3].

In the artificial ground freezing method (AGF), freezing pipes are placed vertically into the ground and frozen horizontally to make frozen earth wall (FEW). It has been used for mineral mining of shield tunnel for a long time. Recently, there are some cases that AGF is used to the containment of contaminated soil [4].

In Fukushima Nuclear Power Plant Decommissioning Project, FEW of approximately 30m in depth and 1,500m in extension is being built, so as to reduce groundwater inflow to the destroyed reactor building until the countermeasure is completed for preventing contaminated water entering into the reactor building [5]. It is expected for FEW to exert an effect to decrease the contaminated water generation [5]. However, for long-term stable operation, it was necessary to clarify permeability change of freeze-thawed soil in the case that FEW is partially thawed because power supply may be stopped by another earthquake shock. The permeability of freeze-thawed soil was studied by two test types. (1) The horizontal freeze-thaw test: Freezing was conducted horizontally and a permeability test was conducted vertically. (2) the vertical freeze-thaw test: Freezing was conducted vertically and permeability test was performed vertically [6]. The test result revealed that permeability of freeze-thawed soil was strongly affected by test pressure and the permeability obtained from the horizontal freeze-thaw test was greater than that obtained from the vertical freeze-thaw test [7]. The cause of this was what the void ratio of the low-temperature side considerably increased in the horizontal freeze-thaw test. The vertical freeze-thaw test revealed the relationship between void ratio and permeability of the freeze-thawed soil, and a method to experimentally predict permeability of freeze-thawed soil has been proposed from the void ratio distribution obtained by horizontal freeze-thaw test [1].

This time, the author's concern is unfrozen soil in front of freezing soil. In order to manage FEW with constant thickness during the maintenance period, the location of the IL which finally generated near the boundary between FEW and unfrozen soil (final IL) is fixed, and therefore it is expected that the thickness of final IL increases with time and SCs generate in unfrozen soil by intense dehydration.

Fig. 1 shows freezing status in the horizontal freeze-thaw test. A number of horizontal cracks like SCs in unfrozen soil and ILs in frozen soil were observed. The water flow that passes SCs may dramatically increase permeability. Therefore, this study aimed at clarifying permeability change of unfrozen soil due to SCs that generates in the unfrozen side in front of the final IL, and investigated permeability change of unfrozen soil by the horizontal freeze-thaw test.

2. Purpose

The purpose of this study is to clarify the permeability change of unfrozen soil in front of freezing soil. Therefore, the followings were conducted.

(1) In order to clarify the permeability change of unfrozen soil in front of freezing soil, step-freezing was carried out in a horizontal freeze-thaw test which reproduced AGF and the permeability of the unfrozen soil in front of freezing soil was measured.

(2) In order to clarify that the degree of SCs generation affects the permeability of unfrozen soil in front of freezing soil, the horizontal freeze-thaw test was conducted

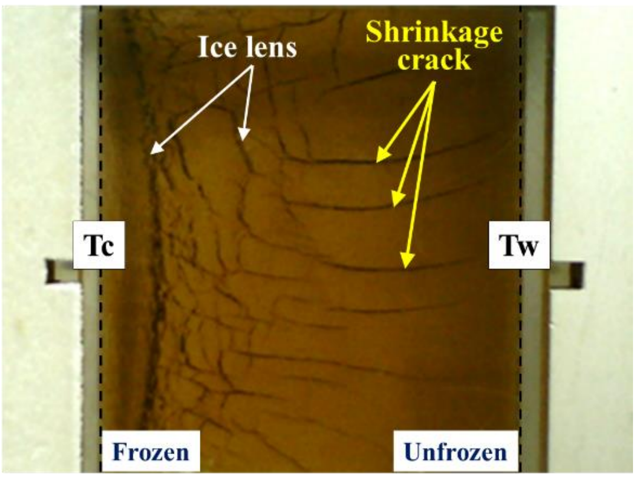

Fig. 1 IL and SC generated during the horizontal freeze-thaw test.

on the different conditions in test pressure and temperature gradient.

3. Test method

3.1 Test specimen

Table 1 shows the physical properties of the sample soil. The sample soil was adjusted to the water content 1.5 times greater than the liquid limit and was vacuumed and then kept in the laboratory for 24 hours at 20℃ and consolidated up to pre-consolidation pressure P =500 kN/m^2. Thereby the specimen was formed rectangle shape with length b = 8cm, width w = 7cm and height h = 7cm.

3.2 Test condition

Table 2 shows test conditions. In order to clarify permeability change of the unfrozen soil in front of freezing soil, test pressure p and temperature gradient dT/dx were varied in the test. As test conditions, p = 50 kN/m^2 and dT/dx = 1.25 ℃/cm were applied for KS1, and p = 100 kN/m^2, dT/dx = 2.50℃/cm for KK62.

Table 1 Properties of Kizuchi clay.

Soil particle density	Liquid limit	Plastic limit	Grain size		
ρ_s	w_L	w_P	Sand	Silt	Clay
g/cm^3	%	%	%	%	%
2.702	54.5	22.1	0.9	31.5	67.6

3.3 Horizontal displacement restrained freeze-thaw and vertical permeability test

Fig. 2 shows the horizontal displacement restrained freeze-thaw and vertical permeability test. In the horizontal freeze-thaw test, the specimen was freeze-thawing horizontally with the horizontal displacement restricted and a permeability test was performed in the vertical direction. This test device consists of a top plate, a bottom plate, two cooling plates, and two acrylic side plates. The cooling plates were placed in both sides of the specimen and were cooled at Tw and Tc. Test pressure p was applied vertically and vertical displacement h_v was measured. Their temperatures were measured with temperature sensors. Water intake tank was connected to the cooling plate on the Tw side, and the weight of water intake and drainage during freeze-thaw was measured. The acrylic plate of 5cm in thickness was installed on the side of the specimen, and generated ILs and SCs were observed. A burette was connected to a bottom plate and permeability tests were conducted.

Fig. 3 shows temperature condition during the horizontal freeze-thaw test. The horizontal freeze-thaw test performed in three steps. Step1 was the phase of before freezing, Step2 was that

Table 2 Test conditions.

No.	Pre-consolidation Pressure	Test Pressure	Temperature gradient	Cooling temperature	
	P	p	dT/dx	Tw	Tc
	kN/m^2	kN/m^2	°C/cm	°C	°C
KS1	500	50	1.25	5→3→5	5→-7→5
KK64	500	100	2.50	5→10→-10→5	5→-10→-10→5

Freeze type: Step, Water supply: Open, Freeze-thaw cycle: n=1

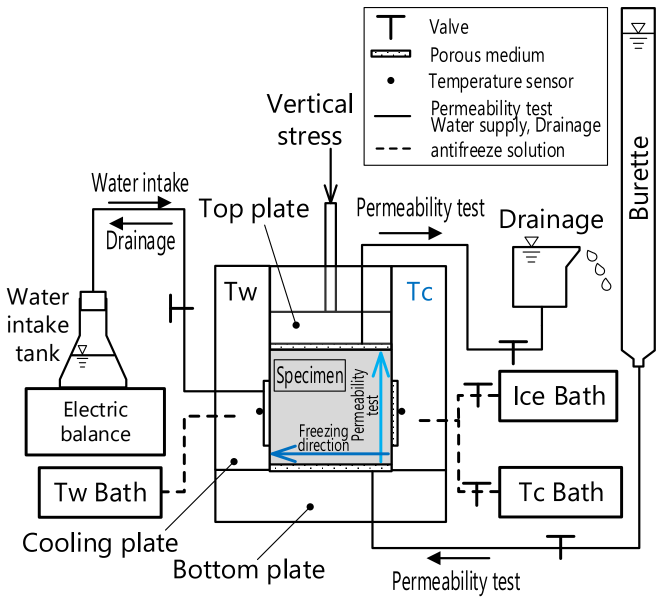

Fig. 2 Test system.

of freezing and Step3 was that of thawing.

Fig. 3(a) shows the result of KS1. In Step1, the cooling temperatures were Tc = Tw = 5℃ respectively. The permeability k_u of unfrozen soil was measured. And then the cooling temperatures were Tc = 0℃, Tw = 3℃ respectively and these temperatures kept for about 6 hours. In Step2, the cooling temperatures were Tc = -7℃, Tw = 3℃ respectively. The permeability k_{hu} of unfrozen soil in front of freezing soil was measured. In Step 3, the cooling temperatures were Tc = Tw = 5℃. The permeability k_t was measured.

Fig. 3(b) shows the result of KK64. In Step1, the cooling temperatures were Tc = Tw = 5℃ respectively. The permeability k_u of unfrozen soil was measured. And then the cooling temperatures were Tc = 0℃, Tw = 10℃ respectively and these temperatures kept for about 40 hours. In Step2, the cooling temperatures were Tc = -10℃, Tw = 10℃ respectively. The permeability k_{hu} of unfrozen soil in front of freezing soil was measured. In Step 3, the cooling temperatures were Tc = Tw = 5℃. The permeability k_t was measured.

The specimen was divided into 8 equal parts from Tw to Tc (the distance from Tw to Tc was b = 8cm) after the test, and water content was measured for computing void ratios.

3.4 Consolidation permeability test

For comparison with the permeability obtained by the horizontal freeze-thaw test, a consolidation permeability test was performed with unfrozen soil. The consolidation permeability test was the test for which the falling head permeability test and standard consolidation test were combined. The specimen was made by consolidation and was set to the standard consolidation apparatus and loaded progressively from 9.8 kN/m^2 to 628 kN/m^2 with an increment ratio of 1. A falling head permeability test was performed for 24 hours after each consolidation stage.

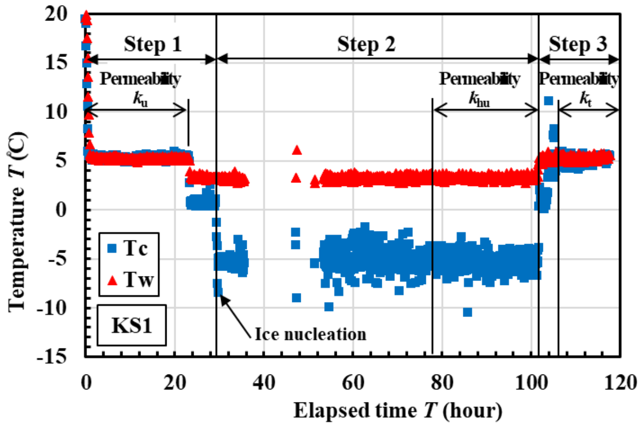

(a) KS1

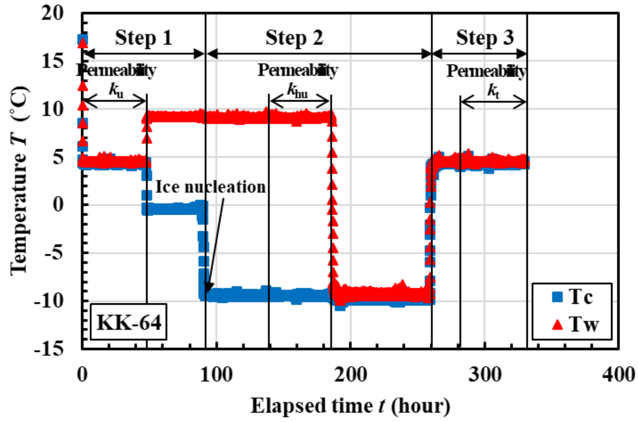

(b) KK64

Fig. 3 Temperature condition during the horizontal freeze-thaw test.

4. Result

4.1 Vertical displacement and water intake

Fig. 4 shows the vertical displacement with elapsed time. Vertical displacement h_v of KS1 and KK64 continued increasing from the start of freezing and did not converge at t' = 150 hour. A permeability test in Step 2 was performed. In KK64 with great test pressure p, h_v at the time of starting the permeability test in Step2 was h_v = 0.5 mm. In KS1 with small p, h_v at the time of start the permeability test in Step 2 was h_v = 2.4mm. The h_v of KS1 was approximately 5 times as great as that of KK64. During the permeability test

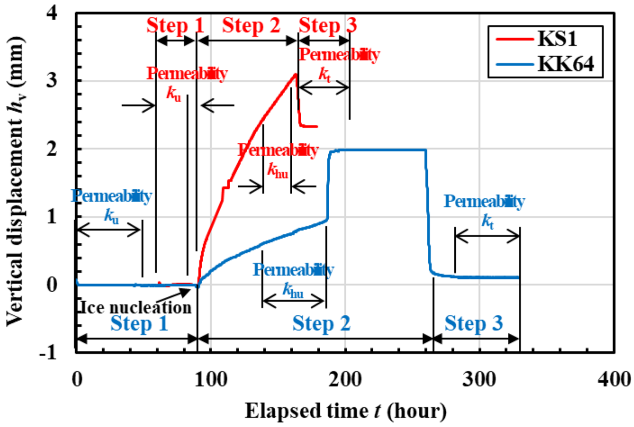

Fig. 4 Vertical displacement with elapsed time.

of Step2, h_v continued increasing even when water intake from Tw was stopped. For h_v in at the end of Step 3, h_v = 2.4 mm for KS1 and h_v = 0.1 mm for KK64.

Fig. 5 shows the water intake and drainage with elapsed time. Water intake and drainage V of KS1 and KK64 suddenly drained just after the start of freezing then they turned to intake. The water intake velocity of V was 0.04 cm^3/hour for KS1 and 0.03 cm^3/hour for KK64. The final V was greater by approximately 1 cm^3 for KS1 than before freezing and became smaller by approximately 1.8 cm^3 for KK64 than before freezing.

4.2 Void ratio distribution

Fig. 6 shows the void ratio distribution of freeze-thawed soil. The void ratio e_0 was the void ratio of unfrozen soil. The void ratio e' was the void ratio of freeze-thawed soil. In KS1 and KK64, The void ratio e' was greater than e_0 in the Tc side and was smaller than e_0 in the Tw side. In KS1 and KK64, e' at Tw decreased to approximately e' = 0.75. The range in which e' is smaller more than e_0 was 2 cm from Tw for KS1 and 4cm from Tw for KK64. In the range of what e' is greater than e_0, e' of KS1 increased overall from Tc to 5.5cm from Tc, and e' = 0.95 at the maximum. e' of KK64 was almost the same as e_0 till 1.5cm from Tc while it suddenly increased at 2.5cm and 3.5cm from Tc and e' = 1.15 at the maximum. It was recognized that e' was greatest around the final IL. It was supposed that e' lowered more than e_0 was caused dehydration by water intake to the final IL. It was inferred that the permeability of the range where e' was smaller than e_0 was measured as k_{hu} in the permeability test in Step 2.

4.3 Relationship between void ratio and permeability

Fig. 7 shows the measured permeabilities of initial unfrozen soil, unfrozen soil in front of frozen soil and freeze-thawed soil with elapsed time. Permeability k_{hu} was the permeability of unfrozen soil in front of freezing soil calculated by subtracting the amount of

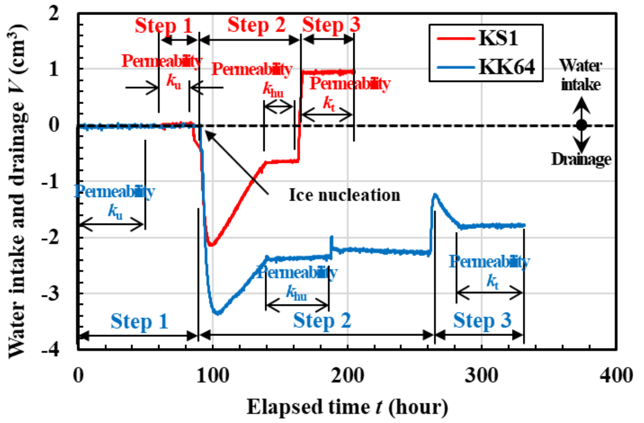

Fig. 5 Water intake and drainage with elapsed time.

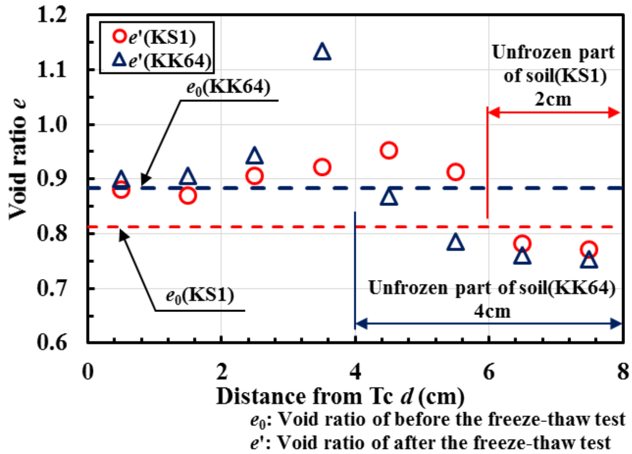

Fig. 6 Void ratio distribution.

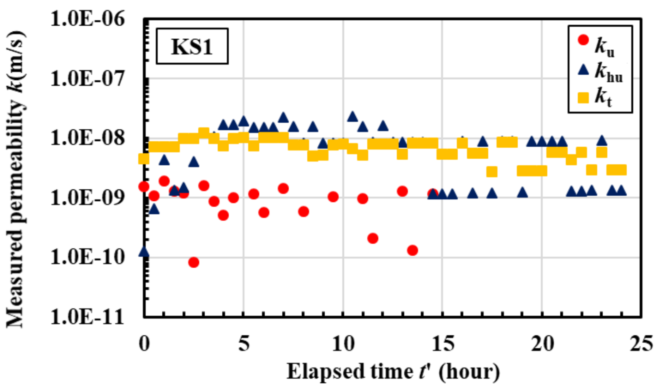

(a) KS1

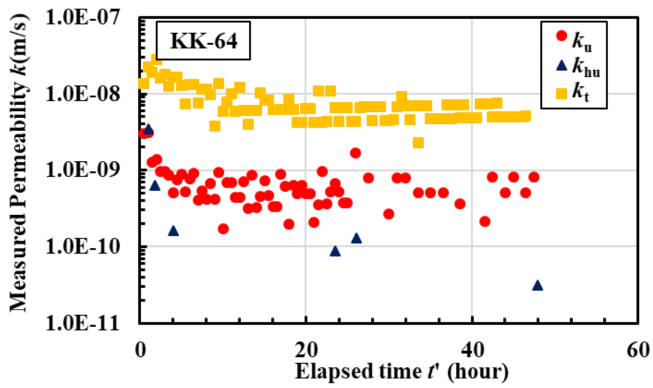

(b) KK64

Fig. 7 Permeabilities during freeze-thaw test.

water intake and drainage V change 0.04 cm^3/hour (KS1) and 0.03 cm^3/hour (KK64) in Fig. 5 from the water head difference of the burette in the permeability test. And a cross-sectional area of flow for calculating k_{hu} was assumed the range of $e' < e_0$. k_t was the permeability of freeze-thawed soil. k_u was the permeability of unfrozen soil. k_{hu} and k_t were greater than k_u in KS1, while k_{hu} was smaller than k_u in KK64.

Fig. 8 shows the relationship between the average of void ratio and that of measured permeability. Average of measured permeability was the permeability which was averaged the measured permeabilities from 4 hours to the end of the permeability test. The average of void ratio e_{ave} corresponding to k_{hu} was the value obtained by averaging e of the unfrozen soil in front of freezing soil. In KS1, k_{hu} increased by approximately 20 times compared with k_u. In KK64, k_{hu} was approximately 0.2 times as great as k_u. The permeabilities k_t of KS1 and KK64 almost correspond with each other, and they increased more considerably than k_u.

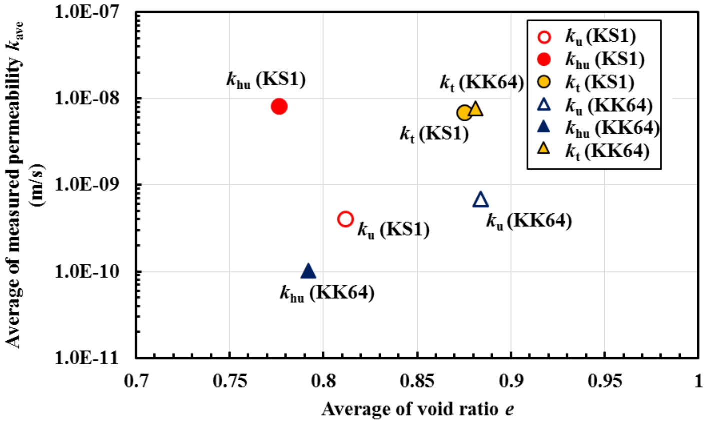

Fig. 8 Void ratio and permeability.

Fig. 9 shows observation of the specimen during Step3 of KK64. Marks of ILs were observed around the center of the specimen. Marks of ILs were recognized in KS1 too. Therefore it is supposed that this ILs trace acted as a water path so k_t was greater than k_u. Since k_{hu} of KS1 almost corresponds with k_t, crack that acted as a water path might have observed in the specimen inside even in the unfrozen soil during Step2 for KS1.

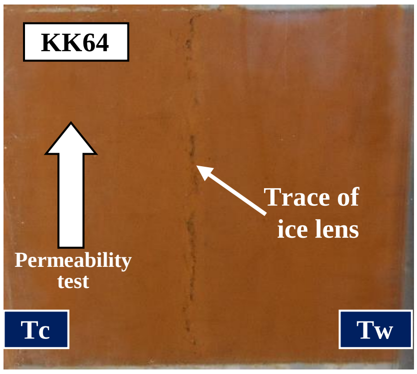

Fig. 9 Marks of ice lens observed during Step3.

Permeability of unfrozen soil in front of freezing soil k_{hu} of KK64 decreased more than k_u. Since the void ratio of unfrozen soil in front of freezing soil, as shown in Fig. 6, was not constant, the permeability of the soil with a low void ratio may have strongly influenced k_{hu}.

The relationship between the void ratio and the permeability with unfrozen soil obtained from the consolidation permeability test was shown in Equation (1) as follow.

$$k_i = 1.026 * 10^{-12} * \mathrm{EXP}\,(7.369 * e) \quad (1)$$

The Permeability k_i was computed from substituting the void ratio given by the horizontal freeze-thaw test into Equation (1). Computed permeability k' was obtained by substituting the permeabilities into Equation (2) in Fig. 10.

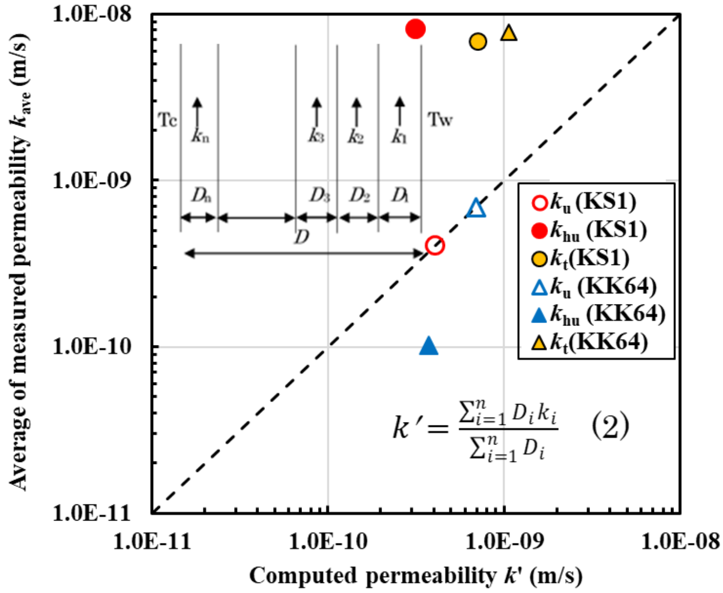

※Computed permeability from void ratio of freeze-thawed soil

Figure 10 Computed and measured permeabilities.

Fig.10 shows the relationship between the computed permeability and the average of measured permeability by the permeability test of the horizontal freeze-thaw test. k_{ave} was smaller than k' in k_{hu} of KK64. In other words, it cannot be said that k_{hu} of KK64 was lowered by decreased the void ratio distribution of the unfrozen soil in front of freezing soil. The k_{ave} was considerably greater than k' in k_{hu} of KS1. SCs may have influenced the considerable increase in permeability of unfrozen soil in front of freezing soil seen in KS1.

5. Conclusions

The results of this study are summarized below.

(1) In these tests, the vertical displacement h_v increased during freezing. On the other hand, the water drained from the soil at the start of the freezing, and then the water took into the soil during freezing.

(2) The void ratio of freeze-thawed soil located between Tc and the final IL was greater than that of unfrozen soil. The void ratio near the final IL considerably increased. On the other hand, the void ratio of unfrozen soil in front of the final IL decreased.

(3) The measured permeability k_{hu} was the permeability of unfrozen soil in front of freezing soil. k_{hu} was computed by subtracting the water intake from the burette and considering the cross-sectional area of unfrozen soil.

(4) In the smaller test pressure, k_{hu} was greater than the permeability of the unfrozen soil k_u and almost equal to the permeability of the freeze-thawed soil k_t. In contrast, in the greater test pressure, k_{hu} was smaller than k_u.

(5) Marks of ILs were observed during the thawing in KS1 and KK64. It is supposed that this Mark acted as a water path so k_t was greater than k_u. Since k_{hu} of KS1 almost corresponds with k_t, the cracks in the specimen inside of unfrozen soil in front of freezing soil might act as a water path.

(6) In the smaller test pressure, the measured permeability of the unfrozen soil in front of freezing soil was greater than the permeability computed by substituting the void ratio of the unfrozen part of soil during freezing into the unfrozen soil's relational equation between void ratios and permeabilities. This result indicated that the permeability of the unfrozen soil in front of freezing soil was influenced by the shrinkage cracks.

Acknowledgments

This study was supported by JSPS Grants-in-Aid for Scientific Research Grant Number JP17H03307.

The major part of the tests was carried out as a graduation study by Mr. Shohei Miyagi, Mr. Ryuki Sugihara, Ms. Mai Yoshikawa at the Department of Civil and Environmental Engineering, Setsunan University.

References

[1] Hirose, G., Ito, Y., “Experimental estimation of permeability of freeze-thawed soils in artificial ground freezing”, *Proceedings of the International Scientific Conference Transportation Geotechnics and Geoecology*, Procedia Engineering, Vol189, pp.332-337(2017).

[2] Chamberlain, E. J., “Effect of freezing and thawing on the permeability and structure of soils”, *Engineering Geology*, Vol.13, pp. 73-92(1979).

[3] Benson, C. and Othman, M. A., “Hydraulic conductivity of compacted clay frozen and thawed in situ”, *Journal of Geotechnical Engineering*, Vol.119, No.2, pp.276-297 (1993).

[4] Wagner, A. M., “Creation of an artificial frozen barrier using hybrid thermosiphons”, *Cold Regions Science and Technology*, Vol.96, pp.108-116(2013).

[5] http://www.meti.go.jp/earthquake/nuclear/osensuitaisaku/committtee/osensuisyori/2018/pdf/020_04_00.pdf, (2018, in Japanese).

[6] Hirose, G. and Ito, Y., “Experimental study on the permeability change of fine-grained soil by freeze-thaw effect”, *The 11th International Symposium on Cold Regions Development*, USB 6-2 IC-013 (2016).

[7] Hirose, G., Ito, Y., Ishikawa, T. and Akagawa, S., “Experimental Prediction of Permeability of Freeze-Thawed Fine-Grained Soil”, *Journal of JSCE*, Vol.6, Issue 1, pp. 156-166(2018).

Study on the unfrozen water content to understand the engineering properties of saturated fine-grained soils

Kosuke Tsukamoto
Master Student
Setsunan University
Japan
18m205tk@edu.setsunan.ac.jp

Yuzuru Ito, Professor, Setsunan University, Japan

Summary

In order to understand the engineering properties of a fine-grained soil, it is extremely important to understand the state of pore water. However, it is almost impossible to measure the state of pore water directly. In this paper, the use of a freezing test was challenged for this purpose. By dropping the specimen temperature, the pore water existing in the fine grain soil gradually freezes. This time the amount of either frozen or unfrozen water may be related to the soil's engineering parameters.

Usually, measurement of unfrozen water has been conducted under unloaded conditions by using some very sophisticated methods[1)]. In this study, frozen and unfrozen water measurement was carried out by volume expansion principal under the loaded condition using a small cell of diameter Φ=6cm and height h=2cm. Because of the small cell size, the temperature distribution can be maintained uniformly and thus we can measure unfrozen water accurately.

In this study, the coefficient of permeability was evaluated by using the frozen porosity and the frozen void ratio. As a result, the following conclusions were obtained; (1) In the normal consolidation condition, the newly defined frozen void ratio is greater with a smaller load p. And the unfrozen void ratio e_u is greater with a greater load p., (2) The relationship between void ratios (e_f, e_0) and the permeability k_p presents that the frozen void ratio e_f represent permeability more precisely than initial void ratio e_0., (3) Similarly, the frozen porosity n_f, which is the cross-sectional area of water path in a soil, may be better represent k_p than initial porosity n_0., (4) In other words, we can propose very simple equations to explain the coefficient of permeability k_p as,

$$k_p=c_1\times e_f \qquad k_p=c_2\times n_f$$

where, c_1, c_2: constants.

Keywords: frozen void ratio e_f, unfrozen void ratio e_u, coefficient of permeability k_p, frozen porosity n_f $=e_f/(1+e_0)\times100$ (%), initial porosity $n_0=e_0/(1+e_0)\times100$ (%), frozen void ratio function $e_f^3/(1+e_0)$, initial void ratio function $e_0^3/(1+e_0)$.

1. Background

A saturated fine-grained soil consists of only soil particles and pore water. In such soils, like clay and silt, the pore water close to the soil surface is strongly attracted by the surface force of the soil particles. Therefore, pore water of fine-grained soil is roughly divided into the adsorbed water which is attracted by soil's surface force, and the free water which is not affected. However, their boundaries are not clear, because the adsorption force becomes weaker according to the distance from the soil's surface.

It was considered that engineering properties of fine-grained soil have some relationship with properties and quantities of such pore water influenced by the soil's surface force. For example, it is inferred that the characteristic that adsorption water has a viscosity in inverse proportion to the distance from soil surface due to the surface force of fine-grained soil[2)] influences the permeability or consolidation characteristics of the fine-grained soil. It was thought that it is the reason why there exists soil with a coefficient of permeability that is from 1,000 times to 1 million times different even with the same void ratio[3)].

On the other hand, measurement of frozen and unfrozen water has been conducted by some very sophisticated methods. But the influence of the initial void ratio and loading has been ignored. In this study, the authors measure frozen and unfrozen water carried out by a method using a volumetric expansion method change when the phase changes from water to ice[4] under loading condition. And we have tried to clarify the relationship between frozen or unfrozen water to the coefficient of permeability.

2. Purpose

The method to obtain the amount of unfrozen water in the freezing soil developed by the authors utilizes volume expansion principal at the time when water freezes. Before experiments have been performed under loading condition with a specimen of diameter Φ=10cm and height h=3cm in +20˚C constant temperature indoor. Because, temperature difference could not be ignored on the top and bottom faces of the specimen[5] we developed a smaller specimen cell of diameter Φ=6cm and height h=2cm in this study, to avoid the difference of temperature distribution, and performed frozen and unfrozen water measurement under normal consolidation condition in a cold room at +3˚C. By using obtained frozen void ratio e_f and unfrozen void ratio e_u, the relationship with the coefficient of permeability k_p and parameters were examined.

Table 1 Physical property of the sample soil.

Sample	Soil particle density ρ_s (g/cm^3)	Liquid limit LL (%)	Plastic limit PL (%)	Particle size distribution Sand (%)	Slit (%)	Clay (%)
Fujinomori 16N	2.705	45.5	23.4	3.7	46.3	50.0
Kizuchi 16N	2.702	54.5	22.1	0.9	31.5	67.6

Table 2 Experimental conditions.

Sample soil	Preconsolidation /Confining pressure $P = p$ (kN/m^2)	Initial void ratio e_0
Fujinomori 16N	39.2	1.142
	78.5	1.064
	157	1.015
	314	0.930
	628	0.840
Kizuchi 16N	39.2	1.161
	78.5	1.065
	157	0.975
	314	0.906
	628	0.816

Cooling temperature: +3˚C →0˚C →-0.7˚C →-1.0˚C →-1.5˚C →-2.0˚C →-3.0˚C →-5.0˚C →-10˚C →-20˚C.

3. Experimental method

3.1 Specimen preparation

Table 1 shows the physical properties of the sample soil. The water content of the sample soil was adjusted at the level 1.3 times higher than the liquid limit (LL) and thoroughly mixed. The specimen was made by preloading with predetermined pressure after deaeration. Consolidation test (JIS A 1217, 1218) is then conducted and the coefficient of permeability k_c was obtained. Further, the coefficient of permeability k_p can be obtained directly by performing a falling head permeability test after each loading stage.

3.2 Frozen and unfrozen water measurement

Fig. 1 shows the frozen and unfrozen water measurement device. This device was set in a temperature-controlled cold room. Cooling plates were placed on the top and bottom ends of the acrylic cell to freeze up the specimen from the top and bottom. The specimen was made in the same way as (3.1) and was set on the acrylic cylinder cell of diameter Φ= 6cm and height h=2cm. The specimen was put in the cold room of +3˚C to maintain the temperature during the experiment. In order to measure the temperature of both ends of the specimen, P_t sensors (reading 0.01˚C) were set for the top and bottom sides. In addition, the thermocouples (reading 0.1˚C) were set on the three points of the top and bottom sides each, six points in total.

Anti-freeze (the ethylene glycol solution for which concentration is adjusted so that it cannot be frozen at over -20˚C) was circulated from the top plate to the bottom plate from the freezing bath. Freezing starts from 0˚C and the temperature was gradually lowered to -0.7, -1.0, -1.5, -2.0, -3.0, -5.0, -10 and -20˚C and changed so that it started to rise again. The plates were kept at 0˚C for more than 12 hours to make the specimen temperature distribution uniform. After that anti-freeze at -0.7˚C flows for 1 to 3 hours. The pore water existed as a liquid state even below 0˚C. In order to start freezing, the anti-freeze set to -10˚C was circulated from an ice nucleation bath. For 15 seconds, the temperature was returned to -0.7˚C. After confirming displacement change.

Fig. 2 shows the temperature change of the top and bottom plates. The temperature was lowered gradually from 0˚C to -20˚C. Fig. 3 shows displacement change with elapsed time. Frozen water volume V_{wf} is computed from the frozen water height h_{wf} by Eq. (1) and specimen's cross-sectional area A, and frozen void ratio e_f is obtained from the ratio with soil particle volume V_s. The unfrozen void ratio e_u is calculated by subtracting the frozen void ratio e_f from the initial void ratio e_0. Specifically, they are computed as follows.

$$h_{wf}=\frac{\Delta d}{0.09} \quad (1), \quad V_{wf}=h_{wf}\times A \quad (2),$$

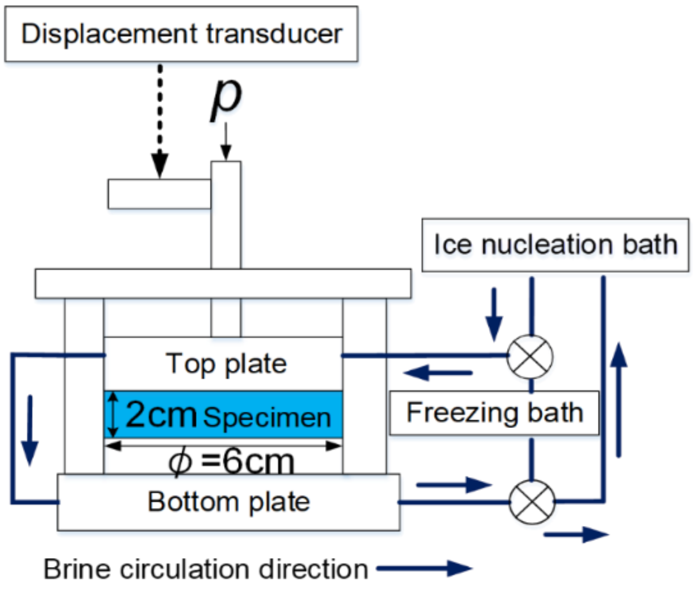

Fig. 1 Frozen and unfrozen water measurement device.

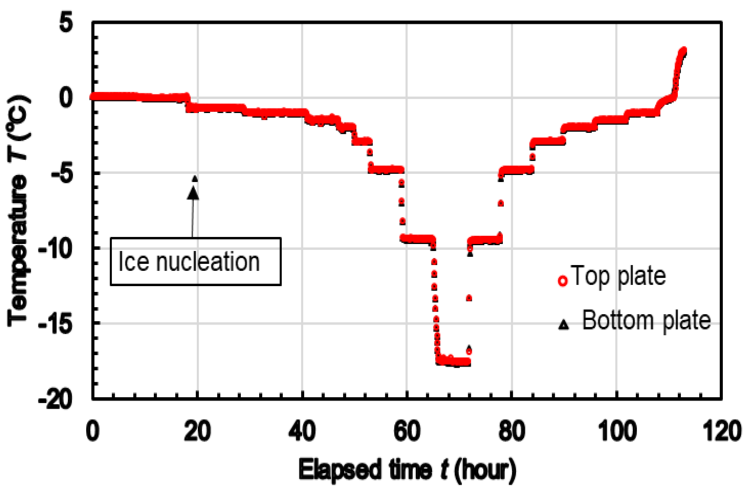

Fig. 2 Temperature change with elapsed time.

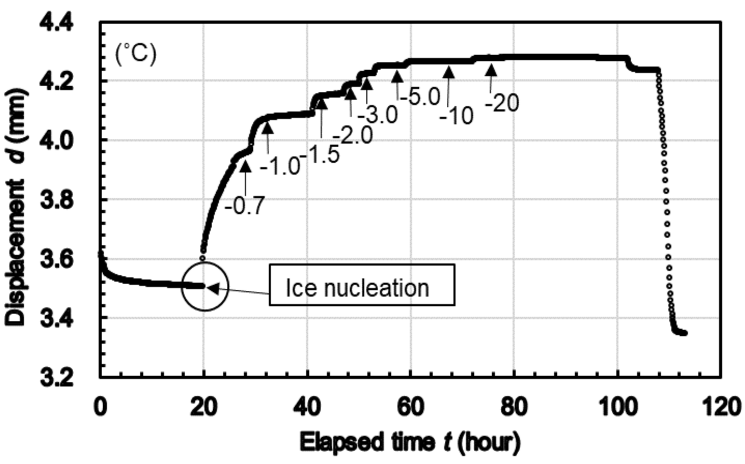

Fig. 3 Displacement change with elapsed time.

$$e_f = \frac{V_{wf}}{V_s} \quad (3), \quad e_u = e_0 - e_f \quad (4)$$

where, Δd: displacement (cm), 0.09: volume increment ratio from water to ice, V_{wf}: frozen water volume (cm^3), V_s: soil particle volume (cm^3), and A: specimen's cross-sectional area (cm^2), e_u: unfrozen void ratio, e_0: initial void ratio.

Frozen porosity n_f is defined as follows.

$$n_f = e_f/(1+e_0) \times 100 \quad (5)$$

Finally, the void ratio function in Kozeny-Calman equation[6] is replaced by e_f and defined as frozen void ratio functions as follows.

$$e_f^3/(1+e_0) \quad (6)$$

4. Result and discussion

4.1 Frozen and unfrozen water heights with temperature *T*(˚C)

Fig. 4 shows the relationship between frozen water height h_{wf} and unfrozen water height h_{wu} with temperature T(˚C). This figure shows that most of the pore water freeze up with the temperature just below 0˚C and, after that rest of the unfrozen water gradually freezes.

4.2 Frozen void ratio e_f, unfrozen void ratio e_u, and temperature *T*(˚C)

Fig. 5 shows the relationship between frozen void ratio e_f in normal consolidation state (P=p) and temperature T(˚C). It is observed that e_f increases with a decrease in temperature T(˚C). The e_f sharply increases from 0˚C to -2˚C and after that, it changes slowly. It is also observed that the e_f increases with a smaller load p.

Fig. 6 shows the relationship between the unfrozen void ratio e_u and temperature T(˚C). It is shown that the e_u is decreasing with lowering temperature. Especially, the e_u sharply decreases from 0˚C to -2˚C and after that, it changes slowly.

4.3 Frozen void ratio e_f, unfrozen

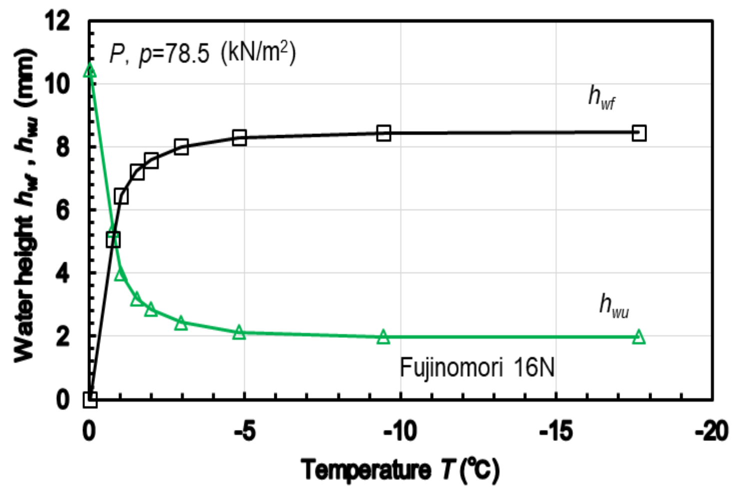

Fig. 4 h_{wf} and h_{wu} with temperature.

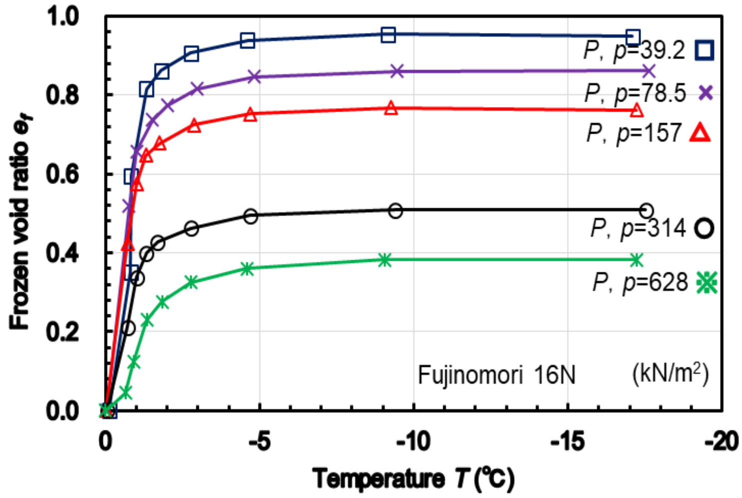

Fig. 5 Fujinomori 16N's frozen void ratio e_f.

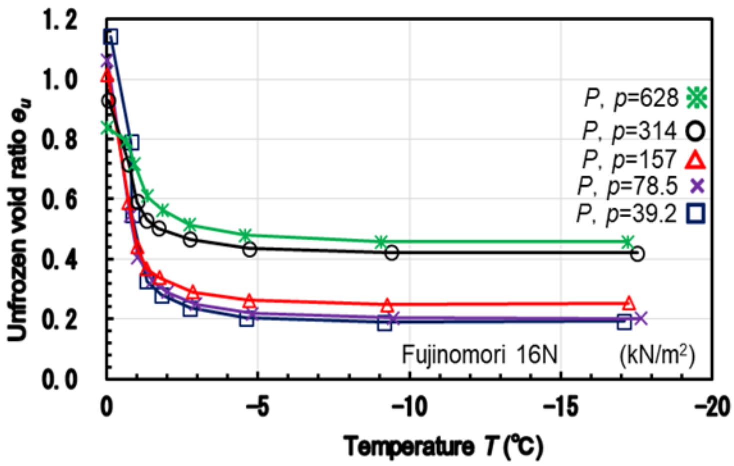

Fig. 6 Fujinomori 16N's unfrozen void ratio e_u.

void ratio e_u, initial void ratio e_0, and coefficient of permeability k_p

Fig. 7 shows the relationship the frozen void ratio $e_{f(T^\circ C)}$, initial void ratio e_0, and coefficient of permeability k_p in Fujinomori 16N clay where k_p is from the falling head permeability test. Frozen void ratio $e_{f(T^\circ C)}$ is computed at each freezing temperature, and $e_{0(+20^\circ C)}$ is the initial void ratio e_0. This figure shows that the e_f, k_p indicated on a normal scale and e_0 increase with a decrease in preload P (= experimental load p). Moreover, the amount of frozen water at in -0.7˚C is greater in smaller load and smaller in greater load. When the specimen temperature decreases below -0.7˚C, the amount of newly frozen water each step appears to be almost the same. The relationship line of e_f and k_p move from left to right in parallel. This indicates that water drained by consolidation is the water existed away from the soil's surface frozen at the temperature close to 0˚C, and we believe that such a state of water influence k_p. Since the e_f-k_p line passes the origin at approximately -1.5˚C, water content governing the k_p is water content frozen at the temperature from 0˚C to -1.5˚C, we presume. As for the relationship between e_f and k_p, it was read from the figure that k_p increases by around 2 times while e_f's increase 2 times. It can be inferred that void defined by the frozen void ratio affect the permeability.

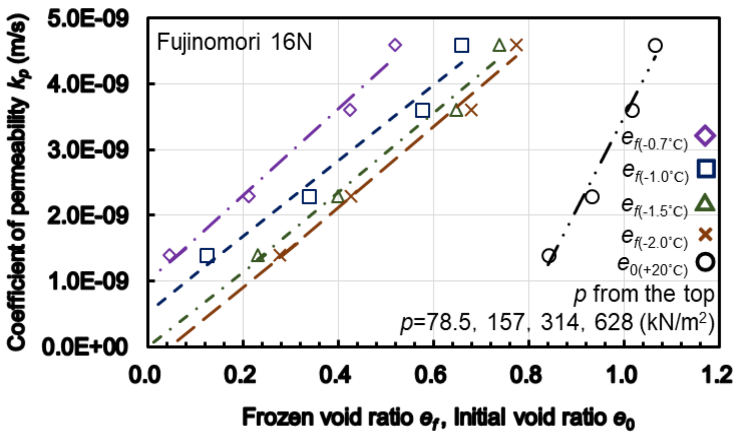

Fig. 7 Void ratios (e_f, e_0) and k_p of Fujinomori 16N.

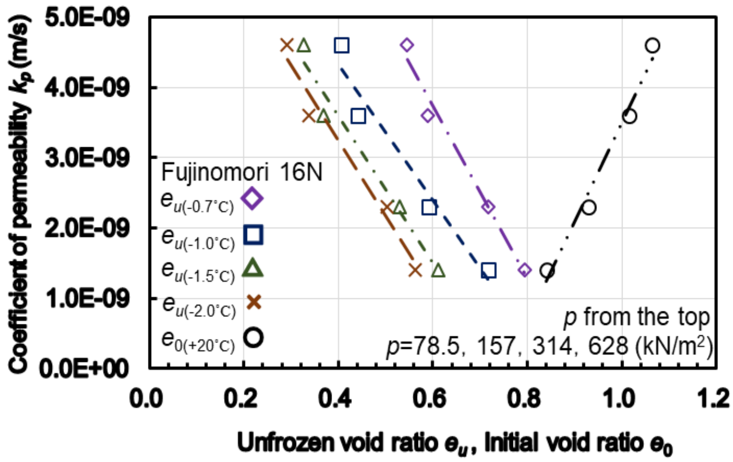

Fig. 8 Void ratios (e_u, e_0) and k_p of Fujinomori 16N.

Fig. 8 shows the relationship of the unfrozen void ratio e_u, initial void ratio e_0, and coefficient of permeability k_p indicating the relationship opposite to Fig. 7. $e_{u(T^\circ C)}$s are computed at each temperature in the freezing test, and $e_{0(+20^\circ C)}$ is initial void ratio e_0. The e_u-k_p line indicates the gradient opposite to that in Fig. 7, and it moves from right to left in parallel with the temperature drop. k_p is greater in a smaller load and smaller in greater load. It is indicated that there exists the water that strongly adheres to soil particle under greater load and is unfrozen even at colder temperatures.

4.4 Frozen porosity n_f, initial porosity n_0, and coefficient of permeability k_p

Fig. 9 shows frozen porosity n_f, initial porosity n_0, and coefficient of permeability k_p. The n_f-k_p relationship moves from left to right in parallel same as Fig. 7. The figure shows that the k_p increases 2 times when n_f increases 2 times. It is inferred that the void defined by e_f affects the permeability. Moreover, since the n_f-k_p line passes the origin at about -1.5˚C, the water contributing water flow in Fujinomori 16N is the water frozen from 0˚C to -1.0˚C or -1.5˚C.

4.5 Frozen void ratio e_f, unfrozen void ratio e_u, and temperature T(˚C)

Fig. 10 shows the relationship between frozen void ratio e_f and temperature T(˚C) of normal consolidation state (P=p). This indicates that the e_f increases when the temperature T(˚C) decreases. The e_f sharply increases from 0˚C to -2˚C but its increment becomes smaller after that. Moreover, it is understood that the e_f increases with a decrease in the experimental load p. This figure indicates that the relationship is as same as that in Fig. 5.

Fig. 11 shows the relationship between unfrozen void ratio e_u and temperature T(˚C) that indicates the relationship inverse to Fig. 10. The e_u is smaller whenever temperature T(˚C) decreases. Although unfrozen void ratio e_u sharply decreases from 0˚C to -2˚C, after that the change becomes smaller and finally constant. In this way, Fig. 11 indicates a relationship is as same as that shown in Fig. 6.

4.6 Frozen void ratio e_f, unfrozen void ratio e_u, initial void ratio e_0, and coefficient of permeability k_p

Fig. 12 shows the relationship between the frozen void ratio e_f, initial void ratio e_0, and the coefficient of permeability k_p in the Kizuchi clay. k_p was measured by the falling head permeability test. Frozen void ratio $e_{f(T˚C)}$s are computed at each freezing temperature, and $e_{0(+20˚C)}$ is the initial void ratio e_0. The e_f becomes greater with smaller test load p, and k_p becomes also greater. Moreover, the amount of water that freezes at each freezing temperature is greater in smaller load and smaller in greater load, same as Fig. 7. The almost the same amount of water freezes when the temperature drops at each steps regardless of a magnitude of the load. The relationship line of e_f-k_p move from left to right in parallel. This is similar to the case of Fujinomori clay. It can be said that water drained away under consolidation is the water located away from soil particle surface which freezes at temperatures close to 0˚C. We presume that such water influences the magnitude of permeability k_p. Since the e_f-k_p line passes the origin at approximately -2.0˚C, water content governing the coefficient of permeability is the water frozen from 0˚C to -2.0˚C, we presume. For the relationship between frozen void ratio e_f and coefficient of permeability k_p, the figure shows that the coefficient of permeability k_p increases by around 2 times when frozen void ratio e_f increases 2 times. It is inferred that the void defined by the frozen void ratio e_f affect influence on the permeability.

Fig. 13 shows the relationship of the unfrozen void ratio e_u, initial void ratio e_0, and coefficient of permeability k_p

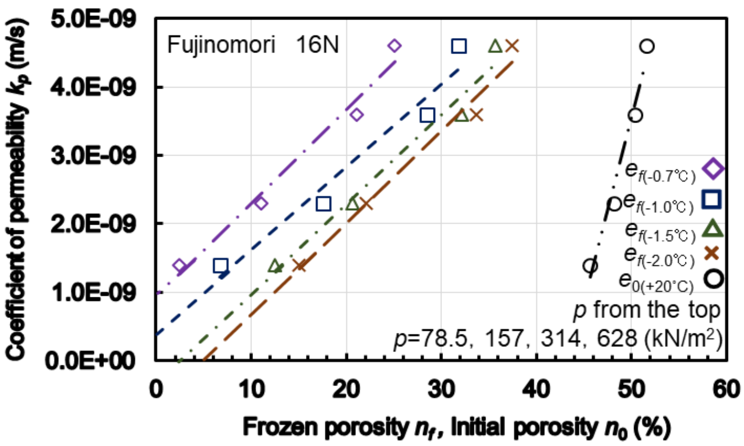

Fig. 9 Porosities (n_f, n_0) and k_p of Fujinomori 16N.

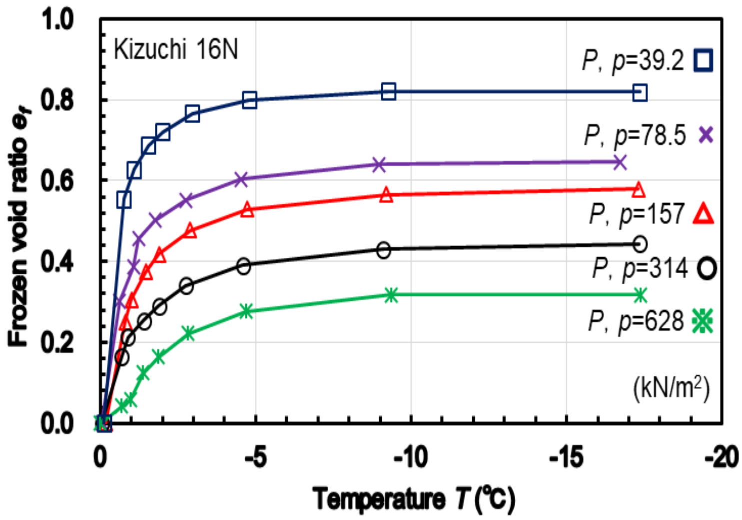

Fig. 10 Kizuchi 16N's frozen void ratio e_f.

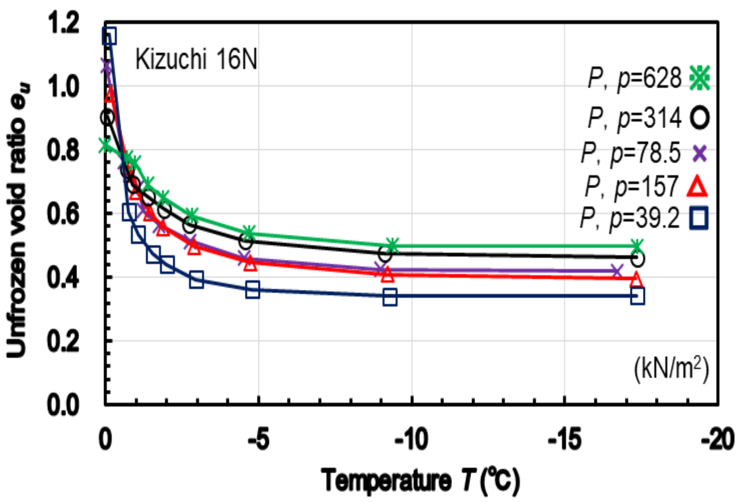

Fig. 11 Kizuchi 16N's unfrozen void ratio e_u.

indicating the relationship opposite to Fig. 12. The k_p is measured from the falling head permeability test. $e_{u(T^\circ C)}$s computed at each freezing temperature, and $e_{0(+20^\circ C)}$ is the initial void ratio e_0. The e_u-k_p line indicates the gradient inverse to that in Fig. 12, and it moves from right to left in parallel with the temperature drop. k_p becomes greater under lower load, and smaller under higher load. It is indicated that there exists the water that strongly adheres to soil particles under greater load and remains unfrozen at a colder temperature.

4.7 Frozen porosity n_f, initial void porosity n_0, and coefficient of permeability k_p

Fig. 14 shows frozen porosity n_f, initial porosity n_0, and the coefficient of permeability k_p. The n_f, n_0, and k_p become smaller with increasing load p. The n_f-k_p relationship moves from left to right in parallel same as Fig. 9. Since the n_f-k_p line passes the origin at approximately -1.5 to -2.0˚C, the water contributing water flow in Kizuchi 16N is the water frozen at over -1.5 to -2.0˚C. As for the relationship between n_f and k_p, it can be read from the figure that the k_p increases 2.1 times while n_f increases 2 times. It is inferred that the void defined by frozen void ratio e_f affects the permeability.

4.8 n_f, n_0, and k_p of Fujinomori and Kizuchi clays

$n_{f(-1.5^\circ C)}$ and n_0 of Fujinomori 16N in Fig. 9, and $n_{f(-2.0^\circ C)}$ and n_0 of Kizuchi 16N shown in Fig. 14, were extracted and plotted in Fig. 15. The frozen porosity n_f, initial porosity n_0, and the coefficient of permeability k_p becomes smaller with increasing load p. From Fig. 15, n_f of Fujinomori 16N and Kizuchi 16N intersect at x = 2, while n_0 of Fujinomori 16N and Kizuchi 16N does not intersect at the x-axis. The coefficient of permeability k_p is considered to be increasing based on x = 2.

4.9 Frozen void ratio $e_f^3/(1+e_0)$, initial void ratio function $e_0^3/(1+e_0)$, and coefficient of permeability k_p

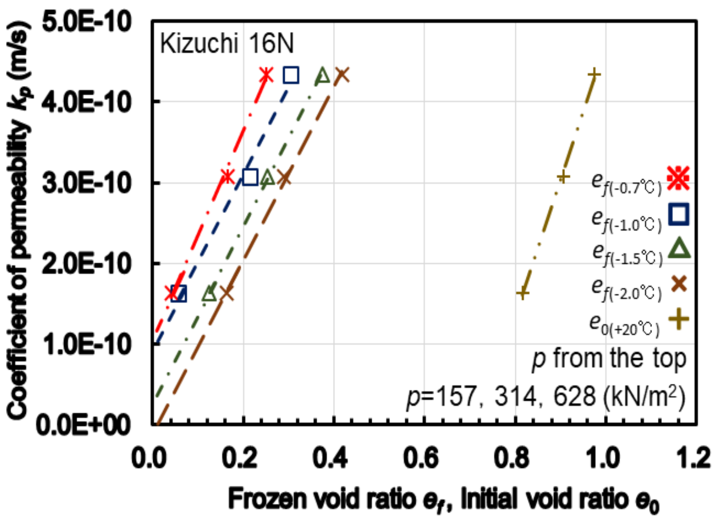

Fig. 12 Void ratios (e_f, e_0) and k_p of Kizuchi 16N.

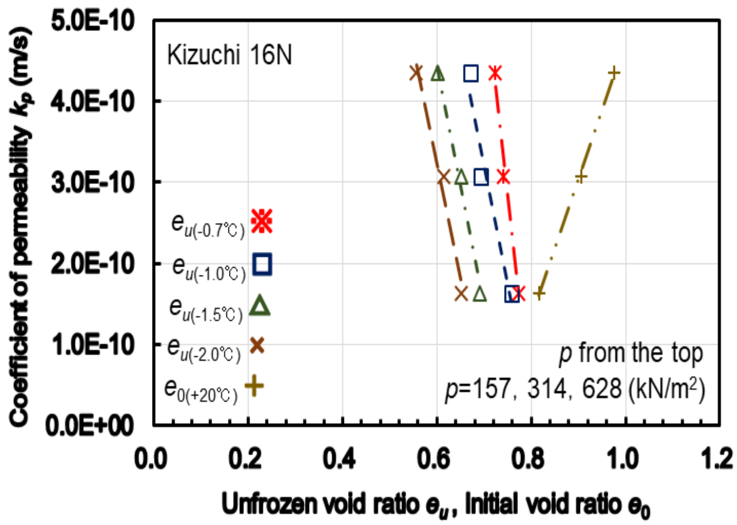

Fig. 13 Void ratios (e_u, e_0) and k_p of Kizuchi 16N.

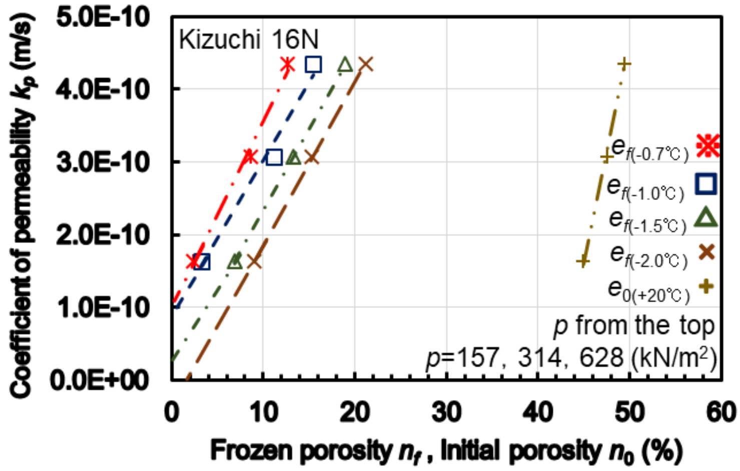

Fig. 14 Porosities (n_f, n_0) and k_p of Kizuchi 16N.

Like Fig. 15, Fig. 16 shows the void ratio functions ($e_f^3/(1+e_0)$, $e_0^3/(1+e_0)$), and coefficient of permeability k_p. The void ratio functions ($e_f^3/(1+e_0)$, $e_0^3/(1+e_0)$), and k_p becomes smaller under greater load p. Every line moves to the Y-axis direction. And it is not easy to explain the coefficient of permeability k_p close to the Y-axis. Compare with Fig. 15, the relationship between frozen void ratio function and the k_p were not clear.

Overall we can propose a very simple relationship to explain the coefficient of permeability k_p as,

$$k_p=c_1\times e_f \quad (7), \qquad k_p=c_2\times n_f \quad (8)$$

where, c_1, c_2: constants.

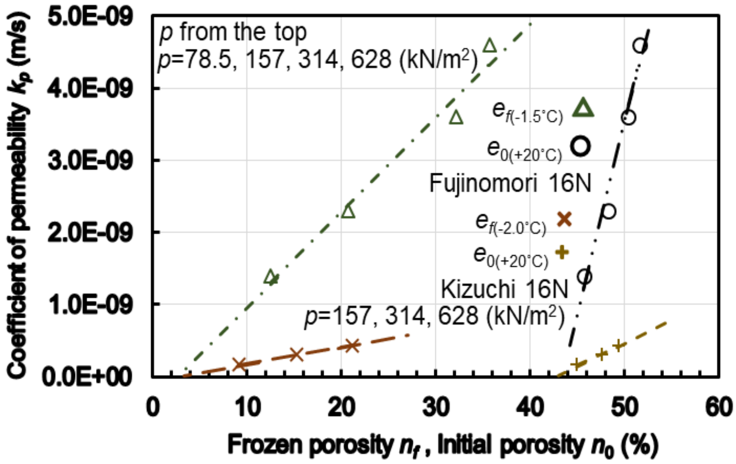

Fig. 15 Porosities (n_f, n_0) and k_p of Fujinomori 16N, Kizuchi 16N.

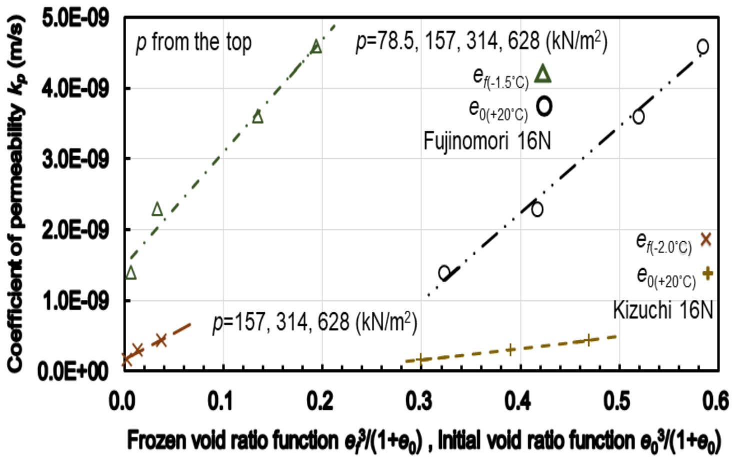

Fig. 16 Void ratio functions ($e_f^3/(1+e_0)$, $e_0^3/(1+e_0)$) and k_p of Fujinomori 16N, Kizuchi 16N.

5. Conclusions

[1] Measurement of frozen and unfrozen water was conducted to understand the relationship between the state of pore water and the coefficient of permeability k_p of saturated fine-grained soil.
[2] In the normal consolidation condition, the newly defined frozen void ratio e_f is greater with a smaller load p. And the unfrozen void ratio e_u is greater with a greater load p.
[3] The relationship between void ratios (e_f, e_0) and the coefficient of permeability k_p presents that the frozen void ratio e_f represent permeability more precisely than initial void ratio e_0.
[4] Similarly, the frozen porosity n_f, which is the cross-sectional area of water path in soil, may be better represent coefficient of permeability k_p than initial porosity n_0.
[5] Overall we can propose very simple equations to explain the coefficient of permeability k_p as,

$$k_p=c_1\times e_f \qquad\qquad k_p=c_2\times n_f$$

where, c_1, c_2: constants.
[6] As for void ratio functions ($e_f^3/(1+e_0)$, $e_0^3/(1+e_0)$), their relationship with coefficient of permeability k_p is not clear.

Acknowledgements

This study was supported by JSPS Grants-in-Aid for Scientific Research Grant Number JP17H03307. A part of the tests was carried out as a graduation study by Mr. Kenta Tsuru, Mr. Shota Nakayama at the Department of Civil and Environmental Engineering, Setsunan University.

Reference

[1] Kikutani, Y., Takahasi, S., Haraguchi, M., and Akagawa, S., “Temperature dependence

Unfrozen water Thickness on Clayey Soil”, The 37th Geotechnical Research Presentation, pp. 1169-1170, 2002. (in Japanese)
[2] Mitchell, J.K., and Soga, K., “fundamentals of soil behavior”, pp. 153-154, 2005.
[3] Ito, Y., and Butsuen, N., “Relationship between the permeability and adsorbed water in fine-grained soils”, The 47th Geotechnical Research Presentation, pp. 303-304, 2012.
[4] Push, R., “Unfrozen water as a function of clay microstructure”, *Proc*. *1st Int*. Symp. Ground Freezing, Elsewier Sci. Pub. Comp., Amsterdam, pp. 157-162, 1979.
[5] Mori, S., and Yamanaka, H., “Relationship between measurement of unfrozen water amount under loading condition and engineering properties of soil”, Setsunan University graduation thesis, 2016. (in Japanese)
[6] Lambe, T.W., and Whitman, R.V., “Soil Mechanics, John Wiley & Sons”, pp. 110-111, 1948.

EDUCATION AND TRAINING

Strengthening Arctic engineering competences through higher education – the Nordic Master in Cold Climate Engineering

Gunvor Marie Kirkelund
Associate Professor
Department of Civil Engineering
Technical University of Denmark
Denmark
gunki@byg.dtu.dki

Assistant Professor Arttu Polojärvi, Department of Mechanical Engineering, School of Engineering, Aalto University, Finland
Professor Jukka Tuhkuri, Department of Mechanical Engineering, School of Engineering, Aalto University, Finland
Professor Knut V. Høyland, Department of Civil and Environmental Engineering, Norwegian University of Science and Technology, Norway

Summary

The Nordic Master in Cold Climate Engineering offers students to study Arctic Engineering and develop Arctic competences, which are sought for by the industry. This two-year double degree master level engineering education is offered within the Nordic Five Tech alliance and includes courses taught in Svalbard (UNIS) and Greenland (DTU Campus Sisimiut). That the students are experiencing the Arctic is one of the main added values of this education and contributes to the development of Arctic competences for the students according to Kolbs learning cycle.

Keywords: Arctic technology, Arctic engineering, joint programme, double degree, graduate studies

1. Introduction

Cold climate engineering has an increasingly important role to play to ensure a sustainable development of the Arctic. With the increasing activities and investments, through exploration of natural resources and accessibility due to opening waters, there is a need for engineers with competences and skills tailored for this region. Aalto University in Finland, the Norwegian University of Science and Technology (NTNU) and the Technical University of Denmark (DTU) are classical higher education engineering institutions, graduating hundreds of engineers annually. The three universities have all long traditions within Arctic and Antarctic research, closely linked to the countries national Arctic strategies and location in the North. Regardless of this cold region focus, a full master programme in Arctic engineering has not been offered at any of the universities. In the Arctic strategy of the Nordic Five Tech alliance, developing a joint master programme, utilising and combining the universities competences was recommended. On this basis, the Nordic master programme in Cold Climate Engineering was developed and welcomed its first students in 2016 [1]. This programme uses existing courses at each university to offer a 2 years Master of Science programme where the students earn a double degree. This presentation aims at emphasising how the Arctic engineering competences are developed during the Nordic Master in Cold Climate Engineering.

2. Approach

There are three tracks of the programme: Land, Sea and Space. In Table 1, the specialisation within each track and the two universities involved are shown. The students at the Land track spend 1 semester in Sisimiut, Greenland. There is also a possibility for the Land track students to study 1-2 semesters at UNIS, Svalbard. For the Sea track students, the students can, depending on their university 1, study 1-2 semesters at UNIS. Currently, there are no scheduled courses in the Arctic for the Space track students. The students currently admitted in the programme are international and highly motivated for their studies [1].

Table 1 Track specializations of the Nordic Master in Cold Climate Engineering [1]

Semester	**Land track**	**Sea track**		**Space track**			
	Arctic Geoengineering	***Arctic Ships and Off-shore structures***		***Mapping and navigation***		***Earth Observation Techniques***	
1	DTU	Aalto	NTNU	DTU	Aalto	DTU	Aalto
2	DTU, Campus Sisimiut	Aalto	NTNU (UNIS)	DTU	Aalto	DTU	Aalto
3	NTNU (UNIS)	NTNU (UNIS)	Aalto	Aalto	DTU	Aalto	DTU
4	NTNU	NTNU	Aalto	Aalto	DTU	Aalto	DTU

The additional Arctic competences are gained through the courses in Greenland (DTU) and Svalbard (UNIS/NTNU) where the teaching is to a large extend based on field work, taking advantage of the Arctic nature right outside the classroom and courses at Aalto, DTU and NTNU where active learning through Arctic case studies and focus in courses. These courses and the whole master programme itself takes offset in the Kolb learning cycle [2], see Fig. 1.

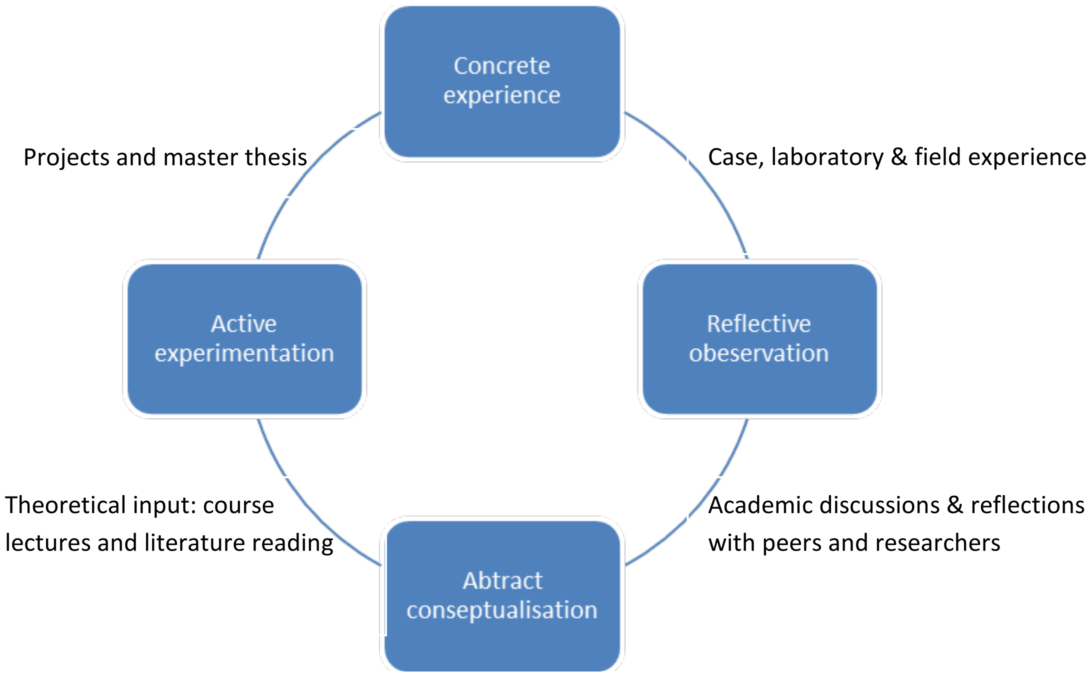

Fig. 1 Kolbs learning cycle implemented in the Nordic Master of Cold Climate Engineering

The students' concrete experience can be achieved through work at e.g. the Aalto Ice tank, cold room facilities at DTU and NTNU, as well as through field work in Svalbard and Greenland or through cases used in courses. The discussions and reflections are supported through the courses and by the Arctic and discipline specific research teams at the universities through e.g. seminars, workshops, conferences. Adding to the students' conceptual knowledge; general competence, technological specialization and elective courses are studied to build a strong base of technical and generic competences. This also means that each student will gain a strong basis within the classical engineering focus of each track and thus eligible for employment in other regions than the Arctic. Finally, the master thesis is when the student's demonstrate their knowledge and innovation within a relevant topic. Master thesis topics can be linked to specific research projects (e.g. PhD, NPA or

H2020 projects) or to research needs raised from industry and stakeholders. At graduation, the students will apart of having a strong academic profile also have obtained generic competences such as group work, working in teams of different international and educational background, oral and written communication and planning and executing field/lab work and projects. In many of the programme's courses the learning approach is linked to cased based teaching. When using cased based teaching, real life situations and group work is a starting point for learning. Cases can be especially useful when dealing with engineering in cold and Arctic environments where projects require a need for rethinking traditional approaches, e.g. with construction on permafrost, ship transport in ice-filled waters and communication in high latitudes. Using real cases strengthens innovation and creativity skills of the students, skills which are highly relevant when contributing to the Arctic and Nordic regions development.

3. Conclusion

The first candidates of the Nordic Master in Cold Climate Engineering graduated in 2018. Throughout their studies the students are developing both general and specific Arctic engineering competences through their courses. These competences are especially important for developing sustainable solutions in the Arctic and also highly valuable to the stakeholders in the Arctic and Nordic region.

References

[1] KIRKELUND G. M., TUHKURI J., HØYLAND K. V., Development of a joint Nordic master in cold climate engineering within the Nordic five tech alliance. Proceedings of ICERI2017 Conference, Seville, Spain. 2017, 0291-0299.

[2] KOLB D.,"*Experiential learning: Experience as the source of learning and development*." Englewood Cliffs, NJ: Prentice-Hall, 1984.

Science with Artic Attitude-
Doctoral Training at the University of Oulu, Finland

Riitta Kamula,
Coordinator
Kvantum Institute, University of Oulu
Finland
riitta.kamula@oulu.fi

University Lecturer Aulikki Herneoja, Oulu School of Architecture, Chair of DTC TNS, University of Oulu, Finland
Professor Björn Klöve, Kvantum Institute, University of Oulu, Finland
Coordinator Karita Saravesi, University of Oulu Graduate School, University of Oulu, Finland

Summary

University of Oulu, Finland has carried out multidisciplinary research-based higher education and doctoral training activities focusing on northern and arctic issues from its establishment. In recent years, the University has made structural changes both in doctoral training and in high-level research. Partly these changes are due to the changed funding system of the universities in 2010, and the changes to doctoral training system in Finland on 2011. This paper describes the current doctoral training system and the strategic research funding tools of the University of Oulu. The paper also discusses the impacts of the changes to doctoral training in the University of Oulu.

Keywords: Arctic research, doctoral training, research funding

1. Introduction

University of Oulu, Finland has been multidisciplinary from its establishment in 1958 with its three faculties of Philosophy, Technology and Medicine. Faculty of Philosophy was composed in the beginning only of natural sciences. In addition to these faculties, the Teacher Training College was incorporated in the University. The University, situated in the Northern Finland, has always focused on issues related to northern and arctic areas.

In Finland, doctoral training is part of the three-tier university degree system, and only universities may award doctorates. Different administrative levels regulate and develop the training through decrees, guidelines, recommendations, and policies. Earlier the Finnish universities were tightly under the administration of the state, and the Finnish Ministry of Education was in charge for their activities. The autonomy of Finnish universities increased in 2010, when the university funding structure changed. The universities now have the overall responsibility also for doctoral training and its development [1].

In 2011, Finnish Ministry of Education and Culture terminated the nationwide doctoral training system, and after that, the structures and practices of doctoral training have developed to different directions among the Finnish universities. University of Oulu decided to adopt a single graduate school model to support systematic doctoral training, and established in 2011 University of Oulu Graduate School, UniOGS. UniOGS started gradually, and it has developed its processes continuously ever since. In addition to processes, UniOGS together with the University has introduced also drastic structural changes in the University's doctoral training and the related high-level research.

2. Doctoral training organization at the University of Oulu

Doctoral training at the University of Oulu changed drastically when the University established a university–wide graduate school UniOGS, which started its activities on 1.8.2011. Following the national aims of the doctoral training and principles formulated by the European Commission, and in line with the strategy of the University of Oulu, the main goal of the Graduate School is to provide the framework and conditions for high-quality, research-driven doctoral training to all of its doctoral students.

UniOGS has adopted standardized practices for doctoral training, changed the application process for the admission of students, renewed study requirements, developed supervision and follow-up processes, and processes related to the doctoral dissertation. By promoting the development of effective student-supervisor relationships, founded on both motivation and commitment, UniOGS creates a favorable environment for the planning, execution and timely completion of doctoral studies tailored to each student.

UniOGS has also developed and harmonized doctoral training processes and requirements in all fields and faculties. These processes and support systems enable graduation in four years of full-time studies. The doctoral degree includes always research work for the thesis, publication and public defense of the thesis, and, depending on the discipline, 20 to 50 ECTS credits of courses and/or other research-related activities. To support and ease the path to doctorate, UniOGS has gathered in one web page almost everything the doctoral candidates and supervisors need to know, about in the order of progress of doctoral training. The page includes links to forms and thorough instructions.

Research units and doctoral programs are responsible for providing field-specific studies and multidisciplinary training in collaboration with focus institutes, whereas the UniOGS provides support and ensures equal opportunities for students to complete the doctoral degree, by providing general and transferable skills courses, monitoring the studies, and by taking care of the administration of doctoral study rights and degrees.

The optimal duration of doctoral training corresponds to four years of full-time study, but it can be completed in a longer time in a case of part-time work. During the studies, students acquire proficiency to work at doctoral level tasks. After completing the degree, the new doctor will have skills to solve problems with scientific methods in academia, administration, private enterprise, or other sectors, and should therefore have good employment opportunities.

2.1 Responsible parties in doctoral training

Doctoral training includes, in addition to educational activities, also research-related activities. Because of this, the actors in doctoral training represent both education and research. All the parties have responsibilities to develop doctoral training from their point of view. A loose description of the parties and their responsibilities is in Table 1.

One of the main actors is UniOGS. Shortly, UniOGS has the responsibility of admission processes, it defines study requirements and finally grants and grades the doctoral degrees. UniOGS core consists of the Dean, Vice Dean and UniOGS-coordinators.

All doctoral candidates, who have study rights in UniOGS, have been registered in one of the four Doctoral Training Committees. The Committees lead doctoral training processes in their fields. Each DTC is comprised of professionals from its fields of expertise.

The four focus institutes of the University of Oulu implement the strategy of the University and promote its high-quality interdisciplinary research profile. The key tasks are to support research and co-operation in the focus areas of the University. In doctoral training, the focus institutes operate together with UniOGS in their fields of responsibility in all the research-related activities.

All doctoral candidates, who have study rights in UniOGS, have been registered in one of the four UniOGS Doctoral Programs. The doctoral programs started in the beginning of 2017. The doctoral programs operate in the middle ground of research and education, and they are committed both to UniOGS and the focus institutes. The programs provide field-specific doctoral training supporting the timely completion of the doctoral degree.

Table 1 The main actors in doctoral training of the University of Oulu

UniOGS / Doctoral Training Committees	**Doctoral Programs**	**Focus institutes**
– Doctoral training processes, study rights, general and transferrable courses, support for field specific courses – Doctoral program board and chair – Under the Vice Rector of Education	– Doctoral program coordination; doctoral training and university-funded positions – Under focus institutes and UniOGS	– Development of doctoral training in the joint body – Foster top-level research projects – Under the Vice Rector of Research
DTC HBS - Health and biosciences	**HBS-DP** - Health and biosciences	**Biocenter Oulu**
DTC HS - Human sciences	**HS–DP** - Human sciences	**Eudaimonia Institute**
DTC ITEE - Information Technology and Electrical Engineering	**ITEE-DP** - Information Technology and Electrical Engineering	**InfoTech Oulu**
DTC TNS - Technology and natural sciences	**TNS-DP** - Technology and natural sciences	**Kvantum Institute**

UniOGS provides framework and conditions for high-quality, research-driven doctoral training for all students of the University of Oulu. Each doctoral training plan should be defined in a way that the doctoral degree can be completed within a time equivalent to four years of full-time studies. By promoting the development of effective student-supervisor relationships, founded on both motivation and commitment, UniOGS aims to create a favourable environment for the planning, execution and timely completion of doctoral training tailored to each student.

Doctoral training committees accept degree requirements proposed by the degree programs, and are responsible for doctoral student selections including numbers, criteria for admission, and evaluation of applications. Each DTC also approves changes of supervisors and appoints additional supervisors, and appoints follow-up group members. DTC accepts Doctoral Training Plans and grants permissions for pre-examination and appoints the pre-examiners of doctoral theses, grants permissions to defend the doctoral theses and appoints the pre-examiners, opponent and Custos. Finally, DTC approves and grades the doctoral theses.

The four UniOGS Doctoral Programs provide field-specific doctoral training supporting the timely completion of the doctoral degree. However, the research groups and units arrange most of the field-specific courses, and the doctoral programs award funding for these courses. The courses and other activities organized by the doctoral programs are open to all doctoral candidates. The programs have strong connections with local, national, and international research communities, which generates multi-disciplinary, high-quality training environments.

Focus institutes coordinate multidisciplinary research and doctoral training in the five strategic research focus areas of the University of Oulu. In addition, focus institutes organize and develop open access research infrastructure services for research groups in the University of Oulu and the local communities, e.g. companies. The institutes also coordinate specific tasks of the University, and support research in the faculties by fostering high-level research projects. The institutes coordinate the strategic research projects of the University but also new openings in the focus areas. The institutes coordinate and participate in preparation of new research applications.

3. Doctoral training and research in the University of Oulu

University of Oulu have adopted the seven principles for innovative doctoral training, developed in the framework of the European Research Area [2]. The University follows the national and international requirements for open science and research, develops the prerequisites of high-quality scientific research with quality assurance and promotes responsible conduct of research with courses on research ethics and good research practice. High-quality research infrastructures support organized research, as well as maintain and develop research capacity. Tenure track program and other career possibilities attract and retain international research talents [3].

In the University of Oulu, doctoral training is an essential part of its high-level scientific research and researcher training. The sustaining concept for the research in the University is “Science with arctic attitude”, which arises from the northern location of the University. The University aims to solve global challenges by combining multidisciplinary approaches, high-quality research, and fruitful collaboration.

The strategy of the University is based on five thematic, internationally important research focus areas. The selected five multi-disciplinary focus areas of research and arctic cooperation are *Digital solutions in sensing and interactions; Understanding humans in change; Earth and near-space system and environmental change; Creating sustainability by materials and systems;* and *Molecular and environmental basis for life-long health.* Activities in arctic research and education relate to all focus areas. To support doctoral training, the University has directed funding for four-year doctoral student positions through spearhead and emerging projects, but also through open calls.

Spearhead projects are funded from the University of Oulu’s strategic research funding for the multidisciplinary, internationally reviewed 4-year projects. In the first round, the University granted funding to 48 spearhead projects, each consisting of one fully funded post-doctoral researcher position and one or two partially funded doctoral student positions. The projects were selected through a peer-review by a scientific evaluation committee. The research projects and the related doctoral training are implemented in research groups of the faculties of the University.

The emerging projects program consists of the allocation of partially funded doctoral training positions to emerging research themes within the context of the four strategic focus institutes. Five 4-year doctoral student positions were allocated to each focus institute for 2018-2022, totaling to 20 positions. The program aims to connect research across disciplines with top research groups in the University of Oulu. The program facilitates linking of best practices and best science to a larger part of the university´s research, and open up new channels to improve the impact of top science. The structure of this strategically funded research maximizes the input by offering young post-doctoral researchers funding in a form of funded doctoral student positions.

UnioGS doctoral student positions will be distributed to all fields of doctoral training in the University. The total amount of these partially funded positions will be 120. The unit of the main supervisor of the selected student is supposed to cover rest of the funding. The call for applications in these positions will open in spring 2019.

Research units and groups offer in their projects every now and then additional funded doctoral student positions for a maximum period of four years.

All the funded positions for over six month-periods are announced in open calls, also internationally. This way the research groups will be able to employ the best young researchers in their projects.

3.1 Doctoral training in figures

Finnish Ministry of Education and Culture (FMEC) sets the targets for annual higher education decrees to ensure good possibilities for employment. In addition to total targets, FMEC also defines targets for each institute; and on Bachelor and Master's levels, also for different fields of studies. This dates back to the fact that all higher education is a big investment both on personal side of view but also from the society.

The annual target for the total number of granted doctoral degrees in Finland has been 1600 new doctors, however, this has been recently lowered to 1500 annual doctorates. Despite of that, the mean annual number of new doctorates during 2008-2017 have been 1733 [4], exceeding the target by eight per cent (Fig. 1). The current annual goal of the University of Oulu is 150, when earlier it was 160. The number of doctoral degrees granted in the University have been on the average 163 doctorates during the last ten years in 2009-2018.

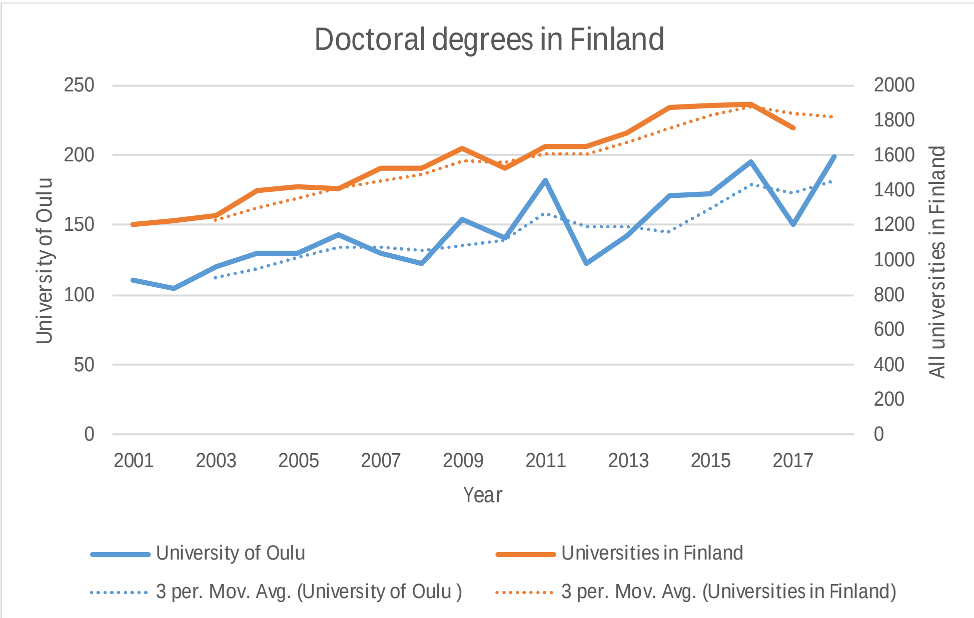

Fig. 1 Doctoral degrees in Finland on 2001-2017 and in the University of Oulu on 2001-2018

From 2001, the annual number of new doctoral degrees have increased slowly but quite steadily in Finland. In individual universities the annual numbers of graduates variate more but the trend is the same in the long run. There are some nationwide but also university-level changes, which have affected the annual numbers of doctoral degrees. The nationwide changes are e.g. the renewed funding system of the universities in 2010, and introduction of passive register in 2016. In the University of Oulu, additional big changes in doctoral training have been the introduction UniOGS in 2011 and the unconditional requirement to register in UniOGS for doctoral study rights in 2015.

Currently, the number of doctoral students registered in UniOGS is about 2100. Of these, about 30 % are in passive register. This means that they are not able to take any steps towards their doctoral degree. Students end up in passive register, if they have done nothing related to their doctoral studies within the last two years – taken courses, updated their doctoral study plans, involved in doctoral training activities e.g. by arranging own follow-up group meetings. However, study rights can be activated quite easily.

4. Discussion

In Finland, systematic doctoral training was introduced in 1995 in a form of a nationwide graduate school system, which was funded by the Finnish Ministry of Education. By 2012, the expanded system consisted of 1600 partially funded 4-year doctoral student positions in 112 graduate schools. In 2011, Finnish Ministry of Education and Culture decided to terminate this system, and each university were given the right to develop their own doctoral training systems [1].

University of Oulu established the University of Oulu Graduate School, UniOGS, which has now the overall control to doctoral training in the University. Ever since its start-up it has develop and harmonized both the processes but also the structure of doctoral training. In spring 2015, UniOGS carried out a survey among its doctoral students as a part of research-based development of doctoral training [5]. Doctoral students' experiences of doctoral training were analyzed in terms of three complementary aspects of the training: the doctoral dissertation process, supervision, and doctoral studies. The results of the survey and the related research have been used to develop UniOGS.

The changes in doctoral training system in the University of Oulu have had clear impacts, which can be noticed in the increased variations in the annual number of new doctorates around the changes. In 2011, the threat of change increased the annual number of doctorates, which then resulted to a sharp drop and gradual increase in the annual number of new doctorates. The same happened again around 2015, when all the students, who had doctoral study rights, were forced to follow the new doctoral training processes.

University of Oulu supports considerably its research related doctoral training by offering partially funded four year doctoral student positions through three main tools: spearhead projects, emerging projects and open doctoral student positions. The number of these positions is in total 120, which makes it impressive instrument to keep doctoral training and high-level research close to each other.

UniOGS as well as the University of Oulu keep on developing their processes to support research-related research. The future will show how these changes appear in the annual numbers of new doctorates in the University. However, the Finnish Ministry of Education and Culture have the final word when it negotiates with each of the universities in four year intervals, and in the same connection, may change its funding model of the universities. This is one way the Ministry can try to regulate the nationwide number of new doctorates.

References

[1] Kamula R et al 2013. Systematic doctoral education in Finland since 1995. - Planning for Sustainable Regions, ISCORD 2013. Proceedings of the 10th International Symposium on Cold Regions Development, June 2-5, 2013, Ancharge, Alaska. Zufelt, Jon E. Reston, American Society of Civil Engineers. 75-86

[2] Principles for Innovative Doctoral Training. 2011. https://cdn5.euraxess.org/sites/default/files/policy_library/principles_for_innovative_doctoral_training.pdf

[3] Pietilä M. 2015. Tenure track career system as a strategic instrument for academic leaders. European Journal of Higher Education. Vol 5, No 4, 371-378, https://www.tandfonline.com/doi/full/10.1080/21568235.2015.1046466

[4] Statistics Finland. https://www.stat.fi/til/yop/2017/yop_2017_2018-05-08_tie_001_en.html (retrieved 16.4.2019)

[5] Pyhältö Kirsi et al 2016. Summary report on doctoral experience in the UniOGS graduate school at the University of Oulu. Acta Universitatis Ouluensis. F, Scripta academica 11. http://jultika.oulu.fi/Record/isbn978-952-62-1084-1

INFRASTRUCTURE

Effect of Frost-heaving Depression on Slope Surface by Vegetation Base Material in Cold Region

Atsuko Sato
Senior Research Engineering
Civil Engineering Research Institute for Cold Region
Japan
atsuko@ceri.go.jp

Osamu Hatakeyama, Civil Engineering Research Institute for Cold Region, Japan
Japan

Summary

Many cases of slope surface protection structures suffering damage due to frost heaving have been reported in Hokkaido and other cold and snowy areas. On the other hand, some cases of shallow frost because of a small amount of frost heave in areas where vegetation bedrocks were constructed have been reported. Considering these cases, we thought that the construction of vegetation bedrocks on a slope surface may be able to reduce the frost depth of slope surfaces to protect them from damage due to frost heaving. This report discusses the results of an experiment constructing some vegetation bedrocks on a slope surface and measuring the frost depth to prove the effectiveness of the vegetation bedrock. The results show that the construction of vegetation bedrocks can reduce the frost depth of a slope surface.

Keywords: Frost-heaving, Slope Surface, Vegetation base, Cold Region

1. Introduction

The occurrence of frost heave damage on sloped surfaces has been reported in cold areas such as Hokkaido located in the northern Japan [1]. Among the various slope protection methods available, use of vegetation may effectively insulate sloped surfaces from cold weather in cold regions [2] [3] and provide surfaces on which snow can accumulate more easily to form an additional layer of insulation [4]. However, a variety of factors are expected to influence the effectiveness of these potential insulators, such as vegetative coverage, weather, soil and the time of the year when slope protection was implemented. The use of vegetation to protect sloped surfaces from frost heaves is still being studied, and its effects should be assumed to be supplementary. It would therefore be premature to incorporate this method into actual slope protection designs at present. In this research project, we studied the susceptibility of sloped surfaces covered by various plant growing media with varying insulating capabilities to freezing.

2. Examples of frost heave damage on sloped surfaces in cold regions and preventive measures

In cold regions, slopes formed by removing soil from the ground sometimes collapse due to the formation of frost heaves in winter and which then melt in early spring (Figure 1). Frost heave develops when the temperature, soil property, and water levels reach a certain threshold [5]. Thus, frost heaving can be prevented by making any of these three conditions unfavorable to it. In this project, we investigated measures to maintain sufficiently high soil temperatures to prevent the development of frost heaves.

a. Cut slope surface by frost heaving

b. Damaged cut slope surface after frost heaving and thawing

Fig. 1 Case of damaged cut slope surface by frost heaving

3. Construction method

In Hokkaido, slopes formed by soil removal are commonly covered with a plant growing medium, while slopes formed by adding soil to the ground are often covered with turf. In this project, we applied these two practices to protect natural slopes and measured the soil temperatures within them [6] [7].

We applied various plant growing media to sloped surfaces at the CERI Tomakomai Test Field on December 26 and 27. Plant growing media -composed of woodchips, local soil, fertilizer and other ingredients in various proportions (Table 1) -were applied to sloped surfaces to form medium layers 5, 10, 15 and 20 cm in thickness. We also measured the thermal conductivity of plant growing media using a thermal conductivity meter that operates using the principle of the transient hot wire method.

Table 1 Mix proportion of the vegetation base material (Per 1 batch)

Name	Quantity
chip	1.89 m^3
Sieve soil	0.81m^3
Greening promotion growth base material	1.500 liter
Microbial material	2.7 liter
Soil fungus active material	24.3 liter
Erosion inhibitor	2.70 kg
Aggregate	0.41 kg
Advanced chemical fertilizer	16.2 kg

The depth to which soil freezes beneath protective vegetation is expected to fluctuate depending on the growing conditions of the vegetation. These growing conditions are in turn subject to various influences. However, we assumed that the use of turf - in which soil and plant (leaves and roots) components are closely associated - may maintain a relatively constant soil freezing depth because even when the plant components die, the soil component would remain to serve as an insulation layer. We experimentally covered sloped surfaces with a turf layer 2 cm in thickness in the CERI Tomakomai Test Field, Hokkaido, in late October.

Fig. 2 Examples of special gabion box

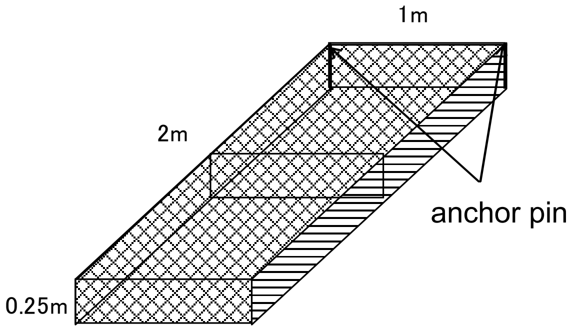

Fig.3 Outline of special gabion box

Some sloped surfaces in Hokkaido are covered with special 25 cm thick gabions to protect them from erosion caused by spring water (Figure 2 and Figure 3) [1] [8]. When properly installed, these gabions respond to the vertical movement of sloped surfaces driven by frost heaving, freezing of water and melting of ice and are effectively permeable to early spring snowmelt and underground water seepage. Previous studies demonstrated that the use of a mixture of gravels and compost to cover the ground reduced soil freezing depth [9]. Thus, in this research project, we studied the effect of special gabions filled with a gravel-compost mixture on soil freezing depth. The main component of the compost was bark from hardwood and coniferous trees. The gravel-to-compost ratio by volume was adjusted to 12.5%, 25% and 50%. We carried out this experiment in a suburb of Kushiro in mid-December.

In another study in eastern Hokkaido, we installed special gabions above a subsurface drainage and formed a plant growing medium layer above them [10]. This treatment was intended to protect slopes formed by removing soil from the ground, which had been damaged by frost heaving, by providing sloped surfaces with both insulation (by means of a plant growing medium) and drainage (by means of a drainage path and gabions). Installation was carried out in January and February.

Figure 4 provides schematic diagrams showing various slope protection treatments. For each studied surface, air temperature and soil temperature were measured hourly at approximately 10 cm depth intervals perpendicular to the sloped surface using temperature sensors for two to three years. The soil freezing depth -at which soil temperature is expected to be 0°C -was estimated using the soil temperature measurements.

4. Results

4.1 Insulating effect of plant growing media

Ministry of Land, Infrastructure and Transport Hokkaido Development Bureau, recommends that plant growing media no greater than approximately 10 cm in thickness be applied to sloped surfaces.[8)] However, to determine the relationship between the thickness of plant growing media and soil freezing depth, we applied media in thicknesses greater than 10 cm. An applied medium 15 cm in thickness was capable of firmly remaining on sloped surfaces, while an applied medium 20 cm in thickness appeared susceptible to sliding. However, we confirmed that the latter was capable of securely remaining on sloped surfaces with gradients of 1:1.5 when applied to a height of up to 1.8 m measured vertically from the bottom of the slope.

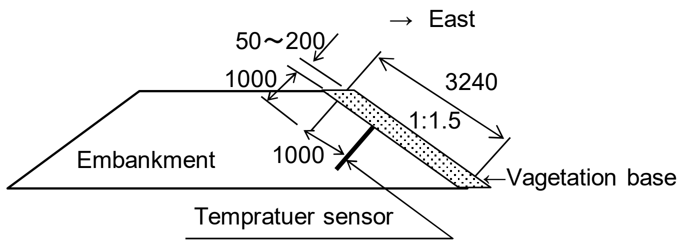

a. Vegetation base construction

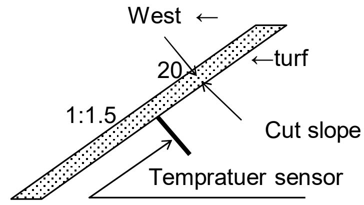

b. Turf constrction

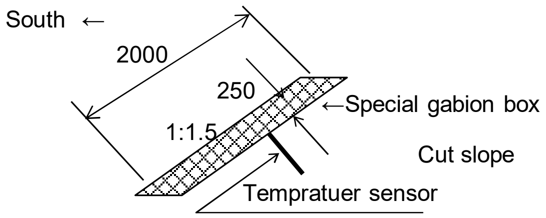

c. Spesial gabion box is contained gravel and compost mixed construction

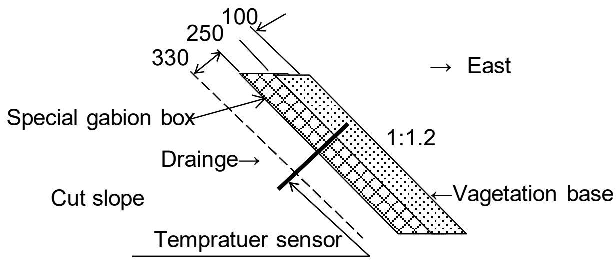

d. Special gabion box and vegetation base

Fig.4 Schematic of construction

The thermal conductivity of plant growing media varied from 0.6 to 1.0 W/mK depending on its water content. Its conductivity was found to be lower than that of earth and sand, which is generally higher than 1 W/mK [11]. Thus, we concluded that the application of a plant growing medium to sloped surfaces may be capable of reducing the soil freezing depth.

We estimated the soil freezing depth (0°C) under a plant growing medium layer using soil temperature measurements. For three years, we measured the thickness of the medium layer and the soil freezing depth in slopes formed by adding soil to the ground (Figure 5). Soil freezing depth was shallower with a plant growing medium than without: the thicker the plant growing medium layer, the shallower the soil freezing depth. The soil freezing depth of uncovered sloped surfaces remained 30 cm or greater during the two years of measurements after the onset of the experiment. By comparison, the soil freezing depth of the covered sloped surfaces progressively decreased over time, from 15 cm or less during the first measurement year to 10 cm or less during the second measurement year. No plant growth was observed on the uncovered sloped surfaces during the two measurement years. By contrast, plant growth was observed on the covered sloped surfaces as early as the first measurement year, which was attributed to migration of seeds into the applied medium from the surrounding environment and seeds that existed in the medium when it was prepared (Photo 6). The insulation provided by a plant growing medium and the snow cover formed in winter appeared to reduce the freezing of sloped surfaces. Thus, we concluded that the application of a plant growing medium can reduce soil freezing depth.

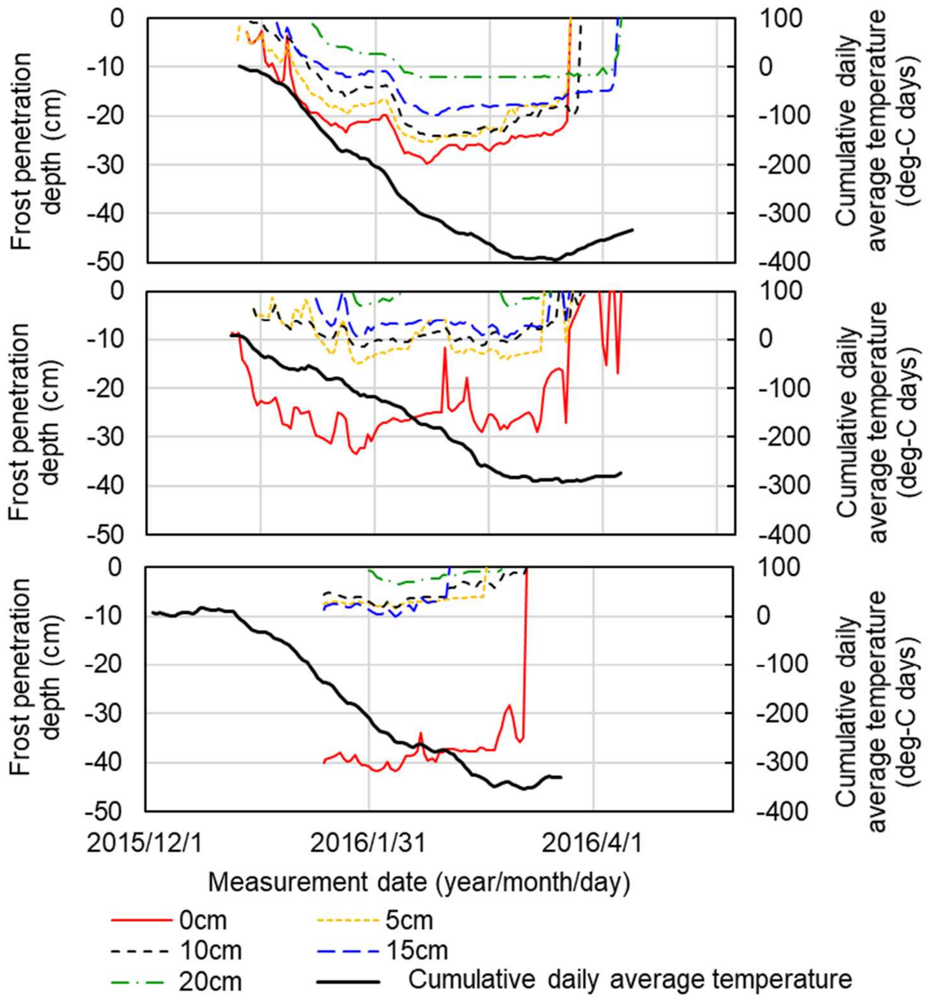

Fig. 5 Thickness of vegetation base material and freeze depth of embankment

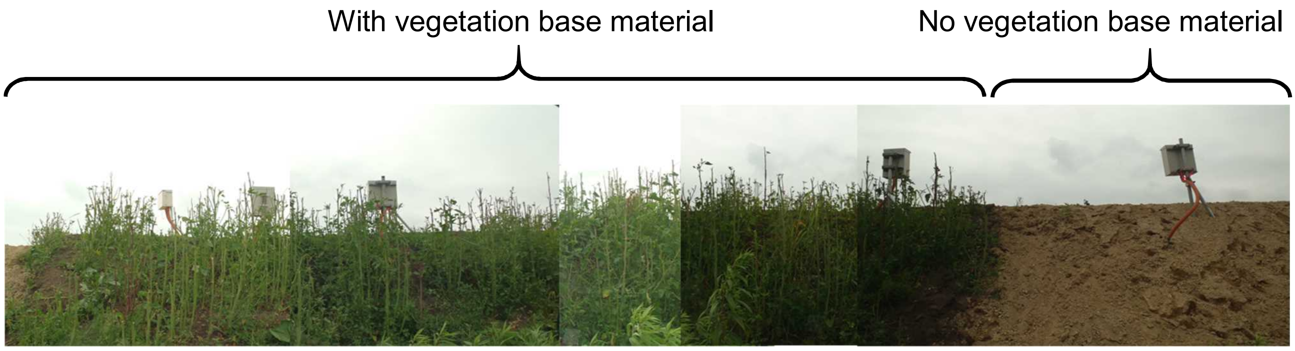

Fig. 6 Plant condition on slope

4.2 Insulating effect of turf

Figure 7 compares the soil freezing depth of turf-covered and uncovered natural ground. Because the freezing depth of the uncovered ground was greater than 50 cm -the depth of the deepest temperature sensor - we were unable to measure it accurately. The freezing depth of the turf-covered ground was shallower than that of the uncovered ground throughout the two measurement years, indicating that turf cover is capable of decreasing soil freezing depth.

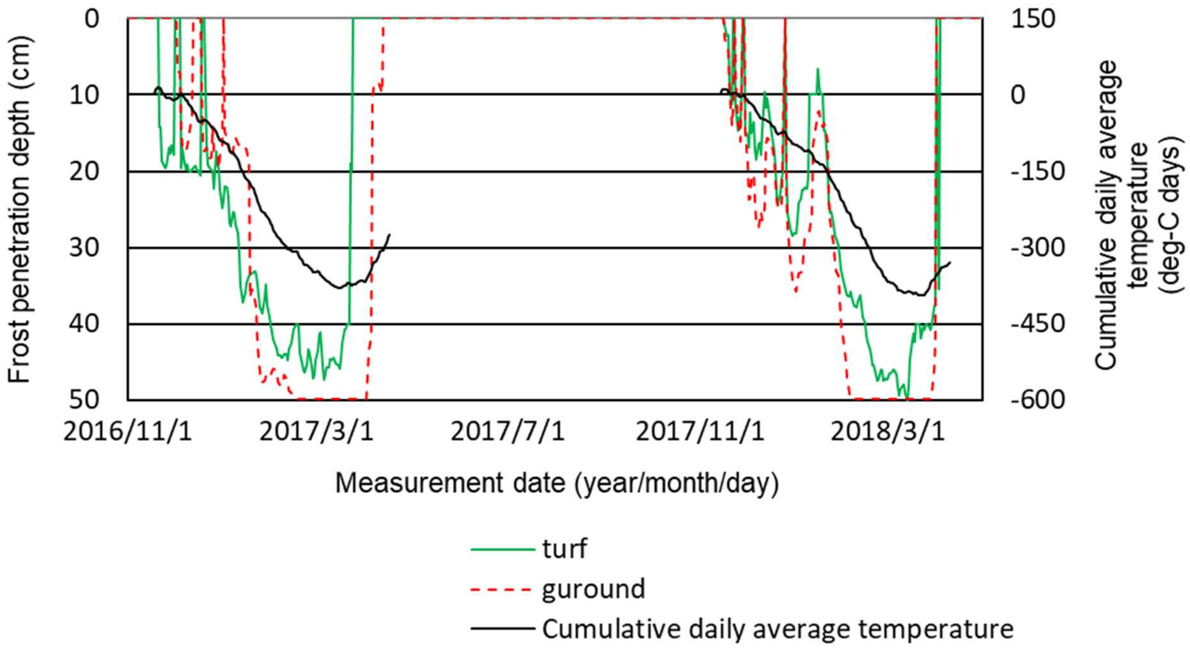

Fig.7 Freezing depth of the ground of turf construction site

4.3 Insulation effect of special gabions filled with a gravel-compost mixture

Figure 8 shows the soil freezing depths of slopes formed by removing soil from the ground, which were then covered with special gabions filled with a gravel-compost mixture. During the first measurement year, freezing depth tended to be only slightly shallower for the gravel-compost mixture than for gravels alone. No clear difference in soil freezing depth was identified between the different compost contents. These results indicated that soil freezing depth is unlikely to be reduced by the application of special gabions 25 cm in thickness filled with a gravel-compost mixture.

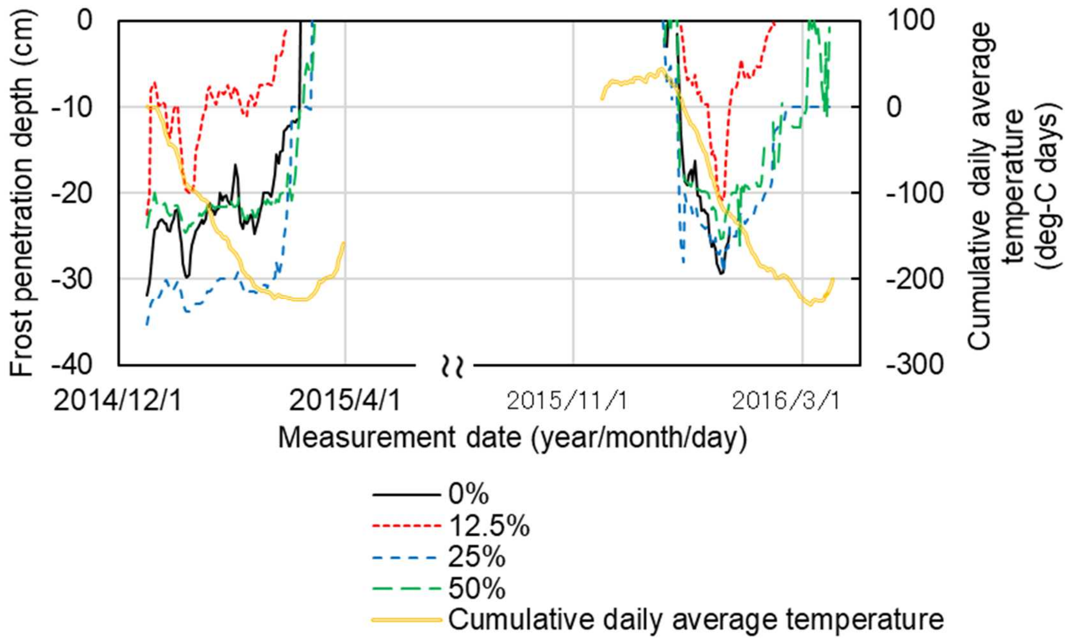

Fig.8 Freezing depth of the ground at installation site of special gabions filled with a gravel-compost mixture

4.4 Combined insulation effect of special gabions and a plant growing medium

Figure 9 shows the soil freezing depth of sloped surfaces covered with special gabions and a plant growing medium. A drainage path 30 cm in depth stretched 3 cm below the gabions. During the two measurement years, we observed soil freezing depths of approximately 10 cm, leaving the upper portion of the underground drainage path to be surrounded by frozen soil. However, the soil surrounding the bottom part of the drainage path remained unfrozen at 1°C during the first measurement year and approximately 2°C during the second measurement year. These results indicated that the proper functioning of the drainage path had been preserved when it was combined with the application of gabions and a plant growing medium. Before this treatment was applied to the slope surface, we conducted a drilling survey and found that the soil freezing depth of the slope was approximately 60 cm, compared to the 10 cm observed after this treatment was applied, indicating that the treatment provided a substantial insulation effect. Figure 10 shows the studied slope surface covered with vegetation in the summer of the first measurement year. Vegetation coverage may provide additional insulation.

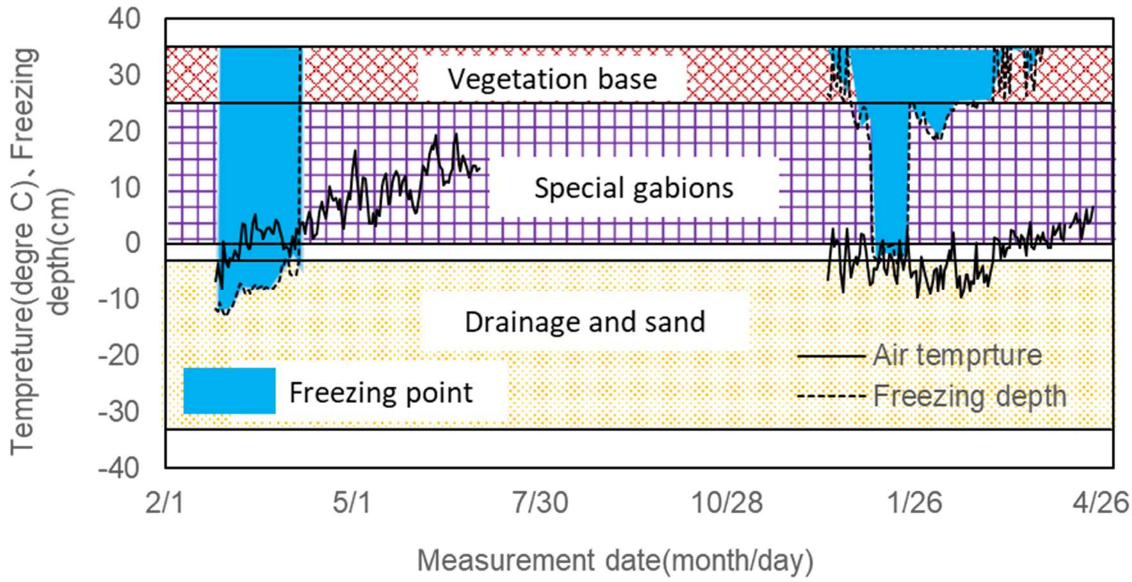

Fig.9 Freezing depth of slope surface by special gabions and vegetation base material

Fig. 10 Vegetation appearance on the slope surface of construction the following year

5. Summary

We covered slope surfaces with a plant growing medium as a means of insulating them and thereby prevent frost heaving. We then monitored soil temperature in the following years. We found:

(1) A layer of a plant growing medium up to approximately 20 cm in thickness can be applied to slope surfaces. The thicker the medium layer, the greater its effect in reducing soil freezing depth. Vegetation that grows naturally on a plant growing medium may facilitate the formation of snow cover on slope surfaces in the winter.
(2) A turf cover may reduce freezing depth in the soil below slope surfaces.
(3) Installation of special gabions filled with a gravel-compost mixture only slightly reduced soil freezing depth.
(4) Combined installation of gabions and a plant growing medium layer above a drainage path reduced soil freezing depth.

Conclusions

Our study revealed that the freezing of slope surfaces can be diminished by installing a layer of a plant growing medium or turf on them. In future studies, we plan to investigate the effect of various combinations of plant growing medium ingredients on soil freezing depth. The methods of reducing slope surface freezing using plant growing media, if established, may also be effective in repairing slope surfaces damaged by frost heaves. We intend to verify this in future studies.

References

[1] Study Group Concerning an Investigation and Design Method of Frost-Heaving Countermeasure, "*Investigation and design manual for frost protection of slopes (Draft)*", Public Interest Incorporated Association, The Japanese Geotechnical Society, Hokkaido Branch, 2016, pp.4.

[2] Takashi Ono. "A method to estimate frost heave affected to earth reinforcement", *52rd Annual Technical Report Meeting of the Hokkaido Branch of the Japanese Geographical Society*, 2012, pp.9-14.

[3] Mingyu Yang, Dahu Rui, Kuniyuki Ueno, Teruyuki Suzuki and Satoshi Yamashita, "Behavior of sodding slope in freeze-thaw process and countermeasure for frost heaving damage, Properties of Embankments in Winter Earthwork", *47rd Annual Technical Report Meeting of the Hokkaido Branch of the Japanese Geographical Society*, 2007, pp.205-210.

[4] Public Interest Incorporated Association, Japan Road Association, "*Guideline for Road Earthwork, Cutting Ground and Slope Stabilization*", 2009, pp.186.

[5] Japanese Society of Soil Mechanics and Foundation Engineering, "*Soil Freezing*", 1994, pp.116–117.

[6] Atsushi Nogami, Toshihiro Hayashi and Atsuko Sato, "Anti-frost-heaving measure in the cut slope in the cold region by a special gabion box with heat insulation(Part 2)", *52rd Japan National conference on Geotechnical Engineering*, 2017, pp.729-730.

[7] Atsuko Sato, Takahiro Yamanashi, Teruyuki Suzuki and Shinichiro Kawabata, "Heat retentive effect of vegetation base material in embankment slope", *50th Japan National Conference on Geotechnical Engineering*, 2015, pp.131-132.

[8] Hokkaido Regional Development Bureau, Ministry of Land, Infrastructure, Transport and Tourism, *Road Design Guidelines*, 2018, 1-4.

[9] Atsuko Sato, Teruyuki Suzuki, Tetsuya Kubo and Satoshi Nishimoto, "Reduction of frost heave depth using compost for geotextile-reinforced earth walls", *Grosynthetics Engineering Journal No.27*, Japan Chapter of International Geosynthetics Society, 2012, pp.189-192.

[10] Akira Ando, Kazutaka Takase and Atsuko Sato, "On spring water and frost heave countermeasure on cut slope surface", *the 52th Hokkaido Regional Development Bureau Technical Presentation*, 2009.

[11] Japan Road Association. "*Road Earthwork Guideline*", 2009, pp.389.

Biological Activated Carbon filtration in contaminated water treatment using two activated carbons at Casey Station, Antarctica

Jack G. Churchill
Department of Chemical Engineering
The University of Melbourne
Australia
j.churchill2@student.unimelb.edu.au

Sally L. Gras[1,2,4], Daniel Wilkins[3], Tim Spedding[3], Geoff W. Stevens[1], Kathryn A. Mumford[1*]
[1] Department of Chemical Engineering, The University of Melbourne, VIC 3010, Australia.
[2] The Bio21 Molecular Science and Biotechnology Institute, The University of Melbourne, VIC 3010, Australia.
[3] Australian Antarctic Division, Channel Highway, Kingston, Tasmania 7050, Australia.
[4] The ARC Dairy Innovation Hub, The University of Melbourne, VIC 3010, Australia.
[*]Author for correspondence, mumfordk@unimelb.edu.au

Summary

At Casey Station, a major Australian Antarctic research station, fuel spills have occurred. The response to mitigating the environmental impact resulting from these spills has led to the development and implementation of hydrocarbon remediation technologies forming an important component of the Australian Antarctic science program. A particular challenge in this environment is treating contaminated groundwater during excavation, due to the diurnal freeze/thaw cycle in the contaminated active layer and permafrost. Initially a groundwater pump and treat operation utilised granular activated carbon (GAC) filtration in the 2015/16 summer season. Given the high logistical cost of operating in remote regions, development of a sustained biological activated carbon filtration process was seen as an attractive alternative and trialled in the 2017/18 Antarctic summer season.

Use of native Antarctic microbes was required to prevent introduction of non-native species. Biological Activated Carbon (BAC) uses a combined biophysical process to adsorb contaminants to the carbon surface, while sustaining a biofilm that is capable of degrading the contaminants. In this study, two activated carbons were compared. Their performance in hydrocarbon removal and biodegradation were assessed. GC1200 (ACT Technologies) is a 100% microporous carbon derived from coconut husk. GS1300 (ACT Technologies) is a meso- and microporous carbon derived from sub-bituminous coal. This paper presents the field results of water sampling in the 2017/18 season and analyses the development of a biological activated carbon filtration process using the native Antarctic microbes at Casey Station, Antarctica.

Treatment of total recoverable hydrocarbons was shown to have occurred successfully, though only a small number of samples were taken. During treatment, removal of ammonium and increased levels of nitrate in both GS1300 and GC1200 filter outlets indicate the presence of active nitrifying bacteria, suggesting some level of biological community has been established. Literature from previous studies into *in situ* Permeable Reactive Barriers utilising ammonia supplementation to GAC beds indicates that the dominant native degrader of diesel fuels, *Burkholderiales,* can also participate in nitrifying communities.

Further work analysing the GAC media particles for evidence of biofilms, via scanning electron microscopy and genetics studies, is required to confirm the formation of biofilms. Further results analysing petroleum hydrocarbon biodegradation indices from the GAC/BAC media is the next step in determining the establishment of a BAC process using native microbes.

Keywords: Remediation, Activated Carbon, Bioremeditation, Water Treatment, Antarctica, Cold Regions

1. Introduction

The growing presence of human activity in Antarctica and the subantarctic over the last sixty years has resulted in significant environmental impacts, challenging the perception of the continent as a pristine environment. With the adoption of the Environmental Protection Protocol in Madrid, 1998, the development of remediation practices to minimise human impacts has become an important part of Antarctic science programs [1]. While generally oil pollution in Antarctica is low in comparison to other regions of the world, and the spatial extent is relatively small, the impact is disproportionate as the human settlements are concentrated in the ice-free areas on the Antarctic coastline which consists of less than 6000 km^2 (around 0.04%) of the total continental area.

In October 2015, a Special Antarctic Blend diesel fuel spill was detected at Casey Station [2]. Snow cover meant that the extent of the spill was hard to delineate. Site response involved recovering and treating contaminated snow and conducting a soil sampling program to delineate the spill extent. A >4000 L spill was detected over an area in excess of 800 m^2, including in the foundation of a new wastewater treatment building under construction [3]. Figure 1 shows near surface (0-40cm) soil sample locations delineating the extent of total petroleum hydrocarbon contamination across the site prior to excavation works. Delineation showed that diesel fuel had migrated to the north-east along preferential flow pathways in fractured bedrock...

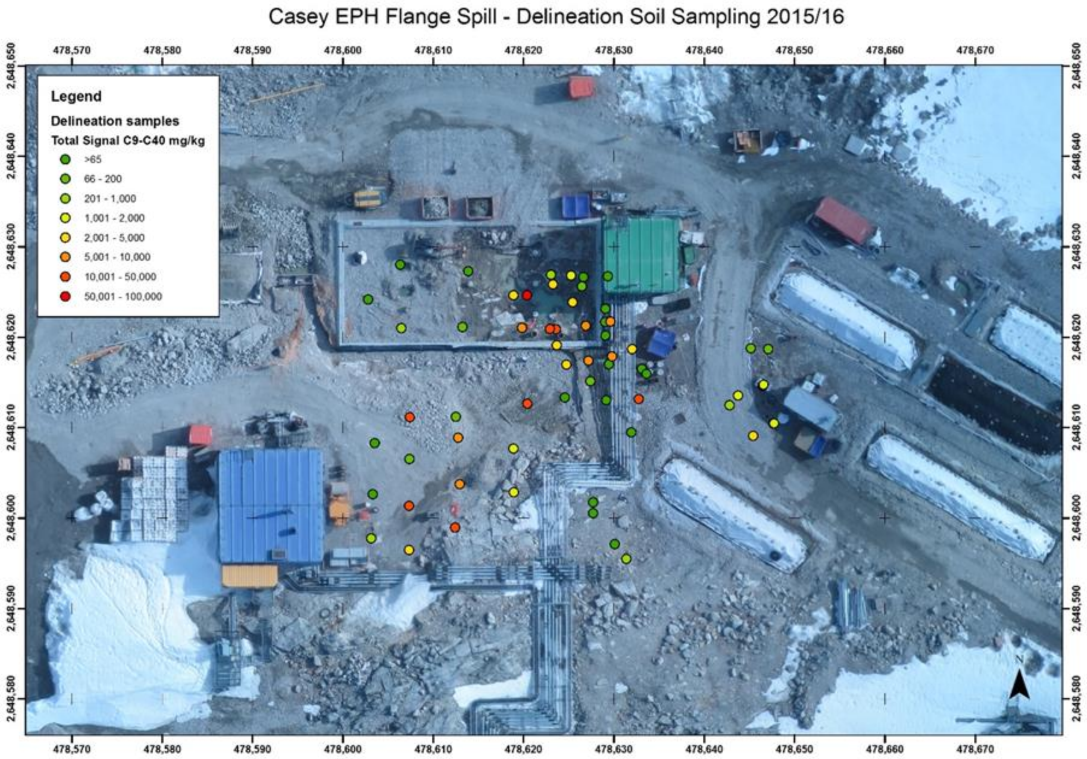

Fig. 1 Initial delineation soil sampling showing the 2015 fuel spill at Casey Station, Antarctica. Long white rectangles are the biopile remediation works. The concrete rectangle is the footprint of the new wastewater treatment building, and showed significant contamination in the southeast corner. Background photomosaic was developed from drone imagery acquired in March 2016 [4] Coordinates are in WGS84 / UTM 49S.

Large scale remediation of contaminated soil in Antarctica is rare, but ex situ biostimulation methods have shown to be a cost-effective and more environmentally appropriate method than excavation and repatriation of contaminated soil [2]. However, a potential environmental risk is the mobilisation of contaminants in meltwater as a result of excavation [5]. Excavation influences the depth of the active layer (the soil zone experiencing seasonal freeze/thaw) and exposes the permafrost, potentially increasing the downwards migration of water and light non-aqueous phase liquids (NAPL). At this site, the initial fuel spill response involved removing and bunding the contaminated snow, and actively pumping LNAPL which pooled in test pits in the frozen soil. Later remediation work involved the excavation of the soil active layer which contained both contaminated soil and fuel encapsulated in ice pockets. This exposure of the active layer can lead to the melting of permafrost layers and the release of NAPL, creating a high contaminant mobilisation risk. Large volumes of contaminated meltwater require treatment prior to discharge, making contaminated water treatment a key issue in excavation operations in Antarctica. At this site, a mobile water treatment container was used to treat contaminated groundwater.

1.1 Mobile Water Treatment Plant Design and Operation

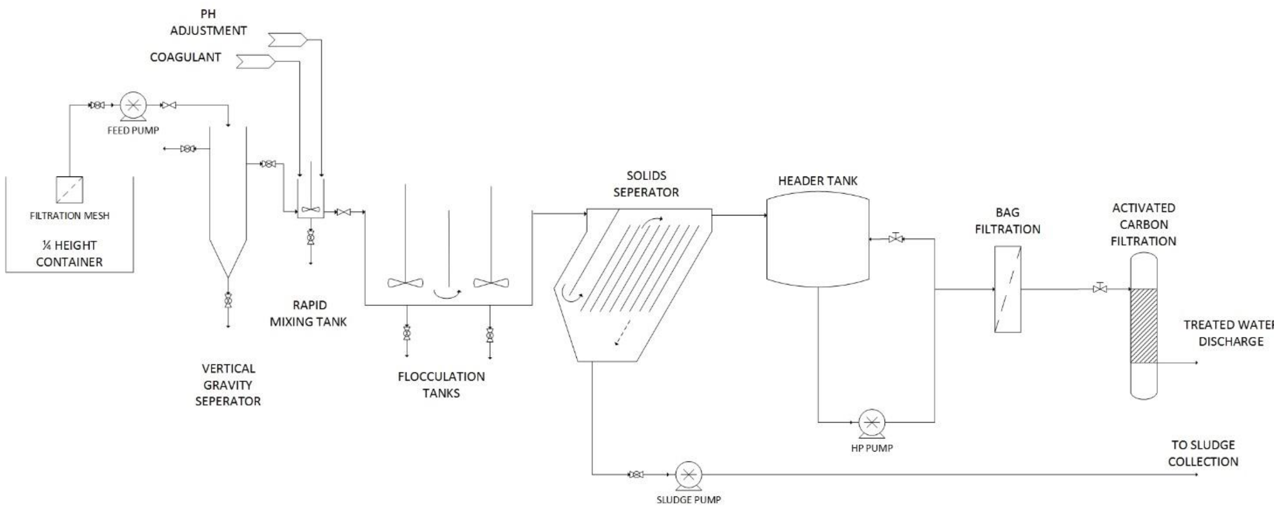

Fig. 2 The mobile water treatment plant process diagram.

To address the issues of quarantine and contaminated waste disposal while still utilising the highly effective removal mechanisms of activated carbon filtration, the development and trial of granular activated carbon and biological activated carbon filtration was proposed for the treatment of the petroleum hydrocarbon contamination, retrofitting an existing mobile water treatment plant [6] previously used in heavy metal remediation (Fig 2.). The ion exchanger columns were replaced with new columns to house activated carbon. The new activated carbon columns were sized at 1.4 m x 0.4 m ID, with four columns installed. Plumbing upgrades were made to allow for different flow configurations as seen in Fig. 3.

Operation during the 2017/18 summer season was conducted using the same plant infrastructure. Contaminated water was pumped from groundwater extraction wells, biopile leachate [2], and meltwater from snow that had been contaminated by the fuel spill. The produced water was stored in a 7,000 L capacity heated container before entering the mobile water treatment plant at a flowrate of 16 L/min. Upon entering the water treatment plant (Fig. 2), the water was contacted with a gravity separator with oleophilic surfaces designed to remove free non-aqueous liquid product. This was followed by receiving a dose of dissolved ferric chloride to achieve a coagulant concentration of approximately 30 mg/L in a rapid mixer. Following the flash contact of the coagulant to the process stream, flocculation was allowed to occur in slow mixers. The process stream was then passed through an inclined plate gravity separator to remove flocculated solids from the process stream. The clarified water was then passed through polypropylene 5 micron bag filter (FSI Filters) to remove remaining sediment.

This filtered and clarified water entered the activated carbon filtration system. The flow was split between two columns (Fig. 3, Column 1 and Column 2) and allowed an Empty Bed Contact Time (EBCT) of approximately 18.5 min. The effluent of each column was passed through a second column (Column 2 and Column 4, respectively) containing a 50:50 mixture of GC1200 GAC and Clinoptilolite, a natural zeolite, before being discharged to a Permeable Reactive Barrier [7]. The columns were filled to leave 300 mm headspace, with the flow entering at the top of the column via a flow distributer.

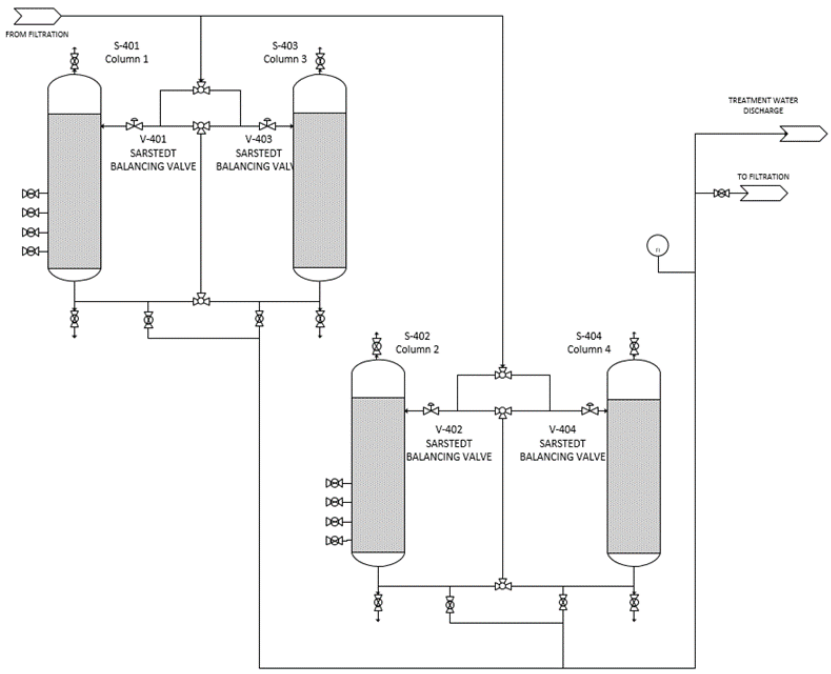

Fig. 3 The plumbing and installed column configuration, allowing for highly flexible flow configurations.

1.2 Granular Activated Carbon and Biological Activated Carbon Filtration

Granular Activated carbon is a widely used adsorbent for removal of hydrophobic (often organic) compounds from aqueous systems utilizing the high selectivity and adsorption capacity of the material, especially for low concentration solutions. These properties make it an ideal media for use in petroleum hydrocarbon removal in Antarctica. However, media saturation and the application of a cautionary management approach to avoiding contaminant breakthrough require large volumes of activated carbon to be used. In the remote Antarctic operating environment, there are significant costs associated with the logistics of shipping large volumes of raw material. There are quarantine and contaminated waste disposal issues with the return of hydrocarbon-saturated media to Australia. The development of a continuous process that involves degradation of the hydrocarbon contamination provides a more sustainable and economic remediation alternative.

Biological Activated Carbon (BAC) filters have been used for the treatment of wastewater for several decades, making use of the high adsorption capacity for removal of organic compounds and biological processes for degradation of the same compounds. This was speculated to be due to the biological system being able to access substrates from both the bulk fluid phase, and the adsorption surface. However, the proof of regeneration of the activated carbon remains somewhat elusive, remaining an ongoing area of interest [8][9]. This simple and advantageous system has been investigated since, in an attempt to improve the performance and cost-effectiveness of activated carbon in the wastewater industry.

Previous applications of GAC in Antarctica have focused on the use of hard, microporous (100% of pores smaller than <2 nm) and steam activated coconut-derived activated carbons for *in situ* applications, primarily as Permeable Reactive Barriers (PRBs) due to material hardness that protected against freeze-thaw stresses. It was suggested that Biological Activated Carbon is a combination of an adsorption and biodegradation phase, whereby a feed rich in carbon enters the filter and is adsorbed to the surface of the activated carbon and degraded from the bulk liquid phase by the biofilm, and a bioregeneration phase, where a carbon-poor feed enters the filter [9]. In the bioregeneration phase, the biofilm degrades both the little carbon source present in the bulk liquid, causing chemical gradient driving force for desorption of adsorbed carbon sources. The desorbed carbon sources are also degraded in this nutrient limited environment. In contrast to other explanations, such as exo-enzymes, this is considered the more likely method and matches well with the high variability of feed streams in both municipal and industrial wastewater treatment feed streams [8].

With knowledge from emerging research into BAC filtration and the necessity to reduce material costs and transport in Antarctica, an understanding of how to develop a BAC process for petroleum hydrocarbon contaminated water in a quarantine restricted region was considered. In this research, the performance of two activated carbons are compared in a full scale mobile water treatment plant. In the experiment presented here, the activated carbons are used in a “high load, low load” BAC filtration operation, where the feed water is received during the operational hours of the day (approximately 8am to 6pm) and where warm water is recirculated through the filters after operational hours with no new contaminated feed water.

2. Materials and Methods

In previous Antarctic applications, the physical stresses of the freeze thaw environment on *in situ* Permeable Reactive Barriers dictated that a hard GAC was required, leading to the choice of a coconut-husk derived carbon with high microporous capacity. The chosen GAC was GC1200 (Activated Carbon Technologies), with the properties outlined in Table 1. [10] However, micropores may limit the mass transfer kinetics, and correspondingly increase the size of the mass transfer zone and decrease the carbon usage rate. As such, a second GAC was chosen for use in the GAC filtration system. Derived from sub-bituminous coal and utilised in municipal water treatment plants in Australia, GS1300 (Activated Carbon Technologies) has roughly the same microporous volume as the GC1200, but also contains a large mesopore volume. This may allow for better kinetic uptake of contaminants, and encourage attachment of biofilms with the rougher surface allowing better protection against shear forces in the filter.

To ensure a biological presence on the filters, an inoculation procedure was used. The columns were loaded with GC1200 in Column 2 and GS1300 in Column 1. Prior to operation a 200 L broth of a microbial culture was prepared for inoculating the columns. Tap water was used from the station to prepare a Bushnell Haas broth at a concentration of 3.27 g/L [11]. This broth is designed to have all the requisite nutrients except a carbon source, necessary for the growth of hydrocarbon degrading bacteria. A spike of Special Antarctic Blend diesel (SAB) was added to a concentration of 7 mg/L in the broth. Finally, soil samples from the EPH flange spill sight were collected and centrifuged. The supernatant liquid (~40 mL) was then used to inoculate the broth, with the broth left to sit for 192 h at 20° C.

Water samples were analysed at two National Association of Testing Authorities Australia (NATA) accredited facilities. Ammonia, Nitrate and Nitrite samples were analysed at Analytical Services Tasmania by flow injection analysis, while Total Recoverable Hydrocarbon (TRH), monoaromatic hydrocarbons (MAH), Benzene, Toluene, Ethyl-benzene and xylene (BTEX) and polyaromatic hydrocarbons (PAH) samples were analysed at Eurofins Australia.

Table 1. The properties of the two activated carbons, used in both Antarctic and municipal water treatment systems.

Material Properties	*GC1200 Activated Carbon*	*GS1300 Activated Carbon*
Supplier	*ACT Pty Ltd*	*ACT Pty Ltd*
Raw material	*Coconut Husk*	*Sub-bituminous coal*
Activation	*Thermal*	*Thermal*
Physical form	*Granular*	*Granular*
Total pore volume (cm^3/g)	*0.458*	*0.933*
Micropore fraction (%)	*100*	*47*
Mesopore fraction (%)	*0*	*53*

3. Results

3.1 Total Recoverable Hydrocarbon Removal

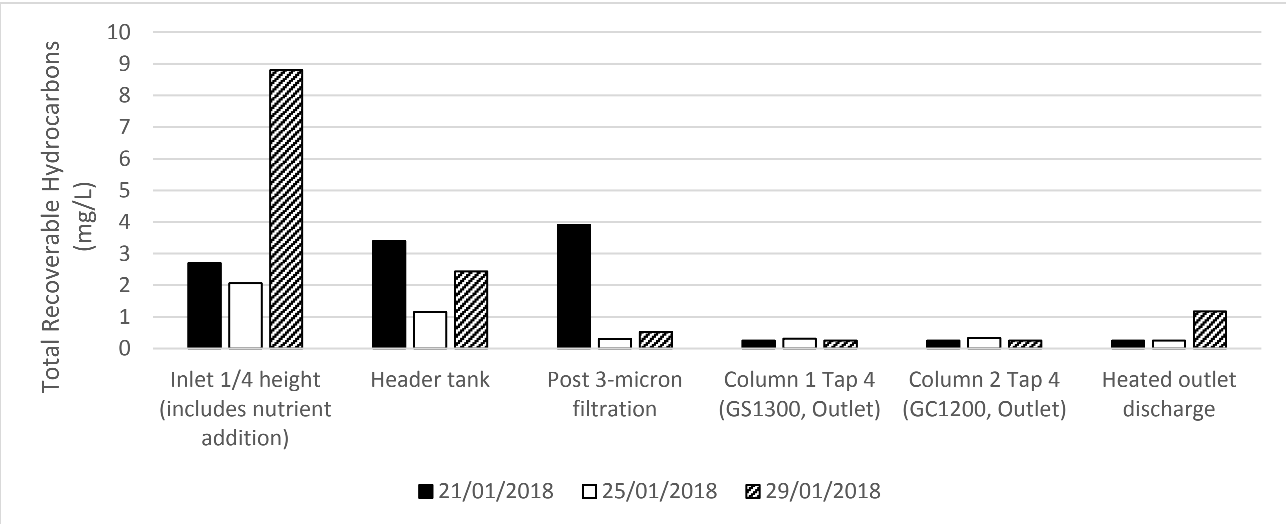

Fig. 4 Total recoverable hydrocarbon (TRH, mg/L) detected in each stage in the water treatment process.

Across the two different BAC column outlets, effluent samples did not exceed 0.33 mg/L and except for on the 25/01, the effluent concentrations were below the method reporting limit of 0.25 mg/L (Fig. 4). The column outlet showed discharge concentrations of below 0.25 mg/L on the 23/01 and 25/01, but showed a concentration of 1.760 mg/L on 29/01. This is higher than the other concentrations upstream until the header tank.

3.2 Nitrogen Removal

Figure 5 displays analytical results for water samples taken from 23/01/2018. These samples correspond with treating a fertiliser-loaded water source diluted with pumped water. Ammonia is shown to be removed by approximately 77% at the effluent, compared to the influent. The bulk of this removal is expected to occur via cation exchange in the zeolite media in the final two columns. This is seen in the large reduction between the Column 2 Tap 4 sample and the Heated outlet discharge. Notably, the Column 1 Tap 4 appears to show a larger reduction of ammonia as compared to Column 2 Tap 4. In the BAC experiment, the system was designed to promote proliferation of biological activity in Column 1 and 2. The decreased ammonia and increased nitrate in the Column 1 effluent suggests that nitrification may be occurring. For the 23/01/18 sampling round, nitrate and nitrite concentrations decrease from the inlet to the outlet by 91.7% and 99.9% respectively. The removal coincides with treatment in the final two columns, suggesting that some removal is being achieved. However, zeolite is a cation exchange material and does not have a discrete mechanism for anion (i.e. nitrate) removal. For the water sampling program on 25/01 and 29/01 (Figure 6 and Figure 7), clear removal is not seen for any of the different nitrogen contaminants. The effluent samples on 25/01 and 29/01 have levels of nitrate, nitrite and ammonia below that of the effluent on the 23/01, suggesting that removal only occurs at high concentrations.

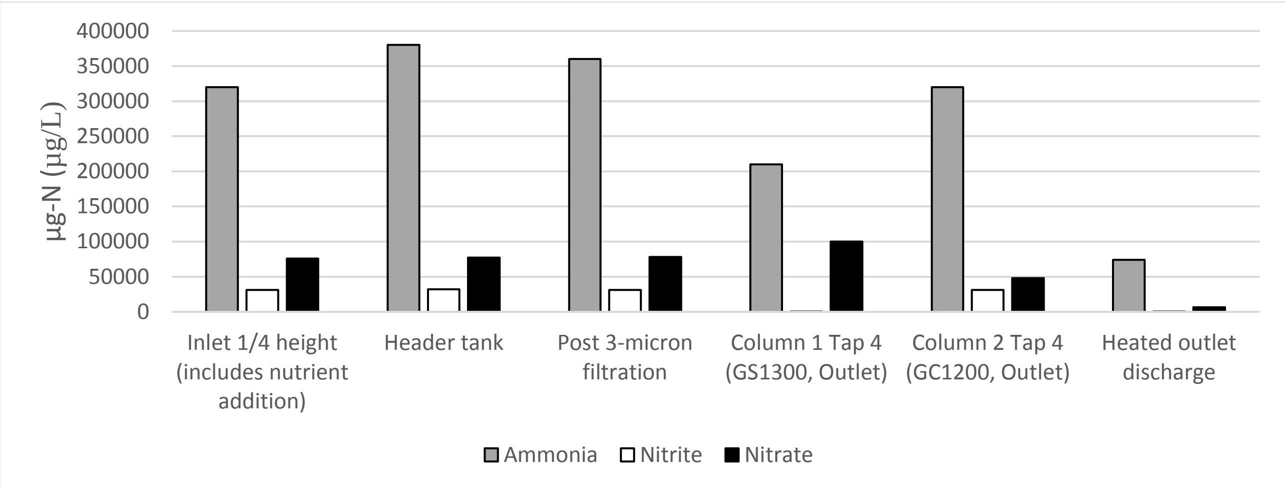

Fig. 5 Ammonia, nitrite and nitrate readings on 23/01/18 (130 h mark).

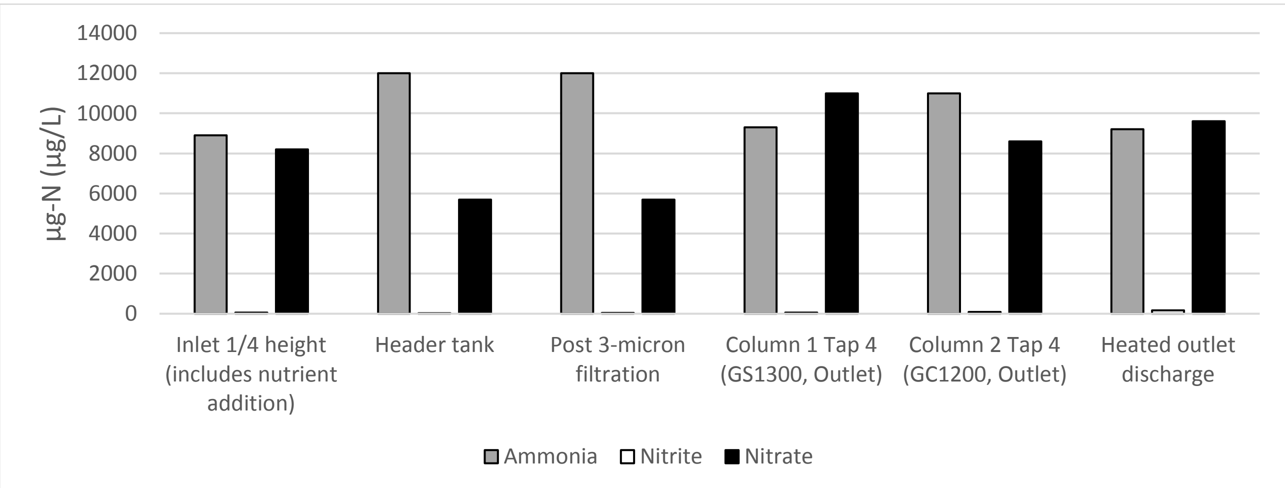

Fig. 6 Ammonia, nitrite and nitrate readings on 25/01/18 (177 h mark).

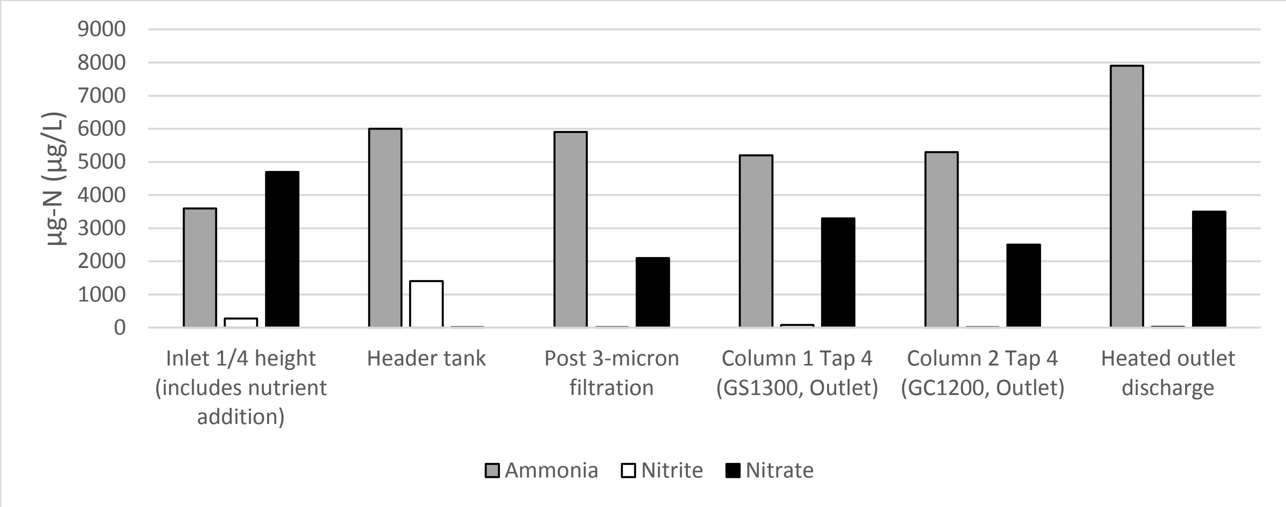

Fig. 7 Ammonia, nitrite and nitrate readings on 25/01/18 273 h mark).

The effluent at the different timepoints had ammonia levels consistently above the Australian and New Zealand Environment and Conservation Council (ANZECC) freshwater trigger value for slightly to moderately disturbed freshwater ecosystems as total ammonia-N of 2180 – 2570 µg/L (ANZECC, 2000 - Table 8.3.7). Similarly, a moderate reliability trigger value (at 95% protective concentration) for nitrate was 700 µg/L, a number that was exceeded in all effluent samples (ANZECC, 2000 - Page 8.3-169). It is important to note that the influent concentrations on 23/01 are irregularly high in an attempt to both treat a one-off high nutrient loaded source, and to show the performance of the water treatment container under those circumstances. The influent and effluent concentrations were not typical of day to day operation, and were not reflective of the concentrations of these nutrients in the receiving water body. Biopile leachate water, the main source of nitrogen contamination, showed a maximum ammonia concentration of 170 mg-N/L on 13/01/18 with an average of 36 mg/L and a maximum nitrate concentration of 89 mg-N/L on 13/01/18 with an average of 23 mg/L. These sources were regularly mixed with low nutrient, hydrocarbon contaminated groundwater prior to treatment. However, the point discharge of the water treatment container in this range of nitrogen levels on the 25/01/18 and 29/01/18 shows that the treatment plant (as designed) was not effective at treating wastewater with a high nitrogen load.

4. Discussion, Conclusions and Acknowledgements

4.1 Discussion

The total recoverable hydrocarbons results from water sample analysis indicate that removal of aqueous organic contaminants can be achieved with the current plant design and operational parameters. The combined sediment removal and dissolved hydrocarbon removal via the presence of granular activated carbon is effective, and these results indicate that both activated carbons have removed TRH from the wastewater stream. At 80,000 L of treated water during the 300 hours of operation, a carbon usage rate of 0.57 g/L (a measure of mass of carbon per volume of water treated) was obtained before the carbon was replaced. In results not presented here, the TRH levels of the activated carbon themselves showed that the material was not saturated during the BAC experiment and breakthrough had not fully occurred. Clear limitations exist in the low sample frequency of the water samples, minimising the ability to draw definitive conclusions about the effectiveness of the setup over extended periods of operation. These limitations highlight the logistical difficulties we encountered as a result of the cold and remote operating environment, with analysis of samples only able to be performed in mainland Australia.

By themselves, the TRH results do not indicate whether the establishment of a biological community of hydrocarbon degraders was successful, or whether one GAC outperformed the other. However, analysis of the nitrogen components shows some potential indication of biological activity. In Fig. 5, Column 1 (GS1300) shows a greater removal of ammonia than Column 2 (GC1200). Column 1 also shows a higher amount of nitrate present at the column exit compared to the column inlet, while Column 2 shows a steady amount. This occurred at an abnormally high concentration of nitrogen in the feed water due to a spike from a fertiliser enriched source. 47 hours after the spike (Fig. 6) the same results are seen, though Column 2 (GC1200) appears to also show some nitrification with decreased ammonia levels relative to the influent and increased nitrate levels. 147 hours after the spike (Fig. 7) the same is seen again, though a high ammonia level is seen in the column effluent, potentially as a release from the zeolite in the two polishing columns following the activated carbon columns. Previous analysis of hydrocarbon degrading microbes in Antarctica in the *in situ* PRBs has been conducted, and focused on the effects of nutrient addition (predominantly in the form of ammonium supplementation) [12]. These results showed that in laboratory flow cells using soil sourced from Casey Station and also in PRB samples, the order *Burkholderiales* (*Betaproteobacteria)* dominated on GAC particles. This order is a putative hydrocarbon degrader, and is associated with preferentially removing short to mid-chain-length alkanes in diesel. It has been found elsewhere to be dominant in BAC filtration systems [13]. Additionally, it was found that on controlled nutrient release materials (predominantly as ammonium-loaded zeolite), nitrification had been observed, with *Burkholderiales* remaining largely abundant. This order includes members which have been shown to undertake nitrification and denitrification roles in water treatment settings [13].

4.2 Final Comments

These results show only a small picture of the designed Antarctic Biological Activated Carbon process. While there is some indication of bioactivity in the apparent nitrification that appears to compliment previous data, further analysis of the GAC media is necessary. To validate whether contaminant breakthrough occurred, and to apply other techniques to ascertain biological activity the petroleum hydrocarbon levels on the activated carbons will be analysed. This should allow for direct comparison of the two carbon products, and allow for comment on their efficacy. Further to this, scanning electron microscopy will be undertaken to view the surface of preserved activated carbons to see the presence of microbes, while preserved genetics samples can be analysed to determine the presence of hydrocarbon degraders specifically. These research methods all rely on preservation then analysis of samples outside of the station, with long hold times - a reality based on the logistical and quarantine issues of operating in remote and protected environment of Antarctica. Future research will focus on batch and rapid small-scale column tests of specific micropollutants present in SAB diesel, to create mathematical relationships to estimate the breakthrough profiles and carbon usage rates of the two activated carbons.

4.3 Conclusions

A mobile water treatment plant initially designed for treating heavy metal contaminants during excavation of an Antarctic tip site was retrofitted to replace ion exchange columns with activated carbon filtration columns. The columns were filled with two types of activated carbons to remove diesel-origin petroleum hydrocarbons as a result of a recent fuel spill. They were inoculated with a culture of indigenous Antarctic hydrocarbon degrading bacteria and operated in a high-load, low-load system designed to bioregenerate the activated carbon products and maximise their longevity. Water samples taken during operation indicate that treatment of petroleum hydrocarbons by the plant was successful, and that there was some indication of potential nitrification in the two filters. The more mesoporous carbon appears to have outperformed the harder microporous carbon in nitrification. Further investigation of the activated carbon materials themselves are necessary, and we acknowledge that the small number of samples sizes analysed in this paper are related to logistical issues, which highlight the difficulty of operating in cold and remote regions.

4.4 Acknowledgments

The authors gratefully acknowledge the financial support of Australian Antarctic Science Project 4029 and Project 4036 and The Particulate Fluids Processing Centre. Jack Churchill is funded from an Australian Postgraduate Award. Sally Gras is supported by The ARC Dairy Innovation Hub (IH120100005).

References

[1] SNAPE, I., ACOMB, L., BARNES, D. L., BAINBRIDGE, S., ENO, R., FILLER, D. M., PLATO, N., POLAND, J. S., RAYMOND, T. C., RAYNER, J. L., RIDDLE, M. J., RIKE, A. G., RUTTER, A., SCHAFER, A. N., SICILIANO, S. D. and WALWORTH, J. L. "Contamination, regulation and remediation: an introduction to bioremediation of petroleum hydrocarbons in cold regions". In: FILLER, D. M., BARNES, D. L. and SNAPE, I. (eds.) *Bioremediation of Petroleum Hydrocarbons in Cold Regions*. Cambridge, United Kingdom: Cambridge University Press.

[2] McWatters, R. S., Wilkins, D., Spedding, T., Hince, G., Raymond, B., Lagerewski, G., et al. "On site remediation of a fuel spill and soil reuse in Antarctica" *Science of the Total Environment*. Vol. 571, 2016, pp. 963-973

[3] MCWATTERS, R., ROWE, R. K., WILKINS, D., SPEDDING, T., HINCE, G., RICHARSON, J. and SNAPE, I., "Modelling of vapour intrusion into a building impacted by a fuel spill in Antarctica" *Journal of Environmental Management*, Vo. 231, 2019, pp. 467-482.

[4] POTTER, S. Sensefly eBee (drone) imagery of Casey and Wilkes. Australian Antarctic Division. 2016 (updated 2017). https://data.aad.gov.au/metadata/records/AAS_5024_drone_imagery_Bailey_Peninsula_2015-16/citation

[5] NORTHCOTT, K. A., SNAPE, I., CONNOR, M. A. and STEVENS, G. W. "Water treatment design for site remediation at Casey Station, Antarctica: site characterisation and particle separation", *Cold Regions Science and Technology*. Vol. 37, 2003, pp. 169-185

[6] NORTHCOTT, K. A., WOODBERRY, P., SNAPE, I. and STEVENS, G. W., "Water treatment to prevent contaminant dispersal during remediation of cold regions contaminated sites", *Cold Regions Science and Technology*, Vol 48, 2007, pp. 92-104

[7] MUMFORD, K. A., RAYNER, J. L., SNAPE, I., STARK, S. C., STEVENS, G. W. and GORE D. B, "Design, installation and preliminary testing of a permeable reactive barrier for diesel fuel remediation at Casey Station, Antarctica", *Cold Regions Science and Technology,* 2013, Vol. 96, pp. 96-107

[8] AKTAŞ, O. and ÇEÇEN, F. "Bioregeneration of activated carbon: A review" *International Biodeterioration & Biodegradation,* Vol. 59, 2007, pp. 257-272

[9] ABROMAITIS, V., RACYS, V., VAN DER MAREL, and P., MEULEPAS, R. J. W. "Biodegradation of persistent organics can overcome adsorption–desorption hysteresis in biological activated carbon systems", *Chemosphere*, Vol. 149, 2017, pp. 183-189

[10] FREIDMAN, B. L., GRAS S. L., SNAPE, I., STEVENS, G. W. and MUMFORD K. A. "A bio-reactive barrier sequence for petroleum hydrocarbon capture and degradation in low nutrient environments" *International Biodeterioration & Biodegradation*. Vol. 116, 2017, pp. 26-37

[11] BUSHNELL, L. D, and HAAS., H. F. "The Utilization of Certain Hydrocarbons by Microorganisms." *Journal of Bacteriology* Vol. 41, 1941, pp. 653-73.

[12] FREIDMAN, B. L., SPEIRS, L. B. M., CHURCHILL, J. G. GRAS S. L., TUCCI, J., SNAPE, I., et al. "Biofilm communities and biodegradation within permeable reactive barriers at fuel spill sites in Antarctica." *International Biodeterioration & Biodegradation*, Vol. 125, 2017, pp. 45-53

[13] NIEMI, M. R., HEISKANEN, I., HEINE, R. and RAPALA, J. "Previously uncultured b-Proteobacteria dominate in biologically active granular activated carbon (BAC) filters" *Water Research*. Vol. 43, 2009, pp. 5075-5086

Granulated ferrochrome slag's capasity to resist resilient deformations

Laura Raerinne
Student of Engineering
Destia Oy
Finland
laura.raerinne@destia.fi

Summary

This paper introduces the use of granulated molten ferrochrome slag in road structure material based on its properties and especially its resilient deformation behavior. Ferrochrome slag is produced in ferrochrome production. Ferrochrome slag is processed to by-products and granulated molten ferrochrome slag (OKTO insulation) is one of these by-products. OKTO insulation is coarse-grained material and because of its properties, for example thermal insulating capacity, hydraulic properties and good load-bearing capacity, it is mainly used in drainage course in road structures.

This paper is based on a master's thesis of the author. One part of thesis was a literary survey about resilient deformation behavior of unbound coarse-grained road structure materials. Researches about this are mostly about natural materials, but because OKTO insulation is also unbound, coarse-grained and granular material, some of these research results can be generalized to resilient deformation behavior of OKTO insulation. One important goal of thesis was to update OKTO insulation's elastic module (E), which represents material's capacity to resist resilient deformations and which is used in designing road structures with Odemark's formula. This updating was done with cyclic triaxial tests and building the experimental structures in Tornio. OKTO insulation's resilient deformations behavior was compared to filter sand, which was used as reference material. When OKTO insulation is sufficiently compacted, it is well-founded to use 100 MPa for OKTO insulation's E-modulus.

Keywords: recycled material, granulated ferrochrome slag, resilient deformations, permanent deformations, road structure, Master's Thesis, cyclic triaxial tests, experimental structures

1. Production process of granulated ferrochrome slag

Granulated ferrochrome slag is a processed by-product from manufacturing process, in which refined chromite is heated to high temperatures and reduced to metallic ferrochrome. Ferrochrome is an essential part of stainless steel. [1]

Chromite is mined from Kemi Mine. Kemi Mine is an only ferrochrome mine in Europe Union area. Chromite ore is refined and after that it is transported to Tornio, where Outokumpu's Tornio plant is located. In this plant refined chromite is reduced to metallic ferrochrome via electric-arc furnace process. Molten ferrochrome sinks to the bottom of the furnace. Ferrochrome slag layer stays above molten ferrochrome. [1] Ferrochrome slag consists of irreducible oxides and chromite and accessory substances (like quartzite). [2] Mineralogy of ferrochrome slag is represented below.

Table 1 OKTO insulation's mineralogy [1]

Mineral	Percentage value
SiO_2	30 %
Al_2O_3	26 %
MgO	23 %
Fe_{TOT}	4 %
Cr	8 %
CaO	2 %

Amount of ferrochrome production is about 530 000 t / a and amount of ferrochrome slag is about 650 000 t / a. Ferrochrome slag is processed to standardized, CE marked by-products, which have tight quality control. OKTO aggregate is manufactured from air-cooled ferrochrome slag by crushing and OKTO insulation is manufactured from molten ferrochrome slag through granulation. Amount of OKTO insulation produced is about 500 000 t/a. [1] [3] OKTO insulation is presented in picture 1.

Fig. 1 OKTO insulation

2. Properties of granulated ferrochrome slag

Because of the manufacturing process and mineralogy, OKTO insulation is homogenous, compact, porous and granular material, which has only very little fine fraction. OKTO insulation's fraction is 0-11. Outokumpu Chrome Oy has published design manual for using of OKTO insulation and OKTO aggregate (2010). OKTO insulation's properties presented in this chapter are from that manual. [1] Design manual will be updated later this year.

2.1 Technical and mechanical properties

OKTO insulation's typical grain size distribution is presented in figure 2. It fits to the grain size distribution area of filter sand. That area is defined in the road structures' design manual, which is published by the Finnish Transport Infrastructure Agency (in Finnish: *"Väylävirasto"*). In Finland, road structures are designed using Odemark's formula, in which road structure materials have given E-moduli. These given E-moduli are based on grain size distribution of materials and experiments of these material's behavior on specific layer in road structure. In figure 2 are represented these E-moduli areas for filter sand. [4]

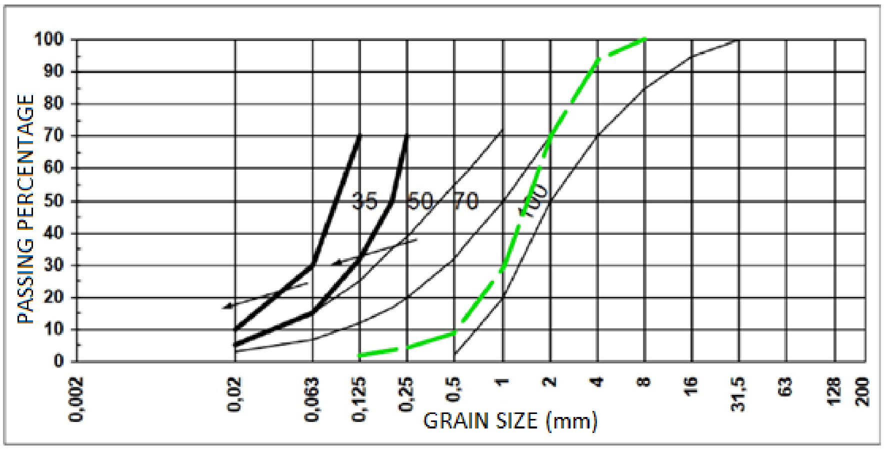

Fig. 2 OKTO insulation [1][4]

OKTO insulation's E-modulus was estimated to be 100 MPa, because of its typical grain distribution (Fig 2) and results from the earlier experimental structures. However, the amount of OKTO insulation produced has doubled after the introduction of the third furnace, so there was a need to research OKTO insulation's capability to resist resilient deformations and update its E-modulus. [1] [3] OKTO insulation's other defined technical and mechanical properties are presented in table 2.

Table 2 OKTO insulation's properties [1]

Property	Value
Maximum dry density	17,9…18,4 kN/m3
Optimum water content	7,0…10,5 %
Friction angl	39...42 ˚
Cohesion	27 kPa

2.2 Thermal characteristics, frost susceptibility and hydraulic properties

Because OKTO insulation is porous material, it has good thermal insulation properties. Its thermal characteristics are defined via results from laboratory testing and experimental structures. [1]

In road structure design manual designing against frost heave is based on calculated frost heave. Material's thermal insulation capacity is represented as equivalence coefficient compared to filter sand's thermal insulation capacity. Filter sand's equivalence coefficient is defined as 1. OKTO insulation's thermal insulation capacity is defined from its thermal conductivity values and its equivalence coefficient is 1,5. OKTO insulation insulates better than filter sand. [1] [4]

OKTO insulation's height of capillary rise varies from 100 mm to 300 mm. Material's frost susceptibility is represented as amount of frost swelling (%). Because of its grain size distribution, capillarity and results from frost heave tests, OKTO insulation is classifies as frost resistant material and its frost swelling is 0 %. [1] [4]

3. Using granulated ferrochrome slag in road structure

Because of its characteristics, OKTO insulation it is mostly used in drainage courses in street or road structures. Ferrochrome slag products have been used in infra structures for decades. Nowadays by-products processed from ferrochrome slag are classified as products, not waste. Also, solubility of detrimental elements is small. Ferrochrome slag products can be used without environmental license. [1] [3]

Main marketing area of OKTO insulation is about 150 kilometers from Tornio's plant, for example it is used in Oulu. OKTO insulation doesn't harden in structures, so it is particularly used in streets, which have municipal engineering. Orderer's and designer's attitudes towards recycled materials are also in important role when it comes to using OKTO insulation. [3]

Final costs for using OKTO insulation instead of filter sand or other natural crushed aggregates depends on many things. OKTO insulation has better thermal insulation capacity than sand. If road structure is built to the frost-susceptible subsoil, thickness of the drainage course is thinner when using OKTO insulation instead of filter sand. Material is needed less, and excavations will be lower. Transportation cost also varies depending availability of the filter sand on the area. [3]

4. Granulated ferrochrome slag's capasity to resist resilient deformations

In Finland designing the road structures is based on designing adequate structures for defined traffic loads. Road structures is supposed to resist repeated traffic loads without too big permanent deformations, which are the main reason for damages in the road structures. Road structure designing is done using target bearing capacities. Bearing capacity represents structure's stiffness and structure's capacity to resist resilient deformations. Road structures are designed using Odemark's formula, in which every road structure material has specific E-modulus. [4] E-moduli represents material's capacity to resist resilient deformations. Quality control of build road structures is also mostly based on road structure's bearing capacity, not structure's capacity to resist permanent deformations. This is understandable, because coarse-grained structure materials' capacity to resist both resilient and permanent deformations are affected partially by the same factors, like density and stress level. [5] [6]

4.1 Results from literature survey about unbound granular road structure materials

Unbound, granular materials consist of lots of particles. When material is under a stress, for example from repeated traffic load, stresses will pass on to other particles via contact points. Unbound, coarse-grained road structure materials can't withstand any tension. That's why stresses cause triaxial compression to these materials. Stresses can cause either permanent or resilient deformations to materials.

Researches concerning granular material's capacity to resist resilient or permanent deformations are mostly made for natural materials, like sand, gravel and crushed aggregate. For example, Brecciaroli & Kolisoja have gathered in their literature review results from these researches. Resilient response of material is mostly influenced by the level of applied stresses and the moisture content and density of the material. Permanent response of material is affected by several factors, like stress level, moisture content, density and physical properties of aggregate particles. [5] Because OKTO insulation is coarse-grained, granular, unbound and permeable to water, many of these results can be applied with reserve to the OKTO insulation's deformation behavior.

4.2 Results from the experimental structures

To define OKTO insulation's E-module and to observe what affects to OKTO insulation's construction properties, part of the master's thesis was to analyze test results from experimental structures. Four experimental structure parts were built to Tornio, part to the pedestrian and bicycle way. OKTO insulation or filter sand was used in drainage courses and layer thickness of drainage courses varied within experimental structure parts. Thicknesses of sub-base, base course and road pavement were the same for all experimental structure parts. E-module of the filter sand based on its grain size distribution varied from 50 MPa to 70 MPa.

From experimental structures was done density tests, plate bearing tests and falling weight deflectometer tests. With help of these test results and other observations, effects of different compaction methods and other prevailing circumstances was estimated.

Plate bearing test's results made from surface of base course was used to estimate E-modulus of OKTO insulation. There were differences in building the experimental structure parts, for example compression methods varied. Also subsoil type under the experimental structures varied. Because of all that, calculation and comparison to the reference material was not so straightforward. Measured bearing capacities was compared to calculated bearing capacities. Calculations were done with Odemark's formula and with different subsoil types. Regarding calculation results from best compacted experimental structure parts, it is well-founded to use E-moduli of 100 MPa to OKTO insulation when designing road structures with Odemark's formula.

4.3 Results from the cyclic triaxial tests

OKTO insulation's resilient deformation behavior was examined with cyclic triaxial tests. Tests were done in Earth & Foundation Engineering Laboratory in Tampere University. OKTO insulation's behavior was compared to filter sand's behavior. Filter sand's E-modulus was defined to be 100 MPa due to its grain size distribution.

Cyclic triaxial tests were done for five samples of OKTO insulation and two samples of reference sand. M_r-moduli of these samples were determined by cyclic triaxial tests and material parameters K_1 and K_2 from these results. After that it is possible to use formula 1 to estimate material's M_r-moduli.

$$M_r = K_1 \left(\frac{\theta}{\theta_o}\right)^{K_2}, \qquad (1)$$

where M_r = resilient modulus (kPa), θ = sum of the principal stresses (kPa), θ_0 = reference stress (1 kPa) and K_1, K_2 = material parameters, which are bounded to the specific density and moisture content of the material. M_r-moduli of samples calculated with K_1 and K_2 are presented in picture 3.

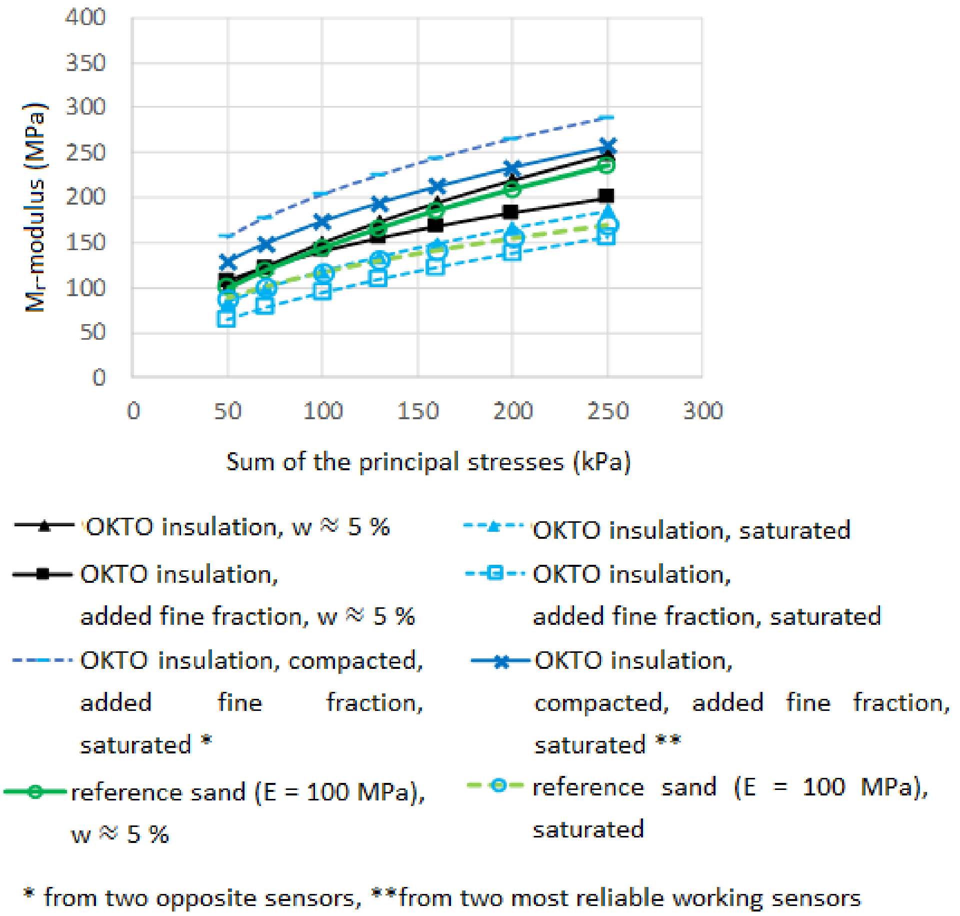

Fig. 3 Calculated resilient moduli of samples [7]

As can be seen in picture above, in comparable conditions and when taken account of precision of measurement, resilient moduli of OKTO insulation are same than reference material's resilient moduli. That also supports using 100 MPa for OKTO insulation's E-modulus when designing road structures with Odemark's formula.

5. Conclusions

OKTO insulation's capacity to resist resilient deformations behavior was researched via experimental structures and cyclic triaxial tests. Results from these together support that it can be recommended to use 100 MPa for OKTO insulation's E-modulus, when designing road structures with Odemark's formula. When building road structures from OKTO insulation, it is very important to compact OKTO insulation enough and do compacting with enough thin layers.

References

[1] KALLIO H., HOLAPPA T. & TIKKAKOSKI A. *"OKTO-rakennustuotteiden suunnittelu- ja rakentamisohje tie-, katu- ja maarakenteissa",* Outokumpu Oy, 2010, pp. 44.

[2] ANTTILA, J. *"Kromin liuottaminen ferrokromikuonasta ultraääniavusteisesti peroksidipohjaisten reagenssien avulla",* University of Jyväskylä, 2016, pp. 67.

[3] MUSTANIEMI, J., interview by Sanna Torniainen, 2017.

[4] LIIKENNEVIRASTO, *"Tierakenteen suunnittelu"*, Liikenneviraston ohjeita 38/2018, 2018, pp. 139.

[5] BRECCIAROLI F. & KOLISOJA P. *"Deformation behaviour of railway embankment materials*

under repeated loading: Literature review.", Publications of Finnish Rail Administration A 5/2006, 2006, pp. 214.

[6] KALLIAINEN A., LUOMALA H., JÄNISKANGAS T., NURMIKOLU A. & KOLISOJA P. "Radan eristys- ja välikerrosten tiiviys- ja kantavuustutkimus" Liikenneviraston tutkimuksia ja selvityksiä 10/2011, 2011, pp. 156.

[7] VUORIMIES, N. & KOLISOJA, P. *"Testausselostus MPR/255/2018"*, 2019, Tampere University, pp. 45.

Valorisation of Greenlandic municipal solid waste incineration bottom ash as sand substitute in mortar

Gunvor Marie Kirkelund
Associate Professor
Technical University of Denmark
Denmark
gunki@byg.dtu.dk

MSc Benjamin A. R. Ebert, Technical University of Denmark, Denmark
MSc Cosmin-Cristian Florian, Technical University of Denmark, Denmark

Summary

In Greenland waste has traditionally been dumped at open disposal sites combined with uncontrolled incineration. In the mid 1990s the first waste strategy was implemented and as a result, simple and small municipal solid waste incineration (MSWI) plants were taken into use in towns and settlements primarily to minimize the amount of waste at the disposal sites. Between 6,000 – 15,000 tons MSWI bottom ash is produced annually in Greenland and is disposed of at the open disposal sites without leachate collection or encapsulation. The MSWI bottom ash could have value as a secondary resource in construction work, as most construction materials are imported. This would contribute to solving the problem of disposal and possible related environmental problems in the vulnerable Greenlandic environment. This study investigated the use of incineration ash, particularly bottom ash, as a sand substitute in mortars. The ash was taken from two of Greenland's six incinerator plants, located in the two biggest cities: Nuuk, the capital, and Sisimiut. Mortar samples with up to four different substitution percentages of sand (5%, 10%, 20%,100%) were tested. The main properties studied were the compressive strength (curing time 7, 14, 28 and 90 days) and the leaching behaviour of the mortars containing ash, in comparison to a reference mix. The characteristics of the ash samples showed that the heavy metal content in the Sisimiut ash contained high amounts of lead and zinc, while the Nuuk ash contained high levels of copper and chromium and the resulting elevated leaching of these metals in the ashes. The compressive strength results after 28 days of curing showed that the mortar samples with 5 % sand replacement with bottom ash have a compressive strength 42-47 MPa compared to the reference (55 MPa). At higher percentages, comparing a replacement of 20% and 100% sand with Sisimiut bottom ash, no significant strength difference was found, while maintaining strength of almost 70% of the reference at 35 MPa. The early strength development was slower for the mortars containing bottom ash compared to the reference.
The leaching results showed that the level of heavy metals in the eluate are significantly lower for the mortar samples, compared to those from tests done directly on the ashes, thus including them into a mortar matrix reduces the leaching significantly. In addition to this, the use of bottom ash as aggregate appears to have high potential in mortar, with strength values approaching those of the reference mixes and could have potential for use a local secondary resource.

Keywords: Waste, concrete, circular economy, secondary resources

1. Introduction

Waste strategy was introduced in Greenland in the late 1990s and with this municipal solid waste incineration (MSWI) was implemented in the six major cities to reduce the waste volume and recover the energy. Fly ash and bottom ash are particulate residues of waste incineration. Annually, Greenlandic incinerators produce between 6,000 – 15,000 tons of MSWI bottom ash, which is dumped or used as cover material on the local disposal sites, and 200 tons fly ash, which is shipped to Norway for disposal due to its high environmental impact. Waste landfills in Greenland do not have control of either leachate or gas, which means that the surrounding air, soil and water are prone to contamination [1]. The possibility to use MSWI ash as a construction material would provide an alternative and ensure that Greenland can reach acceptable economic and environmental standards and contribute to the circular economy.

Valorization of bottom ash has used as secondary material in road construction due to its similarity to natural aggregates [2]. In concrete production, the use of pre-treated bottom ash has been tested as aggregate, with promising results and possible uses in non-structural elements [3-7]. The properties of bottom ash in cement was also studied and have shown that the inclusion of pre-treated ash had little effect on the strength of the created cement [8-10]. For finding an efficient use of the bottom ash in concrete, the replacement of aggregate with ash has been studied at different ratios. Zhang and Zhao [11] tested at 0, 30, 50, 70% by weight. Pera et al. [12], tested at 50% and 100% aggregate replacement. They concluded that compressive strength decreases as substitution percentage increases. In addition to this, swelling and cracks were visible on the samples, possibly due to the reaction between metallic aluminum and cement. Kirkelund et al. [13] studied the use of Greenlandic incineration fly ash and bottom ash as a secondary resource in mortar. The results showed that substitutions of 5% cement with fly ash and 5 % sand with bottom ash in the same mortar mix reduces the compressive strength of the mortar, but that bottom ash and sand have similarities [14] that indicate a potential use as a secondary material, especially if pre-treated. The study also showed that the workability of the mortar is reduced and the setting times delayed, proportional to ash replacement. Kirkelund et al. [15] found that the use of Greenlandic bottom ash as subbase in road construction is possible, with small modifications to the size distribution done prior to use.

In this study, Greenlandic MSWI bottom ash from the incinerators of the two largest towns, Nuuk and Sisimiut, was characterized and tested to determine the usability of the ash as sand substitute in mortar production and evaluated as a construction material, both from a structural and environmental point of view.

2. Materials and methods

2.1 Experimental materials

Bottom ash was collected from Nuuk and Sisimiut incineration plants, from the containers collecting the bottom ash after the grate furnace. The bottom ash was stored at room temperature in sealed plastic containers until the experimental work. Sea sand 0-4 mm, Rapid Aalborg Cement, CEM I 52.5 N and distilled water were used for mortar mixing.

2.2 Pre-treatment of bottom ash

Large pieces of metal, ceramic and glass in the bottom ashes were removed. Then, the ashes were separated in fractions larger than 4 mm and fractions lower than 4mm by the use of a sieve. The bottom ash fraction lower than 4 mm was further used for analysis and testing. Parts of the Sisimiut bottom was further separated into seven size groups and then mixed as to create an ash mixture with a size distribution similar to that of the sea sand used. This was done in order to test if changing the size distribution of the bottom ash to resemble that of the sand has an impact on the properties of the ash.

2.3 Analytical methods

Particle size distribution of the two bottom ashes was performed by sieving. The water content was measured by heating the bottom ash at 105ºC for 24 hours and expressed in percentage of weight of ash before drying. Loss on ignition (LoI) was measured as weight loss at 550ºC after one hour. pH was measured in 1 M KCl at a liquid to solid ratio (L/S) of 5 and after 1 hour of agitation, pH was measured by a Radiometer Analytical pH electrode. The heavy metal content was measured on acid digested (DS 259) bottom ash samples by induced coupled plasma-optical emission spectrometry (ICP-OES). A modification of the leaching test DS/EN 12457-1, where 40 g of material/crushed mortar was mixed with 80 ml of distilled water (liquid to solid ratio 2) and the sample was agitated for 24 h. pH was measured in the suspension, which was filtered before metal analysis by ICP-OES. Ash mineralogy was studied by X-ray powder diffraction (XRD), for identification of major crystalline phases. The instrument was a PANalytical X'Pert Pro operating at 45 mA and 40 kV applying Cu Ka radiation with a 2HX'Celerator detector. The samples were scanned in the range of 4–70 2 H within 2.5 h. The diffractograms were interpreted by using the ICDD PDF-4 database for minerals.

2.4 Mortar mixing and testing

In total, 13 different mortar mixes were made, see Table 1. Besides a reference sample with virgin materials, mortar mixes with 5, 10 and 20 % substitution of sand with bottom ash were made for the raw and sorted Sisimiut bottom ash and Nuuk bottom ash. Additionally, two mortar mixes with only use of bottom ash rather than sand were made with the raw and sorted Sisimiut bottom ash.

Table 1 Mortar mixtures

Sample name	Bottom ash	Sand	Cement	Water	Pre-treatment
REF	0	1350	450	225	-
SIS-5-R	67.5	1282.5	450	225	-
SIS-10-R	135	1215	450	225	-
SIS-20-R	270	1080	450	225	-
SIS-100-R	1350	0	450	225	-
SIS-5-S	67.5	1282.5	450	225	Sorted
SIS-10-S	135	1215	450	225	Sorted
SIS-20-S	270	1080	450	225	Sorted
SIS-100-S	1350	0	450	225	Sorted
NUK-5	67.5	1282.5	450	225	-
NUK-10	135	1215	450	225	-
NUK-20	270	1080	450	225	-

The consistency of the fresh mortars were measured as the flow value according to DS/EN 1015-3:1999, with a stainless steel mould with 50 mm height. The setting times with a Vicat apparatus according to DS/EN 196-3, with the modification that mortar was used instead of cement paste. The initial setting time was found the first time the Vicat needle sunk 6±3 mm and the final setting time when the needle only penetrates the mortar specimen up to 0.5 mm from the bottom of the specimen.

Each mix was cast in 160×40×40mm steel prism mould, covered with plastic foil and stored at room temperature until demoulding 20-24 h after casting. The mortar samples were cured in distilled water in different containers, according to the type of ash that was used. Compressive strength was tested after 7, 14, 28 and 90 days for all Sisimiut bottom ash and the reference sample and for mortars with Nuuk bottom ash, compressive strength was tested after 7, 14 and 28 days according to DS/EN 196-1:2005. One mortar prism was divided into two by a three-point loading setup, and thereafter the compressive strength measurements were made on the two samples of each prism on a 40×40 mm test area with a Toni Technik 300 tons compressive test machine, totally six measurement for each mortar mixture. All 28 days samples were collected and further crushed to particles smaller than 4 mm and used for leaching tests.

3. Results and discussion

3.1 Material characteristics

The characteristics for the bottom ashes are shown in Figure 1 and Table 2. They all have an alkaline pH and highest concentrations of Cu, Pb and Zn. The low organic content, shows that the incineration process was performed at a sufficient temperature. Metal leaching from the bottom ashes were above the Category 3 [16] for Pb and Zn in the untreated Sisimiut bottom ash, Pb in the sorted Sisimiut bottom ash and Cr, Cu and Pb for Nuuk bottom ash. Exceeding these limits make these bottom ashes unsuited for reuse for geotechnical purposes, i.e. road construction from an environmental point of view. The particle size distribution (Fig. 1) shows that the raw bottom ashes are less sorted than sand and cannot directly be compared and the Sisimiut bottom ash was more fine grained than the Nuuk bottom ash. The main minerals in the bottom ashes were quartz and Ca-containing minerals.

Table 2 Bottom ash characteristics

	Sisimiut bottom ash	Sorted Sisimiut	Nuuk bottom ash	Category 3 limits [16]
pH	12.6	12.6	12.0	-
Water content (%)	0.2	0.15	22.4	-
Organic content (%)	0.2	0.04	0.85	-
Al (g/kg)	19.8	22.1	47.4	-
Cd (mg/kg)	3.1	2.0	2.0	>0.5
Cr (mg/kg)	63.0	49.8	98.7	>500
Cu (mg/kg)	4100	3600	10200	>500
Pb (mg/kg)	2210	750	337	>40
Zn (mg/kg)	4300	3500	5590	> 500
Main minerals	SiO_2, $CaCO_3$, $Ca(OH)_2$, $CaAl_2Si_2O_8$, (Na, Ca)Al(Si,Al)$_3$O$_8$	SiO_2, $CaCO_3$, $Ca(OH)_2$, $CaAl_2Si_2O_8$, (Na, Ca)Al(Si,Al)$_3$O$_8$	SiO_2, $CaCO_3$, TiO_2	-
Leaching				
Al (mg/l)	3.6	0.55	483	-
Cd (mg/l)	<0.002	<0.002	<0.002	0.04
Cr (mg/l)	0.24	0.09	**0.76**	0.5
Cu (mg/l)	0.20	0.04	**3.4**	2
Pb (mg/l)	**1.3**	**5.3**	**0.26**	0.1
Zn (mg/l)	**1.4**	0.79	0.24	1.5

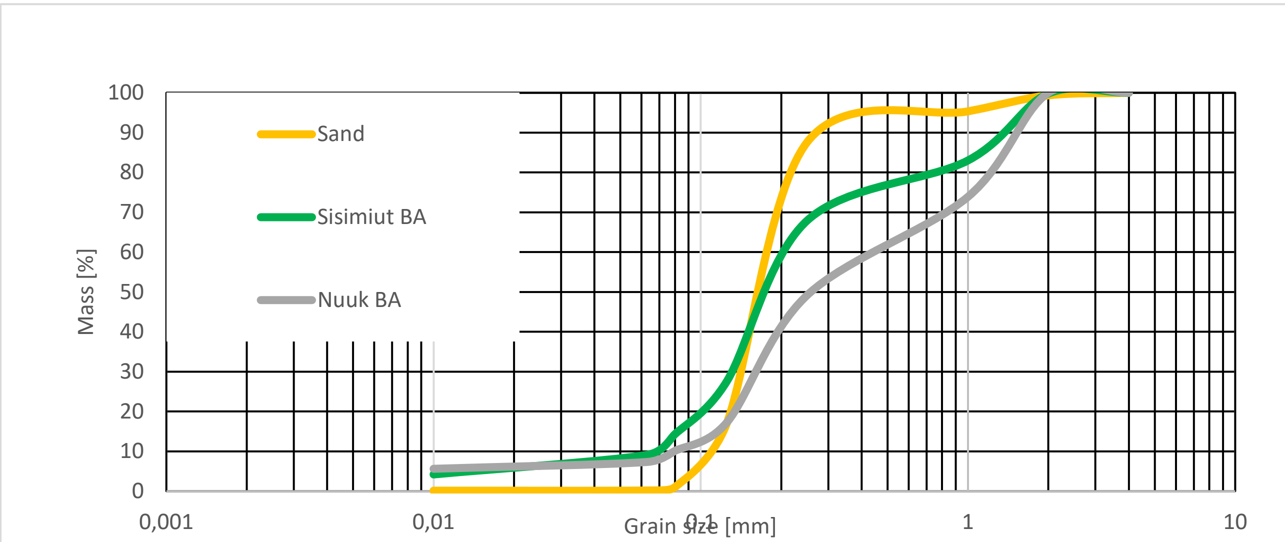

Fig. 1 Particle size distribution

3.2 Workability and setting time

The observed workability of the fresh mortar, appeared to be the same, between the reference mix and the mortar mixture with 5% sand replacement with ash. However, as the ash percentage increased, the workability decreased. This behavior has been observed by others and is expected to be due to the larger fraction of small porous particles [11], which is seen in Fig. 1. For samples with 100% sand substitution, the mixture showed almost no bonding between the aggregate particles, and the water/cement ratio of the 100% mixtures was then increased to 0.67 to be able to cast the mortar samples. The fresh mortar consistency results of the 5% ash containing mortars are shown in Fig. 2. They show the values for the average flow diameter, expressed in millimeters. At low substitution percentages, the samples appear to have a good consistency, even surpassing that of the reference samples. The Nuuk ash mortar has the highest flow values, of around 140 mm, even if the Nuuk bottom ash had larger particles than the Sisimiut bottom ash.

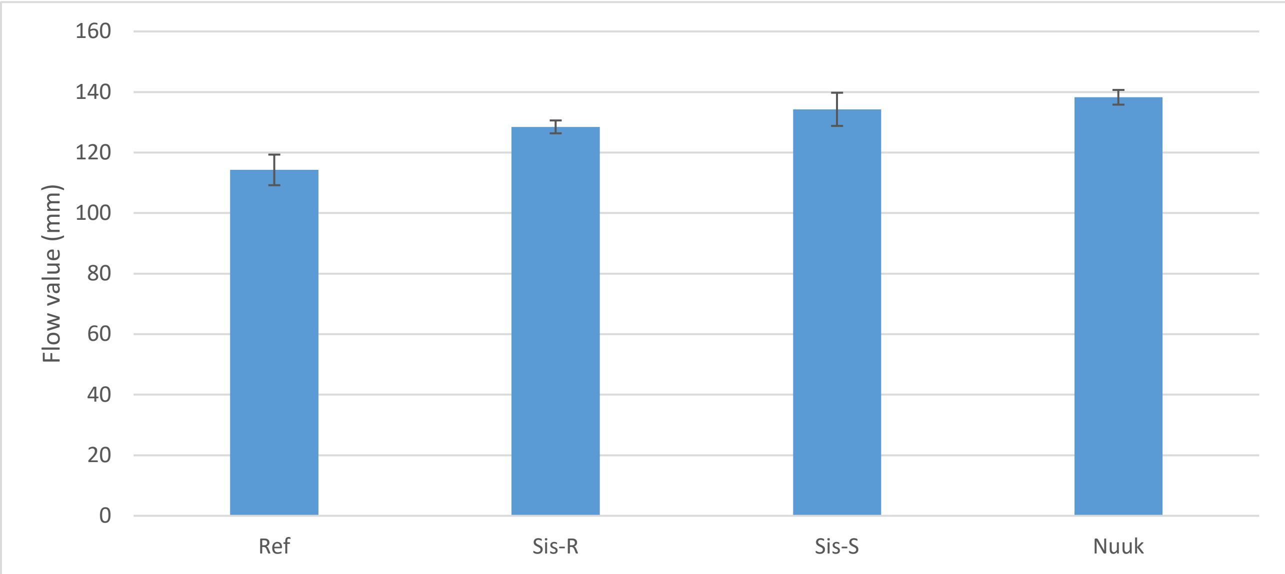

Fig. 2 Flow values of mortar mixes

Setting time measurements were also performed on the 5% substitution mortar mixtures. The results showed that the addition of the ash decreases the initial setting time of the mortar, as seen in Fig. 3.

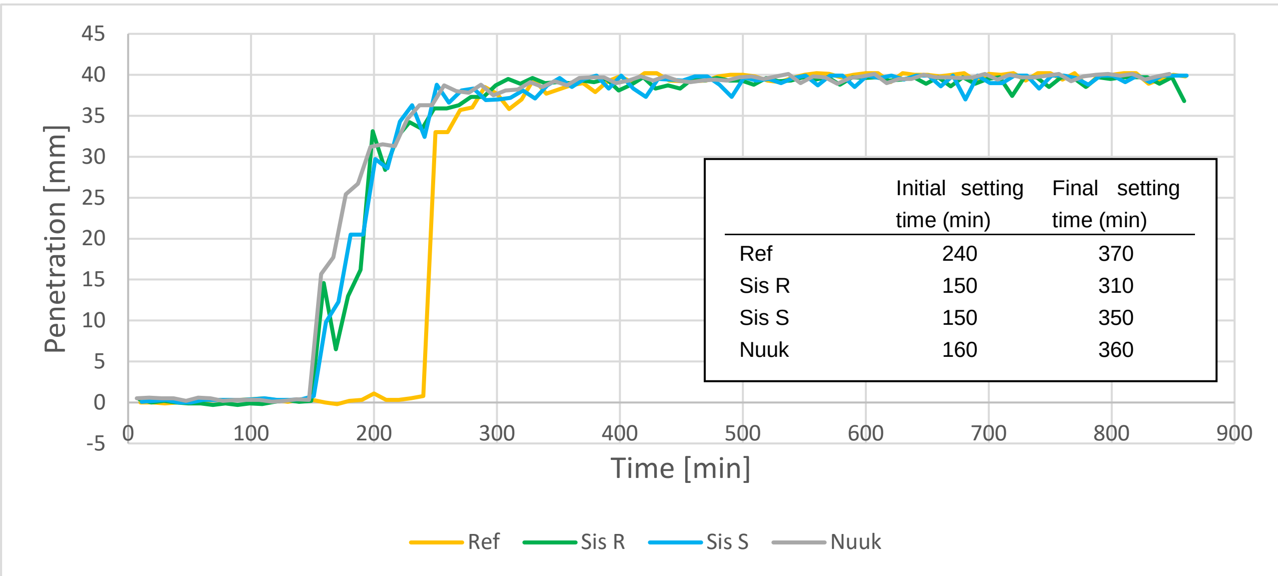

Fig. 3 Setting time measurements

The mortars containing the bottom ash had a initial setting time 80-90 min faster than the reference mix. There appears to be no significant difference between the ash types themselves on the intial setting times, with Nuuk BA having a setting time only 10 min slower than the Sisimiut BA. Kurdowski [17] states that the presence of chlorides, sulphates, nitrides and nitrates may act as factors for accelerated setting and strength development of cementitious mixtures, by improving the hydration process and increasing the heat evolution. This phenomenon can prove to be very advantageous in arctic regions, as the water in the mix is exposed to the cold environment for a shorter period of time and it should be tested at colder temperatures.

3.3 Mortar volume and density

The volumes of the 28 days cured samples are shown in Fig. 4. At 5 % sand substitutions, the Sisimiut BA samples have a volume close to that of the reference sample, within a 1% increase. However, as the substitution increases, the volume of the samples increases with almost 5%.
In addition to this, large voids and cracks in the mortar samples was observed, which can be resulting from gas formation between any metallic aluminium in the bottom ash and cement, in water, a behavior observed in other researches done on use of bottom ash in concrete or mortars [18]. A solution for this was given by Pera et al. [12], supported by Pan et al. [10], where it is recommended to wash the ash prior to use, allowing the metallic aluminum particles to be depleted and preventing the release of hydrogen during the curing period. In addition to this, the washing of the ash also helps remove soluble salts and heavy metals, which is expected to ultimately increase the performance of the mortars [10].

Contrary to the expectations, the ashes containing 100% ash in place of sand did not have a significant volume increase. The 100 % raw ash samples had an increase of only 2%, while the sorted ash sample volume was almost identical to that of the reference. For the Nuuk ash, the volumes of all the mortars were similar to the reference, with volume differences of less than 1%.

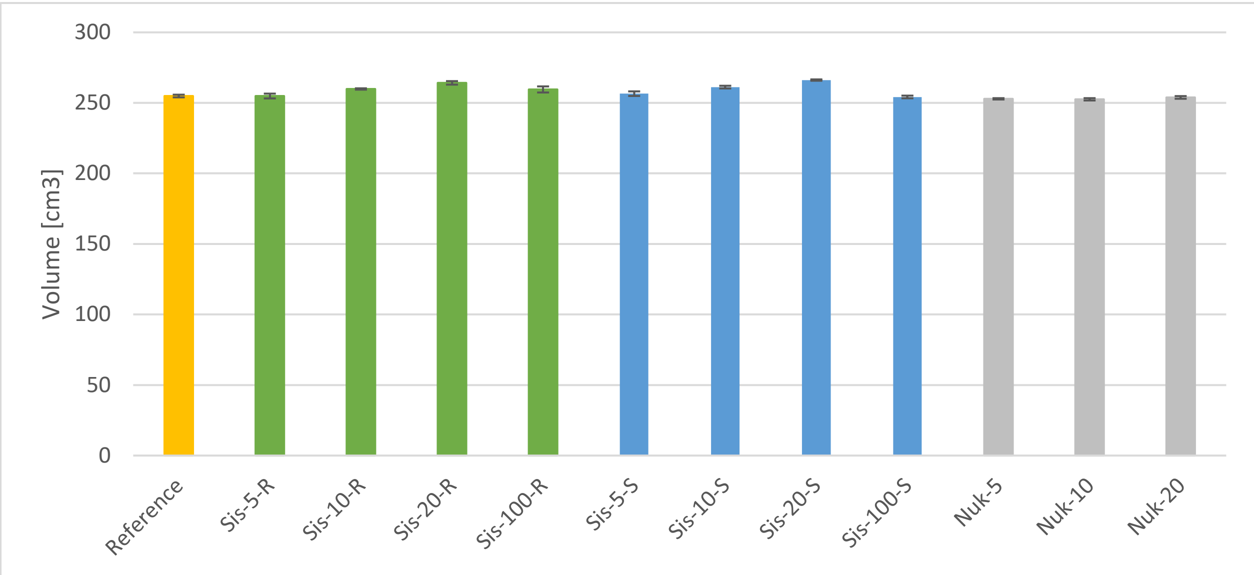

Fig. 4 Volumes of mortar samples cured for 28 days

Another thing observed was that the density of the samples is affected by the ash substitution. This was also observed by others in previous research done on bottom ashes [19, 20], which showed that the density of the concrete decreases with the addition of the bottom ash.
The density of the mortar samples, at 28 days, can be seen in Fig. 7.

The BA samples appear to have similar densities, in relation to the amount of ash they contain (Fig. 5). For the 5% BA mortars, the decrease in density is of up to 4% compared to the reference. The density reduction is more visible for the 100% BA mortars, where the decrease is of almost 11% compared to the reference. This decrease is caused by the more porous structure of the bottom ash compared to sand. Overall, the mortar samples maintain a density similar to that of normal-weight concrete, with values within 2,151 kg/m^3, for the 5% Sisimiut raw BA, and 2041 kg/m^3, for the 20% Sisimiut sorted BA. The values of the 100% BA mortar densities lower than 2000 kg/m^3.

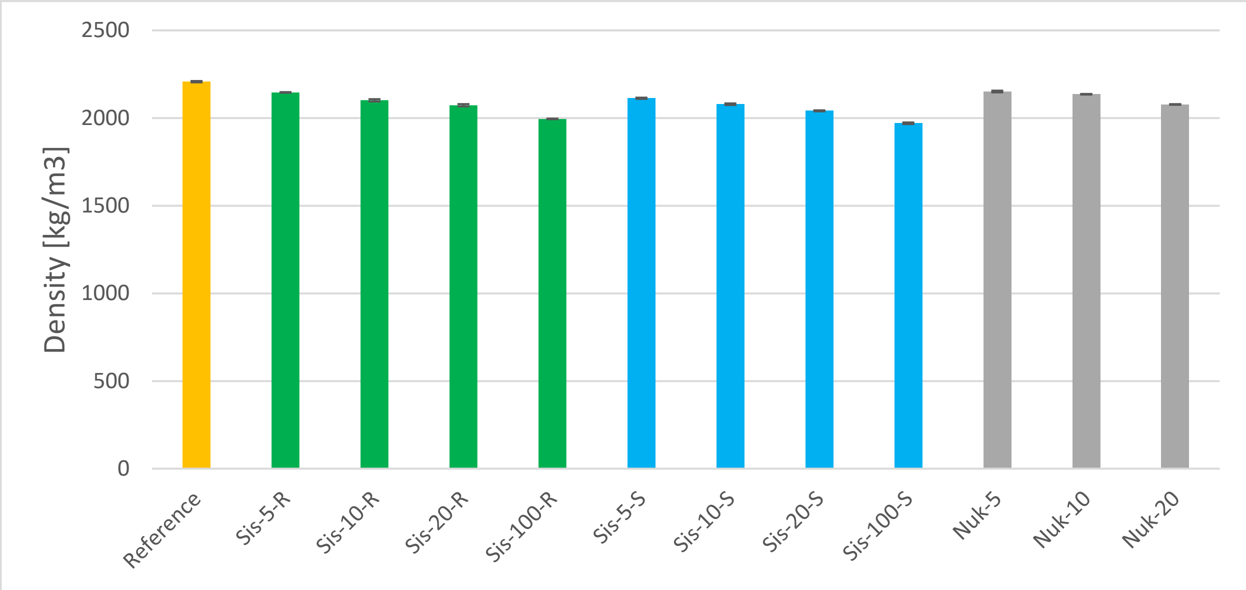

Fig. 5 Densities for mortars cured for 28 days

3.4 Compressive strength

The compressive strength development of the mortar samples can be seen in Fig. 6. The samples containing bottom ash have a lower compressive strength than the reference, which is mostly linked to a more porous structure of the bottom ash than the sand, but possibly also the particle shapes. In addition to this, the strength of the mortars is decreasing, as the percentage of ash is increased. Comparing the samples containing 5 and 10% of the Sisimiut BA, it can be seen that they have

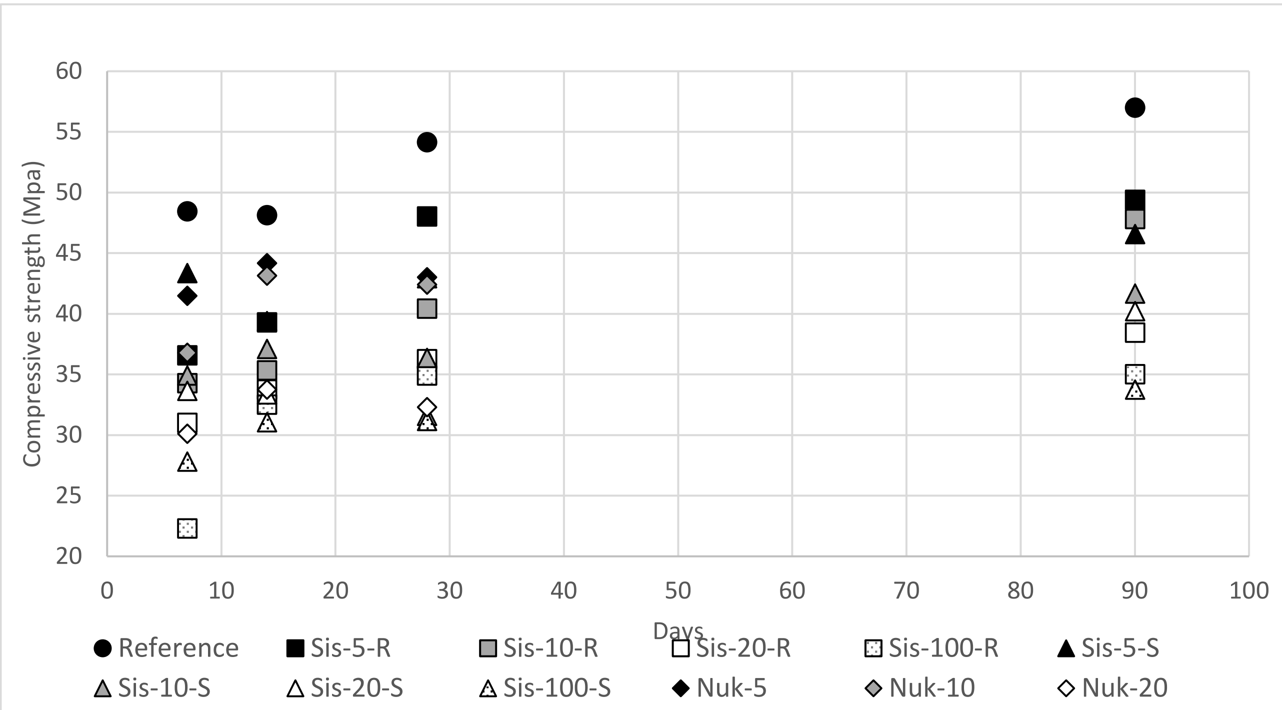

Fig. 6 Compressive strength measurements

similar strength development over the 90 days curing period. The mortar samples have a high early

strength, seen for the 28 days curing period, with only limited increase in strength until 90 days. The sample containing Sisimiut raw BA appear to have a lower early compressive strength than the ones containing Sisimiut sorted BA, for both substitution levels of 5 and 10%. After 90 days, however, the strength of Sisimiut raw BA mortar was higher than the Sisimiut sorted BA mortar.
Mortar samples containing Nuuk BA were only tested at three curing periods, of 7, 14 and 28 days. It can be seen that all three Nuuk mixtures show a similar strength development over time, with a quick early strength development, at 14 days, which slowly decreases until they reach 28 days age. This is opposite to the reference mix, which shows the strength increase from 14 to 28 days of curing.
For the mortar containing the Sisimiut raw ash, the highest strength was given by the samples with 5% BA. The strength of the mortar was 48 MPa, almost 90% that of the reference. Samples with 10% BA showed a strength of 40 MPa, 75% that of the reference. The surprising results came from mortars with 20% and 100% BA, which had an almost identical strength, with the 20% mortar showing a greater deviation. The strength values were of around 35 MPa, which is over 60% that of the reference. This also suggests that a considerable amount of ash could be used in the fabrication of 100% BA mortar, having a strength similar to those of lower percentages.
The mortar samples containing the sorted Sisimiut BA had compressive strengths similar to those of the mortar with the raw Sisimiut BA. However, the strength of the mortars with sorted ash was only 90% of those with the raw BA. The highest value was, as expected, given by the mortar with 5% sorted BA, of 43 MPa, while the 20% and 100% BA samples showed a strength of almost 32 MPa.
The mortar samples containing the Nuuk ashes also had surprising results, considering the high water content of the ash. Mortar mixtures with 5% and 10% Nuuk BA had a similar compressive strength of almost 43 MPa, while the 20% BA mortar had a strength of 32 MPa.

3.5 Leaching

Metal leaching concentrations from the mortars were significantly lower than the leaching concentrations from the bottom ashes themselves. This is due to dilution of the bottom ash into the mortar mix, but also stabilisation of the metals in the mortar matrix. Cd leaching from all samples were below the detection limit of 20 µg/l, while Cr, Cu and Zn leaching from the mortars were in the range of 20 – 65 µg/l. Pb leaching showed highest concentrations of all metals and a relation between increased leached concentrations and increased amount of bottom ash in the mortar samples can be seen for Pb. Pb leaching from the reference mortar, Sis-5-R and Nuk-5 was below the detection limit of 20 µg/l. For the Sisimiut samples, the mortars containing raw bottom ash showed Pb leaching of 20 µg/l, 0.25 mg/l and 1.4 mg/l for the Sis-10-R, Sis-20-R and Sis-100-R samples respectively. For the sorted Sisimiut mortar samples, the highest leached concentation was 0.34 mg/l for Sis-100-S and for Nuuk mortar samples, 25 µg/l for Nuk-20. Pb is mobile at higher pH levels than other heavy metals and the higher Pb leaching is probably linked to the alkaline pH of the mortar.

4. Conclusion

The present study was performed to determine the potential use of Greenlandic MSWI bottom ash as a sand substitute in mortar. For the two tested bottom ashes, levels of heavy metals were high, especially for cadmium, copper, lead and zinc and exceeded the leaching concentrations for reuse for geotechnical purposes.
There appeared to be no significant improvement in consistency or compressive strength of the mortars by size sorting the Sisimiut ash. Taking into account the extra treatment step this would create combine with the strength results given by the mortar, size sorting as pre-treatment for this ash is not necessary.
The mortar density for samples containing bottom ash substitution up to 20% classified the mixtures as normal-weight, while 100% BA mortars fell into the light-weight category. The mortar mix strength showed promising results. At 5% substitution, the strength was 48 MPa for raw Sisimiut BA, 42 MPa for Nuuk BA and sorted Sisimiut BA. Even at higher percentages, of 100% raw Sisimiut BA substitution, the mortar showed a strength of almost 32 MPa. The immobilization of heavy metals in the mortar matrix seems to reduce the leaching considerably, with only Pb showing high values. This, however, could be decrease with prewashing of the ash. Prewashing could also remove substances that causes the volume increase of the mortars, and therefore prewashing of ash should be included in further studies.

Overall, the use of bottom ash as substitute for sand in the making of mortar has proved to be an acceptable solution to the problems posed by waste landfilling. The strength values of the mortar fall within acceptable limits for the use as structural elements in the construction industry, with significantly lower impact on the environment than the current situation.

References

[1] EISTED R., CHRISTENSEN T.H., "Waste management in Greenland: current situation and challenges", Waste Management and Resources, Vol. 29, 2011, pp. 1064–1070.

[2] TORALDO E. and SAPONARO S. "A road pavement full-scale test track containing stabilized bottom ashes", Environmental Technology, Vol. 36, No. 9, 2015, pp. 1114–1122.

[3] JANSEGERS E. (1997), "The use of MSWI bottom ash in hollow construction materials", in Waste Materials in Construction: Putting Theory into Practice. Elsevier B.V., 1997 pp. 431–436.

[4] GINES, O. CHIMENOS J.M., VIZCARRO A., FORMOSA J., ROSELL J.R., "Combined use of MSWI bottom ash and fly ash as aggregate in concrete formulation: Environmental and mechanical considerations", Journal of Hazardous Materials, Vol. 169, No. 1–3, 2009, pp. 643–650.

[5] CIOFFI R. COLANGELO F., MONTAGNARO F., SANTORO L., "Manufacture of artificial aggregate using MSWI bottom ash", Waste Management. Vol. 31, No. 2, 2011, pp. 281–288.

[6] SORLINI S., ABBA A. and COLLVIGNARELLI, C., "Recovery of MSWI and soil washing residues as concrete aggregates", Waste Management, Vol. 31, No. 2, 2011, pp. 289–297.

[7] DEL VALLE-ZERMENO R., FORMOSA J., CHIMENOS J.M., MARTÃNEZ M., FERNÃNDEZ A.I., "Aggregate material formulated with MSWI bottom ash and APC fly ash for use as secondary building material", Waste Management, Vol. 33, No. 3, 2013, pp. 621–627.

[8] FILIPPONI P., POLETTINI A., POMI R, SIRINI P., "Physical and mechanical properties of cement-based products containing incineration bottom ash", Waste Management, Vol 23, 2003, pp. 145–156.

[9] CHEESEMAN C. R., MAKINDE, A. and BETHANIS S., "Properties of lightweight aggregate produced by rapid sintering of incinerator bottom ash"', Resources, Conservation and Recycling, Vol. 43, 2005, pp. 147–162.

[10] PAN J. R., HUANG C., KUO J.S., LIN S.H., "Recycling MSWI bottom and fly ash as raw materials for Portland cement", Waste Management, Vol. 28, 2008, pp. 1113–1118.

[11] ZHANG T. and ZHAO Z., "Optimal Use of MSWI Bottom Ash in Concrete", International Journal of Concrete Structures and Materials, Vol. 8, No. 2, 2014, pp. 173–182.

[12] PERA J., COUTAZ L., AMBROISE J., CHABABBET M., "Use of incinerator bottom ash in concrete", Cement and Concrete Research, Vol. 27, No. 1, 1997, pp. 1–5.

[13] KIRKELUND G. M. , OTTOSEN L.M., JENSEN P.E., GOLTERMANN P., "Greenlandic waste incineration fly and bottom ash as secondary resource in mortar", International Journal of Sustainable Development and Planning, Vol. 11, No. 5, 2016, pp. 719–728.

[14] KIRKELUND G. M., DIAS-FERREIRA and JENSEN P. E. "Characterization of particulate residues from greenlandic mswi for use as secondary resources". In Proceedings of the International Conference Materials, Systems and Structures in Civil Engineering 2016: Workshop on Cold Region Engineering : 2016, pp. 27-36. Nyt Teknisk Forlag.

[15] KIRKELUND G.M., JOERGENSEN A.S., INGEMAN-NIELSEN T., VILLUMSEN A., "Characterisation of MSWI bottom ash for potential use as subbase in Greenlandic road construction". Proceedings of the 4th International Conference on Engineering for Waste and Biomass Valorisation, Porto, Portugal 2012. Eds: Nzihou A.; Castro F.

[16] Miljøstyrelsen, 2015. "Bekendtgørelse om genanvendelse af restprodukter og jord til

bygge-og anlægsarbejder (Restproduktbekendtgørelsen)" BEK nr 1414 af 30/11/2015 (in Danish).
[17] KURDOWSKI W., "Cement and Concrete Chemistry", Dordrecht: Springer Netherlands, 2014.
[18] QUENEE B., LI G., SIWAK J.M., BASUYAU V., "The use of MSWI (Municipal solid waste incineration) bottom ash as aggregates in hydraulic concrete", Waste Management Series, Vol. 1(C), 2000, pp. 422–437.
[19] FERRARIS M., SALVO M., VENTRELLA A., BUZZI L., VEGLIA M., "Use of vitrified MSWI bottom ashes for concrete production", Waste Management, Vol. 29, No. 3, 2009, pp. 1041–1047. .
[20] REITERMAN P., HOLCAPEK O., KRAUSOVÁ A., SYC M., KEPPERT M. "High-Volume Municipal Solid Waste Incineration Bottom Ash Concrete", Key Engineering Materials, Vol. 722, 2016, pp. 181–186.

Tasks and Technical Developments toward the Shallow Undergrounding of Utility Lines in Cold Regions

Keisuke Iwata
Researcher
Scenic Landscape Research Unit,
Civil Engineering Research Institute for Cold Region (CERI)
Japan
iwata-k@ceri.go.jp

Yasuaki Matsuda, Scenic Landscape Research Unit, CERI, Japan
Tetsuo Takahashi, Scenic Landscape Research Unit, CERI, Japan

Summary

In this study, tasks and technical developments of undergrounding in cold region and rural area are considered, and to clarify the mechanism of freezing for stagnant water in underground pipes and the influence of such freezing on optical cables, an outdoor exposure experiment was done using stagnant water and specimens that reproduced curved pipelines. Under the conditions of this experiment, no problems were found with the undergrounding of cables shallower than the frost penetration depth. It is considered that, as long as there is space for water to move away from the frozen portion of the pipe, the shallow burial of pipes carrying cables is possible even if there is the possibility that stagnant water in the pipe will freeze.

Keywords: Undergrounding of Utility Lines, Shallow Undergrounding, Cold Region, Experiment

1. Introduction

1.1 Present situation of utility-pole removal program in Japan

The utility-pole removal program in Japan has been promoted, aiming at the conservation of historic streets and promotion of sightseeing, in addition to the prevention of disasters, preservation of safe and comfortable passing spaces, and formation good landscapes and a living environment (Fig.1).

The program includes the “Undergrounding Transmission Networks Program”, “Plan for Promoting a Program for No Utility Poles” and other programs to remove roadside utility poles.
Since 1980, utility poles have been removed, mainly by laying power lines underground, from arterial roads in urban districts, tourist areas with historic townscapes, and housing areas developed by the private sector.

However, it is pointed out that those undergrounding of utility lines in Japan has lagged far behind the US, Europe and parts of Asia. Comparing with major cities in Europe and Asia, the No Utility Pole ratio is 100% in London, Paris and Hong Kong, but only 7% for Tokyo’s 23 Wards and 5% in Osaka (Fig.2). Moreover, Comparing with total length of low-voltage power line in whole country, Japan has the

Fig.1 Impact of utility poles and cables on the roadside landscape

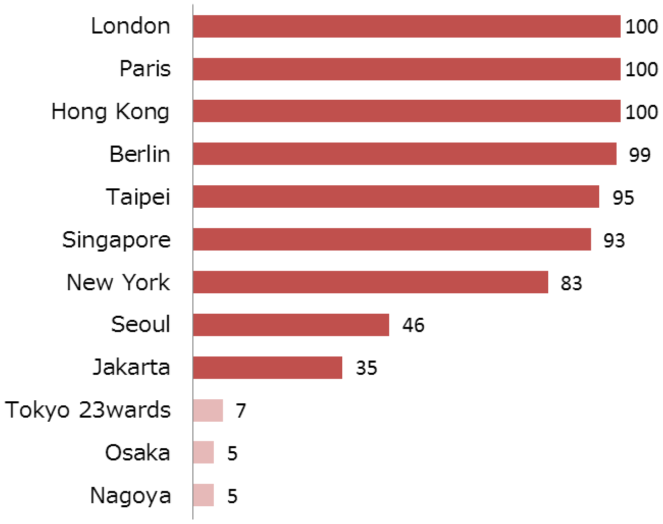

Fig.2 Comparison of Non-pole ratio （%）

※London, Paris, Hong Kong, Berlin, Singapore, New York, Seoul: Cable Distance Base
※Taipei, Jakarta, Japan: Road Distance Base

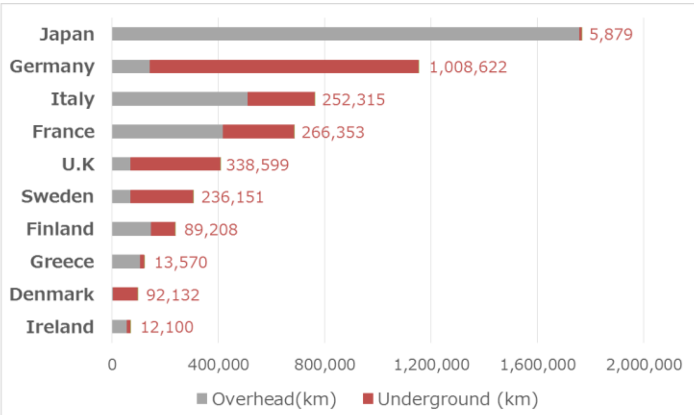

Fig.3 Comparison of Total length of electric power lines (km)

greatest length of these counties, but the least length of underground line. The undergrounding ratio is only 0.3% in Japan.(Fig.3)

The history of this lag, and the reasons for it, were mainly caused by high initial costs and lowly efficient compared with overhead lines.
To promote the undergrounding of utility lines, it is essential to reduce the high installation costs and improve efficiency.

In light of the above, in December 2016, the “Act for Promoting the Undergrounding of Power and Utility Lines” took effect. Because of this law, it has become a legal obligation for power and utility businesses and manufacturers to develop low-cost technologies for undergrounding utility lines.

1.2 Necessity of shallow undergrounding in cold region

Shallow undergrounding is one of the low-cost technique. Reduction in the depth of burial results in a substantial decrease in the need for excavation and back-filling work, and thus costs and work period are curtailed.

Therefore, the Ministry of Land, Infrastructure, Transport and Tourism established the Technical Investigation Committee for Low-Cost Undergrounding in September 2014. The Committee re-

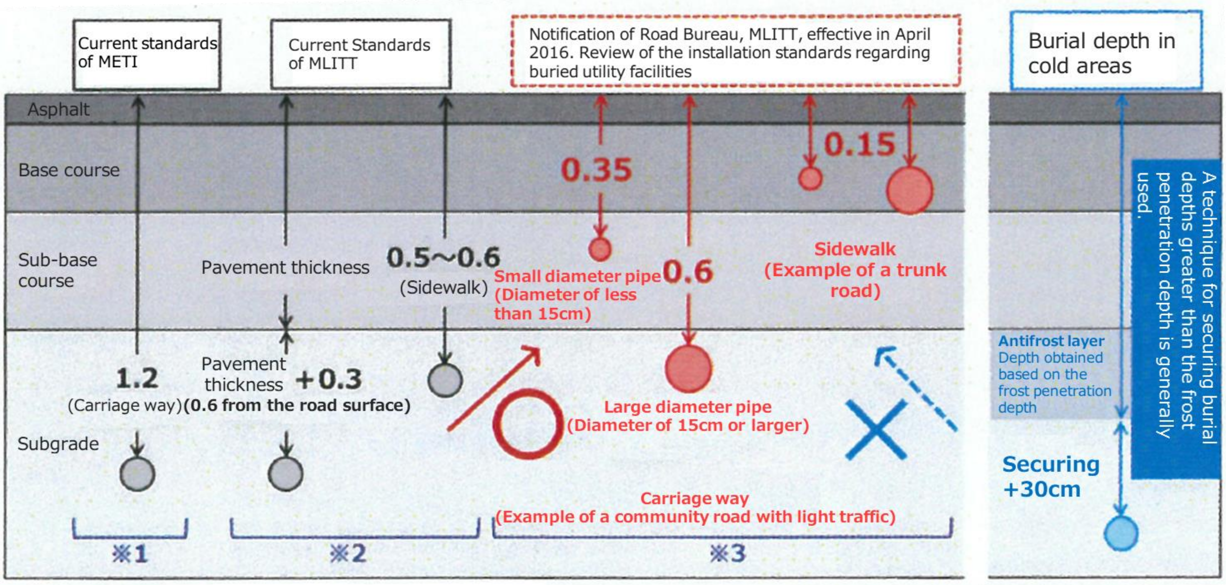

Fig.4 Comparison of standards for the burial depth in Japan

examined the Installation Standard on Burial of Utility Cables. The standard was relaxed so as to allow the laying of utility cables more shallowly underground than before in April 2016 (Fig.4)..

While, in cold regions such as Hokkaido prefecture, Japan, utility pipelines and cables are buried deeper than the frost penetration depth to protect against malfunctions in electric and telecommunication lines and cable pipelines caused by freezing for stagnant water in underground pipes and frost heaving. However, when determining the safe depth for the undergrounding of utility lines and pipes, there is the possibility of overestimation.

2. Preceding studies on undergrounding utility cables

2.1 Technological problems in shallow layer undergrounding

Iwata et al (2016), to clarify technological problems in formulating standards for shallow layer undergrounding, conducted a survey on the existing standards undergrounding utility facilities and a survey on various problems regarding undergrounding utility facilities in cold areas through field survey and interviews with related business operators.

The surveys revealed two major potential problems. One problem is the freezing of stagnant water in pipelines. This problem is crucial particularly for communication cables, which do not generate heat, unlike power cables. The stagnant water in pipelines expands when it freezes and may cause functionality of the communication cables to deteriorate.

The other problem is the irregular heaving settlement of pipelines and cables caused by freeze and thaw of the ground around them.

2.2 Basic laboratory experiment

Iwata et al.(2017), to clarify the influence of the freezing of stagnant water on communication cables in pipelines, conducted a basic laboratory experiment on freeze and thaw of communication cable specimens. The specimens were 1m-long closed pipes that contained optical cables and water. To reproduce the conditions of stagnant water in the pipeline, two patterns of specimens ware prepared. One was fully filed water and the other was half filled with water. In this experiment, communication functionality deterioration or cable disconnection did not occur under either conditions.

The results of this experiment show that pressure from frozen water in a pipeline does not affect the communication functionality of optical cables when the cables are short and straight. But, it is necessary to understand the influence of deformation of the cables from the bends in a long pipeline laid underground in actual cases. The influence of freeze and thaw on the functionality of the cable, when compression and extension occur at the bends, also needed to be clarified.

3. Outline of outdoor exposure experiment

Following the basic laboratory experiment, an outdoor exposure experiment was done using stagnant water and specimens that reproduced curved pipelines. The optical cable was installed in the piping filled with stagnant water, the amount of optical cable was measured.

Table.1 Outline of the experiment

Date	January 23 to 29, 2017
Place	CERI / Civil Engineering Research Institute for Cold Region
Method	Outdoor Exposure Experiment

3.1 Specimens of experiment

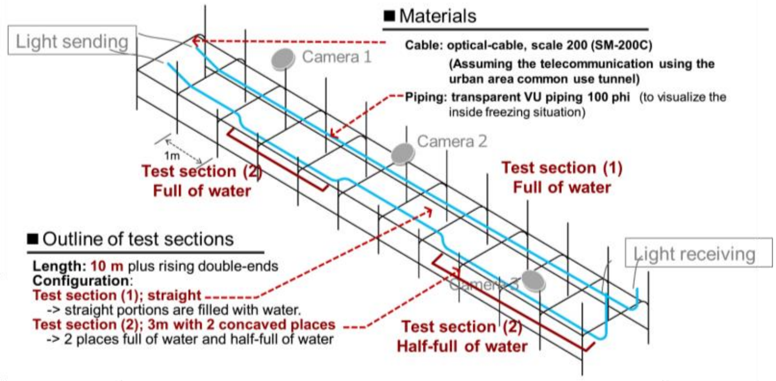

Fig.5 Specimens of the experiment

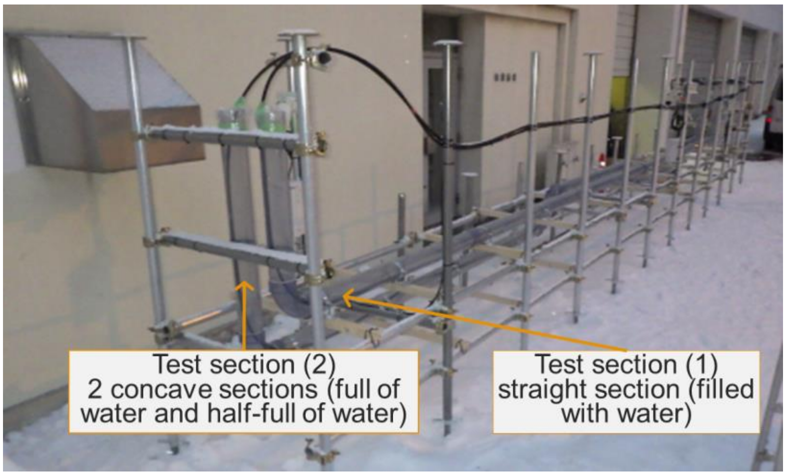

Fig.6 Specimens of the experiment

Specimens of the experiment is shown as Fig.5 and Fig.6. The length of specimens are 10m plus rising double-end. Test section 1 is straight portions which are filled with water. Test section 2 is 3m with 2 concaved places which are filled with water and half-filled with water.

Optical cable of 200 scale is used in specimens assuming the telecommunication using the urban area common use tunnel. And transparent VU piping 100phi was used to visualize the inside freezing situation.

3.2Measurement of communication attenuation

Communication functionality was continuously measured for 24 hours every day during experiment. The cross section of optical cable and Measurement points are shown in Fig.00. Communication attenuation P is shown in the following

P=P1-P2

Where P: Communication attenuation, P1: Sending optical reading, P2: Receiving optical reading

Fig.7 Pattern diagram of communication attenuation measurement

Pattern diagram of communication attenuation measurement is shown as Fig.7. Sending optical reading P1 is average reading measured beforehand using test cable. Receiving optical reading P2 is measured at the edge of cables.

3.3 Verification method of communication functionality

Standard circuit loss Ps（1.32 dB）, Calculated according to the Japanese Industrial Standards and CC-Link association, was used. When the loss P is less than the allowable circuit loss Ps, it was judged that the communications performance is not affected.

4. Results and considerations

The result of measurement is shown as Fig.8. The water before freezing moved to the open space, and neither damage to the optical cable nor communication attenuation was confirmed. No effect of the freeze expansion of the stagnant water in the piping on the cable was observed under the compression situation of the indoor freeze experiment. According to the freezing mechanism observed by the outdoor experiment, ice was generated along the piping wall, and the center portion of the piping was considered difficult to freeze.

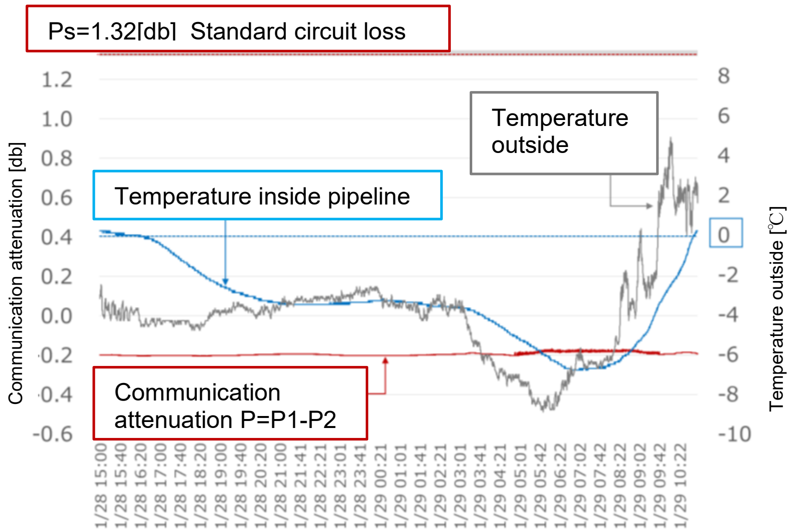

Fig.8 Result of Experiment (Test section 1)

Based on the above experiment results, it is feasible to employ shallow layer undergrounding in cold regions, because it is thought that considerable compression and extension do not affect the optical cables under the condition where there are open spaces for the water to move in the pipeline even when part of the water freezes.

This experiment could not confirm the effect of water freezing in cases of long burial distance, long freezing period, and damage or aging degradation of the cable.
From now on, the investigation of the freezing situation in construction fields will be performed to verify conditions in which the shallow underground burial in the cold district succeeds.

References

[1] IWATA K., KABASAWA H., and 2 others(2016), "Development of Technologies for Shallow Layer Undergrounding of Utility Cables in Cold Regions", Monthly Report of the Civil Engineering Research Institute for Cold Region, Vol.758, pp.44-49.

[2] IWATA K., KABASAWA H., and 2 others(2017), "An Experiment and Discussion on Stagnant Water in the Optical Pipeline –Assuming the Shallow Layer Installation in Cold Regions-", Monthly Report of the Civil Engineering Research Institute for Cold Region, Vol.767, pp.38-42.

New Finnish Guideline on Frost Protection

Seppo Saarelainen Dr
Aalto University, Roussa Ltd, Finland
(ssaarel5@gmail.com)

Henry Gustavsson MSc., University Teacher
Aalto University, Finland
(henry.gustavsson@aalto.fi)

ABSTRACT: Specific guidelines for various structured on ground, open to outdoor temperatures, have been compiled in Finland since late 70'ies. They have been updated since publication several times. They differed slightly as well on the climate parameters as on the soils description. In 2011, effort was started to harmonise the common soil description and climatic conditions and to edit different codes of practice into one reference publication suitable to the basis of national building and infrastructure standards.

KEYWORDS: frost protection, frost heave, building foundations, infrastructure, code of practice, Finland.

1 Introduction

The guideline consists of the description of design climate parameters in Finland, theoretical and practical approach to frost penetration and frost heaving in the ground, design properties of frost insulation materials, and design recommendations for various structures on or in the ground. The frost considerations for winter construction are treated, as well.

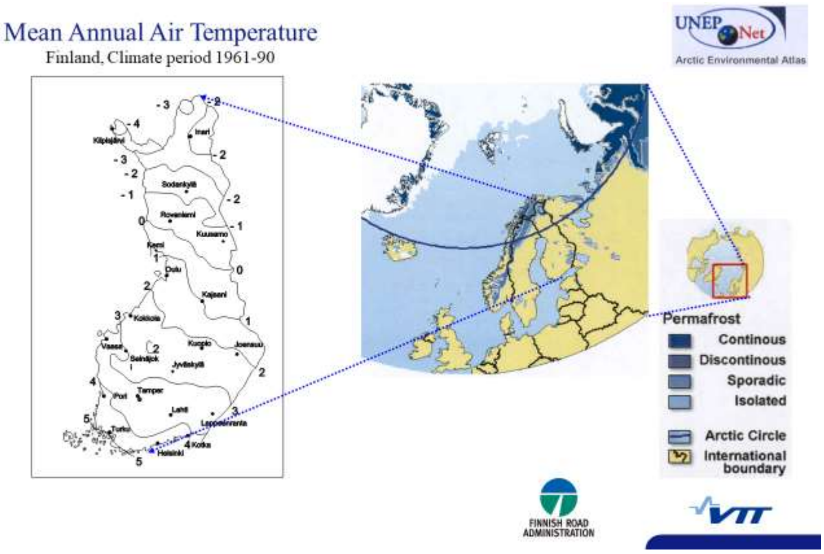

Fig 1. Mean annual air temperature in Finland (Saarelainen S. (ed.). 2013).

2 Common background

2.1 Climatic description

The general part the publication contains climatic data on the variation of freezing and thawing indice and annual mean air temperatures, based on observed daily air temperatures at 30 sites in Finland during 30 years. The are presented in the maps (Fig1)

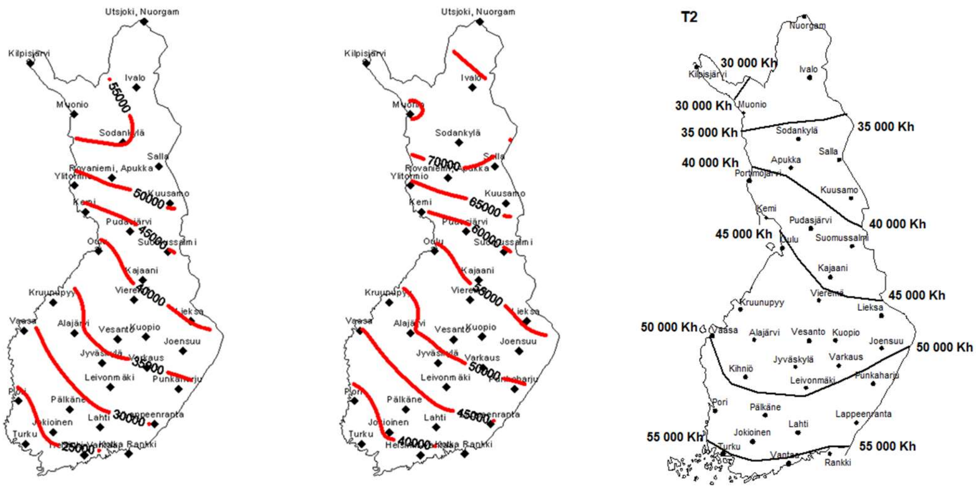

Fig 1. Maximum freezing index, Kh, occurring in 10 years (left) and in 100 years (middle). Mean thawing index, Kh (right) (Saarelainen S. (ed.). 2013).

2.2 Freezing and frost heaving of ground

Thermal and freezing properties of soils are estimated using the modified Kersten method (Berg et al., 1980).

Numerical modelling was applying tested computer methods to estimate frost penetration in multilayer systems and frost heaving.

Frost susceptibility as a classifying characteristic is estimated considering the soil type and grain size distribution. Frost heaving is estimated using frost heave coefficient SP or swelling degree. SP can be determined using frost heave tests on natural specimens (Fig 2), estimated using clay content (Fig 3), or back-calculated from site observations (Fig 4). In the pavement code of practice, swelling-degree values are presented for various subgrade soil types.

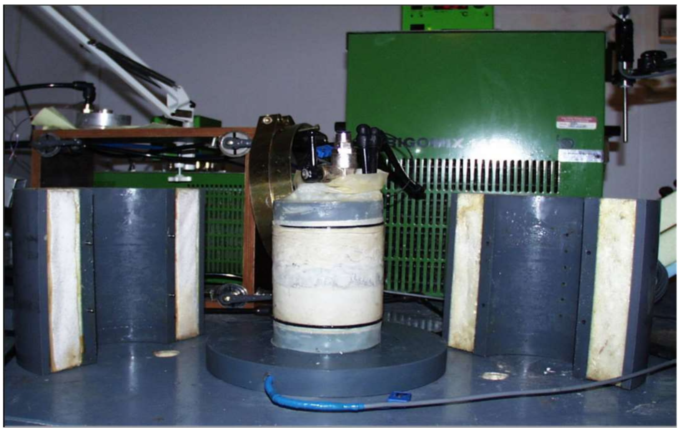

Fig 2. Determining the frost-heave coefficient with a laboratory frost heave test.

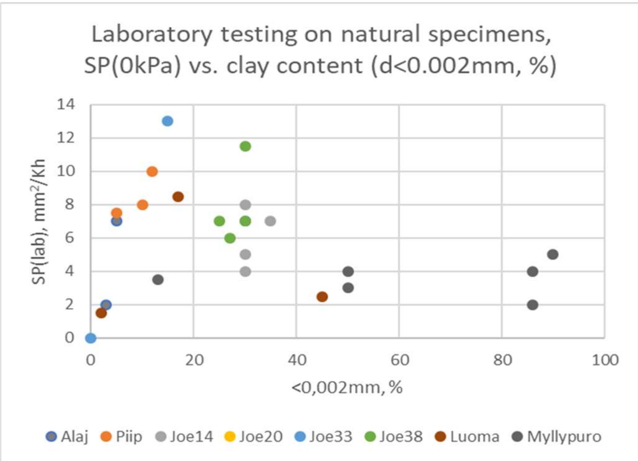

Fig 3. SP from frost heave tests on natural specimens, vs. clay content (Saarelainen

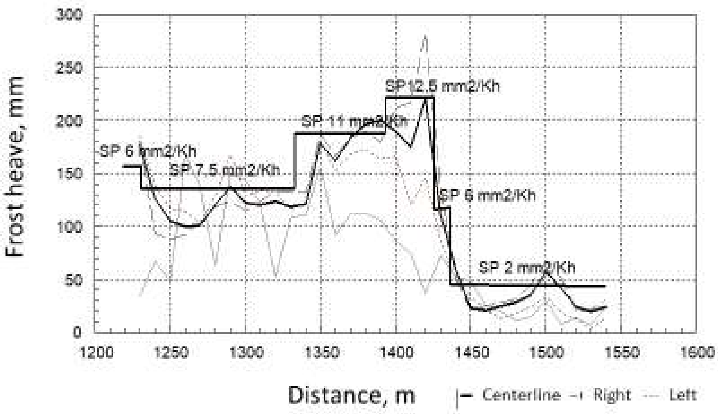

1992, Saarelainen et al. 2015, Sinnathamby, G et al. 2017).

Fig 4. Estimating frost heave coefficients from site observations in Rovaniemi, Northern Finland, on Pappilantie, in the spring of 1997.

2.3 Frost insulation materials

Application of thermal insulation in frost protection may be in same cases rational, Especially in the pavement repair or lack of non-frost susceptible aggregates. The effective thickness of the insulation depends on local moisture conditions, eg. drainage.

recommended design values fo most common insulation materials are presented. They are illustrated in Table 1.

The nomination "XPS 200" means an extruded polystyrene board, which will compress less than 200 kPa at a compression of 10%.

Table 1. Recommended design thermal conductivity for some most common insulation materials.

Product	$\lambda_{dec,}$ W/Km Normal drainage condition	$\lambda_{dec,}$ W/Km Severe drainage condition
Extruded polystyrene		
XPS 200	0.041	0.045
XPS 300	0.041	0.045
XPS 400	0.045	0.06
XPS 500	0.045	0.06
Expanded polystyrene		
EPS 120	0.05	0.06
EPS 200	0.041*)	0.05*)
EPS 300	0.041*)	0.05*)
EPS 400	0.041*)	0.05*)
Lightweight expanded clay (LECA)		
KS 420	0.16	0.20

*) Type approval concerns EPS-products Isora Super 200, 300 and 400. For other EPS-products, design values of product category "EPS 120" are applied.

2.4 Frost protection of structures

The individual codes of practice define the design winter (risk of damage), design principles, proper materials and structures, examples of frost design and drainage needs. Here, only titles are listed to describe contents of each item.

Frost protection of buildings (warm, semiwarm, unheated**)**

Design climate. Design principles. Materials and structures. Frost design. Drainage. Specific demands and general descriptions for installations

Frost protection of cold structures (retaining walls etc.)

Design climate. Design principles. Materials and structures. Frost design. Drainage. Specific demands and general descriptions for installation

Frost protection of trafficed yards

Transition structures. Principles (incorrect, recommended).

Frost protection and thermal insulation of subsurface pipelines

Design climate. Design principles. Materials and structures. Frost design. Drainage. Specific demands and general descriptions for installations.

Frost protection of streets

Design climate. Design principles. Materials and structures. Frost design. Drainage. Specific demands and general descriptions for installation.

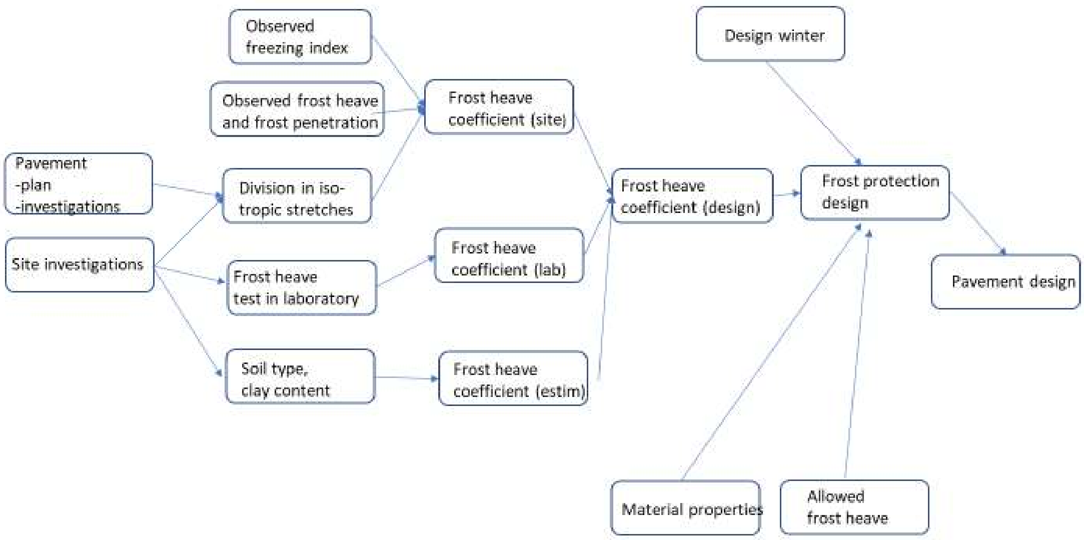

Fig 5. Frost heave design of roads and streets

Frost protection of roads

Design climate. Design principles. Materials and structures. Frost design. Specific demands and general descriptions for installations/culverts.

Frost protection of railways

Design climate. Design principles. Materials and structures. Frost design. Specific demands and general descriptions for installations.

Thermal insulation of traffic tunnels

Design climate. Design principles. Materials and structures. Frost design. Specific demands and general descriptions for installations

Frost protection of bridges

Design climate. Design principles. Materials and structures. Frost design Specific demands and general descriptions for installations.

Frost protection of specific structures (winter sport facilities, cold storages, heated structures, harbours etc.)

Design climate. Design principles. Materials and structures. Frost design. Specific demands. References.

Temporary frost protection during construction

Design climate. Design principles. Materials and structures. Frost design. Thaw control. Specific demands and general descriptions for installations.

3 CONCLUSIONS

The earlier, separately compiled and in various civil engineering disciplines guidelines were harmonised and edited in a common form. It presents a good basis for engineering applications and a useful textbook for education.

4 ACKNOWLEDGEMENTS

Authors will present their gratitude to authors original guideline papers, and to The Finnish Association of Civil Engineers.

5 REFERENCES

Berg RI., Guymon GL. & Johnson TC. 1980. Mathematical model to correllate frost heave of pavements with laboratory predictions. Hanover NH., US Army CRREL, Report 80-10. 54p.

Sinnathamby, G, Gustavsson, H, Korkiala-Tanttu, L, Cervera, CP & Koskinen, M 2017, Case study: frost heave and thaw settlement under an ice rink. *Environmental Geotechnics* , vol. 4, no. 2, pp. 103-112. https://doi.org/10.1680/jenge.15.00047

Saarelainen, Seppo; Gustavsson, Henry; Korkiala-Tanttu, Leena; Tieaho, Ilkka. Applying site and laboratory studies to determine frost-heave coefficient. XVI European Conference on Soil Mechanics and Geotechnical Engineering (ECSMGE). Edinburgh, 13.-17.September 2015. ed. / D M Smith; P J L Eldred; D G Toll. London : ICE Publishing, 2015. p. 22-36.

Saarelainen S. 1992. Modelling frost heaving and frost penetration at some observation sites in Finland. The SSR model. Espoo, Technical Research Centre of Finland, Publication 95. 119p.
Saarelainen S. (ed.). 2013. Routasuojaus – rakennukset ja infrarakenteet (Frost protection – buildings and infrastructure, in Finnish. Helsinki, Finnish Assocoation of Civil Engineers, Publication RIL 261-2013. 257p.

CONSTRUCTION TECHNOLOGIES

Ultimate theoretical span lengths for snow and ice arches and vaults

Esko Järvenpää
Senior Bridge Specialist
University of Oulu, WSP Finland
Finland
esko.jarvenpaa@wsp.com, Esko.Jarvenpaa@oulu.fi

Antti H. Niemi
Senior Research Fellow
Structures and Construction Technology Research Unit, University of Oulu
Finland

Summary

The article discusses the theoretical basis for the design of arch and vault structures. In the design of arches and vaults, it is essential to realize that the optimal shape of the arch is determined by the loading. This article clarifies the use of parabolic shapes in snow structures. If parabolic shape is used, it is required that, the vertical load is constant along the arch. This means that the snow thickness in the arch changes so that the thickness is smallest at the base.

Catenary, the shape of a hanging chain, is another well-known shape. We show analytical and numerical calculations yielding the optimal parameters for the catenary arch. It is demonstrated that the compression stress in a catenary arch is minimized when the span-to-height ratio of the catenary arch is 2,96.

Snow vaults should be compressed structures. This means that the arch thrust line should lie within the middle third of the arch cross section. The compression line is a familiar concept historically as a stone and concrete vault design principle. In snow and ice structures, the compression line should be designed to travel along the axis of the arch, resulting in a uniformly distributed compression stress in the cross section. The general design principle is to retrieve the moment-less shape of the structure, that is, to design the shape so that the thrust line is centric.

The extreme theoretical spans can be achieved when the moment-less arch is designed such that its compressive stress is uniform across the arch. The article illustrates the dimensions of a constant stress arch, a catenary arch, and a parabolic arch when the design is based on the same compressive stress level. The theoretic ultimate span and the shape of the constant stress snow arch is found when the span-to-height ratio is close to unity.

Guidelines for designing snow arches and vaults have been published. It should be noted that theoretically the correct form is the shape of the centreline of gravity of the arch. Because the snow structures have rather thick cross-sections, the shape of the inner surface of the vault may be different from the optimal shape of the centreline. The article presents calculations that illustrate this.

Keywords: snow and ice construction, constant stress arch, ultimate span, form-finding

1. Introduction

Snow and ice are common building materials in cold regions and they are employed especially in important tourist attractions. The biggest event in the world is probably the annual snow sculpture festival in Harbin, China. In Finland, e.g. the snow castle constructed annually in Kemi (Fig. 1) and the snow hotels in Lapland provide memorable experiences for travellers. Igloos are a traditional form of snow structures. In this context, it is worth mentioning the article “The Igloo and The Natural Bridge as Ultimate Structures” [4].

Fig. 1 Inside the snow castle in Kemi (2019).

Design guide for snow structures published by the Finnish association of civil engineers (RIL) is an exceptional publication for snow construction [1]. The code is also available in English [2]. According to these instructions, design of snow and ice structures should be based on theoretical structural calculations. Practical instructions are provided in case detailed design calculations cannot be made. Based on field tests, the Lapland University of Applied Sciences has published practical guidelines for the authorities responsible for snow structures [3].

Snow structures are typically made of artificial snow. Its material properties can be described in terms of design quantities such as density of snow, compression strength, tensile strength, creep, viscosity, modulus of elasticity, etc. The properties of ice have been studied more extensively in context of structural engineering when structures are constructed in water and must resist ice loads. In ice structures one can rely more precisely on the results of calculations than on snow structures. The properties of the test pieces made in the research work of the practical structures of snow structures play a significant role. The dimensions of the test structures should precisely follow the calculated shape [5].

Self-weight is the primary load for snow and ice arches and vaults. The resulting compression force is a key quantity of interest. Even a relatively small eccentricity of the compression force may cause a large bending moment and the snow arch will deflect significantly and finally collapse. Correcting the deflection by adding snow just worsens the situation.

2. Arch shapes

2.1 History

Bridge builders of the Roman Empire knew how to build stone arches. Ottoman time-lapse also includes numerous historical arch bridges. Graphical design techniques were used for remarkably demanding structures and in the past graphical statics was a separate course in technical universities. Fig. 2 is from the book of engineering mechanics used in the Helsinki University of Technology [6].

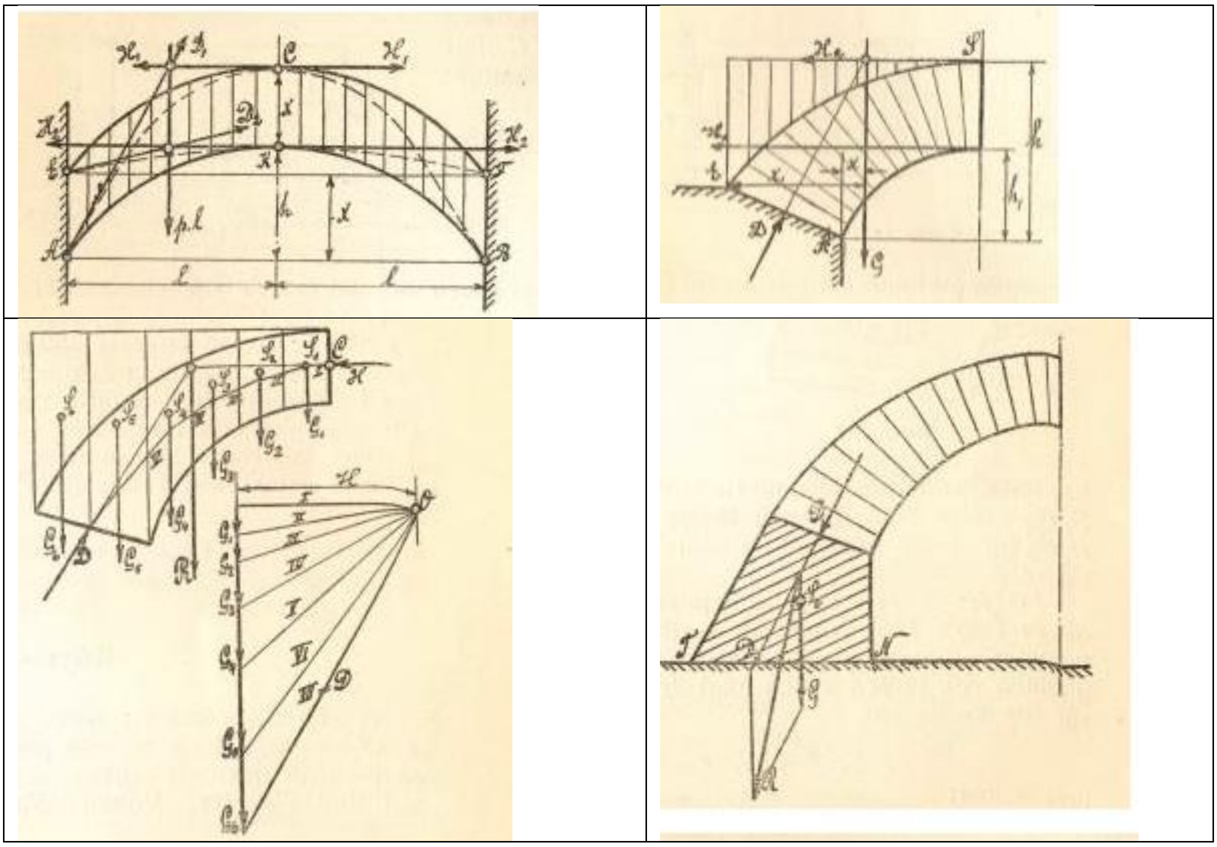

Fig. 2 Stone arch graphics. Teknillinen mekaniikka (1924) by Hugo Ahlberg.

2.2 Parabolic arches

In order to obtain a moment-less structure for the parabola, the vertical load carried by the structure must be constant. For snow and ice arches, this means that the thickness of the arch decreases as it approaches the arch springing line (*Fig.3*). The figure demonstrates a realistic snow parabola with a 24 m span and a rise relation of *l/h* = 2,0. At the top of the arch, the thickness of the snow is 2,0 m and 0,894 m at the base in this case. The unit weight of the snow is 5 kN/m^3 and the stress at the base is 0,15 MPa. The structure is not a very effective snow structure as our following results will reveal.

The equation of the parabola with the span *l* and the height *h* is

$$y = \frac{4h}{l^2}x^2. \tag{1}$$

If the thickness of the snow at the crown is *t,* then the thickness along the arch is

$$t = \frac{1}{\sqrt{1+k^2}} \tag{2}$$

where

$$k = \frac{dy}{dx} = \frac{8h}{l^2}x. \tag{3}$$

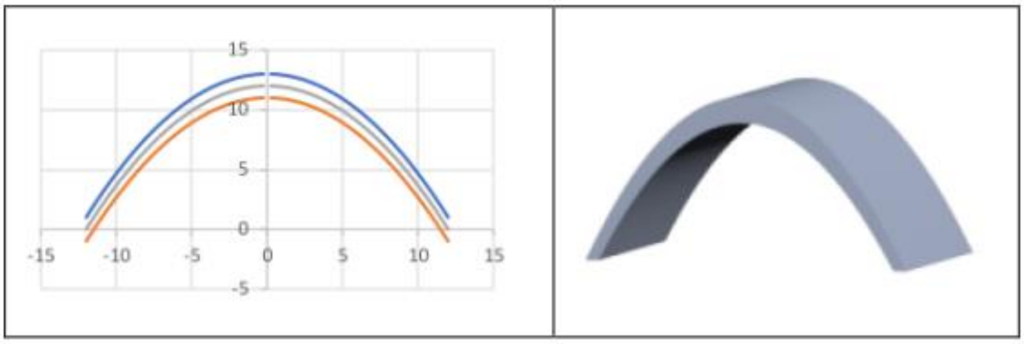

Fig. 3 Realistic parabolic vault with span of 24 m and rise relation l/h = 2. The snow thinkness at the crown is 2,0 m. Compression max 0,15 Mpa.

The ultimate span for a parabolic arch can be calculated by finding the rise which minimizes the axial force at the arch base.

Setting the arch span and the vertical load to unity, the horizontal force becomes

$$H_x = \frac{1}{8h} \tag{4}$$

The axial force *R* at the arch base is then

$$\mathrm{R} = \mathrm{H_x}\sqrt{1 + \mathrm{k}^2} \tag{5}$$

and the cross-sectional area *A* of the arch is

$$A = \frac{1}{\sqrt{1+k^2}} \tag{6}$$

The compression stress σ at base is

$$\sigma = \frac{R}{A} = H_x(1 + k^2) \tag{7}$$

Taking *k* as defined by Eq. (3) at $x = \frac{1}{2}$ and *l = 1,* the stress becomes

$$\sigma = \frac{1}{8h} + 2h. \tag{8}$$

which has a minimum at *h= 1/4.*

In other words, the minimum stress is found when *l/h = 4,0* so that the maximum span for which the stress does not exceed 0,15 MPa is 30,0 m.

2.3 Catenary arches

The equation of the catenary arch is the same as inverted hanging chain:

$$y = -a\cosh(\frac{x}{a}) \tag{9}$$

where the parameter *a* = *H/w* is defined in terms of the horizontal force at the arch springing line *H* and the constant weight of the cross-section *w* along the arch. The moment-less arch for general loads have also been analyzed recently in [7].

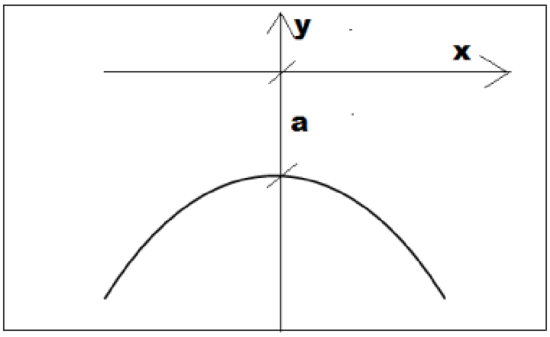

Fig. 4 Catenary arch.

2.3.1 Minimum axial force and maximum span length for the catenary arch

For simplicity, we choose the weight as unity so that *w* = 1 and *H* = *a*. The axial force *R* of the arch, as a function of *a,* is then

$$R = a\sqrt{1 + (\frac{dy}{dx})^2} \tag{10}$$

For the arch having a unit span length 1, the maximum axial force at the spring line *x* = *l/2* is

$$R = \mathrm{a}\sqrt{1 + (\sinh(\frac{1}{2a}))^2} \tag{11}$$

The axial force *R* is minimized at a^* = 0,416778. The height of the arch, having unit span length, is then

$$h = a^* \cosh(\frac{1}{2a^*}) - a^* = 0{,}337662. \tag{12}$$

which gives the rise relation *l/h*=2,962 for the minimum axial force. The minimum material amount of the caternay, for chosen stress level of the arch is found by using the same rise relation.

The value gives the length of the catenary needed between the two bearing points which results the minimum axial force.This information can be used in practice.
The half-length of the catenary is

$$\frac{l}{2} = \int_0^{1/2}\sqrt{1 + (\sinh(\frac{x}{a^*}))^2}\mathrm{d}x = 0.628868 \tag{13}$$

so that the total arch length is *l* = 1.257736.

The thickness of the snow is here constant along the arch. This information makes it possible to find the ultimate span length for constant thickness snow and ice arches and vaults.

We can calculate the maximum span of snow catenary assuming the unit weight of the snow of 5 kN/m^3 and allowing the compression stress level of 0,15 MPa.

Application of equation (11) with the above data yields

$$0{,}15 = 0{,}005 * l * a^* \sqrt{1 + (\sinh(\frac{1}{2a^*}))^2} \quad (14)$$

which can be solved for l = 39,76 m.

Fig. 5 shows a catenary arch with rise relation l/h = 2,0 and span length 38 m. The thickness of the arch is 2,0 m and the unit weight of the snow is 5 kN/m^3. The compression stress at the base is 0,15 MPa. The structure is in practice an effective snow structure.

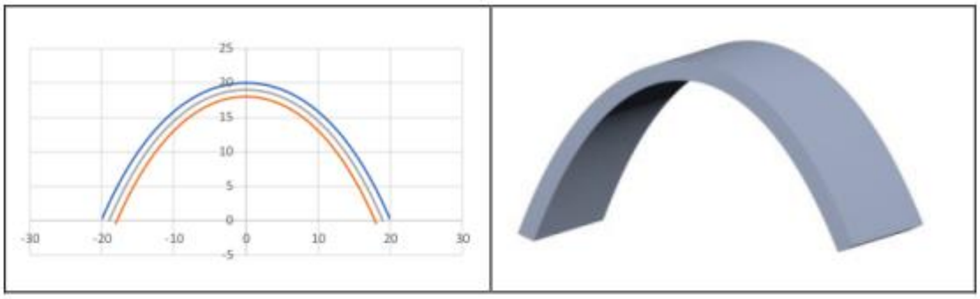

Fig. 5 Catenary vault, span 38 m, l/h = 2,0, snow thickness 2,0 m, compression max 0,15 MPa

3 Constant stress arch and form-finding

There exists few analytical studies of constant-stress arches, see e.g. [8,9] and the references therein. For practical engineering purposes, the shape of the constant-stress arch and the axial forces can be found by iterative vector algebra calculation. In the iteration of the constant stress arch, one shall take into account the change of cross-section area, which follows the size of the axial force in the arch. In addition, to obtain good accuracy, one needs to change the location of the self-weight points for each bar member. The difference to catenary iteration is that the weight point is not in the midpoint of the element like in the catenary bar member.

It has been shown in [8] that the ultimate span length limit for constant stress arch is

$$\boldsymbol{l_{max}} = \frac{\boldsymbol{\pi}}{\boldsymbol{k}} \quad (15)$$

where $\boldsymbol{k} = \frac{\rho g}{\sigma}$. (16)

For snow arch, using the values $\boldsymbol{\rho g}$ = 5 kN/m^3, and $\boldsymbol{\sigma}$ = 0,15 MPa, the theoretic maximum span length is 94,25 m. The rise relation of the arch is then very close to unity. *Fig. 6* shows the snow arch shape using the maximum span length when the thickness of the arch at the crown is 4,0 m.

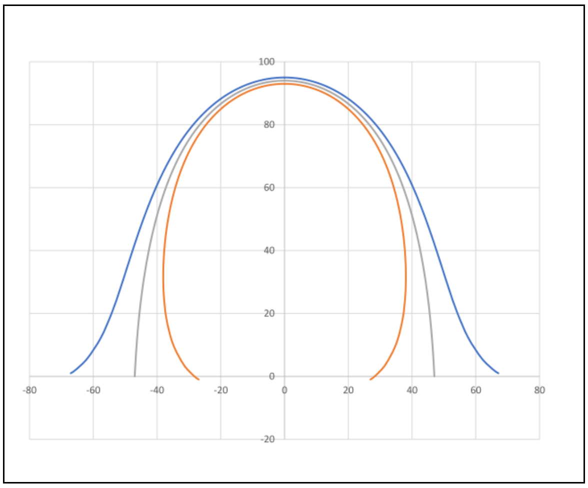

Fig. 6 Constant stress snow arch shape, span 94 m, stress 0,15 MPa and l/h = 1.

In addition, we solve the constant stress arch with the same unit weight and maximum stress of 0,15 Mpa but take the rise ratio *l/h* = 2 and the thickness of the snow is at the crown 2,0 m and at base 7,2 m. *Fig. 7* shows the geometry of the center line of the arch and the outer and inner surfaces. The span length is 77,60 m.

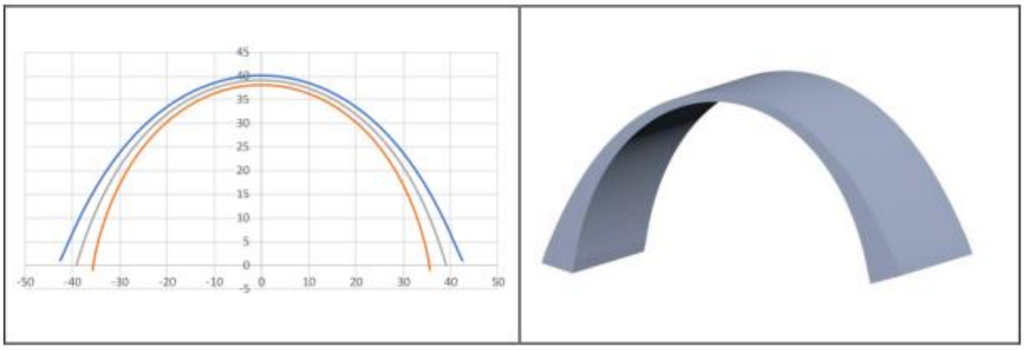

Fig. 7 Constant stress snow arch, span 77,5 m, compression 0,15 MPa, l/h = 2.

4 Discussion

4.1 Guidelines for arches and vaults

It should be noted that the above calculations consider only axial strains while bending and shear strains are neglected. In this case, the compression stress on the surface of the snow and on its central axis prevails throughout the cross section. However, the calculations reveal the correct snow thickness in order to obtain constant stress moment-less structure.

It is important to note that the shape of the catenary should follow the central axis of the arch. The shape of the inner surface of the arch is no longer the shape of the catenary. The picture below illustrates the shapes of the central axis of the catenary and constant stress arch (*Fig. 8*). The picture shows the top surfaces and the lower surfaces when the inside height of the both vaults is 5 m. The distance of the inner surface of the arch at the bottom level is 10 m.

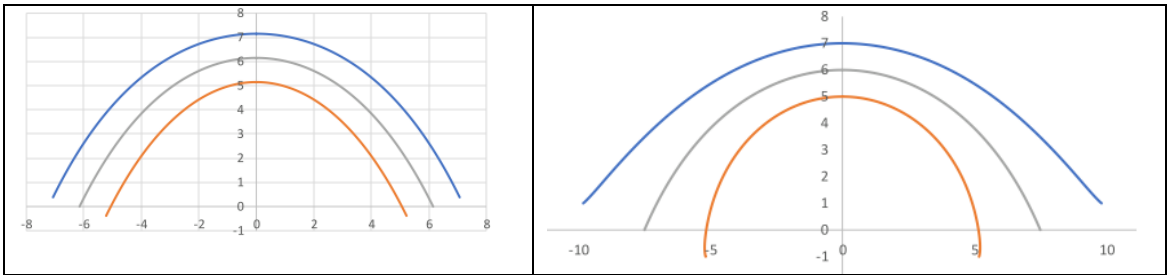

Fig. 8 The shape catenary and constant stress arch, inner span 10, free height 5,0m

4.2 Comparison of structural dimensions

The 3D illustrations made from the examples listed above clarify the differences between different types of arches. The calculated three different types of vaults are shown in the same scale in *Fig. 9*. The thickness of the snow at the crown in each arch is 2,0 m and the maximum stress at base is 0,15 MPa. The unit weight of snow is 5 kN/m^3. The differences are quite large.

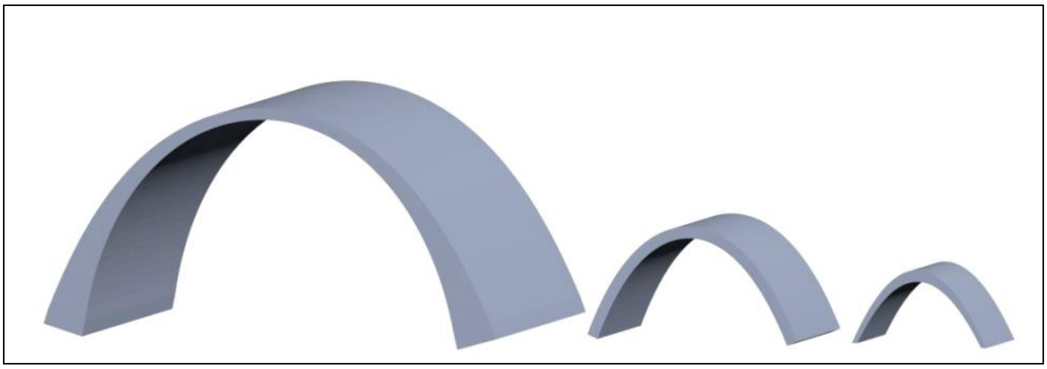

Fig. 9 Three arches l/h = 2, compression stress 0,15 MPa, snow thickness at crown 2,0 m, arches are in the same scale.

5 Concluding remarks

If the proposed theoretical forms can be realized in practice, structural problems should be minimized. The best structures can be probably obtained by using artificial compacted snow, where the mould structures and snow thicknesses are designed based on calculations and the snow deformations are taken into account by exploiting the knowledge from experimental research. When doing testing, it is important that the research test models use theoretically correct shapes of catenary and constant stress arch based of centre line geometry. The theoretically optimal span lengths for snow and ice arches and vaults seems to be much larger than generally known.

.

References

[1] RIL 218-2001. Lumirakenteiden suunnitelu- ja rakentamisohjeet. ISBN:951-758-419-9.

[2] RIL 218-2002., “Snow constructions- General rules for design and construction”. ISBN 951-75

[3] RYYNÄNEN K., “Safe Snow and Ice Construction to Arctic Conditions”, Lapland University of Applied Sciences, Rovaniemi, Finland., *The Interconnected Artic – UArctic Congress 2016.* DOI 10.1007/978-3-319-57532-2-28.

[4] HANDY R.L., “The Igloo and the Natural Bridge as Ultimate Structures”, *Engineering Research Institute and Civil Engineering Dept. Iowa.,* Arctic 1973.

[5] LINTZEN N., EDESKÄR T., “Study on basic material properties of artificial snow”, Luleå University of Technology, Sweden, 2012.

[6] AHLBERG H., “Teknillinen mekaniikka”, *Werner Söderström Osakeyhtiö*, Helsinki 1924,pp. 90-91.

[7] LEWIS W., “Mathematical model of a moment-less arch”. *Royal Society Publishing Proceedings A 472:20160019,* School of Engineering, University of Warwikc

[8] MARANO C., TRENTADUDE P., PETRONE F.,“Optimal arch shape solution under static vertical loads”, “*Acta Mechanica “,* DOI:10.1007/s00707-013-0985-0, 2014.

[9] FAIRCLOUGH H., GILBERT M., PICHUGIN A., TYAS A., FIRTH I., “Theoretically optimal forms of very long-span bridges under gravity loading”. *Proceedings of the Royal Society A.*

Lessons from a fibre composite building in Antarctica

Mark Pekin
Project Engineer – Antarctic Infrastructure
Australian Antarctic Division
Tasmania, Australia
mark.pekin@aad.gov.au

Summary

The Australian Antarctic program constructed a medium sized fibre composite building at its Davis station in Antarctica over the period 2006 - 2011. This building adopted a structural steel frame that was clad with bespoke fibre-composite insulating panels. The adoption of fibre composite cladding was undertaken to improve thermal performance of the building, whilst also reducing the Antarctic effort in terms of resources and personnel, hence cost.

The building uses the inherent strength within large fibre composite panels to minimise the steel framing requirements. It also uses the fibre-glass skin of the panel to be the internal wall cladding, hence reducing the need for additional lining. This lowered the Antarctic construction costs by reducing the overall work and ensuring a smaller installation team.

The building has now been in operation for seven years and the fibre-composite panels have suffered to some extent from both the elements and human usage: some damage has occurred at the highly stressed areas of the panels due to the range of temperature and their extremes; ultra-violet light has also impacted on panels that are subjected to significant sunlight; and physical damage is evident where people, materials and vehicles access the building.

Despite these problems, the fibre-composite panels have proven to be strong, durable and thermally efficient and the building has more than achieved the design intent.

Keywords: Antarctica, Australian, building, fibre-composite, structural

1. Introduction

Australia's Davis research station is located in east Antarctica, approximately 4100km south south west of Perth, Western Australia. Davis is positioned on the coastal edge of the Vestfold Hills - an area of ice-free land approximately 400km^2 in size and is about 20km from the edge of the continental ice sheet.

Most of the buildings at Australia's Antarctic stations derive from the station rebuilding program which Australia commenced in the late 1970s to replace the original station establishment "huts". The program resulted in the development of the distinctive Australian ANtarctic BUilding System (AANBUS), where heavy steel framed buildings were clad in standard cool room panels. The laminated cool room panels were adopted due to their light-weight nature and standard fabrication techniques.

Although these AANBUS buildings have been highly successful, they were labour intensive to construct, very limited in flexibility and have resulted in cold-path and moisture ingress issues. Furthermore, due to the labour intensive nature of the AANBUS construction methodology, considerable limitation of ship's berths and available beds on station, limited science occurred during this 20 year rebuilding period. As a result, any future buildings required a modified approach so that the impact to the Antarctic science program was minimal.

2. Design approach

During the late 2000s, a new living quarters building was designed and constructed at Davis. This new building adopted a different building technique than the traditional AANBUS approach in order to minimise the impact to the science program. The fibre-composite building approach was developed where the exterior insulating panels would become part of the structural capacity of the building, enabling more work to be carried out in Australia, resulting in much less effort on station. This building comprised of large exterior fibre-composite thermal panels secured to an internal steel frame.

Finite element modelling of the proposed building led to the structural design of both the exterior insulating panels and that of the structural steel supporting frame. The much larger panels and the minimalistic steel supporting frame greatly reduced installation time and effort, reducing the construction personnel required on station, particularly over summer when maximum demand for science occurs. However, the fibre-composite panels did create their own specific challenges.

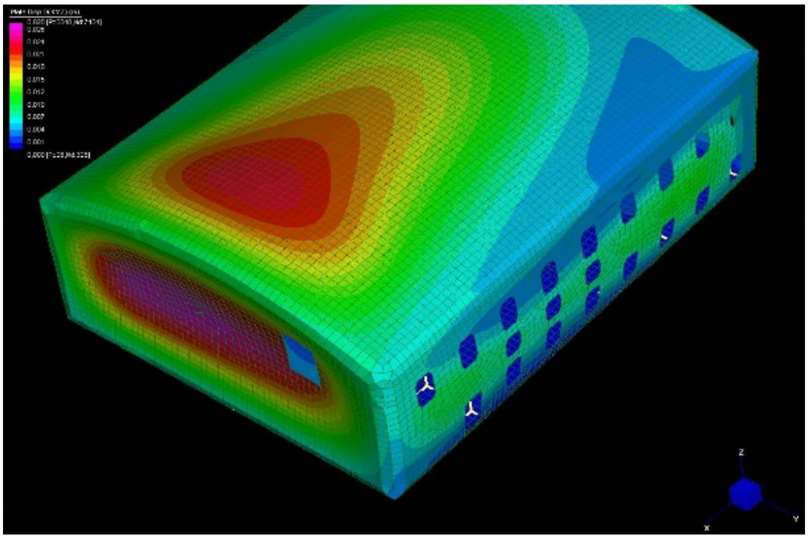

Fig 1
Finite element testing was undertaken to better understand key stress locations.

(Source: AAD)

2.1 Wind design

Wind loads are the dominant design load on Antarctic buildings, and wind load guidelines for Australia stations were developed using statistical analysis of daily maximum extreme values recorded at each of the Australian stations. Much of the coast of Antarctica experiences some of the Earth's strongest winds due to a combination of low pressure systems, generally born over the Southern Ocean, and the 'katabatic winds', caused by the flow of cold air down from the intensely cold interior of this domed shaped continent. Wind speeds often exceed hurricane force for several days at a time with maximum gusts up to 280kph (McEwan, 1985). Due to the dome shape of Antarctica, strong winds are typically very predictable in terms of direction. The 'katabatics' as they are known provided a serviceability design wind of 72m/s in one direction and 48m/s for all other directions.

Since the early 1980s, an ultimate design wind of 90m/s (320kph) has been adopted for all of Australia's Antarctic buildings. The wind velocity used for ultimate case was a 1.5% probability of occurrence of a design wind within the 25 year life of the structure. The 1.5% probability approach was the design philosophy for all post-disaster buildings in Australia at the time. It equated to an ultimate wind velocity with a 1670 return period – 90m/s (Antarctic Structural Group, 1984).

During the austral winter of 2017, a wind speed of 107kts (55m/s) was recorded at Davis. There was no discernible damage to the panels, only minor impact damage as a result of airborne rocks.

2.2 Structural design

The design of the main structural steel support framework was tailored to maximize the advantage of the inherent panel strength. A very stiff portal frame was developed to transfer the critical wind loads from the panels into the frame and then to the ground via the foundations (Figure 2). This approach enabled the building to have minimal secondary steel, but did require the panel design to accommodate for this. Particular attention was paid during detailed design of the main frame to ensure structural integrity throughout at all stages of the construction process.

Three-dimensional modelling was used to evaluate the structural and thermal properties of the panel system. The wall panels were designed to span the full height of the building (maximum of 8.1m) and needed to be able to deal with positive pressures in the order of 4.4kPa with localized pressures of 8.8kPa (suction) on the roof adjacent to the leading edge.

Fig 2 - The structural frame has very little secondary steel, which greatly reduced installation time on station & transport volume on the resupply ship.

2.3 Panel design

The fibre-composite panels are approximately 210mm thick and contain 5mm fibre-glass “skins” (Figure 3) encompassing two layers of 100mm extruded polystyrene insulating boards and typically weighed between 750-900kgs. The panels were laid up using the internal “skin” as the main shell of the panel. This shell contained the insulating foam and laminated timber stiffening beams. The external outer “skin” of the panels was fitted over the main shell similiar to a lid of a shoe-box.

Typically a timber picture frame around the edge of the panel was installed to provide the necessary stiffness within the panel to cater for the design loads (Figure 4). Other laminated timber beams were installed at key locations to enable mechanical fixing of the panels to the structural steel frame, along with other locations where mechanical fixings were required (windows, doors, etc.).

Fig 3 - Laying up the internal skin of the panel

Fig 4 - Installing the laminated timber beams

3. Design successes

3.1 Panel fixings

A significant advantage of the adopted approach was that panel fixings could be undertaken from the inside of the building, rather than the AANBUS approach of fixings through the entire panel. This approach eliminated the 'cold-path' of the steel fixing from the external side of the building into the warm building interior. The panel fixing method adopted utilized stainless steel coach screws that not only improved panel durability and thermal performance, but also eliminated the need for scaffolding during construction – both a time saving and an improvement in overall safety.

Testing was undertaken at the University of Tasmania (Figure 5) to not only confirm the structural capacity of the proposed panel fixing technique, but the number, depth and spacing, of the coach screws. This fabrication approach also resulted in a completely sealed fibre-composite panel, producing a comprehensive vapour seal and eliminating the problems associated with previous cladding methods.

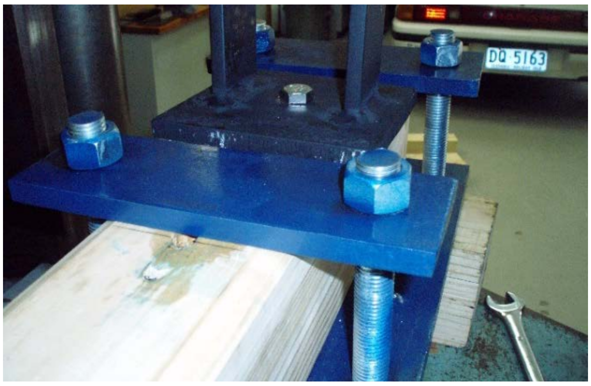

Fig 5 - Testing of panel fixings at the University of Tasmania - Hobart

Fig 6 - Oversized holes were punched into the steel frame for the panel fixing bolts

3.2 Thermal challenges

The use of a steel building frame clad with fibre-composite panels was predicted to result in considerable variation in thermal expansion acompared to the fibre-composite panels. The construction of the steel frame was carried out during the 2008/09 summers, with the installation of the fibre-composite panels undertaken the following summer in January 2010. The fibre-composite panel/structural steel frame interaction was modelled and the predicted differential thermal expansion within the building quantified. The steel frame was erected and the fibre-composite panels installed at an ambient temperature of around 0°C, however the building is operated at a constant internal temperature of 20°C. The 9m high and 22m long steel frame was predicted to expand up to 2.5mm more per metre than the fibre-composite panels. Oversized holes were punched into the structural steel and large steel and teflon washers used to accomodate for this differential expansion (Figure 6).

The steel frame did expand as predicted and the initial "gaps" between panels grew from 8mm to typically 15-20mm. Silicone rubber tubing (30mm diameter) was squeezed between the panels to create a seal during this warming process so that heat would remain within the building as the 'gap' between the panels increased. The final panel joints were then filled with a series of silicone sealant seals.

3.3 Static electricity

A potential drawback of the fibre-composite panels was the build-up of electrostatic charge due to the action of wind over the outer fibre-glass 'skin' of the building in the dry Antarctic atmosphere. To accommodate for this, a carbon cloth layer was incorporated in the outer skin of the panels to conduct electrostatic charge to earth via a drain wire. The carbon cloth layer also provided a more robust outer surface and hence better protection from debris impact during extreme winds. To date, static electricity issues within the living quarters building is less than that for the AANBUS style buildings.

4. Design failures

The cladding of Antarctic buildings is subjected to harsh environmental conditions. The temperature range across the year results in considerable stress in the cladding. During winter at Davis, the temperature often drops to well below -30°C; whilst during summer the surface of the fibre composite panels on sunny days has been measured (IR camera) to be as much as 50°C. This 80°C change has resulted in considerable thermal expansion/contraction on the outer "skin" of the fibre-composite panel across the year. Whilst the -30°C (and colder temperatures) were well known, it was the high surface temperatures during summer that has resulted in damage of the outer "skin", particularly at the window voids.

4.1 Delamination

Delamination of the joint between the internal and external fibre-glass "skins" has occurred at a number of windows on the north-west side (Figure 7). These window joints were manufactured as a glued butt joint and the thermal variation has resulted in too much stress for the glue used. This failure is only evident along the north/western face that receives high solar radiation – the other three sides either have no windows or face southward and hence have much lower solar radiation.

The butt joint (circled in dashed red in Fig 8) was designed to provide support for the windows, especially those subjected to high negative pressures during high wind events.

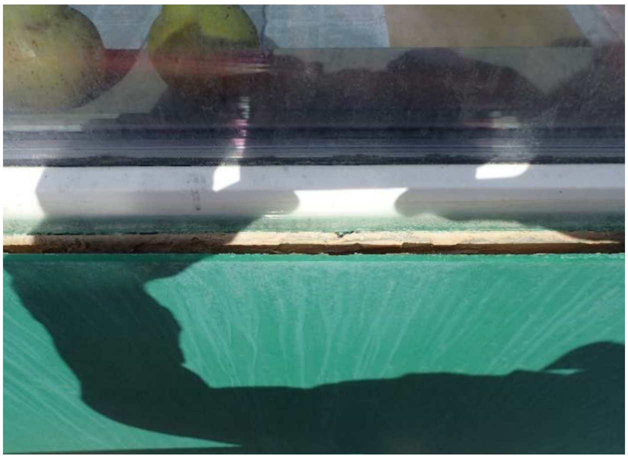

Fig 7 - Delamination of the outer "skin" away from the main body of the panel – snow melt enters here.

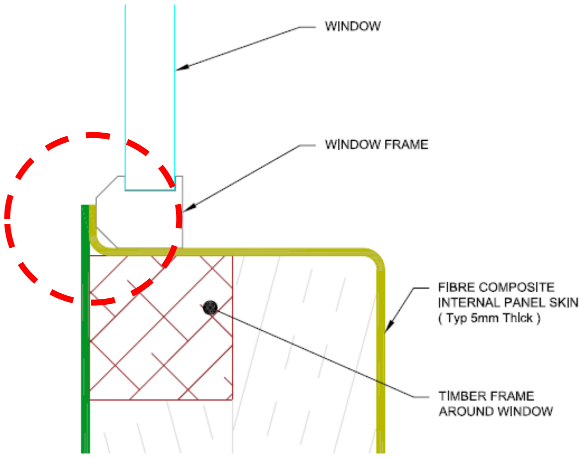

Fig 8 - A detail of the "butt" joint between the two fibre-glass "skin" of the panel at the windows.

Where the panel's internal and external fibreglass "skins" joined around the edge of the panel, this interface was designed as a slip joint and has not suffered from any delamination at all. Clearly the butt joint in the two "skins" at the window required an alternative approach, whilst still providing support for the windows.

4.2 Diagonal cracking

Diagonal cracking has occurred at the square corners of the window voids in the external shells. These sharp square corners were a poor design detail and the resultant cracking due to thermal stresses should have been predicted. Curved and/or thickened corners should have been considered and tested. Again, this diagonal cracking is only evident along the north/western face that receives high solar radiation (Figures 9 & 10).

Previous repair works undertaken on station have not improved the issue, rather the incorrect application of these repairs has resulted in similar cracking due to a lack of understanding by the repairer. Additionally, the aesthetic looks very poor.

Fig 9 – Delamination and cracking

Fig 10 – Cracking through a "repair"

The detail of square internal corners on the window voids in the outer shell was a poor decision – exacerbated by delamination.

4.3 UV fading

During the 1980s it became evident that a thinning of the concentration of ozone in the stratosphere was occurring each summer over the Antarctic continent. This "hole" in the ozone greatly reduces the natuaral atmospheric screening of ultra-voilet light and results in greater UV radiation impact to Antarctic facilities. This impact of ultra violet radiation was understood during the design phase, and a UV stabilised gel-coat was adopted for the external panel "skin". However, this UV stabilised gel-coat has not been able to deal with the extreme level of ultra violet light. The panels on the north east & north-west wall and roof panels are subjected to significant sun and have become very faded. The panels on the southern face of the building are much brighter. Although not critical to the structural or thermal integrity of the building, the aesthetic is very poor (Figure 11).

Fig 11 – The Living Quarters after seven summers of ultra violet radiation (2017) – D Thost.

5. Conclusions

The construction of a new Living Quarters at Davis adopted a fibre-composite approach in an attempt to resolve a number of issues that the Australian Antarctic program had with its traditional AANBUS building approach. The adopted fibre-composite building approach resulted in a building that could be staged to suit the fiscal constraints of the day, meet transport logistics to Antarctica, and maximize the amount of work that could be undertaken in Australia. It also enabled simpler, quicker and safer construction than the AANBUS building approach, minimizing the impact on day-to-day station operations, and the science research programme.

However, the fibre-composite approach wasn't without it's challenges and a number of design decisions have caused on-going maintenance concerns. The panels have been very successful with respect to their structural and thermal aspects. However, after seven years in service – the effects of multiple Antarctic summers is clearly evident. The fibreglass external "skin" of the panels that have receive considerable exposure to the sun has suffered from cracking, delamination and fading. Many of these issues could have been prevented by better detailing during the design stage.

Alternatively, it may have been better to construct the panels in reverse, with the interface between the internal and external "skins" on the inside of the building. This approach would have the join between the two panel "skins" located where the temperature is very stable, and solar radiation would be minimalised. This approach would not have corrected the fading of the panels due to the high ultra-voilet radiation that the Antarctic continent receives each summer.

This said, the building has now been operating successfully as the station's Living Quarters for the past seven years, despite some maintenance work being required on the external fibre-composite panels. It has been thermally very efficient and has required changes to the building's air handling system in order to 'cool' the building on hot days during summer.

ACKNOWLEDGMENTS

Many thanks to so many people who worked on this project, particularly those expeditioners who spent months, even years in some cases away from home constructing this building. Also a special thanks to the Infrastructure Engineer at the time who had the courage to try something different in such an extreme location.

REFERENCES

[1] ANTARCTIC CONSTRUCTION GROUP, "Design of the cladding system for use on Antarctic projects.", Department of Housing and Construction, Reston, Melbourne, Australia. 1984

[2] McEwan R.A., "Construction in Antarctica", 12th Biennial Conference, Concrete Institute of Australia, Melbourne, Australia, 1985.

All Figures by Author unless noted otherwise.

Basic Study on Mechanism of Frost Damage to Bricks in Cold Regions

Dai Nakamura
Associate Professor
National University Corporation Kitami Institute of Technology
JAPAN
dnaka@mail.kitami-it.ac.jp

Dr. Takayuki Kawaguchi, Kitami Institute of Technology, JAPAN
Dr. Tatsuya Watanabe, Kitami Institute of Technology, JAPAN
Dr. Shunzo Kawajiri, Kitami Institute of Technology, JAPAN

Summary

We have discovered that the possible cause of cracks in the brick is frost damage at the two places in Kitami City, Hokkaido. To clarify the crack occurring mechanism of bricks in this research, we conducted a field survey, an exposure test, and an indoor model experiment. From these results, we have confirmed that the closed freeze-thaw gives cracks to the brick.

Keywords: Cold Regions, Brick, Frost Damage, Freeze-Thaw, Closed Freeze-Thaw

1. Introduction

When porous material such as a brick is applied to buildings and civil-engineering works in a cold and snowy region, it always has trouble called frost damage. In Kitami City, Hokkaido, Japan, we found cracks in bricks that were expected to occur due to frost damage at a private house's flowerbed and a railway station's parking lot. Such cracks are not limited to the city and have been identified all over Hokkaido.

Since old times, many researchers have worked on frost damage to porous materials and expressed a variety of views. It has generally been said that the phenomenon, in which frost damage is given to porous building materials, such as bricks and concrete, happens due to a rise in volume when pore water is frozen (e.g. Thomas [1] and Watson [2]). The following describes a typical theory, provided by Powers, et al. [3], who explained the frost damage mechanism of concrete. They state that in the frost damage to concrete, when pore water is frozen, the volume increases by 9 percent, which moves unfrozen water and raises the pressure (water one), resulting in cracks. This is the basic theory of the frost damage mechanism of concrete. However, Powers, et al. [3] conduct a detailed investigation of the frost damage emerging mechanism in the inside of porous material, but do not take account of air temperature variation caused in the winter of an actual cold area.

In this research, we made efforts to clarify the crack generating mechanism of bricks identified in Kitami City, Hokkaido by taking winter's air temperature variation into consideration. First of all, we conducted a field survey of the two places where cracks were observed in the City to grasp how the bricks cracked. Next, we simulated the private house's flowerbed to conduct an exposure test, and then carried out an indoor model experiment.

2. Field Survey

Fig.1 shows cracks caused in the bricks installed in the private house's flowerbed. The bricks were installed diagonally so that the upper part protruded from the ground surface and the lower part was buried in the ground. The cracks appeared in parallel with the ground surface, and some of them had a large opening that divides one brick into two parts. Cracks of bricks sat near to the ground surface or in the top of the upper part. Most of them were arranged with the face pointing to the south, so they were exposed to plenty of sunshine in the daytime.

Fig. 2 shows cracks caused in the brick wall of the station's parking lot. The parking lot was surrounded by the brick wall, and the top-line bricks projected from the second-line ones. We discovered that cracks occurred in the projecting part of the top-line bricks as shown in Fig. 2, that they included cracks with a large opening dividing one brick into two parts, and that many bricks came off as a block. All the bricks other than the top-line ones had almost no cracks, so their soundness was kept. Like the bricks installed in the flowerbed, the cracked brick wall was arranged with the face pointing to the south, so they got plenty of sunshine in the daytime.

The field survey results above suggest that the frost damage to the bricks at the two places in Kitami City follows the same mechanism, although the installation methods are different.

3. Exposure Test

In this research, we made efforts to clarify the frost damage mechanism by reproducing the bricks installed in the private house's flowerbed in our campus.

Fig. 3 shows the exposure test site. We made a hole 100 cm long, 140 cm wide, and 30 cm deep at the site and refilled it with soil for gardening. After that, we arranged seven bricks extracted from the flower garden and conducted the exposure test.

Table 1 lists the basic physical properties of a brick 210 mm long, 100 mm wide, and 60 mm thick. We installed the bricks so that they stood diagonally and their faces pointed to the south as shown in the flowerbed. Note that snow was removed to keep the effect of the cold sufficiently high in winter.

We installed 15 thermal sensors in or on the bricks to analyze the brick temperature variation. Fig. 4 shows the detailed sensor installation points. The sensor, a thermocouple, was attached with an adhesive. In this research, we created a temperature distribution chart from the resulting temperature data. We found the temperature between two adjacent sensors by using linear interpolation in steps of 5 mm. A data logger automatically measured the brick and air temperatures mentioned above every hour. In late February 2010, we observed cracks in the bricks. Fig. 5 shows an example of them. The

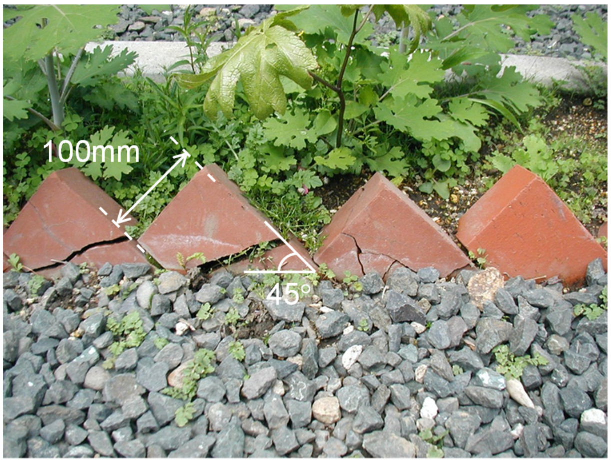

Fig. 1 Frost Damage of bricks in the flowerbed

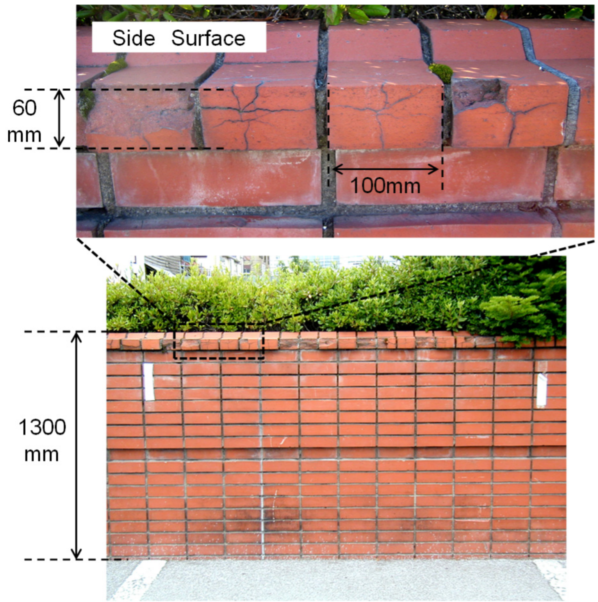

Fig. 2 Frost Damage of bricks in the brick wall

Fig. 3 Appearance of exposure test site

schematic depiction in the figure indicates the crack emerging points. From Fig. 5, we can see that a brick with no crack on February 23 had a crack on the 24th. This means that the brick cracked during the night.

Fig. 6 shows the temperature distribution from dawn to night on February 23. At dawn, the distribution of the bricks consists of negative temperatures, so it is expected that the bricks are frozen as a whole. After that, as the sun is rising and the bricks are getting sunshine, the ice in upper part of the bricks is starting to thaw almost one-dimensionally and the surface temperature is changing to positive values. We think that along with this change, the ice formed in the pores thaws in the upper part of the bricks protruded from the ground surface. After that, the night comes with the lower part of the bricks frozen, resulting in featured temperature distribution in which the night cold surrounds the upper part of the bricks with negative temperatures. This suggests that the thawed part during the daytime is refrozen because it was confined in the night cold. Such a refreezing

Table.1 Basic physical properties of brick extracted from the flower garden

Water Absorption Ratio (%)	12.2
Porosity (%)	24.9
Bulk Density (g/cm^3)	2.01
Apparent Density (g/cm^3)	2.68

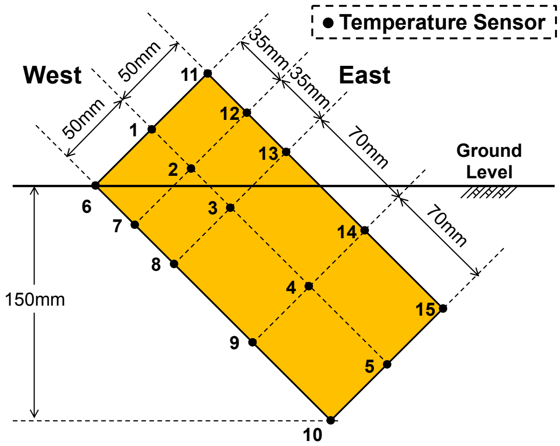

Fig. 4 Detail of sensor installation points

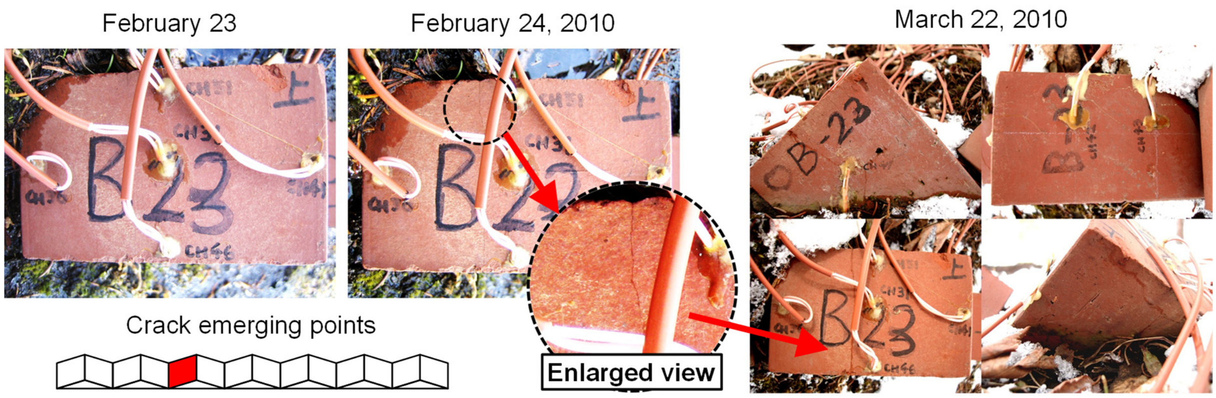

Fig. 5 Crack of the brick that occurred on February 23 & 24, 2010

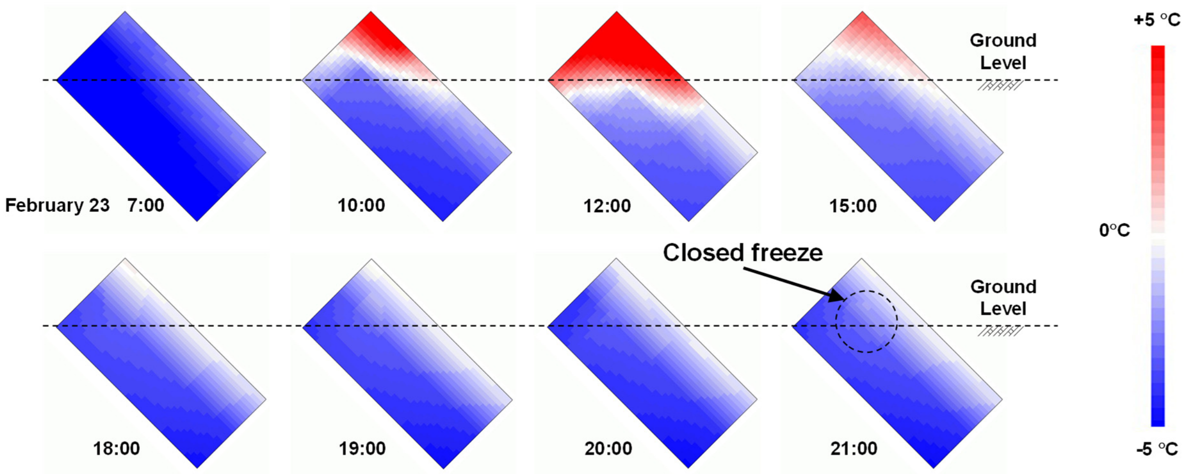

Fig. 6 Temperature distribution from dawn to night on February 23

phenomenon confines and freezes the water contained in the upper part of the bricks and increases the internal pressure, resulting in cracks in the brick. In this research, we define the freezing and thawing phenomenon with this temperature distribution as a closed freeze-thaw.

4. Frost Damage Emerging Mechanism of Bricks Inferred from the Exposure Test Results

From the exposure test results, we have presumed the frost damage mechanism as follows:

Fig. 7 schematically shows the mechanism of frost damage to the bricks installed in the private house's flowerbed. The bricks, which are completely frozen until the deepest part due to the night cold in later winter, are thawing from the surface as they are being exposed to sunshine in the daytime. Along with this change, the brick inside has a temperature gradient and the 0 °C line moves to the deep part. Above the line, the ice formed in cracks and pores is thawing. After that, the line reaches the ground surface and the ice starts to thaw in the upper part of the bricks. Since the sunshine of later winter is weak, the ice does not thaw completely. The lower part of the bricks remained frozen, but when the night comes with this condition kept, the unfrozen part in the daytime is confined and refrozen due to the night cold. Accordingly, we think that the water in the upper part of the bricks is confined and frozen and the internal pressure increases, resulting in cracks in the brick.

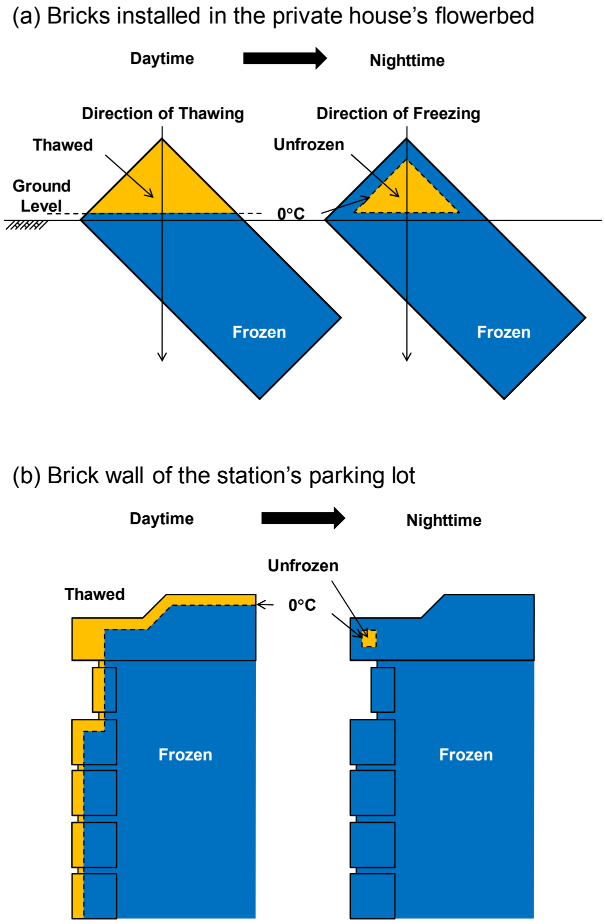

Fig. 7 Schematic image of the mechanism of frost damage that occurs in brick

The brick wall of the station's parking lot experiences the same phenomenon as the flowerbed—in the projecting part of the top-line bricks, the water is confined and frozen, resulting in a rise in internal pressure and cracks in the brick.

5. Verification based on an Indoor Model Experiment

In this experiment, we used ordinary bricks sold on the market. Table 2 lists the basic physical properties. There was no difference in properties between the ordinary and flowerbed bricks. Each brick was 210 mm long, 100 mm wide, and 60 mm thick. We used a vacuum pump to deaerate the bricks in distilled water for 24 hours and then humidified them for several days until the mass did not change. Because of such forced humidification, we believe that all the test pieces are in a water-saturated state.

We installed the bricks in a plastic container as shown in Fig. 8. They were piled diagonally in the same fashion as the ones at the site where frost damage occurred in Kitami City. The container had three bricks, and the surrounding space was full of weathered volcanic ash collected in Kitami City. The ash had a grain density of 2.557 g/cm^3 and an

Table.2 Basic physical properties of ordinary brick sold on the market

Water Absorption Ratio (%)		12.2
Porosity (%)		24.7
Bulk Density (g/cm^3)		1.98
Apparent Density (g/cm^3)		2.63
Compressive Strength (MPa)	Dry Condition	51.6
	Wet Condition	45.4
Tensile Strength (MPa)	Dry Condition	3.64
	Wet Condition	3.73

optimum moisture content of 32.5%. For the experiment, we adjusted the moisture content so that it was about 30%.

We installed 15 thermal sensors in the brick to analyze the brick temperature variation. Fig. 9 shows the detailed sensor installation points. The sensor, a thermocouple, was attached with clay. The numeric values in the figure represent the sensor numbers. In this research, we created a temperature distribution chart from the resulting temperature data. We found the temperature between two adjacent sensors by using linear interpolation in steps of 5 mm. A data logger automatically measured the brick and air temperatures mentioned above every minute.

Fig. 8 Appearance of the freeze-thaw experiment

During the experiment, we used a fixed-point camera to take a picture of the bricks and to observe how the brick changed its state in the freezing and thawing processes. The shooting interval was one minute.

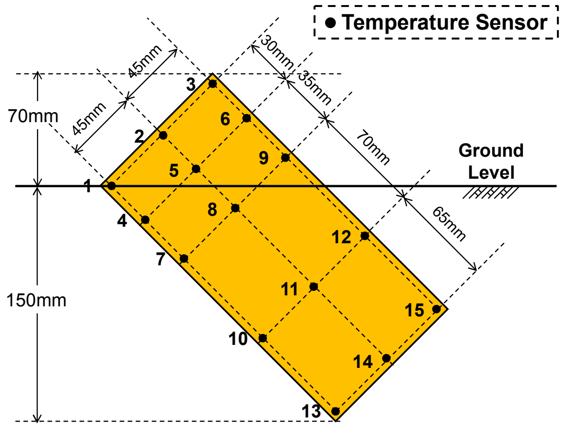

Fig. 9 Detail of sensor installation points

To freeze the bricks, we put the container mentioned above in a low-temperature chamber whose temperature was set at -25 °C. In the thawing process, we took the container out of the chamber and left it to stand in a room whose temperature was set at +20 °C. The freezing and thawing cycles were repeated twice. The following presents a detailed description of the freezing and thawing method. In the 1st freezing cycle, the brick is frozen until all the thermal sensors reach negative values. In the 1st thawing cycle, the upper part of the brick starts to thaw, but the cycle stops when Sensor 5 shown in Fig. 9 presents a positive value; that is to say, the brick does not thaw completely at the end of the 1st cycle. At the start of the 2nd freezing cycle, the brick consists of frozen and unfrozen parts, and the boundary is present between Sensors 5 and 8 indicated in Fig. 9. When the brick is refrozen in such a condition, its upper part has a closed unfrozen area surrounded by the frozen area.

Fig. 10 shows the brick states before and after the freezing and thawing processes. Cracks occur in part of the brick protruded from the ground surface, and they are formed in parallel with the ground or diagonally. This crack emerging state is very similar to that checked in the bricks installed in the private house’s flowerbed shown in Fig. 1.

The following describes the possible causes of such cracks that we posit. In the case of the closed freeze-thaw, when the brick is refrozen, the part below the freezing face has higher strength because the pore water is frozen. Therefore, no crack occurs toward the lower part of the brick. In the brick installation method used in this research, the lower part of the brick is farther from the free face than is the upper part protruded from the ground surface. As a result, we think that cracks occur in the closed part with high internal pressure and develop horizontally or diagonally toward the near free face.

Fig. 11 shows changes over time in brick internal and air temperatures. Note that of the 15 thermal sensors installed, only Sensors 2, 5, 8, 11, and 14 installed along the centerline of the brick are used to plot the measured values. The numerical values in the legend correspond to the sensor numbers in Fig. 9. From Fig. 11, we can see that Sensors 11 and 14 are once kept at about 0 °C in the 1st

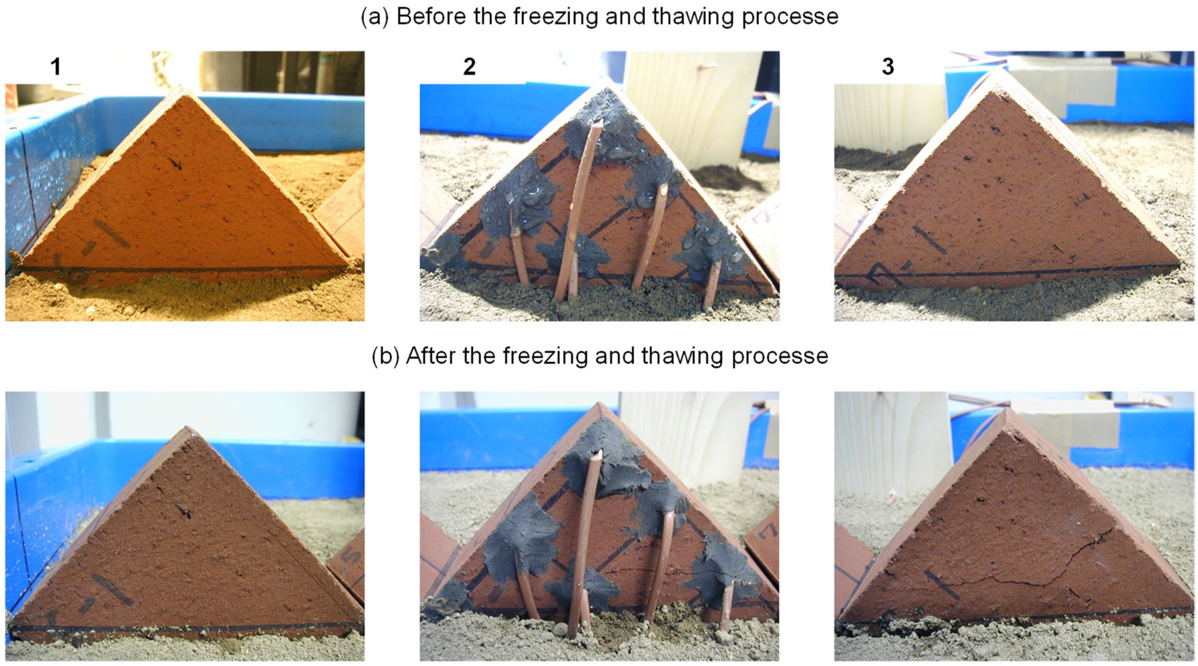

Fig. 10 Appearances of bricks before and after the freezing and thawing processes

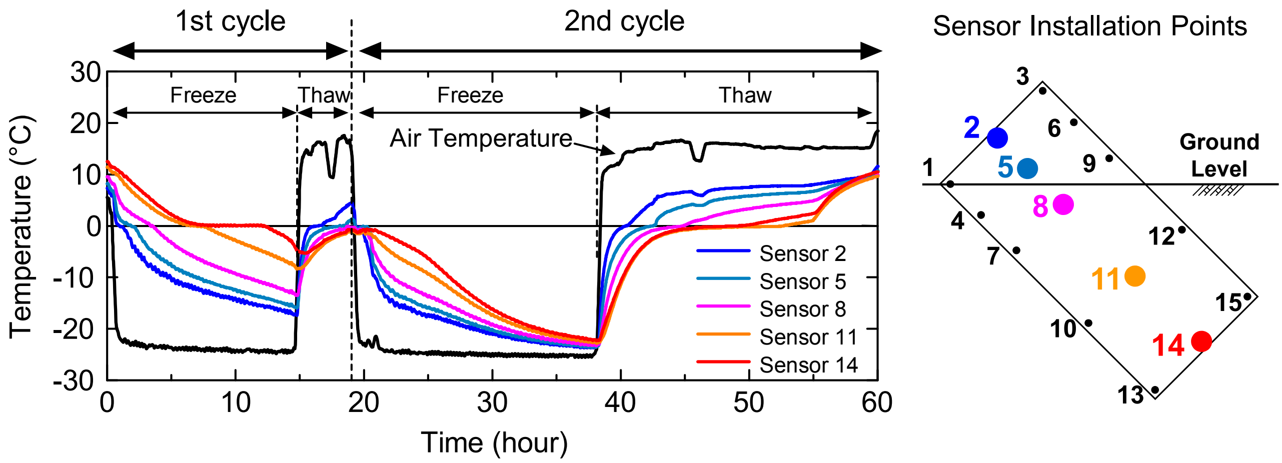

Fig. 11 Changes over time in brick internal and air temperatures

freezing cycle. The other sensors also show the same behaviour for a short time. This means that the pore water in the brick is frozen. In the 1st thawing cycle, after Sensors 2 and 5 are kept at about 0 °C, the temperature increases. This is because the pore ice in the brick thaws and changes to water. Meanwhile, Sensors 8, 11, and 14 are still kept at about or below 0 °C, so the pore ice remains formed.

Fig. 12 presents a temperature distribution chart in the 2nd freezing cycle and a picture of the crack developing state taken by the fixed-point camera. Just after the freezing cycle starts, the upper part of the brick remains unfrozen at a positive temperature near 0 °C, while the lower part is frozen at a negative temperature. Part of the brick protruded from the ground surface is cooled down due to the surrounding cold, and the 0 °C line moves and gradually envelops the unfrozen part. We can see that water drops occur on the brick surface 20.27 hours after the experiment starts. As they are confined and frozen, the water moves to the center of the brick, the pore water pressure increases and pushes latent cracks in the brick, and finally the cracks develop toward the surface. All the protruded brick parts have negative temperatures 20.33 hours after the experiment starts, but the temperatures increase again and change to positive values 20.42 hours after. We think that latent

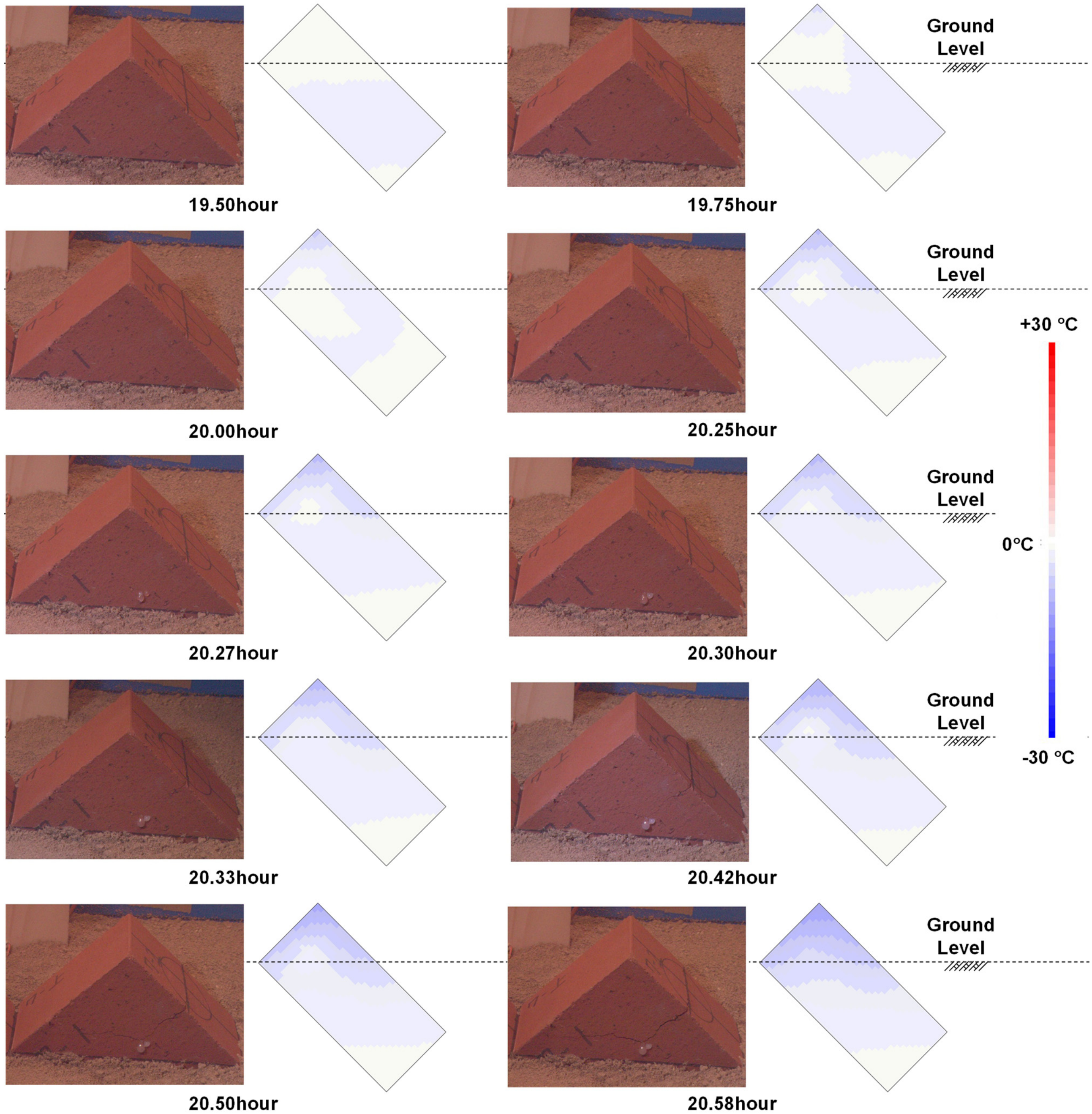

Fig. 12 Temperature distribution charts in the 2nd freezing cycle and pictures of the crack developing state

heat is generated when phase change from water to ice occurs in the pore water in a supercooling state. At the same time, hairline cracks occur in the brick. Therefore, we think that the cracking occurs because the pore water is frozen and the internal pressure increased in phase change to the pore ice is higher than the tensile strength of the brick. After that, the brick is cooled down continuously and the opening width of the crack is large as the temperature decreases.

The experiment results above clarify that the closed freeze-thaw cracks the bricks. Moreover, we have found that cracks occur in the brick in two freezing and thawing cycles or substantially in only one closed freeze-thaw cycle. This suggests that the internal pressure produced by the latter cycle is large enough to break the brick in a single freezing cycle. We posit that the closed freeze-thaw has the possibility of occurring not only in brick structures but also in exposed natural stones and masonry buildings.

As mentioned above, we believe that the indoor model experiment conducted in this research correctly reproduces the cracked bricks in Kitami City. However, the test pieces used in the experiment are in an almost water-saturated state, so the moisture content is very different from the actual one. Moreover, the freezing temperature adopted is lower than the air temperature measured in the exposure test, which we believe makes it easy for the brick to have cracks. We will clarify the relationship between the moisture content and freezing temperature of bricks and degradation caused by the closed freeze-thaw.

6. Conclusions

We have discovered that the possible cause of cracks in the brick is frost damage at the two places in Kitami City, Hokkaido. To clarify the crack occurring mechanism of bricks in this research, we conducted a field survey, an exposure test, and an indoor model experiment. Main results obtained in our research are summarized as follows.

• Field survey
(1) Many cracks occur in bricks installed in a place that points to the south and that gets plenty of sunshine.
(2) The projecting part of the brick has cracks.

• Exposure test
(1) The brick has cracks in the latter part of winter from late February to late March.
(2) At that time, the brick has the following featured temperature distribution. After the brick is completely frozen until the deepest part due to the night cold in late winter, the surface temperature changes to positive values because of sunshine in the daytime. Next, the night comes with the lower part of the brick frozen and the night cold gives the brick a closed temperature distribution in which the upper part is surrounded by negative temperatures. The part thawed in the daytime is confined and refrozen due to the night cold, and the water in the upper part of the brick is also confined and frozen. As a result, the increasing internal pressure gives cracks to the brick.

• Indoor model experiment
(1) We have confirmed that the closed freeze-thaw gives cracks to the brick. Moreover, we have found that it occurs in two freezing and thawing cycles, or substantially in only one closed freeze-thaw cycle. This suggests that the internal pressure produced in the latter cycle is high enough to break the brick in a single freezing cycle.

We are confident that the results above are very significant as notes for how to apply porous material such a brick to structures in a cold region such as Hokkaido.

References

[1] Thomas, W.N., "*Experiments on the Freezing of Building Materials*", Building Research Technical Paper, Building Research Station, Great Britain, No.17, 1938, pp.146.
[2] Watson, A., "Laboratory Tests and the Durability of Bricks. VI. The Mechanism of Frost Action on Bricks", *Transactions of the British Ceramic Society*, Stoke-on-Trent, England, Vol. 63, No. 11, 1964, pp. 663-680.
[3] Powers, T.C. and Brownyard, T.L., "Studies of the physical properties of hardened cement paste", *Journal of the American Concrete Institute*, Vol.18, No. 8, 1947, pp. 933-969.

Stress analysis and calculation of pile foundation caused by the lake ice

Jiliang Wang [1], Chenxi Zhang[2]

Jiliang Wang
Senior Engineer r
Heilongjiang Province Academy of Cold Area Building Research
China
wangjiliang@sohu.com

Chenxi Zhang,
Heilongjiang Province Academy of Cold Area Building Research,
China

Summary

With the development of urban construction, most of structures were built in the lake by use of pile foundation, such as gallery road, pavilion and observation deck. In cold regions, lake water freeze to ice in winter, which would cause the horizontal and friction stress on the pile, and even to lead to different destroys on the pile foundations built in lake. This paper focuses on the damage of lake ice to the pile foundation of a gallery road built in Heilongjiang province, China. The stress conditions and damage reason were analyzed first, then the calculation method of the horizontal force caused by lake ice on pile foundation was proposed. Finally, the analysis conclusions and the solution of this engineering problem were also given.

Keywords: lake ice, pile foundation, horizontal force, calculation method.

1. Introduction

More and more buildings in the lake, such as trestles, viewing platforms, photovoltaic power stations and so on, were built in cold regions. In northeast of China, there are horizontal or vertical effects of ice on buildings in the lake when it is used in the winter. Different degrees of damage were found in many engineering structures[1,2], which caused much economic losses. Generally, for dams and piers in rivers, the damage caused by ice pressure usually occurs during the spring drift ice age, but for piles in lakes, it often occurs during the ice formation period. For example, on November 24, 1998, a three-storey building at a lakeside near Harbin collapsed due to static ice pressure, while the engineering accident in this paper occurred on November 20. Therefore, for the pile foundation in the lake, the ice pressure should be fully considered from the design stage in order to avoid quality accidents. Taking the pedestrian trestle project of Sanyong Lake in Daqing as an example, causes of the breakage and inclination of bridge piles were analyzed in the paper, which could be a reference for future design.

2. Project overview

2.1 Overview of trestle design

Daqing Sanyong Lake Trestle Bridge is located in Sanyong Lake, Daqing City, Heilongjiang Province, which was built on November 6, 2013. The water area of Sanyong Lake is more than 3.1 million m^2, and the length of the trestle bridge is 2300 m, which is the longest trestle bridge in China. Superstructure of bridge: the I-shaped steel is adopted as main girder continuous structure and horizontal connection, a bridle iron is set at the pier, support and upper main girder are connected by bent cap of I-shaped steel. The steel support, steel bent cap and longitudinal steel main girder are welded together; Substructure: The static pressure pre-stressed high-strength concrete pipe pile (model is PHCA-400(95)-8.0) is adopted, the depth of pile in soil is about 6m, while the bridge deck and railings are made of wood structure.

2.2 Geological survey

An engineering geological survey was carried out on the damaged section of the bridge in February, 2018. The stratum is divided into six layers within the depth range revealed by the borehole. From top to bottom: (1) ice water; (2) silt; (3) clay; (4) silty clay; (5) clay; (6) clay. The lithological characteristics of each soil layer are described as follows:

(1) Ice water: Ice thickness is 0.60 m~0.80 m and water depth is 1.90 m~2.00 m during survey; (2) Silt: the soil is black-grey, containing humus and a small amount of grass roots, flow plastic, and the thickness of this layer is 0.50m-0.80m; (3) Clay: the soil is grey brown to brown, deposited, homogeneous, strong viscous, high compressibility, plastic, and the thickness of this layer is 3.10 m to 4.05 m. (4) Silty clay: the soil is grey brown, deposited, homogeneous and plastic, and the thickness of this layer is 2.00m~2.80 m; (5) Clay: the soil is grey brown, deposited, homogeneous, viscous and plastic, and the thickness of this layer is 0.70m~2.20m. (6) Clay: the soil is brown, deposited, homogeneous, strong stickiness and hard plastic, and the layer has not been drilled through.

2.3 Accident overview

The staff heard a click coming from the trestle at afternoon in November 20, 2017. 34 piles were found to be broken and 59 piles were inclined during the inspection on the afternoon of November 21, which had an impact on the safe operation of the bridge, then the bridge was stopped using. However, no new fracture was found being occurred after November 22, while the ice thickness was detected to be 40 cm and there is a phenomenon of ice surface uplift on November 23, 2017. As shown in Fig.1(a), it is the broken pile of trestle, and one of the inclined pile is shown in Fig.1(b).

(a) (b)

Fig.1 broken and inclined pile of trestle

3. Analysis of the action of ice on piles

There are interaction problems with water and ice during the operation of structure in the lake. The effect of ice on piles can be divided into vertical and horizontal ones. Vertical action is due to the downward pulling force on the structure caused by the falling water level when the ice layer freezes together with the structure, or the upward pulling force on the structure caused by the rising water level of the ice layer. Horizontal action can be divided into static ice pressure and dynamic ice pressure. The dynamic ice pressure refers to the impact and friction of moving ice blocks on structures driven by wind and current. The static ice force refers to the destructive effect of ice and ice sheet on the structure during ice growth and after freezing (the pressure caused by ice expansion with temperature rising). This paper will focus on static ice pressure.

The damage of this project occurred on November 20, which is in the stage of the ice layer occurrence. Therefore, only the static ice pressure is considered. The ice surface is uplifted when the accident happens, so only the upward freeze-pull force is considered, while the downward pull force of the ice layer is not considered.

3.1 Vertical force acting on piles by ice

There are few domestic studies on tangential frost heave force of piles caused by temperature rise and expansion of ice layer, and there is no specific calculation method in relevant codes. Generally, the tangential frost heave force of piles is calculated by referring to method for the frozen soil, but the value of the tangential frost heave force is different for different scholars.

3.1.1 Formula for calculating uplift force of piles caused by ice expansion：

$$T_\tau = n_f q_f u z_0 \tag{1}$$

Where T_τ is maximum Freeze Drawing Force of Single Pile; n_f is the influence coefficient of freezing depth is 1.0; q_f is the tangential frost heave force produced by ice on piles, 110 kPa-150 kPa; u is pile circumference; z_0 is ice thickness.

According to the above formula, the uplift force on the pile is 75 kN when the ice thickness is 38 cm, while the maximum uplift force of piles at ice thickness of 0.9 m is 170 kN.

3.1.2 The ultimate uplift bearing capacity of single pile is calculated according to "Technical Code for Building Pile Foundation" JGJ94-2008:

$$T_{\mathrm{uk}} = \sum \lambda_i q_{sik} u_i l_i = 0.7\times20\times1.256\times1.0+0.7\times70\times1.256\times5=325.3\text{kN} \tag{2}$$

Where T_{uk} is Standard value of ultimate uplift bearing capacity of foundation pile； u_i is Pile circumference, while u can take πd for equal diameter piles; q_{sik} is standard values of ultimate lateral resistance of layer i soil on pile side surface are 20 kPa for muddy clay and 70 kPa for silty clay; λ is anti-pulls coefficient for 0.7.

3.1.3 Checking calculation of uplift bearing capacity according to "Technical Code for Building Pile Foundation" JGJ94-2008:

$$\mathrm{T}_\tau = \eta_{\mathrm{f}} q_{\mathrm{f}} u z_0 \leqslant T_{\mathrm{uk}} / 2 + N_{\mathrm{G}} + G_{\mathrm{P}} \tag{3}$$

Where T_{uk} is Standard value of Uplift Ultimate Bearing Capacity of single pile below standard frozen depth line; N_G is standard values of building self-weight, pile cap and its upper soil weight above the bottom of pile cap supported by piles; G_p is Pile self-weight and floating weight below groundwater level.

When the ice thickness of the pile is 0.9m, the calculation shows that the formula

$T_\tau = \eta_f q_f u z_0 \le T_{uk}/2 + N_G + G_P$ is satisfied, therefore, the pile will not be pulled up by ice, and the pipe piles with a length of 8m satisfies the requirements of uplift resistance.

3.2 Checking calculation of static ice pressure of ice to pile

According to the national industry standard "Code for Design of Freeze Resistance of Hydraulic Structures (GB/T50662-2011)", the static ice pressure acting on the independent piers can be calculated by the following formula:

$$F = mfB\sigma c \tag{4}$$

Where *m* is the plane shape factor of pier-column leading edge, for circle is 0.9; *f* is the compressive strength of ice, 0.75 MPa; *B* is front width of piers at ice action elevation, m; c is the thickness of ice block, taking the 0.7~0.8 times of maximum value for the beginning of drifting ice. *σ* is the extrusion strength of ice. Generally, it is 0.75 MPa at the beginning of drifting ice and 0.45 MPa at the later stage.

3.3 Computing model

When the ice layer temperature rises and expands, the static ice pressure acting horizontally on the pile is produced. The calculation sketch of the column under static ice pressure shows that the pile top can be deformed according to the damage picture of the pile, so the pile top can be regarded as articulation.

3.4 Checking calculation of bearing capacity of piles

The actual ice thickness at the time of the accident is 38 cm, and the horizontal static ice pressure acting on a single pile is calculated according to the formula F=0.9x750x0.4x0.4=108 kN. The damage of trestle occurred on November 20 when the ice layer was thin for only 38 cm. The maximum thickness of ice layer in Daqing area was 1 meter according to the regulations, and then the design value of static ice pressure could be obtained according to the formula: F=0.9x750x0.4x0.8=216 kN. The PHC (A) - 400 (95) - 8.0 pile is selected, whose design value of shear bearing capacity of pile body is 146 kN referring to the relevant atlas.

According to the calculation, the shear capacity of the pile is greater than the static ice pressure when the ice thickness is 38 cm, while it is less than the static ice pressure when the ice thickness is 80 cm. However, the ice thickness is 38cm when the pile is destroyed, and the bridge has been running for nearly five years, which means that the most dangerous time is not the initial stage of drifting ice, but the freezing period. It also means that the static ice pressure of the pile may be smaller at this time, while the static ice pressure calculated at the initial stage of drifting ice is larger.

3.5 Analysis of static ice pressure

It is necessary to find the reasons for piles are damaged when the ice thickness is 38 cm, but not when the ice thickness is 80 cm. It is known that there are many factors affecting the ice pressure value. On the one hand, they are the conditions of ice itself and environment, such as initial ice temperature, temperature rise rate, ice surface size, shape, impurity content, crack state, and so on, on the other hand, they are constraints, such as reservoir shape, strength and stiffness of slope protection materials, and so on. But the ice pressure calculated by any formula should not be greater than the limit ice pressure.

Ice temperature is one of the main factors affecting ice pressure, which is closely related to temperature. According to literature 1, the relationship between ice surface temperature and atmospheric temperature is T=0.8T_a, T_a is atmospheric temperature, and the relationship between atmospheric temperature increment and average ice temperature increment of surface ice layer (0-15cm) is T_a=2T_i from 8:00 to 14:00 am. The relationship between surface average ice temperature increment rate S1 (℃/h) and second layer (15-30cm) average temperature increment rate S2 (℃/h) is S1=0.4S2, and the influence of atmosphere temperature on ice layer is mainly in 30cm - 40cm, has little effect on the deeper ice temperature. When the accident happened, the ice thickness was about 38cm.

Referring to the meteorological data of Daqing in November 2017, the temperature change chart is as follows:

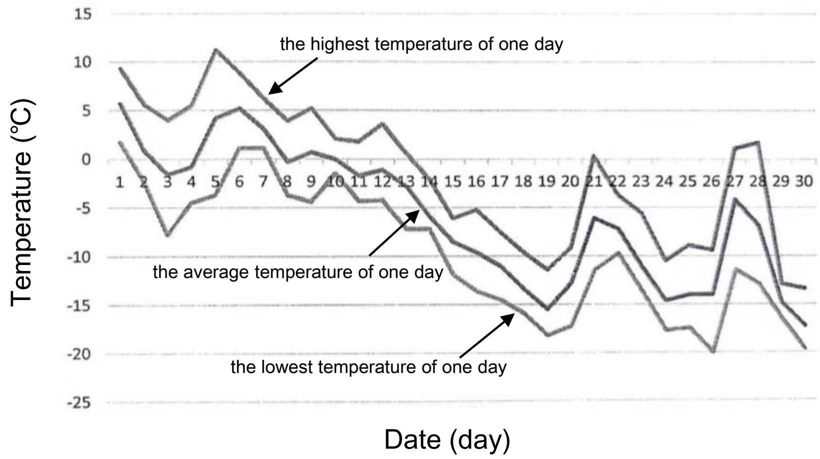

Fig.2 temperature change on November, 2017

From the Fig.2, it can be seen that the temperature began to drop from November, 13 to 19, but rise from November, 20 to 21. The sound of destruction was heard by the staff on the afternoon of November, 20, then it was found that the pile was broken on the afternoon of November, 21. So the breaking time of the pile should be in the afternoon of November, 20. The lowest temperature of November, 20 is -17.2 degrees, and the highest temperature is -9 degrees, so the temperature rises 8 degrees. The ice surface temperature on the November, 20 is about -12 degrees at 8 a.m. and - 7 degrees at 2 p.m. According to the design code for freezing resistance of hydraulic structures, the compressive strength of ice can be 1200 kPa when the average daily temperature is 15 degrees. If the static ice pressure is calculated directly referring the value, then F = 0.9 x 1200 x 0.4 x 0.38 = 164 kN, which is greater than the shear strength of the pile by 146 kN.

According to the analysis, the static ice pressure calculated according to the maximum ice thickness is larger than the design value of the shear strength of the pile. If the pile is designed according to the code, there should be no quality accident. The static ice pressure should be calculated less in the design of the bridge pile.

4. Conclusion

Piles in lakes in cold regions are affected by ice in operation. The main effects of ice on piles are vertical and horizontal. Pile damage caused by static ice pressure often occurs during the freezing period. Ice pressure during freezing period can reach 1250 kPa. If static ice pressure is calculated according to the design code for freezing resistance of hydraulic and hydraulic structures, when ice thickness is calculated by 0.8 times of maximum ice thickness, static ice pressure is 750 kPa, which can also meet the application requirements. The effect of ice on piles should be fully considered in design calculation so as to avoid similar quality accidents.

References

[1] Jialian Qi, Jinglong Pan, Yuguan Wang. Ice-damage analysis for structures standing in water in cold regions. Journal of Harbin University of C.E. & Architectures, 2002, 25(3): 45-48.

[2] Bomeng Xu. Analysis and calculation of ice-pressure in reservoir. Water Resources and Hydropower Engineering, 1985, 11(4): 16-21.

[3] JGJ94-2008. Technical Code for Building Pile Foundation.

[4] GB/T50662-2011. Code for Design of Freeze Resistance of Hydraulic Structures

ROAD CONSTRUCTION AND MAINTENANCE

Surface softening on gravel roads

Jaakko Nurmi
Planner
Destia Oy
Finland
jaakko.nurmi@destia.fi

Summary

This paper introduces the research about the phenomenon and mitigation measures of surface softening on gravel roads. Methods used were literature study, expert interviews and excursions to gravel roads. The surface weakening caused by thawing of frozen soil and road structures was excluded from this study. This paper is based on author's thesis research about surface softening on gravel roads.

Surface softening has become a common phenomenon on Finnish gravel roads as the weather conditions have become more favorable. Due to climate change, average temperature and precipitation are expected to continue rising especially in the northern latitudes and thus surface softening may be expected to become even more common. Typically the phenomenon takes place during the rainy periods of autumn, but even a short summer rain might cause gravel road's wearing course to turn soft if the traffic and the properties of the wearing course are adequate.

Other factors promoting the phenomena are e.g. malfunctions of drainage and certain parameters of wearing course material. Such aggregate properties are e.g. minerology, fines content and chloride content. However, when planning the repairs, the road's condition in its entirety should be considered. The problem might not be resolved only by renewing the wearing course, if additional causes for the problem lie in the subgrade, faulty drainage system or structures.

In the interview study interviewees pointed out that spring thaw weakening, surface softening, changed climate and limited maintenance budget cause greatest challenges in gravel road maintenance. It was hoped that more co-operation would take place between contractee and contractor in planning of maintenance. Setting the objective for planning was pointed out to be important, as the qualities expected for wearing course may be conflicting. It was admitted that there is a need for further development to increase the knowledge and know-how related to gravel road maintenance among both authorities and contractors.

Keywords: gravel roads, surface softening, soft gravel road surface, moisture related damage, gravel road maintenance, surface weakening, wearing course

1. Introduction

Each of the last three decades has been warmer than any decade since the mid-17th century. As a result of the climate change the atmosphere and oceans have become warmer. It has been estimated, that the 30-year sequence between 1983 to 2012 has been the warmest in 1400 years. The rise in average temperature from year 1880 to 2012 has been calculated to be 0.85 °C. Although the climate is expected to become warmer in the long run, annual average temperatures are still going to vary and thus also cause challenges to road maintenance. [1]

The most critical projected changes in Finland when considering gravel road surface softening are winter seasons becoming milder and previous snowfall raining as liquid water. This will result in the road surfaces staying moister and not frozen for a longer period of the year, which creates favorable conditions for surface softening to occur. Climate change is also expected to cause summers to become warmer, which increases the need for dust control on gravel roads. [2]

However, there seldom is only one reason for problems occurring in the wearing course. Often the problems are a result of joint effect of microclimate, wearing course properties and drainage malfunctions.

2. Backround

2.1 Gravel roads in Finland

Finnish gravel roads can be divided into two different groups. Built gravel roads usually have a clear layer structure, which consist of wearing course and base course. Additionally, there may also be sub base and filter course or geotextile. See fig. 1.

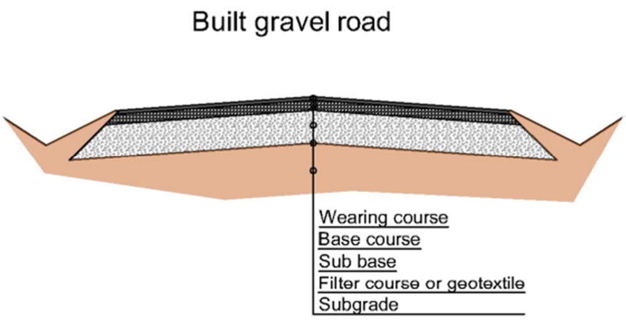

Fig. 1 Built gravel road

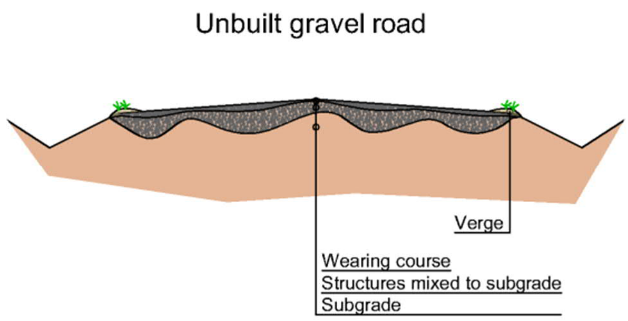

Fig. 2 Unbuilt gravel road.

However, most of the gravel roads in Finland are unbuilt, see fig 2. They have been formed by gradually widening old cart tracks and thus they lack proper structure.

In some cases the unbuilt gravel roads have only been maintained by spreading more graveling aggregate and thus the road has no other structures besides the wearing course. Wearing course may also have been mixed with the subgrade over time due to frost heave and traffic loading. In these cases the structure is usually thickest in the ruts whereas in the middle and on the sides it may be rather thin. Furthermore, sections suffering most of spring thaw weakening on unbuilt roads may have been repaired with structure containing geotextile, base course and wearing course, which results in varying structure conditions on same gravel road. [3, 4]

Year 2017 the total length of state-maintained roads in Finland was 77 993 kilometers. The length of state-maintained gravel roads was 27 245 kilometers, which means that 35 % of state roads were gravel roads. Total kilometreage on state roads was 38 299 million vehiclekilometers per year, of which 893 million vehiclekilometers (2,3 %) was on gravel roads. Throughout the 2010s the total kilometreage has grown while there has been decreasing trend on kilometreage on gravel roads. [5, 6]

Despite the low utilization rate, gravel roads have significant task in serving the Finnish society and business sector. It has been estimated, that as much as 60 % of industrial transports either depart or arrive to low volume roads. Typically, these roads are also the only links to and from rural areas and thus the mobility of people and goods, social equality and possibilities for development are dependent on the road and its condition. [7]

Since the beginning of 21st century dismantling the pavement and building a gravel or aggregate wearing course has been considered and option instead of repaving the road. This has been justified with the lower maintenance costs and increased driving comfort of wearing course when compared to poor conditioned pavement and on low volume roads. However, often the proposition to dismantle the poor conditioned pavement meets resistance. Paved road is considered an acquired right and a sign of higher standard of living. Often the residents living along a paved road about to be turned to a gravel road are concerned, that the condition of gravel road will be even worse than the current pavement, which is full of potholes and at the end of its lifecycle. The most common reasons to object turning paved road to a gravel road are breakage of vehicles due to potholes and loose gravel, and nuisance or harm to real properties and vehicles by dust and mud. [8]

3. Surface softening on gravel roads

3.1 Soil suction theory

The most important soil suctions affecting unbound aggregate's mechanical behaviour are matric suction, osmotic suction and cryo-suction, which is present in cold regions. Total suction consist of matric and osmotic suction and it reflects the energy needed to release the free water. Matric suction is mainly affected by material's porousness, size of the pores and fines content. Osmotic suction is dependent on the amount of ionic substances. Soil suction properties form powers between earth particles on porewater, and thus increase gravel road's wearing course's bearing capacity. As the water content of the material increases, the suction properties of the material weaken. Sufficiently high water content might lead to wearing course turning plastic under traffic load. [9, 10, 11]

High total suction increases the risk for surface softening. On the other hand low total suction might lead to loose wearing course and dusting problems. Dusting is usually prevented by adding salt to the road surface, which increases the osmotic suction and thus may increase the risk of surface softening during rainy periods. Tube Suction test (TS-test) may be used to evaluate aggregate's susceptibility to water. Test is conducted by compacting aggregate to a tube and placing it on water. TS-value is determined by measuring the dielectricity on top of the sample. TS-value depicts the suction properties of the sample. Aggregate classification based on TS-value is presented on table 1. [10, 11, 12]

Table 1. Estimation of wearing course material quality based on TS-value [4, 12].

Dielectricity value (TS-value)	Quality	Procedures
< 8	Total suction of the wearing course is too low. Risk is great for dusting and wearing course wearing out.	Increasing the fines content or salting should be considered to prevent dusting.
8−12	Lower limit for optimal value.	Fines content may be increased by gravelling if needed.
12−16	Upper limit for optimal value.	When planning gravelling attention should be paid to the fines content of wearing course and material added. Functionality of drainage (crossfalls, ditches) should be ensured.
> 16	Wearing course binds too much water. Probability of surface softening during rain is high.	Salt and fines content of the wearing course should be investigated to determine the cause of possible surface softening. Functionality of drainage (crossfalls, ditches) should be ensured.

Pylkkänen [13] investigated gravelling aggregate used on gravel roads suffering of surface softening in Vaasa area, Finland. It was found out that TS-value was over 16 on nine out of thirteen samples taken from stock piles of gravelling aggregate. Although TS-value was not measured from wearing course, it may be presumed that value would have been even higher. [13]

3.2 Mineralogy

Stone consist of chemical substances in crystalline form: minerals. Stone's mineral content effects on its strength and weathering properties. During temperature fluctuation minerals expand and shrink differently, which causes difference in erosion durability. Also mechanical stress from traffic causes material to pulverize on gravel road's wearing course. Stone strength is affected by the size of mineral grains and the way they are joined. Fine-grained, glasslike and dense stones are tougher than coarse-grained stones. Mineral strength consists of the size and charge of the atoms and lattice texture determined by these properties. [14]

Especially micaceous stone has been observed to be problematic and to pulverize on unbound layers so much, that material's grain size distribution has turned to more frost susceptible [14, 15]. This is due to the low abrasion resistance of aggregates containing mica. Pylkkänen found that graveling aggregate used on roads suffering of surface softening typically contained mica mineral biotite more than 10 %.

Miskovsky et al. [16] studied the effect of mineral consistency and structure of Swedish granitoids to aggregate quality. It was found that increase in quarts and feldspar content rose the resistance towards abrasion of the aggregate. There also seemed to be a slight indication that increase in mica content would decrease the abrasion resistance. [16]

4. Interview study

To survey problems and development needs in gravel road maintenance an interview study consisting of ten oral interviews was conducted. Nine people were interviewed individually and two people as a pair. Three supplementary written answers were also received. Selection of the interviewees aimed to include viewpoint of contractees, contractors and researchers. Interviews were conducted as semi-structured. Questions were sent to the interviewees in beforehand, and target was on the questions corresponding each interviewee's core knowledge. Interviews were recorded, and then essential parts were transcribed.

Interviewees' emphases varied somewhat, but all of them mentioned one or more of the following to be the greatest challenge in gravel road maintenance: spring thaw weakening, autumntime surface softening, changed climate and low budget in road maintenance. Ensuring the functionality of the drainage system on the whole was considered to be most important in planning and executing gravel road maintenance.

4.1 Climate change

All the interviewees mentioned climate to have changed during their career or at least having heard of the changes from older colleagues. Autumntime surface softening on gravel roads was mentioned to be one of the most visible changes. The phenomenon was considered to be relatively new in Finland and to have become common during the last 15 years. Conditions for surface softening have become more favorable as greater part of previous snowfall rains as water and also the beginning of winter has delayed. Conditions are also more favorable for spring thaw weakening, as rains raise the groundwater table already during autumn. Also the beginning of winter has started to happen stepwise which makes it challenging to estimate the final freezing of the wearing course. Thus, there's a possibility that the wearing course will be left uneven for the entire winter, if the last levelling isn't scheduled correctly.

Another change has been prolonged droughts during summer times, which causes dusting problems. Spring time levelling has to wait until the wearing course dries after winter. But if the wearing course gets too dry and no rain is expected, levelling cannot be done at all as it would result a loose and dusting wearing course. Thus, climate change increases the importance of situation awareness and rapid capacity to act in maintenance of gravel roads.

4.2 Surface softening on gravel roads during autumntime

Surface softening during autumn and early winter was mentioned to take place regularly at least in Southern and Central Finland, Häme, Savonia and Southern Ostrobothnia. Unbuilt gravel roads on subgrades with low permeability such as clay grounds are most susceptible towards surface softening. Surface thaw weakening during spring was also acknowledged to be common, but less harmful due to usually appearing for only couple of days or weeks. Some of the interviewees characterized autumntime surface softening as a persistent nuisance which is almost impossible to prevent.

The phenomenon was told to be tedious as there is little to be done during the time of occurrence. Spreading more coarse gravel on the road offers a temporary solution but might bring up problems elsewhere as the amount of gravel to be spread is fixed per year. The only resolution for the problem was reckoned to be freezing of the wearing course, as warm and sunny weather needed for the drying of the wearing course is usually absent during autumn and winter. Thus phenomenon should be prevented proactively, such as optimized gravelling and levelling and profiling of gravel road during spring and early fall, while the wearing course is still in decent condition and not too dry or soft.

The most common causes for surface softening were mentioned to be weak quality of graveling material and deficiencies on crossfalls. Also heavy traffic was reckoned to effect on the severity of surface weakening. No new means to prohibit the phenomenon that wouldn't have been introduced in instructions and researches already came up in the interviews. Instead a question arose whether everything is really done to fix the situation in comparison to resources available.

It was found problematic, that origin or technical properties of the gravelling aggregate spread cannot be easily investigated. In order to learn from procedures done on gravel roads, better exploitation of documentation was pointed out to be vital. Currently documentation is done for quality control purposes of the moment, but usually data is forgotten after that. At worst cases this has lead to a state in which same mistakes are repeated as no learning is happening.

4.3 Gravelling procedure and aggregates

Most of the interviewees mentioned, that optimization of gravelling aggregate to existing wearing course should be promoted. However, there was uncertainty about the basis of optimization as demanded material properties for preventing surface softening and dusting are somewhat conflicting. Dust prevention by salting was reckoned to be relatively easy and cost-effective, which would support prioritizing prevention of surface softening when choosing gravelling aggregate. Dusting wasn't either considered to cause danger to traffic unlike softened and slippery wearing course.

There was variation among interviewees about suitable properties for gravelling aggregate. Especially contractors considered the minimum demand of 8 % for fines content to be too high. Some of the contractees and researchers were worried that the aggregate being spread doesn't meet the requirements and is too coarse. Both contractors and contractees hoped, that planning of gravelling would happen more in co-operation between both parties.

Currently gravelling and levelling is done both on spring and autumn. It was mentioned, that shaping the wearing course while its softened during autumn might make the situation even worse. Thus it was suggested, that gravelling and levelling work on roads suffering of surface softening should be considered to be done in spring just after thaw has properly melted. However, in order to do this successfully information of the roads suffering of surface softening would be needed. Also the real cause for the surface softening should be identified in order to allocate the repair measures correctly.

Contractees pointed out that there is a great variation in execution of gravelling between different contractors. Some do the levelling and gravelling exactly as it is instructed in the contract documents. However, it was stated that most contractors choose the aggregate purely based on the price and transport distance. This aggregate was described to be typically coarser than instructed and being spread without breaking the wearing course, which leads to significant spoilage as the aggregate rolls off the hard surface. It was told, that the required levelling before gravelling is done rarely and the wearing course is compacted even more seldom. This was believed to be because of lack of understanding for the importance of these procedures. It was also reckoned, that the condition of gravel roads is often perceived as irrelevant which leads to lower quality of work.

Insufficient funding was mentioned to have increased repair deficit on gravel road network. Especially harmful effects were told to be decrease in ditch drainage maintenance and gravelling. Thinning of wearing courses raised concern. Too thin wearing course cannot be levelled as the blade would pick stones from structure or sub base.

5. Excursions to gravel roads

5.1 Backround

Excursions to gravel roads were made to observe autumntime surface softening. Gravel roads in Nokia area were selected as destinations, as they are well known to suffer of surface softening during autumn. Surface softening was detected for the first time on most of the Tottijärvi and Vesilahti areas' gravel roads during autumn 2005. Feedback of softened road surfaces from road users started coming already on autumn 2004. In research carried out later on it was found that the cause for the phenomenon lied in poor quality gravelling aggregate, which contained plenty of mica mineral biotite.

Test structures were constructed on road 12995 (Hautaantie) to investigate a solution for the problem:

- reshaping the road surface and opening the ditches,
- replacing the old wearing course with good quality crushed aggregate,
- gravelling with crushed gravel and
- gravelling with crushed aggregate (macadam, without fines).

In this case the best option was found out to be peeling off the old wearing course and replacing it with good quality crushed aggregate [17]. Most of the gravel roads in Nokia were repaired in autumn 2018 by either replacing the wearing course or levelling the wearing course to correct profile depending on the severity of surface softening.

5.2 First excursion September 2, 2018

The first excursion was done in the beginning of September to observe the gravel roads while surface softening and reparations were not yet expected to take place. Roads visited were road 2501 (Sarkolantie ja Kutalantie) ja road 12995 (Hautaantie). Precipitation of 0.3 mm had been measured the previous day [18]. In open areas the gravel road surfaces were dry, and dusting took place. In forested areas road surfaces were a bit moister, but not softened. On Kutalantie it was observed, that narrow sections of the gravel road were in better condition compared to wider sections. On wide sections the road profile had flattened to almost concave form and ruts had formed to vehicle paths.

Fig. 3 On the left unrepaired section on road 12995 (Hautaantie) on September 2, 2018. On the right renewed wearing course on road 12995 (Hautaantie) September 2, 2018.

On road 12995 the unrepaired sections of wearing course (fig. 3, left) seemed soft and loose compared to the repaired section’s new wearing course, which was smooth and dense (fig. 3, right).

5.3 Second excursion October 5, 2018

Second excursion was done to road 13765 (Jokivarrentie) and road 2991 (Härkäläntie), which were being repaired during the time of excursion. For comparison road 12995 (Hautaantie) was visited. On roads 13765 and 2991 the micaceous wearing course was yet untouched. Precipitation of 3.0 mm and 2.2 mm had been measured for previous day and excursion day respectively. There had been three days of dry weather before the rainy days. [18]

Fig. 4 On the left minor surface softening on road 2991 (Härkäläntie). On the right softened wearing course on road 13765 (Jokivarrentie).

On both roads 13765 and 2991 the wearing course had softened due to traffic load and rainfall (fig. 4). The road surfaces had softened also on the sections with crossfalls sufficient for drainage to function properly. The machinery used for the repair work may have had some effect for the softening. The wearing course had softened to the depth of couple centimeters and it felt slippery while driving, even though the precipitation of previous days was only 5 mm.

Fig. 5 Road 12995 (Hautaantie). On the left dense wearing course on the repaired section. On the right softened wearing course on the unrepaired section.

On road 12995 the wearing course on the repaired section was in good condition (fig. 5, left). On the unrepaired section the wearing course had softened (fig. 5, right). There had not been repair work taking place on the road, so the softening had happened due to regular traffic and precipitation. There were deficiencies on the crossfalls on the softened sections of the road.

5.4 Third excursion November 2, 2018

Third excursion was done to roads 13765 (Jokivarrentie) and 12995 (Hautaantie). At this point the wearing course on road 13765 had been replaced. The intention was to observe the functionality of the new wearing course and check if surface softening had become worse on road 12995. There had been a rainless period between October 26 till 29 and from October 30 to November 2 the precipitation had been 2.8 mm, of which 1.6 mm rained during the excursion day.

Fig. 6 On the left new wearing course on road 13765 (Jokivarrentie). On the right unrepaired wearing course on road 12995 (Hautaantie).

It was observed, that on road 13765 the new wearing course performed better than the old one (compare fig. 6 left and fig. 4 right). It was dense and even and didn’t feel slippery while driving. On road 12995 surface softening was not significantly worse or better than during second excursion (compare compare fig. 6 right and fig. 5 right). On the repaired section of road 12995 there was no softening.

6. Discussion and conclusions

Surface softening has become common on Finnish gravel roads since the beginning of 21st century. Most common causes for surface softening are poor quality gravelling aggregate and lacks in roads surface drainage. During the excursions an observation was made, that even minor rainfall can cause surface softening, if the quality of the wearing course is weak.

Gravelling aggregate’s susceptibility to surface softening can be estimated for example by measuring fines content, mineral consistency, TS-value or chlorinity. In addition to properties mentioned before water is also needed for surface softening. Due to climate change greater par of the previous snowfall is expected to rain as liquid water. As it is impossible to control the weather for the time being, the focus should be on proactive prevention of surface softening by optimized selection of the gravelling aggregate and ensuring the surface drainage of the road. Too small crossfalls often lead to surface softening and forming of potholes soon after levelling. Verges (fig. 2) are also especially harmful, as they prevent rainwater from flowing to the ditches. To support the proactive prevention of the phenomenon, the information of gravel roads suffering of surface softening is needed. One way to acquire this information is by the means of crowdsourced data collection by for example installing measurement devices to third party vehicles, which drive the same routes regularly. In the interviews it was found out that digitalization is hoped to offer possibilities for planning of maintenance and learning from effects the work done.

Interviewees stated that climate change has brought also other challenges to gravel road maintenance. These include for example stepwise beginning of winter and other weather phenomena which are hard to project, such as droughts. Also the meager funding and varying structural condition of grave roads was considered to make planning of gravel road maintenance challenging. The new contract model introduced fall 2018 was hoped to offer better chances to improve and increase co-operation between contractors and contractees. It might turn out to fruitful to investigate and report the practical changes brought by the new model after couple of years.

Some of the interviewees were worried about the state of the knowledge and know-how related to gravel road maintenance. Guidelines, education and guided introductions are significant ways to promote knowledge. Currently there is guidelines available rather comprehensively. However, it is hard to estimate how well parties working on road maintenance have found and gotten themselves familiar with these guidelines. Thus while writing the guidelines the target audience should be considered in its entirety. Sessions of education and guided introductions are ways more independent of individual’s interest to self-learning to increase the knowledge and know-how among people working on gravel road maintenance.

References

[1] RUOSTEENOJA K., ”Ilmastonmuutos v. 2013: Luonnontieteellinen perusta. Yhteenveto päätöksentekijöille suomeksi”, *Intergovernmental Panel on Climate Change (IPCC) Ilmatieteen laitos*, 2014. Available: https://ilmatieteenlaitos.fi/documents/30106/42362/ipcc5-yhteenveto-suomennos.pdf/4332dffb-da72-41c9-a23d-24215c5cbbac.

[2] RUOTOISTENMÄKI A., VALKEISENMÄKI A., VENÄLÄINEN A., MÄKELÄ O., SIPILÄ J., JYLHÄ K., SAVOLAINEN S. and LAAPAS M., ”Ilmastonmuutoksen vaikutus tiestön hoitoon ja ylläpitoon”, *Tiehallinnon Selvityksiä 8/2009*, Tiehallinto, Helsinki, 2009, pp 80. Available: https://julkaisut.liikennevirasto.fi/pdf2/3201122-v-ilmastonmuutoksen_vaikutus_kunnossapitoon.pdf.

[3] THE ROADEX NETWORK, “Suunnittelu pysyviä muodonmuutoksia vastaan”, *The ROADEX Network webpage*, 2007. Available: https://www.roadex.org/fi/e-learning/kurssit/pysyvat-muodonmuutokset/7-suunnittelu-pysyvia-muodonmuutoksia-vastaan/.

[4] LIIKENNEVIRASTO, ”Sorateiden kunnossapito”, *Liikenneviraston Ohjeita 1/2014*, Liikennevirasto, Helsinki, 2014. Available: https://julkaisut.liikennevirasto.fi/pdf8/lo_2014-01_sorateiden_kunnossapito_web.pdf.

[5] LIIKENNEVIRASTO, ”Tietilasto 2009”, *Liikenneviraston tilastoja 2 2010*, Liikennevirasto, Helsinki, 2010. Available: https://julkaisut.liikennevirasto.fi/pdf3/lti_2010-02_tietilasto.pdf.

[6] LIIKENNEVIRASTO, ”Tietilasto 2017”, *Liikenneviraston tilastoja 5/2018*, Liikennevirasto, Helsinki, 2018. Available: https://julkaisut.liikennevirasto.fi/pdf8/lti_2018-05_tietilasto_web.pdf.

[7] PERÄLÄ, M., VALKEISENMÄKI, A., WECKSTRÖM, L. and PENTTINEN, O., ”S 14 Vähäliikenteisten teiden taloudellinen ylläpito Yhteenveto”, *Tiehallinnon Selvityksiä*, Tiehallinto 2006.

[8] MERILÄINEN, A. and RUONAKOSKI, A., ”Soratieksi palauttamisen vaikutukset tienpitäjän ja tienkäyttäjän näkökulmista”, *Tiehallinnon Selvityksiä 39/2007*, Tiehallinto, Kuopio, 2007. Saatavissa: https://www.doria.fi/bitstream/handle/10024/139382/4584tie.pdf?sequence=1&isAllowed=y.

[9] FREDLUND, D.G. and RAHARDJO, H., *“Soil mechanics for unsaturated soils”*, John Wiley & Sons, New York, 1993.

[10] SAARENKETO, T. and AHO, S., “Managing spring thaw weakening on low volume roads. Problem description, load restriction policies, monitoring and rehabilitation”, *Roadex Publications*, 2005. Available: http://www.roadex.org/wp-content/uploads/2014/01/2_3-Spring_Thaw_Weakening_l.pdf.

[11] PYLKKÄNEN, K. and NURMIKOLU, A., ”Routa ja routiminen ratarakenteessa”, *Liikenneviraston tutkimuksia ja selvityksiä 22/2015*, Liikennevirasto, Helsinki, 2015. Available: https://julkaisut.liikennevirasto.fi/pdf8/lts_2015-22_routa_routiminen_web.pdf.

[12] SAARENKETO, T., ”Tube suction test: sitomattomilla murskeilla suoritettujen rengastestien tulokset”, *Tielaitoksen Selvityksiä 20/2000*, Tielaitos, Rovaniemi, 2000. Saatavissa: http://www.doria.fi/bitstream/handle/10024/138942/4142tie.pdf?sequence=1&isAllowed=y.

[13] PYLKKÄNEN, K., ”*Vaasan tiepiirin pintakelirikkoiset soratiet*”, Tampereen teknillinen yliopisto, Tampere, 2008. Available: https://julkaisut.liikennevirasto.fi/pdf2/3201092-v-pintakelirikkoselvitys.pdf.

[14] KAURANNE, L.K., GARDEMEISTER, R., KORPELA, K. and MÄLKKI, E., ”*Rakennusgeologia II*, *Toinen korjattu painos”,* Otakustantamo, Espoo, 1972.

[15] YLIHEIKKILÄ, T., ”Kemiallisen koostumuksen vaikutus murskeiden vedenherkkyyteen”, *Tielaitoksen Tutkimuksia*, Tielaitos, Oulu, 1998.

[16] MISKOVSKY, K., DUARTE, M.T., KOU, S.Q. and LINDQVIST, P., “Influence of the mineralogical composition and textural properties on the quality of coarse aggregates”, *Journal of Materials Engineering and Performance, Vol. 13(2)*, 2004, pp. 144-150.

[17] VALKONEN, A., telephone interview 3rd of August 2018.

[18] ILMATIETEEN LAITOS, ”Paikallissää. Havaintojen lataus”, *Ilmatieteen laitos, webpage,* available: https://ilmatieteenlaitos.fi/havaintojen-lataus#!/.

Development of sustainable binder for concreting in the arctic region

Katja Ohenoja
D.Sc., Postdoctoral researcher
Fibre and particle engineering research unit
University of Oulu
Finland
katja.ohenoja@oulu.fi

MSc. Hoang Nguyen, MSc. Jouni Rissanen, MSc. Elijah Adesanya, PhD Paivo Kinnunen & Prof. Mirja Illikainen, University of Oulu, Fibre and Particle Engineering research unit, Finland

Summary

New ways to utilize industrials residues from the arctic area and to reduce CO_2 emissions of winter concreting are needed. In this paper, we will give an overview to some of our recent findings in the field. We have studied alternative cementitious materials and their durability in freeze-thaw test. These alternative materials are ladle slag (LS), phosphogypsum, bottom ash from municipal solid waste incineration, and biomass fly ash from energy industry. Our results show that it is possible to produce durable 100% eco-mortar from industrial residues from northern area.

Keywords: cement replacement, frost resistance, freeze-thaw, green concrete, sustainable concrete

1. Introduction

The construction industry is a major industry in the arctic and sub-arctic region, and it is a leading player to accelerate economic growth in those regions. A prerequisite for successful utilization of rich natural resources at arctic region (metal ores, oil, gas, energy and forest) is evidently infrastructure development: the road network, railways, harbors, and energy systems have to be constructed and this should be done in a sustainable manner. On the other hand, already existing mining, metal and energy industries generate large amounts of inorganic solid residues such as mine tailings, slags and ashes. These residues are currently mostly disposed of even if they could be partially used as a raw material for construction materials. Construction industry has challenges at arctic region when taking into account the long period of cold weather and long transport distances. In the arctic and sub-arctic areas, extreme cases with temperatures below -25°C combined with long transportation distances from concrete plant to casting site puts additional demands to the normal winter concreting. The most commonly used method for casting at subzero temperatures needs electrical current, warm water, or building up heated tents surrounding the structure. All of these techniques are energy intensive and they lead to increased CO_2 emissions. Therefore, new ways to utilize industrials residues from the arctic area and reduce CO_2 emissions of winter concreting are needed. We have studied alternative cementitious materials and their durability in freeze-thaw test. These alternative materials are ladle slag (LS), which is an under-utilized slag from steel manufacturing process (2,7 Mt/a in EU) [1]. In this work we present the results about hydration of ladle slag with and without gypsum (G) and the freeze-thaw durability of these samples. We also studied bottom ash from municipal solid waste incineration (MSWI) as an aggregate in LSG system. Also other northern industrial side streams, fly ashes from peat and wood combustion [2,3] were studied as a partial cement replacement materials.

2. Materials and methods

2.1 Materials

Ladle slag (LS) used was supplied by SSAB Europe Oy (Raahe Finland). To increase reactivity, the as-received slag was milled below 10 μm using a ball mill for 2 hrs with a ball filling ratio of 60%. Commercial grade gypsum (G) (VWR, Finland) was used as a co-binder with the slag to produce an ettringite system. Sand used in mortars was CEN Standard sand (CEN-Standard Sand, Normensand GmbH). Municipal solid waste incineration (MSWI) bottom ash (MSWIBA) used as aggregates was supplied by Suomen Erityisjäte. Citric acid (product code C1949 by Tokyo Chemical Industry Co., Ltd., Japan) was employed as a retarder for the reaction between LS and G. A melamine-based chemical (commercial name: Melment F10 provided by BASF, Germany) was used as superplasticizer. Polypropylene fibers (provided by Saint Gobain Brasil with some following physical and mechanical properties: length 12 mm, diameter 12 μm, Young's modulus 9 GPa, and tensile strength 910 MPa) were employed as fibrous reinforcement, and a sodium polymethacrylate agent named Darvan 7-N (supplied by Vanderbilt, USA) was employed as fiber dispersing agent. The dose of Melment F10 and Darvan 7-N were 0.5% and 1%, respectively, by weight of total binder mass.

Two different fly ashes were used. Fluidized bed combustion fly ash (FBCFA) used in this study originated from circular fluidized bed combustion of peat and wood. Conventional coal fly ash (CFA) fulfilling standard EN 450-1 originating from pulverized combustion of coal was used. Cement used in this study was sulfate resistant Portland cement, type: CEM I 42,5 N -3R (SR-sementti, Finnsementti). Sand used in mortars was CEN Standard sand (CEN-Standard Sand, Normensand GmbH). Super plasticizer (SP) used in mortars was polycarboxylate based (SemFlow ELE 20). The chemical composition of the starting materials is shown in Table 1.

Table 1. The chemical composition of the starting materials in wt.%.

	CaO	SiO_2	Al_2O_3	Fe_2O_3	MgO	SO_3	Others
LS	51.0	8.3	27.9	1.1	6.3	0.8	4.6
Gypsum	41.4	1.0	0.1	0.1	0.5	53.8	3.1
MSWIBA	16.7	39.5	11.4	12.8	2.2	2.6	14.8
FBCFA	12.0	30.8	15.1	26.7	2.5	3.5	9.4
CFA	4.2	54.8	20.9	7.2	1.9	0.4	10.6

2. Methods

2.1 Mix design

The mix design for samples (4x4x16cm) was done by first blending the dry materials together in a Kenwood mixer for 1min and then de-ionized water was added to mix. The subsequent mixing followed mostly EN-196-1 standard. The preparation of PP-LSG sample was detailed in [4]. It is worth noting that it usually took 20–25 minutes to complete the mixing process for one batch of PP-fibre mortar. The mix designs are described in Table 2.

Table 2. Mix proportions of the eco-mortars [in grams] studied in this work.

Sample id	Slag	Gypsum	Cement	Fly ash	Sand	MSWIBA	Fiber volume fraction [%]	w/b
LSG	630	270	-	-	900	-	-	0.45
MSWIBA-LSG	630	270	-	-	-	900	-	0.45
PP-LSG	630	270	-	-	900	-	2	0.45
Ref. OPC	-	-	450	-	1350	-	-	0.45
20% FBCFA	-	-	360	90	1350	-	-	0.45
20% CFA	-	-	360	90	1350	-	-	0.45

*W/B is water-to-binder ratio

2.2 Methods

The mechanical performance of samples were assessed after 28 d of curing and different aging cycles by uniaxial compressive loading, conducted by a Zwick device (load cell of maximum 100 kN). The compressive strength was measured by loading halves of the prismatic bending specimens with loading speed of 2.4 kN/s according to EN 196-1.

Different artificial aging procedures were conducted in a climatic chamber Weiss WK3-180/40 (Germany) for 28 days cured samples. LSG-MSWIBA was exposed to temperature change ranging between -18 °C to +20°C according to PD CEN/TS 12390-9:2016 standard. Each cycle consist of mortars exposure to -18 °C for 13 h and 3 h at +20 °C. The transitions from plus to minus and vice-versa took 3h and 5h. The specimens were submitted to 50 freeze-thaw (F-T) cycles. LSG and fly ash mortars were exposed to freeze-thaw cycles according to modified ASTM standard C-666. After the mortars were cured 28 days, they were put in small plastic boxes (three prisms per box) and water was added to the box so that mortars were half immersed in water during the experiment. Each cycle consist of mortars exposure to -18 °C for 2 h and 2 h at +15 °C. The transitions from plus to minus and vice-versa took 2h. For LSG and PP-LSG the duration of aging process was approximately 2 months with approximately 180 cycles. The cycles were divided into 90 'cold' and 90 'warm' cycles, and changed every 45 cycles. In the 'cold' cycle, the temperature ranged from 5° to -20°C, while in the 'warm' cycle, the temperature varied from 10° to 30°C. It is worth noting that the aging scheme was designed to simulate the climate of cold regions based on the actual temperature recorded in Oulu (Finland) in 10 year from 2008 to 2018. One single cycle lasted for 8 h. Specimens were fully covered by curing solution, which is a combination of sodium chloride and sodium sulfate (SL), or just water (W). Both LSG and PP-LSG were aged by SL based on [5].

The environmental leaching test for LSG-MSWIBA mortars after 28 days of curing was done according to SFS-EN 12457-2. The samples were crushed to particle sizes below 4mm before leaching test. The leached values were then compared with earth construction act 843/2017.

3. Results

3.1 Ladle slag-gypsum binder

LSG shows a very good freeze-thaw resistance after 300 cycles (see Fig 1). After 300 cycles of freeze-thaw, LSG still attained a good residual compressive strength (i.e., 30 MPa). Interestingly, the residual compressive strength of LSG after 120 cycles increased by roughly 25% in comparison to the sample before aging. This is probably due to some further reactions in the ettringite system that led to the formation of some new hydrated products. After 120 freeze-thaw cycles, the compressive strength of LSG decreased slightly, but still obtained approximately 30 MPa compressive strength.

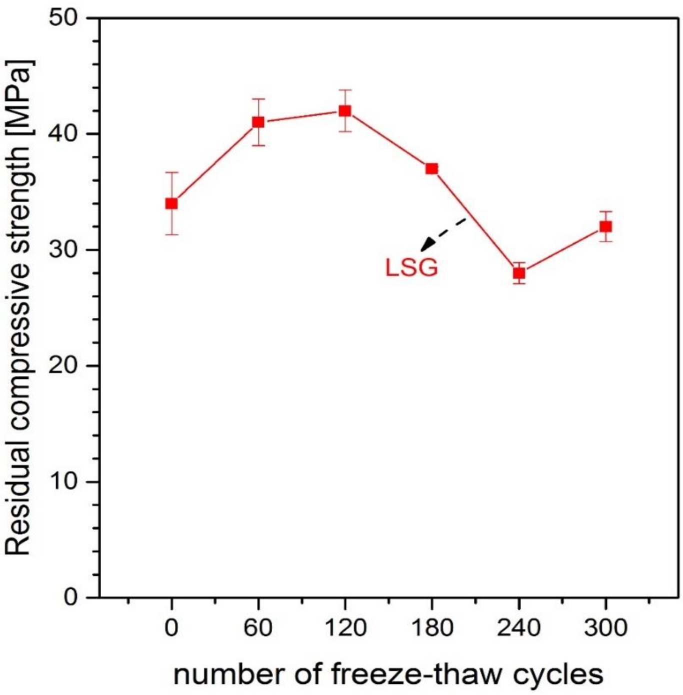

Fig 1. Residual compressive strength of HLS and LSG mortars after freeze-thaw cycles.

3.2 Ladle slag-gypsum and MSWI bottom ash eco-mortar

In this section the aim is to study 100% eco-mortar in which LSG is used as a binder and MSWI bottom ash as an aggregate. Before freeze-thaw test, the mortars average compressive strength was determined to be approximately 13 MPa (see Fig 2). In the first 20 cycles, the mortars experienced reduction strength caused by the initial induction of temperature variations on the internal structure of the mortars. However, at 30 cycles the strength significantly increased peaking at 14 MPa, more than the reference sample. This is attributed to the further formations of ettringite in moist environment as for pure LSG too. However, the last 20 cycles had an effect on the residual strength, experiencing an overall 23% loss at the end of the experiment compared with the reference sample. Still after 50 cycles residual strength was 8 MPa. Therefore this eco-mortar could be used for example in earth construction. We measured also the environmental leaching of crushed mortar (<4mm) and it fulfilled limit in Finnish earth construction act (843/2017).

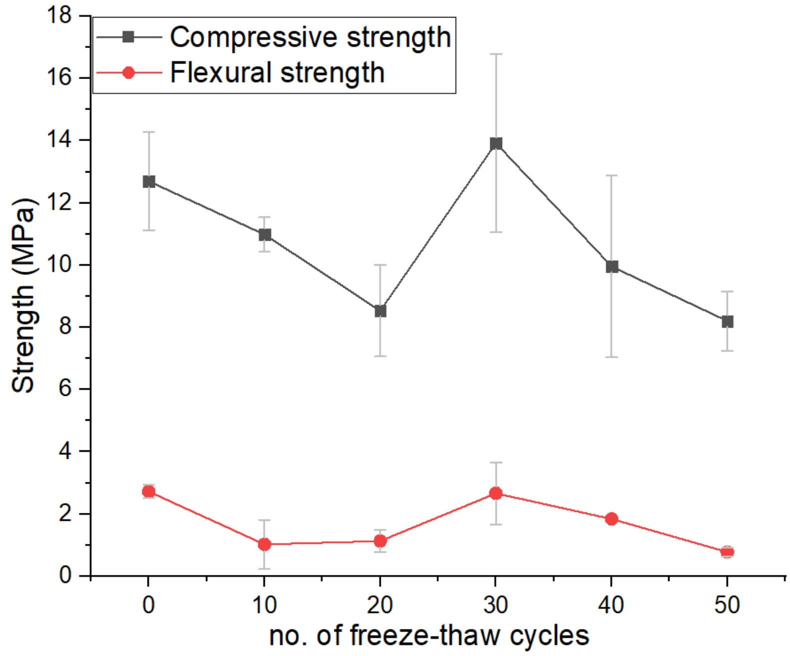

Fig 2. Residual compressive strength of MSWIBA-LSG mortar after freeze-thaw cycles.

3.3 Fiber-reinforced ladle slag-gypsum cement under physical and combined physical-chemical attack

In this section, the aim was to reinforce LSG binders with fibres, and to study freeze-thaw durability of these mortars in salt water (SL). PP-LSG in SL gradually decreased the compressive strength, while the reference LSG was completely spoiled after the aging, as shown in the Fig 3. The composite slightly reduced the compressive strength by roughly 11% after 180 freeze-thaw cycles. PP fibers seemed to delay the crack propagation under the attacks and led a slow diffusion of sulfate and chloride ions. As a consequence, only a slight decrease in the compressive strength of PP-LSG in SL was recorded. In contrast, the unreinforced LSG suffered the combined physical and chemical attacks leading to a negligible strength after only 90 freeze-thaw cycles. This result highlighted the important role of PP fibers in retaining the mechanical properties and leading to a good durability under such harsh conditions.

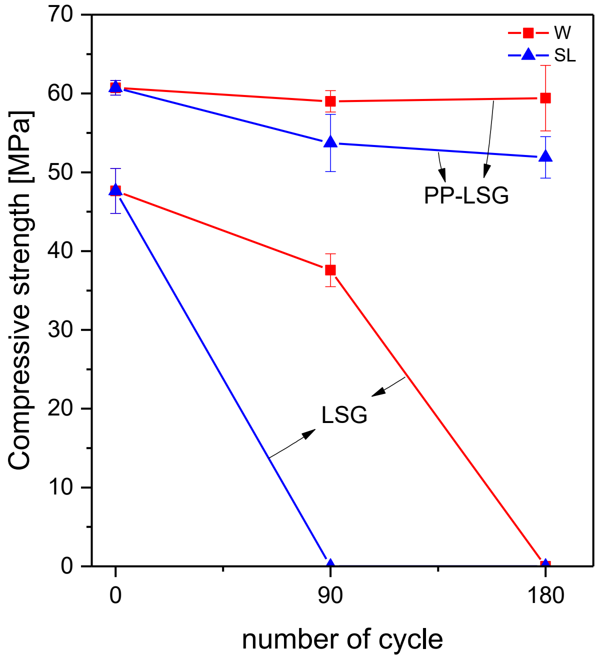

Fig 3. Compressive strength of LSG and PP-LSG in W and SL after 90 and 180 freeze-thaw cycles in comparison to its initial state.

PP-LSG in W still obtained very good residual compressive strength, while the composite in SL reduce its compressive strength slightly after 2 months of aging. Fig 3 shows the compressive strength of materials in different aging periods and environments compared to its initial state. The composite kept its compressive strength around 60 MPa after 2-month aging in W. In contrast, in SL, the composite decreased the compressive strength by roughly 11% after the same aging period. In this investigation, the freeze-thaw cycles might accelerate the chemical attacks attributed to the presence of Cl^- and SO_4^{2-} ions in the solution, and thus the residual compressive strength of PP-LSG slightly dropped. On the other hand, the main attacking mechanism of PP-LSG in W is physical factor, in which the water uptake in the developed composite expanded under freeze-thaw cycles and eventually caused volume expansion. The PP fibers, in both cases, play a very important role in terms of controlling the crack propagation and hence delaying the degradation of PP-LSG.

The plain LSG was attacked by both physical and chemical factors and degraded after 180 cycles. The residual compressive strength of LSG in W was approximately 82% after 90 cycles and completely spoiled after 180 cycles. Under the harsh marine conditions of SL, the plain LSG degraded after 1 month of aging due to some chemical reactions between ions in SL and LSG. These results confirmed the vital role of PP fiber reinforcement in terms of improving the durability of ettringite-based binder under such very aggressive conditions.

3.4 Fly ashes as a partial cement replacement

In this section the aim was to study eco-mortars in which cement was partially replaced with fly ash. Mortar containing 20% FBCFA had similar compressive strength compared to reference (see Fig 4). This result suggest that FBCFA produced hydration products which had positive impact on compressive strength. In the case of CFA, pozzolanic reactions were probably slower, which could explain lower compressive strength of 20% CFA mortar. In freeze-thaw test 20% CFA mortar suffered severe damage during the experiment and compressive strength could not be determined after 90 cycles. Reference and 20% FBCFA mortar suffered well: their freeze-thaw resistance was 83-90%.

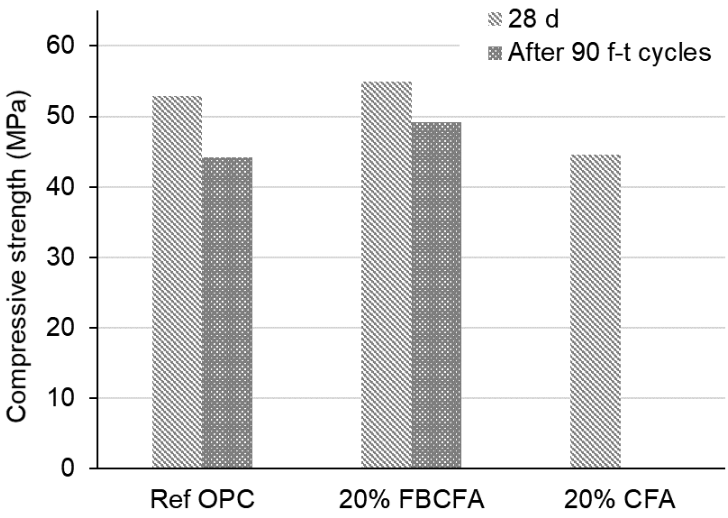

Fig 4. 28 d and residual compressive strength of mortars containing fly ashes before and after freeze-thaw cycles.

4. Conclusions

We presented here promising eco-mortars and their freeze-thaw durability. Ladle slag-gypsum binder is promising eco-binder to be used in harsh conditions. It has superb durability in freeze-thaw tests: at the beginning it actually gain more strength due to more reactions in a water. The residual compressive strength after 300 cycles was almost the same with the un-cycled materials. If mortar is exposed even more harsh conditions (salt water and frost) fibres can be used to increase the durability. Mortars, in which 20% of cement was replaced with biomass fly ash from fluidized bed combustion had similar compressive strengths compared to reference mortars after 28 d curing. Mortars containing conventional fly ash from pulverized coal combustion had slightly lower compressive strengths. FBCFA mortar had good freeze-thaw resistance, which was even slightly better compared to reference specimen, whereas mortar, containing conventional CFA, suffered from severe damage during the experiment.

References

[1] ADESANYA E., OHENOJA K., KINNUNEN P., and ILLIKAINEN M., “Alkali Activation of Ladle Slag from Steel-Making Process”. Journal of Sustainable Metallurgy, 2017; Vol. 3, pp. 300–10.
[2] OHENOJA K., WIGREN V., ÖSTERBACKA J., and ILLIKAINEN M., “Applicability of Fly Ash from Fluidized Bed Combustion of Peat, Wood, or Wastes to Concrete”, Waste Biomass Valorization, 2018, pp. 1–10.
[3] RISSANEN J., OHENOJA K., KINNUNEN P., and ILLIKAINEN M., “Partial Replacement of Portland-Composite Cement by Fluidized Bed Combustion Fly Ash”, Journal of Materials in Civil Engineering, 2017, Vol. 29.
[4] NGUYEN H., KINNUNEN P., CARVELLI V., MASTALI M., and ILLIKAINEN M., “Strain hardening polypropylene fiber reinforced composite from hydrated ladle slag and gypsum”, Composites Part B Engineering, 2019; Vol. 158, pp. 328–338.
[5] LIU H., ZHANG Q., LI V., SU H., and GU C., “Durability study on engineered cementitious composites (ECC) under sulfate and chloride environment”, Construction and Building Materials, 2017; Vol. 133, pp. 171–181.
[6] ADESANYA” E., SREENIVASAN H., KANTOLA A.M., TELKKI V.-V., OHENOJA K., KINNUNEN P., and ILLIKAINEN M., ”Ladle slag cement – Characterization of hydration and conversion”, Construction and Building Materials, 2018; Vol. 193, pp. 128–134.

Formation Mechanism of Spontaneous Corrugation on Road Surface due to Moving Vehicles

Shunji Kanie, Dr.
Professor
Faculty of Engineering, Hokkaido University
Japan
kanie@eng.hokudai.ac.jp

Hao Zheng, Dr., Hokkaido University, Japan
Aiko Ikeda, Graduate School of Engineering, Hokkaido University, Japan
Kai Hashimoto, Graduate School of Engineering, Hokkaido University, Japan

Summary

Washboard road on snowy-icy road in Hokkaido is a well-known phenomenon. It spontaneously appears several times a year due to moving vehicles. However, the formation mechanism has not yet been verified physically and mathematically. The authors developed their original experimental apparatus to reproduce the spontaneous corrugation on dry-sand condition in laboratory, and report their findings through the experiments as well as their proposal of a numerical model.

Keywords: Spontaneous corrugation, Sand surface, Moving vehicle, Formation, Mechanism, Indoor experiment, Numerical model

1. Introduction

In winter Hokkaido, appearance of washboard road on snowy-icy road is broadly known as a mysterious phenomenon. It spontaneously emerges on snowy-icy road several times a year due to moving vehicles, and it endangers motor drivers and pedestrians because of lack of friction between road surface and tires. Fig. 1 (a) shows a typical example of washboard road on snowy-icy road observed in Hokkaido. However, the formation mechanism has not yet been verified physically and mathematically as well as the formation process. Therefore, it is almost impossible to predict the occurrence and to apply some effective countermeasures for prevention. In order to establish a maintenance technology for washboard road, the authors are investigating this phenomenon with an indoor reproduction experiment [1] and field observation by time-lapse cameras [2]. This paper aims to introduce the results of indoor experiments with a simple numerical model to understand the fundamental mechanism of spontaneous corrugation on dry sand.

The phenomenon of spontaneous formation on unpaved road has been known for long time. Fig. 1 (b) shows an example of washboard road on dry gravel road [3]. In Japan, Takeshita et al. [4] reported their observation results about the corrugation appeared on unpaved road in 1954 with the phrase of ‘Soroban (Abacus in Japanese) road’. They considered that the washboard road is likely to occur when the surface material is in dry condition. For example, corrugation on unpaved road is frequently observed during summer because moisture in soil easily evaporates into the air. They also mentioned the phenomenon is caused by both of external and internal factors. The former is the natural frequency of vehicle decided by the combination of spring coefficient and damping performance equipped on the suspension of vehicle. On the other hand, the latter is material properties of surface. Whereas cohesive moist clay is not likely to scatter, dry and fine sand is easily rolled up and blown off by the centrifuge of rotating wheel. The mobility of surface material is thought as an important factor of the formation.

Similarly in Europe, various researchers have studied the phenomenon with empirical and theoretical approaches [5] [6] [7]. Interesting is that similar corrugation pattern also appears on farmland when an agricultural tractor drags plow or hoe [8]. The authors developed their original experimental apparatus to reproduce the phenomenon in laboratory. Since the model scale of the experiment including the model vehicle is rather small, we adopted fine granular sand as a surface material and investigated the growing process of corrugation. In this paper, we introduce some interesting findings in the experiments as well as our numerical model to explain the formation process on dry sand surface.

(a) Snowy Icy Road

(b) Unpaved Road [3]

Fig. 1 Examples of Corrugation Patterns

2. Indoor Reproduction Experiment

The authors introduce here the indoor reproduction experiment with dry sand. We have understood that the physical mechanism of the formation on dry sand cannot sufficiently explain the occurrence of corrugation on snowy-icy road and we may have to learn the physical formation of penitentes [9]. However, fundamental knowledge of the phenomenon could be accumulated through the experiments with dry sand.

2.1 Experimental Setup

The experimental apparatus consists of a self-rotating track (Fig.2 (a)) and a seesaw-shaped oscillator (Fig.2 (b)) equipped with a laser displacement sensor. The outer and inner boundaries of the track are 50 cm and 41 cm in diameter respectively, and the gap between two circular boundaries is filled with surface material of road. As our standard experimental condition, we adopted dry granular sand, called as Toyoura sand with an average particle size of 0.2 mm. The rotation velocity of the track can be tuned from 0 up to 20.0 rounds per minute (rpm) precisely, and the maximum velocity of the rotating track is about 0.5 m/s. The seesaw-shaped oscillator is fixed at the end of a cantilever beam extending from the rotational axis of the track. The time-dependent change in height of the surface material is observed by a laser displacement sensor with sampling frequency of 100 Hz set just behind the oscillator. (Fig. 3).

The seesaw-shaped oscillator plays a key role in our reproduction experiments. The total length of the arm is 14.2 cm, and an attachment simulating a wheel is mounted at one end of the arm. In this experiment, the attachments do not roll unlike a real wheel of vehicle and are simply dragged on the road surface. On the other hand, pendulum is loaded at the other end as a counterweight to control the natural frequency of the oscillator as well as the loading magnitude at the contact with road surface. The middle part of the seesaw arm is mechanically suspended by a soft spring which promotes the vertical oscillation of the attachment.

At the beginning of the experiments, the self-rotating track revolves at a slow speed of 3 rpm for 2 minutes to make the surface flat. Then, the rotating velocity is increased to an experimental value, and the track keeps revolving continuously for 7 minutes. The change in height of the road surface is measured with a laser displacement sensor.

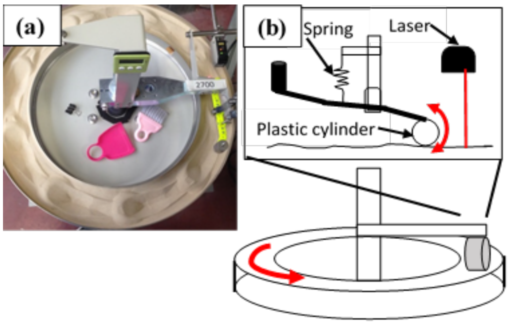

Fig. 2. Experimental Apparatus

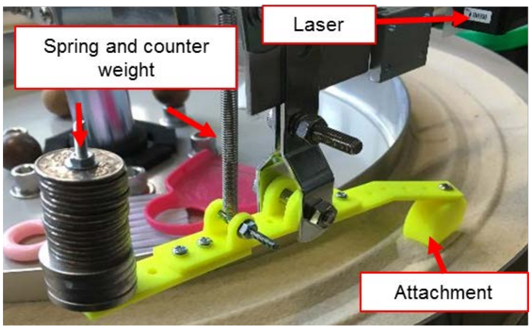

Fig. 3 Seesaw-shaped oscillator

2.2 Experimental Results

The experiments were conducted with various velocities of the track rotation increased from 10 rpm to 19.5 rpm. Fig. 4 on the next page shows running spectrums of corrugation in which the colors indicate the height of surface. The horizontal axis of the figure represents the location of track, and the vertical axis stands for the number of rotations. At the beginning of the rotation located at the bottom of the vertical axis, for example, the horizontal zones along the axis are colored with light green in any cases. It means that the height of surface is almost flat in any place of the rotating track. By keeping the experimental velocity of rotation, the road surface gradually waves from the initial flat condition. Accumulating the number of rotation towards upward direction in the figure, the areas are colorized with red and blue because the corrugation gradually grows. By those figures, the growing processes of corrugation are visualized. Interesting is that the convex part of the corrugation slowly shifts in backward or in forward, and the shifting directions are depending on the rotation velocity. In addition, the maximum height of the wave is increasing with the rotation velocity. At the rotation velocity of 9.0 rpm shown in Fig. 4 (a), the surface was kept flat throughout the experiment and no waves were observed. As the rotation velocity increases, the amplitude of the wave is gradually increased.

Table 1. shows the number of waves formed on the track at the end of each experiment, the maximum amplitude of the road surface and the frequency of the wave on road surface. We used an oscillator with a natural frequency of 1.66 Hz in those experiments. We found that the faster the track rotation velocity is, the earlier the formation of wave begins. From this table, it is recognized that the maximum amplitude of the wave gradually increases with the rotation velocity, and it converges to around 20 mm at the rotation velocity of 16.5 rpm or larger. As the rotation velocity of the track increases, the wave length also increases while the wave number on the track decreases. As a result, the peak frequency of the wave shown on the track keeps almost constant at approximately 2.25 to 2.44 Hz. and it is larger than the natural frequency of the oscillator. From those above, it can be seen that the occurrence of corrugation is greatly depending on the rotation velocity of the track.

Table 1. Comparison of Experimental Corrugation

Velocity (rpm)	Wave Number	Max Amplitude (mm)	Peak Frequency (Hz)
10.5	14	11.77	2.25
12	12	12.66	2.34
13.5	10	16.17	2.25
15	9	19.01	2.25
16.5	9	20.41	2.44
18	8	20.07	2.44
19.5	7	19.37	2.25

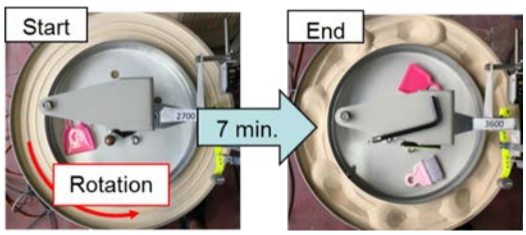

Fig. 5 Examples of surface conditions

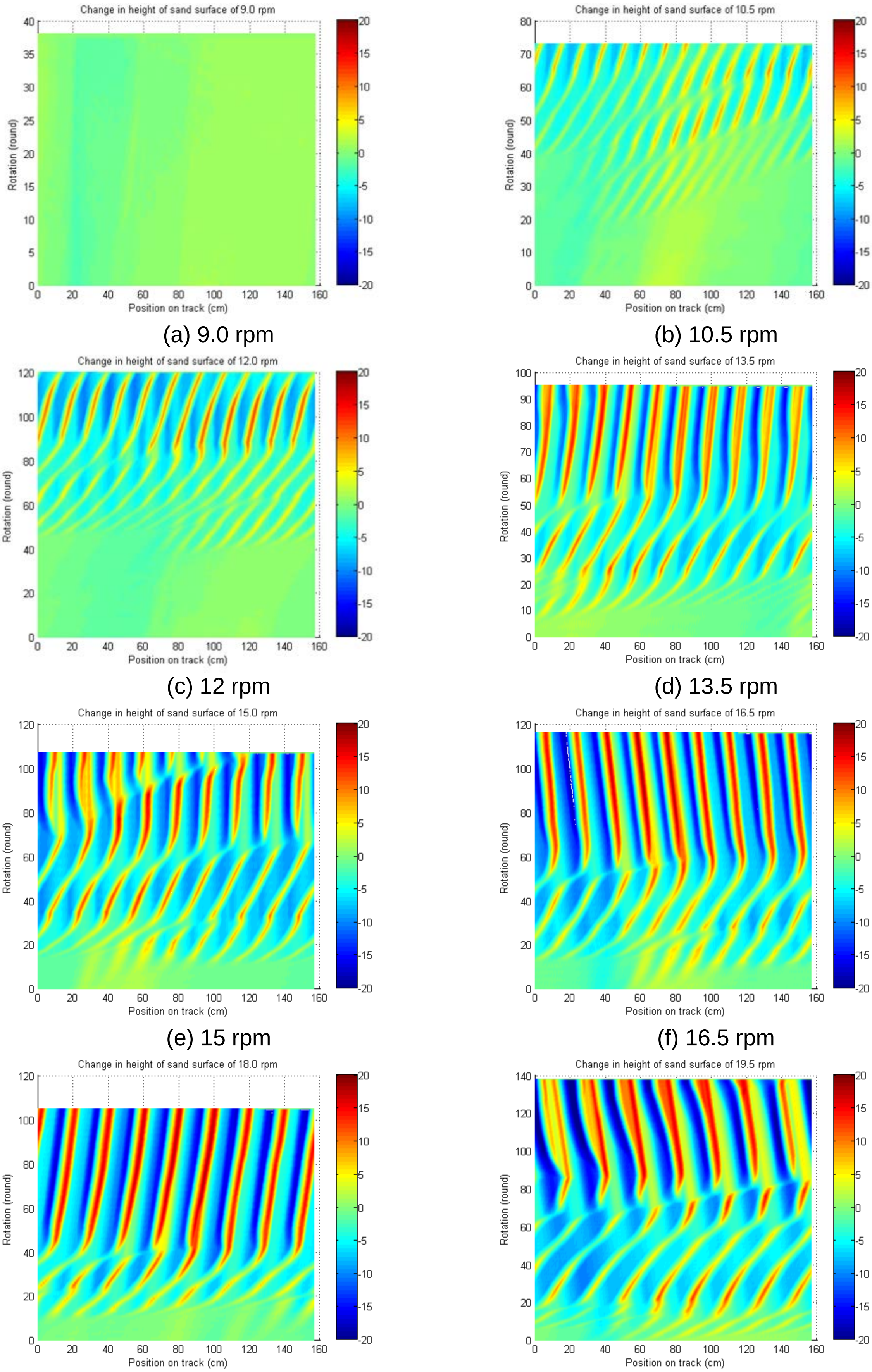

(a) 9.0 rpm (b) 10.5 rpm

(c) 12 rpm (d) 13.5 rpm

(e) 15 rpm (f) 16.5 rpm

(g) 18 rpm (h) 19.5 rpm

Fig 4 Running Spectrum of Each Track Rotation Velocity

2.3 Effects of Shapes and Surface Materials

In order to confirm the shape effect of the attachment on the formation of corrugation, we prepared several different shapes of the attachments as shown in Figure 6 in addition to the cylindrical one. Three attachments in triangular shape have different tip angles of 60, 90 and 120 degrees, and a hemisphere is another type of the attachment. All the attachments are made of acrylonitrile butadiene styrene plastic. According to our literature survey, washboard road appears not only on unpaved road with sand or gravel but also on farmland by dragging plow or hoe. The attachments in triangular shape are modelling plows with different contact angles to the surface. The authors thought that the contact angle to the surface along the longitudinal direction is one of the important factors to decide the shape of corrugation. Similarly, the contact angle to the surface in the transverse direction might give some effect on the shape. Then, a hemisphere-shaped attachment was provided in addition to the standard type of attachment in cylindrical shape. We conducted the reproduction experiments using those attachments.

(a) Tip angle of 60 (b) Tip angle of 90 (c) Tip angle of 120 (d) Hemisphere (e) Cylinder

Fig. 6 Various shapes of attachment

At the same time, the authors thought that the material property of surface is another factor to determine the formation of corrugation. We changed the moisture content of sand from dry to over saturated conditions. Since there are plenty of combinations with shape of attachment, material property and rotating velocity, we summarized the results in Table 2 as an example of comparison. The tip angle of triangular attachment shown in this table is fixed at 90 degrees and the results for moisture content of 70% is compared with those under dry and over saturated conditions. The figures in the table are indicating the wave numbers on the track after the convergence.

It can be said that the triangular attachment is likely to generate corrugation on the road surface by comparing the results of triangular attachments with those by cylindrical attachments under wet conditions. On the other hand, spontaneous corrugation is likely to occur under less moist condition of the surface material and this fact endorses the findings by Takeshita et al [4]. In Fig. 7, the running spectrums of the experimental results are shown to compare the effect of moisture content. The shape of the attachment for those is a cylindrical one.

Based on the study above, it became obvious that the deformation ability of surface material is very important as well as the shape of attachment. In order to propose a mathematical model for spontaneous corrugation, the authors decided to verify the deformability of material by a penetration test described in the next section.

Table 2 Wave Numbers under different conditions

Sand Condition		Shape of Attachment	Rotation Velocity (rpm) 12 rpm	15 rpm
Dry		Cylinder	11	8
		Triangular	10	8
Wet	Around 70 %	Cylinder	Slightly	Slightly
		Triangular	13	10
	Over Saturated	Cylinder	None	None
		Triangular	13	9

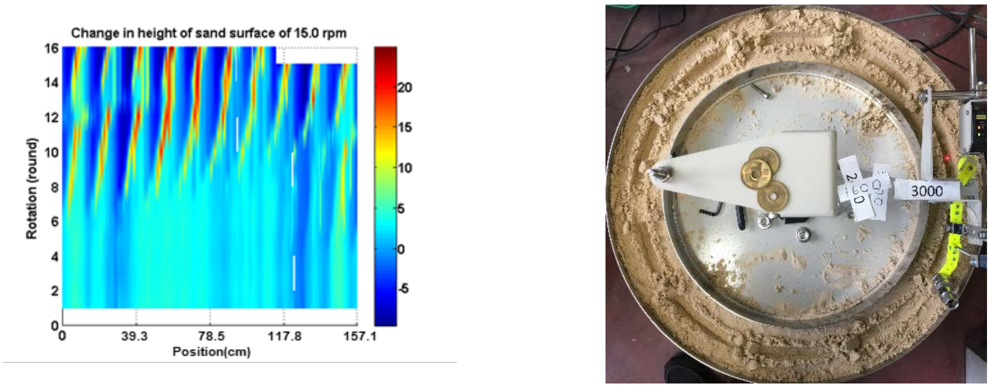

(a) Moisture Content of 12 %

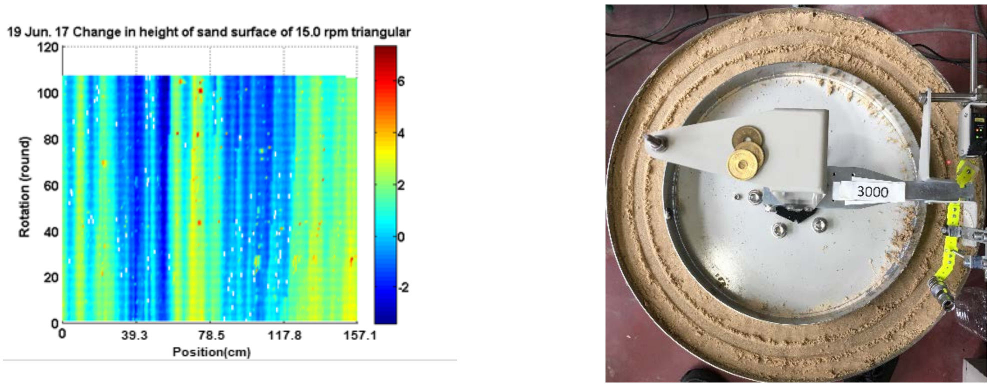

(b) Moisture Content of 41 %

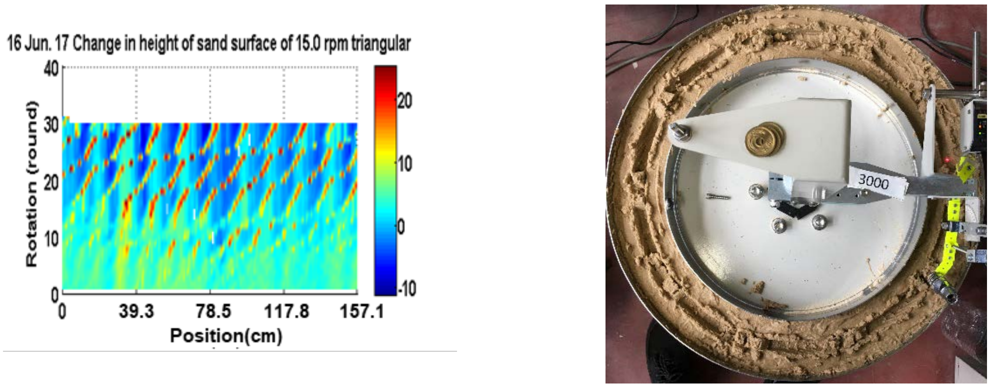

(c) Moisture Content of 69 %

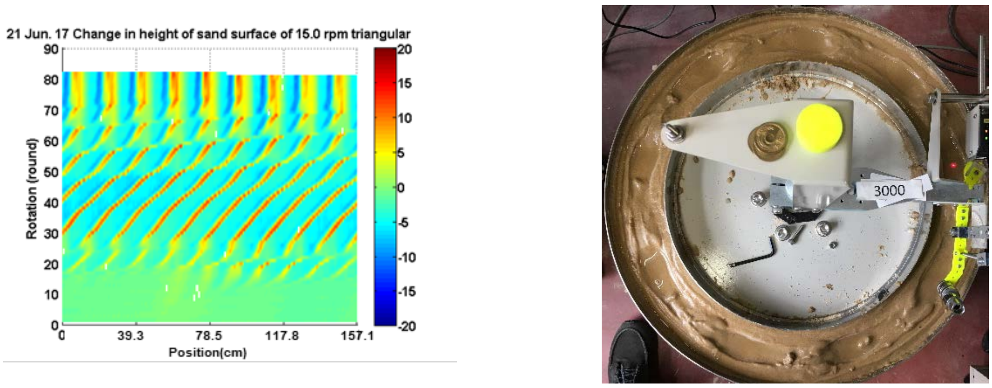

(d) Moisture Contents of 100 % and more (Over Saturated)

Fig 7 Experimental Results with Different Road Surface Condition

3. Penetration test

Due to some action of force transmitted by wheel, the sand surface deforms and migrates. As a result, it finally causes the formation of washboard road. Then, it is obviously important to know the deformation ability of surface material due to the interaction between the wheel and the surface. The authors provided a penetration test device to confirm the deformation ability of sand.

3.1 Experimental setup

Fig. 8 shows the penetration test device. The attachment modelling a wheel is gradually settled down into the test material, and the penetration depth is simultaneously measured by a laser displacement sensor. The magnitude of force transmitted to the material through the attachment is recorded by an electronic balance installed at the bottom of the material. The downward force magnitude is controlled by the pendulums put at the top, and the maximum load applied to the material is approximately 5 N. By repeating the loading and unloading three times, we investigated the relationship between the penetration depth and the magnitude of force. As a fine sand material, we used Toyoura standard sand which is same as the material used in the reproduction experiments. When the attachment penetrates to the deepest position under the maximum load, the loading phase is terminated. In the unloading phase, on the contrary, a displacement-control procedure cannot be applied because the deformation of sand surface has already been in inelastic range. The unloading is completed when the loading magnitude shows no changes around 0 N.

3.2 Relationship between displacement and Force

Fig. 9 illustrates the relationship between the penetration depth and the downward force for the cylindrical attachment with dry sand. After the first cycle of loading and unloading, the sand surface has already been deformed in inelastic range. In the loading phase, the displacement linearly increases with the force magnitude regardless of the repetition. However, the increment in the displacement for the first cycle is much smaller than those of second and third cycles because the surface material has been sufficiently compacted and migrated after the first cycle. In other words, the deformation ability of the material is lessen during the first cycle. In the unloading phase, the displacement shows a slight recovery from the deepest position, and this fact is another evidence for that the material has been deformed in plastic range.

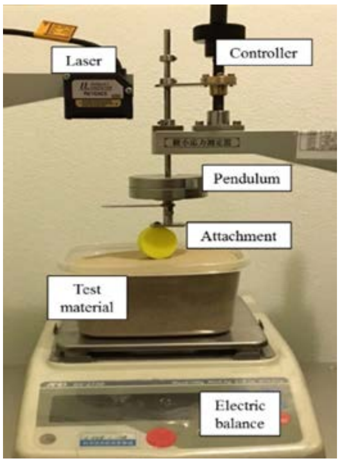

Fig. 8 Penetration Test Instrument

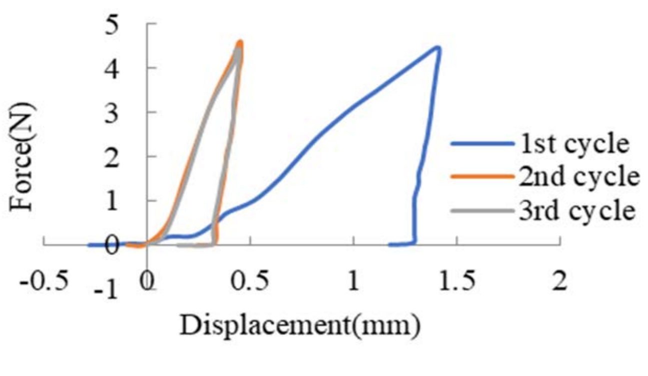

Fig 9 Relation between depth and force magnitude

For comparison of shape effect, Fig. 10 shows the experimental results of the relationship between the penetration depth and the force magnitude in their first cycles. It can be seen that the gradient of the graph in the first cycle differs by the shape of attachment. Those results seem very natural because the steepness in the tip angle has a significant effect on the penetration ability. For example, the triangular one with a tip angle of 60 degrees is easily settled down with the least force magnitude, and when the tip angle becomes larger from 60 to 120 degrees, greater force is necessary to obtain a same penetration depth. Comparing the gradients of the cylindrical and hemisphere ones, we also found clear difference between those, and the difference is caused by the shape effect in the transvers direction to the driving track. From those results, it can be concluded that the smaller the contact angle between the attachment and the horizontal surface becomes, the larger the force magnitude to induce a same penetration is.

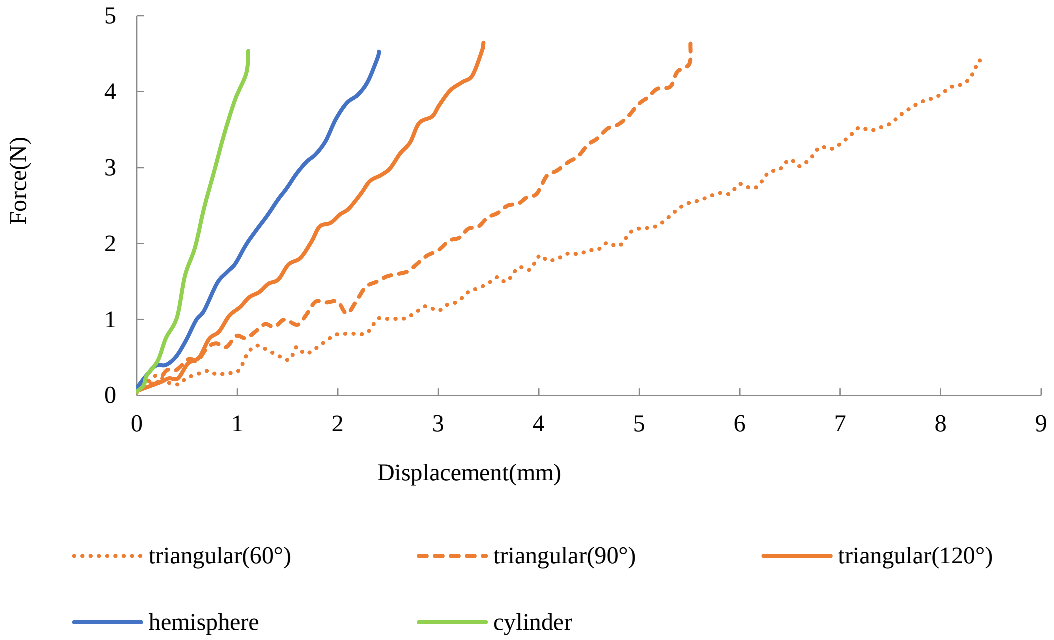

Fig. 10 Relationship between Displacement and Force for Different Shapes of Attachment

4. Numerical Model and Analysis

The dynamic motion of the oscillator can be described by a simple equation for single degree of freedom as shown in Equation (1). The oscillator has a counterweight representing m at the tail and a spring with a spring coefficient of k near the middle of the arm. We set a damping coefficient of suspension as c. The height of the attament is expressed as x, and the external force applied to the attachment from the road surface is given as F. As shown in Fig. 11, the top surface of the road is assumed as z and the reaction force from the road material is assumed to work only when the attachment touches the road surface. The magnitude of the force is estimated as a function of (z-x) and the linear constant of A is decided by the penetration test. Since the road surface deforms plastically in the experiment, the deformation of the road surface caused by F never behaves elastically and it is assumed that the height of surface keeps its deformed position after unloading.

$$m\ddot{x} + c\dot{x} + kx = F(t) \tag{1}$$

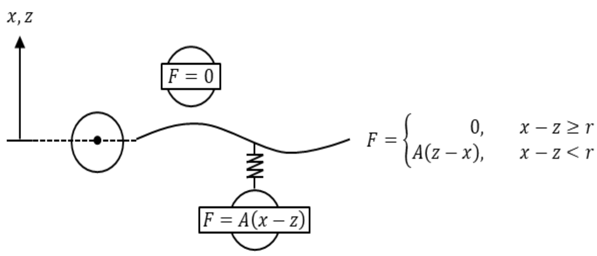

Fig. 11 Setting of External Force F

In the numerical model, it is necessary to give some initial roughness on the surface to promote the spontaneous corrugation. We adopted a sinusoidal wave with an amplitude of 1 mm. In order to confirm the effect of initial condition, we gave different wave frequencies of 1, 2, 4 and 8 Hz as an initial roughness. Fig. 12 shows the calculation results with different initial conditions. However, the formation processes of those look very similar regardless with the trequency of initial roughness, and the model satisfactorily immitates the formation process. Fig. 13 compares the relationships between the rotation velocity of the track and the wave number on the road surface by the numerical analysis with those observed by the experiments. The natural frequencies of the oscillators are 1.49 Hz for the analysis and 1.46 Hz for the experiments. The wave numbers of those are similarly decreasing with increase in the rotation velocity of the track. Even though the analytical solution slightly underestimates the wave numbers observed in the experiments, those difference comes from the evaluation in the migration of surface material due to the plastic deformation and it can be improved by the modification in the migration modelling of surface material. The authors are convinced of that the numerical model we proposed is practically applicable for the estimation of the formation process.

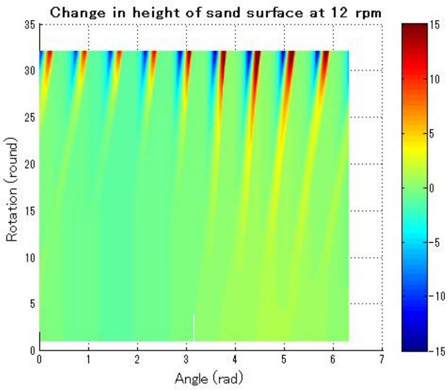

(a) Initial Wave Frequency: 1

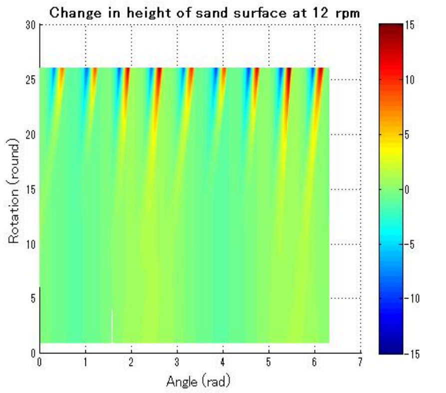

(b) Initial Wave Frequency: 2

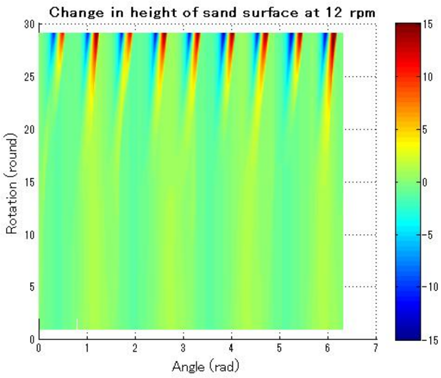

(c) Initial Wave Frequency: 4

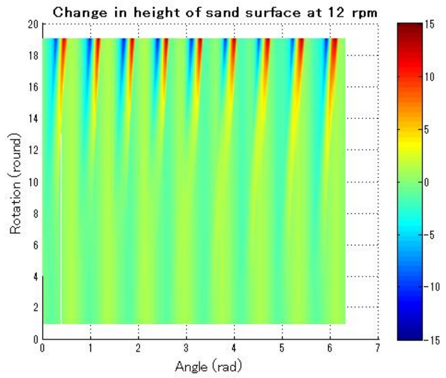

(d) Initial Wave Frequency: 8

Fig 12 Comparison of Running Spectrums with Different Initial Fluctuation

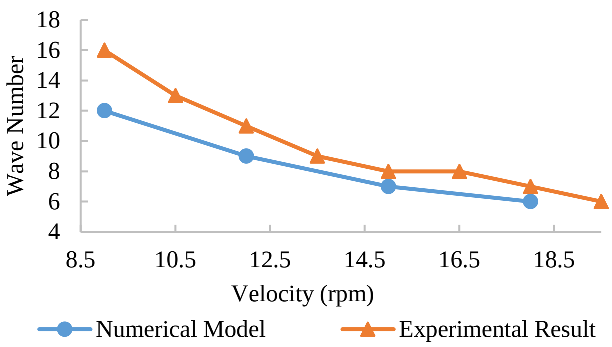

Fig 13 Relationship between Track Rotation Velocity and Wave Number

5. Conclusions

We investigated the spontaneous corrugation patterns of dry sand on the self-rotating track formed by the oscillator. It is confirmed that the rotation velocity of the track is one of the dominant factors for the formation of corrugation and the amplitude of the wave increases with the rotation velocity. The effect of the shape of the attachment is also verified by the experiments as well as the effect of the moisture content of surface material. By the penetration test, relationship between the vertical displacement driven into the test material and the force applied from the attachment was discussed. As a result, the relationship between the displacement and the force can be expressed as a linear function for loading and unloading but the behaviour of the material shows an inelastic property. The dynamic motion of the oscillator is calculated by a time-domain technique with a simple model of single degree of freedom. By introducing the plastic deformation of the surface material based on the penetration test, we successfully constructed a numerical model for imitating the corrugation process even if it may need some modification on the movement of surface material for more precise simulation. The authors are now improving the oscillator which has a revolving attachment like a real wheel, and are investigating the phenomenon more realistically. We believe that the accumulation of knowledge on the spontaneous corrugation with dry sand leads to the elucidation of formation mechanism of the phenomenon on snowy-icy road and it contributes to the establishment of road management technology in winter Hokkaido.

Acknowledgement

This work was supported by KAKENHI Grants No. 16K01278 of Japan. The authors would like to express our gratitude to Yasuhiro Kaneda and Yasuhiro Nagata of Hokkaido development engineering center (DEC) as well as Mr. Teeranai Gartoon Srimahachota, a doctoral candidate of our school.

References

[1] SRIMAHACHOTA, T., ZHENG, H., SATO, M., KANIE S. and SHIMA, H., "Dynamics of washboard road formation driven by a harmonic oscillator", *Physical Review. E*, Vol. 96, Issue 6, 062904, 2017.

[2] KANIE, S., ZHENG, H., YOKOMISE, D., KANEDA, Y., NAGATA Y. and MASAKI, Y., "A study on a growing process and its conditions of Soroban road based on observation with fixed point cameras (in Japanese)", *Proceedings of Hokkaido Chapter of the Japan Society of Snow and Ice*, Annual Report on Snow and Ice Studies in Hokkaido, Vol.35, 2016, pp.55- pp.58

[3] MAYS, D. C. and FAYBISHENKO, B. A, "Washboards in unpaved highways as a complex dynamic system", *Complex 5*, 2000, pp.51- pp.60

[4] TAKESHITA, H. and KOBAYASHI, K., "Soroban road: Corrugation of roads with gravel (in Japanese)", *Road Engineering & Management Review*, Vol.54, Issue 2, 1954, pp.69 – pp.71.

[5] BOTH, J. A., HONG, D. C. and KURTZE, D. A., "Corrugation of roads", *Physica A* 301, Elsevier, 2001, pp.545-pp.559

[6] TABERLET, N., MORRIS, S. and McELWAINE, J., "Washboard road: The dynamics of granular ripples formed by rolling wheels", *Physical Review Letters*, PRL 99, 068003. The American Physical Society, DOI: 10.1103/PhysRevLett.99.068003, 2007

[7] BITBOL, A., TABERLET, N., MORRIS, S. W. and MCELWAINE, J. N., "Scaling and dynamics of washboard roads", *Physical Review E* 79, 061308, The American Physical Society, DOI: 10.1103/PhysRevE.79.061308, 2009.

[8] PERCIER, B., MANNEVILLE, S., MCELWAINE, J. N., MORRIS, S. W. and TABERLET, N., "Lift and drag forces on an inclined plow moving over a granular surface", *Physical Review E* 84, 051302, The American Physical Society, DOI: 10.1103/PhysRevE.84.051302, 2011

[9] CLAUDIN, P., JARRY, H., VIGNOLES, G., PLAPP, M. and ANDREOTTI, B., "Physical processes causing the formation of penitentes", *Physical Review E* 92, 033015, The American Physical Society, 2015

PEHKO Project – Implementing ROADEX Recommendations for Rural Road Asset Management in Finland

Timo Saarenketo
Ph.D., Adj.prof., CEO
Roadscanners Group
Finland
timo.saarenketo@roadscanners.com

CEng. Ron Munro, Munroconsult Ltd., Scotland
MSc. Annele Matintupa, Roadscanners Oy, Finland

Summary

"Urbanization" is currently one of the trend words into day´s discussion, but at the moment it is still the case that almost half of the world's population live in rural areas. For these people roads will be the only transportation route in the future and their roads will need to satisfy the increasing needs of transportation, mobility and connectivity services for the foreseeable future.

The big problem with rural roads is that the funding for condition management of European road networks has been constantly decreasing over the last decades. And when the needs of high traffic volume road networks have been increasing this has led to a reduction in the management budget for low volume roads. That is why, when the first ROADEX project started in 1998, one the key challenges for road owners was how to keep the condition of their rural road networks at such a level to ensure safe roads and the sustainable development of local livelihoods.

The ROADEX Projects and later ROADEX Network has been a series of technical co-operations between a range of roads organisations across Northern Europe that shared rural public and forest road related information and research. ROADEX has executed numerous research and pilot projects all with the common general goal of "how to do more with less". A number of excellent findings with a high potential to increase productivity and increase savings have been made without compromising quality. Results have been published in a range of reports and the goal of this report is to summarize their benefits and savings by example case studies' calculations wherever possible.

Since 2015 the ROADEX ideas for rural road asset management have been tested "full scale" in the PEHKO project in Finland. The project´s goal is to improve practices and policies in paved road maintenance and management and thereby improve the condition of the paved road network, or at least keep it at the current level using less resources. This is being done by focusing on three targets: 1) Improving daily maintenance, especially drainage. 2) Applying new NDT methods in the diagnostics of paved roads. These techniques allow engineers to focus rehabilitation measures exactly on the problem sections and address the root. 3) Changing maintenance policies from reactive to more proactive maintenance, allowing maintenance crews to fix the potential problem sections before serious pavement damages appear.

The PEHKO project has now been under way for three years and preliminary results have exceeded expectations. The last calculations of the impact of the new, improved and focused methods on annual paving costs were made in 2018. The calculated annual costs fell by as much as 26% in Central Finland and 22% in Lapland. With these encouraging results it is expected that the target of 50% reduction in calculated annual paving costs can be reached by 2025.

This paper will present experiences about how ROADEX recommendations have been used in practice in the PEHKO project to improve the productivity of asset management of rural roads in Northern Europe.

Keywords: Pavement Performance, Road Maintenance, Innovative Engineering Solutions

1. Introduction

The ROADEX Network is a technical collaboration of forest and public roads organisations across Northern Europe that share road related information and research. The collaboration started as a European Union pilot in 1998 and over the intervening period, and projects, has grown into a centre of information for all things concerning sustainable rural roads. This includes issues as diverse as road condition management, vehicle and human vibration, socio-economic impacts, through to climate change adaptation and measures to mitigate environmental impacts. A wide range of new technologies and policies have been developed for accurate road survey and monitoring, winter maintenance operations, forest road management and the use of road friendly trucks.

Over its 20 years of existence ROADEX has also executed numerous research and pilot projects all with the common general goal of "how to do more with less" [1]. A number of ground-breaking findings with high potentials to increase productivity and increase savings have been made without compromising quality. Results have been published in a range of reports. A summary of the potential benefits and savings of the ROADEX project results and recommendations has been published by Leviäkangas [2].

The most comprehensive project implementing, and further developing, ROADEX findings and recommendations has been the PEHKO 2015-2025 project in Finland [3]. The PEHKO project is largely based on long term work, carried out by the ROADEX projects and the ROADEX Network within the Northern European Road Agencies, and on Roadscanners' own product development. The basic idea and goal for the PEHKO project is to improve the practices and policies in paved road maintenance and management and thereby improve the condition of the paved road network, or at least keep it at the current level using less resources. This is being done by focusing on three targets: 1) Improving daily maintenance, especially drainage. 2) Applying new NDT methods in the diagnostics of paved roads. These techniques allow engineers to focus rehabilitation measures exactly on the problem sections and address the root. 3) Changing maintenance policies from reactive to more proactive maintenance, allowing maintenance crews to fix the potential problem sections before serious pavement damages appear. Two 10 year R&D pilot projects were commenced in 2015 in Lapland and Central Finland, and good experiences from these led to a further 10 year pilot, which started in 2018 in the different climatic and traffic conditions in Southern Finland.

2. ROADEX

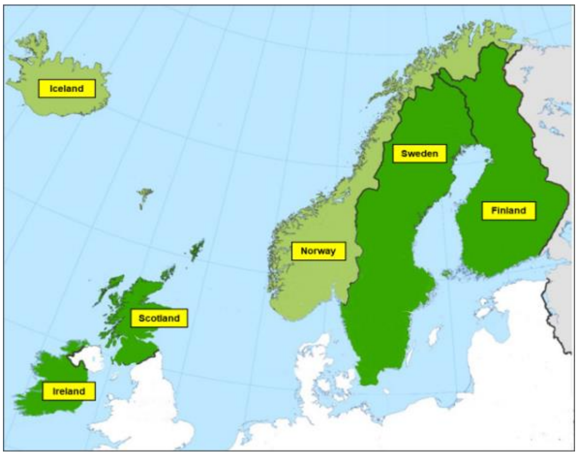

Fig. 1. The ROADEX Network areas.

The ROADEX Network currently comprises 12 partner organizations: Transport Scotland, The Highland Council, Forestry Commission Scotland and Comhairle nan Eilean Siar from Scotland; the Northern Region of the Norwegian Public Roads Administration; the Northern Region of the Swedish National Road Administration; the Lapland Centre for Economic Development, Transport and the Environment; The Finnish Transport Agency, The Icelandic Road Administration; The Department of Transport Tourism and Sport, The Road Management Office and The Department of Agriculture, Food and the Marine from Ireland (Figure 1). This Network is the custodian of the legacy of the ROADEX co-operations since 1998 comprising website, social media, knowledge centre, e-learning packages, co-operation outputs and technical reports.

The aim of the Network is to continue to advance the management of low volume roads at all levels through state-of-the-art strategies and technologies. In particular, in the context of ISCORD, this means furthering the development of improved strategies and practices in cold regions for better road drainage, dealing with freeze-thaw cycles, winter maintenance and mitigating the effects of climate change. This includes issues as diverse as road condition management, vehicle and human vibration, socio-economic impacts, through to climate change adaptation and measures to mitigate environmental impacts. In addition a wide range of new technologies and policies have been developed for accurate road survey and monitoring, winter maintenance operations, forest road management and the use of road friendly trucks.

Some examples of the types of issues being addressed by ROADEX are given below.

Drainage

It is generally accepted that the key to a sustainable road [4, 5, 6] is a well-working drainage system. Road structures work well in dry conditions, roads with poor drainage develop problems quickly, and especially in winter. ROADEX has shown that keeping the drainage in good condition is crucial for the long term performance of a road [7, 8, 9]. Most notably, it has been demonstrated that where the drainage is kept in good condition the pavement lifetime can be increased by 1.5-2.0 times. ROADEX has established a drainage analysis technique [10] that combines laser scanner, thermal camera, and ground penetrating radar to identify critical drainage sections on a route that need regular monitoring and maintenance. All surveys are logged to GPS for accuracy and repeatability. When these surveys are brought together, and analysed in an integrated fashion, a 3D cloud model (Figure 2) and visual picture can be assembled to accurately identify where and what works should be carried out.

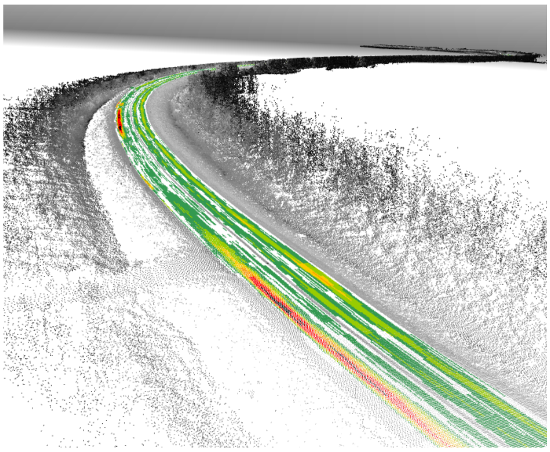

Fig. 2. 3D cloud model of road showing increase in rutting at a private access.

Climate change adaptation

The ROADEX Partners recognise the threats of climate change and committed themselves to investigating possible mitigation and adaptation measures to keep their networks sustainable. All partners were invited to complete a questionnaire (Figure 3) on their view on the likely effects of climate change and possible measures discussed accordingly. The ROADEX report "*Climate Change Adaptation*" [11] sets out a range of cost-effective and sustainable measures that can be brought into daily engineering management, and integrated into policies and regulation in the same way that health & safety and environmental issues are currently considered. It is recognised that good adaption is part of a continuous process that needs to be regularly reviewed and updated as new information comes to light. An example of a typical consideration is freeze-thaw cycles. The frequency of freeze-thaw cycles has been increasing across Northern Europe in recent years. The ROADEX report "*Developing Drainage Guidelines for Maintenance Contracts*" [9]. and the ROADEX elearning lesson on "*Drainage*" (www.roadex.org). set out good practice measures to deal with the effects of freeze-thaw cycles. Depending on the likely scale and scope of frost damage the ROADEX project offers several policies and techniques for managing roads during the spring thaw weakening period.

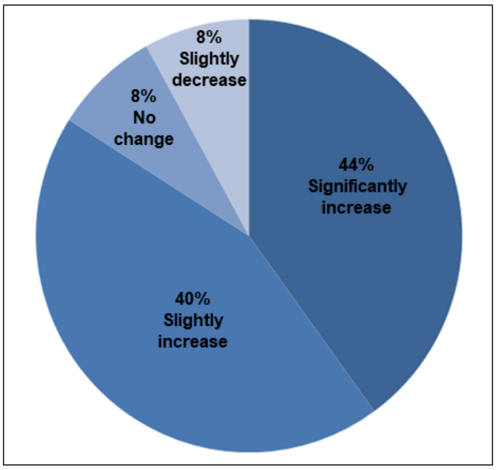

Fig. 3. Results of the questionnaire on the impacts of climate change to freeze-thaw cycles

Winter maintenance

Winter maintenance is a major consideration for the ROADEX Network countries [12], and in all countries in the cold regions of the world. Apart from keeping roads free from snow and ice, ROADEX has also shown that winter maintenance operations themselves [13, 14, 15] can have a great effect on pavement damages, and the lifetime of road pavements, if not addressed. Examples of these are delayed snow removal from the road shoulders (Figure 4), overly extensive use of de-icing salt, and ice-clogged culverts causing water to infiltrate into the road structures. A well working drainage system can help mitigate these, and it is therefore essential that drainage monitoring and maintenance should be continued through the winter period as well as summer.

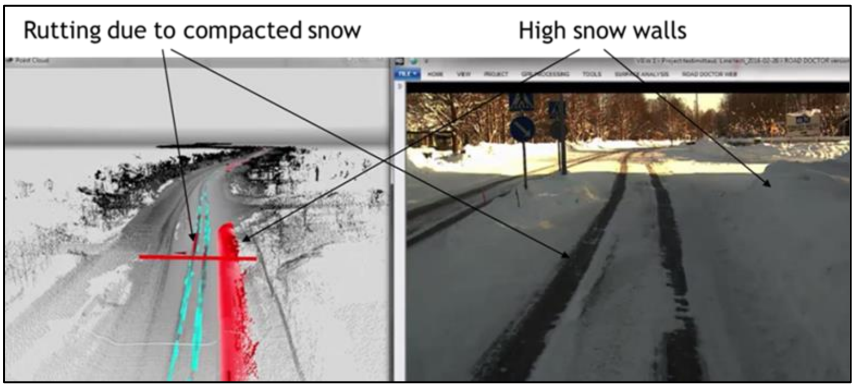

Fig. 4. Rutting due to compacted snow and high snow walls are major traffic safety hazards for road users during winter time.

Vehicle and human vibration due to road condition

ROADEX carried out a number of research projects [16, 17] and case studies into the effects of road surface condition (Figure 5) and road geometry on driver health. The work included in-cab surveys of truck ride vibration on live public and forest roads in Finland, Norway, Scotland and Sweden. Research was undertaken into the effectiveness of tyre pressure control systems in reducing ride vibration in the cab. The impact of road maintenance standards on truck drivers' working environment was also investigated. The work concluded that road condition did have an effect on driver vibration, and that all of drivers in the trucks tested recorded unacceptably high levels of the EU 8hr daily vibration dose A(8).

Fig. 5. Vibration recorded on a patched road.

Environmental guidelines & checklist


Fig. 6. Dust in maintenance operations.

ROADEX has carried out a number of studies on the environmental issues that should be considered when planning road construction or maintenance [18, 19, 20]. The "*Environmental Guidelines - Results of a Study on Environmental Practices and Regulations*" aims to be a working manual, concentrating on the environmental practices that should be carried out for road works on low volume roads and is accompanied by a checklist for designers. The report concludes that sensibly organized routines and proper use of resources will lead to savings in money and resources. The checklist sets out a range of good practice measures and provides guidance on dealing with waste, noise and vibrations, dust (Figure 6) and exhaust gases, contaminated soil, natural environment, and water.

Road friendly vehicles & tyre pressure control

ROADEX has been a pioneer in the use of road friendly vehicles and tyre pressure control (TPC) systems on timber haulage vehicles across the Northern Periphery (Figure 7.) [21, 22]. TPC had not been used in Scotland or Finland before being piloted in the Scottish Highlands in ROADEX in 2006. It had been trialled in Sweden. Since 2006 however the numbers of trucks equipped with TPC have grown annually in Scotland and Sweden, and as a result of ROADEX Finland and Ireland have also started to introduce TPC on a limited number of timber trucks. Alongside this development ROADEX has also been promoting road friendly tyres and offset axle arrangements to spread loads across multiple wheelpaths. Timber haulage companies are now seeing the business and driver health benefits that can arise from having TPC systems fitted. This is particularly the case on weak public rural roads where public road organisations and forest agencies are coming under increasing pressure to permit timber haulage operations along weak public roads to support local communities and industries.

Fig. 7. TPC and tyre testing.

Socio-economic impacts of road conditions on low volume roads

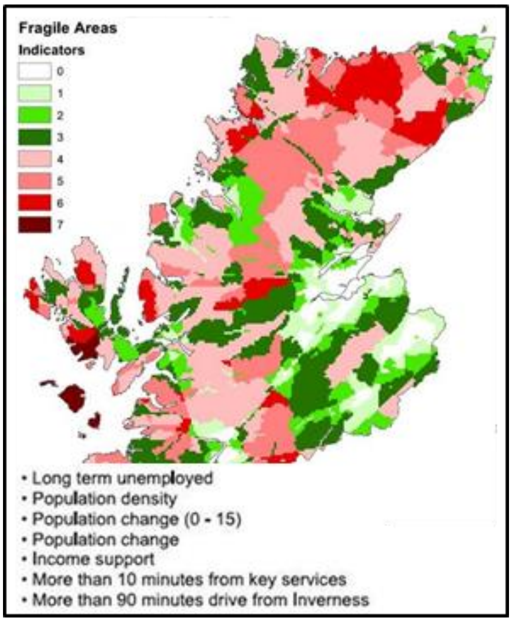

Fig. 8. Map of fragile areas in Scotland.

ROADEX does not only restrict its research to the engineering aspects of roads, it also actively carries out research into the socio-economic arguments for rural roads leading to rural communities and their industries, and their funding [23, 24]. These researches report that socio-economic needs have to be considered in the wider context when considering the importance of roads for people, companies and societies in rural areas, as they are essential lifeline routes for their communities. The results of ROADEX investigations show that identifying and mapping fragile areas (Figure 8), lifeline roads and the transportation needs for people and businesses is an effective way to calculate the rural road user needs of an area. ROADEX has developed a "*Transportation Need Index*" that combines fragility, lifeline class and the accessibility needs for people and businesses in an area. This information can thereafter be used to set minimum service levels and give a robust way of ranking the importance of low volume roads against other competing budgets.

Dissemination of ROADEX materials

It is the aim of the ROADEX Partners that the collected ROADEX material is disseminated as widely as possible to inform all end users, from politicians to engineers in the field, of the benefits and savings that can be accrued from using ROADEX technologies [25]. Dissemination is currently being carried out through a combination of reports, knowledge centre and elearning lessons in the ROADEX website at www.roadex.org, as well as through social media sites, seminars and conferences.

3. PEHKO 2015-2025 Project

3.1 Background

ROADEX benchmarking has shown that the decline in national budgets for paved roads has caused increasing pavement deterioration rates in many countries that will soon lead to major problems on national networks. This trend can be clearly seen from Figure 9, that shows the development of paving budgets and length of poor quality paved roads in Finland 2005-2016. Falling budgets have led to the fact that low traffic volume areal and connecting roads are now suffering from inadequate funds. In addition trends towards heavier truck total weights and maximum allowed axle loads have exacerbated this, as have the newer generations of tyre types with smaller footprints [26]. Climate change is also likely to have an effect through the impact of seasonal changes on road networks. All of these cause extra stresses on pavements as well as unbound pavement structures. To counter this, research on new methods and policies is now needed to address the growing problems.

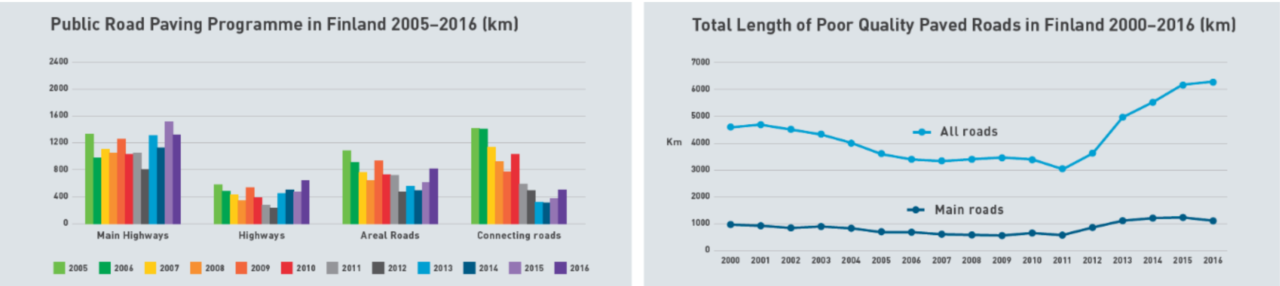

Fig. 9. Public road paving budgets (left) and the rise of poor quality paved roads (right) in Finland 2005-2016.

With this background the PEHKO project was started in 2015 in cooperation between The Finnish Transport Infrastructure Agency, Roadscanners and The Centres for Economic Development, Transport and the Environment of Lapland, Central Finland [3], and from 2018 Uusimaa area (Figure 10). The total length of the paved road network in PEHKO areas is roughly 2400 km. The goal of the project was to develop and test new and innovative methods to improve the productivity of the maintenance and care of paved roads to increase the pavement lifetime. A further aim is also to provide new information on the life cycle costs of various roads and the factors that increase these costs and cause premature damage to pavements. In other words, the goal is to identify the "weakest links" on our paved road networks that are increasing asset management costs, and to develop repair and maintenance measures that address the real root causes of the problems.

Fig. 10. PEHKO pilot areas in Finland.

The PEHKO project partners set themselves a very ambitious financial goal by requiring that in 2025, the annual pavement costs in the pilot areas should be about 50% lower than the current computational costs (= annual paving budget + annual backlog). This would mean that in 2025 (and 2028 in the Uusimaa area) the PEHKO roads should be able to be maintained in good condition at the current cost level of about € 130-140 million without increasing the budget backlog. However, it should be noted that at the same time the costs of daily maintenance would be expected to increase slightly from the current level.

Efforts have also been made in the PEHKO project to take into account the requirements of future digitalisation and intelligent traffic. For this reason digital point cloud models were developed from the entire road network surveyed and all the collected data linked to these models. This makes it possible to gather accurate historical data and to move forward to proactive maintenance based on the monitoring results.

3.2 Survey Techniques and Asset Management Process

Fig. 11. Roadscanners Road Doctor Survey Van (RDSV) with laser scanner, GPS and IMU behind the van, and GPR antennas and cameras on the front of the van.

The Road Doctor Survey Vehicle (RDSV), developed by Roadscanners Oy (Figure 11), and the continuous Traffic Speed Deflectometer (TSD) developed by Greenwood, Denmark, have been used in the diagnostics and condition monitoring of the PEHKO pilot project road network. This has proven to be a very good combination for the functional and structural condition analysis of the roads [27]. And at the same time it has been possible to map even small changes in the pavement surface and road surroundings. RDSV data is collected throughout the road network annually and TSD measurements every fifth year.

Road structures and upper part of subgrade are measured with the RDSV using Ground Penetrating Radar (GPR) with 2GHz and 400 MHz antennas. Road surface roughness is measured with 3D accelerometer. Surface shape and rut depth are measured with laser scanner + IMU + GPS combination. Using this combination crossfall, slope inclinations and depths of ditch bottoms can also be surveyed. The TSD measures the pavement deflection under a 10 ton axle load at traffic speed (80km/h) using doppler sensors. All data analysis is carried out using Road Doctor® software developed by Roadscanners.

The basic asset management process used in the PEHKO pilots is described in the following:
1. Surveying the paved road network using new techniques, locating the problem sections and their root causes.
2. Identifying road sections that are still in good condition, but are close to the end of their service life, ie before visual damages can be seen. These sections are paved with a new and thicker pavement.
3. Identifying road sections suffering from inadequate daily maintenance. These sections are treated by raising the standards of daily maintenance and improving practices.
4. Locating rapidly damaging paved road sections and diagnosing the root causes of these damages. A focused rehabilitation plan is prepared for each section and executed.
5. Continuing annual monitoring of the entire road network. This involves launching proactive maintenance operations immediately if the monitoring results indicate an increased risk of pavement damage. The effectiveness of various treatments and remedies is also monitored.
6. Repeating steps 1-5

3.3 Preliminary results of implementation of ROADEX and PEHKO policies

PEHKO project data from the Lapland and Central-Finland areas has now been analysed for the first three years, but so far only the basic data collection has been gathered from the Uusimaa area in Southern Finland. The economic analysis has however already shown that the worst 10-20% road sections take roughly the half of the annual paving costs. Also the contributing factors that can be related to these 10-20% sections have been identified and they are the following.

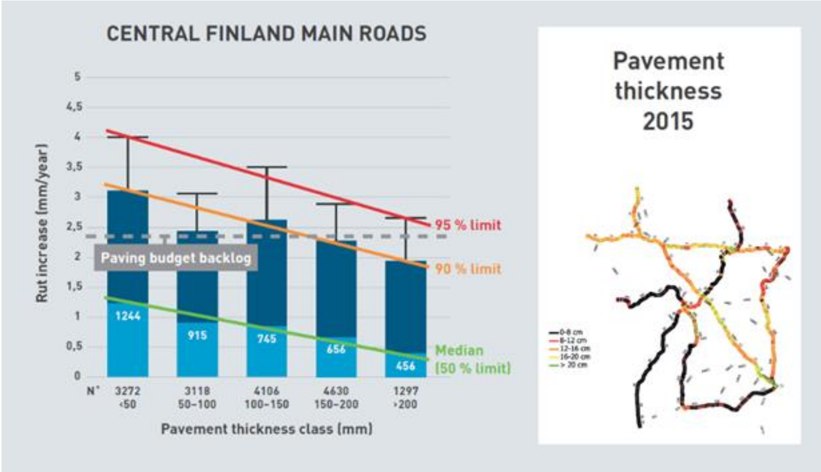

Fig. 12. Statistical analysis showing the distribution of annual rut increase rates at different pavement thickness class (left) of main roads, and pavement thickness map (right) of Central-Finland PEHKO area. Current paving backlog limit is roughly 2.4 mm/year.

1. Heavy trucks on road sections with weak subgrade. This is a big problem especially on road sections resting on peat. However PEHKO project has found that steel grid structure has proven to perform well in these sections
2. Heavy trucks and thin pavements (<150 mm). This is a fast increasing problem with the new heavier trucks and new tyre types. Figure 12 shows that high annual rutting increase values are concentrated on road sections with thin pavements and that a great part of the paved road network still has pavement thicknesses of less than 80 mm.
3. Pavement quality, including aggregate quality, creep, remix pavements, poor quality patching, etc. Pavement quality can also be a problem in thicker pavement sections.
4. Poor daily drainage maintenance. This applies mainly to private access road junctions, or to poorly performing side ditches. Private access road culvert problems are cheap to fix and the latest update in Finnish law requires the road owner to maintain them.
5. Pavement deterioration problems due to inadequate winter maintenance. This can be as a result of delayed snow removal from road shoulders that PEHKO has shown to have a great impact on shoulder deformation and roughness.
6. The extensive use of de-icing salt on thin pavements. This is a recently discovered cause for increasing rut growth rates. It can be a problem on high volume roads but needs more research.

After three years of PEHKO asset management procedures, and focusing maintenance actions on weak links, results achieved so far have been very promising. Improved maintenance operations have had a very positive influence in decreasing the rutting speed of the different road classes (Table 1), and the total savings in annual costs have been between 22-26%. A particularly remarkable issue is the trend on connection roads. On these roads nothing else has been done other than winter maintenance operations have been intensified by early snow bank removal.

Table 1. Development of calculated annual paving costs (€/m/year) on PEHKO pilot areas from 2015-2016 to 2017-2018.

Road class	Lapland 2015-2016 €/m/year	Lapland 2017-2018 €/m/year	Improve-ment	Central-Finland 2015-2016 €/m/year	Central-Finland 2017-2018 €/m/year	Improve-ment
Main roads	2,72	2,17	23%	2,59	1,72	34%
Areal roads	1,92	1,64	16%	2,10	1,73	18%
Connecting roads	2,35	1,91	22%	2,32	1,89	18%
All roads	2,47	2,00	22%	2,38	1,75	26%

4. Conclusions

According to the United Nations 54% of the world's population now lives in urban areas, a proportion that is expected to increase to 66% by 2050. That means that 1 in 3 of us will still be living in rural areas with increasing needs of transportation, mobility and connectivity services for the foreseeable future. Currently, the main digitalization discussions in the transport sector have focused on solutions for urban areas but this does not mean that the challenges for rural areas should be forgotten.

The PEHKO project has only been in place for the last three years, but results show clearly that ROADEX recommendations for improving the productivity of road asset management by using new road condition monitoring techniques based on diagnostics, focused rehabilitation and proactive maintenance can lead to major savings in annual paving budgets. This means that in the future available budgets can be effectively spent, and more of the limited resources can be allocated to low volume rural roads also.

For this to happen, road asset management and maintenance can no longer be based decisions based on fixed time cycles. Road users' demands are changing, traffic is changing, vehicles are changing and maintenance has to reflect these changes also. Maintenance measures need to be based on continuous road structural and functional condition monitoring and data analysis, and be focused on solving the actual problems developing in the road.

The ROADEX and PEHKO projects have given new ideas and tools to solve the forthcoming challenges with rural road networks in cold climate areas, but these technologies and policies can be implemented also in other areas including in the asset management of main road networks.

References

[1] MUNRO, R. (2012) "THE ROADEX PROJECTS 1998-2012, Project History and Index of Reports", ROADX IV.

[2] LEVIÄKANGAS, P. (2015) "Evaluation of ROADEX Benefits and Savings", ROADEX IV

[3] TAPIO, R., LEHTINEN, J., YLINAMPA, J. and SAARENKETO, T. (2016) "PEHKO Project 2015-2025, increasing the productivity of paved road management in Finland" Proceeding of EAPA Conference, Prague 2016. Digital Object Identifier (DOI): dx.doi.org/10.14311/EE.2016.144

[4] JOHANSSON, S. and JOHANSSON K. (2007) "Road Condition Management Policies, Tests and Development of Proposal", ROADEX III.

[5] JOHANSSON, S. et al (2004) "Road management policies for low volume roads – some proposals", ROADEX II.

[6] JOHANSSON, JOHANSSON, K. and S. EKEDAHL, F, (2007) "Policies for Forest Roads - Some Proposals", ROADEX IV

[7] BERNTSEN, G. and SAARENKETO, T. (2005) "Drainage on low traffic volume roads", ROADEX II.

[8] AHO, S. and SAARENKETO, T. (2006). "Managing Drainage on Low Volume Roads", Executive Summary, ROADEX III.

[9] SAARENKETO, T. (2007). "Developing Drainage Guidelines for Maintenance Contracts", ROADEX III.

[10] MATINTUPA, A. and TUISKU, S. (2012) "New Survey Techniques in Drainage Evaluation, Laser Scanner and Thermal Camera", ROADEX IV.

[11] HUDECZ, A. (2012) "Climate Change Adaptation", ROADEX IV.

[12] NOREM, H. (2001) "Winter Maintenance Practice in the Northern Periphery - extended Summary and Conclusions", ROADEX I.

[13] SAARENKETO, T. (2006) "Monitoring Low Volume Roads – Executive Summary", ROADEX III.

[14] AHO, S. and SAARENKETO, T. (2006) "Design and Repair of Roads Spring Thaw Weakening", Northern Periphery, ROADEX III.

[15] AHO, S. and SAARENKETO, T. (2005) “Managing Spring Thaw Weakening on Low Volume Roads”, ROADEX III.
[16] GRANLUND, J. (2008) “Health Issues Raised by Poorly Maintained Road Networks”, ROADEX IV.
[17] [14] GRANLUND, J. (2012) “Vehicle and Human Vibration due to Road Condition”, ROADEX IV.
[18] ULLBERG, J. (2004) “Environmental guidelines”, ROADEX II.
[19] ULLBERG, J. (2004) “Environmental Checklist – a pocket guide to working on site”, ROADEX II.
[20] ULLBERG, J. (2006) “Environmental Guidelines – Executive Summary”, ROADEX III.
[21] DAWSON, A. and KOLISOJA, P. (2006) “Managing Rutting in Low Volume Roads- Executive Summary”, ROADEX III.
[22] MUNRO, R. and MACCULLOCH, F. (2008) “Tyre Pressure Control on Timber Haulage Vehicles”, ROADEX IV.
[23] JOHANSSON, S. (2004) “Socio-economic impacts of road conditions on low volume roads”, ROADEX II.
[24] JOHANSSON, S. (2006) “Socio-economic Impacts of Road Conditions on Low Volume Roads”, ROADEX III.
[25] SAARENKETO, T., MUNRO, R. and MATINTUPA, A. (2012) “ROADEX benefits and savings – achieving more with less” ROADEX report. www.roadex.org
[26] VARIN, P. and SAARENKETO, T. (2014) “Effect of axle and tyre configurations on pavement durability – a prestudy” ROADEX report. www.roadex.org
[27] HERRONEN, T., MATINTUPA, A. and SAARENKETO, T. (2015) “Experiences with Integrated Analysis of TSD, GPR and Laser Scanner Data”, International Symposium Non-Destructive Testing in Civil Engineering, Proceedings, Berlin 2016.

SPECIAL ISSUES - SNOW AND ICE

EFFORTS TO FORECAST ICY ROAD SURFACE SLIPPERINESS LEVELS IN WINTER IN SAPPORO, HOKKAIDO, JAPAN

Fumiyoshi KAWAMURA
Business Services Section Group Leader
Japan Weather Association Hokkaido Regional Office
Japan
fumi@jwa.or.jp

Seiya UEDA, Japan Weather Association, Japan
Hisae NIKAIDO, Japan Weather Association, Japan
Yasuhiro KANEDA, Hokkaido Development Engineering Center, Japan
Yasuhiro NAGATA, Hokkaido Development Engineering Center, Japan
Naotoshi KANEMURA, Sapporo Information Network Co., Ltd., Japan
Yoshifumi WATANABE, Sapporo Information Network Co., Ltd., Japan
Hiroshi HOSHINO, Civil Engineering Services Co., Ltd., Japan
Sapporo Winter Life Promotion Council

Keywords: icy road surface slipperiness forecasts, prevent pedestrians' fall accidents

1. Introduction

In Sapporo, pedestrians who fell severely enough to require ambulance transport to the hospital in winter have numbered about 1,000 a year. On December 21, 2014, the number of the pedestrians who fell severely enough to require ambulance transport to the hospital (hereinafter referred to as "injured fallers") recorded 163 that exceeded 57, the maximum number of those in a day in the past. In recent years, the number tends to get increased. In 2016-2017 and 2017-2018 winters, the number exceeded 1,300. This rapid increase in the number of severely injured fallers is making the municipal lifesaving service in winter in Sapporo too busy to fulfill its duty.
The authors have been engaged in the project to provide the public with icy road surface slipperiness forecasts (hereafter referred to as "the forecasts") in Sapporo through the Internet since 2006-2007 winter as a measure to prevent wintry pedestrians' fall accidents. The slipperiness forecasting project is named as "TSURUTSURU YOHOU" in Japanese. "TSURUTSURU" means very slippery state. The forecasts express the road surface slipperiness by three levels based on the road surface conditions that are assumed by the latest weather forecasts including expected air temperatures and snowfalls. The three levels of road surface slipperiness are defined as: Level 3, extremely slippery; Level 2, moderately slippery and Level 1, somewhat slippery.
As of today since 2015-2016 winter, in cooperation with the Sapporo City Fire Department and the media including television and radio stations and newspaper publishers, the authors have issued road surface slipperiness forecasts to prevent pedestrians' fall accidents. This study reports the results of those efforts, verifying actual data.

2. Winter Slip-and-Fall Accidents

2.1 Outline of Sapporo

2.1.1 Location and Climate

Although the city is farther south to most of the major cities in Europe and North America, Sapporo's annual mean temperature is 8.5 °C, and winters are quite snowy (Fig. 1).

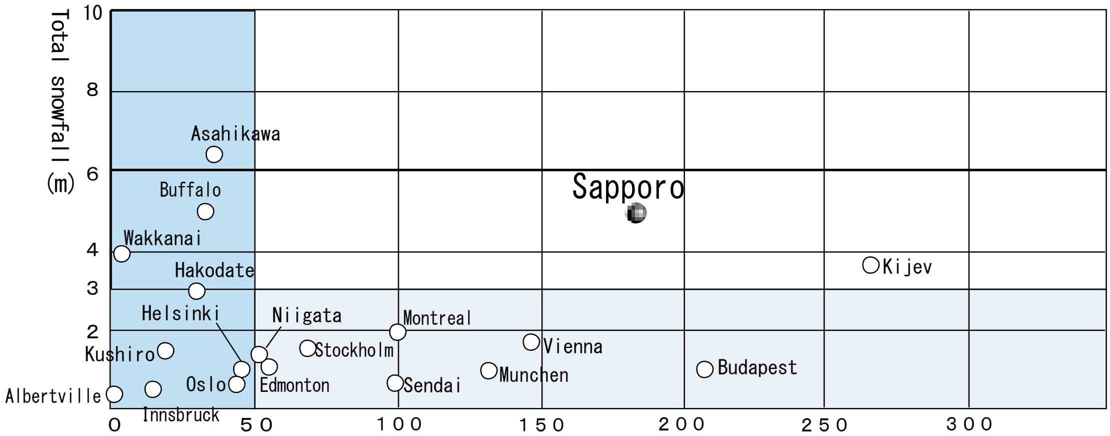

Sapporo annually sees about 5 m snowfalls. This ranks it among the snowiest large cities of the world.

Fig. 1 Population and annual snowfalls of snowy cities

2.2 Injurious falls

Fig. 2 shows the number of injured fallers for each winter from 1983-1984 to 2017-2018. Since the use ban on studded tires took effect in 1991 in Sapporo, the number of injured fallers in winter has been rapidly increasing. Such fallers in winter have numbered about 1,000 per year.

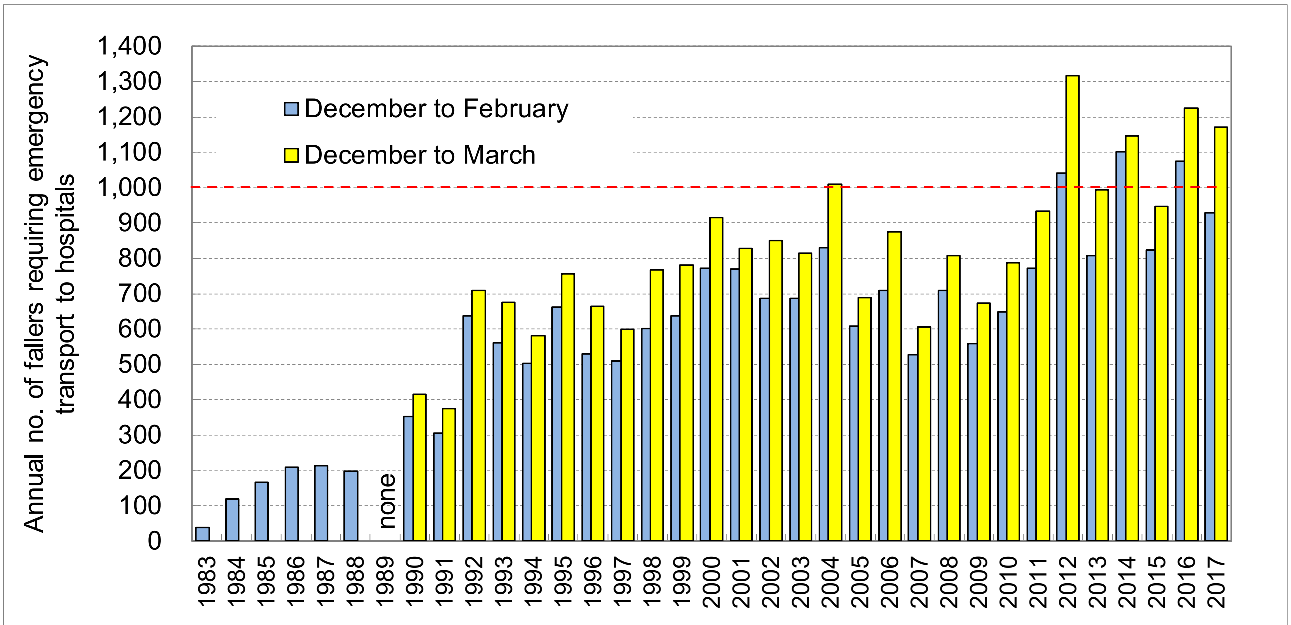

Fig. 2 Annual no. of fallers requiring emergency transport to hospitals (1983-2017)

Fig. 3 shows the percentage of hourly no. of injured fallers to the total during 2017-2018 winter. The peak hours recording injured falls are from 7:00 am to 10:00 am. Almost the same trend is seen every winter because those hours fall on the hours of people's commuting to schools or workplaces.

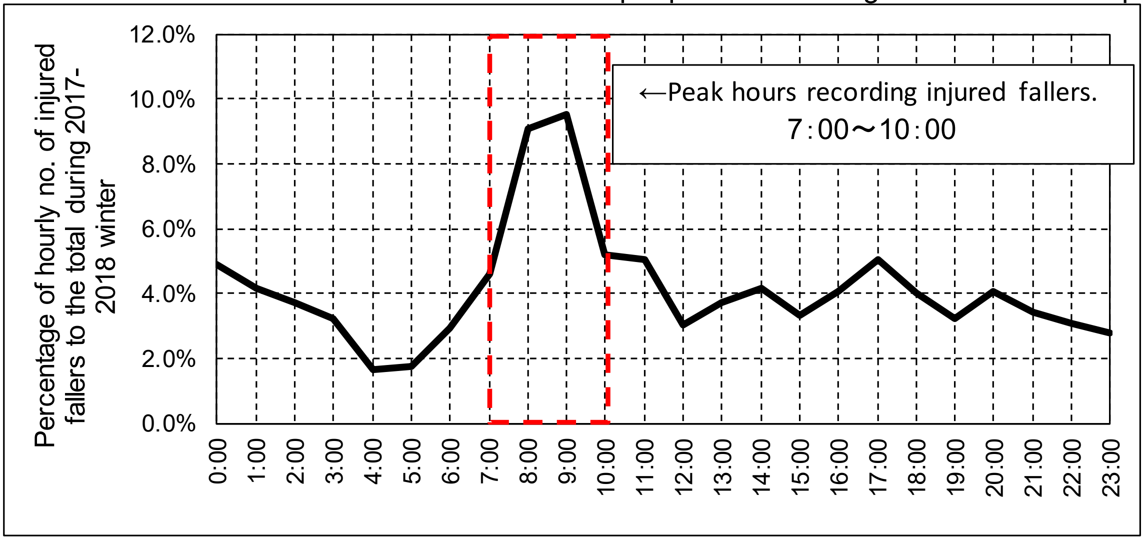

Fig. 3 Percentage of hourly no. of injured fallers to the total during 2017-2018 winter

3. Efforts to issue the forecasts to prevent fall accidents

The icy road surface slipperiness level forecasts are issued on the basis of the meteorological information including air temperature and snowfall forecasts and accumulated snow depths. The visual road surface state monitoring results are also taken into consideration for the forecasts. The snow surface slipperiness to be forecasted is expressed with the three levels of slipperiness: Level 3, extremely slippery; Level 2, moderately slippery and Level 1, somewhat slippery. The typical Level 3 road surface states are introduced in Photo 1 and Photo 2.

Photo. 1 Icy walkway surface at Level 3 resulting from compacted snow that melted first and was frozen up later due to temperature dropping.

Photo. 2 The road surface with rains or moist snowfalls was rapidly frozen at Level 3, while being packed.

Photo. 1

Photo. 2

To issue the forecasts, the weather conditions that are likely to cause icy road surfaces have been categorized to make them reflect the road surface slipperiness as precisely as possible. The state of fallen risks are commented on some specific places that are significantly risky. The forecasts and other information to prevent fall accidents are provided to the public from 17:00 to 10:00 am next day through the Walk Smart website (http://tsurutsuru.jp/) that is operated by the Winter Life Promotion Council (Fig. 4). Further, because the highest no. of injured fallers in a day was recorded in 2014-2015 winter, the information has also been provided through newspapers and TV and radio broadcasts since 2016-2017 winter.

Fig. 4 Image of the Walk Smart Website (in English and Japanese)

4. Examination of the accuracy of the icy road surface slipperiness level forecasts

4.1 The percentage breakdown of the forecasts by level

The two graphs of Fig. 5 show the percentage breakdown of the no. of days when the forecasts were issued by level for the two winter periods, 2016-2017 and 2017-2018, about 100 days each.

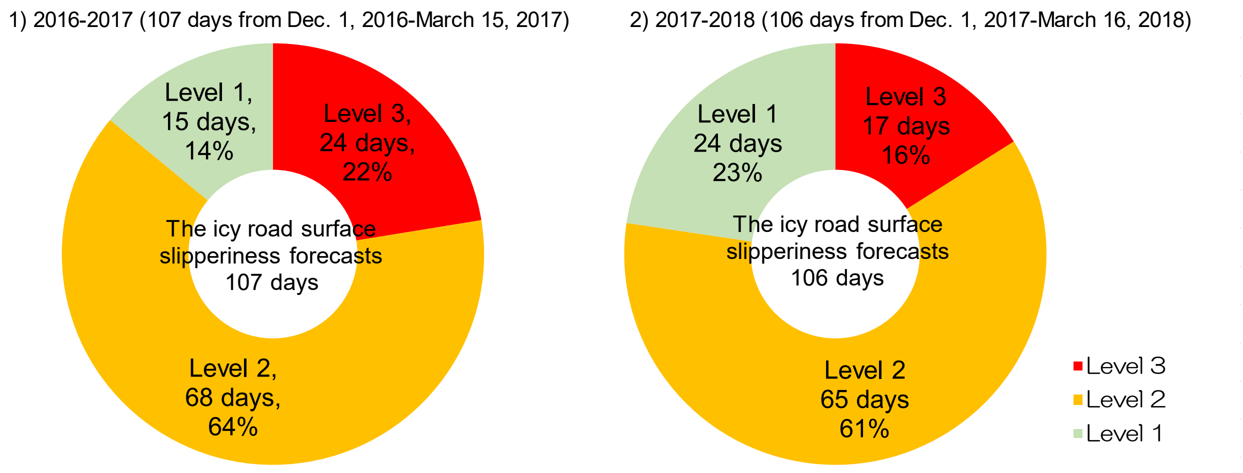

Fig. 5 Percentage breakdown of the icy road surface slipperiness forecasts by level for 2015-2016 and 2016-2017 winters.

4.2 Accuracy of the forecasts in comparison to on-site visual observation results

In the winters when the forecasts had been issuing, visual observations of icy road surface state (hereinafter referred to as VO) at three or more points had been conducted on weekdays at some point of time during the hours from 07:00 am to 10:00 am, which are the riskiest hours of fall accidents. The average VO results evaluating the road surface state by the same criteria as those of three forecast levels were compared with the forecasts to examine their accuracy. Because the visual observations were conducted only on weekdays, the no. of the days when VO were conducted in 2016-2017 winter was 81 and in 2017-2018 winter, it was 89. Fig. 6 compares the VO results and the forecasts in 2016-2017 winter 1) and in 2017-2018 winter 2).
The table 3) and 4) organize the comparison results of 1) and 2) , respectively to examine the accuracy of the forecasts. The evaluations of the forecasts' accuracy are classified to three levels: the same as VO, lower than VO, higher than VO. During 2017-2018 winter, the same as VO numbered 57 taking 64% of the total forecasts followed by 11 of lower than VO , 12.4% and 21 of lower than VO, 23.6%. Compared with those during 2016-2017, 11.1, 64.2 and 24.7, respectively, the accuracy of the forecasts during 2017-2018 is almost the same. Focusing on the day when the forecast and/or VO indicates level 3, the forecasts accuracy was examined for the two winter periods. The results of 2017-2018 period were: the no. of the day the same as VO: 8; lower than VO: 4 and higher than VO: 6, 44%, 22.2 % and 33.3 %, respectively. Compared with those during 2016-2017 winter, the no. of "the same as VO" has increased from 6, 28.6% to 8, 44.4%, while the no. of "lower than VO" has decreased from 12 (57.1%) to 6 (33.3%).

1)

2016-2017 winter		VO results: Level 1	Level 2	Level 3	Sum
Forecasts	Level 1	7	6	0	13
	Level 2	8	39	3	50
	Level 3	0	12	6	18
	Sum	15	57	9	81

[days]

2)

2017-2018 winter		VO results: Level 1	Level 2	Level 3	Sum
Forecasts	Level 1	11	7	0	18
	Level 2	15	38	4	57
	Level 3	2	4	8	14
	Sum	28	49	12	89

[days]

3)

ALL	Lower	9 days	11.1%
	Same	52 days	64.2%
	Higher	20 days	24.7%
forecast and/or VO indicates level 3	Lower	3 days	14.3%
	Same	6 days	28.6%
	Higher	12 days	57.1%

4)

ALL	Lower	11 days	12.4%
	Same	57 days	64.0%
	Higher	21 days	23.6%
forecast and/or VO indicates level 3	Lower	4 days	22.2%
	Same	8 days	44.4%
	Higher	6 days	33.3%

Fig. 6 Comparison of the visual observations results and the forecasts

4.3 Comparison of the forecasted road surface slipperiness risk levels and the no. of injured fallers

Table. 1 compares the forecasted road surface slipperiness levels and the greatest no. of injured fallers for each 1-3 levels during 2016-2017 and 2017-2018 winters. As for 2016-2017 winter, the higher the forecasted slipperiness level is, the more injured fallers are recorded. However, during 2017-2018 winter, on the days with Level 2 or Level 1 slipperiness saw more injured fallers than on a day when Level 3 was forecasted. The day for Level 2 was March 9, 2018 and that for Level 1 was Dec. 6, 2017. The reasons why the greater numbers of injured fallers than that for Level 3 were recorded could be unstable weather in the beginning of early December and March that fall on the beginning of winter and spring, respectively. During those periods, ups and downs of air temperatures tend to repeat, so that snow on the road surface repeats thawing and freezing, which is led to quite slippery road surfaces. And, pedestrians do not get used to slippery road surfaces in the beginning of winter, which may also be the reason why many people fall in early winter (Fig. 7).

Table. 1 The average and maximum no. of injured fallers per day by forecasted road surface slipperiness level

Year	No. of injured fallers	Level of forecasted road surface slipperiness: Level 1		Level 2		Level 3	
2015	Average no.	8		10		13	
	Max. no.	39	2015/12/26(Sat)	50	2015/12/27(Sun)	39	2015/12/29(Tue)
2016	Average no.	9		9		18	
	Max. no.	23	2017/2/17(Fri)	39	2017/1/7(Sat)	53	2016/12/28(Wed)
2017	Average no.	9		10		16	
	Max. no.	43	2017/12/6(Wed)	56	2018/3/9(Fri)	34	2018/2/26(Mon)

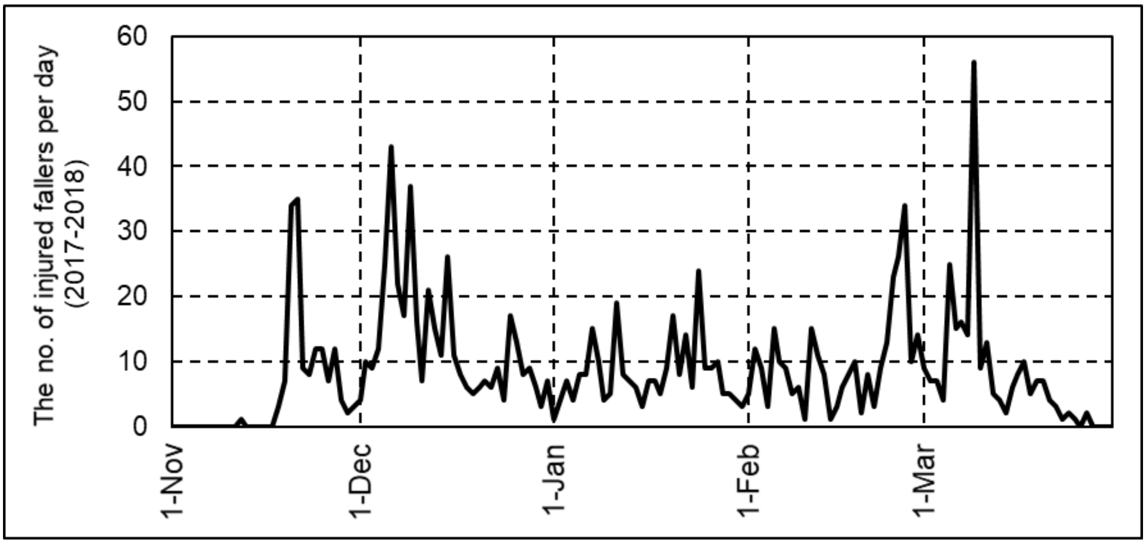

Fig. 7 Changes in the no. of injured fallers per day (2017-2018)

5. Conclusions

The icy road surface slipperiness level forecasts provision has started in 2006 and it has extended to be provided through media in 2015. Through those efforts, the public awareness of the slippery road surface risk has increased. The forecasts' accuracy has also increased by the development of data analysis measures and the accuracy examinations to improve the forecasts. However, not a few people still fall on icy roads and get injured. The efforts to provide the icy road surface slipperiness forecasts will continue to further increase the awareness of the public to the fall risk in winter.

Acknowledgements

The authors appreciate the fire department of the City of Sapporo who has offered the data of the injured fallers and volunteers who has kindly reported the information on road surface slipperiness state.

References

[1] HOSOTANI et al., "Current State of Winter Pedestrian Fall Accidents in Sapporo", Proceedings of ISCORD2007, 2007.

[2] KAWAMURA et al., "Efforts to Prevent Pedestrian Slip-and-Fall Accidents in Winter in Sapporo", Proceedings of ISCORD2010, 2010.

A Study on Evaluation Method of Fall Over Risk in Winter Walkway Using Smartphones

Akira Saida
Researcher
Civil Engineering Research Institute for Cold Region, PWRI
Japan
saida-a@ceri.go.jp

Roberto Tokunaga, Senior reseacher of Civil Engineering Research Institute for Cold Region, PWRI, Japan
Takerou Watanabe, Graduate student of Hokkaido University, Japan
Shin-ei Takano, Professor of Hokkaido University, Japan

Summary

As winter slip-and-fall accidents involving pedestrians have been increasing with the progress in population aging in recent years, clarification of the levels of slip-and-fall risks in winter walking space has been becoming increasingly important for road administrators and road users. Road administrators require determination of risk-prone locations in order to take measures against slip-and-fall accidents, and road users are able to avoid risk locations based on the determined risk information. However, a simple and useful method for assessing such slip-and-fall risk quantitatively, in real-time, and for wide areas, which is necessary for realizing the provision of this important information, has not yet been established.
Toward developing a method to resolve that problem, the authors developed a smartphone application for measuring the walking behavior of the pedestrians by using sensors in their smartphones, and conducted an experiment with human subjects under various snow and ice road surface conditions. This experiment and the following examination aimed at obtaining a useful set of data, which will contribute to assessing the risk of slip-and-fall accidents in winter walking space.
The results of this examination demonstrated that the level of acceleration amplitude from walking tends to differ according to the condition of the snow- and ice-covered road surface. This tendency was observed in many experiment subjects with varying locations of the smartphone on the bodies of the subjects. This experiment suggests the possibilities of obtaining useful information for assessing the risk of slip-and-falls on snow- and ice-covered road surfaces based on the walking acceleration measured by using the acceleration sensor in smartphones.

Keywords: Winter road maintenance, winter slip-and-fall accident, smartphone, gait analysis

1. Introduction

1.1 Background to this study

Slip-and-fall accidents involving pedestrians on the snow-covered or icy surfaces of roads and sidewalks occur frequently, mainly in the cold and snowy regions, and have been an issue. For example, in recent years, Sapporo City had over 1000 cases per winter of ambulance transport of persons who were injured in slip-and-fall accidents in walking spaces. This number tends to be increasing because of factors that include progressing population aging.[1] Providing information on the level of slip-and-fall risk, which changes hour-to hour, is estimated to be effective for pedestrians to prevent slip-and-fall accidents because they will be able to be well prepared before they go out, for example, by changing their routes or wearing slip-resistant shoes.[2] Furthermore, an understanding of the details of the slip-and-fall risks in winter walking spaces is important for road administrators in selecting the road/sidewalk sections that require snow removal and spreading of anti-skidding materials intensively.

Based on the above, a method to temporally and spatially determine and evaluate the slip-and-fall risk of winter walking space is considered to be indispensable in the future sophistication of winter road management. There have been several attempts to assess the slip-and-fall risks of winter walking spaces as discussed below.

1.2 Existing studies on detecting and determining the conditions of winter walking space

As a method for evaluating the slip-and-fall risks in winter walking spaces, Hashimoto[3],[4] analyzed the tendency of occurrences of slip-and-fall accidents by using the data on ambulance transport of winter slip-and-fall accidents recorded by the Sapporo City Fire Department. Shintani et al. [5] analyzed the tendency in occurrences of slip-and-fall accidents by using data from the fire department on the number of occasions of ambulance transport of persons injured in slip-and-fall accidents. They also clarified, by using fixed point video shooting, conditions under which the persons who fell were not injured as seriously as those requiring ambulance transport. The method for clarifying the risk locations for pedestrians using the ambulance transport data has advantages including finding the location and time of accidents, such as information including the sex, age, and other details of persons who slipped and fell. With this method, however, events such as occurrences of falls that were not as serious as those requiring ambulance transport and slips that did not end in falls were not found, and clarification of the locations or time of potential slip-and-fall risk is difficult. Real-time detection of risk locations for pedestrians and real-time evaluation of the level of slip-and-fall risk by using the above described method are extremely difficult.

The method used in Sapporo City [6] is an example case of a method for clarifying the level of slip-and-fall risk in winter walking spaces. In this case, data on visually determined road surface conditions and still images of road surface conditions are collected by volunteers. The collected data are aggregated for each ward and determined as real-time information on the slipperiness of the sidewalks in the central areas of the city. In this case, the volunteers need to manually report on the road conditions from the observation location, which is a considerable burden on the volunteers. Furthermore, the reported conditions vary depending on the subjectivity of the volunteers. The problem with this method is that quantitative, detailed and comprehensive risk assessment is difficult because it uses the results of road condition reports observed at fixed points.

For measuring the conditions of the snow- and ice-covered surface of the carriageway, a method for linear measurement of skid resistance of the road surface using a traction type device [7] and a noncontact method for determining road surface conditions using the reflection of a light wave [8] have been proposed. By using these methods, the conditions of the carriageways are able to be clarified quantitatively and in real time. The measurement equipment for these methods is large and expensive. Using such methods for risk assessment of slip-and-fall is extremely difficult.

The existing assessment methods for slip-and-fall risk in winter walking space needs to be improved to be a quantitative and real-time method, and for wide areas. Ease of conducting the assessment is also required. It was reported that a practical method for assessing slip-and-fall risks in winter walking spaces that covers all these requirements has not yet been realized.[9]

1.3 Purpose of this study

To realize a quantitative, real time, and economical method for assessing the risks of walking in winter spaces, which have been issues to be solved in past studies, this study aims at proposing an improved method using smartphone sensors. In this paper, the development of a smartphone application for measuring the walking behavior of pedestrians will be discussed, and the results of a gait measurement experiment, after which an investigation on obtaining useful data for walking risk assessment was done, will be reported.

2. A walking risk assessment method using smartphone sensors

The smartphone, which has quickly disseminated in recent years, has various built-in sensors. Particularly, an acceleration sensor and GPS are in almost all types of smartphones, because these two sensors are indispensable in realizing basic smartphone functions (i.e., rotating the screen

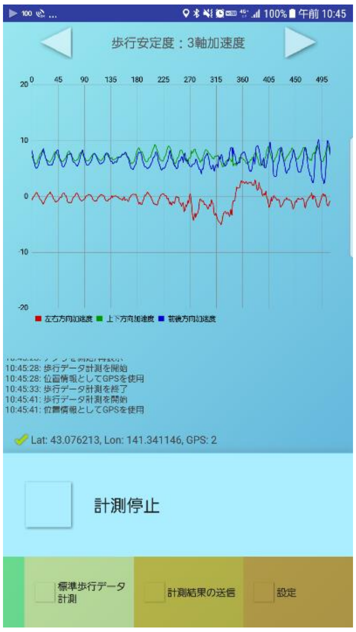

Fig. 1 Application for obtaining the acceleration sensor data

according to the orientation of the terminal and detecting the present location). In this study, we focused on these sensors, and attempted to investigate the possibility of assessing the walking risks by using smartphones. Points examined were whether it was possible to determine the walking risk of a pedestrian based on the walking behavior, which was clarified based on the values of the acceleration sensor, and the present location of the pedestrian, which was detected by the GPS.

The acceleration generated during walking is thought to differ depending on whether the road surface is with or without snow. For example, when a pedestrian is walking on a snow- and ice-covered surface, the amplitude of acceleration is thought to be smaller than that of a pedestrian walking on a dry road surface, because the pedestrian walks carefully on the slippery surface to avoid slip-and-fall. It is estimated that the tendency in walking acceleration (gait) changes with the change in the snow and ice conditions on the road surface.

In this study, we developed, for Android smartphones, an application that reads the acceleration sensor data and location information (Fig. 1), and obtained acceleration data on three axis (upward-downward, right-left, and forward-backward), and the location information. To realize a high accuracy measurement of acceleration during walking and to reduce battery drain, the interval of measurement of the three-axis acceleration was set as 50Hz in this application. In addition to this setting, the sleep function of the CPU was suppressed to avoid occurrences of missing data during the acceleration measurement. The location information was obtained at one second intervals. The positioning was done using the GPS only.

3. Outline of the gait measurement experiment

In this study, the experiment was done at the Tomakomai Winter Test Track owned by the Civil Engineering Research Institute for Cold Region on the nights of January 16 and 17, 2018, to investigate 1) the possibility of obtaining data that are useful in assessing the risk of walking by using the gait measurement application that we developed (Section 2), and 2) the possibility of assessment of slip-and-fall risks of pedestrians of all ages and sexes. An overview of the experiment is shown in Fig. 2. In this experiment, the road sections with three types of surfaces (dry surface, surface with compacted snow, and surface with thin ice film; each of which was 20m in length) were prepared. The coefficient of sliding friction of the road surface was measured by using a portable skid tester, and the surface temperature was measured by using an infrared thermometer. After these measurements, test subject pedestrians, who carried a smartphone, walked on the test sections at

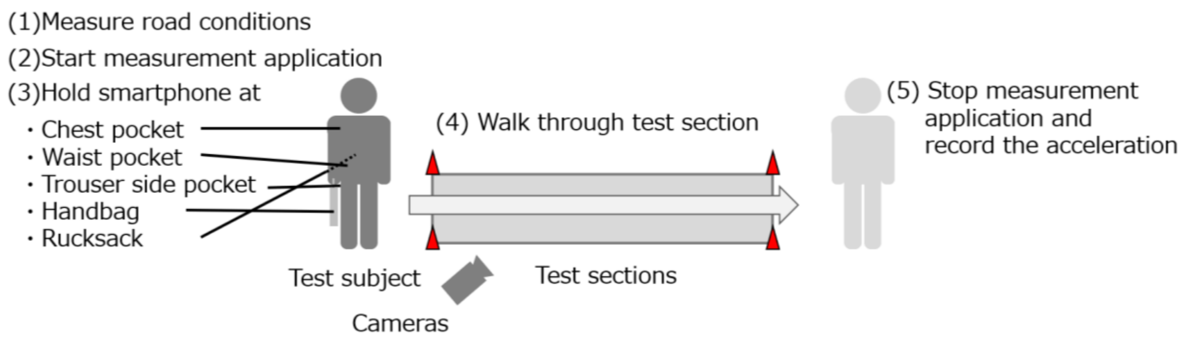

Fig. 2 Overview of the experiment to examine the quantitative assessment method for walking risks

their paces, and their gaits were measured. In this gait measurement, the three-axis acceleration was measured at intervals of 50Hz. The smartphones used were ASUS ZenFone 3 Max ZC520TL, Sony XPERIA AX and XPERIA XZ, SHARP AQUOS PAD SH-05G, and Samsung Galaxy S7 Edge and Galaxy Note 2. The locations on the body of the pedestrians for keeping the smartphone were the chest pocket, waist pocket, trouser side pocket, handbag, and rucksack. During this walking experiment, video shooting of the pedestrians was done. The test subjects, 31 persons from the age of 21 to 65, were recruited through the Winter Life Promotion Council.10) The heights of the test subjects (25 males and 6 females) were in the range of 150cm to 190 cm. The times for which they had lived in cold and snowy regions varied from about 4 to 65 years. The test subjects wore their everyday clothes and comfortable shoes, as well as helmets and other protective gear. To secure safety during the experiment, a person for safety control oversaw the experiment. The detailed information of the experiment, safety issues, points to bear in mind, and privacy protection were explained to the test subjects, and consent was obtained from each of them.

4. Results of the gait measurement experiment and discussion

4.1 Conditions of the experiment road sections

Fig. 3 shows the conditions of the road surfaces of the test sections for the gait measurement experiment. The surface temperatures of the dry, compacted snow, and ice film road surfaces were in the range from -1℃ to -3℃. The coefficient of sliding friction of the road surfaces were 0.6 or higher for the dry surface, around 0.55 for the compacted snow surface, and around 0.35 for the ice film surface.

The surfaces of the dry, compacted snow, and ice film sections were roughly flat. The thickness of the ice film was less than 1mm, and the ice film section had a partially exposed pavement aggregate.

Fig. 2 Conditions of the road surfaces of the test sections

4.2 The walking speed, step length, step time, and number of slips

Table 1 Conditions of the road surfaces of the test sections

Road surface conditions	Walking speed (km/h)	Step length (m)	Step time (sec/step)	Number of slips (time/20m)
Dry	4.40	0.69	0.58	0.00
Compacted snow	4.09*	0.65	0.57	0.17
Ice film	4.16*	0.63*	0.55	0.10

Significance of degree of stability in walking when compared with that for walking on the dry surface:
*：P<0.05; **：p<0.01

Table 1 shows the average walking speed, step length, and step time (the time required for taking one step) and the average of the occurrences of slips for all test subjects. The table also shows the result of a t-test done to know the significance of the decrease in walking speed, step length, and step time compared with those on the dry surface. Significant decreases were observed in walking speed on the compacted snow and ice film sections compared with that on the dry section. On the ice film section, the reduction in the step length compared with that on the dry section was found to be significant, but no significant differences according to the road surface conditions were found in the step time. It was verified that these tendencies were found in all test subjects, irrespective of the age or sex. The number of slips were 0.17 times/20m on the compacted snow section, and 0.10 time/20m on the ice film section. It was found that slips tend not to occur under the condition in which the values for walking speed and step length became small, such as that on the ice film section.

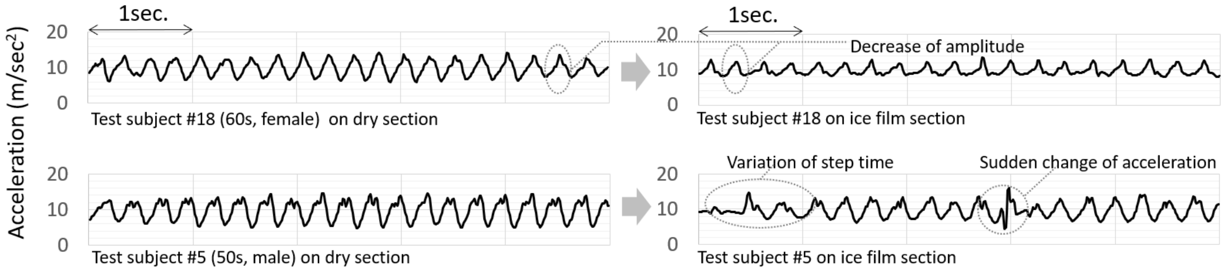

Fig. 4 Upward-and-downward walking acceleration of two test subjects on different road surfaces (smartphone location: chest pocket)

4.3 The walking speed, step length, step time, and number of slips

4.3.1 Time-series changes in the walking acceleration

Fig. 4 shows the time-series changes in the upward-downward acceleration measured from the chest pocket of the test subjects on various road conditions. The walking behavior was generally regular on the dry section, and the amplitude of the walking acceleration was about 10m/sec^2. On the compacted snow and ice film sections, as the result of careful walking to avoid falling, the amplitude of acceleration was about 6m to 8m/sec^2, which is small compared with that on the dry surface. The test subjects avoided slippery-looking spots when they walked on the compacted snow and ice film sections; therefore, unstable gaits, such as irregular step time and irregular changes in the acceleration were observed.

Based on the above results, we examined whether it is possible to evaluate the conditions of snow- and ice-covered road surfaces and the slip-and-fall risks by using the amplitude of acceleration in walking. In this examination, we calculated the acceleration obtained from the results of acceleration measurement done every 5 seconds (number of data points: 250), and considered the standard deviation of the obtained composite acceleration as the level of amplitude in acceleration in walking.

4.3.2 Standard deviation of the acceleration

Table 2 shows the average standard deviation of the acceleration obtained from the measured upward-downward, right-left, and forward-backward accelerations for all test subjects by location of the terminal on the body. The table also shows the results of the t-test done to know whether the decrease in the standard deviation of the acceleration, compared with that on the dry surface, was significant. The standard deviation of the acceleration was the highest for the dry section, followed by that for the compacted snow section and then, that for the ice film section. This tendency was observed in common in the cases, except for those when the location of the terminal was the rucksack. This tendency was also found to occur irrespective of the age, sex, or number of years the subject had lived in cold and snowy areas.

Table 2 The standard deviation of the acceleration (m/sec^2) for each location on the body where the terminals were kept on each road surface condition

Road surface conditions	Chest pocket	Waist pocket	Trouser side pocket	Handbag	Rucksack
Dry	2.70	3.02	3.77	3.20	3.29
Compacted snow	2.56*	2.73*	3.20*	2.79*	3.29
Ice film	2.26*	2.67*	3.03*	2.67*	2.79*

4.3.3 Frequency component of the acceleration

In this study, an evaluation of regularity in the walking behavior of pedestrians was attempted by obtaining the amplitude for each frequency of walking acceleration. The frequency component of walking acceleration was obtained by using the acceleration data in 5.12 second intervals (number of data: 256) and the fast Fourier Transform, and the relationship between the icy road surface conditions and the amplitude of each frequency of walking acceleration was analyzed.

Fig. 5 shows the time-series changes in the acceleration and the frequency component for test subject #30 (male in his 40s), when he walked on the dry section. Fig. 6 shows the time-series changes in the acceleration and the frequency component for the same test subject, when he walked on the ice film section. The acceleration for walking on the dry section (the solid black line in the figure) shows regular changes, and the frequency component of the acceleration (the solid gray line in the figure) indicates a marked increase at about 1.6 Hz. The reason for these was that the step time was nearly constant, at about 0.6 seconds (1.6Hz), and the changes in the acceleration, which was generated at the landing of a foot, occurred at about 1.6 Hz. The acceleration during walking on the ice film section was irregular compared with that during walking on the dry section. The frequency component of the acceleration at about 1.6Hz was smaller than that during walking on the dry section. The frequency component of the acceleration during walking on the ice film section from 1Hz to 2Hz was higher compared with that during walking on the dry section. This is thought to be due to the changes in the step time that occurred in the period from the 1st second to 2nd second, which occurred from irregular gaits in trying to avoid falling.

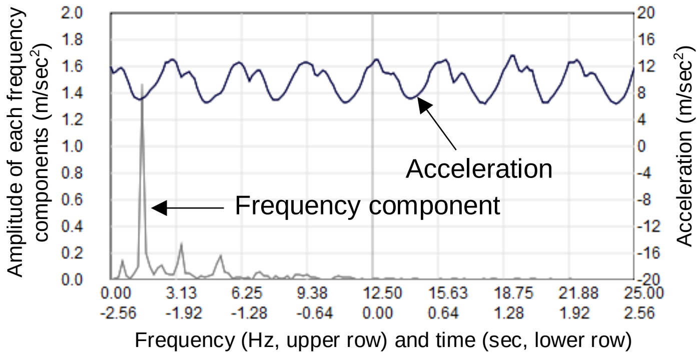

Fig. 5 Time-series changes in the acceleration and the frequency component for walking on dry section

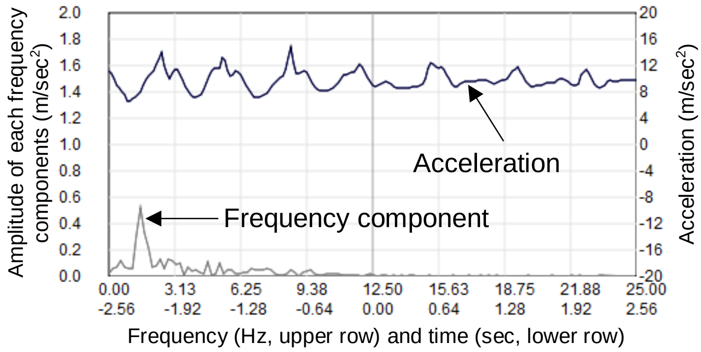

Fig. 6 Time-series changes in the acceleration and the frequency component for walking on the ice film section

The results discussed above demonstrate that the values of acceleration amplification measured by using a smartphone is an important factor in evaluating snow/ice-covered road surface conditions and risk of slip-and-fall. It was also clarified that the level of acceleration amplitude is not necessarily proportional to the number of slips, and that determining the conditions of the icy road surface is difficult only by using the level of acceleration amplitude, depending on the age group of the pedestrian and the location of the terminal on the body. It was suggested that accurate detection of the conditions of icy road surface and accurate assessment of the slip-and-fall risks are possible by considering the degree of regularity in walking, in addition to the level of the acceleration amplitude in walking.

5. Conclusion

In this study, to construct a simple method for assessing the risk of slip-and-fall for a wide area in real time by using smartphones, we developed a smartphone application for measuring the waking behavior of pedestrians, and examined the possibilities of obtaining data that contribute to assessing the risk of slip-and-fall by conducting a gait measurement experiment. The following lists the results and findings of this study.

- We developed a smartphone application for measuring walking behavior (acceleration in walking) by using the acceleration sensor in a smartphone.
- It was found that measurement of walking behavior is possible by using the walking acceleration measured with the above method, irrespective of the type of smartphone.
- When the condition of icy road surface changes, the level of acceleration amplitude for walking changes in many cases, irrespective of the age, sex, or the location of the terminal on the subject's body.
- In light of the above, it was demonstrated that the level of acceleration amplification measured by using the acceleration sensor of a smartphone is an important factor in detecting the snow/ice-covered road surface conditions and assessing the risk of slip-and-fall accidents.
- To perform high accuracy assessments for slip-and-fall risks, it is necessary to use other indexes in addition to the acceleration amplitude in walking, because it is possible to overlook the risk-prone locations, such as the location where slips occur, if only the level of acceleration amplitude in walking is used for determining the risk of slip-and-fall accidents.

We will improve the method proposed in this study, and develop a method for quantitatively assessing the risk of slip-and-fall in winter walking spaces, and examine the possibility of a wide area assessment of the slip-and-fall risks entailed by walking in winter by conducting the risk measurement experiments on actual streets, as shown in Fig. 7 .

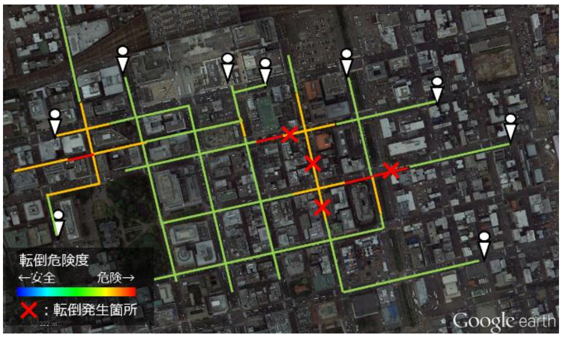

Fig. 7 Conceptual rendering of the assessment of walking risks in which a large number of test subjects participated

References

[1] Yasuhiro Nagata, Yasuhiro Kaneda, and Mami Tomita: An Analysis on Persons who Fell and Were Transported by Ambulance in Sapporo City, Proceedings of the JSSI & JSSE Joint Conference on Snow and Ice Research, p. 113. 2014. 113, 2014.

[2] Anttila, V.: Pedestrians during wintertime-slippery conditions, slipping accidents and information service, Technical Research Center of Finland (VTT), Tiedotteita-Meddelanden 2119, 2001.

[3] Yoshihiro Hashimoto: Analysis on Emergency Dispatch of Ambulances for Winter Slip-and-Fall Accidents (No. 1, The Overall Tendency), Report of Sapporo City Fire Science Laboratory, No. 9, pp. 35-39, 2002.

[4] Yoshihiro Hashimoto: Analysis on Emergency Dispatch of Ambulances for Winter Slip-and-Fall Accidents (No. 2, Susukino District, Relation Between the Weather and Accidents), Report of Sapporo City Fire Science Laboratory, No. 9, pp. 40-47, 2002.

[5] Yoko Shintani, Fumihiro Hara, and Tetsuo Akiyama: Pedestrian Slip and Fall Accidents in the Sapporo City Center in Winter-- Present Situation and Future Countermeasures, Comprehensive Urban Studies, Vol. 85, pp.57-68, 2005.

[6] Hirono Konno, Mami Tomita, Fumiyoshi Kawamura, Yasuhiro Kaneda, Hiroshi Hoshino, Naotoshi Kanamura, and Shin-ei Takano: Construction of A System for Collection and Provision of Winter Road Surface Information by Collaboration with Residents, Proceedings of the JSSI & JSSE Joint Conference on Snow and Ice Research, p. 46, 2010.

[7] Roberto Tokunaga, Makoto Funahashi, Naoto Takahashi, Motoki Asano, and Masamitsu Nakano: A Study on Winter Road Management Sophistication based on Road Surface Friction, Monthly Report of the Civil Engineering Research Institute for Cold Region, No. 661, pp. 11-18, 2008.

[8] Tomoyuki Nakajima, Naoto Takahashi, and Kazutaka Tateyama: Assessment of the Winter Road Conditions using NIR and Microwave, Proceedings of the Japan Road Conference, No. 32, 2017.

[9] Leif Sjögren: Friction requirements on roads, paths and cycleways in summer road condition in Sweden、Proceedings of Road Safety on Five Continents, 2018.

[10] Website of the Winter Life Promotion Council: http://www.winter-life.jp/ (Accessed on Feb. 22, 2019)

Inbound tourism development in cold regions – a case of Hokkaido, Japan

Ayami Saga, MA
Researcher
Hokkaido Development Engineering Center, Japan
saga@decnet.or.jp

Masaaki Abe
Director, Hokkaido Development Engineering Center, Japan

Norihiko Ito, Dr., Eng.
Senior Researcher, Hokkaido Development Engineering Center, Japan

Summary

In 2017, international tourists to Japan numbered 28.89 million, recording the highest with 19.3% increase from that of 2016. Compared with 8.4 million in 2008, it has increased by 345%.
Likewise, the number of inbound tourists to Hokkaido has increased by 400% from 0.69 million in 2008 to 2.79 million in 2017. Those increases have resulted mainly from the relaxation of visa requirements for the tourists from part of Asian countries. Other reasons of the increase are steadfast economic development of those countries and their geographical closeness to Japan. As a result, for all Japan and Hokkaido, Asians take 85% or more of the total inbound tourists.
Though Japan has 43 prefectures and Hokkaido one of those draws about 10% of inbound tourists to Japan.
This paper analyses the background of the popularity of Hokkaido, introducing how Hokkaido is making use of its cold, snowy environment for inbound tourism. Further, the potential of cold regions including Hokkaido as tour destinations toward the future is examined.
Lastly, the risk of global warming that may bring about the destruction of cold regions' tourism is referred.

1. Introduction

The number of inbound tourists to Japan has continued to increase, recording the highest 28.29 million in 2017. The increase is 345%, compared with 8.4 million in 2008 (Fig. 1).
The number of inbound tourists to Hokkaido has also increased by 400% from 0.69 million in 2008 to 2.79 million in 2017 (Fig.2). Those increases have resulted mainly from the relaxation of visa requirements for the tourists from part of Asian countries including China, Indonesia, Thailand, Korea, Vietnam and etc. Other reasons of the increases are steadfast economic development of those countries and their geographical closeness to Japan. As a result, for all Japan and Hokkaido, Asians take 85% or more of the total inbound tourists.
The greatest incentive that is drawing the Asian tourists is cold, snowy environment of Hokkaido. As shown in the chart (Fig. 4), compared with other seasons, more inbound tourists are visiting Hokkaido in the winter season from December to March. Meanwhile, the no. of inbound tourists to Japan is not so greatly different by season (Fig. 3).

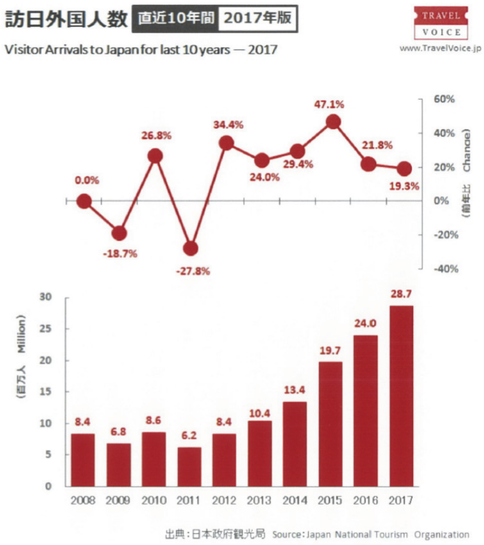

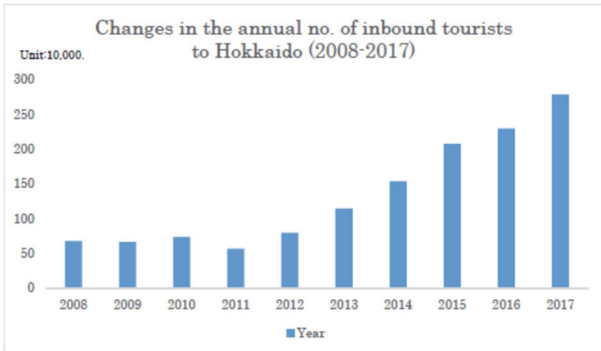

Fig.1 Annual changes in the no. of inbound tourists to Japan (Source: JNTO)

Fig.2 Annual Changes in the no. of inbound tourists to Hokkaido (Source: Hokkaido Gov.)

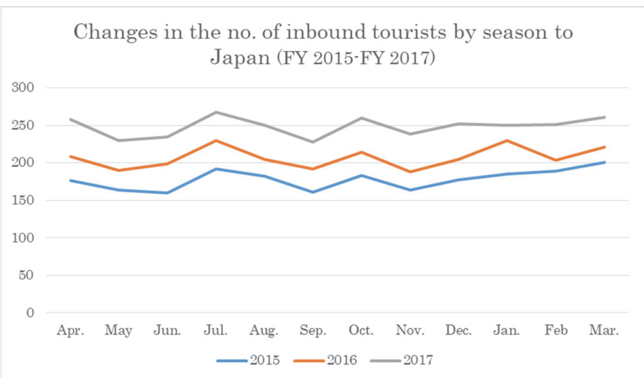

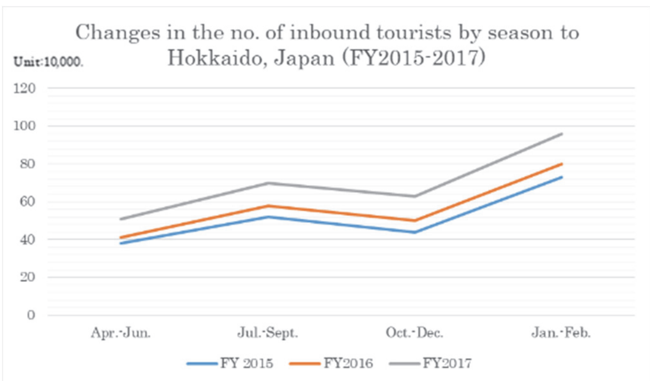

Fig.3 Changes in the no. of Inbound tourists by season to Japan (Data Source: JNTO)

Fig.4 Changes in the no. of inbound tourists by season to Hokkaido, Japan (Data Source: Hokkaido Gov.)

This indicates how much Asian tourists admire Hokkaido as a cold, snowy tour destination. Though the northern Honshu sees heavy snowfalls and the air temperatures there are lower than southern Honshu including Tokyo, compared with Hokkaido, the temperatures are relatively higher. Fig. 5 compares the average temperatures of Aomori City, the capital of Aomori Prefecture, the northern most prefecture of Honshu and those of Abashiri City, one of the popular winter destinations in Hokkaido.

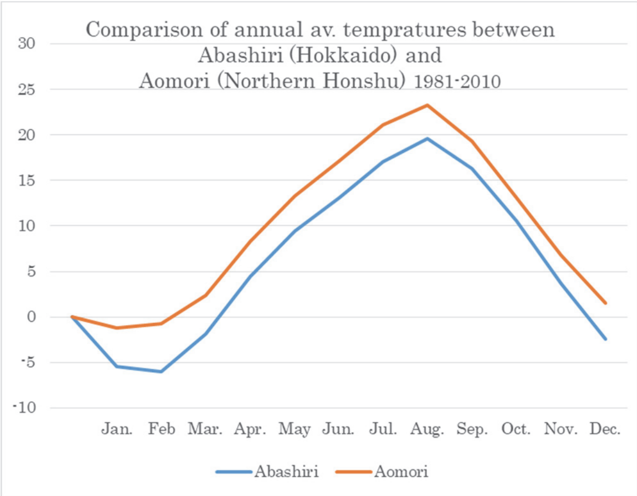

Fig.5 Comparison of annual ave. temperatures between Abashiri (Hokkaido) and Aomori (Northern Tohoku)
(Data Source: Japan Meteorological Agency)

What to be focused is that Hokkaido has been significantly popular among Asian inbound tourists whose countries see no snow. Concerning the accumulated no. of guests from overseas at accommodations by region, Hokkaido takes the third place following Kanto area including Greater Tokyo and Kansai where world-renowned tourism spots, Kyoto and Osaka are located. Hokkaido owes this popularity to the tourism resources characterized by cold, snowy environment which is drawing many tourists. This study introduces how Hokkaido is attracting tremendous inbound tourists, utilizing the cold environment and explores the potential of the tourism in cold regions toward the future.

2. Tourism amusements making use of the cold environment in Hokkaido

The Sapporo Snow Festival has been most famous (Fig. 6), but there are a number of other winter events and programs available all around Hokkaido. While the cold environment and heavy snowfalls are annoying locals, the cold and snow are the natural blessings offering great attractions to tourists, particularly those from non-snowy countries. A number of skiers are swarming in Niseko to enjoy powder snow. Ice floes that appear along the east shore of Hokkaido and rare spices of northern eagles are other winter charms. The ice floes function a vital role to nurture the amazing ecology in east Hokkaido including Shiretoko, a UNESCO World Heritage. They are bringing nutritious fresh water of the Amur River to the Okhotsk Sea, and the nutrition explodes phytoplankton that increase sea creatures that are eaten by birds and animals. The Red-crowned Cranes beautifully dancing in mid-winter, their mating season, are the most popular targets of photographers around the world (Fig. 7). Back-country skiers are enjoying powder snow in the wilderness of the Daisetsu Mountains and Mt. Rishiri in north. Some are snorkeling in frozen Lake Shikotsu that is boasting the purest water quality in Japan (Fig. 8). Those are the secrets drawing a huge number of inbound tourists to Hokkaido.

Fig. 6 Helsinki Cathedral at Sapporo Snow Festival

Fig.8 Winter Snorkeling in Lake Shikotsu

Fig.7 Mating dance of Red-crowned Cranes

Fig.9 The Ainu, Akan, Hokkaido,

3. Potentials of cold regions' tourism in Hokkaido

In the world, adventure tourism market has been rapidly growing. Adventure tourists take about 40% of all the outbound tourists departing from Europe and Americas [1]. The outbound tourists from those continents take about 60% of the world outbound tourists. ATTA (Adventure Travel Trade Association, USA) defines an adventure travel as a travel including two of the three elements: nature, activity and culture.[2] The adventure tourism market value has recently amounted conservatively to 683 billion, showing 21% CAGR since 2012 [4]. We have found that Hokkaido with a vast wild nature that affords countless adventure opportunities perfectly meets the conditions of adventure tourism. Inbound tourists who are visiting Niseko, Hokkaido which has become a world renowned ski resort actually are adventure tourists. Their focus is backcountry skiing enjoying powder. The results of a research conducted by Otaru University of Commerce in 2015[5] targeting 254 overseas tourists in Niseko, 80% of them are from Australia, North America, Europe and New Zealand. For 30% of the total survey targets, the expenditures for the trip in total including air fares range from $4,000 to $10,000. Though the targets include 18.1% of Asians, this expenditure amount seems to reflect the feature of adventure tourists who are relatively upscale people [3]. This suggests that besides the swarming Asian tourists, the cold snowy environment of Hokkaido could draw tourists from the adventure tourism market.
Hokkaido has Ainu culture which also completely meets the culture factor of adventure tourism (Photo 9.). The Ainu are the descendants of Jomon people, the indigenous people to Japan and their culture currently remains only in Hokkaido. The same as other indigenous people, Ainu people are completely nature oriented and have deep knowledge about the nature.

4. Issues about the cold regions' tourism development

The cold regions' tourism resources greatly depend on the cold environment. Therefore, the most serious concern about the tourism is global warming. In recent years, the average atmospheric temperatures on the earth have steadily increased so as the Arctic regions' temperatures do (Fig.10). Actually, unusually high temperatures have been recorded in the Arctic Circle. The average temperatures of Hokkaido has continued to increase the same as in the Arctic regions (Fig. 11).

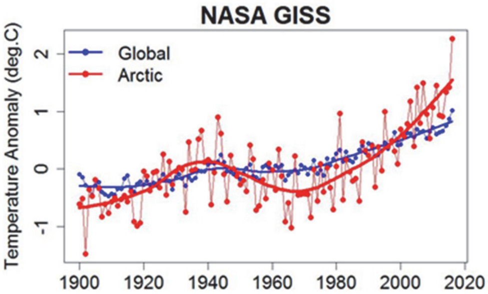

Fig. 10 1898-2015 Global and Arctic temperature changes (Source: NASA/GISS)

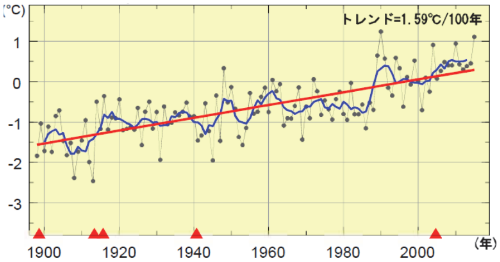

Fig. 11 Changes in the ave. annual temperatures of Hokkaido (Source: Japan Meteorological Agency)

The report of IPCC[6)] indicates that the average temperatures of the Earth have risen about 0.85 °C over the past 100 years. It also definitely mentions that the changes resulting from global warming have been significantly recognized as ocean warming and sea level rises. The global warming phenomenon are caused by radiative forcing whose largest contribution is the atmospheric concentration of CO2 produced by human activities. Scientists say that global warming is progressing faster than expected.

5. Conclusion

As abovementioned, the potential of the cold regions' tourism is huge. Not only in Hokkaido, but in many places in cold regions on the earth as well, untouched pristine nature that allows a number of opportunities to enjoy diverse activities still remains. In addition, unique indigenous people are living there with cold-environment specific cultures. They include Sami in Finland, Yakut, Evenk and many other in Siberia and Eskimo tribes in the USA as well as in Canada. Those places meet all the elements of adventure tourism, which suggests huge potential of cold regions' tourism.
However, if the adverse effects of global warming are getting worse and the cold environment and its blessings such as ice floes and snowfalls disappear, the tourism utilizing them will result in destruction. To minimize the destructive effects of global warming, we need to make desperate efforts to decrease CO2 and other greenhouse gas emissions.

References

[1] Tourism Highlights 2018, UNWTO, 2018, p.14,
[2] Global Report on Adventure Tourism, UNWTO & ATTA, 2014, p.10,
[3] Viren P.P., Murray K.A., Brown T. and Beckmann C., North American Adventure Travelers: Seeking Personal Growth, New Destinations, and Immersive Culture, ATTA, P.6, Oct. 2017
[4] 20 Adventure Travel Trends to Watch in 2018, ATTA, 2018, p.5
[5] Goto H., Miyazaki Y., Praet C., and Lee S., Hokkaido Niseko Ni Okeru Kanko Chiiki Kenkyu（Local Tourism Research in Niseko, Hokkaido), Vol. 67, no. 1, Shogaku Tokyu, 2017, p.303-326
[6] The Physical Science Basis. Contribution of Working Group I to the Fifth Assessment Report of the Intergovernmental Panel on Climate Change, 2013

POSTER SESSION

A Snow and Ice Surface Processing Technique Using Machine for Urban Sidewalks

Masatoshi Makino
Machinery Technology Research Team
Civil Engineering Research Institute for Cold Region, PWRI
Japan
makino-m@ceri.go.jp

Hiroshi Yamaguchi, Civil Engineering Research Institute for Cold Region, PWRI, Japan
Takahiro Shimbo, Civil Engineering Research Institute for Cold Region, PWRI, Japan

Summary

On the sidewalks in urban areas of snowy and cold regions in Japan, uneven slippery snow and ice surfaces are formed. Many pedestrians have slip-and-fall accidents on such sidewalks. Based on the viewpoint of providing a barrier-free traffic environment for all sorts of users, including elderly and people with limited mobility, road surface management that improves the conditions of sidewalks has been required. We experimentally created a technique for processing snow and ice covered sidewalk surfaces, which uses machine processing. This paper reports the usefulness of the technique which we verified through our repeated tests and improvements.

Keywords: Sidewalk, Snow and ice surface, Crushing

1. Introduction

On the sidewalks in urban areas of snowy and cold regions in Japan, uneven slippery snow and ice surfaces are formed because of great changes in air temperatures and treading by many pedestrians (Fig. 1). Many pedestrians have slip-and-fall accidents on such sidewalks. Based on the viewpoint of providing a barrier-free traffic environment for all sorts of users, including elderly and people with limited mobility, road surface management that improves the conditions of sidewalks has been required. As a measure for providing safe walking conditions, road administrators spread anti-skidding materials, such as crushed stone of small-grain sizes, and install “sand boxes” that contain anti-skidding materials so that the citizens themselves are able to spread the materials on slippery sidewalks. However, the effectiveness of spreading anti-skidding materials is short-lived, and when large amounts of materials are spread during the winter, the work volume for recovering the materials increases in spring. On sidewalks in urban areas of Sapporo, snow steps are formed at locations where the sidewalks intersect with access roads or carriageways. Removal of a thickly accumulated snow “steps” on the sidewalk is usually done by using backhoes from the carriageway during the snow hauling works for the carriageway, because such snow removal is not possible with small snow blowers used for sidewalks. An efficient surface processing technique for such areas had also been required.

Fig. 1 Slippery ice covered sidewalk

Therefore, we experimentally created a technique for processing snow and ice covered sidewalk surfaces, which does not depend on anti-skidding materials but uses machine processing. We verified the usefulness of the technique through our repeated tests and improvements.

2. Outline of the winter road surface processing equipment

To create a winter sidewalk processing technique that does not depend only on anti-skidding materials, we focused on an icy road surface crushing technique used abroad, which used equipment with a simple structure and did not require a special power source for crushing ice. By utilizing this technique, we experimentally created an equipment for crushing and removing surface snow and ice from a winter sidewalk.

The purposes of using this surface processing equipment is to improve the sidewalk surface conditions by crushing and leveling the slippery snow and ice surface. This processing equipment consists of an ice-breaking part and a snow-removal part, and is used by attaching them to a small snow blower usually used for snow removal on sidewalks.

2.1 The ice-breaking part

The structure of the ice-breaking part used for this experimental equipment was used abroad mainly for crushing snow and ice surfaces of carriageways. The width of 1.52m of the ice-breaking part was determined based on the width of 1.5m of the small snow blowers used for snow removal on the sidewalks of the national highways in Hokkaido, Japan (Fig. 2).

The main feature of this equipment was a cylindrical rotating body with breaking blades made of round bars with diagonally cut points (Fig. 3). This rotating body was pushed onto the icy sidewalk surface by its own weight and rolled by the propulsion force of the snow blower. Continuous ice crushing was able to be done without using any special power source.

Fig. 2 The initial ice-breaking part attached to a small snow blower

Fig. 3 Ice-breaking blades

The pushing pressure was made to be adjustable by attaching weights (up to 200kg), in addition to the equipment’s own weight (1,230kg).

The icy sidewalk surface is crushed by the ice-breaking blades, which cut into the icy surface and make holes. Then, by the propulsion force of the snow blower, which applies rolling power to the

Fig. 4 An icy sidewalk surface after processing and an ice fragment generated in the work

cylindrical body, the blades dig up the ice surface. Through this crushing process, snow and ice fragments, each of which is about 5cm × 5cm, are generated on the sidewalk (Fig. 4).

To clarify the optimum pushing pressure for snow and ice processing for the sidewalk, an ice crushing test using various weights was conducted. As the result of this test, the crushing depth was from 7mm to 16mm when only the weight of the equipment was applied. It was clarified that effective processing of a slippery icy sidewalk surface was possible even when only the weight of the equipment was used.

The sidewalks of national highways in Hokkaido are paved with standard fine-graded asphalt concrete of 3cm in thickness. When the ice layer on the sidewalk is thin, the crushing blades may cut through the ice layer and touch the pavement. By considering such a condition, an experiment for surveying the influence of the crushing blades on the pavement was done by using a pavement specimen of 30cm in length, 15cm in width and 3cm in thickness, and a full scale (1/1) model with four blades. The condition in which the four blades touch the pavement in the rotating manner was reproduced.

In this experiment, the blade model was pushed to the pavement specimen by using a hydraulic press, and the dimensions of the scratch generated on the pavement specimen and the load at the time when the scratch was generated were measured (Fig. 5 and 6).

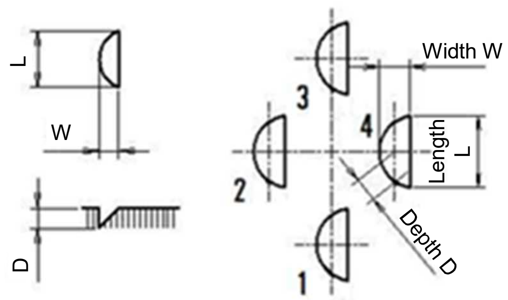

Fig. 5 Locations for measuring the dimensions of the scratch on the pavement specimen

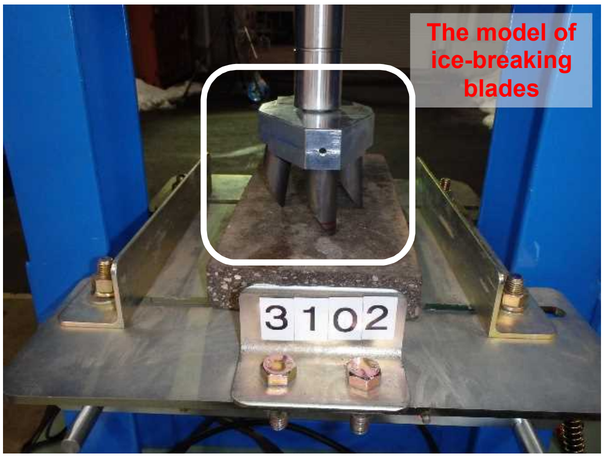

Fig. 6 The experiment using a pavement specimen

According to the results of this experiment using the load up to 1,960N, which was about the same as the weight of the ice-breaking part, the maximum depth of the scratch made by the blade was 2.4mm (Table 1). It was found from the results of this test that one blade causes a scratch of about 2mm in depth on the pavement when the blade directly touches the pavement during the ice-breaking work.

Table 1 The loads and the dimensions of the scratches on the pavement specimen

	Set load (N)		980	1,225	1,470	1,715	1,960
	Actual load (N)		952.0	1,253.6	1,454.4	1,764.2	1,936.8
1	Length	L (mm)	8.8	10.4	11.8	12.5	13.0
	Width	W (mm)	1.7	2.1	2.4	2.6	2.8
	Depth	D (mm)	0.8	1.3	1.6	1.9	2.0
2	Length	L(mm)	6.6	6.9	8.7	9.4	9.8
	Width	W(mm)	1.1	1.3	1.6	1.8	1.9
	Depth	D(mm)	0.5	0.5	0.7	1.1	1.3
3	Length	L(mm)	11.6	12.4	12.9	13.9	14.0
	Width	W(mm)	2.2	2.4	2.6	3.0	2.7
	Depth	D(mm)	1.3	1.5	1.9	2.4	2.2
4	Length	L(mm)	0.0	0.0	0.7	1.2	3.5
	Width	W(mm)	0.0	0.0	0.2	0.2	0.7
	Depth	D(mm)	0.0	0.0	0.0	0.1	0.2

To prevent damage to the pavement covered with thin ice layers, we added to the equipment a function to control the crushing depth (Fig. 7). To control the cutting depth of the ice-breaking blades, height adjustable skid shoes were added to both sides of the frame of the ice-breaking part. Screw-adjustable skid shoes were employed for easy and accurate height adjustment.

Work safety was improved by attaching a guard covering the ice-breaking part to prevent pull-in accidents (Fig. 8).

Fig. 7 The breaking depth control device attached to the ice-breaking part

Fig. 8 The guard for preventing pull-in accidents

2.2 The snow-removal part

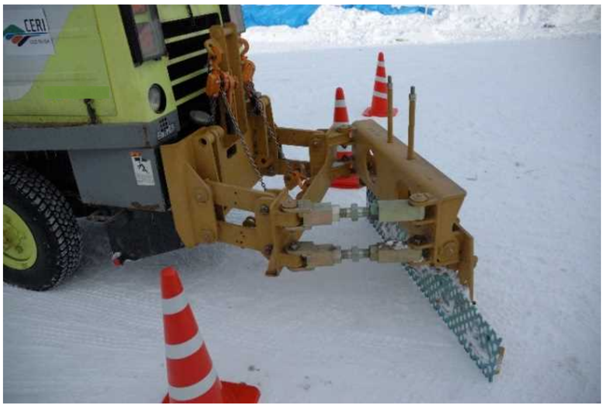

Fig. 9 The initial snow-removal part attached at the rear of the snow blower

A snow-removal part for removing crushed snow and ice from the sidewalk was experimentally created and attached at the rear of the snow blower. A blade in the form of a net was attached to achieve a surface roughening effect, and adjusting the links made it possible to change the direction of snow removal (Fig. 9).

The test to examine the performance of the snow-removal part revealed that the performance is low in terms of following the unevenness of the sidewalk surface, and a considerable amount of snow and ice fragments were left on the sidewalk. The great overhang of the rear part of the blower and the center-pin steering of the vehicle made it necessary for the operator to take particular care not to hit sidewalk fences or other auxiliary road facilities.

Based on the results of this examination, the equipment was improved so that the snow-removal part at the rear of the vehicle was shorter than the initial one, and hydraulic power enabled the lift-and-fall and adjustment of the snow-removal part (Fig. 10). To further improve the performance, a snow-removal edge was attached to the location immediately behind the ice-breaking part (Fig. 11). The effectiveness of the equipment in which the ice-breaking part and the snow-removal part were combined together was examined.

Fig. 10 The improved snow-removal part at the rear of the vehicle

Fig. 11 The snow-removal edge attached immediately behind the ice breaking part

In the examination of the snow-removal part attached at the rear of the vehicle, it was found that this equipment left crushed fragments where unevenness is considerable. In the equipment setting, in which the snow-removal edge was attached immediately behind the ice-breaking part, the amount of crushed ice fragments left on the sidewalk was small and the performance in following the unevenness of the icy surface was improved.

Fig. 12 The improved snow-removal part attached immediately behind the ice-breaking part

In an interview, the operator reported to have felt a lighter load when operating the equipment with the snow-removal edge attached immediately behind the ice-breaking part. The operator expressed that the influence of the extra equipment on the steering was small. The vehicle used for this examination had a front biaxial tandem structure; therefore, it was estimated that the load from snow removal concentrated at the tandem axel and the steering was not influenced by the snow removal load.

After verifying that the performance of the snow-removal part in following the unevenness of the snow and ice on the sidewalk was improved and that the influence of the two parts on vehicle steering was negligible, the location for attaching the snow-removal part was changed to the location immediately behind the ice-breaking part (Fig. 12).

As a main feature, the snow-removal part is moved independently up and down by using a linkage. The equipment follows the unevenness of the icy surface by pushing the ice-breaking part onto the icy surface using its own weight, and the snow-removal part removes the snow and ice crushed by the blades to both sides of the sidewalk.

To push away ice and snow fragments to the right and left, the propulsion angle of the v-shaped blade was set as 74° (Fig. 13). An additional edge of 6cm in height and with a propulsion angle of 90° was attached at the front edge of the plate under the blade. The addition of this edge made it possible for the snow-removal part to evenly touch the sidewalk surface and secure good performance in following the unevenness of the surface.

The lifting and lowering of the snow-removal part for the works and out-of-service traveling is able to be controlled from the operator's seat in the cabin by using the hydraulic cylinders(Fig. 14).

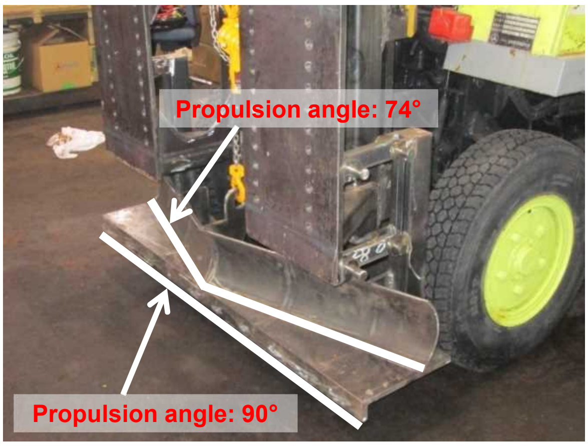

Fig. 13 The angles of the blades

Fig. 14 The hydraulic cylinder for lifting and lowering the snow-removal part

3. Verification of the performance of the improved ice surface processing equipment

Fig. 15 The improved ice surface processing equipment attached to a small snow blower

To verify the performance of the improved processing equipment (Fig. 15), a test on a road surface covered with an ice sheet and created for this test was done, and an adaptability test on a sidewalk in service was also done.

3.1 Processing performance test

Fig. 16 Skid resistance measurement using the ASM

To clarify the changes in the condition of sidewalk surface after the processing, we created an icy road surface in the premises of the Civil Engineering Research Institute for Cold Region (CERI), and conducted a performance verification test. This icy surface was 2m in width, 30m in length and 10cm in thickness. For measuring skid resistance, an American Slip Meter (ASM) (Fig. 16), which is a meter for measuring the skid resistance of floors, was used. Measurement by using the ASM is easy and can be done in a short period of time. The results of the measurement did not conform to the Japanese standards; however, it was possible to clarify the changes in slipperiness of the road surface by comparing the results of measurements taken before and after the processing.

Through this measurement, it was verified that it is possible to break icy surfaces and to remove snow and ice fragments without any problem, even for an icy surface with an average snow density of 777kg/m^3 and an average snow hardness of 264kg/cm^2 (Fig. 17). It was found in the measurements before and after the processing, that the skid resistance after processing increased and that the processing by using this equipment is effective in preventing skidding (Fig. 18).

Fig. 17 Sidewalk surface before processing (left) and that after processing (right)

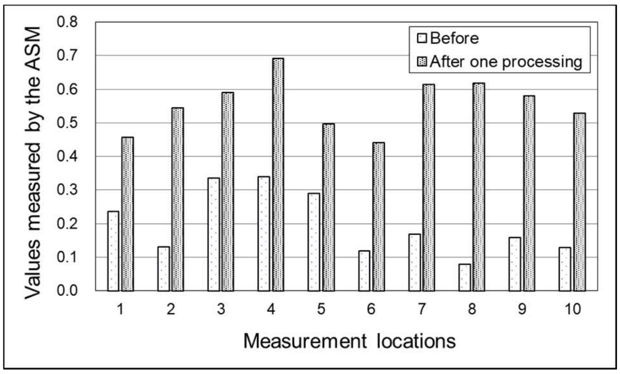

Fig. 18 Skid resistance (of the icy road surface in the premises of CERI)

3.2 The adaptability test on the sidewalk in service

Fig. 19 The snow and ice surface on the sidewalk was crushed into fragments of approx. 5cm × 5cm.

To investigate the maneuverability of the vehicle with this equipment and performance of this equipment on the sidewalk in service, an adaptability test was done on a sidewalk administrated by the City of Sapporo. The test sidewalk surface was that with compacted snow with an average snow density of 739kg/m^3 and an average snow hardness of 145kg/cm^2, which are nearly the same characteristics as those of an ice sheet.

It was verified in this test that the vehicle control stability and workability were equal to those of a snow removal machine (i.e., snow blower) without any additional equipment and that the ice crushing and removing works were carried out without any problem.

A similar test was done on an additional sidewalk administered by the City of Sapporo (Fig. 19 and 20).

Fig. 20 The improved sidewalk surface formed by using the edge of the snow-removal part

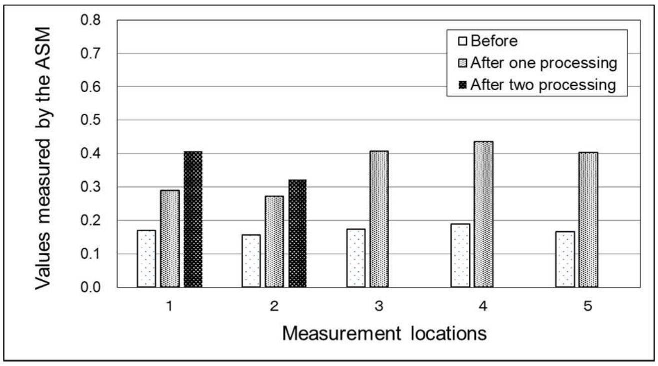

Fig. 21 Skid resistance (sidewalk in service)

The tested sidewalk surface was an ice sheet covered with a compacted snow layer. The average snow hardness of this surface was 158kg/cm^2. The skid resistance increased after the processing. This test clarified that this processing technique was effective in improving the conditions of a slippery surface (Fig. 21).

Fig. 22 Repeated processing was done at the site with an approx. 20cm height difference.

The crushed snow and ice fragments were manually removed onto the road shoulders.

An experimental processing of a part of sidewalk which had a height difference with the other parts of the sidewalk was done. At this location, an approximately 20cm-high snow and ice step was formed from treading by pedestrians (Fig. 22).

The removal of snow steps on the sidewalk, where snow accumulates thickly to form a height difference, is usually done by using backhoes on the carriageway during the snow hauling works for the carriageway. During this experiment, the icy step was repeatedly processed by using the created equipment. The snow and ice fragments generated in the processing were manually removed onto the road shoulders. In the experimental processing, it was verified that processing at the location with a height difference on the sidewalk is also possible by using this equipment.

4. Conclusion

By using an experimentally created snow and ice road surface processing equipment, slippery winter sidewalk surfaces were processed. The effectiveness of this equipment in improving sidewalk surface conditions was verified. The processing of snow steps formed on sidewalks, which was difficult to do with ordinary snow removal works on sidewalks, was found to be possible by using the created processing equipment.

This technique for processing snow and ice covered winter surfaces of sidewalks in Hokkaido, Japan, was verified to be useful.

In cooperation with the road administration offices of the City of Sapporo, we have been continuing the trial use of the improved equipment in the snow removal works by the city to further examine the workability and effectiveness of this technique using the created equipment in actual sidewalk maintenance works.

Experiment on Provision of Visibility Prediction on the Internet during Blowing Snow

Tetsuya Kokubu
Researcher
Civil Engineering Research Institute for Cold Region (CERI)
Public Works Research Institute (PWRI)
Japan
kokubu-t22aa@ceri.go.jp

Hirotaka Takechi, Satoshi Omiya, Joji Takahashi, Masaru Matsuzawa, Civil Engineering Research Institute for Cold Region (CERI), Public Works Research Institute (PWRI), Japan

Summary

On winter roads in snowy and cold areas, traffic hindrances caused by snowstorm-induced poor visibility and snowdrifts due to snowstorms frequently occur and have a significant social impact. In recent years, there have been many cases of disasters related to blowing snow under the influence of rapidly developed low-pressure systems even in the areas where the frequencies of severe blowing snow have been low.

By considering such meteorological changes in winter, our institute has been working on studies for preventing or reducing occurrences of blowing snow related disasters.

The technological measures against blowing snow disasters include physical measures, such as snow hazard control facilities (e.g., snow fences and avalanche prevention forests), and intangible measures, such as information provision. Existing physical measures have been effective in mitigating damage; however, the development of such facilities incurs considerable costs and takes much time. Furthermore, their performances against extreme snowstorms has limitations. To implement immediate and effective measures against blowing snow disasters, it is necessary, in addition to the conventional physical measures, to employ an intangible measure of providing information on the current conditions and prediction for snowstorms.

Our institute has developed a technology for estimating visibility during blowing snow based on the meteorological data (i.e., snowfall rate, wind velocity, and temperature). Since February 2013, we have been conducting an experiment on the provision of visibility prediction information to support drivers in their decision making in case of snowstorms. The subject area of this experiment is Hokkaido, which is in the northern part of Japan, and the experiment uses a website called “Visibility Information during Snowstorm.”

In addition to this information provision for PC users, we started the construction of a website for information provision for smartphone users and an experiment on delivering email alerts.

To clarify the effectiveness of information provision via this website, we checked the number of visitors to the website and conducted a questionnaire survey on them. We found that the number of visitors tended to increase when a snowstorm warning was issued, and about 80% of the users of “Visibility Information during Snowstorm” changed their travel behavior after they visited this website.

Keywords:Blowing Snow , Traveler Information , Internet

1. Introduction

On winter roads in snowy and cold areas, traffic hindrances caused by snowstorm-induced poor visibility and snowdrifts due to snowstorms frequently occur and inflict a significant social impact[1)]. In Hokkaido, which is in the northern part of Japan (Fig. 1), there have been many cases of blowing-snow-related disasters caused by extreme snowstorms under the influence of quickly developed low-pressure systems in recent years. During the snowstorm occurred in Hokkaido in

March, 2013, many national highways were closed for long periods. This snowstorm caused a large scale damage, with 9 persons died from snowstorm-related incidents. As a non-structural countermeasure for these snowstorms, provision of information on the real-time visibility during a snowstorm and on visibility forecast are thought to be important to support the drivers in their traffic-related decision making.

In February 2013, the authors started information provision on the predicted visibilities for the areas in Hokkaido at the "Visibility Information during Snowstorm" website. In addition to these information provision for PC users, we started constructing a website for information provision to smartphone users and conducted an experiment on delivering e-mail alerts in December 2013. We investigated and clarified the effectiveness of this information provision by conducting a questionnaire survey. In this paper, we will report on the summary of these experiment and survey results.

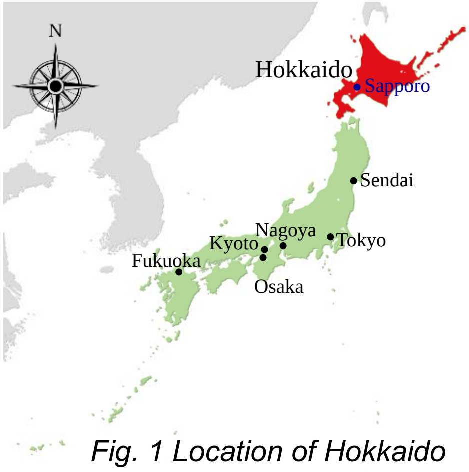

Fig. 1 Location of Hokkaido

2. The present conditions of winter road information provision systems

There are many examples of weather information provision from the road administrators to the road users[2]. Hokkaido Regional Development Bureau, Ministry of Land, Infrastructure, Transport and Tourism has been providing information on road weather (rainfall, wind direction and speed, snow depth, and air temperature) and road traffic including CCTV images and information on road closures on its website[3].

The Federal Highway Administration (FHWA) of the U.S.A conducted a demonstration experiment to call attention of the road users to a particular road weather conditions by using "Clarus", a road weather management program[4]. One part of this experiment was provision of an alert information at "511NY", a traffic information service website of New York State. In this system, alerts on various adverse weather conditions such as those related to snow, freezing, winds, and so on are created by combining the road weather information of Clarus and other weather data, and are provided at the website of "511NY". The Western Transportation Institute (WTI) constructed a website that displays the road and weather conditions in four western states of the U.S.A (California, Oregon, Washington, and Nevada). At this comprehensive information site, various road traffic related information along each route, including Closed Circuit Television (CCTV) images, information on road closures, weather observation data of Clarus, and weather forecast by the National Weather Service (NWS) are provided[3]. Similar efforts as these are carried out in the other states of U.S., too[5]. The University of Maryland's Center for Advanced Transportation Technology Laboratory (CATT Lab) developed "RITIS" system, which issues low visibility warning by using the current visibility data of Clarus[6]. The information provision of the CATT Lab is limited to the registered users.

In the provinces of Ontario[7] and Quebec[8] of Canada, efforts for supporting safe winter driving have been done through provision of information on current visibility during blowing snow, in addition to information on road weather (rainfall, snowfall, freezing and wind direction and speed), road conditions (CCTV images) and road closures. As far as we have researched, no other road administrations than ours, home or abroad, have attempted to develop a technique for predicting visibility hindrances during blowing snow and provide visibility information to support drivers' decision making.

3. Outline of the visibility information provision during snowstorm

3.1 How to create the visibility prediction information

The current and predicted visibility information are created by using the following weather data issued by the Japan Meteorological Agency and a technique for estimating visibility based on the weather conditions, which was developed by our institute (Fig. 2).

Good
(1,000m or longer)
Moderately poor
(500-999m)

・Precipitation, air temperature, wind speed: 5km-mesh data; Issued every 3 hours; 33 hours ahead forecast
・Precipitation: 1km-mesh data: Issued every 30 minutes: The current data and 6 hours ahead forecast

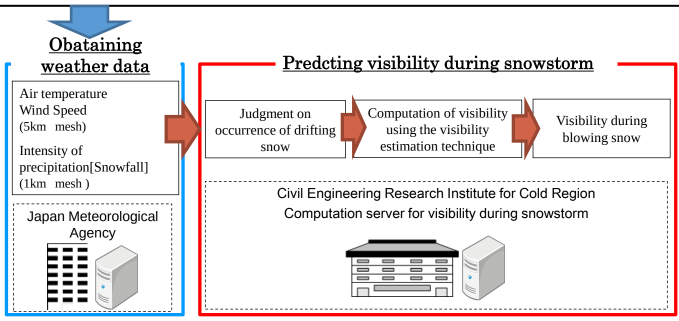

Fig. 2 Flow of computation for the current and predicted visibility during snowstorm

3.2 Outline of the experiment for visibility information provision during snowstorm

The experiment for snowstorm information provision using the Internet has been conducted since February 2013. The outline of the experiment is as follows.

3.2.1 PC version of visibility information during snowstorm

PC version of "Visibility Information during Snowstorm" has been operated since Feb. 1, 2013. The information provided on this website are 1) visibility information during snowstorm; 2) snowstorm information posted by general users; 3) weather warnings and alerts; and 4) information on road closures (Fig. 3). The following will detail the visibility information during snowstorm (Fig. 3-(1)) and the snowstorm information posted by general users (Fig. 3-(2)).

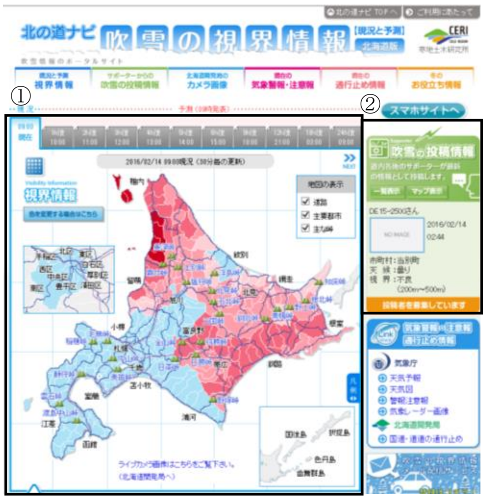

Visibility level

Good
(1,000m or longer)
Moderately poor
(500-1,000m)
Poor
(200-500m)
Very poor
(100-200m)
Severe visibility hindrance
(less than 100m)

Fig. 3 PC version of Visibility Information during Snowstorm
URL：http://northernroad.jp/navi/touge/fubuki.htm

(1) Visibility Information during Snowstorm

The "Visibility Information during Snowstorm" provides information for 1, 2, 3, 4, 5, 6, 9, 12, 18, and 24 hour forecasts. Update for the forecast values are issued
every 3 hours, and update for the current values are issued every 30 minutes. "Visibility Information during Snowstorm" is provided for all areas of Hokkaido which is divided into 221 small areas. Based on the result of a study on driving behaviors of drivers during blowing snow[10], the levels of visibility hindrances are classified into 5 levels of visibility of less than 100m, 100-200m, 200-500m, 500-1000m, and 1000m or longer. The visibility levels for areas in Hokkaido are indicated in five colors (Fig. 3).

(2) Snowstorm information posted by general road users

The "Snowstorm information posted by general road users" which was initiated in January 2011,provides information on visibility on roads contributed by road users using PCs or smartphones on the website.
The disaster information from citizens, which are provided through the social networking services, are very useful[11]. The Fire Defense Agency of Japan has been working on a project to collect

information provided by the general public[12]. The snowstorm-related information provided by the drivers during snowstorms are considered to be very useful.

The contributor (registered user) sends a driving condition information, by imputing on a message field on the web page, which includes the name of the municipality, name of the route, visibility condition, weather, comment (optional), and a still image of the road. The information sent by the contributor is published in two forms, as shown in Fig. 4, on the "Snowstorm information posted by general road users" page. To avoid inadequate posts, registration is necessary for becoming a contributor.

Fig. 4 Viewing window of the "Snowstorm information contributed by general road users"

3.2.2 Smartphone version of "Visibility Information during Snowstorm"

To improve usability of this website for the users who are not near their PCs or caught in blowing snow while driving, we constructed a smartphone version of the website and started provision of services on Dec. 1, 2013 (Fig. 5 (a)). By considering the use of this website by smartphone users, buttons such as "Weather Information" and "Road Closure Information" were displayed on the screen. A function for checking visibility information at the current location of the smartphone user was added. The user is able to obtain visibility information by sending his location information in the latitude and longitude coordinate (Fig.5 (b)).

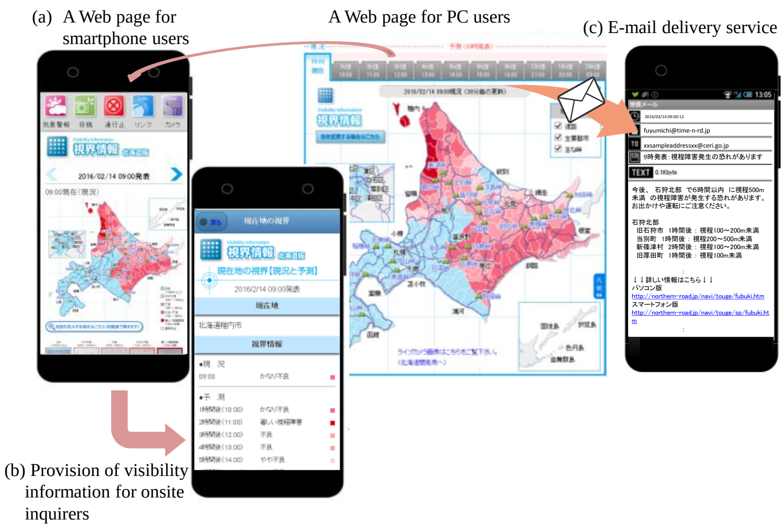

Fig. 5 Overview of the "Visibility Information during Snowstorm"

3.2.3 E-mail delivery service

On Dec. 20, 2013, we started an e-mail delivery service to call attention of drivers in advance to poor visibility.

Table 1 Delivery conditions for the e-mail delivery service

Item	Outline
Area	Possible to select the area subject to the e-mail delivery (Multiple areas can be selected) 【46 areas in Hokkaido; Some areas include multiple municipalities】
Delivery time	Possible to select the time for the e-mail delivery【2 types of delivery time---6 times per day: 6:00, 9:00, 12:00, 15:00,18:00, 21:00; 4 times per day: 9:00, 12:00, 15:00, 18:00】
Predicted visibility	Possible to select the visibility conditions for the e-mail delivery 【3 levels of visibility: Less than 500m, less than 200m, less than 100m】
Predicted hour	Possible to select the prediction delivery hours【2 types: 3 hours ahead, 6 hours ahead】

Based on the e-mail address and delivery conditions shown in Table 1, which are registered by the user in advance, this push-based information delivery service automatically notifies the user of the poor visibility predictions (Fig. 5 (c)).

4. Result of the experiment for information provision during blowing snow

4.1 Result of a questionnaire survey

To clarify the effectiveness of provision of snowstorm visibility information, we conducted a questionnaire survey on the website to the PC and smartphone users. A total of 483 persons responded to the questionnaire.

4.1.1 Result of the survey on “Visibility Information during Snowstorm”

Fig. 6 shows the responses to the question on the purpose of using this site. The first purpose of use was for work or commuting.
The second purpose of use was outings, among which the ratios for private matters, driving, and traveling were high.

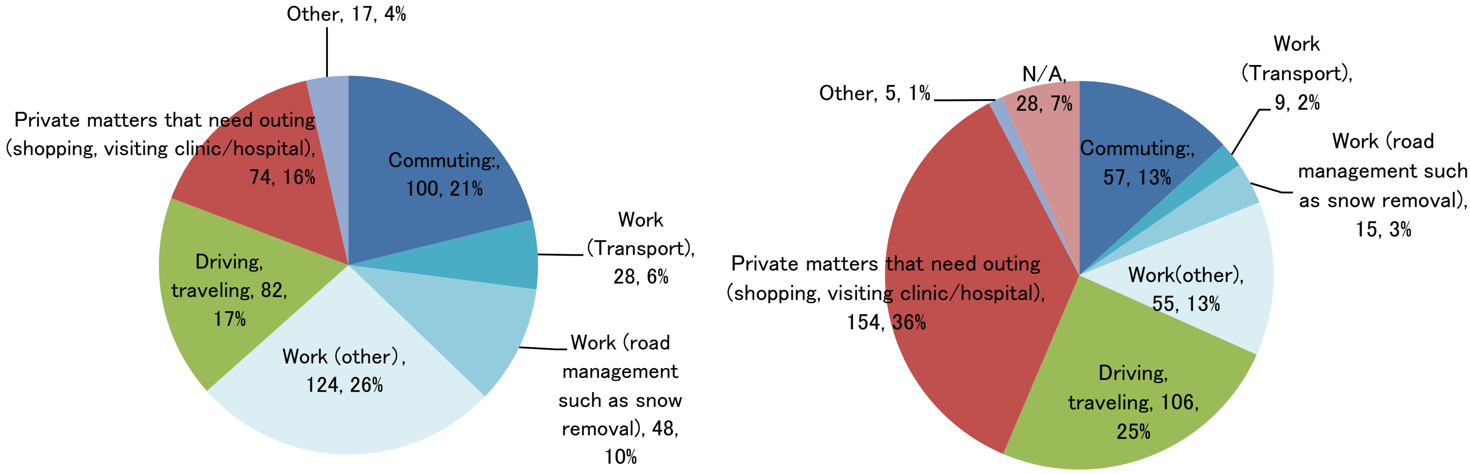

（N=473 10 cases of without answers were excluded)　　（N=429 54 cases of without answers were excluded)

Fig. 6 Purposes of use of “Visibility Information during Snowstorm”
Left: First purpose of the use　Right: Second purpose of the use

Fig. 7 shows the breakdowns of answers to the question that asked about the satisfaction level of the users of PC and smartphone sites. Over 85% of the users answered that they were satisfied (i.e., the ratio including “very satisfied”, “satisfied” and “mildly satisfied”). The reasons for not being satisfied, which includes “very dissatisfied”, “dissatisfied” and “mildly dissatisfied, found as comments in the survey were that, for the PC site, the accuracy of the blowing snow prediction was low; and, for the smartphone site, the image on the screen was hard to read because it was not able to be enlarged with swiping.
Fig. 8 shows the breakdown of the answers to the question that asks the person about the changes he made on his traffic-related behaviors or plan when poor visibility (less than 200m) was predicted at “Visibility Information during Snowstorm”. The respondents answered as “I change my behavior or plan” or “I often change my behavior or plan” accounted for the largest percentage of 79%. Among these respondents, 60% changed their departure time, and 59% canceled their plans for outing or trip. These result clarified that many of the respondents used the blowing snow information and took actions to avoid blowing snow.

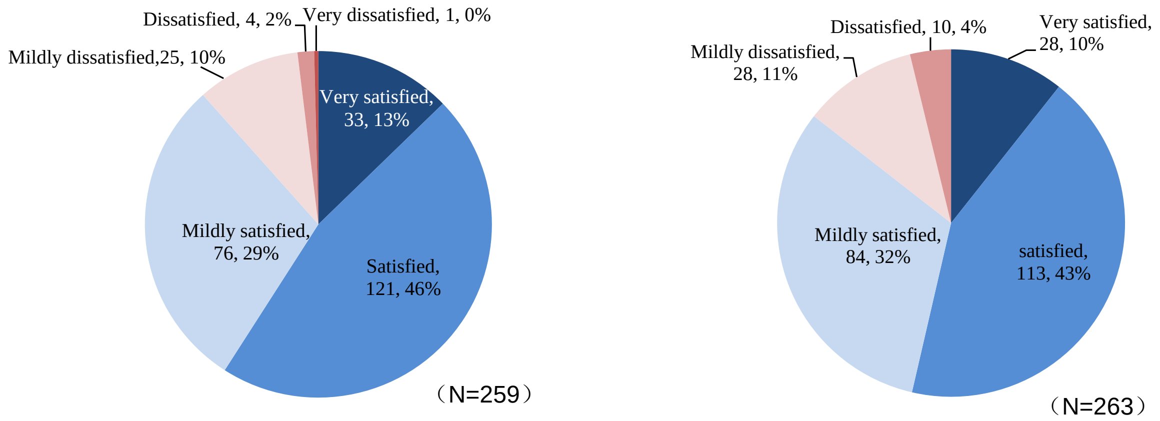

Fig. 7　Level of satisfaction regarding “Visibility Information during Snowstorm”
Left: PC site Right: Smartphone site

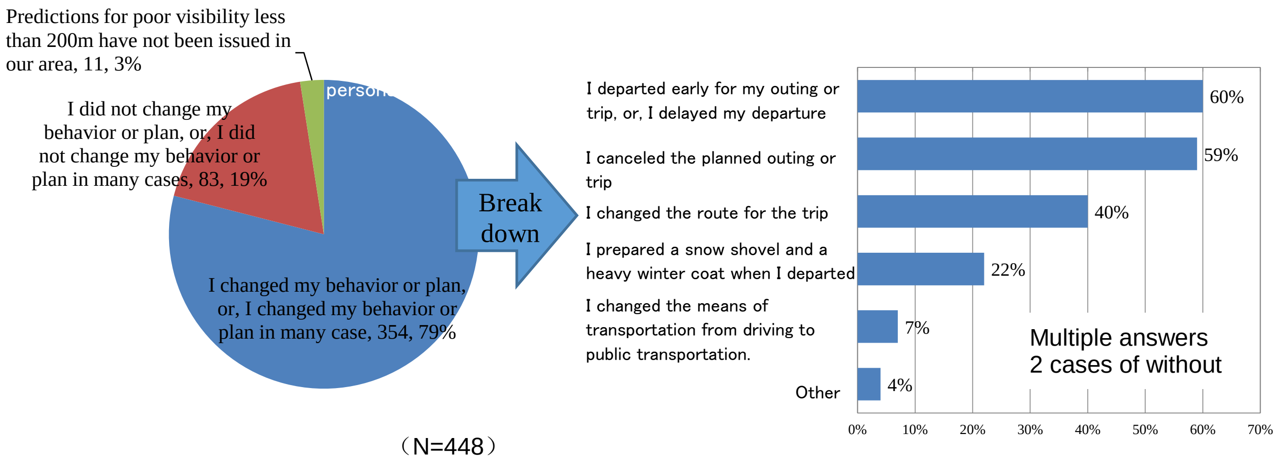

Fig. 8 Change/No change of plans for traffic-related behaviors after checking the blowing snow information

Next, the first purposes of use shown in Fig. 6 were categorized into the higher level groups shown in Table 2. The result of the cross tabulation between the items in Table 2 and the levels of satisfaction in Fig. 7 is shown in Fig. 9. It was found that, for all purposes for use, “satisfied” (the sum of “very satisfied”, “satisfied”, and “mildly satisfied”) exceeded 80%.

Table 2　Categorization of purposes of use for cross tabulation

Categories of use	Purpose of use in the questionnaire survey
Commuting	Commuting
Work	Work (Transport), work (road management such as snow removal) and work (other)
Private matters and other	Driving, traveling, private matters that need outing (shopping, visiting clinic/hospital, etc.), other

Next, the result of cross tabulation of the with/without changes in the traffic-related behavior or plan shown in Fig. 8 and the purposes of use categories shown in Table 2 is shown in Fig. 10. This cross tabulation revealed that the ratio of behavior changes was greater in private matters than in work or commuting.

The reasons for “not changing behaviors or plans” or “not changing behaviors of plans in many cases” were asked. The reasons were cross tabulated by the user category. The result of this cross tabulation is shown in Fig. 11. From this result, it was found that the percentage of respondents who answered that they could not change their plans was greater by about 10%

among the respondents whose purposes of use were “commuting” or “work” than the respondents whose purposes of use was “private matters” or “other”. The reasons for this greater percentage is considered to be from greater time constrains in “commuting” and “work” than “private matters” and “other”. Canceling “commuting” or “work” is often difficult.

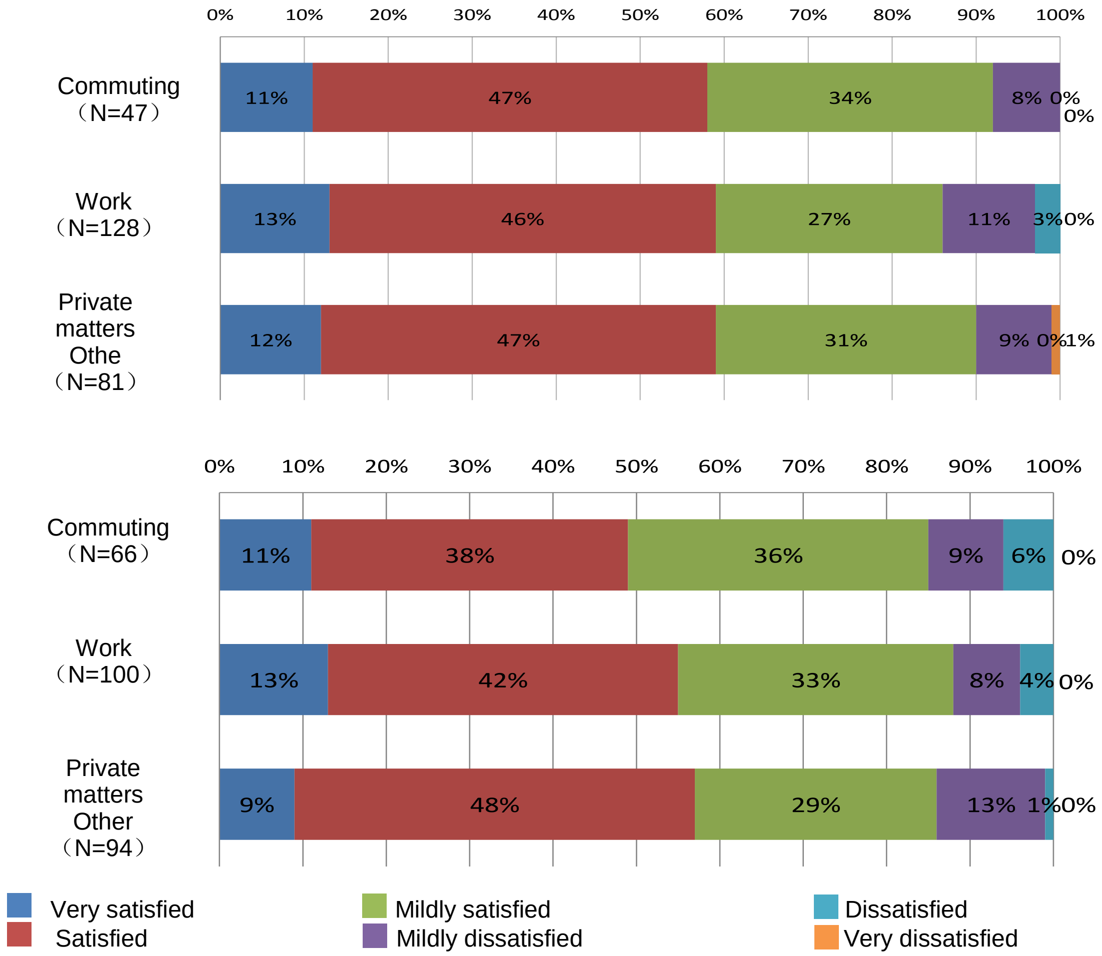

Fig.9 Level of satisfaction regarding “Visibility Information during Snowstorm” (by purpose of use)

Upper: PC site Lower: Smartphone site

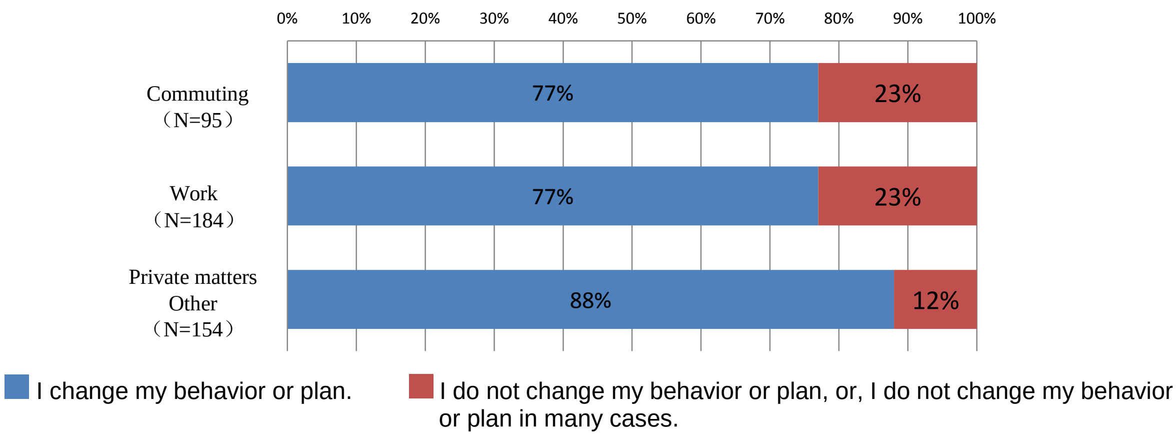

Fig. 10 With/without changes of plans for traffic-related behaviors after checking the Visibility Information during Snowstorm (by purpose of use)

Fig. 11 The reasons for not changing traffic-related behaviors after checking the Visibility Information during Snowstorm (by purpose of use)

4.1.2 Result of the survey on the e-mail delivery service

Fig. 12 shows the responses to the question on the purpose of using the e-mail delivery service. Many of the first purpose of use were work or commuting. The higher ratios of the second purposes of use were outings for private matters, driving, and traveling. This result was found to be the same as that shown in Fig. 6.

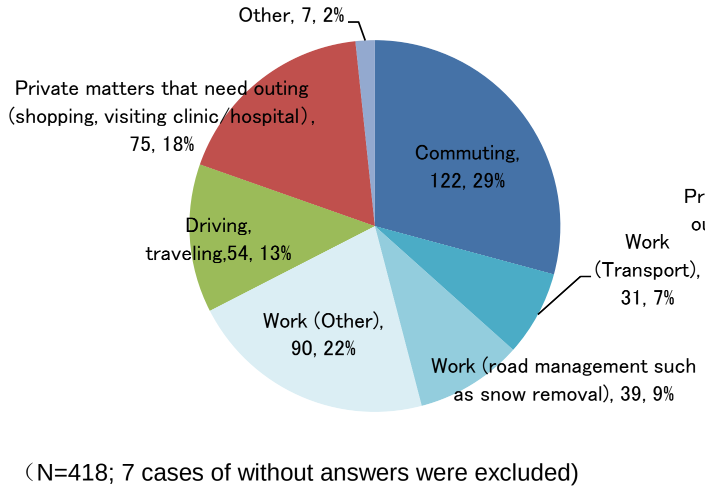

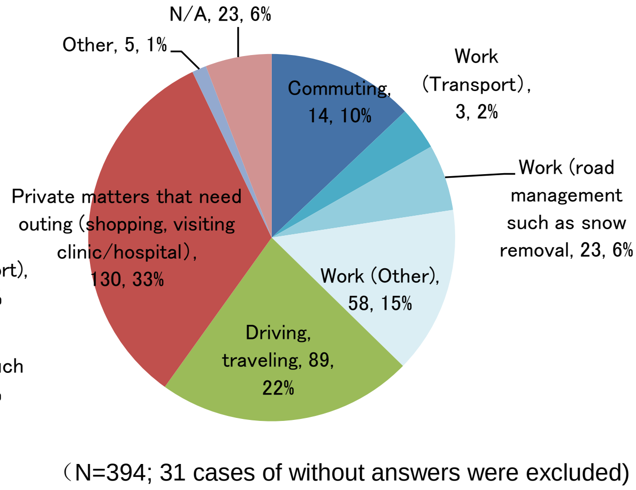

Fig. 12 shows the responses to the question on the purpose of using the e-mail delivery service
Left: First purpose of the use Right: Second purpose of the use

Fig. 13 shows how the users used the information delivered by the e-mail. It was found that 46% of the recipients of the e-mail checked the "Visibility Information during Snowstorm", and 17% checked the weather information. These users were found to proactively collect information after they received the e-mail alert. A total of 63% of the e-mail recipients, which is a large percentage, actively collected information.

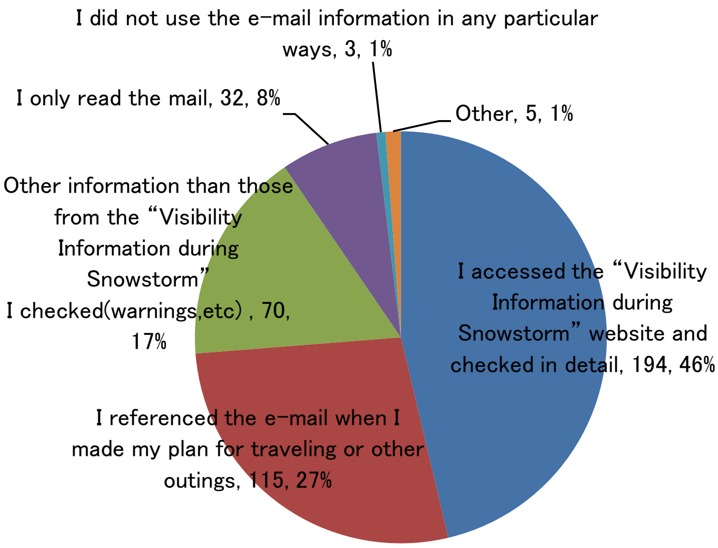

(N=419; 6 cases of without answers were excluded)

Fig. 13 Use of the e-mail

Next, the first purpose of use shown in Fig. 12 was categorized into the higher level groups shown in Table 2, and a cross tabulation of these groups and the level of satisfaction in Fig. 13 was done. The result is shown in Fig. 14. It was found that, when the purpose of driving is "commuting" or "work", the ratios of persons who actively collect information on weather and visibility during blowing snow were high; however, when the purpose of driving is "private matters" or "other", the ratios of persons who change their plans for outings were high.

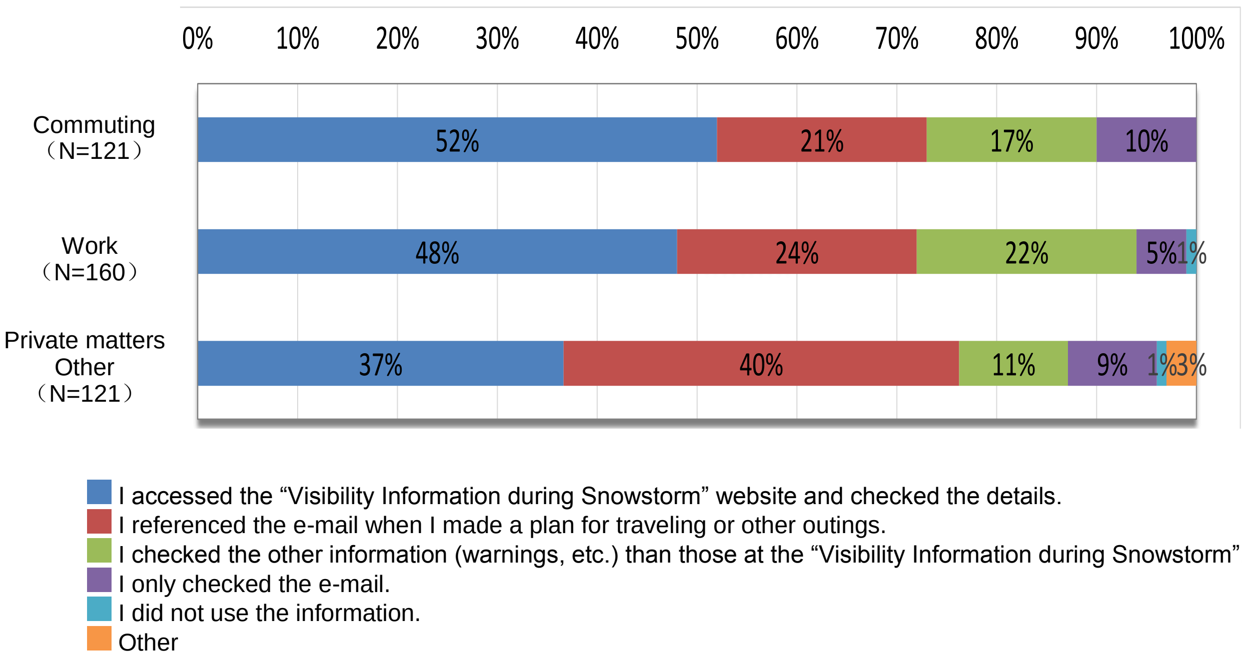

Fig. 14 Use of the information sent by e-mail (by purpose of use)

5. Conclusion

To support the drivers in their decision making in the traffic-related behaviors in case of blowing snow, we conducted an experiment for providing information on visibility during snowstorm. We found the following effectiveness of the information provision in this experiment.

- We conducted a questionnaire survey on the users of the “Visibility Information during Snowstorm” website and clarified that the users of this site changed their traffic-related behaviors after they visited this website. Many of the users changed departure time, canceled trips, and changed their travel routes.
- The result of a questionnaire survey on the users of the e-mail delivery service revealed that many of the users actively collect information after they received e-mail informing of poor visibility.

We are planning to further research on this theme toward future application of this technique in other areas of Japan than Hokkaido.

References

[1] W. A. Nixon., and R. M. DeVries. Extreme Storms in the Midwest US: Case Studies, PIARC, *Proceedings of 14th International Winter Road Congress*, 2014.

[2] Jeremy Duensing. Geospatial Weather Decision Support for Transportation Applications, *Transportation Research Circulars, Number E-C162*,2012, pp. 72-87.

[3] Road Information in Hokkaido website at http://info-road.hdb.hkd.mlit.go.jp/RoadInfo/index.htm（in Japanese）

[4] R.M. Alfelor. ,P.A. Piasano, D. Galarus, and D. Yohanan. Using Clarus Data for Disseminating Winter Road Weather Advisories and Other Weather-Related Alerts, In *Transportation Research Circulars, Number E-C162*, 2012,pp. 223-236.

[5] Federal Highway Administration website, *Best Practices for Road Weather Management*, at http://www.ops.fhwa.dot.gov/publications/fhwahop12046/fhwahop12046.pdf

[6] Federal Highway Administration website. The Integration of Multi-State Clarus Data Visualization Tools at http://ntl.bts.gov/lib/45000/45500/45599/FHWA-JPO-12-008_The_Integration_of_Multi-State_Clarus_Data_into_Data_Visualization_Tools_Final_508.pdf

[7] Ontario 511 website at http://www.mto.gov.on.ca/english/traveller/trip/

[8] Quebec 511 website at http://www.quebec511.info/en/default.aspx

[9] T. Kokubu, H. Takechi, Y. Harada, S. Omiya, M. Matsuzawa, and Y. Sakai: Provision of Visibility Information, *TRIS and ITRD database at* http://docs.trb.org/prp/16-2189.pdf .

[10] Y. Kajiya, M. Matsuzawa, T.Suzuki, K.Tanji, and Y. Nagata: A Study on Driver Behavior during Poor Visibility Due to Snowfall/Snowstorm, *Proceedings of Cold Region Technology Conference*, Vol. 20, Hokkaido Development Engineering Center, Inc,2004, pp. 325-331. （in Japanese）

[11] Prime Minister of Japan and His Cabinet website at http://www.kantei.go.jp/jp/singi/it2/senmon_bunka/pdf/h2903guidebook.pdf. （in Japanese）

[12] Fire and Disaster Management Agency website at http://www.fdma.go.jp/ugoki/h2207/2207_01.pdf. （in Japanese）

Evaluation of frequency of snowfall events using exponential function

Hiroki Matsushita
Senior researcher, Ph.D
Civil Engineering Research Institute for Cold Region (CERI)
Public Works Research Institute (PWRI)
Japan
matsushita-h@ceri.go.jp

Wataru Takahashi and Joji Takahashi, Civil Engineering Research Institute for Cold Region (CERI), Public Works Research Institute (PWRI), Japan

Summary

The suitability of exponential approximation for snowfall events was examined to obtain a simple method for evaluating the frequency of snowfall events exceeding a certain snowfall amount. The frequencies of snowfall events with snowfall amounts at intervals of 10 cm were analyzed using the cases of snowfall amounts greater than 30 cm. Regression analysis showed a strong correlation between the logarithm of frequency and the snowfall amount at a statistically significant level. The frequencies of certain snowfall duration and snowfall intensity also could be approximated to the exponential distribution. Consequently, the exponential function with simple regression analysis can be used in frequency analysis for snowfall events concerning the snowfall amounts, durations, and snowfall intensities. However, we should note the need to: (1) set a suitable interval of classes corresponding to the number of events, (2) set a helpful threshold for planning disaster prevention, in other words, events with a high frequency and small value cannot be expressed using the approximation, and (3) use data observed in a sufficient duration, including extreme events that should be noticed.

Keywords: snowfall event, frequency, snowfall amount, exponential function

1. Introduction

The frequency of phenomena that cause natural hazards is an important factor to consider for prevention and protection measures against the phenomena. In the frequency analysis, probability distributions of extreme values, such as the annual maximum, are commonly used to ascertain the return period, but complex procedures, such as parameter setting, are necessary for fitting the data to the probability distribution [1]-[3]. In addition, using only extreme values means a loss of information of other values that are not extreme but large. On the other hand, all values exceeding a certain threshold are sometimes used to evaluate the frequency of phenomena in peaks over threshold (POT) analysis [2]-[4]. Moreover, it has been known for a long time that the relationship between the frequency and the magnitude of natural phenomena exceeding a certain threshold could be simply approximated to exponential and/or power-law distributions. One of the typical examples is the relationship between the number of occurrences and the magnitude of earthquakes [5]. The suitability of exponential and/or power-law distributions for the frequencies of rain events [6],[7], drought [7],[8], landslide [9], snow avalanches [10], and forest fires [11] also has been examined by much previous research. In particular, long-range correlations underlying the spatial and temporal power-law behavior of dynamic systems were identified as self-organized criticality (SOC) [6],[9],[12],[13]. If the approximation could be applied to phenomena related to snow disasters, the frequency required to plan prevention measures against the phenomena could be easily evaluated also in snowy regions. However, the suitability of the approximation for phenomena related to snow disasters (e.g., heavy snowfall events) has never been examined.

In many analyses on the frequency of snowfall events concerning heavy snowfall, data observed and/or compiled at intervals of one day, such as the daily snowfall amount or daily precipitation, have been commonly used [3],[14]-[16]. However, hourly data should be used for evaluating the frequency of snowfall events, including heavy snowfall during a short period (e.g., a half day), that cause snow avalanches [17],[18]. We examined the suitability of the exponential approximation for snowfall events using hourly data to obtain a simple method for evaluating the frequency of snowfall events exceeding a certain snowfall amount.

2. Methods

To examine the suitability of exponential approximation for the frequency of snowfall events, we used hourly snow depth observed at Minakami (36° 48.0' N, 138° 59.5' E, 531 m a.s.l.) and Kusatsu (36° 37.0' N, 138° 35.5' E, 1223 m a.s.l.) in Gunma prefecture of central Japan. This area is located in one of the regions that were hit by extreme heavy snowfall on February 2014 that caused many snow avalanches on many slopes over a wide area (Fig.1) [17],[19]. The snow depths were observed during the period of 28 winters from November 1989 to April 2017 by the Automated Meteorological Data Acquisition System (AMeDAS) of the Japan Meteorological Agency (JMA).

Snowfall amount S (cm) was defined as the cumulative value of the positive difference in snow depth each hour. Each snowfall event was regarded as ending when the snowfall (i.e., the hourly difference in snow depth ≤ 0 cm) ceased for more than 6 hours. The numbers of snowfall events n with snowfall amounts S at intervals of 10 cm were counted regarding the cases of snowfall amounts S greater than 30 cm. Dividing the number of events n by the years of observation period provides the frequency of snowfall events $F(S)$ (number of events / year) with snowfall amounts S. In this paper, we used the frequencies $F(S\leq)$ based on the cumulative number of snowfall events N from classes of large snowfall amounts at intervals of 10 cm. The frequency $F(S\leq)$ means the occurrence number N of snowfall events per year with snowfall amounts exceeding S cm. To examine the suitability of the exponential approximation for snowfall events exceeding a certain snowfall amount, a regression analysis between the logarithm of frequencies $F(S\leq)$ and the snowfall amounts S was carried out.

In addition to snowfall amount S, we examined the suitability of exponential approximation for the frequencies of snowfall duration and snowfall intensity. The duration D (h) of a snowfall event was obtained from the definition of a snowfall event described above. The snowfall intensity I (cm/h) during each snowfall event was calculated by dividing the snowfall amount S (cm) by the snowfall duration D (h). The snowfall intensity I means the average snowfall intensity during the event. The frequencies of snowfall events with the duration $F(D\leq)$ and the snowfall intensity $F(I\leq)$ were calculated by the same manner as that with snowfall amounts $F(S\leq)$. Air temperatures T (°C) observed hourly during the events at Minakami and Kusatsu provided by the JMA also were used.

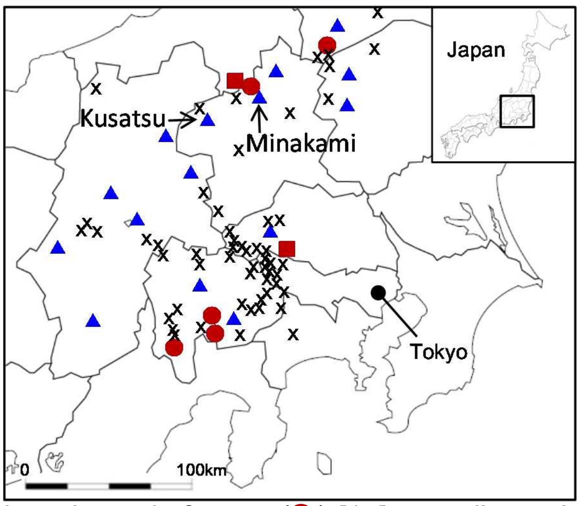

Fig. 1 Locations of avalanche release in forests (●) [17] as well as other avalanches (×) [19] that occurred during extreme heavy snowfall on February 14-15, 2014. Locations of snow sliding through nets and fences for preventing falling rocks (■) and meteorological observatories (▲) of the Japan Meteorological Agency also are shown.

3. Results

3.1 Characteristics of snowfall events

Figure 2 shows the time series of the snowfall events observed at Minakami and Kusatsu during the past 28 winters. The total numbers of the snowfall events at Minakami and Kusatsu are 227 and 49, respectively. At Minakami, shown in Fig. 2a, there are many snowfall events and the snowfall amount exceeded 100 cm in seven events, but extreme events with a large snowfall amount compared to other events are not found there. On the other hand, in Fig. 2b, although the number of snowfall events at Kusatsu is less than that at Minakami, there is an extreme event with a snowfall amount of 122 cm, which is over 30 cm greater than that of other events at Kusatsu.

Figure 3 represents the numbers n and the frequencies $F(S\leq)$ of snowfall events with snowfall amounts S at intervals of 10 cm at Minakami and Kusatsu. The frequencies $F(S\leq)$ shown in Fig. 3 are the occurrence number N of snowfall events per year with snowfall amounts exceeding S. The numbers n and the frequencies $F(S\leq)$ of snowfall events decrease rapidly as the snowfall amount S increases at both the observation points. The frequencies of snowfall events with snowfall amounts over 50 cm and 100 cm are 2.96 (three times per year) and 0.25 (once every four years) at Minakami, and 0.43 (about once every two years) and 0.04 (once every 25 years) at Kusatsu.

3.2 Frequency of snowfall events expressed using exponential function

Figure 4 represents the relationship between the snowfall amount S and the logarithm of the frequency of snowfall events $F(S\leq)$ with snowfall amounts exceeding S at intervals of 10 cm. The vertical axis of this figure is expressed by a natural logarithm, and the logarithm is shown as "ln" in this paper. The solid line is a regression line with coefficient of determination r^2 between the snowfall amount S and the logarithm of frequency $F(S\leq)$. The regression analysis indicates a strong linear correlation between the logarithm of frequency and the snowfall amount at a statistically significant

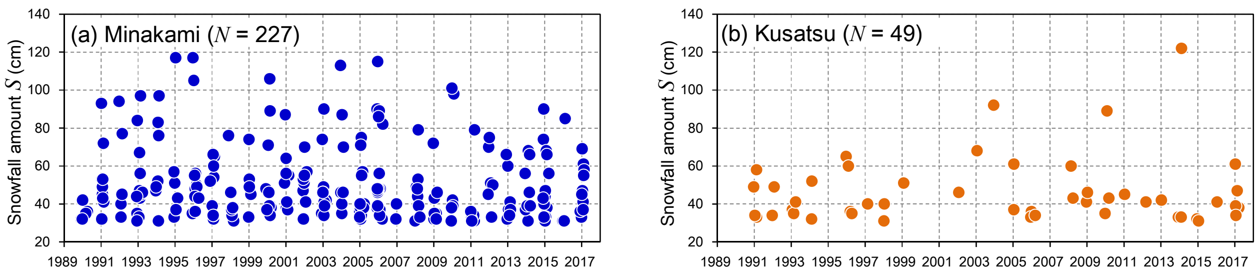

Fig. 2 Snowfall events with snowfall amounts exceeding 30 cm during the period from November 1989 to April 2017 at (a) Minakami and (b) Kusatsu. N is the total number of snowfall events.

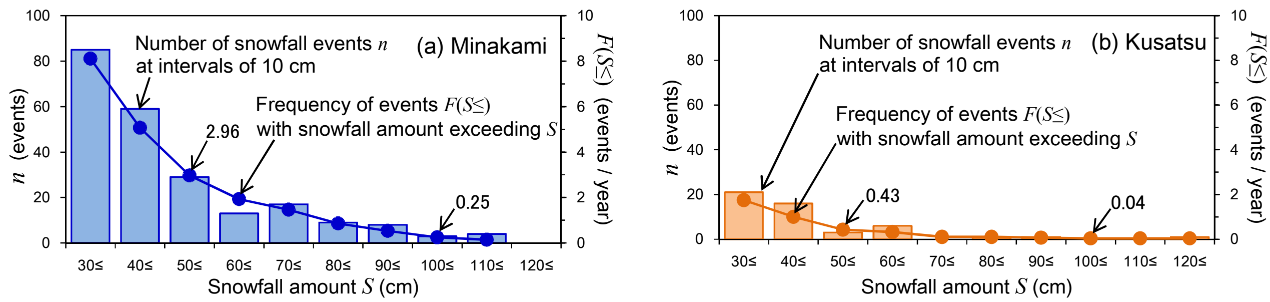

Fig. 3 Numbers of snowfall events n (histograms) and frequencies of events $F(S\leq)$ with snowfall amounts exceeding S (solid lines with closed circles) at intervals of 10 cm at (a) Minakami and (b) Kusatsu.

level of 1 %. The frequencies of snowfall events with snowfall amounts exceeding 50 cm and 100 cm that are estimated from the regression equations are 3.22 and 0.28 at Minakami, and 0.49 and 0.05 at Kusatsu. These estimated values agree closely with the observed values shown in section 3.1. Therefore, the exponential function with simple regression analysis can be used for evaluating the frequency of snowfall events with snowfall amounts exceeding a certain value. In statistical terms, it means that the frequency of snowfall events follows the generalized Pareto distribution (GPD), including the exponential distribution with a shape parameter of zero.

Figure 5 shows the relationship between the snowfall amount S and the frequency of snowfall events $F(S\leq)$, like Fig. 4, but the intervals of snowfall amounts S are changed to 5 cm. Figure 5 also indicates a strong linear correlation between the snowfall amount S and the frequency $F(S\leq)$ at a significant level of 1 %. The frequencies of snowfall events with snowfall amounts exceeding 50 cm and 100 cm that were estimated from the regression equations are 3.30 and 0.28 at Minakami, and 0.48 and 0.05 at Kusatsu. Changing the interval of classes of snowfall amount to small will make it possible to evaluate in detail the frequency of snowfall events with a certain snowfall amount. However, in the case of Kusatsu shown in Fig. 5b, the data distribution takes a shape like steps because few events exist with snowfall amounts exceeding 70 cm and the maximum snowfall amount among the events

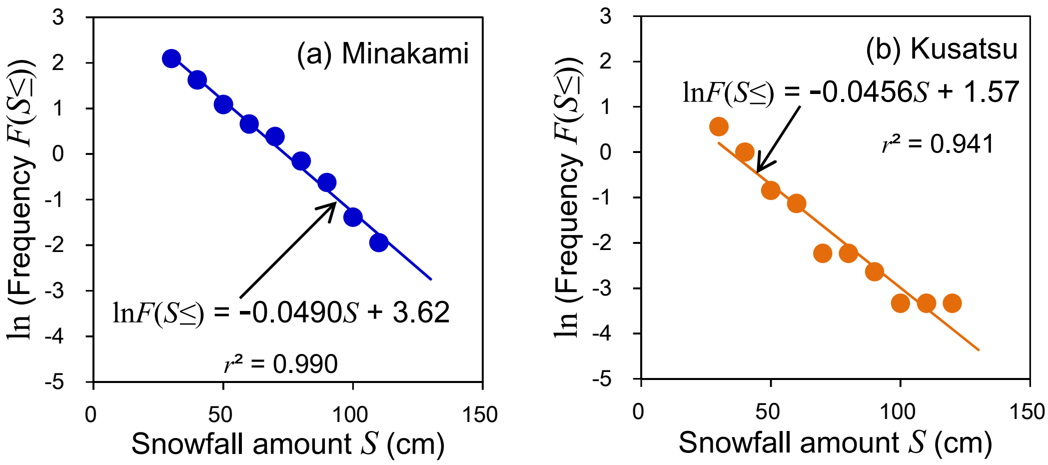

Fig. 4 Snowfall amounts S versus the logarithms of frequencies of snowfall events $F(S\leq)$ with snowfall amounts exceeding S at intervals of 10 cm at (a) Minakami and (b) Kusatsu. The vertical axes are expressed by a natural logarithm. Solid lines represent regression lines with coefficients of determination r^2.

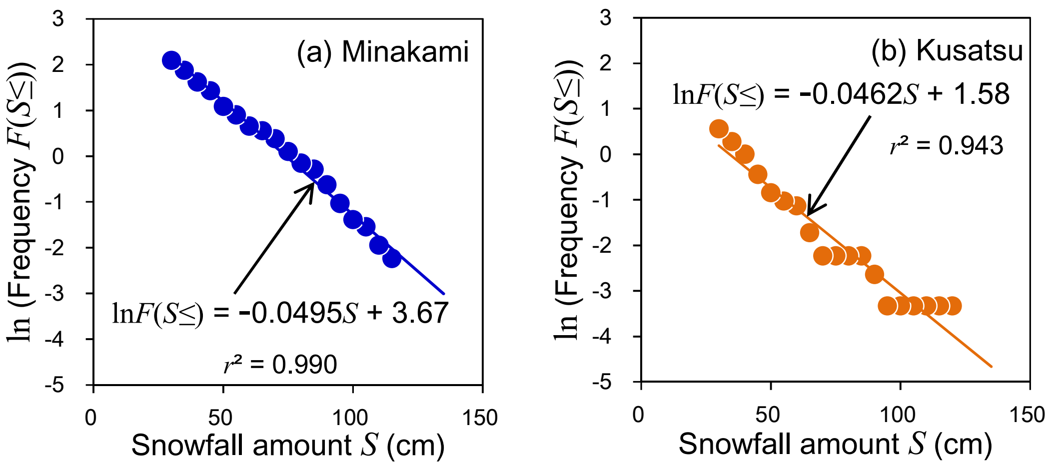

Fig. 5 Same as Fig. 4, but the interval of snowfall amounts S is 5 cm.

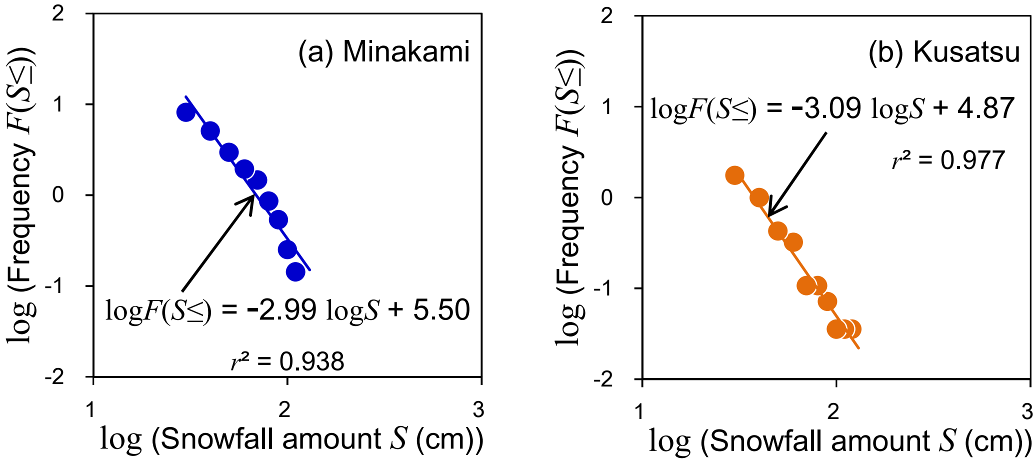

Fig. 6 Same as Fig. 4, but both the vertical and horizontal axes are expressed by a common logarithm.

is over 30 cm greater than that of other events (Fig. 2b). The effect of extreme events on the data distribution is remarkable in the case of snowfall amount at intervals of 5 cm (Fig. 5b) compared with that of 10 cm (Fig. 4b). Although the frequencies $F(S\leq)$ estimated from the regression equations in both the cases of snowfall amounts at intervals of 10 cm (Fig. 4b) and 5 cm (Fig. 5b) are not different, we should note the need to set a suitable interval of classes corresponding to the number of events (i.e., sample size). In particular, the number of events with a large value that should be noticed is very important.

3.3 Frequency of snowfall events expressed using power-law function

Figure 6 shows the relationship between the logarithms of snowfall amount S and of frequency of snowfall events $F(S\leq)$ with snowfall amounts exceeding S at intervals of 10 cm. The logarithms in the figure are common logarithms with a base of 10 and shown as "log" in this paper. In the case of Kusatsu shown in Fig. 6b, the relationship between the snowfall amount S and the frequency $F(S\leq)$ of snowfall events is expressed in a straight line that fits the regression equation at a statistically significant level of 1 %. The frequencies of snowfall events with snowfall amount exceeding 50 cm and 100 cm that were estimated from the regression equation are 0.42 and 0.05, which agree closely with the observed values shown in section 3.1. It means that the frequency of snowfall events at Kusatsu follows the power-law distribution. In contrast, in the case of Minakami shown in Fig. 6a, the relationship between the snowfall amount S and the frequency $F(S\leq)$ of snowfall events is expressed in a curve and does not fit the regression line. The frequency of snowfall events with snowfall amount exceeding 100 cm that was calculated by the regression equation is 0.33 (about once every three years), which was slightly overestimated compared with the observed value of 0.25 (once every four years). Therefore, the power-law function should not be used for evaluating the frequency of snowfall events with large snowfall amounts at Minakami. The suitability of the power-law approximation for the frequency of snowfall events should continue to be examined using the data observed in many other regions.

4. Discussions

4.1 Evaluation for frequencies concerning snowfall duration and snowfall intensity

The factor that characterizes a snowfall event is not only the snowfall amount. Figure 7 represents relationships among the durations D (h), snowfall intensities I (cm/h), and the snowfall amounts S of the snowfall events at Minakami and Kusatsu examined in chapter 3. The figures indicate various types of snowfall events characterized by the duration D and the snowfall intensity I. For example, there are snowfall events with snowfall amount exceeding 30 cm caused by a long duration of snowfall with weak snowfall intensity and/or by a large snowfall intensity in a short period. A long lasting snowfall will require responses for the safety of inhabitants and traffic (e.g., snow removal

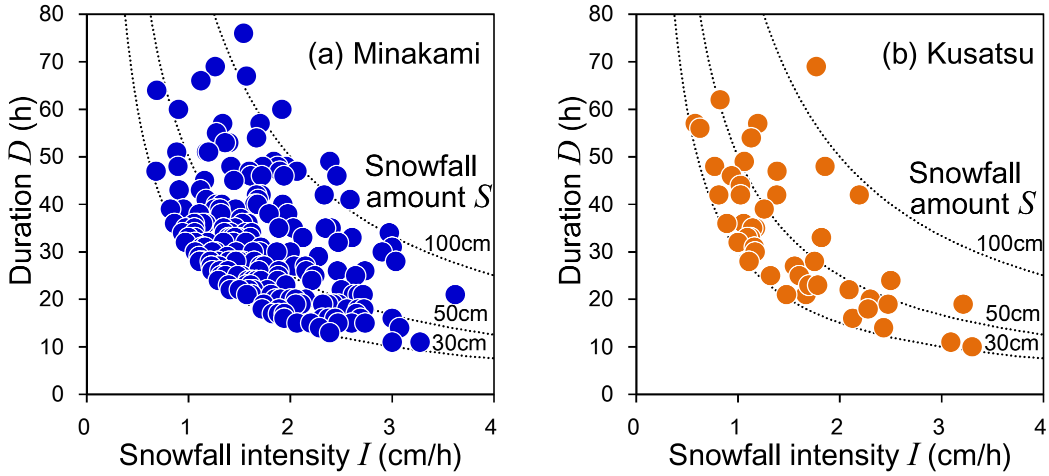

Fig. 7 Relationships among duration D, snowfall intensity I, and snowfall amount S of snowfall events at (a) Minakami and (b) Kusatsu.

and traffic regulations) during a long period. In contrast, heavy snowfall during a short period tends to cause phenomena related to disasters, such as snow accretion on structures and avalanches in mountain areas. In this section, we attempt a simple evaluation of the frequencies of snowfall events concerning the duration D and the snowfall intensity I by using the exponential approximation examined in section 3.2.

Figure 8 shows the relationship between the duration of snowfall D and the logarithm of frequency of snowfall events $F(D\leq)$ with snowfall durations exceeding D at intervals of 10 hours. The regression line in the figure was obtained from the snowfall events, except the events with duration less than 20 hours shown as open circles. The relationship between the frequency of snowfall events $F(D\leq)$ and the snowfall duration D could be represented by the exponential approximation at a statistically significant level of 1 %. However, the snowfall event with duration less than 20 hours did not agree with the regression line. It means that the frequencies of phenomena with a small size and high frequency (i.e., short duration of snowfall in this case) cannot be evaluated using the exponential approximation [6],[9], and setting a helpful threshold for evaluating the frequency of phenomena is

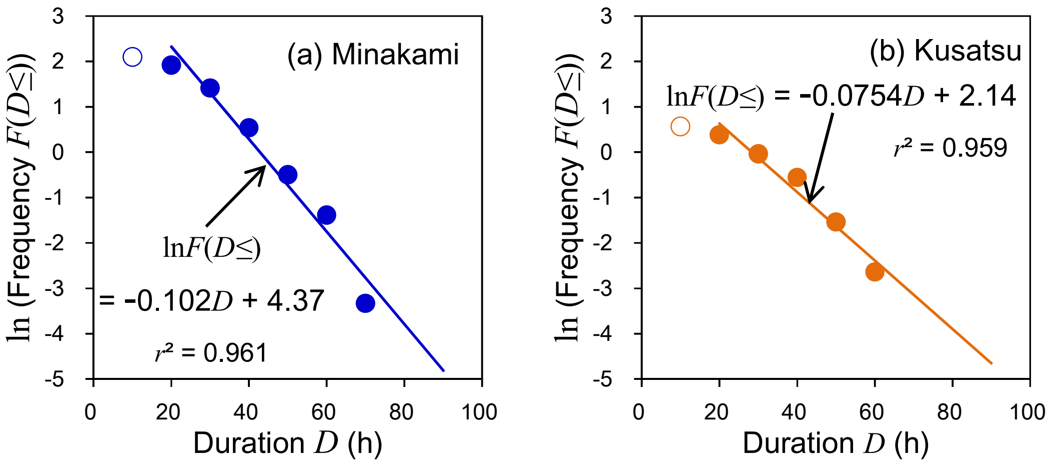

Fig. 8 Durations of snowfall D versus the logarithms of frequencies of snowfall events $F(D\leq)$ with snowfall duration exceeding D at intervals of 10 hours at (a) Minakami and (b) Kusatsu. Regression equations shown as solid lines were obtained from the data except snowfall events with duration less than 20 hours shown as open circles. The r^2 are the coefficients of determination.

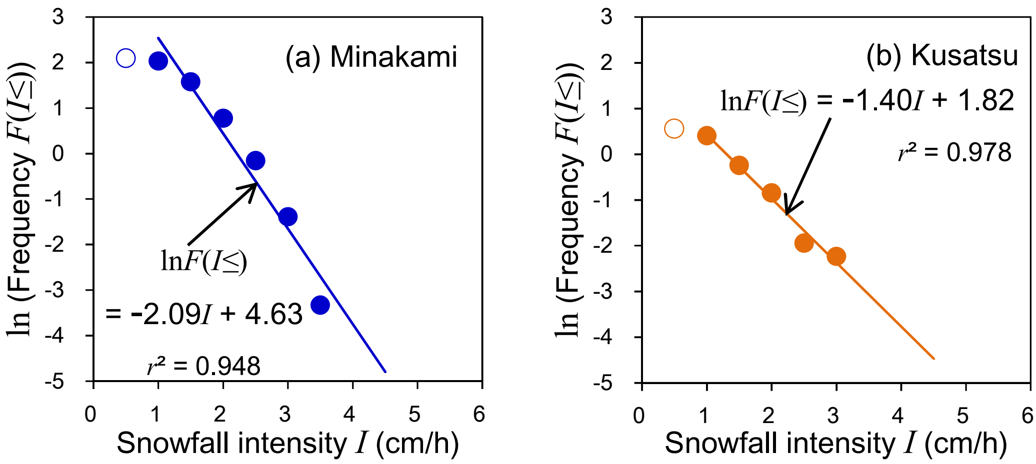

Fig. 9 Snowfall intensities I versus the logarithms of frequencies of snowfall events $F(I\leq)$ with snowfall intensities exceeding I at intervals of 0.5 cm/h at (a) Minakami and (b) Kusatsu. Regression equations shown as solid lines were obtained from the data except snowfall events with snowfall intensity less than 1.0 cm/h shown as open circles. The r^2 are the coefficients of determination.

important. The relationship between the snowfall intensity I and the logarithm of frequency of snowfall events $F(I\leq)$ with snowfall intensity exceeding I at intervals of 0.5 cm/h is shown in Fig. 9. Although the regression line in the figure does not include the snowfall events with snowfall intensity less than 1.0 cm/h shown as open circles, Figure 9 indicates that the relationship between the frequency of snowfall events $F(I\leq)$ and snowfall intensity I also can be expressed in the exponential approximation at a statistically significant level of 1 %.

In addition to the frequency of snowfall amounts, therefore, the frequencies concerning a certain duration and snowfall intensity of snowfall events also can be approximated to the exponential distribution and evaluated by simple statistical analysis. However, we should note the need to set a helpful threshold for planning disaster prevention, in other words, events with a high frequency and a small value cannot be expressed using the approximation.

4.2 Evaluation for frequencies of snowfall events categorized into cases by conditions

One of our purposes in future work is to evaluate the frequency of dry-snow avalanches during snowfall using the exponential approximation for snowfall events associated with conditions for the avalanche releases. The dry-snow avalanches caused by heavy snowfall during a short period are characterized as multi-occurrences in many slopes in a time [18] and releases in forests where the avalanches could not be commonly released [17],[20]. For evaluating the occurrences of the dry-snow avalanches, attention must be paid to the snowfall amount, duration, snowfall intensity, and air temperature during snowfall as meteorological factors [17],[18],[20]. If the exponential approximation could be applied to the snowfall events associated with conditions for the avalanche releases, we could evaluate the frequency of the avalanches. In this section, we examine whether the exponential approximation could apply to the frequencies of snowfall events categorized by the duration of snowfall and the mean air temperature during snowfall.

Figure 10 shows the relationships between the snowfall amounts S and the logarithm of frequencies of snowfall events $F(S\leq)$ in cases categorized by the durations of snowfall D less than 36 and 24 hours at Minakami. The case of all snowfall events shown in Fig. 5 also is depicted in Fig. 10. The N in the figure is the total number of events in each case. In addition, in the cases of snowfall events categorized by the snowfall durations D, regression analyses indicate strong correlations between the logarithm of frequencies $F(S\leq)$ and the snowfall amounts S at a significant level of 1 %. Furthermore, the characteristics of the frequency of snowfall events in each case categorized by the snowfall duration can be found from Fig. 10. The regression lines between the frequencies and the snowfall amounts shift downward in the figure as the number of snowfall events N decreases, it means that the frequencies of snowfall events with snowfall amounts greater than 30 cm decrease as snowfall duration decreases. Moreover, the slopes of regression lines increase as snowfall durations decreases, indicating that the frequencies of snowfall events with large snowfall amount decrease significantly as the duration of the events decreases. However, in the case of snowfall events with duration less than 24 hours, the relationship between the frequency and the snowfall amount was expressed in a shape like steps by sparse data due to only one event with snowfall amount exceeding 60 cm. Therefore, we should note that using data with a sufficient number of events, including extreme one, is important.

Figure 11 shows the relationship between the snowfall amounts S and the logarithm of frequencies of snowfall events $F(S\leq)$ in cases categorized by the mean air temperature T during snowfall at Minakami. The exponential approximation can be used also for evaluating the frequency of snowfall events concerning the air temperature during snowfall. In the case of air temperature below -4 °C, the regression line between the frequencies and the snowfall amounts shifts downward in the figure

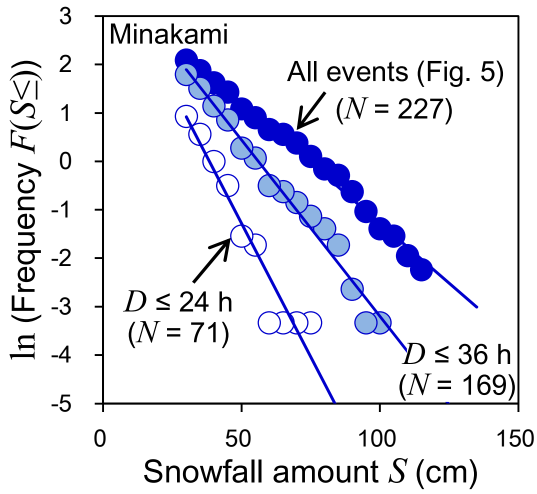

Fig. 10 Relationship between snowfall amounts S and the logarithms of frequencies of snowfall events $F(S\leq)$ with snowfall amount exceeding S at intervals of 5 cm in the cases categorized by snowfall duration D less than 36 and 24 hours at Minakami. The N is the total number of events and the solid line is the regression line in each case.

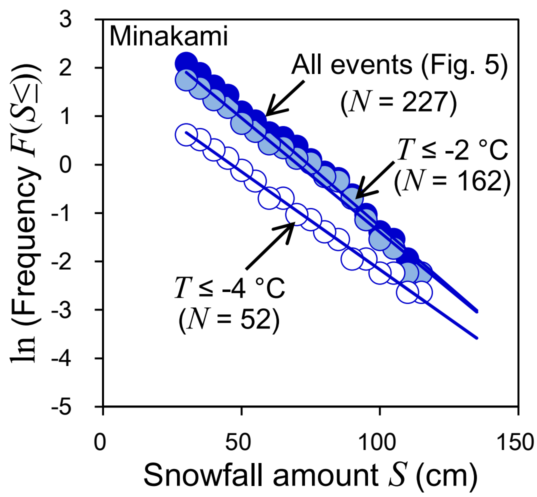

Fig. 11 Same as Fig. 10, but in the cases categorized by the mean air temperature T during snowfall below -2 and -4 °C.

but the slope of the line decreases slightly. Although the number of snowfall events decreases as the mean air temperature decreases during snowfall, the ratio of the number of snowfall events with snowfall amount exceeding 100 cm increases as the temperature decreases.

Consequently, the exponential approximation with simple statistical analysis can be applied for evaluating the frequencies of snowfall events categorized into cases by such conditions as duration of snowfall and air temperature during snowfall. It is likely that the exponential approximation could be used for evaluating the frequency of snowfall conditions associated with dry-snow avalanche releases.

5. Conclusions

We examined the suitability of exponential approximation for snowfall events to obtain a simple method for evaluating the frequency of snowfall events exceeding a certain snowfall amount. Simple regression analysis using the exponential function revealed strong correlation between the snowfall amount and the frequency of snowfall events exceeding a certain snowfall amount at a statistically significant level. Consequently, the exponential approximation can be used in frequency analysis for snowfall events concerning certain snowfall amounts, snowfall durations, and snowfall intensities. However, we should note the need to: (1) set a suitable interval of classes corresponding to the number of events (i.e., sample size), (2) set a helpful threshold for planning disaster prevention, in other words, events with a high frequency and small value cannot be expressed using the approximation, and (3) use data with a sufficient duration, including extreme events that should be noticed.

In the future work, we will apply the exponential approximation to evaluate the frequency of snowfall events associated with dry-snow avalanche release conditions due to snowfall [21].

References

[1] FUJIBE F., "Discussion of fitness analysis for selecting distribution functions in extreme value analysis", *Tenki (Bulletin Journal of the Meteorological Society of Japan)*, Vol. 58, 2011, pp. 765-775. (In Japanese with English abstract)

[2] GHIL M., YIOU P., HALLEGATTE S., MALAMUD B. D., NAVEAU P., SOLOVIEV A., FRIEDERICHS P., KEILIS-BOROK V., KONDRASHOV D., KOSSOBOKOV V., MESTRE O., NICOLIS C., RUST H. W., SHEBALIN P., VRAC M., WITT A., and ZALIAPIN I., "Extreme events: Dynamics, statistics and prediction", *Nonlinear Processes in Geophysics*, Vol. 18, 2011, pp. 295-350.

[3] BLANCHET J., MARTY C., and LEHNING M., "Extreme value statistics of snowfall in the Swiss Alpine region", *Water Resources Research*, Vol. 45, W05424, 2009, doi:10.1029/2009 WR007916.

[4] BEZAK N., BRILLY M., and ŠRAJ M., "Comparison between the peaks-over-threshold method and the annual maximum method for flood frequency analysis", *Hydrological Sciences Journal*, Vol. 59, 2014, pp. 959-977.

[5] GUTENBERG B., and RICHTER C. F., "Frequency of earthquakes in California", *Bulletin of the Seismological Society of America*, Vol. 34, No. 4, 1944, pp. 185-188.

[6] ANDRADE R. F. S., SCHELLNHUBER H. J., and CLAUSSEN M., "Analysis of rainfall records: Possible relation to self-organized criticality", *Physica A: Statistical Mechanics and its Applications*, Vol. 254, 1998, pp. 557-568.

[7] PETERS O., DELUCA A., CORRAL A., NEELIN J. D., and HOLLOWAY C. E., "Universality of rain event size distributions", *Journal of Statistical Mechanics: Theory and Experiment*, P11030, 2010, doi: 10.1088/1742-5468/2010/11/P11030.

[8] DELUCA A., and CORRAL Á., "Scale invariant events and dry spells for medium-resolution local rain data", *Nonlinear Processes in Geophysics*, Vol. 21, 2014, pp. 555-567.

[9] HERGARTEN S., "Landslide, sandpiles, and self-organized criticality", *Natural Hazards and Earth System Science*, Vol. 3, 2003, pp. 505-514.

[10] BIRKELAND K. W., and LANDRY C. C., "Power-laws and snow avalanches", *Geophysical Research Letters*, Vol. 29, 2002, pp. 49-1-49-3.

[11] MALAMUD B. D., MOREIN G., and TURCOTTE D. L., "Forest fires: An example of self-organized critical behavior", Science, Vol. 281, 1998, pp. 1840-1842.

[12] BAK P., TANG C., and WIESENFELD K., "Self-organized criticality: An explanation of the 1/f noise", *Physical Review Letters*, Vol. 59, 1987, pp. 381-384.

[13] SELVAM A. M., "*Self-organized criticality and predictability in atmospheric flows: The quantum world of clouds and rain*", Springer, 2017, pp. 139.

[14] CHANGNON S. A., "Frequency distributions of heavy snowfall from snowstorms in the United States", *Journal of Hydrologic Engineering*, Vol. 11, 2006, pp. 427-431.

[15] SUZUKI H., "Long-term changes in frequency of heavy snowfall and their relation to environmental fields in Japan: Analysis using data observed at meteorological stations and railway stations", *Tenki (Bulletin Journal of the Meteorological Society of Japan)*, Vol. 59, 2012, pp. 333-350. (In Japanese with English abstract)

[16] DANCO J. F., DeANGELIS A. M., RANEY B. K., and BROCCOLI A. J., "Effects of a warming climate on daily snowfall events in the Northern Hemisphere", *Journal of Climate*, Vol. 29, 2016, pp. 6295-6318.

[17] MATSUSHITA H., and ISHIDA K., "Characteristics of snow avalanche release in forests during a heavy snowfall event", *Proceedings of International Snow Science Workshop (ISSW)*, 2016, pp. 556-560.

[18] HARADA Y., TAKAHASHI W., MATSUSHITA H., and ISHIDA K., "Characteristics of avalanche occurrences during heavy snowfall within a short period: Case study of the south Tokachi region in Hokkaido", *Proceedings of Cold Region Technology Conference*, Hokkaido Development Engineering Center, Vol. 33, 2017, pp. 187-192. (In Japanese)

[19] IZUMI K., KAWASHIMA K., IYOBE T., and MATSUMOTO, T., "Characteristics of avalanche accidents caused by heavy snowfall in mid-February, 2014", *Report of Grant-in-Aid for Special Research*, Japan Society for the Promotion of Science, KAKENHI 2590003, pp. 111-118. (In Japanese)

[20] MATSUSHITA H., TAKAHASHI W., MATSUZAWA M., and TAKAHASHI J., "Conditions associated with dry-snow surface avalanche releases in deciduous forests", *Journal of Snow Engineering of Japan*, Vol. 34, No. 4, 2018, pp. 55-67. (In Japanese with English abstract)

[21] MATSUSHITA H., TAKAHASHI W., and TAKAHASHI J., "A simple evaluation of dry-snow avalanche hazard using meteorological data", *Proceedings of International Symposium on Mitigative Measures against Snow Avalanches and Other Rapid Gravity Mass Flows*, Siglufjörður, Iceland, April 2019. (Submitted)

Biological treatment of organic waste in cold regions – a case study from Sisimiut, Greenland

Gunvor M. Kirkelund
Associate Professor
Technical University of Denmark
Denmark
gunki@byg.dtu.dk

Monika Skadborg, Technical University of Denmark, Denmark
Monica Nielsen Technical University of Denmark, Denmark
Leire Díez Larrea, Technical University of Denmark, Denmark
Charlotte Scheutz, Technical University of Denmark, Denmark
Rasmus Eisted, Ramboll Environment & Health, Denmark and The Danish Environmental Protection Agency, Denmark

Summary

In 2014, Qeqqata Kommunia, Greenland, initiated a pilot project in Sisimiut to reduce the amounts of landfilled waste by source separation of organic waste and subsequent composting. One year after the first batch of compost was produced, this fieldwork study was carried out with the aim of characterising the composition of the organic waste that is composted and assessing the compost quality to evaluate its potential utility as plant growth medium or biocover to reduce methane emissions from the landfill. Both organic waste and compost was analysed for LoI, water content, pH, EC, TC, TKN, C/N, P_{tot}, K, Ca and heavy metals. The compost was additionally analysed for S_{tot}, CH_4 oxidation rates and respiration rates. The organic waste consisted mainly of food residues with low contents of impurities and was overall appropriate for composting, except for a low pH value, which can be balanced with aeration or addition of CaO. The compost was limited for use as plant growth medium by several parameters which indicated immaturity, high content of wood and impurities. High respiration rates and low CH_4 oxidation rates further indicated immaturity of the compost. The study found potential for collecting organic waste and composting in the Arctic. However, the compost quality and maturity should be improved by more efficient composting. Improvement could be achieved by reducing the wood content mixed into the organic waste and by applying a higher mixing frequency during the composting process.

Keywords: Compost, waste management, Arctic, Greenland, biological treatment, organic waste, source separation

1. Introduction

The waste management system in Greenland consists mainly of landfilling and incineration. The incineration plants lack capacity resulting in growing piles of combustible waste in landfills. In addition to causing aesthetic problems, the landfills contribute with emissions of the greenhouse gas methane (CH_4). Methane has a global warming potential around 28 times greater than that of CO_2 (averaged over 100 years and not including climate feedbacks) [1], and studies show, that landfills produce 8 % of global anthropogenic methane emissions [2]. One solution for limiting landfill CH_4 escape is the utilization of biocovers. A biocover enhances methanotrophic bacteria, which oxidise CH_4 when it diffuses through the biocover [3].

To tackle the problems with the capacity in the waste system, a pilot project was initiated in 2014 in Sisimiut to reduce landfilling by valorizing the organic waste as compost that can be used as either plant growth medium or biocover. One year after the first batch of compost was produced, this fieldwork study was carried out. The purpose was to characterise the composition of source separated organic waste, to evaluate if this waste is suitable for composting, and furthermore to evaluate the composting processes by assessing the maturity and quality of the compost with a view to utility as a plant growth medium or a biocover.

1.1 Composting pilot project

The pilot project was initiated in 2014 in Sisimiut by Qeqqata Kommunia. It was an important aspect of the project to find methods for source separation and treatment of organic waste that are applicable also in other settlements in the Arctic region. In the pilot project 3 supermarkets, 8 canteens and restaurants, and 400 households participated, equivalent to 43 % of the supermarkets, 80 % of the canteens and 20 % of the households, respectively. After collection and manually removal of the largest impurities, the organic waste was homogenized by shredding. This was done immediately to avoid the waste freezing in the cold climate (average temperature -2 °C [4]). The compost was produced in a container from shredded organic waste mixed approximately 1:1:1 w/w with shredded wooden pallets and snow. Wooden pallets are abundant in Sisimiut and were chosen as bulky material to provide structure to the compost as wood is a scarce resource in Greenland. The composting container was a rebuild shipping freeze container with installed floor and walls to make space along the sides for ventilation. To melt the snow and kick-start the exothermic composting processes (during a 2 weeks period), excess heat from the waste incineration plant was connected to the container. This was switched off when the biological processes started. The biological processes warm the air, which rises through the material to the roof where it was pumped to the bottom to repeat the ventilation cycle. After the 2 weeks kick-start period, the container is emptied and the compost material is piled up in windrows for maturation.

2. Methodology

Waste collection, waste sorting and sampling of waste and compost was carried out in August 2015 in Sisimiut. The samples were transported to Denmark where the laboratory experiments took place in the autumn of 2015. Unfortunately, due to lack of manpower, the pilot project was shot down and the compost material was left in the container to the end of the following summer of 2016. The samples presented in this paper are taken from the abandoned pile of compost material.

2.1 Organic waste sampling

In total, 1.6 tonnes of source separated organic waste was collected during one week from the three different participating sources: Supermarkets, canteens/restaurants and households. Buckets were filled and weighted with organic waste in order to measure the total amount of organic waste. Every fourth bucket, in total 394 kg, was sorted into organic and non-organic fractions which were weighed in wet weight. In addition, the residual household waste from 92 of the households participating in the organic waste collection was collected and sorted into organic and non-organic fractions to evaluate the efficiency of organic waste separation. Samples for chemical analysis were taken from landfilled organic waste collected over four weeks.

2.2 Compost sampling

Three random samples from the pile of shredded organic waste (waste samples) were collected, and another three samples after addition of shredded wood chips (mixed waste samples).

For compost samples, the locations are shown on Fig. 1.

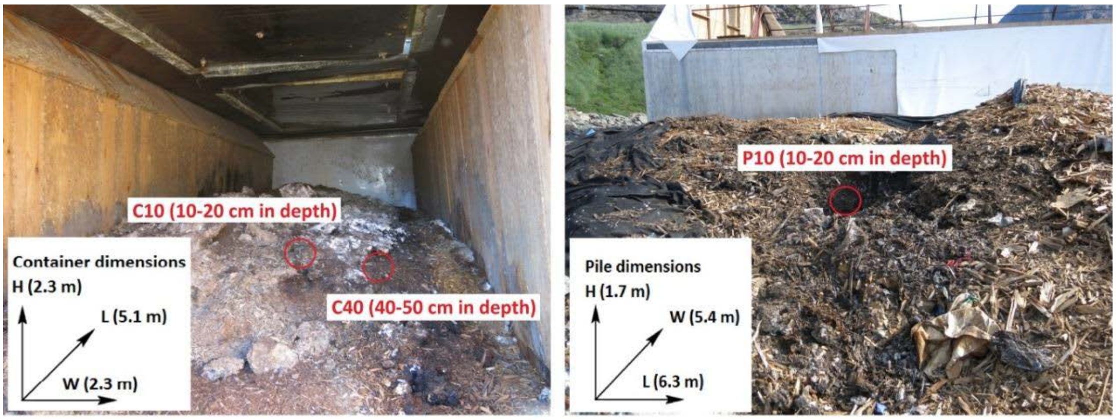

Fig. 1 Sample sites in container (left) and pile (right) including dimensions.

The sample C10 was from the top 10 – 20 cm of the container, where the compost was heterogeneous and dry, whereas the sample C40 was taken 40-50 cm from the top of the container, as below 30 cm in depth the compost was more homogeneous and moist. The compost in the pile was heterogeneous and the structures of the initial compost material were easily recognised, for instance wooden pallets. No change in the heterogeneity of the compost was observed in depth and thus only one sample was taken from the pile in the depth 10-20 cm (P10). The samples were stored in a refrigerator (2-4°C) until analysis.

2.3 Chemical analysis

Both waste and compost samples were dried at 105 ºC for 24 h and subsequently crushed until a homogenized sample was achieved. Moisture content was calculated after drying. To measure the loss on ignition (LoI) the samples were heated at 550 ºC for 1 hour. pH was measured potentiometrically in a suspension of waste and 1M KCl at a ratio of 1:2.5 and for the compost at a ratio of 1:10 after 1 hour of agitation. Further, pH and electrical conductivity (EC) of the compost samples were measured in a suspension of compost and distilled water, in the ratio 1:10. Total carbon and sulphur (TC and S_{tot}) content were determined using a LECO Induction Furnace CS-200. Nitrogen content was determined by the Kjeldahl method. The samples were digested after DS 259 by mixing 1.0 g of sample with 20 mL 7.3 M HNO_3 and heated at 200 kPa (120°C) for 30 min. The liquid was then filtered through a 45 µm filter and diluted to 100 ml. After digestion, the concentration of As, Ca, Cd, Cr, Cu, Fe, K, Mg, Mn, Na, Ni, P, Pb and Zn was measured by induced coupled plasma-optical emission spectrometry (ICP-OES). The Kjeldahl, LECO and digestion analysis were made in triplicates for the waste and waste mix samples and in five replicates for the compost samples.

Batch incubation tests were performed as in Pedersen et al. [5] to assess CH_4 oxidation rates and respiration rates. To determine the CH_4 oxidation, 50 g (wet weight) of compost was added to 300 mL infusion bottles sealed with gas-tight rubber septa. 40 mL air was removed with a syringe and 40 mL of CH_4 was added, and the samples were left overnight for the bacteria to adapt to the presence of CH_4. The bottles were ventilated in a fume hood for 30 min, and resealed with gas-tight rubber septa. 140 mL of air was removed with a syringe and 40 mL of CH_4 and 100 mL of O_2 was added. The composition of gas in the bottles was measured with a gas chromatograph (GC Trace 1300, Thermo Fisher Scientific, USA) approximately every third hour for four days and every eighth hour in the following week. To avoid anaerobic conditions in the bottles, O_2 was added multiple times when the concentration approached zero. This was necessary for all three replicates of P10, where in total 720 mL O_2 was amended, and of C10 where in total 170 mL O_2 was amended. The experiment to determine oxygen consumption and CO_2 production was executed in the same way, except that only O_2 was added.

3. Results and discussion

3.1 Efficiency of organic waste separation

The distribution of the material fractions for the collected organic waste from each source is presented in Fig. 2. Totally; 1600 kg organic waste was collected, corresponding to 710 kg from canteens and restaurants, 870 kg from supermarkets and 20 kg from households, representing a normal production for one week from the participators. Surprisingly, only 1 % of the organic waste was collected from the households. Most of the organic waste containers at the households were empty and the collected organic waste fraction from households contained 18 % non-organics (plastic wrappings, metal, glass and other impurities) and 9 % paper (including the paper bags used to collect the organic waste). Simultaneously, 32% of the residual waste collected from the same households consisted of organic waste and this shows that the source-separation of organic waste at households had limited success. Of the collected organic waste, 44 % originated from the canteens and restaurants and 55 % from supermarkets. Non-organics accounted for 3.9 % of the total waste from the canteens and restaurants, slightly more than in the waste from the supermarkets (2.7 %) and this result showed a significantly better separation than from the households. In general, the waste from supermarkets consisted of entire pieces of vegetables, fruits and bread.

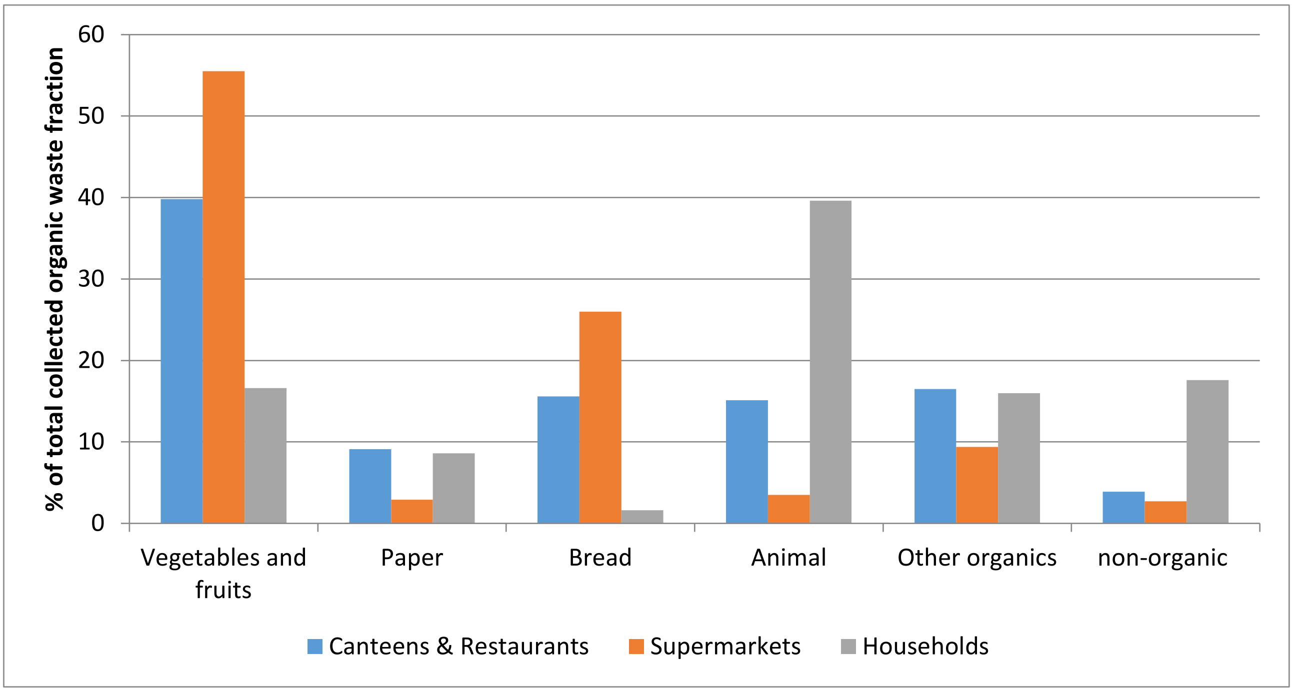

Fig. 2 Material fractions of the organic waste sorted in the canteens, supermarkets and households in percentages.

3.2 Characteristics of organic waste and mixed waste

The chemical characteristics of the organic waste and mixed waste (organic waste, shredded wood pellets and snow/water) is shown in Table 1.

Table 1 Average chemical composition of organic waste and mixture of organic waste and wood chips.

Chemical parameter	Organic waste	Mixed waste	Biowaste Greenland [6]	Biowaste Norway [7]	Wood chips [8]
LoI [%]	83.7 ± 0.3	86.6 ± 0.8	-	-	-
Water content [%]	48 ±13	52 ± 3	62.6	69.4-70.3	-
pH	5.3 ± 0.3	5.1 ± 0.4	-	4.9 - 6.1	4.7
TC/TOC [$\%_{dw}$]	23.4 ±11.2	16.1 ± 1.9	49.2	47.7 -48.1	55.2
TKN [$\%_{dw}$]	1.1 ±0.6	0.7 ± 0.1	3.7	2.3-2.9	0.1
C/N [-]	21	23	13	16.6-20.6	552
P_{tot} [$\%_{dw}$]	0.2 ± 0.06	0.1 ± 0.01	1.3	-	-
K [$\%_{dw}$]	0.4 ± 0.1	0.3 ± 0.02	0.7	-	-
Ca [$\%_{dw}$]	0.8 ± 0.2	0.6 ± 0.06	2.1	-	-
Mg [$\%_{dw}$]	0.2 ± 0.06	0.3 ± 0.05	0.2	-	-
Na [$\%_{dw}$]	0.3 ± 0.01	0.2± 0.02	0.8	-	-
Mn [$mg \cdot kg^{-1}$]	82 ± 26	97 ± 5.2	23.2	-	-
Fe [$\%_{dw}$]	0.74 ± 0.28	0.80 ± 0.05	0.02	-	-
As [$mg \cdot kg^{-1}$]	12.2 ±1.6	57.9 ± 8.2	3.53	-	-
Cd [$mg \cdot kg^{-1}$]	0.3 ± 0.1	0.3 ± 0.1	0.26	-	-
Cr [$mg \cdot kg^{-1}$]	12.2 ± 5.0	15.8 ± 1.9	1.27	-	-
Cu [$mg \cdot kg^{-1}$]	27.2 ± 9.0	26.5 ± 2.6	8.63	-	-
Ni [$mg \cdot kg^{-1}$]	12.1 ± 3.6	20.1 ± 8.2	1.38	-	-
Pb [$mg \cdot kg^{-1}$]	28.2 ±10	27.8 ± 1.8	0.24	-	-
Zn [$mg \cdot kg^{-1}$]	42.8 ±5.7	43.8 ± 4.7	34.1	-	-

The optimum moisture content for composting ranges from 40 to 70 %, with an ideal value of 60 % [9]. Other similar studies reported higher values of 60 % in the biowaste fraction of the general waste from several households in Sisimiut [6], 62.3 % in the source-separated food waste from households and stores in Norway [7] and between 84 and 93 % in the source-separated food waste from some restaurants and groceries in Canada [10].

The ideal pH for composting is between 7-8 [11]. Lower pH values in the range 4.8-5.5, were measured in all samples. Similar low values have been measured for source-separated biowaste in Scandinavia [12-13]. pH values below 6 are often related to slow decomposition and low compost quality but aeration or addition of CaO are possible measures to reduce acidity [14].

The balance between organic carbon and nitrogen is a key parameter to ensure microbial performance during the composting process. The suitable range of C/N ratios is 20-35 [15]. C/N ratios of the samples were in the range 19.8 – 26.8 suggesting appropriate nutrient availability. Some trace elements were present in significantly higher amounts in the mixed waste for composting than previously found in waste. This could be related to the presence of non-organic impurities. This explanation is supported by the different sorting methods in the studies: Eisted & Christensen [6] analysed the biowaste fraction of the general waste, which was sorted by specialists, while the waste in the current study was sorted at the source, increasing the probability of impurities.

3.3 Compost characteristics and quality

Table 2 and 3 provide an overview of the results from the chemical characterization of the compost samples and the batch incubation experiments. For assessment of the suitability of the compost as a growth medium and as biocover, recommended quality criteria from literature are shown. The common ranges given are typical declarations for kitchen waste compost used for landscaping.
The organic matter content is a key property to determine optimal moisture content for methane oxidation and Pedersen et al. [5] found an optimal water content of 52 % in compost with an organic matter content of 52 %. However, values for optimal water content for methane oxidation in compost with similar elevated LoI as found in this study were not found in literature. The low water content of C10 inhibits methane oxidation, however mixing of the compost can result in more homogeneity in

the water content, and if it is still too low, water can be added.

Table 2 Chemical composition in averages of compost samples. Values outside one standard deviation of the common range are in bold. QC = Quality criteria.

	Sample C10	Sample C40	Sample P10	Common range [11, 16]	QC (growth media) [11, 16,17]	QC (biocover) [5, 18,19]
Temperature [ºC]	14	14	50-55	-	-	-
LoI [%]	**83.7** ± 0.3	**86.6** ± 0.8	**76.4** ± 0.7	35 – 75	35 – 75	>15
Water content [%]	**29.5** ±1.7	63.3 ± 1.4	41.4 ± 5.0	40 – 75	40 – 75	≈52
pH_{KCl}	**5.7** ± 0.1	**6.2** ± 0.1	**5.2** ± 0.3	7.2 - 8.5	7.2 - 8.5	5.5 - 8.5
pH_{H2O}	**5.8** ± 0.0	**6.3** ± 0.1	**5.5** ± 0.1	7.2 - 8.5	7.2 - 8.5	5.5 - 8.5
EC [$mS{\cdot}cm^{-2}$]	**6.5** ± 0.6	3.0 ± 0.1	1.0 ± 0.0	1.5 - 4.0	0.3 - 0.6	<4
TC(≈TOC) [$\%_{dw}$]	**44.3** ± 1.8	**41.7** ± 2.7	**38.0** ± 3.2	19 - 25	19 - 25	>7
TKN [$\%_{dw}$]	**2.7** ± 0.1	1.5 ± 0.2	2.0 ± 0.1	1.7 - 2.1	1.7-2.1	>0.5
C/N	15.8	25.6	19.0	9.0 -14.7	9.0 -14.7	≈15
P_{tot} [$\%_{dw}$]	**0.9** ± 0.01	0.2 ± 0.03	**0.1** ± 0.01	0.2 - 0.3	0.2 - 0.3	>0.3
S_{tot} [$\%_{dw}$]	0.2 ± 0.0	0.1 ± 0.0	0.1 ±0.0	0.1-0.2	0.1 - 0.2	-
K [$\%_{dw}$]	**0.9** ± 0.03	0.4 ± 0.06	**0.2** ± 0.02	0.4 -0.7	0.4 - 0.7	-
Ca [$\%_{dw}$]	1.4 ± 0.2	**0.4** ± 0.06	0.6 ± 0.09	0.6 – 6.7	0.6 – 1.5	-
Mg [$\%_{dw}$]	0.17 ± 0.01	0.1 ± 0.02	0.07±0.01	0.1-1	0.02 -0.1	-
Na [$\%_{dw}$]	**1.3** ± 0.2	**0.7** ± 0.1	0.2 ± 0.02	-	< 0.3	-
Mn [mg/kg]	84.9 ±10.7	89.5 ±14.4	65.7 ± 8.8	-	20 – 80	-
Fe [$\%_{dw}$]	**0.08** ± 0.01	0.19 ±0.05	0.22±0.08	-	0.12 -0.25	-
As [$mg{\cdot}kg^{-1}$]	**30.2** ± 1.6	**57.9** ±8.2	16.8 ±3.6	-	<25	-
Cd [$mg{\cdot}kg^{-1}$]	0.3 ± 0.1	0.3 ± 0.1	0.2 ± 0.1	-	<0.8	-
Cr [$mg{\cdot}kg^{-1}$]	37.6 ± 2.2	33.7 ± 5.3	22.0 ± 3.8	-	<100	-
Cu [$mg{\cdot}kg^{-1}$]	40.3 ± 2.7	56.6 ± 9.0	57.4 ±12.0	-	<1000	-
Ni [$mg{\cdot}kg^{-1}$]	1.8 ± 0.3	**38.0** ± 2.7	3.4 ± 0.4	-	<30	-
Pb [$mg{\cdot}kg^{-1}$]	4.8 ± 0.8	22.0 ±3.4	31.9±17.1	-	<120	-
Zn [$mg{\cdot}kg^{-1}$]	199 ± 30.0	224 ± 24.1	93.2 ±14.9	-	<4000	-

Waste usually has acidic pH values until degradation and volatilization of the organic acids starts, then the alkalinity increases [11]. The low pH suggest that the compost samples were not fully degraded, and that C40 was more degraded than C10 and P10. This was expected since C40 was the oldest part of the compost. This is corroborated by the slightly lower pH in the fresh waste mixture used as compost material (Table 2). The acidity of the compost samples will limit the flora diversity to acidophilus, unless the compost pH is neutralised, for instance by addition of CaO [11]. All samples had a pH within the range for optimum growth and activity of methanotrophs (5.5 – 8.5) [19].

C10 had an elevated EC compared to the common range for kitchen waste compost, and all samples exceeded the recommended range for using the compost as growth medium. Few plants can grow in media with EC > 1.20 $mS{\cdot}cm^{-1}$, and plant growth is therefore likely limited by EC values in C10 and P10. Methanotrophs are tolerant to high EC and previous studies observed no change in methane oxidation rate at EC <4 $mS{\cdot}cm^{-}$ [20]. Thus, the only sample where methane oxidation was possibly limited by EC was C10.

Total organic carbon can be estimated as LoI divided by 1.8 [18]. However, using this approximation would result in a TOC higher than the measured TC. TOC was therefore assumed to equal TC, thus assuming negligible content of inorganic carbon. Only an insignificant difference in TC of the different samples was observed, suggesting that the heterogeneity of the compost did not influence the availability of organic carbon. TC values were higher than the recommendations for use as growth medium. This is in agreement with the LoI and the high content of wood which has a high C/N ratio [8]. Although TC in all samples was higher than recommended, examples exist of compost with comparable carbon content [10] and a TC of up to 60 is not considered a problem for plant growth [21]. However, to achieve C/N ratios of 9.0 – 14.7, correspondingly high N contents are required which has in some cases caused problems for plant growth [21].

TKN is often a limiting factor for plant growth [11]. The sample C40 had a TKN within the recommended range, P10 was within one standard deviation, and C10 was elevated. Lack of N can limit microbial activity and restrict the degradation of carbon compounds [10]. For use as biocover material a C/N ratio of 15 is recommended. TKN might therefore be limiting for methane oxidation. Since the compost did not appear fully degraded, a lower TOC and thus a lower C/N ratio can be expected over time [11].

The P_{tot} of C40 was within the recommended range for kitchen waste compost. The P_{tot} of P10 was lower than recommended which may limit plant growth if the compost is used as growth medium. Phosphorous is an essential nutrient for methanotrophs and a P_{tot} >0.3% is required [3]. This threshold value was only fulfilled by C10. Thus methanotrophic growth may be limited in C40 and P10. All samples had S_{tot} values within the recommended range for growth media and S_{tot} is thus not expected to limit plant growth.

C10 had elevated values for K, Mg, Na and low Fe compared to the recommendations. C40 had elevated Na values and low Ca and Mg values. P10 had low K content. Micronutrients are necessary for plant growth, and too low values can limit the growth. On the other hand, too high concentrations may inhibit the absorption, transport processes and utilization of other nutrients with similar chemical properties as they compete with one another [22]. For use of compost as biocover, no recommendations for micronutrient contents were found. Since the contents of Ca for P10 and C40 are respectively in the low end of and lower than the recommended range, lime can be added to increase the pH without exceeding the threshold. However, as C10 and C40 were both from the container, it is recommended that the compost is mixed during composting to get a more homogeneous product and a complete picture of how much lime can be added.

Compost exceeding the limit values for metals cannot be used for edible plant growth. C10 and C40 exceeded the limit value of As by 20% and 55% respectively, thus the compost is not safe to use for growing plants. The contents of Cr, Cu, and Zn were below the limit value for compost in all samples, but it was in some samples above the limit for soil used for plant growth. Therefore, even if the As and Ni contents could be minimized, plants should not grow directly in the compost but rather in a mix of compost and soil. These results were surprising since the organic waste used to produce the compost was found to have lower contents of these metals, making it safe to produce compost from. Since the content of metals had a large variance across samples, the elevated levels may have been due to contaminants in those parts of the compost sampled, and not reflect an elevated level in the compost on average. Another possibility is that metals were introduced to the compost during the shredding and mixing process, either from the equipment or from contaminated soil at the landfill where the pile of organic waste was stored.

The temperature was only logged in the container during the first three months of the composting process. The temperatures in the pile were not logged. However, the temperature log for the first three months in the container reveals that the compost reached 70ºC [23] in 60 hours as recommended to achieve hygienisation [11]. Even though the temperature initially secured hygienisation in the compost, mice were observed in the container which raised concern about possible contamination during storage.

The O_2 consumption rates (Table 3) are used to indicate the degree of maturity, which is important both for the potential of using the compost as a plant growth medium and as a biocover. C10 and P10 were determined to be “not finished” and C40 was “fresh” according to the maturity index presented by Christensen [11]. Only “stable” compost can be used as plant growth medium [11], meaning none of the samples can be utilized as growth media for plants until further degraded. C40 was expected to be more mature than C10 and P10 as it had been in the container for a longer time and had better conditions for degrading such as higher moisture content. This was confirmed, however none of the samples had the maturity required to be used as biocover.

Table 3 Resipiration and methane production rates for compost sampels. (1st) = first batch incubation experiment. (2nd) = second batch incubation experiment.

	C10	C40	P10	Common range [5,11]
O_2 consumption (1^{st}) [µg O_2· g_{dw}^{-1}·h^{-1}]	**70** Not finished [11]	**29** Fresh [11]	**124** Not finished [11]	<20 [5] Stable or very stable [11]
O_2 consumption (2^{nd}) [µg O_2·g_{dw}^{-1}·h^{-1}]	**111** Not finished [11]	**42** Fresh [11]	**148** Not finished [11]	<20 [5] Stable or very stable [11]
CO_2 production (1^{st}) [µg CO_2· g_{dw}^{-1}·h^{-1}]	117	80	148	4.3-73 [5]
CO_2 production (2^{nd}) [µg CO_2· g_{dw}^{-1}·h^{-1}]	103	52	133	4.3-73 [5]
CH_4 oxidation rate [µg CH_4· g_{dw}^{-1}·h^{-1}]	**0.1** (2^{nd})	**0.3** (1^{st})	**0.1** (2^{nd})	0.8-125 [5]

The initial methane oxidation test performed indicated that C40 oxidized CH_4 at a rate of approximately 0.3 µg·g_{dw}^{-1}·h^{-1}, as all CH_4 was oxidized within four days. C10 and P10 showed no CH_4 oxidation within two weeks. When the experiment was repeated with more replicates, the results were different. C40 did not oxidize any CH_4, while C10 and P10 initiated CH_4 oxidation within a week, however only at low rates compared to what was found in literature for more mature compost. The low methane oxidation rates were expected both due to the low maturity and due to other factors such as the content of water and phosphorus. The results indicate, that there may be potential for methane oxidation by the microorganisms in the compost, but at this time it is only at low rates and not consistently observed in all replicates. It is therefore recommended to test the methane oxidation rates in the compost again, when more mature.

The necessity of increasing the temperature to initiate the composting process during the winter 2014 indicates that degradation of waste and thus methane production will be slow if even existent for fresh waste during the winter. However, the measured temperature in the compost pile standing outside the container was approximately 55°C, which suggests that the degradation was ongoing, and thus degradation of waste can happen without aids during summer. The same was observed in Yellowknife, Canada where a composting process using the turned windrow method and regular irrigation successfully produced finished compost after two summers [24]. Degradation could possibly also occur during winter for material that has already started degradation, if the degradation process itself can sustain a sufficiently high temperature to keep the microorganisms active in the isolated middle of the material. The self-heating ability is especially high in fresh material and decreases with maturity [11]. Due to the degradation, CH_4 production is expected at the landfill and a biocover would be relevant. In order to conclude whether the compost is suitable for use as biocover, maturity must be achieved before further testing. A second test will preferably also include field conditions, as low temperatures (5-10°C) have been found to slow down methane oxidation [25]. Field studies have shown temperature dependency of biocover efficiency but also in some cases elevated temperatures in CH_4 oxidation layers of biocovers even during cold periods [26]. However this has yet to be investigated under Arctic conditions. Another factor that would be relevant to investigate is the grain size distribution of the material, especially if the recommendation of adding less wood is followed. The grain size influences porosity and permeability [27]. This has been shown to influence biocover efficiency [28].

4. Conclusion

The source separation of organic waste from households was inefficient as shown by high content of impurities in the organic fraction, and a high organic content in the residual fraction. The source separation from restaurants, canteens, and supermarkets was efficient and showed potential for composting a large fraction of the organic waste in Sisimiut. The chemical analysis showed that the composition of the source-separated organic waste was suitable and safe for compost production. However, after one year of composting, the compost was not mature enough to be used as either growth media or biocover. If the compost should be used as a growth medium, the composting process should be improved by lowering the content of woodchips, adding more water, mixing more frequently, and avoiding contamination of the organic waste with metals. The methane oxidation rates should be tested again when the compost has become more mature to conclude if the compost can be used as a biocover.

5. Acknowledgements

Naalakkersuisut (the Government of Greenland) and Qeqqata Kommunia are thanked for financing this project.

References

[1] MYHRE G., SHINDELL D., BRÉON F.-M., COLLINS W., FUGLESTVEDT J., HUANG J., KOCH D., LAMARQUE J.-F., LEE D., MENDOZA B., NAKAJIMA T., ROBOCK A., STEPHENS G., TAKEMURA T. and ZHANG H., "Anthropogenic and Natural Radiative Forcing. In: *Climate Change 2013: The Physical Science Basis. Contribution of Working Group I to the Fifth Assessment Report of the Intergovernmental Panel on Climate Change*," Cambridge University Press, Cambridge, United Kingdom and New York, NY, USA, 2013.

[2] BLANCO G., GERLAGH R., SUH S., BARRETT J., D CONINCK H. C., MOREJON C. F. D., MATHUR R., NAKICENOVIC N., AHENKORA A. O., PAN J., PATHAK H., RICE J., RICHELS R., SMITH S. J., STERN D. I., TOTH F. L. and ZHOU P. , "Drivers, Trends and Mitigation*. In: Climate Change 2014: Mitigation of Climate Change. Contribution of Working Group III to the Fifth Assessment Report of the Intergovernmental Panel on Climate Change*," Cambridge University Press, Cambridge, United Kingdom and New York, NY, USA, 2014.

[3] HUBER-HUMER M., RÔDER S. and LECHNER P., "Approaches to assess biocover performance on landfills," *Waste Management*, vol. 29, pp. 2092-2104, 2009.

[4] CHRISTENSEN J. H., OLESEN M., BROBERG F., STENDEL M. and KOLDTOFT I., "*Fremtidige klimaforandringer i Grønland: Qeqqata Kommune*," Danmarks Meteorologiske Institut, København, 2016.

[5] PEDERSEN G. B., SCHEUTZ C. and KJELDSEN P., "Availability and properties of materials for the Fakse Landfill biocover," *Waste Management*, vol. 31, pp. 884-894, 2010.

[6] EISTED R. and CHRISTENSEN T. H., "Review: Characterization of household waste in Greenland," *Waste Management*, vol. 31, pp. 1461-1466, 2011.

[7] SUNDBERG C., FRANKE-WHITTLE I., KAUPPI S., YU D.,ROMANTSCHUCK M., INSAM H. and JÖNSSON H., "Characterisation of source-separated household waste intended for composting," *Bioresource Technology*, vol. 102, pp. 2859-2867, 2011.

[8] HONG J. H. and PARK K., "Wood chip biofilter performance of ammonia gas from composting manure," *Compost Science & Utilization*, vol. 12, pp. 25-30, 2013.

[9] EVANS G., "*Biowaste and biological waste treatment"*, London: James & James, 2001.

[10] MORIN S., LEMAY S. and BARRINGTON S., "An urban composting system. Paper No. 03-612," in CSAE/SCGR 2003 meeting, Quebec, Montreal, 2003.

[11] CHRISTENSEN T. H., *Solid Waste Technology & Management*, Chichester: John Wiley & Sons, Ltd, 2011.

[12] EKLIND Y., BECK-FRIIS B., BENGTSSON S., EJLERTSSON J., KIRCHMANN H., MATHISEN B. and NORDKVIST E., "Chemical characterization of source-separated organic household waste," *Swedish Journal of Agricultural Research*, vol. 27, p. 167–178, 1997.

[13] NORGAARD E. and SORHEIM R., "Tiltak for å sikre rask etablering av varmkompostering ved behandling av bioavfall (Measures for the establishment of thermal composting when treating biowaste," Norsk Jordforbedring & Jordforsk, 2004.

[14] FERNANDES F., VIEL M., SAYAG D. and ANDRÉ L., "Microbial breakdown of fats through in-vessel co-composting of agricultural and urban wastes," *Biological Wastes*, vol. 26, p. 33–48, 1988.

[15] HAUG R. T., "*The practical handbook of compost engineering*", Boca Raton, USA: Lewis Publishers, 1993.

[16] BEK. nr. 1001 af 27/06/2018, Bekendtgørelse om anvendelse af affald til jordbrugsformål (Slambekendtgørelsen), København: Miljø- og Fødevareministeriet, 2018.

[17] LECHNER P., HEISS-ZIEGLER C. and HUMER M., "Reducing greenhouse gas emissions: How composting and compost can optimize landfilling," *BioCycle* , vol. 43 , no. 9, pp. 31-37 ,

2002 .
[18] MOR S., VISSCHER A. D., RAVINDRA K., DAHIYA R. P., CHANDRA A. and CLEEMPUT O. V., “Induction of enhanced methane oxidation in compost: Temperature and moisture response,” *Waste Management* , vol. 26, p. 381–388, 2006.
[19] HUMER M. and LECHNER P., “Alternative approach to the elimination of greenhouse gases from old landfills,” *Waste management & Research*, vol. 17, pp. 443-452, 1999 .
[20] GEBERT J., GROENGROEFT A. and MIEHLICH G., “Kinetics of microbial landfill methane oxidation in biofilters,” *Waste Management*, vol. 23, pp. 609-619, 2009.
[21] Crop Nutrition Laboratory Services, “*Manure Compost Analysis Report, April 2014*,” Crop Nutrition Laboratory Services ltd, Nairobi, 2014.
[22] FAGERIA V. D., “Nutrient Interactions in Crop Plants,” *Journal of Plant Nutrition* , vol. 24, no. 8, pp. 1269-1290 , 2001.
[23] JUNGERSEN M., “*Qeqqata Komunia Pilotprojekt med Kompostering*,” Qeqqata Komunia, Sisimiut, 2014.
[24] RIPLEY S., “Yellowknife Centralized Composting Pilot Project Final Report,” *Ecology North*, Yellowknife, 2012.
[25] BÖRJESSON G., SUNDH I. and SVENSSON B., “Microbial oxidation of CH4 at different temperatures in landfill cover soils,” *FEMS Microbiology Ecology*, vol. 48, pp. 305-312, 2003.
[26] KJELDSEN P. and SCHEUTZ C., “Reduction of methane emission from landfills using bio-mitigation systems – from lab tests to full scale implementation,” Istanbul, 2014.
[27] NAZAROFF W. W. and ALVAREZ-COHEN L., “*Environmental Engineering Science”*, 1st ed., New York: John Wiley & Sons, Inc., 2001.
[28] KHOSHAND A. and FALL M., “Hydraulic and thermal conductivity of compost based biocover,” Montréal, 2013.

Zhanbolat Anuarbekovich Shakhmov, PhD,
Head of Civil Engineering department, Associate Professor
L.N. Gumilyov Eurasian National University
Kazakhstan
zhanbolat8624@gmail.com

Askar Zhussupbekov, L.N. Gumilyov Eurasian National University, Kazakhstan
Gulshat Tleulenova, L.N. Gumilyov Eurasian National University, Kazakhstan
Aigerim Karagulova, L.N. Gumilyov Eurasian National University, Kazakhstan

INFLUENCE OF CLIMATIC DATA TO SEASONALLY FREEZING SOIL GROUND IN KAZAKSHTAN

Summary

The construction of the foundation in seasonally frozen soil ground in Astana (the capital of Kazakhstan) is the most urgent problem today. Unfortunately, one of the factors that negatively affected the stability of the soil base is the freezing of the soil base and consequently the loss of their stability as a result of thawing. Foundation design in areas of seasonal frozen soil ground depends on the choice of an appropriate foundation depth and protection of foundation from the effects of frost action, particularly where there is frost susceptible soil. Under certain conditions, harmful frost action effects may arise sharply. The cyclical nature of seasonal freezing and thawing is complex thermo-physical processes, entailing consequences, such as frost heaving and glaciation of soil layers, and, subsequently, sediment development, leading to deformations of buildings and structures. The application of the results of the calculation of seasonally frozen soils can determine the optimal depth of the foundations [1,2].

Keywords: frost swelling, glaciation, optimal depth, seasonally frozen soil, deformation.

1. Introduction

There are many investigations provided and analysed about frost action process. The most urgent problem regarding to this topic is the research of freezing in construction. There are done much investigation in laboratories about frost action in soil in next countries Russia, Scandinavian countries, USA, Canada, Japan, Korea [3,4].

The climate of Astana is a sharply continental temperate climate zone.It locates in the valley of the Ishim river. Ishim at a great distance from all the oceans, Astana is characterized by very severe winters and dry summers. The winter period is an average of 5 months, during which soils are exposed to negative temperatures, which lead to deformations of buildings and structures. The depth of soil freezing is 205 cm [5]. The frost action is general word, which include many meanings such as frost heaving, heaving force, unfrozen moisture content, frost depth and so on. Frost heaving is main dangerous factor for stability of foundation. Much research are done for investigation how influence moisture content, negative temperature, soil type to frost heaving development during freezing process [6, 7]. The influence of frost action could be damageable and accidental not only to buildings, but also very dangerous for stability and settlement of underground infrastructures. Thermal insulation design for underground utilities and how backfill materials, geometry, thickness of insulation studied by researchers from Canada [8].

The geotechnical conditions of the territory of Astana are represented by a diverse complex of soils: loam with interlayers and sandy loam lenses; sandy loam; medium-sized sands with lenses of sandy loam; gravel sands; clay. The problem of designing and building on heaving soils is particularly acute in Astana due to the increasing volumes of construction (Fig. 1).

Fig. 1 Unique architectural buildings in Astana

2. Methodology

The basic laws of freezing at a specific site are determined by the conditions of heat exchange on the soil surface, its composition and state. The depth of freezing depends mainly on the following four characteristics: average annual soil temperatures, annual amplitudes of surface temperatures, soil composition and moisture content. The solution of particular problems for cases of freezing during continuously occurring phase transitions, as well as taking into account the processes of moisture migration, has shown that the movement of the phase boundary downward in many cases can occur according to the law of moisture migration. It has shown that the movement of the phase boundary downward in many cases can occur according to the law $df(f) = \alpha t$, where $\alpha>0$ – constant, determining the rate of freezing and depending both on the boundary conditions in the temperature and humidity problems, and on the entire set of heat and mass transfer characteristics, t -time.
The exact solution of the classical Stefan problem can be described in a similar way by the specified expression. An approximate solution for determining the depth of seasonal freezing by the LS method. Leibenzon produce on the basis of dependence in the form $d_f(t) = \alpha t$, in which α is determined by the indicators of the physical properties of the soil, the temperature of the frozen and thawed layers and phase transitions. Thus, the analysis of theoretical solutions to the problems of the depth of soil freezing in a wide range of parameter values included in the calculation formulas shows that, in a generalized form, the patterns of change in the depth of seasonal freezing throughout the territory of Kazakhstan can be expressed by the equation

$$d_{fn}=\alpha t \quad (1)$$

where α - generalized characteristic of the freezing rate, $m/s^{/2}$
t - time for the period of freezing, s

Numerous observations by foreign authors at experimental sites beyond the depth of seasonal freezing confirm this pattern. These sites are located in areas where the maximum depth of freezing is from 1.5 to 3.5 m or more. These observations also confirm the validity of determining the normative depth of seasonal freezing in accordance with the recommendations of SNiP 2.02.01-83 *, i.e. according to the equation

$$d_{fn}=d_o M_t \qquad (2)$$

Where d_0 -- the value taken depending on the type of freezing soil in the range from 0.23 to 0.34; M_t – the sum of the absolute values of mean monthly negative air temperatures during the winter in the area under consideration.

Equation (2) complies with the requirements of the aforementioned “Stefan Problem” solutions for estimating the freezing depth obtained without any conditions for limiting this depth. An analysis of the original formula, given in the mandatory annex of SNiP 2.02.04-88, shows that it is based on a decision with certain clarifications concerning the temperature at which the soil begins to freeze. Thus, along with rigorous theoretical solutions to the problems of estimating the temperature fields of freezing (thawing) soils when solving many design and foundation issues, the depth of seasonal freezing (thawing) can be determined on the basis of the pattern described as an expression of equation (1). This expression was used in the development of a theoretical method for predicting moisture accumulation in the freezing soil layer and the amount of frost heaving of the soil foundations in the problems considered below.

3. Study Area and Datasets

For preliminary calculations, the normative freezing depth is allowed to be determined according to a schematic map (Fig. 2).

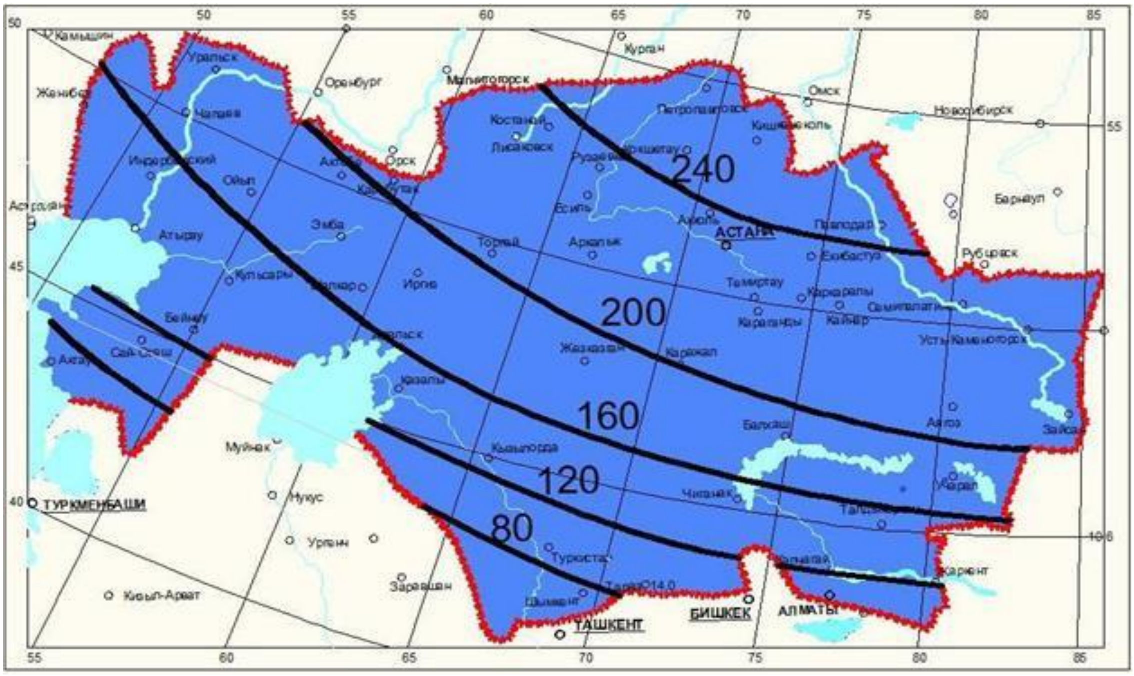

Fig. 2 Schematic map of the normative freezing depths

The map was compiled to estimate the depth of freezing for loams and clays. Therefore, when determining the depth of freezing soils of other varieties, the value of normative freezing found on the map should be multiplied by the ratio $d_0/0.23$, here d_0 corresponds to the soils of the considered site. The value of d_0 for areas composed of soils that are not uniform in depth is determined as the weighted average of the depth of the seasonal freezing layer.

To determine the temperature regime of the soil ground of shallow foundations, pipelines and other structures with insulating elements, a nonlinear two-dimensional (flat) or three-dimensional (spatial) problem is solved using the finite element method. The most convenient for design is the program TEMP / W. However, this program does not take into account the migration of moisture to the freezing front, in contrast to the “Thermoground” program, developed by specialists from neighboring Russia. When determining the depth by time, the temperature field in these programs is found at the mean (standard) temperature of the soil on the surface and its duration, which does not allow for the distribution of negative temperature over the depth of frost penetration when interacting with the sources of radiation embedded in the soil.

It is considered that the temperature of the soil varies slightly each year, which allows the processing to be limited to relatively short series of observations. The distribution of mean monthly, decadal values of the soil temperature at depths of 0.2 ... 3.2 m is considered to be normal.

To extend a series of parallel observations of the distribution of soil temperature and the maximum penetration depth of 0 ° C into the ground for surfaces cleaned and untreated from snow (5 years), known methods of ratios and temperature differences over the freezing depth were used.

The large scatter of soil temperature in areas of Kazakhstan for cleaned and untreated snow surfaces is explained by the influence on the freezing of a large number of factors (humidity and groundwater level, snow thickness, soil type and density, topography and microrelief, vegetation, etc.). Moreover, such a determining factor as an index of freezing, equal to the sum of the products of the absolute values of negative temperatures for a time

$F=T_i/\Delta t_i$ (3)

changed slightly by observation posts. Below, in tabular and graphical form, the results of the calculation of the index of freezing for the last 17 years in Astana are presented.(Fig.3,tab.1)

Table 1 Freezing Index in Astana

I	II	III	XI	XII	year	F, freezing index $^{o}C\cdot day$
-14.1	-14.8	-1.9	-2.0	-12.4	2001	1354.8
-6.3	-5.6	0.9	-2.5	-17.8	2002	978.9
-13.6	-15.1	-9.3	-6.9	-9.5	2003	1634,2
-14.8	-9.6	-7.5	-1.4	-12.8	2004	1398,9
-14.3	-19.1	-3.2	-2.3	-10.5	2005	1471,8
-23.0	-10.7	-1.6	-3.2	-7.0	2006	1375,2
-8.5	-10.9	-9.0	-4.4	-12.9	2007	1379,6
-21.5	-13.6	0.2	-0.9	-11.4	2008	1427,7
-13.5	-16.0	-4.5	-4.0	-14.0	2009	1560
-19.4	-20.0	-6.7	0.2	-12.6	2010	1759.7
-18.5	-13.6	-7.4	-8.8	-15.0	2011	1912.7
-16	-18.5	-3	-5	-19	2012	1846
-11.5	-11	-2	-2	-7.5	2013	1019
-15	-16.5	-2	-7	-9.5	2014	1493,5
-14.5	-8.5	-4.5	-5	-4.5	2015	1116,5
-12.5	-5.5	-1.5	-9.5	-9.5	2016	1167,5
-10	-12	-4.5	0	-18.5	2017	1359

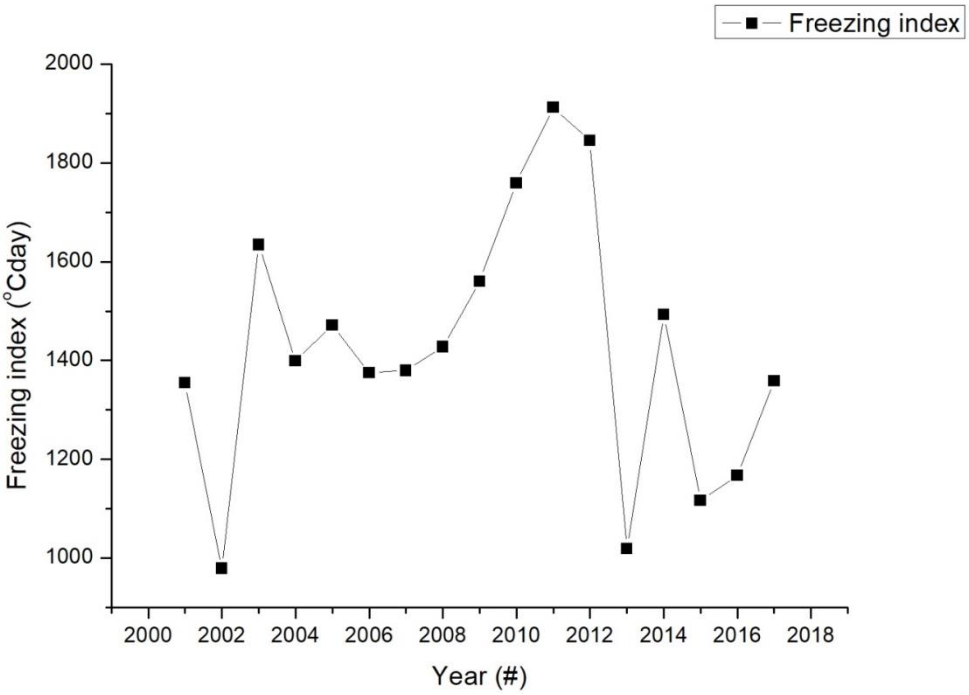

Fig. 3 Freezing Index in Astana

The penetration depth of 0 ° C in the soil at the actual humidity is determined by the formulas

$$d_{f,w} = k_{df} d_{f,c} \quad (3)$$

$$k_{df} = d_{f,w} / d_{f,n} \quad (4)$$

where k_{df} – coefficient taking into account the effect of moisture on the depth of soil freezing.

These equations are provided for definition of foundation depth in the project stage of future construction.
To determine the depth of frost penetration, the d_o coefficient is used, which depends on the type of soil. For loams and clays - 0.23; sandy sands, fine and silty sands - 0.28; gravel, coarse and medium sands - 0.30; coarse soils - 0.34.

year	M_t, °C	d_{fn}, m (clay and silts)	d_{fn}, м (loam, fine sand, silty sand)	d_{fn}, м (gravelly sand, coarse and medium)	d_{fn}, м (coarse soils)
		1	**2**	**3**	**4**
2001	45,2	1,55	1,88	2,02	2,29
2002	32,2	1,31	1,59	1,70	1,93
2003	54,4	1,70	2,07	2,21	2,51
2004	46,1	1,56	1,90	2,04	2,31
2005	49,4	1,62	1,97	2,11	2,39
2006	45,5	1,55	1,89	2,02	2,29
2007	45,7	1,55	1,89	2,03	2,30
2008	47,4	1,58	1,93	2,07	2,34
2009	52,0	1,66	2,02	2,16	2,45

2010	58,7	1,76	2,15	2,30	2,60
2011	63,3	1,83	2,23	2,39	2,71
2012	61,5	1,80	2,20	2,35	2,67
2013	34,0	1,34	1,63	1,75	1,98
2014	37,0	1,40	1,70	1,82	2,07
2015	37,0	1,40	1,70	1,82	2,07
2016	38,5	1,43	1,74	1,86	2,11
2017	45,0	1,54	1,88	2,01	2,28

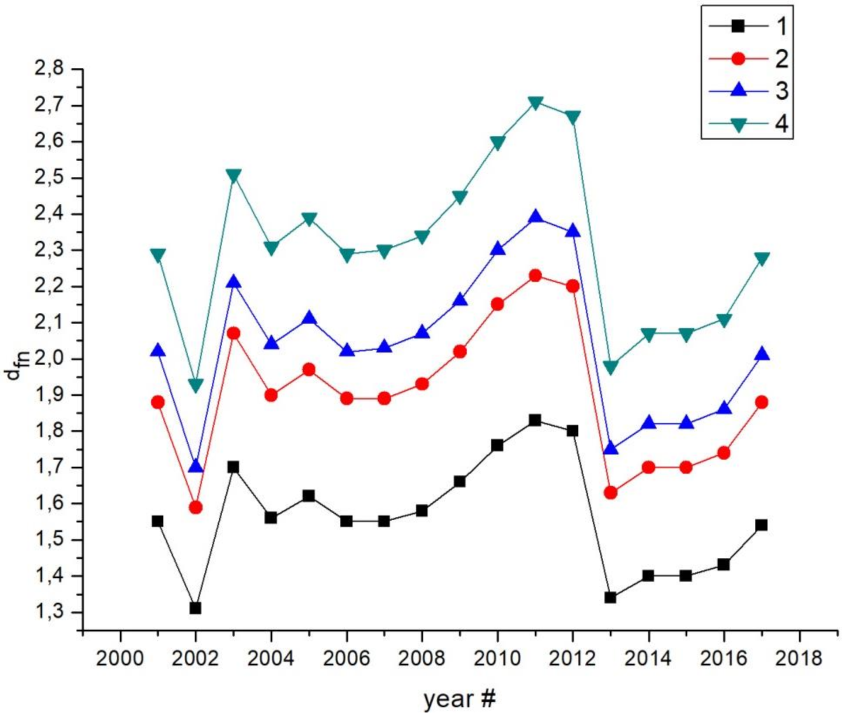

Fig. 4 Frozen depth (d_{fn}) of soil ground depend on soil type

The Figure 4 illustrates freezing depth of soil ground depend on its type. The freezing index is also used for determination of freezing depth of soil. The results shows the freezing depth changing about to 20% from minimum to maximum amount during 2000 and 2018. However, amount of year are not enough for proposing some solid argumentation or conclusion about some rule of freezing depth variation.

Conclusion

The article presents the results of an analytical calculation that can be used in the design of foundations. In particular, one can observe cyclical changes in the freezing index. Freezing index has enough high variation during only about 20 year. Also, there are presented results of frozen depth depend on freezing index. Some data show minimum results in 2002, 2013. While maximum results demonstrated according figures in 2003, 2011 in Akmola region of Kazakhstan. No doubt, further research should be done for more better analyzing in this region, because many infrastructure and resident constructions build and planning to build in near future.

References

[1] SHAKHMOV Z., TLEUBAYEVA A., SMAGULOVA E., UTEPBERGENOVA L., TOGABAYEV Y., BAZARBAYEV D., “Analyzing of soil ground to frost heaving of structures”, *8th Asian Young Geotechnical Engineers Conference*, Astana, Kazakhstan, 2016, pp. 47-50.
[2] ZHUSSUPBEKOV A., SHAKHMOV ZH., LUKPANOV R., TLEULENOVA G., “Frost depth monitoring of pavement and evaluation of frost susceptibility at soil ground in Kazakhstan”, *19th International Conference on Soil Mechanics and Geotechnical Engineering*, Seoul (Republic of Korea), 2017, pp. 1455-1458.
[3] KARLOV V.D., Foundations and foundations on seasonally frozen heaving soils, Saint Petersburg, 2007, p.87.
[4] ZHUSSUPBEKOV A., SHIN E., SHAKHMOV ZH., TLEULENOVA G., “Experimental study of model pile foundations in seasonally freezing soil ground”, *International Journal of Geomate*, Vol. 15, Issue 51, 2018, pp. 85-90.
[5] TELTAYEV B., SUPPES E., “Temperature in pavement and subgrade and its effect on moisture”, *Case Studies in Thermal Engineering*, Vol. 13, 2019.
[6] LARSON L.L., KIEMNEC G.L., JOHNSON D.E., “Influence of freeze-thaw cycle on silt in sagebrush steppe of Northeastern Oregon”, *Rangeland Ecology & Management,* Vol. 72, 1, 2019, pp. 69-72.
[7] Xu J., Wang Q., Ding J., Li Y., Wang S., Yang Y., “Frost heave of irrigation canals in seasonal frozen regions”, *Advances in Civil Engineering,* Vol. 2019, 2019,
[8] Liu H., Maghoul P., Shalaby A., “Optimum insulation design for buried utilities subject to frost action in cold regions using the Nelder-Mead algorithm”, *International Journal of Heat and Mass Transfer,* Vol. 130, 2019, pp. 613-639.
[9] Pylkkanen K., Nurmikolu A., Guthrie W., Argyle H., “Measurements and modeling of frost depth in railway tracks”, *Proceedings of the International Conference on Cold Regions Engieering,* 2015, pp. 123-134.
[10] Shi Y., Niu F., Lin Z., Luo J., “Freezing/thawing index variations over the circum-Arctic from 1901 to 2015 and the permafrost extent”, *Science of the Total Environment,* Vol. 660, 2019, pp. 1294-1305.